University of Molise
Department of Bioscience and Territory

PhD course in Bioscience and Territory

XXXIV Cycle

AGR/05

PhD research project:

Atmospheric particulate matter (PM) removal by deposition on leaves: analytical evaluation and applications to biomonitoring and to nature-based solutions (NbS)

PhD candidate

Martina Ristorini

164322

Supervisors

Prof. Vittorio Garfì

Prof. Carlo Calfapietra

Prof.ssa Silvia Canepari

Prof.ssa Chiara Baldacchini

PhD coordinator

Prof. Giovanni Fabbrocino

Academic year: 2020/2021

Index

Acronyms

a.d.	Aerodynamic diameter
AA	Ascorbic acid
AAS	Atomic absorption spectroscopy
BC	Black carbon
DCFH	Dichlorofluorescein
DTT	Dithiothreitol
EC	Elemental carbon
EC	Electrical conductivity
ES	Ecosystem service
HSRS	High spatial resolution samplers
HVS	High volume sampler
IC	Ionic chromatography
ICP-MS	Inductively coupled plasma mass spectrometry
ICP-OES	Inductively coupled plasma atomic emission spectroscopy
LAI	Leaf area index
LVS	Low volume sampler
NbS	Nature-based solution
OC	Organic carbon
OP	Oxidative potential
PAH	Polycyclic aromatic hydrocarbon
PM	Particulate Matter
PMF	Positive matrix factorization
POP	Persistent organic pollutant
R_a	Aerodynamic resistance
R_b	Boundary resistance
R_c	Surface resistance
R_{tot}	Total resistance
SEM/EDX	Scanning Electron Microscopy coupled with Energy Dispersed X-ray
SIRM	Saturation Isothermal Remanent Magnetization
TOC	Total Organic Carbon
UV-Vis	Ultraviolet and visible

V_d	Deposition velocity
VF	Vacuum Filtration
VOC	Volatile organic compounds
WSOC	Water soluble organic carbon
XRF	Energy-dispersive X-Ray fluorescence

Description and objectives of PhD thesis

The present PhD research project investigates the removal mechanism of atmospheric particulate matter (PM) by deposition on tree leaves, in urban and industrial areas. This study aims to identify and validate new analytical procedures for the assessment of PM leaf deposition and to exploit them to test the capability of leaves as alternative, low-cost and passive PM samplers with biomonitoring or air mitigation purposes.

Some of the most used experimental techniques for the quantification and characterization of leaf deposited PM are reviewed (Chapter 2) and compared to each other (Chapter 3). Namely, leaf microanalysis by Scanning Electron Microscopy coupled with Energy Dispersed X-ray (SEM/EDX) is tested and validated on several leaf samples collected from different species and from specific nature-based solutions (NbS). The proposed procedure allows the combined chemical and physical characterization of leaf deposited PM, thus being able to provide information on particles density (number of particles per unit leaf area), size distribution, chemical composition and finally through the combination of these parameters, mass of removed particles. Vacuum filtration (VF) gravimetric procedure, based on leaves washing and subsequent filtration of washing solutions, is also applied and tested to this aim. Then, a chemical fractionation procedure based on the characterization of both leaf washing solutions and membrane filters by means of electrical conductivity (EC), ionic chromatography (IC), inductively coupled plasma mass spectrometry (ICP-MS), UV-Visible spectrophotometer, total organic carbon analyzer (TOC) and inductively coupled plasma atomic emission spectroscopy (ICP-OES) is validated, thus allowing to achieve information on both the water-soluble and insoluble fraction of leaf deposited PM. Results obtained from the three approaches are compared, in order to prove their efficiency and to highlight their main limitations. PM water-soluble fraction quantified by means of the chemical fractionation results to be proportional to the washing solutions EC, while the insoluble fraction of coarse particles ($PM_{2.5-10}$) results to be consistent with the gravimetric VF results. The chemical fractionation proves to be reliable for the estimation of total and inorganic leaf deposited PM, with PM_{10} load values similar to those determined by SEM/EDX.

The potentialities of the characterization of leaf deposited PM for biomonitoring and source apportionment purposes have been explored in connection within two different urban contexts (Terni

and Turin, Italy; Chapter 4). To this aim, and in the first study (Terni), the leaf deposition of specific PM elemental components, known as specific source tracers, is compared to their atmospheric concentrations as obtained by the chemical characterization of PM_{10} membrane filters actively sampled at the same sites. Additionally, and in a second case study in Turin, the PM leaf deposition data obtained by SEM/EDX microanalysis from two NbSs, urban productive gardens and an urban forest, are integrated with the atmospheric concentrations of PM and its elemental components as retrieved by the analysis of the sampled membrane filters (Chapter 5), to evaluate the role and impact of specific emission sources acting in the study area.

In Chapter 5, new insights on the tree leaf efficiency for the removal of atmospheric PM and the improvement of urban air quality are also provided, in connection with the new concept of NbS. In particular, the PM removed by vegetation in three different NbSs realized within the context of the European project H2020 "productive Green Infrastructure for post-industrial urban regeneration': nature for renewal - proGIreg" has been assessed by SEM/EDX leaf microanalysis. The studied NbSs have been realized in post-industrialized context of Turin (Italy), Dortmund (Germany) and Ningbo (China). In each case study, results related to leaf deposited PM and its chemical/physical characteristics are presented as a function of plant species and size fraction. In Turin and Ningbo, PM removal via leaf deposition is evaluated at different NbS, an urban forest, urban gardens and a renatured lakeshore. Specifically for the two NbSs in Turin, results are integrated with those retrieved from the chemical characterization of PM_{10} membrane filters actively sampled at the same sites, as previously described. In the specific case of a renatured landfill in Dortmund (DE), SEM/EDX experimental results are also compared with those obtained by the *i-Tree Eco* model (USDA Forest Service), largely used for assessing the provision of ESs by vegetation in urban areas.

Finally in Chapter 6, the application of new and alternative techniques for the monitoring and spatially-resolved analysis of atmospheric PM is described. All of these additional studies are connected to the potential overcoming of some of the main limitations associated to conventional PM monitoring. These aspects result to be extremely functional for achieving a reliable evaluation of the spatial variability of PM and its main components to be used in the assessment of emission sources impact, and human health exposure. Moreover, and coherently with the aims of this PhD thesis, being able to obtain reliable and high spatially resolved data is extremely useful for a proper validation of data retrieved through the utilization of leaves as low-cost PM samplers and through the chemical and physical characterization of deposited particles. To this aim, newly-developed and low-cost active PM_{10} samplers, the High Spatial Resolution Samplers (HSRS, Fai Instruments, Fonte Nuova, Italy) are employed in a wide and dense network across Terni in central Italy, for the evaluation and

mapping of the spatial distribution of PM_{10} and its main elements. The application of oxidative potential (OP) acellular assays on PM_{10} membrane filters is also reported, to evaluate the relative relevance of single emission source in inducing oxidative stress, thus being recognized as one of the main mechanisms by which PM causes negative effects on organisms. In the same study area, the efficiency of lichen transplants is tested with biomonitoring purposes and for the evaluation of the spatial distribution of persistent organic pollutants (POPs). Then, the Positive Matrix Factorization (PMF) model is applied to chemical data retrieved from the analysis of PM_{10} membrane filters sampled before, during and after the Covid-19 lockdown, to evaluate the chemical profiles of natural and anthropogenic sources and their contribution to PM_{10} mass concentration during these peculiar periods.

Concluding, the results obtained and presented in this PhD thesis provide new insights on the evaluation of atmospheric PM leaf deposition and its main applications. The newly proposed chemical fractionation results to be effective for obtaining detailed information on the water-soluble and insoluble fraction of leaf deposited PM and for increasing the selectivity of PM elemental components as specific source tracers. The comparison with the atmospheric concentrations of PM and its main elemental components, proved the reliability of leaves as low-cost passive PM samplers which can be deployed for the identification of specific emission sources and the evaluation of their impact. Finally, SEM/EDX leaf microanalysis, thus being able to provide a physical/chemical characterization of leaf deposited PM as complete as possible, proved its efficiency for evaluating the species-specific affinity and the efficiency of NbS implemented in urban and post-industrial areas towards this removal mechanism.

1. Introduction

Atmospheric PM is an extremely heterogeneous mixture of solid and liquid airborne particles having different physical and chemical characteristics. The deposition on leaf surfaces is one of the most important removal mechanisms for this pollutant. The process itself is complex and dynamic, thus being influenced by several factors, connected to chemical-physical characteristics of PM, meteorological conditions, and species-specific characteristics of the vegetation. Due to its intrinsic complexity, it is still quite unsure what is the most efficient analytical procedure applicable to the evaluation of this process. On the other hand, being able to effectively characterize leaf deposited PM, in terms of chemical composition, size distribution, morphology, density and solubility, certainly deserves particular interest for its potential application to source apportionment purposes and to the assessment of risk exposure for human health.

In fact, once the different analytical procedures are validated, results obtained can be used to identify and quantify the impact and the role of specific natural/anthropogenic PM emission sources. This is true since chemical and physical characteristics of emitted, and thus leaf deposited PM are strongly affected by the type of emission source and/or process. To this aim, the evaluation of PM leaf deposition with biomonitoring purposes is taken in consideration, thus exploring the potential utilization of leaves as PM passive filters and as a low-cost alternative for high-spatial resolution monitoring networks.

The removal of atmospheric pollutants, and the consequent air quality improvement, is an important ecosystem service (ES) provided by plants, and often exploited within the context of the newly introduced concept of nature-based solution (NbS), especially in highly anthropized areas. The NbS concept includes a wide spectrum of solutions, which are inspired and supported by nature, and it is connected to the addressing of several and cross-cutting challenges, not only related to environmental quality but also to social and economic issues. Within this context, being able to properly assess the efficiency of urban vegetation and/or specific NbSs in the removal of atmospheric PM is important to increase the measurability of their impact and the comparability between different solutions, thus providing also valuable information for stakeholders and decision makers.

1.1 Atmospheric particulate matter (PM)

1.1.1 Definition and Classifications

Atmospheric particulate matter (PM) is an extremely heterogeneous mixture of liquid and solid airborne particles, with aerodynamic diameters ranging from 0.01 to 100 μm (EPA, 1997). The aerodynamic diameter (a.d.) is defined as the diameter of a unit-density spherical particle (1 g/cm^3) having the same aerodynamic properties (and therefore sedimentation rate) of a given particle (John, 2001).

Atmospheric PM includes several types of particles such as dusts, salts, ashes, trace metals and microbiome such as viruses, bacteria, fungi, spores, and pollen. It can be originated by natural or anthropogenic emission sources. Natural ones are mainly wildfires, volcanic eruptions, sea spray and erosion and consequent resuspension of soil and rocks, while anthropogenic activities responsible for PM emission are mainly biomass burning, domestic heating, vehicular traffic, industries, and agriculture.

Depending on their formation mechanism, atmospheric PM can be divided in primary particles, which are directly emitted in the atmosphere, and secondary ones, which originates from the chemical reactions of gaseous precursors in the atmosphere.

Considering the large physical/chemical heterogeneity of PM, several classifications have been proposed and applied. The so-called *modal* classification is based on the probability to find a particle in a certain dimensional class or mode (Figure 1). Airborne particles are therefore classified by their dimension and consequently their mechanism formation. The nucleation mode consists of particles with a.d. less than 0.1 μm (ultrafine fraction), generally emitted by combustion process. The accumulation mode considers those particles ranging from 0.1 to 1-2 μm (fine fraction), which originate from the coagulation or condensation of ultrafine ones. The coarse mode includes particles having a.d. from 1-2 μm to 100 μm, which are associated to mechanical processes, such as abrasive/erosion ones (Puxbaum, 1991).

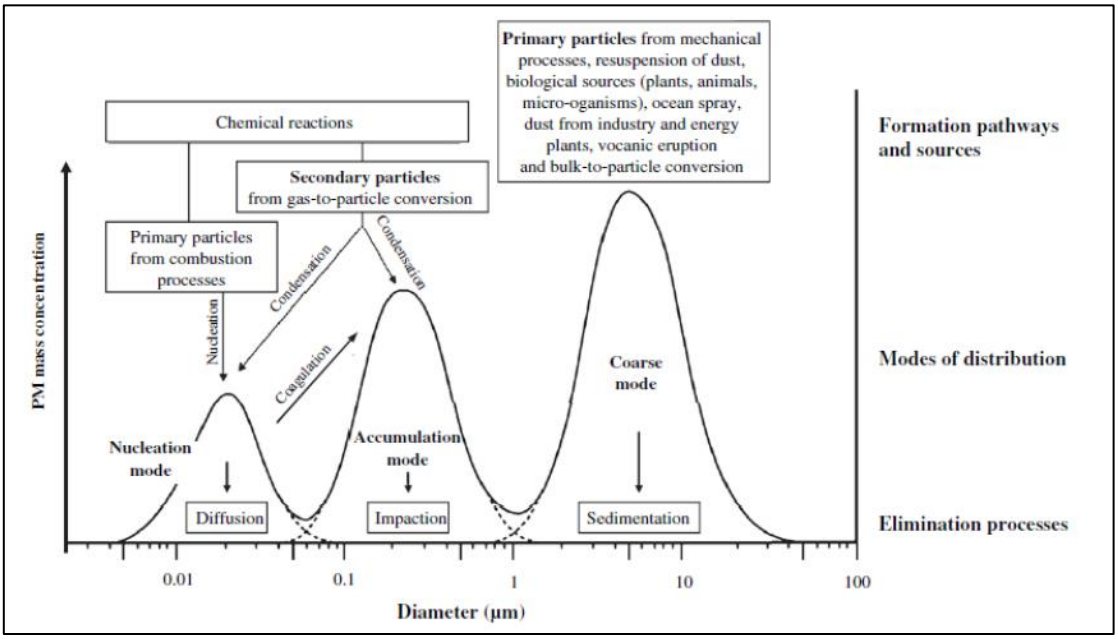

Fig. 1. PM modal classification with details on emission sources and formation processes.

The *dimensional cut-off* classification considers the efficiency of traditional PM sampling systems. PM_x is the fraction of PM collected by a selective sampling head with a 50% efficiency cut-off at X µm a.d. (EC, 1997). The most common sampling heads collect mainly PM_{10} and $PM_{2.5}$ fractions. These conventional samplers show a 50% efficiency in collecting particles with 10 ± 0.5 µm or 2.5 ± 0.5 µm a.d..

Finally, the *dosimetric* classification accounts the capability of atmospheric PM to penetrate at different levels of human respiratory system. Within this latest classification, particles greater than 10 µm are defined as inhalable fraction which can enter the upper part of the respiratory systems (nose and mouth). The thoracic fraction is composed by particles between 5 and 10 µm which can deposit in the lower part (trachea, pharynx, and lungs) and finally the respirable ones which have a.d. less than 2 µm is able to penetrate the gas-exchange region of alveoli. High risk respirable particles are the ones which can determine harmful effect on children and people suffering from cardio-pulmonary diseases (Mark, 1999).

1.1.2 PM chemical composition

Atmospheric PM is characterized by an extremely heterogeneous chemical composition. Its chemical components can be divided into two major classes: macro-components, representing more than 1% of its mass, and micro-components present in trace amount (< 1% of PM mass) (CEN 1998).

Among the so-defined macro-components, it is possible to identify inorganic and organic species. The inorganic fraction is mainly represented by anions (i.e., Cl^-, NO_3^-, SO_4^{2-}, CO_3^{2-}, SiO_4^{4-}), cations (i.e., Na^+, NH_4^+, K^+, Mg^{2+}, Ca^{2+}) and some elements (i.e., Al, Si, Fe). Some of these ions are emitted as primary particles: sodium, magnesium (Na^+ and Mg^{2+}) from marine aerosol together with chlorides (Cl^-) which can be also associated to waste incinerators; silicates (SiO_4^{4-}) and carbonates (CO_3^{2-}) from soil resuspension together with calcium (Ca^{2+}), potassium (K^+), which can be also emitted by wildfires, industrial activities, and agricultural fertilization. Secondary ions are mainly generated by the chemical transformation of three main gaseous precursors: sulfur and nitrogen oxides (SO_x and NO_x) mainly produced by coal and fuel combustion processes (*i.e.*, power plants, heating plants, vehicular traffic; Seufert et al., 1995), and ammonia NH_4^+ coming from stock farms and exhausts from vehicular traffic (Allegrini et al., 1987) or naturally from the microbial activity of soil and sea. These gaseous precursors can react in the atmosphere, through acid-base, oxidation, or gas-particles interactions, thus leading the formation of salts, such as ammonium sulphates and nitrates, which are considered as the main secondary components of PM.

The organic fraction of PM macro-components is mainly represented by organic and elemental carbon (OC and EC), which together represent from 20 to 60 % of the PM mass. EC is directly emitted in the atmosphere by combustion processes (Barone et al., 2006), while OC can derive also from secondary processes which may involve chemical reactions between Volatile Organic Compounds (VOCs) and oxidizing species such as ozone (O_3). This fraction includes compounds that may be very harmful and detrimental to human health, such as alkanes, phenols, carboxylic acids, polycyclic aromatic hydrocarbons (PAHs) and pesticides.

Inorganic micro-components of PM are trace elements coming from both natural and both anthropogenic emission sources. Trace metals may be naturally emitted by soil erosion and resuspension, forest fires (responsible of copper (Cu), lead (Pb) and zinc (Zn) emission), and by volcanic emissions (related to atmospheric concentrations of cadmium (Cd), mercury (Hg), arsenic (As), chromium (Cr) and nickel (Ni)) (Pacyna, 1999). The atmospheric concentrations of these trace metals may be enriched by the significant impact of anthropogenic activities, such as fossil fuel combustion (vehicular traffic and domestic heating) or electricity production. Indeed, these sources are known to be responsible for more than 50% of chromium (Cr), manganese (Mn) and vanadium (V) and almost 30% of other hazardous heavy metals such as Cu, Ni, Pb, Hg and Zn (Moore, 1994). In addition, waste incineration is connected to the emission of trace heavy metals, mainly in the fine fraction (*i.e.*, Cu, Zn, Cd, Sb, Pb, Ca, Cr, Mn, and Ni; Abbas et al., 2001), while soil resuspension from paved roads releases elements mainly in the coarse fraction (*i.e.*, Al, Si, K, Ca, Ti and Fe). Even thought, all these trace elements account for less than 1% of the PM mass, their importance is

associated to utilization as specific tracers with source apportionment scopes. Indeed, the evaluation of the spatial and/or temporal variability of their atmospheric concentrations is connected to the identification and assessment of the impact of their emission sources, both natural and anthropogenic.

1.1.3 PM Health and environmental impact

PM is recognized as one of the air pollutants of greatest concern due to its negative effects on human health and the environment (Kim et al., 2015; Prajapati et al., 2012).
The World Health Organization (WHO) estimates that PM air pollution contributes to approximately 800,000 premature deaths each year (WHO, 2006) and in 2013 the International Agency for Research on Cancer (IARC) classified PM as carcinogenic of Group 1 to humans (IARC, 2013). Both chronic and acute exposure to PM have been correlated with the onset of respiratory diseases, such as asthma, and chronic obstructive pulmonary illnesses. Several epidemiological studies have also reported strong correlations with cardiovascular pathologies, such as myocardial infarction, heart failure and cerebrovascular accidents (Anderson et al., 2012). However, most of these studies, use the PM total mass as exposure indicator, thus ignoring the multiple and potential toxicological effects of the different chemical compounds which constitute PM. This can lead to a misestimation of the overall impact of PM, since it does not account of the bioavailability and interaction with biological systems of single elemental components. In addition to this, the oxidation state, solubility, pH, and ionic strength of each compound need to be considered to properly assess the mobility of each element and therefore their biological interaction and elimination time. In this context, more attention has been given to the evaluation of PM complex chemical composition and the toxic effects of specific PM components, which are emitted by specific emission sources. This results to be extremely important to 1) explain the cause-effect relationship between PM and its elemental components and human health, 2) assess the different biological responses to specific PM physical and chemical properties (Hlavay et al., 2001).

Oxidative potential (OP) of PM is considered one of the most relevant predictive factors for the assessment of PM toxicity (Delfino et al., 2011; Gupta et al., 2019). OP is intrinsically influenced by different physiochemical properties, such as size, surface area and chemical composition, these being able to affect the PM ability to cause oxidation of target molecules (Andrade et al., 2020). Therefore, OP predicts the PM intrinsic capacity to cause damaging oxidative reactions and inflammations and is frequently proposed as a more biologically appropriate metric for addressing human exposure than bulk PM mass concentration. Reactive species can exist on PM or can be generated in vivo by specific compounds, that chemically interacts with fluids and cells in the body. Multiple acellular tests are

developed for quantifying these two phenomena and the related particles oxidative potential (Bates et al., 2019). One group of acellular methods measure the capacity of PM to oxidize certain naturally occurring antioxidants in the human lung lining fluid over time, such as ascorbic acid (OP^{AA}), or a cellular reductant surrogate, such as dithiothreitol (OP^{DTT} assay), using units of time rate-of-change of volume-based concentration (nmol depletion per min per m^3 of sampled air), while particle-bound ROS techniques typically record radical species levels in units of concentration (i.e. 2',7'-dichlorofluorescein, OP^{DCFH}, assay). All these acellular assays have their own sensitivity to different pathways of reactive species formation, to specific PM chemical compounds and therefore also to the impact of specific emission sources. Therefore, the combined application of different acellular methods on the same PM sample is strongly suggested and often considered advantageous in providing insightful assessment of particles OP (Ayres et al., 2008; Lin and Yu, 2020; Manigrasso et al., 2020). Numerous studies have shown that OP^{AA} is mainly related to the redox activity of transition metals, but recent applications show further affinity for organic compounds (Mudway et al., 2004). OP^{DTT} well correlates with both organics (i.e. WSOC, EC, OC, BC, quinones and hydroxyquinones) and transition metals (i.e. Cu and Mn) (Charrier and Anastasio, 2012; Visentin et al., 2016). Lastly, OP^{DCFH} is particularly sensitive to transition metals (i.e., Fe, Ni) and organics (See et al., 2007; Wang et al., 2010).

The main negative environmental effects of PM concern the acidification of natural ecosystems and the interaction with solar radiations. Chemical reactions of gaseous precursors such as sulfur and nitrogen oxides with water vapor can lead to the formation of secondary acids (H_2SO_4, HNO_3, HNO_2). These acidic pollutants can deposit through mechanism of wet or dry deposition, thus causing the acidification of soils, lakes, rivers, seawaters and groundwaters (Morselli et al., 1991). Depending on their chemical composition and size, airborne particles can interact differently with solar radiation. Carbonaceous particles, such as the so-called brown and black carbon can absorb infrared radiation, contributing positively to climate change (Andrae et al., 2006). On the other hand, light-colored particles can reflect sunlight, leading to cooling of the earth surface (Ramanathan et al., 2001). Additionally, effects of PM on vegetation may be associated to a reduction of light required for the photosynthesis and an increase in leaf temperature due to changed surface optical properties. Alkaline dust materials may cause leaf surface injury while other materials may be taken up across the cuticle (Prajapati et al., 2012).

The increasing need to protect human health and the environment from these negative effects has brought to the definition of air quality standards for PM. A key role has been played by the European Union (EU), which has established reference regulations for the reduction of PM atmospheric concentrations, mainly the Directive 1999/30/CE and the Directive 2008/50/CE. These directives

have been transposed by the Italian legislation, respectively by the DM 60/2002 and the Dlgs 155/2010. The first one, has set the PM_{10} daily limit of 50 µg/m^3, which cannot be exceeded more than 35 times a year, and a yearly average value for this specific size fraction of 40 µg/m^3. This legislation also reports limit values and alert thresholds for other hazardous pollutants such as nitrogen and sulfur oxides, carbon monoxide, tropospheric ozone, benzene, and lead (Pb). For the first time, with the Dlgs. 155/2010, a yearly average values of 25 µg/m^3 has been introduced also for $PM_{2.5}$, considered potentially more dangerous, due to its higher capacity of penetrate in the human respiratory system. With this directive a new obligation for the measurement of concentrations of some specific PM components, such as As, Cd, Ni, Hg and Benzo(a)pyrene has been set and new target values have been also provided.

1.1.4 Standard atmospheric PM sampling

PM sampling and measurement procedures are defined by the European Committee for Standardization (CEN), which provides specific standard for PM_{10} and $PM_{2.5}$ (respectively being EN 12341 and EN 14907; CEN, 1998; CEN, 2005). The choice of focusing on these two size fractions is mainly determined by toxicological considerations, since these particles can penetrate the respiratory system, thus being able to affect negatively human health. Conventional PM samplers are composed by a selective sampling head which draw the airflow and discriminate particles of a certain size. Then, the air is conveyed through a membrane filter able to retain the selected particles. Downstream of the sampling line, a pump generates the pressure gradient necessary to create the airflow. Different membrane filters can be used, depending on the chemical analysis to perform after the sampling step. Conventionally, Teflon filters (PTFE) are deployed for the chemical characterization of trace elements (i.e., heavy metals), being characterized by very low blank values. Quartz filters are usually deployed to analyze carbonaceous compounds by means of thermal methods, being extremely resistant to high temperature. PM samplers can be divided in two categories depending on their flow rate: high-volume samplers (HVS) with a constant flow rate of 68 m^3/h and low-volume samplers (LVS) with a flow rate of 2.3 m^3/h. Alternatively, the so-called cascade impactors may be used to separate particles in restricted ranges of a.d, thus being able to sample simultaneously size-segregated membrane filters for subsequent analysis. This sampling system is composed by different stages, sequentially arranged to stop and collect particles that are progressively smaller (Hering et al., 1978).

1.1.5 PM chemical analysis

Once PM is collected on membrane filters, its mass is gravimetrically measured through a microbalance under ambient air conditions and after equilibration at 20 ± 1 °C and 50% ± 5 R.H.
Depending on the final aim, different analytical procedures can be applied for the chemical characterization of sampled PM membrane filters. Carbon fraction of PM, composed by the so-called elemental and organic carbon (EC and OC), is usually determined by means of thermal procedures, which consist of the volatilization and oxidation of the sample and following measure of developed gaseous CO_2. Inorganic ionic fraction can be analyzed by ion chromatography (IC) after the water extraction of sampled Teflon membrane filters. Macro elemental components such as Al, Fe, K, Mg, Ca, Ti, S and Si are conventionally analyzed by non-destructive energy-dispersive X-Ray fluorescence (XRF). Then, micro and trace elements are usually determined by inductively coupled plasma with optical or mass spectrometer detection (ICP-OES or ICP-MS).
For the characterization of water-soluble and insoluble fraction of PM_{10} micro and trace elements, a chemical fractionation procedure (Canepari et al., 2006a) has been developed, validated, and largely applied. The chemical fractionation, based on the elemental solubility, allows to get useful information on the chemical form in which each element is released and this may be typical of its emission source (Templeton et al., 2000). Moreover, the use of the chemical fractioning yields useful information on the environmental mobility of the elements. Indeed, biogeochemical distribution and bio accessibility, health and environmental effects are strongly related to the chemical form of the elements (Canepari et al., 2014; Harrison et al., 2000). This procedure allows to discriminate the water-soluble from the insoluble fraction of each analyzed element and results to be useful in increasing the selectivity of each element as source tracer (Massimi et al., 2020). Each sampled membrane filter is extracted in deionized water and then acid-digested. Afterwards, water-extracted solutions are used for the chemical characterization of anions and cations by IC and of the water-soluble fraction of trace elements by ICP-MS. Acid-digested solutions are employed for the characterization of insoluble fraction of PM elemental components by ICP-MS or ICP-OES.

1.1.6 PM spatially resolved analysis for source apportionment

The evaluation of the spatial distribution of PM and its chemical compounds is essential for a reliable identification of emission sources, the evaluation of particle dispersion over the territory, the assessment of human exposure and the development of focused pollution management strategies.
One of the main difficulties in PM monitoring is attributable to the complex nature of emission sources and to the differences in spatial and temporal scales over which the various components of

PM operate, especially in urban environments (Zwack et al., 2011; Sportisse, 2009). The development of extensive monitoring networks is crucial to provide data on the spatial variability of PM mass concentrations and its chemical components. However, the definition of dense monitoring networks with conventional PM sampling instrumentations is associated to very high costs, both in terms of implementation and both in terms of maintenance. Traditionally, to overcome this limitation, mathematical models can be employed to simulate the dispersion of air pollutants released by specific emission sources. The modelling approach offers a series of advantages, such as the reduction of time and costs and the possibility of covering very large areas. However, the modelling approach also present some limitations, such as reducible error results due to the large number of different sources and the complexity of PM transport and transformation processes, or due to inadequate air quality data input (Massimi et al., 2017; Almeida et al., 2006).

Recently, automatic, and very-low volume PM samplers have been developed with the purpose of allowing spatially-resolved analysis of PM chemical components. This innovative sampler (High Spatial Resolution Sampler, HSRS; FAI Instruments, Fonte Nuova, Rome, Italy) assures long-term (1-2 months) collection of PM and it results extremely suitable for the definition of dense, extensive monitoring networks, thus determining a substantial reduction of in-situ maintenance costs, usually associated to conventional PM samplers (Massimi et al. 2017; Massimi et al. 2019).

To this regard, also the biomonitoring approach can be considered as a low-cost alternative for high spatially-resolved analysis of PM, thus ensuring higher number of monitoring sites applicable to the detection of the impact of specific emission sources. The biomonitoring approach and its main advantages and applications will be deeply discussed in the following paragraphs of this thesis.

As previously described, being able to assess the spatial variability of atmospheric PM and its main chemical components is strictly connected to source apportionment purposes. In this context, source apportionment is a technique used to identify and quantify the emission contribution from different sources at a specific receptor site. Several receptor models are commonly applied in PM source apportionment, including Chemical Mass Balance (CMB), and the multivariate model Positive Matrix Factorization (PMF), which will be furtherly discussed in this study (Pio et al., 2020; Querol et al., 2007; Reff et al., 2007; Paatero and Tapper, 1994). This latter technique has been used extensively for source apportionment of atmospheric PM, with the final aim to 1) reconstruct the chemical emission profiles of specific emission sources and 2) the contribution of each source or so-called factor to the PM mass concentration.

1.2 PM deposition on leaf surfaces

1.2.1 Process description and driving factors

Deposition on leaf surfaces is one of the main removal mechanisms of atmospheric PM, which ensure the abatement of its concentrations and the improvement of air quality. PM deposition involves both *dry* and *wet* processes. While wet deposition is conveyed by meteorological precipitations (mainly rain or snow), dry deposition refers to the direct delivery of mass to the surface (Wu et al., 2018, Dolske and Gatz, 1985). Wet deposition can be divided in *rainout* processes and *washout* ones. The first one occurs, when airborne particles act as cloud-condensation nuclei themselves or they are captured by cloud water and transported to the ground. On the other hand, the direct removal of airborne particles by rain or snow drops as they fall is the so-called *wash-out*. Usually, snow appears to be more efficient in this process, thus being characterized by higher contact surface and slower drop speed (Jennings et al., 1999).

Dry deposition can take place through four different processes, depending on airborne particles size distribution: *brownian diffusion, interception, inertial/turbulent impaction and gravitational settling or sedimentation* (Petroff et al., 2008a). *Brownian diffusion* concerns the deposition of ultrafine particles with a.d. $\leq$ 0.1 μm. Instead, airborne particles with a.d. ranging from 0.1 to 1.0 μm are usually subjected to mechanisms of *interception* or *impaction*. The first one takes place when particles of small inertia pass in the vicinity of an obstacle and are held back, since the distance between the particle center and the surface is smaller than its diameter (Fuchs, 1964). *Impaction* mechanisms usually occur when airborne particles collide with the obstacle surface due to their large inertia. Finally, *sedimentation* is mainly driven by typical gravitational forces, and it represents the main deposition mechanism for larger airborne particles (a.d. $\geq$ 1.0 μm). The size distribution of particles is also able to affect their specific deposition velocity (V_d) and therefore their deposition rate (Nowak et al., 2006). Deposition velocities for super-micrometer particles result to increase with their size, while for sub-micrometer ones, V_d usually decrease with it. Minimum deposition velocities are reported for particles in the 0.1 - 0.3 μm range (Lin and Khlystov, 2012). V_d is often described as the reciprocal of resistance to deposition, R_{tot}, which is the sum of the aerodynamic resistance (R_a), boundary resistance (R_b) and surface resistance (R_c) (Davidson and Wu, 1990). R_a is influenced by meteorological conditions, and except for larger particles, it is considered small compared to the other resistances and it is usually set to zero. R_b regulates the transfer of particles through the boundary layer adjacent to the surface, while R_c depends on the adsorption capacity of the surface itself.

Differences among the results obtained by studies focused on this removal process, show the influence of numerous driving factors, thus proving its complexity and dynamicity. Besides the

described physical and dimensional characteristics, also other PM variables can influence its efficiency. For instance, the solubility of PM and its chemical components can affect the interaction with leaf surfaces and therefore their deposition and retention. Among the driving parameters able to affect PM deposition on leaf surfaces, meteorological variables certainly play a key role. This is the case of wind speed and direction which drive the interaction between the airflow and vegetation canopies (Wang et al., 2015), and relative air humidity which can interfere with the size distribution of hygroscopic airborne particles and change their deposition properties (Janhall, 2015). On the other hand, the amount, duration, and intensity of precipitations are mainly related to the wash-out and removal of leaf deposited particles. Also in this case, the efficiency of rainfall events in reducing the number of accumulated particles varies depending on their size distribution (Przybysz et al., 2014).
Several studies have also underlined the differential efficiency of plant species towards deposition (Rasanen et al., 2013, Saebo et al., 2012). This is strictly related to the impact of peculiar characteristics of the vegetation. Structure, size, height, and space configuration of urban vegetation itself and of single trees, crowns or branches result to be relevant in influencing the deposition of atmospheric PM (Chen et al., 2016, Deng et al., 2019). Parameter such as the porosity of the crown is often considered to evaluate the efficacy of specific green barriers, thus allowing at intermediate values, the passage of the airflow and of airborne particles and therefore their deposition. On the other hand, and at lower values, porosity can determine a lower infiltration capacity of particles and considerably reduce leaf deposition (Barwise and Kumar, 2020). Even though, crowns still represent the larger surface area of a tree, suitable for PM deposition, species-specific values of leaf area, which is usually quantified through the calculation of the leaf area index (LAI, expressed as m^2 of leaf area / m^2 of ground area), can determine a different removal efficiency (Perini et al., 2017). At a lower scale, also leaf structure and macro-, micro-morphology need to be taken in account. Leaf shape, margin and thickness can also act as driving factors for PM dry deposition (Weeraddoky et al., 2017), thus being related to higher or lower deposition rates. The enhancement of the on-leaf deposition of PM is often described in association with greater leaf roughness. This is strictly related to the presence, density and also dimension of leaf microstructures such as, trichomes, stomata pores and generally grooves, which can increase leaves roughness and favor PM deposition and retention (Li et al., 2019). All these factors can act singularly in influencing the deposition rate of atmospheric PM. However, more attention is needed on the interaction and combination of single driving factors (Sgrigna et al., 2020; Leonard et al., 2016), to be able to efficiently replicate and properly evaluate this process.

1.2.2 Analytical evaluation of leaf deposited particles

Due to the high complexity of the on-leaf deposition processes and the heterogeneity of atmospheric PM, to date it is still unclear which is the most efficient analytical procedure applicable to its evaluation and to the chemical and physical characterization of leaf deposited particles.

In the last few years, the scientific community have investigated this process, both in controlled environments and in field conditions, and both through modelling and experimental approaches.

Regarding the experimental approaches used for the evaluation of PM deposition on leaf surfaces, analytical techniques such as atomic absorption spectroscopy (AAS), x-ray fluorescence spectroscopy (XRF) and alternatively inductively coupled plasma with optical or mass spectrometer (ICP-OES or ICP-MS) can be used for the elemental characterization of leaves surfaces (Richardson et al., 1995; Power et al., 2009; Sawidis et al., 2011; Tepanosyan et al., 2021). However, since these techniques are usually applied to the characterization of the whole leaf, it results to be difficult to discriminate whether the detected elements are connected to deposition processes or to other form of exposure (i.e., adsorption from the soil). Another approach is represented by Saturation Isothermal Remanent Magnetization (SIRM), which calculates the magnetization retained by a sample after exposure to a large magnetic field (Matza and Maher, 1999). This rapid, cost-effective, and non-destructive technique can be employed for the detection of ferro(i)magnetic fraction of deposited PM (Hofman et al., 2013). Vacuum filtration (VF) procedure (Dzierzanowski et al., 2011) is a gravimetric technique used for the quantification of leaf deposited and size-segregated PM, which is based on leaves washing and subsequent filtration of the washing solutions through membrane filters with decreasing porosity. Main limitations of this procedure are connected to the lack of a chemical characterization of deposited particles, and the fact that hygroscopic PM cannot be detected, since the washing solution is an aqueous one. Moreover, chemical, and physical characteristic of PM may favor its encapsulation within leaf surfaces, thus mining the efficiency of this procedure (Terzaghi et al., 2013). Plants products may be brought in solution and without a proper chemical characterization, it is impossible to discriminate them from deposited PM. The impact of these limitations on the VF efficiency for the evaluation of the amount of leaf deposited PM has been proved through the intercomparison with data retrieved with other analytical techniques or from air quality stations (Baldacchini et al., 2019; Sgrigna et al., 2015).

Scanning Electron Microscopy coupled with Energy Dispersive X Rays Spectroscopy (SEM/EDX) can be applied for the evaluation of the number, size, morphology, and elemental composition of leaf deposited particles, thus representing one of the most efficient analytical techniques applicable to this aim. Among these systems, high vacuum electron microscopy has higher resolution, but usually consists of large and high-cost instrumentations. Moreover, injected electrons may accumulate on

non-conductive sample surface, thus disturbing the imaging process (surface charge effect). For this reason, and for biological samples such as leaf surfaces, metallization and freezing steps are required. On the other hand, low vacuum electron microscopy is characterized by a lower resolution and usually works only with Back Scattered Electrons, useful for the detection of elements with higher atomic mass, such as transition or heavy metals. Through this instrumentation, surface charge effects are reduced, and no metallization step is required. Long-time analysis, due to the spatial scale of the single data collected (hundreds of micron square of leaf area per image) and lack of information on the carbon/organic fraction of leaf deposited PM, represent the main limitation of this technique.

Eddy covariance (EC) towers are often used to measure PM fluxes, thus providing evidence for the relationship between PM deposition and resuspension (Fares et al., 2016; Guidolotti et al., 2017). EC provides direct measurement of the net surface-atmosphere exchange of gases and particles and can operate at high temporal resolution. From a spatial point of view, it requires homogeneous areas. This can lead to results with lower spatial resolution and higher uncertainties, especially in urban areas which are characterized by high spatial discontinuity (Pace et al., 2021).

For what concerns the experiments conducted in controlled environments, wind tunnels are some of the most used. This approach results to be extremely important to properly discriminate the impact of wind directions and intensities towards certain deposition properties (i.e, deposition velocity) of size-segregated airborne particles (Gromke and Ruck, 2007; Beckett et al., 2000). Several models have also been developed and have produced significant and reliable outputs. The *i-Tree Eco* model (USDA Forest, 2019) and *Computational Fluid Dynamics* (CFD) simulations (Jeanjean et al., 2016) are among the most common computational techniques used to estimate PM removal from urban vegetation. The *i-Tree Eco* model has been developed starting from the implementation of the UFORE model (Escobedo and Nowak, 2009) with GIS (Geographical Information System). Within the i-Tree Eco model, PM deposition, resuspension, net flux and, therefore, accumulation on leaf surfaces are estimated by using input data related to meteorological conditions (wind and precipitations), leaf area index (calculated from vegetation biometric data), and atmospheric concentrations of PM. CFD is a branch of fluid mechanics, and it is efficient for simulating the free-stream flow of air and airborne particles and their interaction with surfaces, as defined by specific boundary conditions. Initial validation is usually performed using wind tunnels as experimental apparatus, together with the comparison with previously performed experimental analysis. The modelling approach presents some evident advantages, being in most case easy to use, and being applicable for the simulation of different case studies, which can be characterized by varying meteorological conditions, levels of PM pollution and types of vegetation. However, it also presents several limitations, as in the specific case of the *i-Tree eco* model, 1) the assumption of a constant

deposition velocity (Hirabayashi et al., 2015), with no species-specific parametrization, except for differences between coniferous and evergreen species, and 2) very low rain level threshold for total particle removal (Pace et al., 2018). However, it is important to underline that every modelling approach is needed of a proper validation with experimental data and being usually based on coarse assumptions, it represents a simplification of the deposition process and its driving factors (Pace et al., 2021; Petroff et al., 2008b).

1.2.3 Plants as PM bioindicators and their application in source apportionment

Biomonitoring is defined as the measurement of the response of living organism or so-called bioindicators (Rai, 2016) to changes in their environments. In the last decades, it has been proposed as a valid alternative to air pollution monitoring problems (Moreno et al., 2003). Since plants are immobile and physiologically sensitive to the most prevalent pollutants, they are usually efficient in reflecting local pollution conditions (Hofman et al., 2013). Biomonitoring techniques can be based on the evaluation of anatomical, morphological, and physiological characteristics or on the analysis of trace elements in animals, plants, lichens or mosses, or parts of them, such as the case of tree leaves (Ares et al., 2012).

In this context, the evaluation of leaf deposited PM and the characterization of its chemical and physical characteristics, deserve particular interest due to their potential for 1) the identification of specific emission sources and 2) the risk assessment for human health (Mitchell et al., 2010). Variables such as the elemental composition, size distribution and morphology of deposited PM, is highly related with pollution source apportionment. This is true since each PM emission sources is able to emit particles which are characterized by a given chemical composition, size distribution and morphology (Shen et al., 2019). Once the emission fingerprint of these sources has been evaluated, these parameters can be used as tracer for their identification and for the evaluation of their impact (Kumar et al., 2018). Numerous studies have focused on the potential utilization of leaves as atmospheric PM passive filters (Fusaro et al., 2021; Kardel et al., 2018), which could represent a low-cost alternative to conventional air quality networks. This approach has several advantages, mainly connected to the achievement of air quality data with a higher spatial resolution, since trees are usually widespread, and can ensure higher density of sampling points (Gratani et al., 2008). Especially in urban areas, where the spatial resolution of active PM monitoring is limited due to high investment and maintenance costs, leaf biomonitoring can be seen as a valuable alternative.

The application of analytical techniques such as AAS, XRF or ICP-OES/MS to the chemical characterization of leaf deposited particles, can be also useful for biomonitoring purposes. However, for those elements which are both known as biologically essential and tracers of specific anthropogenic sources, such as iron, zinc and copper, values need to be normalized by subtracting baseline concentrations (Rossini-Oliva and Fernandez Espinosa, 2007) and enrichment factors (EF) may be calculated (Lorenzini et al., 2006). SIRM technique results to be particularly effective for the evaluation of vehicular traffic impact in urban areas (Mitchell and Maher, 2009; Sagnotti and Wrinkler, 2012), since ferro(i)magnetic particles can derive directly by exhaust (combustive) and non-exhaust emission processes (mechanical abrasion of vehicles components) associated to traffic. In Mitchell and Maher 2009, SIRM values of tree leaves exhibited strong correlation with atmospheric PM_{10} concentrations, thus proving to be a robust quantitative proxy for roadside PM pollution.

Finally, the combined provision of both chemical and physical data of leaf deposited particles obtained through the application of SEM/EDX microanalysis, is certainly effective to improve the identification of emission sources (Baldacchini et al., 2019), thus also providing information on particles size and morphology. In this latter study, tree leaves and SEM/EDX have been identified as an efficient and highly spatially resolved system, thus being able to provide information on the differentiated impact of PM emission sources such as soil resuspension, sea spray and vehicular traffic, in the city of Naples. In Baldacchini et al., 2017, SEM/EDX microanalysis applied to the characterization of PM deposited on *P. acerifolia* leaves from 28 different European cities, allowed to efficiently discriminate heavy traffic sites from urban park ones and to discriminate the cities based on the PM composition in connection with the local sources.

It is important to underline that proper validation is needed to prove the efficiency of these biomonitoring approaches. The validation step may include the comparison with data retrieved from already existing air quality monitoring networks (Sgrigna et al., 2015, Baldacchini et al., 2017). However, due to the low density of urban monitoring stations, it is not always possible to ensure their proximity to leaf sampling points, thus compromising the possibility of carrying out a proper comparison.

1.3 Nature-based solutions in urban environments and provided benefits

1.3.1 NbS definition and legislation

Global increase of population and accompanying increment in the number and size of urban areas (UN, 2012) determine an extensive range of negative pressures on natural resources and on the environment (Kabish et al., 2016). It is estimated that 40% of the urban areas that are foreseen to exist by 2030 have already been built, with 66% of world's population living in cities by 2050 (Secretariat of the Convention on Biological diversity, 2012). This accelerated urbanization in combination with climate change impact, are setting new challenges for urban areas, related to the maintenance of living conditions that support human health and well-being (Sarabi et al., 2019). Natural areas degradation with connected loss of biodiversity, noise and light pollution as well as changes in local climate and water regimes are some of the main negative pressures which characterized these areas. In addition, the impact of urban and anthropogenic emission sources contributes considerably to increase air, water and soil pollution (van den Bosch and Sang, 2017).

In this context, more attention has been given to the value of nature in addressing these challenges (Maes and Jacobs, 2015). New and so-called ecosystem-based approaches have been developed, with the first aim to re-nature urban areas and to enhance their resilience toward climate change impacts (Eggermont et al., 2015). A wide spectrum of ecosystem-based initiatives has been promoted by the European Commission (EC) and further integrated into its policies. These include concepts as *ecosystem services*, *green-blue infrastructure*, *urban forest*, *ecological engineering,* and *ecosystem-based management* (Raymond et al., 2017). However, these approaches often focus on short-term goals, and they tend to address single challenges from a distinct perspective. The most recent entry to this discourse is the concept of *nature-based solutions* (NbSs), which are defined by the International Union for the Conservation of Nature (IUCN, 2012, Cohen-Schacham et al., 2016) as *actions to protect, sustainably manage and restore natural or modified ecosystems that address societal challenges effectively and adaptively, simultaneously providing human well-being and biodiversity benefits*. Within Europe, this newly-developed concept has been integrated into the framework program for Research and Innovation "Horizon 2020", which defines NbS *as solutions that are inspired and supported by nature, which are cost-effective, providing simultaneously environmental, social and economic benefits* (EC, 2015). NbS is often presented as an umbrella concept (Pauleit et al., 2017) and as an evolution of previously developed ecosystem-based solutions. However, this concept gives more attention to the integrated and systemic approach, thus being designed for the simultaneous addressing of environmental, social, and economic challenges (van den Bosch and Ode Sang, 2017). Their implementation in highly anthropized areas, results to be associated with benefits for human health and well-being, increased social cohesion and potential for new economic opportunities and green jobs (Xing et al., 2017). As shown in Figure 2, the EU R&I agenda on "Nature-Based Solutions and Re-Naturing Cities", identifies four main goals in which

innovative NbSs can be implemented and which are connected to: sustainable urbanization, restoring degraded ecosystems, developing climate change adaptation and mitigation, and improving risk management and resilience (EC, 2015). Based on these four goals, seven nature-based solutions are recommended to be taken forward by the European Commission and by each Member States (Fig. 2).

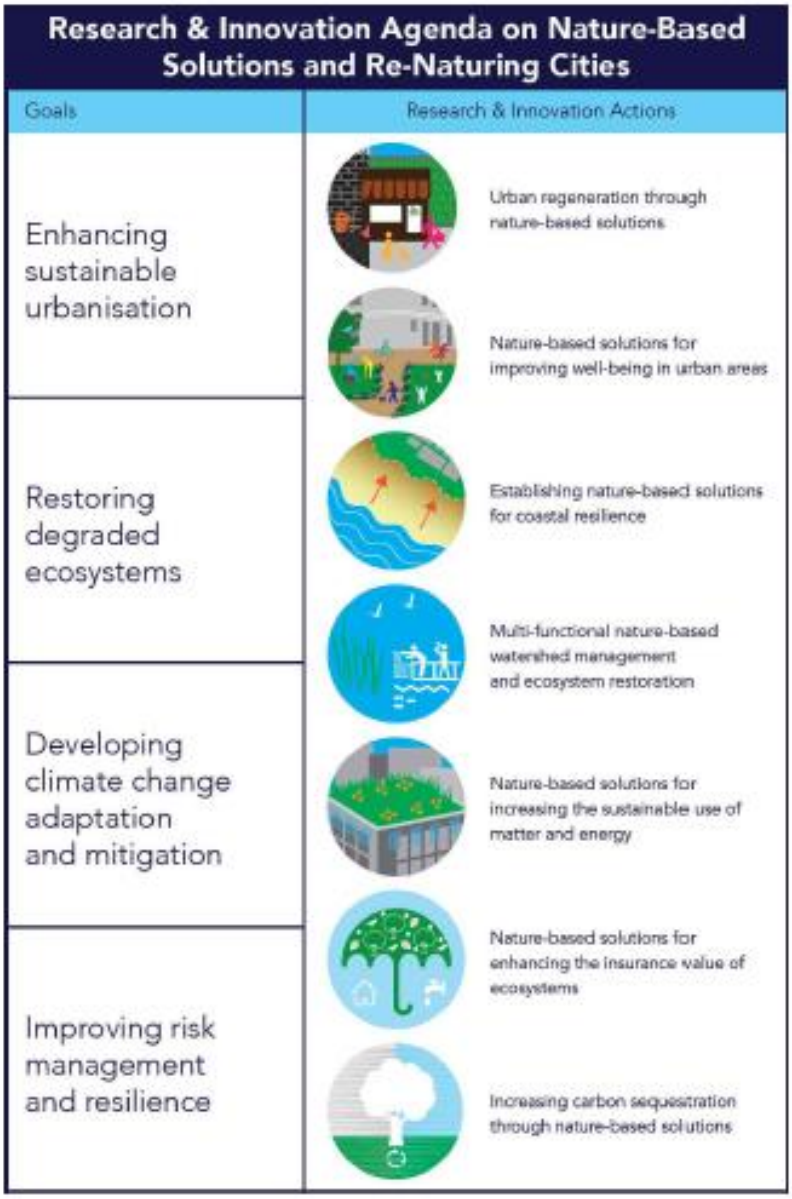

Fig. 2. The four main goals and seven NbSs identified and recommended by the EU R&I agenda on "Nature-Based Solutions and Re-Naturing Cities" (EC, 2015, p. 7)

Practically, the NbS concept includes the implementation of several solutions applicable at different scale, which can range from the improved use of existing ecosystems to the design and construction of new ones (Eggermont et al., 2015). These can vary from ecosystem restoration to greening of grey

surfaces (i.e., green rooftops, wall and greened brownfields), natural flood control and constructed wetlands. These add up to specific NbSs like afforestation, urban parks, street trees, natural and seminatural green spaces, productive gardens, bio-swales and finally green road lines and roundabouts. The coexistence in urban areas of multiple solutions, is connected to the potential and simultaneous addressing of different challenges. In some cases, and due to its intrinsic complexity, the NbS concept may still appears too broad and may allow different interpretations (Nesshöver et al., 2017), thus mining its actual implementation and effective supply of benefits. For this reason, a comprehensive formulation of this concept is needed (Abson et al., 2014), to help stimulate the communication between scientist, policymakers, and citizen, thus underlining the proper overlaps and differences with previously developed concepts.

1.3.2 Provision of ecosystem services

NbSs are strictly connected to the *ecosystem service* (ES) concept (Lafortezza and Chen, 2016), thus considering the potential to improve urban resilience and quality through their provision (Melles, 2005, EC, 2015).

The ES term was firstly introduced in 1970 (Mooney et al., 1997), then fully entering the policy agenda, at the beginning of the 21st century and following projects such as the Millennium Ecosystem Assessment in 2005 (MEA), The Economics of Ecosystems and Biodiversity in 2010 (TEEB), and the establishment of the Intergovernmental Panel on Biodiversity and Ecosystem Services (IPBES) in 2012 (Chaudhary et al., 2015). Since 2012, the Common International Classification of Ecosystem Services (CICES), which present a uniform definition and classification of ESs has been also proposed (Haines-Young and Potschin, 2011).

ESs, mostly defined as *benefits that humans derive directly and indirectly from the processes and functions of an ecosystem* (Costanza et al. 1997), are classified into four main categories: provisioning (i.e., food, raw materials, energy), regulating (i.e., air and water quality, carbon sequestration and storage, pollination), cultural (i.e., aesthetic value, education, and psychological benefits) and supporting (i.e., nutrient cycling and biogeochemistry). The provision of these ESs depends on several factors, related to the specific urban context, the NbS type and species-specific functional traits of the vegetation. For this reason, proper and accurate evaluation, planification and design are needed in the preparatory stages of the NbS implementation to secure the provision of single or combined ESs.

Among the different regulating ESs, the ones connected to the regulation and improvement of air quality are of great interest and extremely coherent with the purposes of this research project. Vegetation can contribute to air quality improvement through the removal of hazardous atmospheric

pollutants. This is the case of gaseous pollutants such as nitrogen and sulfur oxides (NOx, SO_2), tropospheric ozone (O_3), Polycyclic Aromatic Hydrocarbons (PAHs) and Volatile Organic Compounds (VOCs). For all these gaseous compounds, the main removal mechanism is represented by stomatal uptake (Nowak et al., 2006). Once inside the leaf, gases diffuse into intercellular spaces and may be absorbed or react with inner-leaf surfaces (Smith, 1990). Airborne particles can be removed by wet or dry deposition on leaves surfaces. Although PM can potentially deposit on all the external surfaces of the plant (even branches and trunk), leaves certainly represent the larger and more efficient deposition surface for this atmospheric pollutant, due to their spatial configuration and interaction with airflow.

1.3.3 Indicators for NbS environmental impact

Being able to properly assess the NbS environmental impact is firstly connected to the possibility of evaluating their efficiency, increasing the measurability of their effects and the comparability between different solutions (Sparks et al., 2011). This aspect is also connected to the ability of understanding synergies and trade-offs but also costs and benefits associated to the different NbS implementation stages (Queroiz et al., 2015). Finally, it is an important resource for supporting practitioners in the urban planning, design, and sustainable management of new and to-be implemented NbSs, thus learning from existing approaches and experiences (Kabish et al., 2016). However, to date, the evaluation of the environmental benefits provided by NbS still represents a challenge, with most of the attempts mainly following reductionist approaches and focusing only on single solutions, challenge areas or ESs (Salmond et al., 2013). Existing approaches are often not able to cover the simultaneous and cross-cutting provision of co-benefits, which is intrinsically connected to the NbS concept itself (Mouchet et al., 2017).

To this aim, key and common indicators, recommended methods and standardized procedures have been developed and applied. One of the first attempts is represented by the EKLIPSE evaluation framework for NbS, which was developed by an expert group under the auspices of the EC (Sarabi et al. 2019). As reported in Figure 3, this framework uses the ten challenge areas outlined by Raymond et al., 2017 as the basis for evaluating NbS benefits and it considers the synergies and trade-offs among different challenge areas. This framework has later encouraged the drafting of the *Handbook for Practitioners – Evaluating the impact of nature-based solutions* (Directorate-General for Research and Innovation EC, 2021). The Handbook describes a comprehensive set of key indicators and methods, applicable to the assessment of the performance and impact of different types of NbS at different spatial/temporal scales. Moreover, the NbS evaluation framework presented in this

handbook, represents an important reference for future EU policies and activities and a guide for urban practitioners in the development of robust monitoring plans of future or already-implemented NbSs.

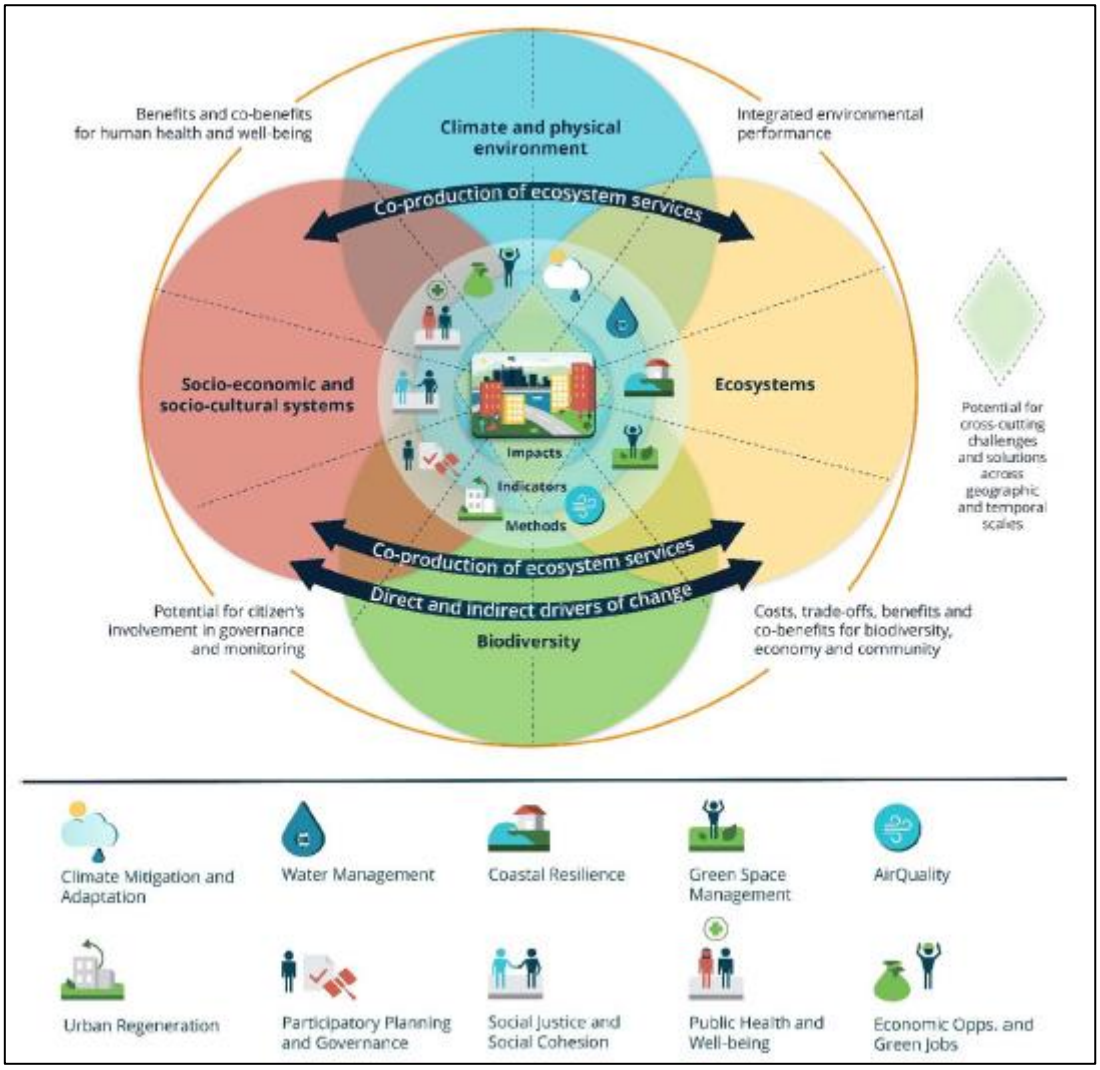

Fig. 3. The NbS assessment framework considering the 10 challenge areas, indicators and methods for assessing NbS impacts within and across challenge areas (Raymond et al., 2017).

For what concerns the evaluation of NbS impact on air quality, and to our interest, several key indicators and recommended methods have been developed and applied. This type of environmental impact can be certainly monitored, through direct measurement near the implemented area, of the air pollutants concentrations, including those traditionally used as air quality criteria, such as PM_{10} (particles with an aerodynamic diameter ≤ 10 μm), $PM_{2.5}$ (particles with an aerodynamic diameter ≤ 2.5 μm), O_3, NO_2, CO, SO_2 and toxic metals (As, Cd, Ni, Pb and Hg). This information can be achieved through the employment of air quality monitoring stations or during apposite experimental

campaigns (ISO, 2018). Concentrations of these atmospheric pollutants detected near the implementation areas are considered themselves as valuable indicators for the NbS impact on urban air quality. However, they can be also used for the calculation of other key indicators, such as the number of days during which threshold values expected for these pollutants are exceeded. Models such as the *i-Tree Eco* (USDA Forest Service, 2019), can be used to achieve information on the removal ability of specific NbSs, through the employment of input data related to land use, biometric information of the vegetation and meteorology. However, the modelling approach results to be more reliable for a larger spatial scale, like the city one, in respect to the NbS one. The application of methodologies which are able to evaluate the pollutant uptake at a lower scale, such as the one of a single tree or lower, may be more suitable and efficient. In this context and specifically for atmospheric PM (mainly PM_{10} and $PM_{2.5}$), the evaluation of deposition of airborne particles on leaf surfaces is considered as one of the key indicators applicable. Even if high uncertainty is still connected to the identification of which is the most efficient procedure, few procedures have been already developed, validated, and applied. To date and as described in the previous paragraphs, these include Vacuum Filtration (Dzierżanowski et al. 2011), able to provide a quantitative estimation of leaf deposited PM mass and leaf microanalysis by Scanning Electron Microscopy (SEM) coupled with Energy Dispersive X-Ray, useful for a comprehensive quali-quantitative characterization of leaf deposited particles (Baldacchini et al., 2017; Directorate-General for Research and Innovation EC, 2021). Once results are obtained, upscaling procedures will be needed to properly evaluate the air quality impact of specific NbS and of urban vegetation.

1.3.4 NbS as biomonitoring tools

The potential of implementing NbS in highly anthropized areas is also related to another important aspect. Indeed, the definition of evaluation frameworks for NBS environmental impacts can bring also to the utilization of NbS itself as low-cost and alternative monitoring stations, able to provide relevant information on the environmental quality of these areas (Larcher et al., 2021). This implies the potential of increasing the spatial resolution of environmental monitoring networks already present in cities. Therefore, NbSs can play the role of real living laboratories, where additional monitoring procedures can be carried out and environmental information can be retrieved. This is strictly connected to the biomonitoring concept, based on the ability of some livings organism to provide quali-quantitative information on certain characteristics of the biosphere (Wolterbeek, 2002). Unfortunately, very few studies have been focused on the potential of NBS as tools for biomonitoring. To date, one of the applications concerns the evaluation of biodiversity and functionality of urban ecosystems, through sampling and monitoring of pollinator species known as reliable and indirect

indicators for these parameters, within implemented NbS, (Ruiz et al., 2013). More attention has been also given to the potential utilization of NbS and urban vegetation to air quality monitoring purposes and this has been true especially for atmospheric PM pollution. Procedures able to quantify and characterize the on-leaf deposition of PM within specific NbS, can also be useful for biomonitoring purposes and for the identification of emission sources (Sgrigna et al., 2016) and the evaluation of their role and impact (Baldacchini et al., 2019). This is true since each natural or anthropogenic source is characterized by specific emission fingerprints, with emitted particles having specific dimensions, morphologies, and of course chemical compositions (Umbria et al. 2014). This latter aspect represents one specific object of the present PhD project, and it will be furtherly and deeply discussed in the following paragraphs of this thesis.

1.3.5 EU Horizon 2020 project – ProGIreg

ProGireg – productive green infrastructure for post-industrial urban regeneration: nature for renewal is funded by the European Union's Horizon 2020 innovation action program and represents one of the main project focused on the NbS implementation and the assessment of their related benefits. Within this project, four front runner cities (Dortmund, Turin, Ningbo and Zagreb) host living labs (LL), in designated post-industrial areas, where innovative NbSs are co-designed, implemented and monitored (website of the project: proGIreg.eu; Figure 4). Key concept of the project is the so-called *Quad-helix model*, which is based on the cooperation between local government, industry, academia and civil society, from co-design to impact evaluation stages of NbS implementation. Eight types of NbSs are defined with the final aim to: 1) improve urban living conditions; 2) reduce vulnerability to climate change and 3) provide measurable economic and social benefits to citizen. The eight types of NbS are the following:

1. Leisure activities and clean energy on former landfills
2. New regenerated soil
3. Community-based urban farms and gardens
4. Aquaponics
5. Green walls and roofs
6. Accessible green corridors
7. Local environmental compensation processes
8. Pollinator biodiversity

Fig. 4. Examples of NbS implemented in the four LL in ProGIreg: a. community-based urban farms in Turin LL; b. Green Wall in Zagreb LL; c. Renatured landfill in Dortmund LL and d. Renatured lakeshore in Ningbo LL (website of the project: proGIreg.eu)

Main target of this project is also the definition of specific monitoring plans for each of these NbSs, able to provide information on their multiple social, economic, and ecological benefits. Specifically, four assessment domains are defined and for each of them, several indicators and related methodologies are described.

For what concerns the *environmental and ecological restoration* domain, several indicators are planned for the evaluation of cross-cutting benefits related to air quality and temperature, carbon impact, biodiversity, and water quality. In addition to these, a specific monitoring tool is dedicated to atmospheric PM biomonitoring, to evaluate the NbS efficiency towards the abatement of this hazardous pollutant. To do so, SEM/EDX is applied to leaves sampled at the beginning and after the NbS implementation, to achieve results on PM removal via leaf deposition. Obtained results, are then upscaled at the LL and at the city level. The application of this monitoring tool within specific NbSs implemented in proGIreg, has been object of this PhD research project, and related results will be discussed in the following paragraphs. This specific monitoring task is relevant for providing useful information on the species-specific and NbS efficiency towards the removal of PM and the improvement of air quality.

References

Abbas, Z., Steenari, B. M., Lindqvist, O. 2001. A study of Cr (VI) in ashes from fluidized bed combustion of municipal solid waste: leaching, secondary reactions and the applicability of some speciation methods. Waste Management, 21(8), 725-739.

Abson, D., Von Wehrden, H., Baumgärtner, S., Fischer, J., Hanspach, J., Härdtle, W., Heinrichs, H., Klein, A. M., Lang, D. J., Martens, P., Walmsley, D. 2014. Ecosystem services as a boundary object for sustainability. Ecological Economics 103, 29–37.

Allegrini, I., De Santis, F., Di Palo, V., Febo, A., Perrino, C., Possanzini, M., & Liberti, A. 1987. Annular denuder method for sampling reactive gases and aerosols in the atmosphere. Science of the Total Environment, 67(1), 1-16.

Almeida, S. M., Pio, C. A., Freitas, M. C., Reis, M. A., Trancoso, M. A., 2005. Source apportionment of fine and coarse particulate matter in a sub-urban area at the Western European Coast. Atmospheric Environment 39(17), 3127-3138. https://doi.org/10.1016/j.atmosenv.2005.01.048.

Anderson, J. O., Thundiyil, J. G. Stolbach, A., 2012. Clearing the Air: A Review of the Effects of Particulate Matter Air Pollution on Human Health. Journal of Medical Toxicology 8, 166–175. https://doi.org/10.1007/s13181-011-0203-1

Andrade, C., Molina, C., Sánchez, L. F., Manzano, C. A., Toro, R., 2020. Exploring the oxidative potential and respiratory deposition of size-segregated particulate matter at an urban site. Journal of South American Earth Sciences, 102957.

Andreae, M. O., Gelencsér, A., 2006. Black carbon or brown carbon? The nature of light-absorbing carbonaceous aerosols, Atmos. Chem. Phys., 6, 3131–3148, https://doi.org/10.5194/acp-6-3131-2006.

Ares, A., Aboal, J.R., Carballeira, A., Giordano, S., Adamo, P., Fernández, J.A., 2012. Moss bag biomonitoring: a methodological review. Science of the Total Environment 432, 143-158.

Ayres, J. G., Borm, P., Cassee, F. R., Castranova, V., Donaldson, K., Ghio, A., Harrison, R.M., Hider, R., Kelly, F., Kooter, I.M., Marano, F., Maynard, R.L., Mudway, I., Nel, A., Sioutas, C., Smith, S., Baeza-Squiban, A., Cho, A., Duggan, S., Froines, J. 2008. Evaluating the toxicity of airborne particulate matter and nanoparticles by measuring oxidative stress potential - a workshop report and consensus statement. Inhalation Toxicology, 20(1), 75-99.

Baldacchini, C., 2019b. Monitoring and Assessment Plan, Deliverable No. 4.1, proGIreg. Horizon 2020 Grant Agreement No 776528, European Commission, 124.

Baldacchini, C., 2019b. Sgrigna, G., Baldacchini, C., Esposito, R., Calandrelli, R., Tiwary, A., Calfapietra, C., 2016. Characterization of leaf-level particulate matter for an industrial city using electron microscopy and X-ray microanalysis, Science of The Total Environment, 548–549, 91-99, ISSN 0048-9697, https://doi.org/10.1016/j.scitotenv.2016.01.057

Baldacchini, C., Castanheiro, A., Maghakyan, N., Sgrigna, G., Verhelst, J., Alonso, R., Amorim, J.H., Bellan, P., Bojović, D. D., Breuste, J., Bühler, O., Cântar, I. C., Cariñanos, P., Carriero, G., Churkina, G., Dinca, L., Esposito, R., Gawroński, S. W., Kern, M., Le Thiec, D., Moretti, M., Ningal, T., Rantzoudi, E. C., Sinjur, I., Stojanova, B., Aničić Urošević, M.,

Velikova, V., Živojinović, I., Sahakyan, L., Calfapietra, C., Samson. R., 2017. How does the amount and composition of PM deposited on Platanus acerifolia leaves change across different cities in Europe? Environmental Science and Technology 51(3):1147–1156

Baldacchini, C., Sgrigna, G., Clarke, W., Tallis, M., Calfapietra, C., 2019. An ultra-spatially resolved method to quali-quantitative monitor particulate matter in urban environment. Environmental Science and Pollution Research 26, 18719–18729 https://doi.org/10.1007/s11356-019-05160-8

Barone, T. L., Lall, A. A., Zhu, Y., Yu, R. C., Friedlander, S. K., 2006. Inertial deposition of nanoparticle chain aggregates: theory and comparison with impactor data for ultrafine atmospheric aerosols. Journal of Nanoparticle Research, 8(5), 669-680.

Barwise, Y., Kumar, P., 2020. Designing vegetation barriers for urban air pollution abatement: a practical review for appropriate plant species selection. npj Climate and Atmospheric Science 3, 12 https://doi.org/10.1038/s41612-020-0115-3

Bates, J.T., Fang, T., Verma, V., Zeng, L., Weber, R.J., Tolbert, P.E., Abrams, J.Y., Sarnat, S.E., Klein, M., Mulholland, J.A., Russell, A.G., 2019. Review of Acellular Assays of Ambient Particulate Matter Oxidative Potential: Methods and Relationships with Composition, Sources, and Health Effects. Environ. Sci. Technol. 53, 4003–4019. https://doi.org/10.1021/acs.est.8b03430

Beckett, K. P., Freer-Smith, P. H., Taylor, G., 2000. Particulate pollution capture by urban trees: Effect of species and windspeed. – Global Change Biology 6, 995–1103.

Canepari, S., Astolfi, M. L., Farao, C., Maretto, M., Frasca, D., Marcoccia, M., Perrino, C., 2014. Seasonal variations in the chemical composition of particulate matter: A case study in the Po Valley. Part II: Concentration and solubility of micro- and trace-elements. Environmental Science Pollution Research 21, 4010–4022, doi:10.1007/s11356-013-2298-1.

Canepari, S., Cardarelli, E., Giuliano, A., Pietrodangelo, A., 2006a. Determination of metals, metalloids and non-volatile ions in airborne particulate matter by a new two-step sequential leaching procedure Part A: Experimental design and optimization. Talanta 69(3), 581-587.

CEN (1998). Determination of the PM10 fraction of suspended particulate matter – Reference method and field test procedure to demonstrate reference equivalence of measurement methods. Brussel (EN12341).

CEN, 1998. Air Quality. Determination of the PM_{10} fraction of suspended particulate matter – Reference method and field test procedure to demonstrate reference equivalence of measurement methods. Brussel (EN12341).

CEN, 2005. Ambient air quality. Standard gravimetric measurement method for the determination of the PM2.5 mass fraction of suspended particulate matter (EN 14907).

Charrier, J. G., Anastasio, C. 2011. Impacts of antioxidants on hydroxyl radical production from individual and mixed transition metals in a surrogate lung fluid. Atmospheric Environment, 45 (40), 7555− 7562.

Chaudhary, S., McGregor, A., Houston, D., Chettri, N., 2015. The evolution of ecosystem services: a time series and discourse-centered analysis. Environ. Sci. Policy 54, 25–34.

Chen, L., Liu, C., Zou, R., Yang, M., Zhang, Z., 2016. Experimental examination of effectiveness of vegetation as bio-filter of particulate matters in the urban environment, Environmental Pollution, 208, Part A, 198-208, ISSN 0269-7491, https://doi.org/10.1016/j.envpol.2015.09.006.

Cohen-Shacham, E., Walters, G., Janzen, C., Maginnis, S., 2016. Nature-based Solutions to Address Global Societal Challenges. IUCN Commission on Ecosystem Management (CEM) and IUCN World Commission on Protected Areas (WCPA), Switzerland.

Costanza, R., d'Arge, R., de Groot, R., Farber, S., Grasso, M., Hannon, B., Limburg, K., Naeem, S., O'Neill, R., Paruelo, J., Raskin, R., Sutton, P., van den Belt, M., 1997. The value of the world's ecosystem services and natural capital. Nature 387 (15), 253–260.

Davidson, C. I. and Wu, Y. L., 1990. Dry deposition of particles and vapors, In S. E. Lindberg, A. L. Page, and S. A. Norton, eds. Acidic precipitation, Springer-Verlag, New York.

Delfino, R. J., Staimer, N., Vaziri, N. D. 2011. Air pollution and circulating biomarkers of oxidative stress. Air Quality, Atmosphere & Health, 4(1), 37-52.

Deng, S., Ma, J., Zhang, L., Jia, Z., Ma, Z., 2019. Microclimate simulation and model optimization of the effect of roadway green space on atmospheric particulate matter, Environmental Pollution, 246, 932-944, ISSN 0269-7491, https://doi.org/10.1016/j.envpol.2018.12.026.

Directorate-General for Research and Innovation (European Commission), 2021. Evaluating the impact of nature-based solutions - A handbook for practitioners. ISBN 978-92-76-22821-9, doi:10.2777/244577.

Dolske, D. A., Gatz, D. F., 1985. A field comparison of methods for the measurement of particle and gas deposition. J Geophys Res. 1985; 90: 2076–2084.

Dzierzanowski, K., Popek, R., Gawronska, H., Sæbø, A., Gawronski, S.W., 2011. Deposition of Particulate Matter of Different Size Fractions on Leaf Surfaces and in Waxes of Urban Forest Species. International Journal of Phytoremediation 13, 1037–1046.

EC, 1997. Working Group on Particles. Position Paper on Ambient Air Pollution by Particulate Matter. http://europa.eu.int/comm.

Eggermont, H., Balian, E., Azevedo, J. M. N., Beumer, V., Brodin, T., Claudet, J., Fady, B., Grube, M., Keune, H., Lamarque, P., Reuter, K., Smith, M., van Ham, C., Weisser, W.W., Le Roux, X., 2015. Nature-based solutions: new influence for environmental management and research in Europe. GAIA - Ecological Perspectives for Science and Society 24, 243–248. http://dx.doi.org/10.14512/gaia.24.4.9.

EPA, 1997. Reference Method for the Determination of Particulate Matter as PM10 in the Atmosphere. Federal Registrer, 62, No 138, Appendix M to part 50.

Escobedo, F.J., Nowak, D.J., 2009. Spatial heterogeneity and air pollution removal by an urban forest. Landscape and Urban Planning 90, 102e110.

European Commission, 2015. Towards an EU Research and Innovation Policy Agenda for Nature-Based Solutions & Re-Naturing Cities: Final Report of the Horizon 2020 Expert Group on Nature-Based Solutions and Re-Naturing Cities, European Commission: Brussels, Belgium.

Fares, S., Savi, F., Fusaro, L., Conte, A., Salvatori, E., Aromolo, R., Manes, F., 2016. Particle Deposition in a Peri-Urban Mediterranean Forestal Environmental Pollution 218, 1278−1286.

Fuchs, N.A., 1964. The Mechanics of Aerosols. Pergamon Press, New York.

Fusaro, L., Salvatori, E., Winkler, A., Frezzini, M. A., De Santis, E. Sagnotti, L., Canepari, S., Manes, F., 2021. Urban trees for biomonitoring atmospheric particulate matter: An integrated approach combining plant functional traits, magnetic and chemical properties, Ecological Indicators 126, 107707, ISSN 1470-160X, https://doi.org/10.1016/j.ecolind.2021.107707.

Gratani, L., Crescente, M. F., Varone, L., 2008. Long-term monitoring of metal pollution by urban trees. Atmospheric Environment, 42, 8273–8277.

Gromke, C., Ruck, B., 2007. Influence of trees on the dispersion of pollutants in an urban street canyon – Experimental investigation of the flow and concentration field. Atmospheric Environment 41, 3287–3302.

Guidolotti, G., Calfapietra, C., Pallozzi, E., De Simoni, G., Esposito, R., Mattioni, M., Nicolini, G., Matteucci, G., Brugnoli, E., 2017. Promoting the Potential of Flux-Measuring Stations in Urban Parks: An Innovative Case Study in Naples, Italy. Agriculture Forestry Meteorology 233, 153−162.

Gupta, T., Singh, S. P., Rajput, P., Agarwal, A. K. 2019. Measurement, Analysis and Remediation of Environmental Pollutants. Springer.

Haines-Young, R., Potschin, M., 2011. Common International Classification of Ecosystem Services (CICES): 2011 Update. Report to the European Environmental Agency, Nottingham.

Harrison, R. M., Yin, J., 2000. Particulate matter in the atmosphere: Which particle properties are important for its effects on health? Science of the Total Environment 249, 85–101, doi:10.1016/S0048-9697(99)00513-6.

Hering, S. V., Flagan, R. C., Friedlander, S. K., 1978. Design and evaluation of new low-pressure impactor. I. Environmental Science and Technology, 12(6), 667-673.

Hirabayashi, S., Kroll, C. N., Nowak, D. J., 2015. i-Tree Eco Dry Deposition Model Descriptions. Syracuse, NY, United States.

Hlavay, J., Polyak, K., Weisz, M., 2001. Monitoring of the natural environment by chemical speciation of elements in aerosol and sediment samples. Presented at the Whistler 2000 Speciation Symposium, Whistler Resort, BC, Canada, June 25–July 1, 2000. Journal of Environmental Monitoring, 3(1), 74-80.

Hofman, J., Wuyts, K., Van Wittenberghe, S., Samson, R., 2013. On the Temporal Variation of Leaf Magnetic Parameters: Seasonal Accumulation of Leaf-Deposited and Leaf-Encapsulated Particles of a Roadside Tree Crown. Science of Total Environment 493, 766−772.

IARC, 2013. Outdoor Air Pollution, IARC Monographs on the Evaluation of Carcinogenic Risks to Humans, 109, ISBN 978-92-832-0175-5.

International Organization for Standardization (ISO), 2018. Sustainable cities and communities — Indicators for city services and quality of life (ISO 37120:2018). Available from https://www.iso.org/standard/68498.html

IUCN, 2012. The IUCN Programme 2013–2016. IUCN, Gland, p. 30.

Janhäll, S., 2015. Review on urban vegetation and particle air pollution – Deposition and dispersion, Atmospheric Environment 105, 130-137, ISSN 1352-2310, https://doi.org/10.1016/j.atmosenv.2015.01.052.

Jeanjean, A. P. R., Monks, P. S., Leigh, R. J., 2016Modelling the Effectiveness of Urban Trees and Grass on PM2.5 Reduction via Dispersion and Deposition at a City Scale. Atmospheric Environment, 147,1−10.

Jennings, S. G., 1999. Wet Processes Affecting Atmospheric Aerosol. Atmospheric Particles.

John, W., 2001. Size Distribution Characteristics of Aerosols in: Baron, P. A., Willeke, K. Aerosol Measurement – Wiley InterScience New York.

Kabisch, N., Frantzeskaki, N., Pauleit, S., Naumann, S., Davis, M., Artmann, M., Haase, D., Knapp, S., Korn, H., Stadler, J., Zaunberger, K., Bonn, A. 2016. Nature-based solutions to climate change mitigation and adaptation inurban areas: perspectives on indicators, knowledge gaps, barriers, and opportunities for action, Ecology and Society, 21 (2). http://www.ecologyandsociety.org/vol21/iss2/art39/

Kardel, F., Wuyts, K., De Wael, K., Samson, R., 2018. Biomonitoring of atmospheric particulate pollution via chemical composition and magnetic properties of roadside tree leaves. Environmental Science and Pollution Research 25, 25994–26004. https://doi.org/10.1007/s11356-018-2592-z

Kim, K., Kabir, E., Kabir, S., 2015. A review on the human health impact of airborne particulate matter, Environment International 74, 136-143, ISSN 0160-4120, https://doi.org/10.1016/j.envint.2014.10.005.

Kumar, A., Elumalai, S. P., 2018. Influence of Road Paving on Particulate Matter Emission and Fingerprinting of Elements of Road Dust. Archives of Environmental Contamination and Toxicology 75, 424–435. https://doi.org/10.1007/s00244-018-0546-6

Lafortezza, R., Chen, J., 2016. The provision of ecosystem services in response to global change: evidences and applications. Environmental Research 147, 576–579.

Larcher, F., Baldacchini, C., Ferracini, C., Vercelli, M., Ristorini, M., Battisti, L., Calfapietra, C., 2021. Nature-Based Solutions as Tools for Monitoring the Abiotic and Biotic Factors in Urban Ecosystems. In: Catalano C., Andreucci M.

B., Guarino R., Bretzel F., Leone M., Pasta S. (eds) Urban Services to Ecosystems. Future City, vol 17. Springer, Cham. https://doi.org/10.1007/978-3-030-75929-2_7

Leonard, R. J., McArthur, C., Hochuli, D. F., 2016. Particulate matter deposition on roadside plants and the importance of leaf trait combinations, Urban Forestry & Urban Greening 20, 249-253, ISSN 1618-8667, https://doi.org/10.1016/j.ufug.2016.09.008.

Li, Y., Wang, S., Chen, Q., 2019. Potential of Thirteen Urban Greening Plants to Capture Particulate Matter on Leaf Surfaces across Three Levels of Ambient Atmospheric Pollution. International Journal of Environmental Research and Public Health, 16, 402. https://doi.org/10.3390/ijerph16030402

Lin, M., Khlystov, A., 2012. Investigation of Ultrafine Particle Deposition to Vegetation Branches in a Wind Tunnel, Aerosol Science and Technology, 46:4, 465-472, DOI: 10.1080/02786826.2011.638346

Lin, M., Yu, J. Z., 2019. Dithiothreitol (DTT) concentration effect and its implications on the applicability of DTT assay to evaluate the oxidative potential of atmospheric aerosol samples. Environmental Pollution, 251, 938-944. https://doi.org/10.1016/j.envpol.2019.05.074

Lorenzini, G., Grassi, C., Nali, C., Petiti, A., Loppi, S., Tognotti, L., 2006. Leaves of Pittosporum tobira as indicators of airborne trace element and PM10 distribution in central Italy, Atmospheric Environment 40 (22), 4025-4036, ISSN 1352-2310, https://doi.org/10.1016/j.atmosenv.2006.03.032.

Maes, J., Jacobs, S., 2015. Nature-based solutions for Europe's sustainable development. Conservation Letters 10 (1), 121-124. http://dx.doi.org/10.1111/conl.12216.

Manigrasso, M., Simonetti, G., Astolfi, M. L., Perrino, C., Canepari, S., Protano, C., Antonucci, A., Avino, P., Vitali, M., 2020. Oxidative Potential Associated with Urban Aerosol Deposited into the Respiratory System and Relevant Elemental and Ionic Fraction Contributions. Atmosphere, 11(1), 6.

Mark, D. 1999. Atmospheric Aerosol Sampling in: Harrison R M and. Van Grieken R E, Atmospheric Particles Vol 5.

Massimi, L., Ristorini, M., Astolfi, M. L., Perrino, C., Canepari, S., 2020. High resolution spatial mapping of element concentrations in PM10: A powerful tool for localization of emission sources, Atmospheric Research, 244, 105060, ISSN 0169-8095, https://doi.org/10.1016/j.atmosres.2020.105060.

Massimi, L., Ristorini, M., Eusebio, M., Florendo, D., Adeyemo, A., Brugnoli, D., Canepari, S., 2017. Monitoring and Evaluation of Terni (Central Italy) Air Quality through Spatially Resolved Analyses. Atmosphere 8, 200. https://doi.org/10.3390/atmos8100200

Massimi, L., Simonetti, G., Buiarelli, F., Di Filippo, P., Pomata, D., Riccardi, C., Ristorini, M., Astolfi, M. L., Canepari, S. 2019. Spatial distribution of levoglucosan and alternative biomass burning tracers in an urban and industrial hot-spot of Central Italy. Atmospheric Research, 104904.

Matzka, J., Maher, B. A., 1999. Magnetic biomonitoring of roadside tree leaves: identification of spatial and temporal variations in vehicle-derived particulates. Atmospheric Environment 33, 4565e4569.

Melles S. J., 2005. Urban bird diversity as an Indicator of human social diversity and economic inequality in Vancouver, British Columbia. Urban Habitats 1(3), 25–48.

Mitchell, R., Maher, B. A., 2009. Evaluation and application of biomagnetic monitoring of traffic-derived particulate pollution. Atmospheric Environment 43, 2095-2103.

Mitchell, R., Maher, B.A., Kinnersley, R., 2010. Rates of particulate pollution deposition onto leaf surfaces: temporal and inter-species magnetic analyses. Environmental Pollution 158, 1472-1478.

Mooney, H. A., Ehrlich, P. R., Daily, G., 1997. Ecosystem Services: A Fragmentary History. Island Press, Washington.

Moore, J. W., Ramamoorthy S., 1994. Heavy Metals in Natural Waters, Springer-Verlag, New York.

Moreno, E., Sagnotti, L., Dinarès-Turell, J., Winkler, A., Cascella, A., 2003. Biomonitoring of traffic air pollution in Rome using magnetic properties of tree leaves. Atmospheric Environment 37, 2967-2977.

Morselli, L. (Ed.). 1991. Deposizioni acide: i precursori, l'interazione con l'ambiente e i materiali. Maggioli.

Mouchet, M. A., Paracchini, M. L., Schulp, C. J. E., Stürck, J., Verkerk, P. J., Verburg, P. H., Lavorel, S., 2017. Bundles of ecosystem (dis)services and multifunctionality across European landscapes, Ecological Indicators, 73, 23-28, ISSN 1470-160X, https://doi.org/10.1016/j.ecolind.2016.09.026.

Mudway, I. S., Stenfors, N., Duggan, S. T., Roxborough, H., Zielinski, H., Marklund, S. L., et al., Kelly, F. J. (2004). An in vitro and in vivo investigation of the effects of diesel exhaust on human airway lining fluid antioxidants. Archives of Biochemistry and Biophysics, 423(1), 200-212.

Nesshöver, C., Assmuth, T., Irvine, K. N., Rusch, G. M., Waylen, K. A., Delbaere, B., Haase, D., Jones-Walters, L., Keune, H., Kovacs, E., Krauze, K., Külvik, M., Rey, F., van Dijk, Inge Vistad, O., Wilkinson, M. E., Wittmer, H. 2017. The science, policy and practice of nature-based solutions: An interdisciplinary perspective, Science of The Total Environment, 579, 1215-1227, ISSN 0048-9697, https://doi.org/10.1016/j.scitotenv.2016.11.106.

Nowak, D.J., Crane, D.E., Stevens, J.C., 2006. Air pollution removal by urban trees and shrubs in the United States. Urban Forestry urban Greening 4, 115-123.

Paatero, P., Tapper, U., 1994. Positive matrix factorization: a non-negative factor model with optimal utilization of error estimates of data values. Environmetrics 5, 111–126. https://doi.org/10.1002/env.3170050203.

Pace, R., Guidolotti, G., Baldacchini, C., Pallozzi, E., Grote, R., Nowak, D. J., Calfapietra, C., 2021. Comparing i-Tree Eco Estimates of Particulate Matter Deposition with Leaf and Canopy Measurements in an Urban Mediterranean Holm Oak Forest, Environmental Science & Technology 55 (10), 6613-6622 DOI: 10.1021/acs.est.0c07679

Pace, R.; Biber, P., Pretzsch, H., Grote, R., 2018. Modeling Ecosystem Services for Park Trees: Sensitivity of i-Tree Eco Simulations to Light Exposure and Tree Species Classification. Forests 9, 89. https://doi.org/10.3390/f9020089

Pacyna, J. M. 1999. Source Inventories for Atmospheric Trace Metals in: Harrison R M and Van Grieken R E, Atmospheric Particles, Vol 5.

Pauleit, S., Zölch, T., Hansen, R., & Randrup, T. B., 2017. Nature-based solutions and climate change – Four shades of Green. In A. Kabisch, N. Korn, H. Stadler, & J. Bonn (Eds.). Nature-based solutions to climate change adaptation in Urban areas: Linkages between science, policy and practice, 29–49 (1st ed.). Springer InternationalPublishing. https://doi.org/10.1007/978-3-319-56091-5.

Perini, K., Ottelé, M., Giulini, S., Magliocco, A., Roccotiello, E., 2017. Quantification of fine dust deposition on different plant species in a vertical greening system, Ecological Engineering 100, 268-276, ISSN 0925-8574, https://doi.org/10.1016/j.ecoleng.2016.12.032.

Petroff, A., Mailliat, A., Amielh, M., Anselmet, F., 2008a. Aerosol dry deposition on vegetative canopies. Part I: Review of present knowledge, Atmospheric Environment 42 (16), 3625-3653, ISSN 1352-2310, https://doi.org/10.1016/j.atmosenv.2007.09.043.

Petroff, A., Mailliat, A., Amielh, M., Anselmet, F., 2008b. Aerosol dry deposition on vegetative canopies. Part II: A new modelling approach and applications, Atmospheric Environment 42 (2008) 3654–3683

Pio, C., Alves, C., Nunes, T., Cerqueira, M., Lucarelli, F., Nava, S., Calzolai, G., Gianelle, V., Colombi, C., Amato, F., Karanasiou, A., Querol, X. 2020. Source apportionment of PM2. 5 and PM10 by Ionic and Mass Balance (IMB) in a traffic-influenced urban atmosphere, in Portugal. Atmospheric environment, 223, 117217.

Power, A. L., Worsley, A. T., Booth, C., 2009. Magneto-biomonitoring of intra-urban spatial variations of particulate matter using tree leaves. Environmental Geochemistry and Health 31, 315–325.

Prajapati, S. K., 2012. Ecological effect of airborne particulate matter on plants. In Environmental Skeptics and Critics, 1(1), 12-22.

Przybysz, A., Sæbø, A., Hanslin, H. M., Gawroński, S. W., 2014. Accumulation of particulate matter and trace elements on vegetation as affected by pollution level, rainfall and the passage of time, Science of The Total Environment, 481, 360-369, ISSN 0048-9697, https://doi.org/10.1016/j.scitotenv.2014.02.072.

Puxbaum, H., 1991. Metal Compounds In The Atmosphere in: Merian E (Edr), Metals And Their Compounds In The Environment, 257-286.

Queiroz, C., Meacham, M., Richter, K., Norström, A. V., Andersson, E., Norberg, J., & Peterson, G., 2015. Mapping bundles of ecosystem services reveals distinct types of multifunctionality within a Swedish landscape. Ambio, 44 Suppl 1(Suppl 1), S89–S101. https://doi.org/10.1007/s13280-014-0601-0

Querol, X., Viana, M., Alastuey, A., Amato, F., Moreno, T., Castillo, S., Pey, J., de la Rosa, J., Sanchez de la Campa, A., Artinano, B., Salvador, P., Garcia Dos Santos, S., Fernandez-Patier, R., Moreno-Grau, S., Negral, L., Minguillon, M.C., Gil, J.I., Inza, A., Ortega, L.A., Santamaria, J.M., Reff, A., Eberly, S. I., Bhave, P. V. 2007. Receptor modeling of ambient particulate matter data using positive matrix factorization: review of existing methods. Journal of the Air & Waste Management Association, 57(2), 146-154.

Rai, P. K., 2016. Impacts of particulate matter pollution on plants: Implications for environmental biomonitoring, Ecotoxicology and Environmental Safety, 129, 120-136, ISSN 0147-6513, https://doi.org/10.1016/j.ecoenv.2016.03.012.

Ramanathan V., Crutzen P. J., Kiehl J. T., Rosenfeld D., 2001. Aerosols, climate, and the hydrological cycle. Science 294, 2119.

Räsänen, J. V., Holopainen, T., Joutsensaari, J., Ndam, C., Pasanen, P., Rinnan, A., Kivimäenpää, M., 2013. Effects of species-specific leaf characteristics and reduced water availability on fine particle capture efficiency of trees, Environmental Pollution, 183, 64-70.

Raymond, C. M., Frantzeskaki, N., Kabisch, N., Berry, P., Breile, M., Nitaf, M. R., Geneletti, D., Calfapietra, C., 2017. A framework for assessing and implementing the co-benefits of nature-based solutions in urban areas, Environmental Science and Policy 77, 15–24. http://dx.doi.org/10.1016/j.envsci.2017.07.008

Reff, A., Eberly, S. I., Bhave, P. V. 2007. Receptor modeling of ambient particulate matter data using positive matrix factorization: review of existing methods. Journal of the Air & Waste Management Association, 57(2), 146-154.

Richardson, D. H. S., Shore, M., Hartree, R., Richardson, R. M., 1995. The use of X-ray fluorescence spectrometry for the analysis of plants, especially lichens, employed in biological monitoring. Science of Total Environment 176, 97–105.

Rossini Oliva, S., Fernández Espinosa, A. J., 2007. Monitoring of heavy metals in topsoils, atmospheric particles and plant leaves to identify possible contamination sources, Microchemical Journal 86 (1), 131-139, ISSN 0026-265X, https://doi.org/10.1016/j.microc.2007.01.003.

Ruiz, J. A., Gutiérrez, M., Porrini, C., 2013. Biomonitoring of Bees as Bioindicators, Bee World, 90:3, 61-63, DOI: 10.1080/0005772X.2013.11417545

Sæbø, A., Popek, R., Nawrot, B., Hanslin, H. M., Gawronska, H., Gawronski, S. W., 2012. Plant species differences in particulate matter accumulation on leaf surfaces. Science of Total Environment, 427-428, 347-54. doi:10.1016/j.scitotenv.2012.03.084.

Sagnotti, L., Winkler, A., 2012. On the magnetic characterization and quantification of the superparamagnetic fraction of traffic-related urban airborne PM in Rome, Italy, Atmospheric Environment 59, 131-140, ISSN 1352-2310, https://doi.org/10.1016/j.atmosenv.2012.04.058.

Salmond, J. A., Williams, D. E., Laing, G., Kingham, S., Dirks, K., Longley, I., Henshaw, G. S., 2013. The influence of vegetation on the horizontal and vertical distribution of pollutants in a street canyon. Science of the Total Environment 443:287-98. doi: 10.1016/j.scitotenv.2012.10.101.

Sarabi, S. E., Han, Q., Georges, A., Romme, L., de Vries, B., Wendling, L., 2019. Key Enablers of and Barriers to the Uptake and Implementation of Nature-Based Solutions in Urban Settings: A Review, Resources 8 (121). doi:10.3390/resources8030121

Sawidis, T., Breuste, J., Mitrovic, M., Pavlovic, P., Tsigaridas, K., 2011. Trees as Bioindicator of Heavy Metal Pollution in Three European Cities. Environmental Pollution 159 (12), 3560−3570.

Secretariat of the Convention on Biological Diversity, 2012. Cities and biodiversity outlook. Montréal, Québec, Canada.

See, S. W., Wang, Y. H., Balasubramanian, R. 2007. Contrasting reactive oxygen species and transition metal concentrations in combustion aerosols. Environmental Research, 103(3), 317-324.

Seigneur, C., 2019. Atmospheric Particles. In Air Pollution: Concepts, Theory, and Applications, 190-238. Cambridge: Cambridge University Press. doi:10.1017/9781108674614.009

Seufert, G., Kotzias, D., Sparta, C., Versino, B., 1995. Volatile organics in Mediterranean shrubs and their potential role in a changing environment. Ecological Studies 117, Springer, New York.

Sgrigna, G., Baldacchini, C., Dreveck, S., Cheng, Z., Calfapietra, C., 2020. Relationships between air particulate matter capture efficiency and leaf traits in twelve tree species from an Italian urban-industrial environment, Science of The Total Environment, 718, 137310, ISSN 0048-9697, https://doi.org/10.1016/j.scitotenv.2020.137310.

Sgrigna, G., Baldacchini, C., Esposito, R., Calandrelli, R., Tiwary, A., Calfapietra, C., 2016. Characterization of leaf-level particulate matter for an industrial city using electron microscopy and X-ray microanalysis, Science of The Total Environment, 548–549, 91-99, ISSN 0048-9697, https://doi.org/10.1016/j.scitotenv.2016.01.057

Sgrigna, G., Sæbø, A., Gawronski, S., Popek, R., Calfapietra, C., 2015. Particulate Matter deposition on Quercus ilex leaves in an industrial city of central Italy, Environmental Pollution, 197, 187-194, ISSN 0269-7491, https://doi.org/10.1016/j.envpol.2014.11.030.

Shen, H., Yang, T., Lu, C., Yuan, C., Hung, C., Lin, C., Lee, C., Jing, G., Hu, G., Lo, K., 2020. Chemical fingerprint and source apportionment of PM2.5 in highly polluted events of southern Taiwan. Environmental Science and Pollution Research 27, 6918–6935. https://doi.org/10.1007/s11356-019-07328-8

Smith, W.H., 1990. Air Pollution and Forests. Springer, New York.

Sparks, T. H., Butchard, S. H. M., Balmford, A., Bennun, L., Stanwell-Smith, D., Walpole, M., Bates, N. R., Bomhard, B., Buchanan G. M, Chenery A. M., Collen B., Csirke, J., Diaz, R. J., Dulvym, N. K., Fitzgerald, C., Kapos, V., Mayaux, P., Tierney, M., Waycott, M., Wood, L., Green, R. E., 2011. Linked indicator sets for addressing biodiversity loss. Oryx 45(03), 411-419. http://dx.doi.org/10.1017/s003060531100024x

Sportisse, B., 2009. Fundamentals in air pollution: from processes to modelling. Springer Science & Business Media.

TEEB – The Economics of Ecosystems and Biodiversity (2011) TEEB manual for cities: ecosystemservices in urban management. www.teebweb.org

Templeton, D. M., Ariese, F., Cornelis, R., Danielsson, L. G., Muntau, H., Van Leeuwen H. P., Lobinski, R., 2000 Guidelines for terms related to chemical speciation and fractionation of elements. Definitions, structural aspects, and methodological approaches (IUPAC Recommendations 2000). Pure Appl. Chem. 72, 1453–1470, doi:10.1351/pac200072081453.

Tepanosyan, G., Baldacchini, C., Sahakyan, L., 2021. Revealing Soil and Tree Leaves Deposited Particulate Matter PTE Relationship and Potential Sources in Urban Environment. International Journal of Environmental Research and Public Health 3;18(19):10412. doi: 10.3390/ijerph181910412.

Terzaghi, E., Wild, E., Zacchello, G., Cerabolini, B. E. L., Jones, K. C., Di Guardo, A., 2013. Forest Filter Effect: Role of leaves in capturing/releasing air particulate matter and its associated PAHs. Atmospheric Environment 74, 378–384.

Umbrìa, A., Galan, M., Munoz, M. J., Martìn, R., 2004. Characterization of atmospheric particles: Analysis of particles in the Campo de Gibraltar. Atmosfera 17, 191–206.

United Nations, 2012. World Urbanization Prospects, The 2011 Revision, United Nations Department of Economic and Social Affairs: New York, NY, USA.

United States Department of Agriculture (USDA) Forest Service, 2019. i-Tree Eco Manual. Northern Research Station, USDA Forest Service. Retrieved from https://www.itreetools.org/resources/manuals/Ecov6_ManualsGuides/Ecov6_UsersManual.pdf

van den Bosch, M., Sang, A. O., 2017. Urban natural environments as nature-based solutions for improved public health – A systematic review of reviews, Environmental Research 158, 373–384. http://dx.doi.org/10.1016/j.envres.2017.05.040

Visentin, M., Pagnoni, A., Sarti, E., Pietrogrande, M. C. (2016). Urban PM2. 5 oxidative potential: Importance of chemical species and comparison of two spectrophotometric cell-free assays. Environmental Pollution, 219, 72-79.

Wang, H., Joseph, J. A. 1999. Quantifying cellular oxidative stress by dichlorofluorescein assay using microplate reader. Free Radical Biology & Medicine, 27, 612–616.

Wang, H., Shi, H., Wang, Y., 2015. Effects of Weather, Time, and Pollution Level on the Amount of Particulate Matter Deposited on Leaves of Ligustrum lucidum. The Scientific World Journal. Article ID 935942. https://doi.org/10.1155/2015/935942

Weerakkody, U., Dover, J W., Mitchell, P., Reiling, K., 2017. Particulate matter pollution capture by leaves of seventeen living wall species with special reference to rail-traffic at a metropolitan station, Urban Forestry & Urban Greening 27, 173-186, ISSN 1618-8667, https://doi.org/10.1016/j.ufug.2017.07.005.

WHO, 2006. WHO Air quality guidelines for particulate matter, ozone, nitrogen dioxide and sulfur dioxide: Summary of risk assessment, Global update 2005. World Health Organization, Available at: http://www.euro. who.int/Document/E87950.pdf.

Wolterbeek, B., 2002. Biomonitoring of trace element air pollution: principles, possibilities and perspectives, Environmental Pollution, 120 (1), 11-21, ISSN 0269-7491, https://doi.org/10.1016/S0269-7491(02)00124-0.

Wu, Y., Liu, J., Zhai, J., Cong, L., Wang, Y., Ma, W., Zhang, Z., Li, C., 2018. Comparison of dry and wet deposition of particulate matter in near-surface waters during summer. PLoS ONE 13 (6): e0199241. https://doi.org/10.1371/journal.pone.0199241

Xing, Y., Jones, P., Donnison, I., 2017. Characterisation of Nature-Based Solutions for the Built Environment, Sustainability 9, 149. doi:10.3390/su9010149

Zwack, L. M., Paciorek, C. J., Spengler, J. D., Levy, J. I., 2011. Modeling spatial patterns of traffic-related air pollutants in complex urban terrain. Environmental Health Perspectives, 119(6), 852-859.

2. Experimental and modelling methods

2.1 Atmospheric PM sampling procedure

In this PhD research project, atmospheric PM_{10} is collected through the utilization of innovative active systems, the High Spatial Resolution Samplers (HSRS, Fai Instruments, Fonte Nuova, RM, Italy). These are low-cost, small, and light instruments that can be easily installed on various supports, such as balconies, railings or light poles (Figure 5), thus being able to access a large number of sampling locations. Key characteristic of HSRS is the very low flow of sampling of 0.5 L/min and a corresponding consumption of 0.2 W for the intake system and a maximum adsorbed electric power of 1 W, instead of 900-1200 W of conventional samplers. This peculiar and low sampling flow allows the collection of PM_{10} on membrane filters for long term periods, usually one or two months, suitable for subsequent chemical characterization. For all these technical characteristics, they are extremely suitable for the definition of dense, extensive, and low-cost monitoring networks. Moreover, being able to work autonomously for long period of time, they determine a substantial reduction of in-situ and maintenance costs, usually associated to the utilization of conventional PM active samplers. HSRS have been evaluated in terms of efficiency and repeatability through the comparison with results obtained from the chemical characterization of membrane filters collected with conventional PM_{10} samplers (Catrambone et al., 2019). This study reported good comparison for stable PM elemental components and high repeatability especially for metals and metalloids. Their efficiency has been also evaluated in the field and in different monitoring campaigns (Massimi et al., 2017; Massimi et al., 2019), which prove their effectiveness for the definition of monitoring networks and the evaluation of 1) spatial variability of PM_{10} and its elemental components and 2) impact of several PM emission sources.

Fig. 5. HSRS – High Spatial Resolution Samplers (Fai Instruments, Fonte Nuova, Italy).

In this study, HSRS are employed in two different study areas in Italy, Terni, and Torino, with the final scope to 1) provide useful information on the spatial and temporal variability of PM and its elemental components, 2) validate the use of leaves as passive PM samplers and the application of leaf deposited particles to biomonitoring purposes. In this context, the long-term collection of PM (usually one or two months) carried out by these innovative systems appears to be extremely useful, being similar to the exposure time of living organisms or bioindicators to environmental pollution. In both study areas, HSRS have been installed in parallel at the leaf sampling locations. In Turin they have been installed at high proximity to the implemented NbSs, while in Terni at differentiated polluted sites characterized by the impact of different emission sources. In both cases, active samplers are installed at least at two meters from the ground, to reduce the impact of natural soil resuspension. Moreover, HSRS are equipped with Teflon membranes with a diameter of 37 mm (PTFE membranes, 2 μm pore size, PALL Corporation, Port Washington, New York, NY, USA) and programmed for bi-monthly sampling periods.

Additionally, in Terni, the HSRS are employed in a wider and dense monitoring network of 23 sampling sites at about 1 km between each other, for the evaluation and mapping of the spatial distribution of PM_{10} mass concentration and its elemental components. These spatially resolved and chemical PM_{10} results are then compared to the ones obtained by the application of acellular oxidative potential (OP) assays (OP_{AA}, OP_{DTT} and OP_{DCFH}), to obtain a detailed evaluation of the ability of specific emission sources and their chemical tracers to induce oxidative stress in living organism. Finally, these data are also employed to validate the use of lichen transplants of *Evernia prunasti* L. and their bioaccumulation as biomonitors for PM pollution and for the identification of emission sources.

2.2 Leaf sampling procedure

Being able to properly plan the collection of leaf samples is extremely important due to the described complexity of the deposition process. Depending on the final scope of the study, sampling sites and therefore plants to be sampled need to be accurately selected. For example, in biomonitoring studies, sites and plants can be identified in proximity to known PM emission sources, such as industries or trafficked streets, or along defined transects. Moreover, a background location must be also selected, far from the direct impact of anthropogenic emission sources, to sample blank reference leaves. To minimize the potential impact of species-specific characteristics of the leaf surface on deposition mechanism, a single species must be chosen. Alternatively, to evaluate the species-specific affinity

towards this removal mechanism, plants from each species must be selected at high proximity to each other, to avoid any variability connected to different exposure conditions. Healthy and mature plants must be considered, thus avoiding abnormal, weak, or unhealthy plants. If the sampling needs to be repeated, selected plants must be marked to be easily recognized in the future.

For each plant, a representative number of branches and leaves must be sampled, and this can also varies depending on the aim of the study. At least three branches should be selected from each plant, sampled from the outer part of the crown. Replicate branches should be sampled with the same cardinal orientation or with specific exposure, for instance towards the prevalent wind direction in the study area. To reduce the impact of soil resuspension, local sources at the ground level or contaminations, branches need to be sampled at a constant height, ranging from two up to six meters from the ground. Furthermore, to reduce any potential influence of meteorological conditions and ensure a significant presence of PM on the leaf surface, branches and leaves must be detached after a constant rainless period. The impact of rain events on the PM accumulation on leaf surfaces is still under debate. It is certain that rain can remove leaf deposited particles mostly depending on their size and chemical composition (Xu et al., 2017). Moreover, only a fraction of the accumulated particles is removed by rain events and it extend depends on both the cumulative amount of rain (typically expressed in mm) and its intensity (expressed in mm/h) (Zhang et al., 2019). To this regard, in a controlled rainfall simulation, Xu et al., 2017 demonstrated that cumulative wash-off rates of leaf deposited PM increased with cumulative amount of rain until 12.5 mm, with this rain amount being able to remove from 51 % to 71 % of leaf deposited PM.

From each replicate branch, healthy replicate leaves should be detached from the same internode, to ensure homogeneous exposure times to atmospheric PM pollution and its deposition. Usually, youngest leaves, which are located at the top of the branch, should be avoided, to ensure a longer exposure period. After sampling, leaf samples can be stored inside paper bags which are properly marked and signed with sampling information (i.e., date, location, species, height of sampling, replicate branch, replicate leaf), to avoid any external contamination.

2.3 Experimental techniques

2.3.1 Scanning Electron Microscopy coupled with Energy Dispersive X-Ray detector (SEM/EDX)

Scanning electron microscopy with energy dispersive X-ray spectroscopy (SEM/EDX) is the best known and most widely-used of the surface analytical techniques. This technique is considered a relatively rapid, inexpensive, and basically non-destructive approach to surface analysis. High

resolution images of surface topography are produced using a highly-focused, scanning beam of primary electrons. The electron beam is focused by one or two condenser lenses into a beam with a very fine focal spot size. The beam passes through pairs of scanning coils or pairs of deflector plates in the electron optical column, typically in the objective lens, which deflects the beam horizontally and vertically over a rectangular area of the sample surface. The primary electrons enter a surface with an energy of 0.5 – 30 kV and generate many low energy secondary and backscattered electrons. Specifically, the intensity of backscattered electrons can be correlated to the atomic number of the element, with brighter particles being characterized by the heavier elemental components. Hence, some qualitative elemental information can be obtained. The incident electron beam may excite electrons in an inner shell of the sample atoms, resulting in the formation of an electron hole within the atom's electronic structure. An electron from an outer, higher-energy shell then fills the hole, and the difference in energy between the higher-energy shell and the lower energy shell is released in the form of an X-ray photon, which has an energy characteristic for each chemical element (Fig. 6). The x-ray released by the electron is then detected and analyzed by the energy dispersive spectrometer (EDX). The resulting spectrum indicates which chemical elements are present in the sample, either locally or overall. In addition, a quantitative distribution of elements can also be calculated using the relative height of the peaks, if the detector has been calibrated for those elements. The depth from where the X-rays originate depends on the material and the used primary electron beam energy.

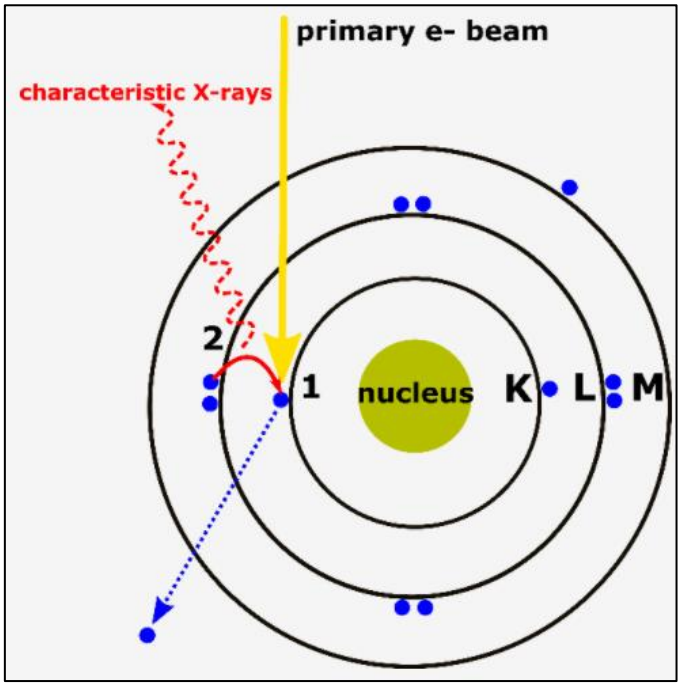

Fig. 6. X-rays are generated using EDX following a two-step process. First, the energy transferred to the atomic electron knocks it off, leaving behind a hole. Second, its position is filled by another electron from a

higher energy shell, and the characteristic X-ray is released (https://www.thermofisher.com/blog/microscopy/edx-analysis-with-sem-how-does-it-work/)

A Phenom ProX (Phenom-World, The Netherlands) scanning electron microscope coupled with an X-ray analyzer (SEM/EDX) and equipped with a charge-reduction sample holder suited for non-metalized biological materials is employed for the chemical/physical characterization of leaf deposited PM. Two portions of about 0.5 cm^2 are cut from each leaf sample, for the micro-analysis of both the adaxial (AD) and the abaxial (AB) leaf surfaces. Portions are cut from the same part of the leaf, except for leaf margins, veins and ribs which can be associated to higher particles accumulation, thus resulting in the risk of overestimated results. These sections are fixed to the head of carbon-based stubs (PELCO Tabs, Ted Pella Inc.) and fluxed with compressed air, to remove any loose particle. The number density and size distribution of leaf deposited particles are determined by ten random SEM images of both the AD and AB surfaces of each sample. Imaging is performed in backscattered electron configuration, with an incident electron energy of 5 keV, in order to limit the surface charging. Each random SEM image is 150 μm × 150 μm wide, with a resolution of 1024 × 1024 pixels (Figure 7a). On these images, PM can be easily distinguished as bright particles, with the color contrast of SEM features being proportional to the atomic number of the elemental components. SEM images are analyzed through Gwyddion software (Nečas and Klapetek, 2012), by applying a color threshold-based grain analysis (Figure 7b; Baldacchini et al. 2017), thus obtaining the number of particles in the image, together with their aerodynamic diameters (expressed as the diameter of the equivalent sphere, d_{eq}). Particles with a d_{eq} comparable with the size of two image pixels are excluded, resulting in a lower cutoff at about 0.3 μm in the diameter of the analyzed particles. Particles with a d_{eq} larger than 10 μm are also excluded from the analysis. Number of particles density are then normalized by scanned leaf area expressed in mm^2, thus obtaining the particles density for both AD and AB surfaces as a function of specific size fraction (usually for $PM_{0.3\text{-}1}$, particles with aerodynamic diameters ranging from 0.3 μm to 1.0 μm, $PM_{1\text{-}2.5}$ with 1.0 μm ≤ a. d. ≤2.5 μm, and $PM_{2.5\text{-}10}$ with 2.5 μm ≤ a. d. ≤ 10 μm).

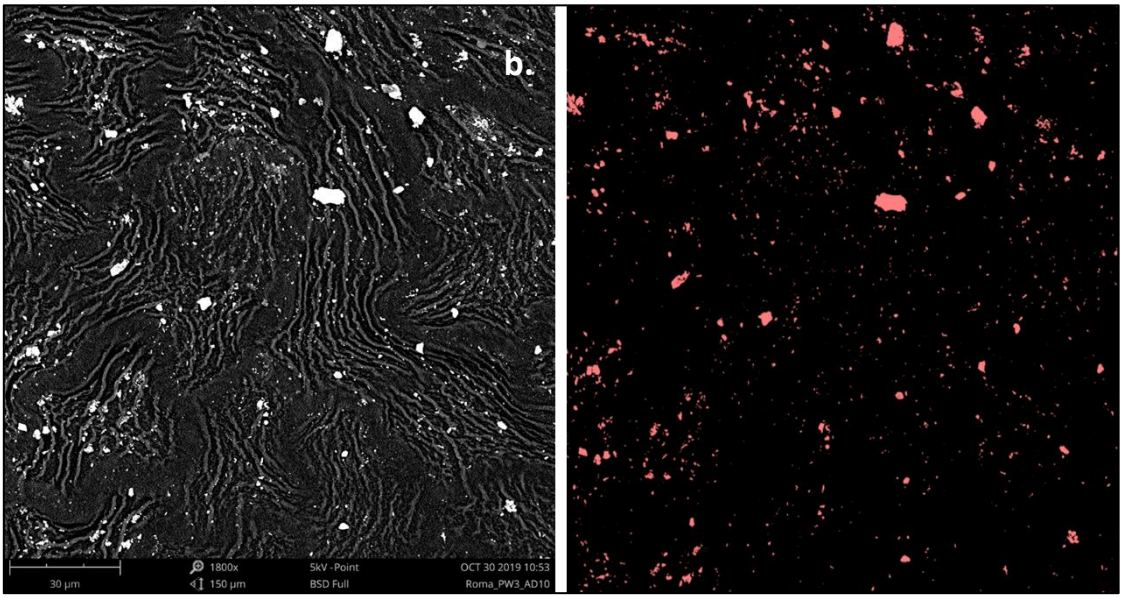

Fig. 7. a) SEM image (150 µm × 150 µm wide, with a resolution of 1024 × 1024 pixels) acquired in backscatter electron configuration and 5 keV and b) application of the color threshold-based grain analysis by Gwyddion software (Baldacchini et al., 2017).

The elemental composition of selected leaf deposited particles is performed through EDX and a dedicated Phenom Pro Suite software. To this aim, five random images of 50 µm × 50 µm scan size (both AD and AB) and the same resolution of 1024 × 1024 pixels, are acquired in backscatter configuration with an incident electron energy of 15 keV. For each of these images, ten particles are selected for EDX analysis. EDX spectra are obtained by positioning the laser beam in the particles' center (Figure 8). In this case, the d_{eq} of EDX particles is obtained by averaging their two main Feret diameters (Merkus, 2009), measured by ImageJ software (Schneider et al., 2012). The main elements identified in the PM are C, N, O, Na, Mg, Al, Si, Cl, K, Ca, Ti, and Fe. Trace elements such as F, P, S, Cr, Mn, Co, Ni, Cu, Zn, Sr, Mo, Sn, Sb, Ba, and Bi can been also observed. Only detected elemental percentages higher than 0.1 % are taken in consideration. C, N, and O are usually excluded due to several reasons, since 1) they can be related to biogenic factors, 2) EDX is known to fail in the correct determination of light elements, and 3) the high values and variability of C and O concentrations as obtained by EDX could hinder the variability of the other elements' concentration, which are the more relevant in terms of pollution.

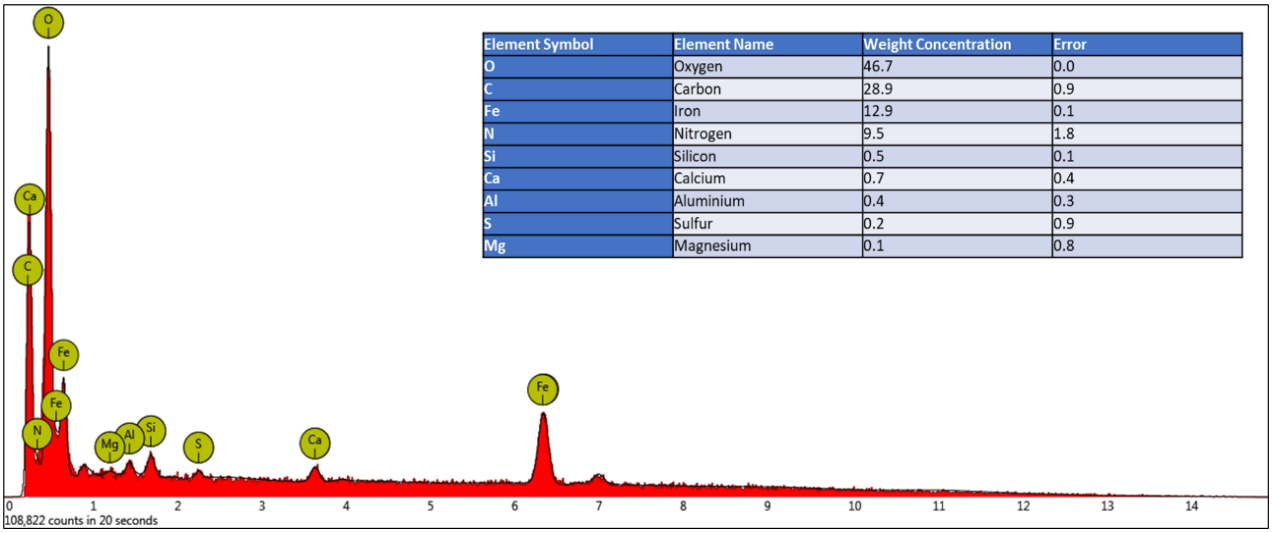

Element Symbol	Element Name	Weight Concentration	Error
O	Oxygen	46.7	0.0
C	Carbon	28.9	0.9
Fe	Iron	12.9	0.1
N	Nitrogen	9.5	1.8
Si	Silicon	0.5	0.1
Ca	Calcium	0.7	0.4
Al	Aluminium	0.4	0.3
S	Sulfur	0.2	0.9
Mg	Magnesium	0.1	0.8

Fig. 8. EDX spectrum and percentage elemental composition of a typical metallic particle.

The weighted volume percentage (W%) occupied by each element x over the N particles selected is calculated multiplying the composition percentage (C) of each element x on each particle i (C_{xi}, as obtained by the EDX software) by the corresponding particle volume (V_i), which is calculated assuming a spherical morphology as $V_i = 4/3\ \pi\ (d_{eq}/2)^3$. Then, for each element, volume percentages are summed together, and this sum is then normalized by using the total volume of all the N analyzed particles (Baldacchini et al., 2017) by following equation 1:

$$W_{\%x} = \frac{\sum_{i=1}^{N} C_{xi} \times V_i}{\sum_{i=1}^{N} V_i} \quad (1)$$

Finally, the mass load of leaf deposited PM is obtained by multiplying the $W_{\%x}$ of each element x, by the total volume of SEM particles (V_{PMtot}, as obtained by the SEM images of the collected leaves) and by the corresponding elemental atomic mass per volume (Am_x; as reported in https://www.webelements.com/periodicity/density/). The obtained quantity is then normalized by the total imaged area (A_{leaf}) (eq. 2), thus resulting in the PM load per unit leaf area, M (expressed in µg cm^{-2}) (Baldacchini et al., 2019).

$$M = \sum_x \frac{W_{\%x} \times V_{PMtot} \times am_x}{A_{leaf}} \quad (2)$$

2.3.2 Washing and Vacuum filtration (VF)

The washing and vacuum filtration (VF) procedure (Fig. 9), firstly described in Dzierżanowski et al. (2011), is a gravimetric technique widely used to quantify the amount of leaf-deposited PM, into different size fractions (i.e., PM_{10} and $PM_{2.5}$). In this study and to this aim, VF procedure is applied to several leaf samples, and its efficiency is evaluated through the comparison with other techniques. Leaf samples are thoroughly shaken in a flask, with a constant volume of deionized water (usually 250 mL or 500 mL) for 5 minutes. Washed leaves are then air-dried, scanned and their surface area is measured using the ImageJ software. Obtained washing solutions are pre-filtered through a 100 µm pores sieve, to remove the coarsest material. Through a vacuum filtration system, leaf washing solutions are consequently filtrated with cellulose filters able to remove particles with diameter larger than 10 µm (code 1250; smallest stopped particle size in the 10–13 µm range, Anoia S.A., Barcelona, Spain) and then larger than 2 µm (code 1244; smallest stopped particle size in the 2–4 µm range, Anoia S.A.). Consequently, particles with diameters between about 2.5 µm and 10 µm ($PM_{2.5\text{-}10}$) can be assumed to accumulate on this second filter. Then, washing solutions are filtered with a 0.2 µm porosity nitrocellulose filter (type CN, LVR > 7, Advanced Microdevices Pvt. Ltd., Ambala Cantt, India), where particles with a diameter ranging from 0.2 µm to about 2.5 µm (i.e., $PM_{0.2\text{–}2.5}$) are expected to accumulate. All filters are dried before and after the filtration in a moisture-controlled oven (Griffin Company) for 40 minutes at 70 °C and are placed into the balance room for 30 minutes, to equilibrate to humidity levels before weighing (R200D Research Analytical Balance, Sartorius, Gottingen, Germany).

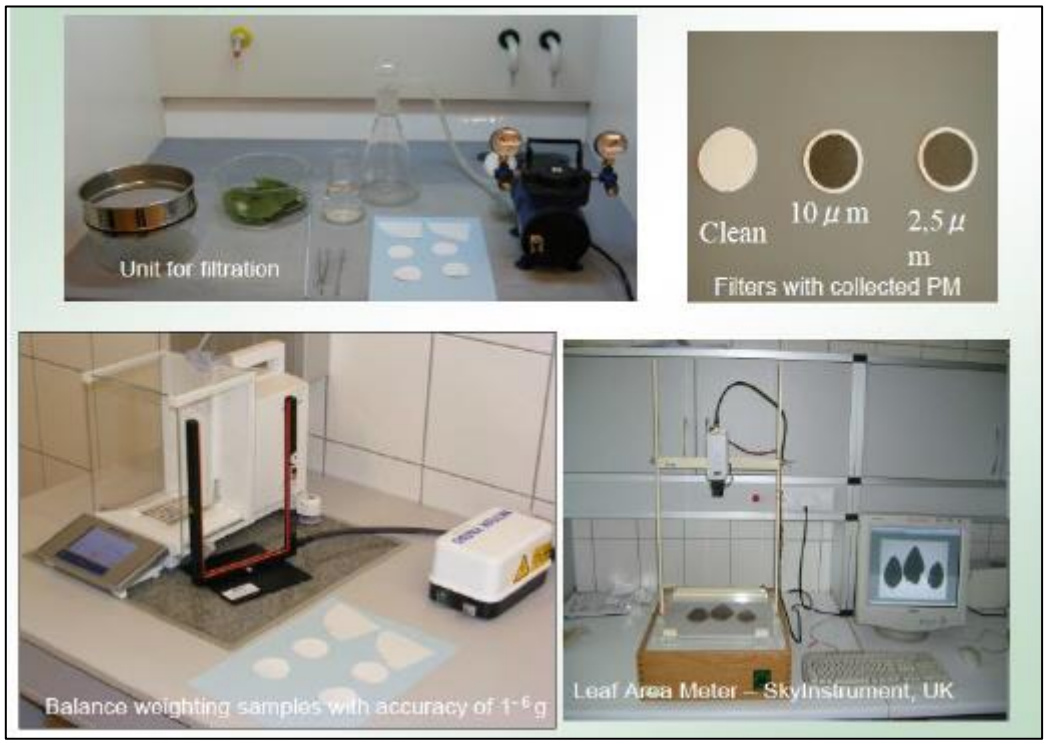

Fig. 9. Equipment and utensils used for washing and vacuum filtration procedure (VF)

The dried mass of filters is obtained at the precision of $\times 10^{-5}$ g, before (T1) and after (T2) filtration. The mass of leaf-deposited PM per unit leaf area is then estimated for each respective size fraction as the difference between T2 and T1 masses, further divided by the total two-sided washed leaf area ($\mu g/cm^2$). This procedure allows to obtain a quantification of the insoluble PM load per unit leaf area of $PM_{2.5–10}$ and $PM_{0.2–2.5}$ that, summed together, provide the total PM_{10} load per unit leaf area. After the 0.2 μm filtration step, a conductometer (Crison Basic 30 conductometer) equipped with standard 5070 platinum cell, is employed for measuring the electrical conductivity (EC) of leaf washing solutions. The conductometer uses a probe to measure conductivity of a solution, which is defined as its ability to conduct electricity. Electrical current flows between two electrodes within the probe set at various distances from each other. Measured values depends on several factors such as the solution's ionic strength, which ions are present and their concentration. Therefore, calibration plays a huge factor in the accuracy of conductometer, as does the temperature. The official unit of measurement for conductivity is mhos/cm or microSiemens per centimeter. Measured EC values are then used to estimate the total dissolved solid (TDS, expressed in mg/mL), thus multiplying the EC by a conversion factor of 0.65 previously identified for freshwaters (Rusydi, 2018). TDS values are then multiplied by the washing solutions volume in mL and divided by the total two-sided washed leaf area in cm^2, to obtain normalized mass results expressed as mg/cm^2.

2.3.3 Chemical fractionation

The chemical fractionation procedure is applied for the characterization of water soluble and insoluble fraction of both PM_{10} elemental components and leaf deposited PM. This procedure has been already optimized and validated for the chemical characterization of the two solubility fractions of airborne PM, actively collected on membrane filters (Canepari et al., 2006a; Canepari et al., 2006b). To be able to apply this procedure also to the chemical characterization of leaf deposited PM, it has been adapted for the analysis of VF materials, both the leaf washing solutions and the membrane filters used for their filtrations. The following procedure results to be effective to overcome the main limitations traditionally associated to the VF procedure, which are associated to the lack of a chemical characterization of leaf deposited PM, and especially of water-soluble particles.

PM_{10} membrane filters

For the analysis of atmospheric PM_{10} actively collected on Teflon membrane filters, firstly, the supporting polymethylpentene ring is removed from each membrane filter, and then filters are

extracted in 10 mL of deionized water for 30 min at 25 °C by means of an ultrasonic bath (Proclean 10.0 ultrasonic cleaner, Ulsonix, Germany). These aqueous solutions are then filtered on cellulose nitrate filters (0.45 m pore size, Merck Millipore Ltd., Billerica, MA, USA) and both the membrane and cellulose nitrate filters are acid digested for 30 min at 180 °C in the microwave oven by using the HNO_3/H_2O_2 mixture (2:1, v/v). The digested solutions are then diluted to 50 mL with deionized water and filtered with syringe filters (25 mm diameter, 0.45 m pore size, GVS Filter Technology, Morecambe, England, UK) before instrumental analysis. Elemental concentrations of both the water-soluble and insoluble fraction are determined by a quadrupole inductively coupled plasma mass spectrometer (ICP-MS, model 820-MS; Bruker, Bremen, Germany) equipped with a glass nebulizer (0.4 mL/min; Analytik Jena AG, Jena, Germany). External matrix-matched standard calibration curves are performed for all the analyzed elements in the 1 - 500 g/L range by serially diluting standard stock solutions (1000 mg/L; Exaxol Italia Chemical Manufacturers Srl,Genoa, Italy). To control the nebulizer efficiency, yttrium (Y) and rhodium (Rh) are set at 5 g/L as internal standards for all measurements and are prepared from standard stock solutions (1000 mg/L; Panreac Química, Barcelona, Spain; Ultra Scientific, North Kingstown, RI, USA; Merck Millipore Ltd.,Billerica, MA, USA). Limits of detection (LODs) for each element in each of the two solubility fractions, are set at 3 times the standard deviation of 10 replicate blank determinations, which are subjected to the same sample preparation and analytical procedure. The used instrumental conditions and the performance of the method are detailed in Astolfi et al. 2018.

Leaf samples

After the 0.2 µm filtration step, and the EC measurement, leaf washing solutions are analyzed by ion chromatography (IC, ICS1000; Dionex Co., Sunnyvale, CA, USA) for the detection of anions such as, Cl^- F^-, NO_3^{2-}, $PO_4^{3.}$ and SO_4^{2-} and by ICP-MS for the detection of the concentrations of both macro and trace elements, as reported in the previous section (Canepari et al., 2006a and 2006b). Ammonium (NH_4^+) is detected by UV-Visible spectrophotometer (50 Scan Varian, Santa Clara, CA United States), following the procedure indicated in the Ammonium-Test, Spectroquant (Merck, Darmstadt, Germany). The chemical characterization of leaf washing solutions is completed by the determination of the water-soluble organic carbon (WSOC), analyzed by TOC-VSCH (Shimadzu, Kyoto, Japan) using the non-purgeable organic carbon (NPOC) procedure (Saarikoski et al., 2008).
VF membrane filters, both the ones corresponding to $PM_{2.5–10}$ and the ones to $PM_{0.2–2.5}$ are acid-digested in a microwave oven, mixed with 2 mL HNO_3 (67%; Promochem, LGC Standards GmbH,Wesel, Germany), 1 mL HF (40%, Suprapur, Merck) and 3 mL HCl (puriss. p.a., Sigma-

Aldrich, Co., St. Louis, MO, USA), to 180 °C for 40 minutes (Astolfi et al., 2020). The acid-digested solutions are diluted in 10 mL of deionized water and then analyzed for the concentrations of elemental components by means of inductively coupled plasma atomic emission spectroscopy (ICP-OES; VISTA-MPX, CCD Simultaneous, Varian) equipped with an inert introduction line. The instrumental conditions used for ICP-OES analysis are detailed in Astolfi et al., 2020.

Instrumentation and analytical procedures

Ion chromatography (IC)

Ion chromatography measures the concentrations of ionic species by separating them, based on their specific interaction with a resin (Weiss and Weiss, 2005). This interaction is mainly affected by species type and size. Sample solutions pass through a pressurized chromatographic column where ions are absorbed by column constituents. As an ion extraction liquid, known as eluent, runs through the column, the absorbed ions begin separating from the column. The retention time of different species determines the ionic concentrations in the sample. A suppressor is used to reduce the background conductance of the eluent and at the same time enhance the conductance of the sample ions. The chromatogram is a record of detector output (electrical conductivity) versus time as the analyte passes through the chromatography system. It usually consists of a series of several peaks corresponding to the different times in which components of the analyte mixture emerge from the column. Each peak represents a separate ion from the sample solution. The elution time, or time it takes for the ion to move through the column, varies for each ion species as they elute from the column separately as the pH and/or ionic strength of the eluent is increased. The concentration of ions moving through the column at a particular time is represented by the height and the breadth of the peaks and can be correlated to the concentration of a particular species in the sample solution. Standards are needed to calibrate the IC to identify peaks and to determine the concentrations of ions. Standards are usually prepared by diluting a multi-ions solution. Deionized water is used as a blank sample to check if the dilutions will not affect measured concentrations and to make sure that there are no significant sources of ions in the instrument.

UV-Visible spectrophotometer and Ammonium-Test

Ultraviolet and visible spectroscopy (UV-VIS) is an analytical technique that measures the amount of UV or visible light that are absorbed by or transmitted through a sample in comparison to a blank sample. This property is influenced by the sample composition, potentially providing information on what is in the sample and at what concentration. This instrumentation is usually composed by a light source, a wavelength selector, and a detector. A single xenon lamp is commonly used as a high

intensity light source for both UV and visible ranges. Monochromators are most used as wavelength selector, thus separating light into a narrow band of wavelengths. It is based on diffraction gratings that can be rotated to choose incoming and reflected angles to select the desired wavelength of light. For all analyses, measuring a blank sample, such as a cuvette filled with a similar solvent used to prepare the sample, is imperative. Quartz sample holders are required for UV examination because quartz is transparent to the majority of UV light. After the light has passed through the sample, a detector is used to convert the light into a readable electronic signal. Also in this case, the construction of a calibration curve is required to accurately determine the concentration of a particular substance in a sample based on absorbance measurements. The absorbance (A) is equal to the logarithm of a fraction involving the intensity of light before passing through the sample divided by the intensity of light after passing through the sample. This fraction is also called transmittance (T), which expresses how much light has passed through a sample. Specifically for the determination of ammonium ion (NH_4^+) a derivatization reaction is employed: in strongly alkaline solution NH_4^+ reacts with hypochlorite ions to form monochloramine. This compound in turn reacts with substituted phenol to form a blue indophenol derivative that is determined photometrically at 690 nm wavelength (Ammonium-Test, Spectroquant, Merck, Germany).

Total organic carbon analyzer (TOC) and the non-purgeable organic carbon (NPOC) procedure

Total Organic Carbon (TOC) is an indirect measure of organic molecules present in water and measured as carbon (Shimadzu Corporation, 2001). Analytical technologies utilized to measure TOC share the objective of completely oxidizing the organic molecules in an aliquot of sample water to carbon dioxide (CO_2), measuring the resulting CO_2 concentration, and expressing as carbon concentration. TOC analyzer discriminates between the inorganic carbon and the CO_2 generated from the oxidation of organic molecules in the sample. The approach used to measure TOC involves subtracting the measured inorganic carbon (IC) from the measured total carbon (TC), which is the sum of these two fractions. The non-purgeable organic carbon (NPOC) procedure (Saarikoski et al., 2008; Williams, 2000) used in this study measures the quantity of total organic carbon (TOC) as non-purgeable organic carbon (NPOC) in water extracts. NPOC is measured by acidifying an aliquot of water extract using 1M HCl, then sparging the sample to strip off any purgeable organic and inorganic carbon. The sample is then injected into a combustion tube that is kept at 720°C. A redox reaction occurs that evolves carbon dioxide gas (CO_2) which is then detected by a non-dispersive infrared (NDIR) detector for NPOC. In this detector, CO_2 molecules absorbs the IR radiation coming from the source, thus reducing the total transmittance of infrared light that reaches the detector. To measure total inorganic carbon (TIC), an aliquot of sample is injected into a bubble chamber. Phosphoric acid

(25 %) is added to the sample which reacts with inorganic carbon to form CO_2. Air is bubbled through the sample and the evolved CO_2 is sent directly to the NDIR detector for TIC analysis.

Inductively coupled plasma mass spectrometry (ICP-MS) and inductively coupled plasma - optical emission spectrometry (ICP-OES)

Inductively coupled plasma mass spectrometry (ICP-MS) and inductively coupled plasma optical emission spectrometry (ICP-OES) are elemental analysis technologies, both characterized by an inductively coupled plasma (ICP) as ionization source. ICP fully decompose a liquid sample into its elemental components and transform those elements in ions. It is typically composed of argon gas and energy is coupled to it using an induction coil to form the plasma. The plasma is a mixture of ions, electrons, and atoms that, at atmospheric pressure, has an extremely high temperature (up to 10,000 K). At these temperatures, most elements easily make the transition from atoms to ions. Before the introduction into the plasma, liquid samples are converted into an aerosol by a nebulizer. In ICP-OES when an atom or ion is excited within the plasma, its electrons move from a lower to higher energy level. Upon relaxation of these electrons to their initial state, energy is emitted in the form of photons. The emitted photons possess wavelengths that are characteristic of their respective elements. One element can have multiple electron excitations and relaxations; therefore, it can have multiple characteristic wavelengths. The liquid sample is introduced into the plasma and the optical system (spectrometer) is used to separate element-specific wavelengths of light and to focus the resolved light onto the detector as efficiently as possible, and the derived signals are processed to quantify the elemental composition.

After the plasma section in ICP-MS, elemental masses of the sample are separated using a mass analyzer. Quadrupole mass analyzers are sequential, so each element is measured in sequence. These analyzers work by combining a radio frequency (RF) alternating current (AC) potential with a direct current (DC) potential over four electrodes, or poles, to create the electric field that sample ions pass through. As the ions pass through this electric field, they gain energy and accelerate. Two of the oppositely placed poles have a positive potential applied to them, and the other two have a negative potential applied. The DC component of the electric field produces a constant force on the ions while they travel through the quadrupole. Because the ions are positively charged from the plasma, the positive poles repel the ions into the center of the mass analyzer, while the negative poles attract the ions away from the center of the quadrupole. The AC component counteracts the effect of the DC component depending on the ion's mass. The size of this stability region is different for each ion mass, so individual masses can be resolved with specific AC/DC potential combinations. Mass resolution is controlled by the ratio of DC against AC potential, and unit mass resolution is easily

achieved. Keeping the ratio constant and increasing the potentials allows each mass in the spectrum to be scanned individually. After mass separation, ions must be detected and amplified to determine their intensities.

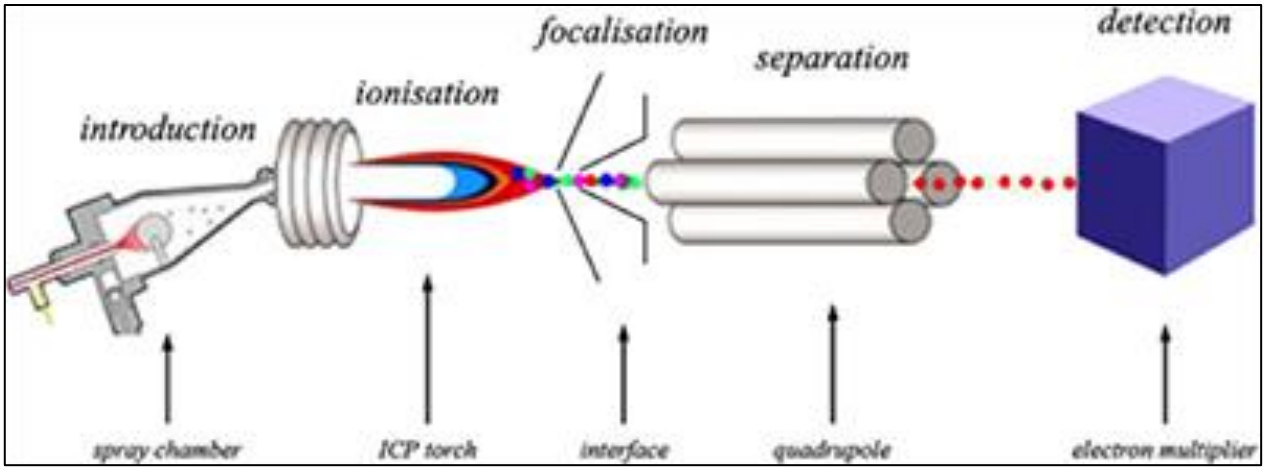

Fig. 11. Schematic of the ICP-MS method (https://nffa.eu/offer/area/technique/?id=6310)

The output of an ICP-MS is numerical, and usually provided in counts per second. Calibration is crucial, thus enabling test sample concentrations to be quantified. A range of standards is tested at the start of the analysis to generate a so-called calibration curve. In this way, instrument response can be correlated to actual analyte concentration within the samples. In addition to this and to compensate for matrix effects and instrument drift, it is important to combine external calibration with internal standardization. This is the most widely used method of calibration in ICP-MS and involves adding the same amount of one or more elements to all measured solutions (blanks, calibration standards, quality control standards, unknown samples, etc.). The response from this element is expected to be the same throughout the assay, so that any variation is assumed to be derived from either matrix effects or instrument drift. A mathematical correction factor is calculated from the relative internal standard response that is then applied to the analytes to correct for both matrix and drift effects. The ideal internal standard for any given analyte is not already present in the sample, has a similar mass and ionization potential as the analyte, and behaves similarly to the analyte, both in solution and the plasma.

2.4 Modelling approaches

2.4.1 *i-Tree Eco* model

The *i-Tree Eco* is one of the most used model for the quantification of urban forest structure, associated ecosystem services (ESs) and value (Selmi et al., 2016). Through its utilization, ESs such as carbon storage and sequestration, air pollution reduction, water runoff reduction, effects on energy consumed by buildings, and some disservices, such as the emission of biogenic volatile organic compounds (BVOCs) can be evaluated (Russo et al., 2016). To this aim, *i-Tree Eco* is designed to use field data from complete inventories of trees or randomly located plots throughout a community, along with hourly meteorological and pollution data (Nowak et al., 2006). Field data required as input for the model are trees biometric or health status information, such as species, total tree height and stem diameter at breast height (DBH, conventionally measured at 1.3 meters from the ground), which can be determined directly in the field by explicit visual inventories. This determination method is relatively easy to learn but remains subjective and prone to errors. Additional data can improve the model accuracy and in our specific case they corresponded to crown base height and width (in meter), percentage of crown missing, crown health, expressed as estimated percentage composed by dead branches and finally crown light exposure. All these data are essential for the modelling of parameters such as the leaf area (LA) and plant dry biomass (Hirabayashi et al., 2012). Instead, hourly meteorological and pollution data can be directly retrieved from the internal model database, and no external data can be employed in the model. Respectively only one station can be chosen for meteorological and pollution data. The removal of atmospheric pollutants such as O_3, SO_2, NO_2, CO and $PM_{2.5}$ is hourly modelled during no-precipitation periods throughout the year, through the evaluation of their deposition (Hirabayashi et al., 2012). To this aim, the pollutant flux (F; in $g/m^2 \times s$) is calculated as the product of the deposition velocity (V_d; in m/s) and pollutant concentration (C; in g/m^3). Deposition velocities are set to zero in the precipitation period (Nowak et al., 2006). For each pollutant considered, deposition velocities are calculated as the inverse of the sum of aerodynamic resistance (R_a), quasi-laminar boundary layer resistance (R_b), and canopy resistance (R_c). The aerodynamic resistance is independent of the air pollutant type, and it is calculated using meteorological data (wind speed and atmospheric stability), while the quasi-laminar and canopy resistance are calculated for each air pollutant (Pace et al., 2018). Each modelled pollutant flux is multiplied for the modelled leaf area (LA) to achieve the mass removed through dry deposition ($PM_{2.5}$) or stomatal uptake (gaseous pollutants) by the vegetation. For each pollutant, *I-Tree Eco* assumes constant V_d with no differentiation among species. Besides different values of LA, which are calculated from biometric data, all canopies are treated equally.

Additionally, the carbon impact is evaluated through the modelling of carbon storage and gross sequestration. Carbon storage describes the amount of carbon stored in the plant dry biomass via the photosynthetic activity, while carbon gross sequestration is the yearly rate of carbon removal from

the atmosphere (Martin et al., 2012). DBH values which are collected as field data and allometric equations are used by the model to calculate the above-ground dry biomass. The below-ground biomass is calculated through the application of a root/shoot ratio of 0.26, then summed together to evaluate the total plant dry biomass. In our specific case, and specifically for trees grown in urban areas, which tend to be shorter than the ones grown in closed canopies, the model also accounts an additional factor of 0.8 to reduce the modelled biomass (Nowak, 1994). Carbon sequestration is evaluated, thus considering a standard diameter growth of tree, which accounts the measured DBH, the crown light exposure, together with the number of frost days in the considered year, able to affect the plant growth rate (Nowak and Crane, 2002). In this research project, the open-source *i-Tree Eco model* (USDA Forest Service, 2019) is employed for the evaluation of the removal of atmospheric pollutants, either gaseous ones (tropospheric ozone O_3, nitrogen oxide NO_2 and sulfur oxide SO_2) or PM (specifically $PM_{2.5}$), together with the carbon impact of woody species located within a specific NbS in Dortmund city (GE).

2.4.2 The *Positive Matrix Factorization*

The Positive Matrix Factorization PMF (Paatero and Tapper, 1994) is a factor analysis technique, in which the fundamental problem is to resolve the identities or/and contributions of components in an unknown mixture (Reff et al., 2007), PMF has been used extensively for source apportionment of atmospheric particulate matter (PM), where the goal is to resolve the mixture of sources that contributes to PM samples. PMF is especially applicable for working with environmental data because it incorporates the variable uncertainties often associated with measurements of environmental samples. This model represents an evolution of previously used methods such as the principal component analysis (PCA). Chemical profiles and contributions of PM from primary sources, such as motor vehicles, residential and industrial fuel combustion, biomass burning, soil dust, and sea salt are typically identified by PMF analyses. Secondary sources, such as atmospheric oxidation of sulphate and nitrate and heterogeneous gas-to-particle conversion reactions on soil dust surfaces, have also been identified. Specifically, the mathematical model is:

$$X_{ij} = \sum_{K=1}^{p} g_{ik} f_{kj} + e_{ij} \quad (3)$$

where x_{ij} is the concentration of species j measured on sample i, p is the number of factors contributing to the samples, f_{kj} is the concentration of species j in factor profile k, g_{ik} is the relative contribution of factor k to sample i, and e_{ij} is error of the PMF model for the species j measured on sample i. In the literature, factors resolved by PMF are often interpreted as sources, although they are not necessarily synonymous. Recently, the graphical user interface-based U.S. Environmental Protection

Agency (EPA) - PMF program (Norris and Brown, 2014; Paatero 1999) has been developed to provide a user-friendly environment to solve PMF model. Initially, all the available species and ambient samples in a dataset are typically considered for source apportionment of PM with PMF, and then analyses are used to exclude specific species, samples, or individual measurements.

In this PhD project, PMF is applied to chemical data obtained by the characterization of PM_{10} membrane filters collected previously, during and after the Covid-19 lockdown. PM monitoring campaign was carried out at three sampling sites in the Rome area (Montelibretti, Sapienza and Saredo), in which 24-h PM_{10} samples were collected and chemically characterized. Final aim is to identify through the application of this model, the chemical profile of emission sources acting in the study area, to apportion mass contribution of sources to measured PM_{10}, before, during and after the lockdown. The lockdown condition of forced abatement of anthropogenic sources offered unique and relevant opportunities to quantify the reduction of the impact of anthropogenic sources of PM. To this aim, the considered chemical components are chosen depending on their ability to selectively trace PM_{10} emission sources, widely documented in previous studies (Sharma et al., 2016; Massimi et al., 2020).

PMF analysis is performed separately at each PM_{10} sampling site with the aim to evidencing possible site-related differences of source impact. The same chemical variables are employed for each PMF to make its outputs comparable among different computations on different sites. Missing data are automatically replaced by median values. Minimum detection limits (MDL) for each chemical compounds are set as mean plus 3 times the standard deviation (SD) of 10 replicate blank determinations, with data below MDL replaced with MDL/2. Uncertainties calculations were based on the approach by Polissar et al. 1998 for data below MDL, and by the equation-based method described by Norris and Brown, 2014 for data greater than MDL. For median-replaced data, uncertainties were calculated as four times the species median. The final input matrices for PMF at the three sites include 29 chemical variables and 94 (Sapienza and Montelibretti) or 75 (Via Saredo) PM_{10} daily samples.

References

Astolfi, M. L., Marconi, E., Protano, C., Vitali, M., Schiavi, E., Mastromarino, P., Canepari, S., 2018. Optimization and validation of a fast digestion method for the determination of major and trace elements in breast milk by ICP-MS, Analytical Chimica Acta, 1040, 49-62.

Astolfi, M. L., Protano, C., Marconi, E., Massimi, L., Brunori, M., Piamonti, D., Migliara, G., Vitali, M., Canepari, S., 2020. A new rapid treatment of human hair for elemental determination by inductively coupled mass spectrometry. Analytical Methods 12, 1906–1918.

Baldacchini, C., 2021. Report on benefits produced by implemented NBS, Deliverable No.4.5, proGIreg. Horizon 2020 Grant Agreement No 776528, European Commission, 146.

Bencharif-Madani, F., Ali-Khodja, H., Kemmouche, A., Terrouche, A., Lokorai, K., Naidja, L., Bouziane, M., 2019. Mass concentrations, seasonal variations, chemical compositions and element sources of PM10 at an urban site in Constantine, Northeast Algeria. J. Geochem. Explor. 206, 106356.

Cai, M., Xin, Z., Yu, X., 2017. Spatio-temporal variations in PM leaf deposition: A meta-analysis. Environ Pollut., 231(Pt 1), 207-218. doi: 10.1016/j.envpol.2017.07.105.

Canepari, S., Cardarelli, E., Giuliano, A., Strincone, M., 2006b. Determination of metals, metalloids and non-volatile ions in airborne particulate matter by a new two-step sequential leaching procedure Part B: Validation on equivalent real samples. Talanta 69, 588–595, doi:10.1016/j.talanta.2005.10.024.

Catrambone, M., Canepari, S., Cerasa, M., Sargolini, T., Perrino, C., 2019. Performance evaluation of a very-low-volume sampler for atmospheric particulate matter. Aerosol Air Qual. Res. https://doi.org/10.4209/aaqr.2019.04.0195.

Hirabayashi, S., Kroll, C. N., Nowak, D. J., 2012. Development of a distributed air pollutant dry deposition modeling framework. Environmental Pollution 171, 9–17.

Martin, N. A., Chappelka, A. H., Loewenstein, E. F., Keever, G. J., 2012. Comparison of carbon storage, carbon sequestration, and air pollution removal by protected and maintained urban forests in Alabama, USA, International Journal of Biodiversity Science, Ecosystem Services & Management 8 (3) 265-272, DOI: 10.1080/21513732.2012.712550

Merkus, H. G., 2009. Particle Size Measurements: Fundamentals, Practice, Quality; Springer Science + Business Media B.V..

Namgung, H.G., Kim, J.B., Woo, S.H., Park, S., Kim, M., Kim, M.S., Bae, G.N., Park, D., Kwon, S.B., 2016. Generation of nanoparticles from friction between railway brake disks and pads. Environ. Sci. Technol. 50, 3453–3461.

Nečas, D., Klapetek, P., 2012. Gwyddion: an open-source software for SPM data analysis. Open Phys 10, 181–188. https://doi.org/10.2478/s11534-011-0096-2.

Norris, G., Brown, S., 2014. EPA Positive Matrix Factorization (PMF) 5.0 Fundamentals and User Guide. EPA PMF 5.0 Manual.

Nowak, D.J., 1994. Atmospheric Carbon Dioxide Reduction by Chicago's urban forest. In Chicago's Urban Forest Ecosystem: Results of the Chicago Urban Forest Climate Project; McPherson, E.G., Nowak, D.J., Eds.; US Department of Agriculture, Forest Service, Northeastern Forest Experiment Station: Radnor, PA, USA, 83–94.

Nowak, D.J., Crane, D. E., 2002. Carbon storage and sequestration by urban trees in the USA. Environmental Pollution, 116(3):381–389. PII: S0269-7491(01)00214-7.

Ottele, M., van Bohemen, H. D., Fraaij, A. L. A., 2010. Quantifying the deposition of particulate matter on climber vegetation on living walls. Ecol. Eng., 36, 154-162. https://doi.org/10.1016/j.ecoleng.2009.02.007.

Paatero, P., 1999. The multilinear engine—a table-driven, least squares program for solving multilinear problems, including the n-way parallel factor analysis model. J. Comput. Graph. Stat. 8 (4), 854–888.

Perrino, C., Canepari, S., Pappalardo, S., Marconi, E., 2010. Time-resolved measurements of water-soluble ions and elements in atmospheric particulate matter for the characterization of local and long-range transport events. Chemosphere 80 (11), 1291–1300.

Polissar, A. V., Hopke, P. K., Paatero, P., Malm, W. C., Sisler, J. F., 1998. Atmospheric aerosol over Alaska: 2. Elemental composition and sources. J. Geophys. Res.-Atmos. 103 (D15), 19045–19057.

Ristorini, M., Astolfi, M.L., Frezzini, M.A., Canepari, S., Massimi, L., 2020. Evaluation of the Efficiency of Arundo donax L. Leaves as Biomonitors for Atmospheric Element Concentrations in an Urban and Industrial Area of Central Italy. Atmosphere, 11, 226. https://doi.org/10.3390/atmos11030226

Russo, A.; Escobedo, F.J.; Zerbe, S. Quantifying the local-scale ecosystem services provided by urban treed streetscapes in Bolzano, Italy. AIMS Environ. Sci. 2016, 3, 58–76.

Rusydi, A. F., 2018. Correlation between conductivity and total dissolved solid in various type of water: a review. IOP Conference Series: Earth Environmental Science 118, 012019

Saarikoski S., Timonen H., Saarnio K., Aurela M., Järvi L., Keronen P., Kerminen V.-M. and Hillamo R., 2008. Sources of organic carbon in □ne particulate matter in northern European urban air. Atmospheric Chemistry and Physic 8, 6281-6295.DOI: 10.5194/acp-8-6281-200

Schneider CA, Rasband WS, Eliceiri KW (2012) NIH Image to ImageJ: 25 years of image analysis. Nat Methods 9:671–675.

Sharma, S. K., Mandal, T. K., Jain, S., Sharma, A., Saxena, M., 2016. Source apportionment of PM 2.5 in Delhi, India using PMF model. Bull. Environ. Contam. Toxicol. 97 (2), 286–293

Shi, J., Zhang, G., An, H., Yin, W., Xia, X., 2008. Quantifying the particulate matter accumulation on leaf surfaces of urban plants in Beijing, China. Atmospheric Pollution Research, 8, 836-842. http://dx.doi.org/10.1016/j.apr.2017.01.011

Shimadzu Corporation, 2001. Total Organic Carbon Analyzer TOC-V User Manual, Analytical & Measuring, Instruments Division, Kyoto, Japan, 2001.

Simonetti, G., Frasca, D., Marcoccia, M., Farao, C., Canepari, S., 2018. Multi-elemental analysis of particulate matter samples collected by a particle-into-liquid sampler. Atmospheric Pollution Research 9 (4), 747–754.

Weiss, J., Weiss, T., 2005. Handbook of Ion Chromatography, Third, Completely Revised and Enlarged Edition. John Wiley and Sons, Inc. 931p. ISBN: 3-527-28701-9.

Williams, 2000. Non-Purgeable Organic Carbon (NPOC): Shimadzu TOC-5050A Total Organic Carbon Analyzer, Institute of Arctic and Alpine Research, University of Colorado, 2000.

Xu, X., Zhang, Z., Bao, L., Mo, L., Yu, X., Fan, D., Lun, X., 2017. Influence of Rainfall Duration and Intensity on Particulate Matter Removal from Plant Leaves. Science of the Total Environment, 609, 11−16.

Zhang, L., Zhang, Z., Chen, L., McNulty, S., 2019. An Investigation on the Leaf Accumulation-Removal Efficiency of Atmospheric Particulate Matter for Five Urban Plant Species under Different Rainfall Regimes. Atmospheric Environment 208, 123−132.

3. Analytical evaluation of PM leaf deposition

As previously described, due to the high complexity of the PM removal mechanism by deposition on leaf surfaces and the very high heterogeneity of atmospheric PM, to date it is still unclear which is the most efficient analytical procedure applicable to its evaluation and to the chemical and physical characterization of leaf deposited particles. This task results to be crucial for several reasons, which are certainly connected to the potential evaluation of the species-specific affinity towards this removal mechanism and the improvement of air quality. Being able to effectively characterize leaf deposed particles is also related to the identification of emission sources and the evaluation of their impact. This latter aspect, connected to the potential application of the evaluation of PM leaf deposition to biomonitoring purposes will be furtherly and deeply discussed in the following Chapter 4.

In the last few years, the scientific community have investigated this process, through the application of several techniques, regarding experiments in controlled environments, model applications and of course experimental approaches.

Vacuum filtration (VF) gravimetric procedure (Dzierzanowski et al., 2011) is one on the most used experimental approach applicable to this aim, thus being able to quantify the amount of leaf deposited particles. Through leaf washing and subsequent filtration of washing solutions by means of membrane filters with a decreasing porosity, VF allows the separation and consequent quantification of leaf deposited PM in different size fractions. Usually, VF does not involve the chemical characterization of leaf deposited particles and does not account of water-soluble particles that may be taken in solution. Moreover, and besides the deposited airborne particles also biological products may be taken in solution and be filtrated, thus potentially determining a misestimation of PM leaf deposition mechanism.

Recently also **Scanning Electron Microscopy coupled with Energy Dispersive X Rays Spectroscopy** (SEM/EDX) has been applied and tested to this aim. SEM/EDX leaf microanalysis proved its efficiency for the chemical/physical characterization of leaf deposited particles, thus being able to provide information on their number, size, morphology, and elemental composition. The combination of these chemical and physical data allows the quantification of the amount of leaf deposited PM in terms of mass per unit leaf area, in different size fractions.

In this PhD project, the efficiency of a **chemical fractionation** procedure for the characterization of both the water-soluble and the insoluble fraction of the elemental components of leaf deposited PM is evaluated (A1). The proposed analytical approach is based on a comprehensive chemical characterization of both VF materials, leaf washing solutions and membrane filters used for their

filtration, based on the integrated application of several analytical techniques (IC, TOC, UV-Vis spectrometer, ICP-MS and ICP-OES).

This procedure is applied on leaves collected in two urban areas of Italy (Naples and Terni), characterized by the presence of different and high-impact anthropogenic PM emission sources.

In Naples, holm oak (*Quercus ilex* L.) leaves were collected from seven sampling sites with different exposure to local PM emission sources, to test the chemical fractionation sensitivity to PM sources. In Terni, leaves were sampled from fifteen species, both trees and shrubs, in the same urban park and with the same exposition toward a well-known air pollution source, to test the suitability of the different tree species to remove atmospheric PM by means of leaf deposition. Ionic concentrations of leaf washing solutions have been compared to their electrical conductivity (EC), to identify a constant coefficient applicable to the quantification of water-soluble leaf deposited PM. Then, results obtained through the chemical fractionation are compared with those from gravimetric V/F and SEM/EDX analyses applied to the same leaf samples, to assess its efficiency and to highlight each technique limitations.

3.1 (A1) Innovative Characterization of Particulate Matter Deposited on Urban Vegetation Leaves through the Application of a Chemical Fractionation Procedure

International Journal of Environmental Research and Public Health (2020), Volume 17, Issue 16, doi: 10.3390/ijerph17165717

Martina Ristorini[1,2], Chiara Baldacchini[2,3,*], Lorenzo Massimi[4], Gregorio Sgrigna[2], Carlo Calfapietra[2]

[1] Department of Bioscience and Territory, Università del Molise, 86090 Pesche (IS), Italy
[2] Institute of Research on Terrestrial Ecosystems (IRET), National Research Council (CNR), 05010 Porano (TR), Italy
[3] Biophysics and Nanoscience Centre, Department of Ecological and Biological Sciences (DEB), Università degli Studi della Tuscia, 01100 Viterbo, Italy
[4] Department of Chemistry, Sapienza University of Rome, Piazzale Aldo Moro, 5, 00185 Roma, Italy
[*] Corresponding author: baldacchini@unitus.it; Tel.: +39-0761357027

Abstract: In this study, we have evaluated the efficiency of a chemical fractionation procedure for the characterization of both the water-soluble and the insoluble fraction of the main elemental components of particulate matter (PM) deposited on urban leaves. The proposed analytical approach is based on the chemical analysis of leaf washing solutions and membrane filters used for their filtration. The ionic concentration of leaf washing solutions was compared with their electrical conductivity, making it a valuable proxy for the quantification of the water-soluble and ionic fraction of leaf deposited PM. The chemical composition of both the water-soluble and the insoluble fraction of PM, resulting from this fractionation procedure, was compared with results obtained by scanning electron microscopy coupled with energy-dispersed X-Rays spectroscopy (SEM/EDX) and processed through chemometrics. Results obtained proved that the proposed approach is able to provide an estimation of total leaf deposited PM and it is highly reliable for the evaluation of the emission impact of different PM sources, being able to increase the selectivity of PM elemental components as specific source tracers; consequently providing useful information also for the assessment of human health risks.

Keywords: air quality; particulate matter; chemical fractionation; pollution source tracers; nature-based solutions

1. Introduction

Among the ecosystem services provided by urban vegetation, its potential to reduce air pollution has become one of the most important objects of investigation, being largely discussed in literature [1–3]. In urban and industrial areas, particulate matter (PM) pollution is considered one of the biggest concerns regarding human health and well-being, its exposure being correlated mainly to cardiovascular and respiratory disorders [4–6]. Airborne PM is a complex mixture of solid particles and liquid droplets characterized by different size, chemical composition, morphology and solubility [7]. Its emission is related both to natural and anthropogenic emission sources (such as vehicular traffic, industrial plants, domestic heating and biomass burning) [8] and

its effects on human health are strongly dependent on its size distribution, chemical composition and solubility [9–11]. Vegetation mitigates PM pollution, since particles can be trapped on leave surfaces through deposition mechanisms [1,12,13]. However, deposition of airborne particles on leaves is a complex and dynamic process, being influenced by numerous parameters. Leaf deposition efficiency depends on particles characteristics, such as their morphology and size [14], but also on species-specific leaf characteristics (such as leaf area, leaf morphology, density of stomata pores and thickness of wax layers) [15–18]. In addition, the density and the porosity of the tree crown, as well as meteorological conditions such as precipitations, wind speed and direction, result to be relevant in influencing the process [12,19,20]. The interaction between vegetation and airborne particles has been the object of a growing number of studies in the last years, which focused, among the rest, on the achievement of information on the chemical composition, solubility, size and morphology of leaf deposited particles. Indeed, these chemical and physical characteristics deserve particular interest due to their potential for the identification of emission sources and for the assessment of the risk exposure for human health [21–23]. The elemental composition and size distributions of leaf deposited airborne particles have been proved to be highly related with pollution source apportionment [24–28], and the use of leaves of urban trees as air passive filters for PM monitoring is emerging as a valid alternative to traditional air quality monitoring networks [29–31]. Indeed, urban trees are widespread, thus providing a high density of potential samplers, corresponding to a higher spatial resolution in PM monitoring with respect to standard air quality monitoring stations [32,33]; this aspect being important for the evaluation of PM emission sources and related human health risks. Moreover, the use of already present trees in the urban context as passive PM samplers results in a substantial reduction of the monitoring activity costs, nullifying those related to the purchase and maintenance of PM sampling instruments. However, to date it is still unclear which is the most efficient analytical procedure applicable to the chemical and physical characterization of leaf deposited particles. Standard spectroscopic techniques such as X-ray fluorescence spectroscopy (XRF), as well as magnetic biomonitoring techniques, such as saturation isothermal remanent magnetization (SIRM), have been largely applied for the detection of leaves elemental concentrations [34,35]. However, these techniques are based on the characterization of the whole leaves, thus making impossible to discriminate whether the detected elements are due to leaf deposited particles or to plant uptake from soil. A different approach has been proposed by Dzierzanowski et al. in 2011 [36]: vacuum filtration (V/F) gravimetric technique is based on leaf washing and subsequent filtration of the washing solution through membrane filters with a decreasing porosity. The weighting of the filters before and after the washing solution filtration allows to gravimetrically assess the amount of leaf deposited PM per unit leaf area into different size fractions, depending on the filter porosity. However, gravimetric V/F has two main limitations: it is not able to provide information on the PM chemical composition (which is essential for source apportionment) and it cannot take into account the soluble part of leaf deposited PM (which is likely dissolved into the washing solution). To date, scanning electron microscopy (SEM) analysis, implemented with energy-dispersed X-ray spectroscopy (EDX), results to be the analytical procedure able to provide the most complete characterization of leaf deposited particles. This technique provides information about the number, size and morphology of PM particles, in addition to information on

their elemental composition [27,31,37–39]. However, SEM/EDX is affected by a main limitation: long analysis time is required to obtain a statistically valid estimation of the PM characteristics per single sample, due to the spatial scale of the single data collected (hundreds of micron square of leaf area per image). In this study, a new approach to characterize inorganic leaf deposited PM particles with a diameter smaller than 10 μm (PM_{10}), which are able to penetrate the human respiratory system, is presented. It is based on the combination of the V/F technique with a chemical fractionation procedure. The V/F of the leaf washing solutions ensures that only material from the leaf surfaces is analysed. The chemical fractionation procedure, which is known to be effective in increasing the selectivity of elements as tracers of PM emission sources [40,41], will extract the PM elemental concentrations from both the insoluble and the soluble part of the washed material, being applied to both filters and washing solutions, respectively. The procedure has been tested on leaves collected in two urban areas of Italy (Naples and Terni), characterized by the presence of different and high-impact anthropogenic PM emission sources. In Naples, holm oak (*Quercus ilex* L.) leaves were collected from seven sampling sites with different exposure to local PM emission sources, to test the chemical fractionation sensitivity to PM sources. In Terni, leaves were sampled from twelve different tree species and four different shrubs species, in the same urban park and with the same exposition toward a well-known air pollution source, to test the suitability of the different tree species to be used as PM passive filters for monitoring purposes. Firstly, the ionic concentrations of leaf washing solutions have been compared to their electrical conductivity (EC), which is expected to be proportional to the total dissolved solid (TDS) in aqueous solutions [42,43]. Then, results obtained through chemical fractionation have been compared with those from gravimetric V/F and SEM/EDX analyses. Finally, the efficiency of the chemical fractionation procedure in increasing the selectivity of the elemental components of leaf deposited PM as specific source tracers was tested through the application of principal component analysis (PCA) applied to the water-soluble and insoluble elemental concentrations. The results obtained in this study prove the reliability of chemical fractionation in the characterization of inorganic leaf deposited PM, as obtained by the V/F procedure, and they represent a further validation for the utilization of leaves as low-cost PM passive filters. Nevertheless, an important warning arises from our results with respect to the choice of the tree species: unreliable data could be obtained from some tree species, likely due to the release of leaf biological material in the washing solutions.

2. Materials and Methods

2.1. Study Areas

Leaves were collected from two urban hot-spots in Italy, characterized by the presence of several PM emission sources, either natural or anthropogenic. The first set of leaves was collected from the urban forest "Real Bosco di Capodimonte" in Naples (Southern Italy). Naples is a densely populated city characterized by typical urban emission sources such as heavy load of vehicular traffic and domestic heating but also by major industrial plants within the urban area [44]. A second set of leaves was collected in Terni, an urban and industrial hot-spot of Central Italy [27,45–47]. In addition to typical PM urban emission sources, such as vehicular traffic

and domestic heating, Terni is characterized by the presence of a wide steel plant in the East of the city and an incinerator in the West [48]. The important presence of anthropogenic PM emission sources, in combination with the peculiar meteorological conditions of the city, located within an intramountain valley, determines the ideal conditions for increasing the accumulation of airborne particles and reducing their dispersion [49].

2.2. Leaf Sampling

In Naples, leaves of holm oak (*Quercus ilex* (L.)), were collected on February, 1st 2017, from seven different sampling sites (NA 1, NA 2, NA 3, NA 4, NA 5, NA 6, NA 7) within the "Real Bosco di Capodimonte" (see Figure 1a): NA 1 within the wood, NA 2 and NA 4 nearest to a high traffic street, NA 3 and NA 5 located between the wood and the meadow, and NA 6 and NA 7 between the wood and a brownfield. A more detailed description of the Naples sampling sites is reported in Baldacchini et al. 2019 [31]. In Terni, leaves were collected from twelve tree species (*Acer saccharinum* L., *Catalpa bignonioides* Walter, *Cedrus atlantica* (Endl.) Manetti ex Carrière, *Celtis australis* L., *Magnolia grandiflora* L., *Platanus acerifolia* (Aiton) Willd., *Populus nigra* L., *Populus tremula* L., *Prunus cerasifera* Ehrh., *Quercus pubescens* Willd., *Robinia pseudoacacia* L. and *Tilia cordata* Mill.), three shrubs species (*Laurus nobilis* L., *Laurus cerasus* L., *Nerium oleander* L.) and *Hedera helix* L., at high proximity from each other within the urban park "Le Grazie" (42° 3303.18" N, 12°3902.03" E) on June, 15th 2017. A more detailed description of the sampling site and sampled species is reported in Sgrigna et al. 2020 [18]. The leaves have been collected, both in Naples and Terni, more than 15 days after the last intense (i.e., precipitation rate higher than 10 mm h^{-1}) rain event.

Figure 1. (a) Location of the seven sampling sites within the urban forest "Real Bosco di Capodimonte" in Naples (Italy). (b) Location of the urban park "Le Grazie" in Terni (Italy), with respect to the main air pollution source (i.e., the steel plant).

Two replicate branches were collected per each sampled plant, both in Naples and in Terni. Sampling height was set at 6 m for trees and at 2 m for shrubs. In Terni, for *H. Helix* (L.), two replicate branches were collected at two different heights (these are reported as *H.e.* A, and *H.e.* B), comparable both to tree and shrub samples. In order to ensure homogeneity among the leaves sampled and avoid potential influence of their age (which could affect the time exposure to airborne PM pollution and the amount of particles deposited [50]), only the

youngest ones were selected in both locations, thus sampling the leaves at the top of the branches [18,31]. All the replicate branches were collected from the external part of the crown, at specific cardinal directions. In Naples, the cardinal direction was selected either toward the sea breeze from South West (sites NA 1, NA 4, NA 5, NA 7), or toward the land wind from North-West (sites NA 2, NA 3, NA 6) [31]. In Terni, all the species were sampled from the East-North-East part of the crown, towards the wind direction coming from the steel plant (see Figure 1b) [27], in order to select leaves under similar conditions, e.g., influenced by the same pollution source [18]. Leaves collected in both locations were preserved in paper bags to avoid external contamination and stored in freezer (−20 °C).

2.3. Vacuum Filtration

For the application of V/F procedure, between 300 and 700 cm^2 of total leaf area were selected from sampled branches; the number of leaves varied depending on the leaf dimensions. Leaves were washed in micro-filtered (0.2 µm) and deionized water (250 mL and 500 mL for Naples and Terni samples, respectively) inside a flask, and hand-shacked for 5 min. Since we are interested in study PM_{10} particles, washing solutions were first filtrated through a 100 µm porosity sieve, to remove the coarsest material. Through a vacuum filtration system, leaf washing solutions were consequently filtrated with cellulose filters able to remove particles with diameter larger than 10 µm (code 1250; smallest stopped particle size in the 10–13 µm range, Anoia S.A., Barcelona, Spain) and larger than 2 µm (code 1244; smallest stopped particle size in the 2–4 µm range, Anoia S.A.). As a consequence, particles with diameter between about 2.5 µm and 10 µm (i.e., $PM_{2.5\text{-}10}$) can be assumed to accumulate on this second filter. Then, washing solutions were filtered with a 0.2 µm porosity nitrocellulose filter (type CN, LVR > 7, Advanced Microdevices Pvt. Ltd., Ambala Cantt, India), where particles with a diameter ranging from 0.2 µm to about 2.5 µm (i.e., $PM_{0.2–2.5}$) are expected to accumulate. After filtration, the washing solutions were collected in falcon tubes and then processed with the chemical fractionation procedure. To obtain the gravimetric determination of PM loads, membrane filters were weighted before and after the filtration (R200D Research Analytical Balance, Sartorius, Gottingen, Germany), and the difference between the two values was assumed to be the mass of the accumulated PM. To equilibrate humidity levels, membrane filters were dried at 65 °C for 40 min in a moisture control oven (Griffin Company, Paoli, PA, USA) before and after the sequential filtration of washing solutions and kept for 30 min into the balance room before weighting. PM mass for each size class were then normalized by the cm^2 of total two-sided area of washed leaves (both abaxial and adaxial surfaces), measured through the optical scanning of the washed leaves and then using ImageJ open-source software [51]. This procedure allowed to obtain a quantification (in terms of mg cm^{-2}) of insoluble PM load per unit leaf area of $PM_{2.5–10}$ and $PM_{0.2–2.5}$ that, summed together, provide the total PM_{10} load per unit leaf area, as reported in Baldacchini et al. [31] and Sgrigna et al. [18]. The same filters used for the gravimetric determination of $PM_{2.5–10}$ and $PM_{0.2–2.5}$ loads were then processed with the chemical fractionation procedure.

2.4. Chemical Characterization of Washing Solutions

Leaf washing solutions were analysed by ionic chromatography (IC, ICS1000; Dionex Co., Sunnyvale, CA, USA) for the detection of Cl^-, F^-, NO_3^{2-}, PO_4^{3-} and SO_4^{2-} and by inductively coupled plasma mass spectrometry (ICP-MS, Bruker 820, Bremen, Germany) for the detection of the concentration of 35 elements (Al, As, B, Ba, Ca, Cd, Ce, Co, Cr, Cs, Cu, Fe, Ga, K, La, Li, Mg, Mn, Mo, Na, Nb, Ni, P, Pb, Rb, Sb, Si, Sn, Sr, Tl, Ti, U, V, W, Zn). The analytical and instrumental conditions used for IC and ICP-MS analysis were previously reported by Canepari et al. [40,41] and by Astolfi et. al. [52], respectively. In addition, ammonium (NH_4^+) was detected by UV-Visible spectrophotometer (50 Scan Varian, Santa Clara, CA United States), following the procedure indicated in the Ammonium-Test, Spectroquant (Merck, Darmstadt, Germany). The chemical characterization of leaf washing solutions was completed by the determination of the water-soluble organic carbon (WSOC), analysed by TOC-VSCH (Shimadzu, Kyoto, Japan) using the non-purgeable organic carbon (NPOC) procedure reported in Saarikoski et al. [50]. Firstly, the concentrations of anionic species such as Cl^-, F^-, NO_3^{2-}, PO_4^{3-} and SO_4^{2-}, obtained through IC, and cationic species such as Na^+, Ca^{2+}, K^+, Mg^{2+} and NH_4^+, obtained through ICP-MS and UV-Vis spectrophotometer, were used to evaluate the ionic balance of each washing solution. Specifically, the ionic balance was evaluated comparing the µmoles of cations (sum of Na^+, Ca^{2+}, K^+, Mg^{2+} and NH_4^+ µmoles) and the µmoles of anions (sum of Cl^-, F^-, NO_3^{2-}, PO_4^{3-} and SO_4^{2-} µmoles) for each washing solution, then averaged over the two replicates for each sampling site in Naples and each Terni species. Since CO_3^{2-} could not be detected through our analytical procedure, its concentration was estimated assuming the balance between µmoles of Ca^{2+} and µmoles of CO_3^{2-}. Total ionic concentration (∑ Ions in mg L^{-1}) was compared to the EC of leaf washing solutions, as obtained by a conductimeter equipped with standard 5070 platinum cell (Crison Basic 30, Crison Instruments, Barcelona, Spain), to verify if a linear relationship exists between them and to quantify the conversion coefficient. Indeed, EC of aqueous solutions is known to be proportional to the concentration of TDS, according to Equation (1), with the conversion coefficient K being dependent on the ion valency [43,53,54]:

$$TDS\ (mg\ L^{-1}) = constant + (K\ x\ EC\ (\mu S\ cm^{-1}) \quad (1)$$

All the concentrations detected in the washing solutions (ions and elements expressed in mg L^{-1}) were further multiplied by the volume of the leaf washing solutions, then normalized by the total two-sided washed leaf area measured for each replicate and averaged for each Naples sampling site and each species sampled in Terni, in order to obtain the concentration of water-soluble species per unit leaf area (mg cm^{-2}).

2.5. Chemical Characterization of Membrane Filters

For each replicate branch, the filters with accumulated $PM_{2.5–10}$ and $PM_{0.2–2.5}$ were transferred into polytetrafluoroethylene (PTFE) vessels, mixed with 2 mL HNO_3 (67%; Promochem, LGC Standards GmbH, Wesel, Germany), 1 mL HF (40%, Suprapur, Merck) and 3 mL HCl (puriss. p.a., Sigma-Aldrich, Co., St. Louis, MO, USA) and subsequently heated in microwave oven (Ethos Touch Control, Milestone, Sorisole, Italy) to 180 ◦C for 40 min, as in previously reported method [55]. The acid-digested solutions were then

diluted in 10 mL of deionized water. The concentrations of 15 elemental components (Al, Ba, Ca, Cr, Cu, Fe, K, Mg, Mn, Mo, Na, P, Si, Sr, Ti) were determined with inductively coupled plasma atomic emission spectroscopy (ICP-OES; VISTA-MPX, CCD Simultaneous, Varian) equipped with an inert introduction line. The instrumental conditions for ICP-OES analysis were described in a previous study in detail [55]. Elemental concentrations were normalized by the total two-sided washed leaf area measured per each replicate and then averaged over each Naples sampling site and each tree species sampled in Terni (shrubs and *Hedera helix* have not been processed at this stage). This procedure allowed us to obtain the elemental concentrations of the insoluble fraction of inorganic leaf deposited particles per leaf area unit (mg cm^{-2}) in two size classes: fine ($PM_{0.2–2.5}$) and coarse ($PM_{2.5–10}$) particles. Then, elemental concentrations per unit leaf area detected in both filters were summed to obtain the load of the inorganic insoluble fraction of leaf deposited PM (mg cm^{-2}) per each size class ($PM_{2.5}$, $PM_{2.5–10}$).

2.6. Scanning Electron Microscopy Analysis

Two leaves from each replicate branch of Naples samples were analysed by a scanning electron microscope (Phenom ProX, Phenom-World, Eindhoven, Netherlands) coupled with an X-ray analyser and equipped with a charge-reduction sample holder suited for biological samples. By combining SEM images of leaf surfaces and EDX spectra of leaf deposited particles, the elemental concentrations per unit leaf area in the PM particles observed and the total leaf PM load (both in mg cm^{-2}), per size fraction, have been obtained, as described in Baldacchini et al., in which results relative to SEM/EDX microanalysis of Naples samples were also reported [31].

2.7. Statistical Analysis

Pearson's coefficients were calculated to highlight statistically significant correlations between the results achieved through the different analytical procedures (chemical fractionation, V/F, SEM/EDX). PCAs were performed on Naples and Terni datasets, using as input variables water-soluble and insoluble elemental concentrations. Both Pearson's coefficients and PCA were obtained using Statistica v 8 (StatSoft Italia srl, Padua, Italy). Graphical outputs were produced by using OriginPro 8.6 (OriginLab, Northampton, MA, USA).

3. Results and Discussion

3.1. PM soluble Fraction: Chemical Characterization of Leaf Washing Solutions and Relationship with Electrical Conductivity

A good ionic balance is observed for soluble PM from Naples samples, since the µmoles of cations turn out to be balanced to the µmoles of anions detected through our analytical procedure, for each washing solution (Figure 2a). On the other hand, the evaluation of the ionic balance of washing solutions related to the species collected in Terni underlines a different behaviour (Figure 1b). Specifically, cations µmoles appear to be higher

than the corresponding anions μmoles for five of the twelve sampled tree species (namely, *Robinia pseudoacacia* L. (R. p.), *Tilia cordata* Mill. (T. c.), *Populus nigra* L. (P. n.), *Cedrus atlantica* ((Endl.) Manetti ex Carrière) (C. a.) and *Populus tremula* L. (P. t.)). This could indicate the presence of anionic species that cannot be detected through our analytical procedure, as it is further suggested by the high WSOC concentrations observed in the washing solutions characterized by the unbalance of ionic species. For instance, WSOC concentration as high as up to 0.59 ± 0.21 mg L^{-1} is measured for *Tilia cordata* L., while ionic balanced species such as *Platanus acerifolia* ((Aiton) Willd.) and *Magnolia grandifolia* L. present in their washing solutions WSOC concentrations as low as 0.010 ± 0.002 mg L^{-1} and 0.0100 ± 0.0005 mg L^{-1}, respectively. Since WSOC analysis does not provide any kind of information about the ionic charge of organic species, it makes impossible to use these concentrations in the evaluation of the ionic balance. However, the high concentrations of WSOC detected for *P. tremula*, *P. nigra*, *C. atlantica*, *T. cordata* and *R. pseudoacacia* could be related to the presence of biological matrices on the leaves. Indeed, when studied by SEM/EDX microanalysis, the leaf surfaces of *P. nigra*, *T. cordata* and *R. pseudoacacia* resulted to be characterized by high accumulation of organic matrices, such as honeydew produced as a response to parasitic infections. For these species, the presence of these organic matrices would be able to totally cover morphological leaves traits, making it impossible to characterize them [18].

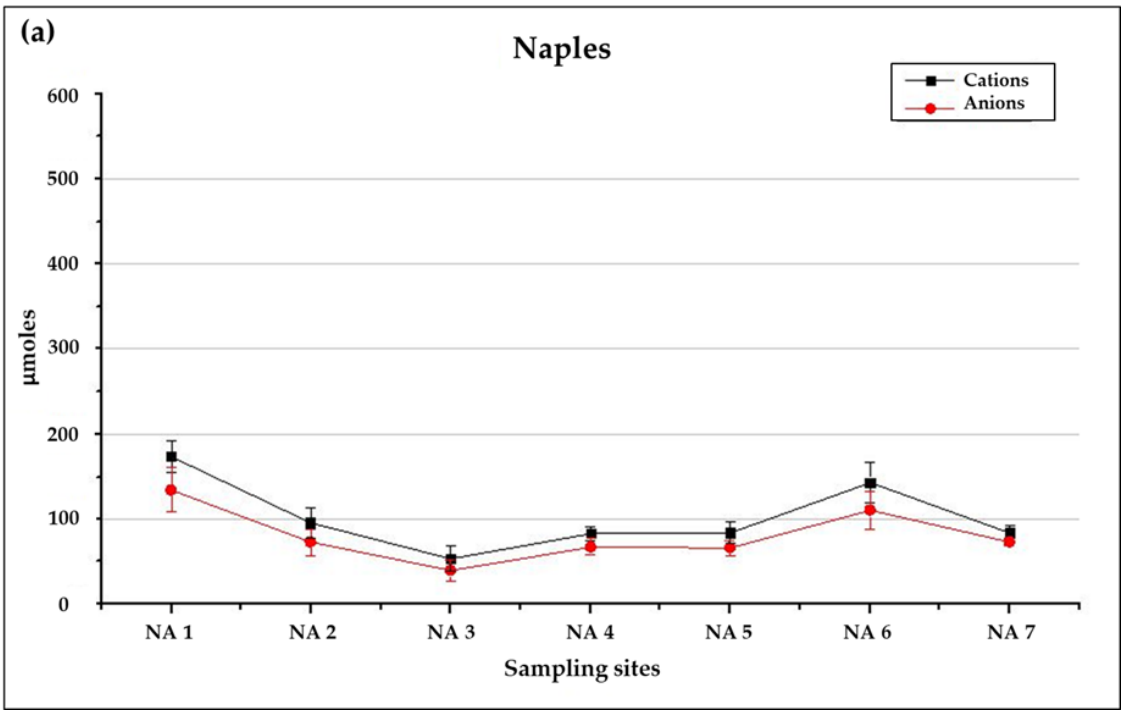

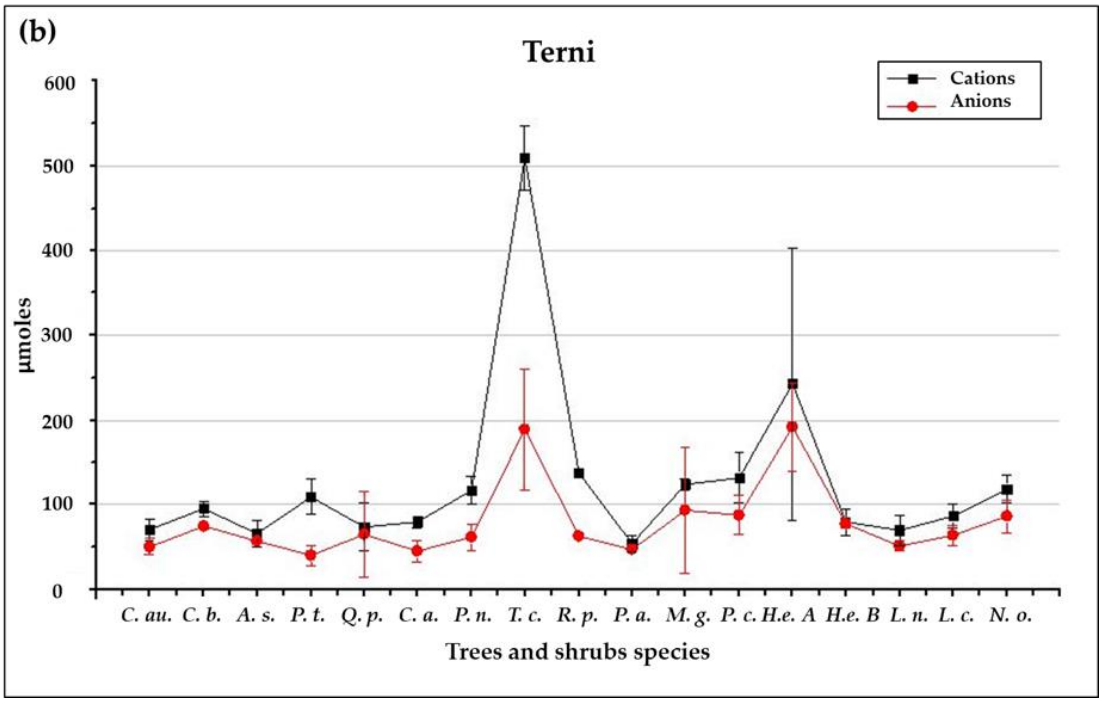

Figure 2. (a) Ionic balance of leaf washing solutions averaged over the two replicate branches of each sampling site in Naples; (b) Ionic balance of leaf washing solutions averaged over the two replicate branches of each tree and shrub species from Terni. Standard deviation between the two replicates are reported.

For *C. atlantica*, the only coniferous species analysed, we hypothesize that the high concentrations of WSOC and the ionic unbalance of its washing solutions may be related to the presence of resins. All these biological matrices may be partially taken in solution, thus affecting the composition of leaves washing solutions. The total ionic concentrations of washing solutions, ∑ Ions (in mg L^{-1}) obtained by ICP-MS, IC and UV-Vis spectrophotometer, are then compared with the corresponding EC (Figure 3). In Naples samples (Figure 3a), except for site NA 6, replicate branches showed a good repeatability, with low standard deviations, for both the EC and the ∑ Ions (standard deviations < 30%). A good linear correlation between the two parameters is obtained ($R^2 = 0.95$), with a conversion coefficient K = 0.64. In Terni samples (Figure 3b), a good repeatability between the two replicate branches is also obtained, both for EC and ∑ Ions results (with standard deviations between the two replicates < 30%). A linear correlation is still observed between ∑ Ions and EC results over the whole Terni dataset, but with a conversion coefficient much lower with respect to that obtained by the Naples dataset (K = 0.44; $R^2 = 0.96$; data not shown). However, by considering only the ionic balanced tree and shrubs species (i.e., *P. acerifolia*, *C. australis*, *C. bignoides*, *A. saccharinum*, *Q. pubescens*, *M. grandifolia*, *P. cerasifera*, *L. nobilis*, *L. cerasus*, *N. oleander* and *H. helix*), the conversion coefficient obtained is again K = 0.64 (as shown in Figure 3b) with a good linear correlation ($R^2 = 0.87$). This discrepancy could be likely due, again, to the presence of biological organic matrices on the leaves of some of the sampled species in Terni that, partially taken in solution, are able to affect not only their ionic balance but also EC measurements (Figure 2b). Indeed, a conversion coefficient of 0.44 has no counterpart in the literature, while 0.64 is already known as the conversion coefficient to be applied to EC values of aqueous solutions characterized by a prevalence of monovalent ions to obtain the corresponding TDS concentrations [43,53,54]. Our data analytically validate the

literature results and confirm the efficiency of this conversion coefficient for most of the species taken in account in this study, both holm oak from Naples and the eleven ionically balanced species from Terni. This suggests that EC measurements could be considered a fast and easy to apply way to quantify the soluble fraction of leaf deposited PM in washing solutions and this deserves particular interest when PM load quantification is performed gravimetrically through V/F, since this procedure cannot provide information on the soluble fraction otherwise. However, the estimation of the soluble PM fraction by EC measurements seems to be reliable only for those species which are not characterized by substantial presence of biological matrices, such as honeydew or resins, on their leaf surfaces. For instance, we have shown that this technique cannot be used with *P. tremula*, *P. nigra*, *C. atlantica*, *T. cordata* and *R. pseudoacacia.*

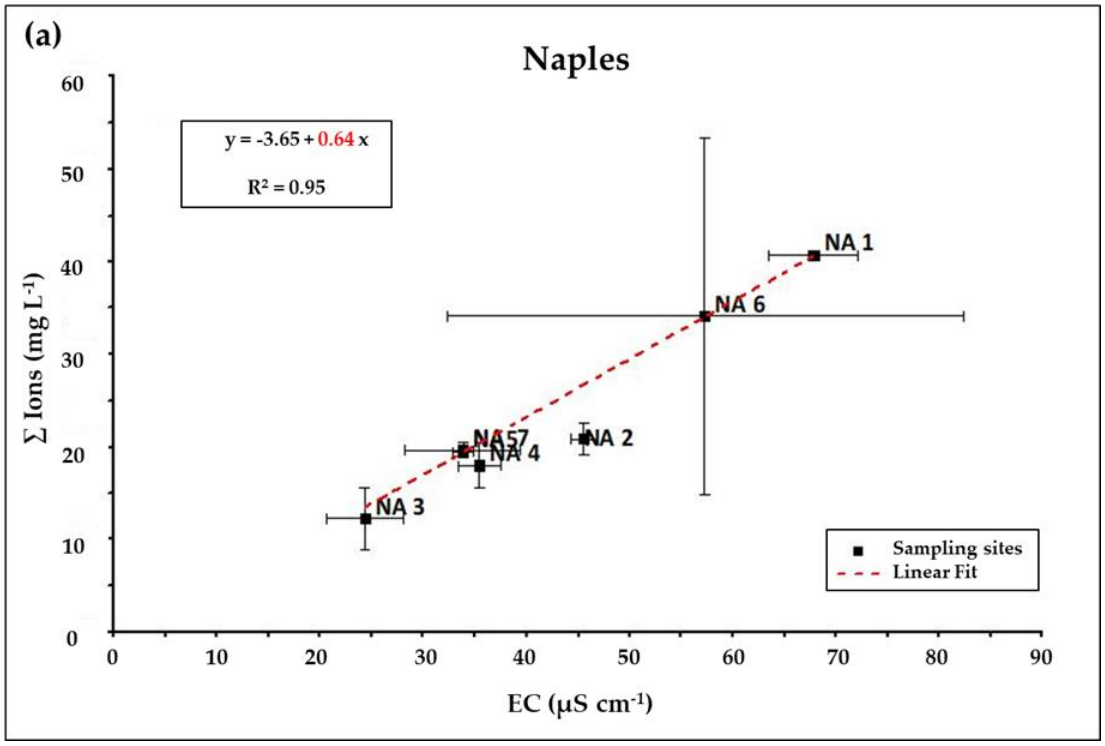

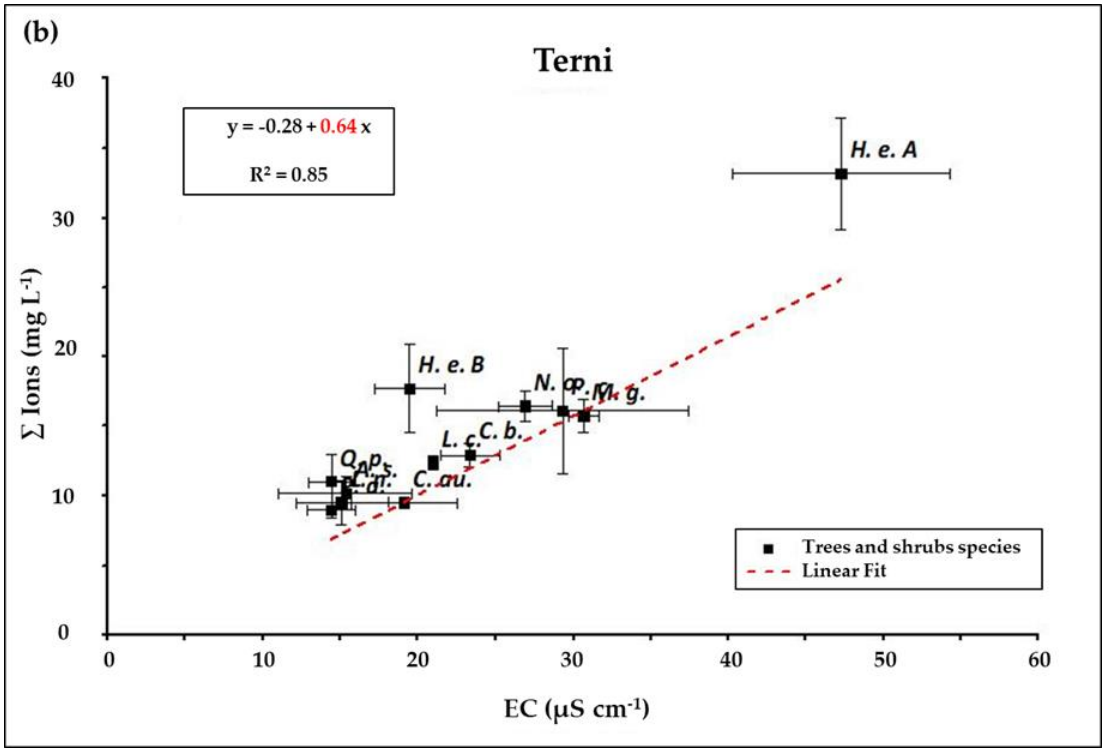

Figure 3. Relationship between ∑ Ions (mg L^{-1}) and electrical conductivity (EC) (µS cm^{-1}) of washing solutions from: (**a**) Q. ilex (L.) leaves sampled in seven sites within an urban forest in Naples; (**b**) leaves from selected tree and shrub species from an urban park in Terni. Values of ∑ Ions (mg L^{-1}) and EC (µS cm^{-1}) are obtained as averaged over two replicate branches. Standard deviations are shown. The linear regressions are obtained by considering only the samples characterized by ionic balanced washing solutions.

3.2. PM Insoluble Fraction: Chemical Characterization of Membrane Filters and Comparison with V/F Gravimetric Results

PM insoluble fraction concentrations per unit of leaf area (in mg cm^{-2}) obtained through the chemical characterization (ICP-OES) of the membrane filters are shown in Figure 3, compared with the gravimetric results obtained by the same filters. The quantification obtained by the chemical fractionation procedure of the insoluble fraction of PM is generally lower than that obtained gravimetrically, except for the case of the coarse PM particles deposited on the holm oak leaves collected in Naples (Figure 4b). This underestimation of the insoluble PM mass when detected through ICP-OES could be due to three main reasons: (a) the lack of information on the chemical speciation of PM elemental components [56–58]; (b) the presence of insoluble organic species that cannot be detected by ICP-OES, such as black carbon particles and polycyclic aromatic hydrocarbons (PAHs) emitted by anthropogenic emission sources like those deriving from combustive processes (e.g., vehicular traffic, domestic heating, biomass, combustion, industrial plants and incinerators) [59,60]; (c) the presence of organic insoluble matrixes of biological origin on the leaf surfaces. For Naples case study, where leaves were collected during the winter season, we could suggest that fine PM ($PM_{0.2–2.5}$) is partially composed by insoluble organic species deriving from domestic heating. These pollutants are known

to be mainly associated to airborne particles in the fine size class (especially ≤ 1 μm) [59,60] and, thus, it would have no (or very little) impact on the coarse particle fraction load, as observed.

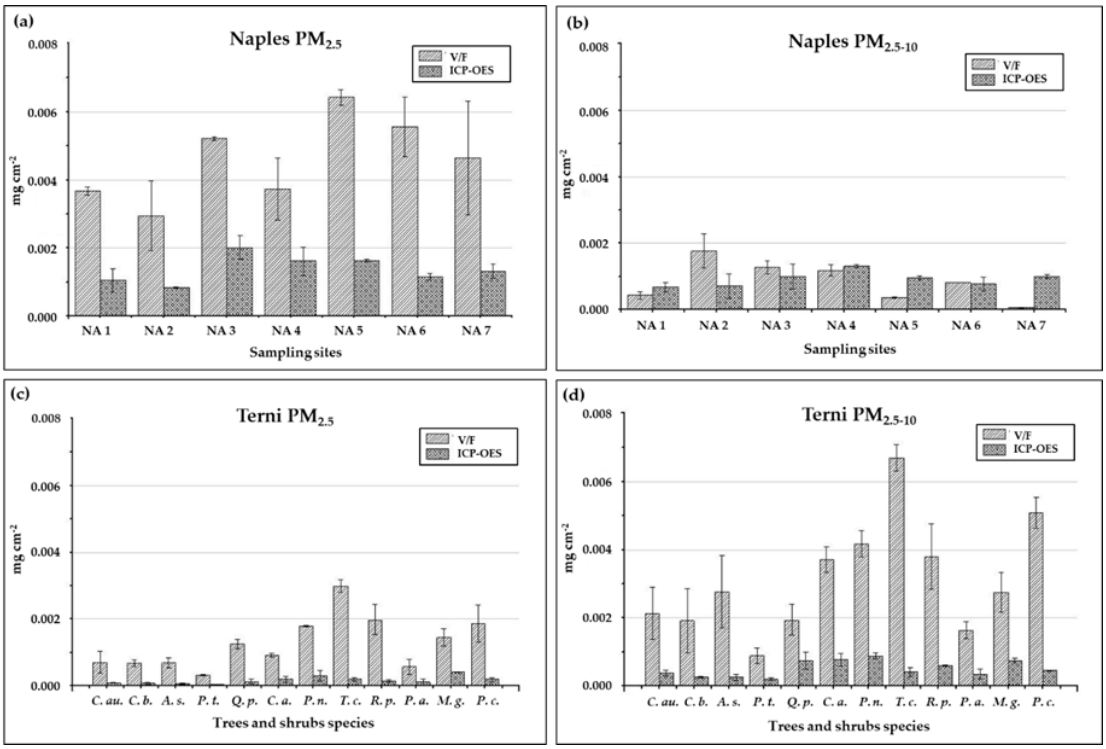

Figure 4. Load of insoluble fraction of leaf deposited particulate matter (PM) (mg cm^{-2}) detected gravimetrically (vacuum filtration, V/F) and through the chemical characterization (inductively coupled plasma - optical emission spectrometry, ICP-OES) of $PM_{2.5}$ (**a**,**c**) and $PM_{2.5-10}$ (**b**,**d**) membrane filters used to filter the washing solutions of the collected urban leaves. Int the different panels are reported data for PM2,5 (**a**) and $PM_{2.5-10}$ (**b**) from holm oak leaves collected in Naples and for $PM_{2.5}$ (**c**) and $PM_{2.5-10}$ (**d**) from different tree species collected in Terni. Tree species are: *Acer saccharinum* (A. c.), *Catalpa bignonioides* (C. p.), *Cedrus atlantica* (C. a.), *Celtis australis* (C. au.), *Magnolia grandiflora* (M. g.), *Platanus acerifolia* (P. a.), *Populus nigra* (P. n.), *Populus tremula* (P. t.), *Prunus cerasifera* (P. c.), *Quercus pubescens* (Q. p), *Robinia pseudoacacia* (R. p.) and *Tilia cordata* (T. c.)). Each bar represents the mean of N = 2 replicates ± standard deviations.

A similar effect is not expected (and, indeed, not observed) for Terni samples, since the sampling has been conducted during summer. However, the sampling site has been selected as strongly exposed to the air pollution coming from a steel factory, and an incinerator is also present close to the city. The high discrepancy observed in Terni dataset, at every size fraction and for each studied species, between the quantification obtained by the two techniques rather suggest that ICP-OES is intrinsically unable to quantitatively measure the insoluble PM characterizing Terni air pollution, likely due to a superimposition of the first two of the above-mentioned reasons. A minor contribution of biological matrixes to the gravimetric values can be also inferred, since four over the five species having gravimetric $PM_{2.5–10}$ load higher than 0.003 mg cm^{-2} are those previously described as showing no ionic balance in their washing solutions (*C. atlantica*, *P. nigra*, *T. cordata* and *R. pseudoacacia*).

3.3. Reliability of Chemical Fractionation Procedure for the Evaluation of PM Emission Sources

Principal Component Analyses (PCAs) based on correlations were performed by using the elemental concentrations per unit leaf area (mg cm^{-2}) as obtained by the chemical fractionation procedure. In order to prove the efficiency of the chemical fractionation procedure in increasing the selectivity of PM elemental components as specific source tracers, for each element, we considered only the concentrations of the solubility fraction (either water-soluble or insoluble one) in which it has its relative highest concentration. Indeed, these fractions correspond to those in which the elemental components are more likely to be emitted by PM sources. Moreover, the elemental concentrations in the selected fractions are also those showing the highest variability between the different samples, per each element. For the insoluble fraction, the concentrations obtained by merging both size fractions ($PM_{2.5}$ and $PM_{2.5–10}$) are considered, thus corresponding to total PM_{10}. The factor coordinates and scores obtained by the PCA for Naples data are reported in Figure 5, where the first two principal components (PCs) are shown. As input variables, the concentration per unit leaf area of the water-soluble fraction of Ca, Mg, Na and Cl together with the ones of the insoluble fraction of Cr, Cu, Fe, Si and Ti are used. The eigenvalues of the two first PCs are at 55.06% and 31.09%, respectively, representing the 86.15% of the total variance. PC1 discriminates sampling sites characterized by high concentration of Mg, Si and Ti in their insoluble fraction (namely, NA 3 and, to a minor extent, NA 6 and NA 7), from those characterized by the presence of Ca, Mg, Na and Cl in the PM soluble fraction (NA 1 and NA 5). PC2 discriminates the sites characterized by high concentrations of Cr, Cu and Fe in the insoluble fraction (NA 2 and NA 4). The clustering of NA 1 and NA 5, discriminated by water-soluble concentrations of Ca, Cl, Mg and Na, which are known elemental components of marine salts, confirms the impact of the South-West marine breeze at these sites. On the other hand, the clustering of NA 2 and NA 4 underlines the emission impact of vehicular traffic at the sites located at high proximity to a trafficked street. Indeed, Cr, Cu and Fe are known to be related to vehicular traffic mechanical-abrasive emission processes, being component of brakes, tire dust and vehicle components [49,61,62]. Leaves collected from NA 2 seemed also to be affected by the South-West marine breeze with relative higher concentrations of marine salts components. Finally, the relative high concentration of Mg, Si and Ti in the insoluble fraction shown by NA 3, together with NA 6 and NA 7, could underline the role of soil resuspension, being these elements often associated to soil compounds. Therefore, the utilization of holm oak leaves, sampled from seven different sampling sites, with different exposure, resulted effective in the identification of the main emission sources acting in this area. In fact, leaves collected from each site, were characterized by distinctive concentrations of those elements, which are known to be tracers for specific emission sources (both natural and anthropogenic). These results prove the efficiency of the chemical fractionation procedure for increasing the selectivity of inorganic PM elemental components as specific source tracers and the utilization of holm oak leaves as efficient passive filters for PM monitoring. Most interestingly, the site clustering obtained by the chemical fractionation data recalls the one previously obtained for the same sampling sites by analysing the holm oak leaves by SEM/EDX data [31]. The factor coordinates and scores obtained by the PCA for Terni tree data are reported in Figure 6, where the first two PCs are shown. As input

variables, the concentrations per unit leaf area of the water-soluble fraction of Ba, Cd, Cs, Mo, Rb, NO_3^{2-}, SO_4^{2-}, PO_4^{3-} and of the insoluble fraction of Cr, Cu, Fe, Ni and Zn, are used. The eigenvalues of the first two PCs are at 40.93% and 20.63%, respectively, representing the 61.56% of the total variance. Based on the factor coordinates (Figure 6a), clear correlations exist among elemental concentrations per unit leaf area, such as: water-soluble Cd and insoluble Ni (positive PC1 values); water-soluble Ba, Cs, Rb, SO_4^{2-} and PO_4^{3-} (negative PC1 values); water-soluble Mo, insoluble Fe and Cr together with NO_3^{2-} (positive PC2 values); insoluble Cu and Zn (negative PC2 values). These elemental clusters can be considered as representative of the different PM emission sources present in Terni: water-soluble Mo and insoluble concentrations of Cr, Fe and Ni, were associated to the emission impact of the steel plant [46,49], since these elements are used as chemical components in the stainless-steel production to increase its ductility, strength and toughness [63]; water-soluble Cs and Rb and ionic species such as $SO_4^{2-}$and PO_4^{3-}could be related to the influence of biomass burning [47,64]; and finally, insoluble Cu and Zn are known to be elemental tracers related to the impact of mechanical and abrasive processes connected to vehicular traffic, being component of brakes and other vehicle parts [65–67]. However, the identification of the main emission sources is only slightly reflected in the case discrimination (Figure 6b): most of the tree species (eight over twelve) are clustered together in the positive PC1 region, without differentiation in PC2.

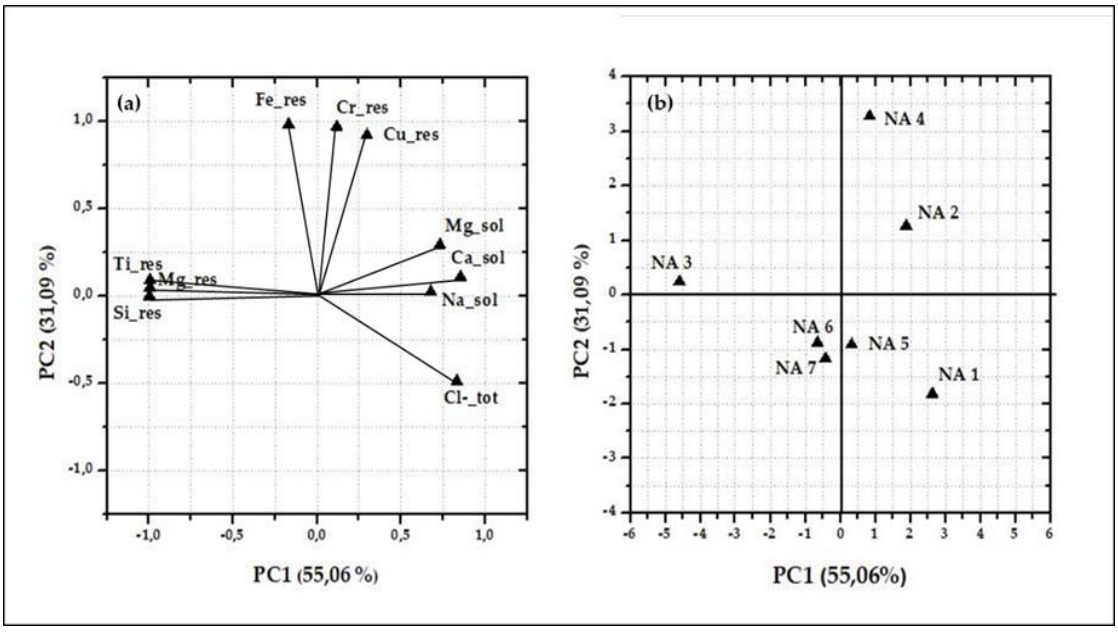

Fig. 5. Biplots of the factor coordinates (a) and of factor scores (b) of the first PCs obtained by correlation PCA of the concentrations per unit leaf area in the water-soluble fraction of Ca, Mg, Na, Cl and in the insoluble fraction of Cr, Cu, Fe, Mg, Si and Ti, detected at the seven sampling sites within the urban forest in Naples.

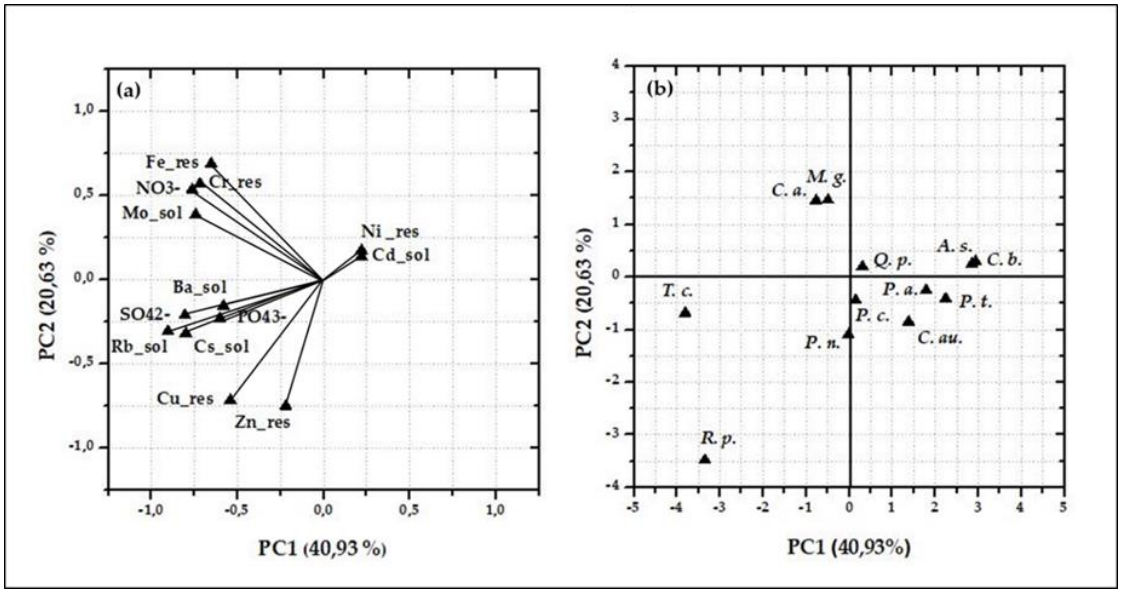

Fig. 6. Biplots of the factor coordinates (**a**) and of factor scores (**b**) of the first PCs obtained by correlation PCA of the concentrations per unit leaf area in the water-soluble fraction of Ba, Cd, Cs, Mo, Rb, NO_3^{2-}, SO_4^{2-}, PO_4^{3-} and in the insoluble fraction of Cr, Cu, Fe, Ni and Zn, as obtained by the twelve tree species sampled in the urban park in Terni, *Acer saccharinum* (*A. c.*), *Catalpa bignonioides* (*C. p.*), *Cedrus atlantica* (*C. a.*), *Celtis australis* (*C. au.*), *Magnolia grandiflora* (*M. g.*), *Platanus acerifolia* (*P. a.*), *Populus nigra* (*P. n.*), *Populus tremula* (*P. t.*), *Prunus cerasifera* (*P. c.*), *Quercus pubescens* (*Q. p*), *Robinia pseudoacacia* (*R. p.*) and *Tilia cordata* (*T. c.*).

This is not surprising, since trees were sampled in the same park and with the same orientation with respect to the main PM source (i.e., the Terni steel factory). However, four species show peculiar PM elemental compositions and are, thus, discriminated: T. cordata (negative PC1), *C. atlantica* and *M. grandifolia* (positive PC2), and *R. pseudoacacia* (negative PC2). Interestingly, three of them (*T. cordata*, *C. atlantica* and *R. pseudoacacia*) are among those characterized by ionically unbalanced washing
solutions, likely due to the accumulation of biological and organic matrices on their leaf surfaces. *T. cordata* leaves are characterized by the highest concentrations of elemental source tracers known to be connected to the emission of biomass burning (i.e., water-soluble Cs and Rb and ionic species such as SO_4^{2-} and PO_4^{3-}). As described previously, this specific emission sources are known to be associated mainly to airborne particles in the fine fraction [59,60]. High accumulation of fine particles on the leaves of *T. cordata* has been previously reported by SEM/EDX microanalysis results [18] and this could be due to the increased PM retention capacity of its leaves because of the presence of honeydew. The leaves of *C. atlantica* and *M. grandiflora* show a relatively high affinity for the emission of the steel plant metals (i.e., insoluble Fe and Cr together with NO_3^{2-} and water-soluble Mo). Both were reported to have high afnity with fine PM [18], likely due to the presence of resins (*C. atlantica*) and trichomes (*M. grandiflora*) on their leaves. *R. pseudoacacia* leaves were mainly characterized by high concentrations of elements associated to the emission of abrasive and mechanical traffic-related emissions, known to be associated to particles in the coarse fraction [65–67]. In Sgrigna et al. *R. pseudoacacia* leaves resulted to be characterized by rough surfaces with deep grooves larger than 1 μm that may be connected to the higher retention of coarse particles [18]. Thus, the PCA performed on Terni tree data

proved again the chemical fractionation efficiency for the individuation of the elemental source tracers of the main anthropogenic PM emission sources acting in the area and also indicated that, despite the twelve tree species leaves were sampled in the same location, some of them show selective affinity for specific PM elemental component. This may be due to the different interaction of particles with peculiar chemical and physical characteristics and the tree leaf species-specific traits, which is an interesting aspect which still deserve further investigations [18].

3.4. Total PM Loads and Single Element Concentrations Per Unit Leaf Area: Comparison between Chemical Fractionation and Scanning Electron Microanalysis

The total inorganic PM_{10} loads of the holm oak leaves collected at the Naples sampling sites have been estimated by summing together the total soluble and insoluble fraction loads obtained by the chemical fractionation and they are shown in Figure 7.

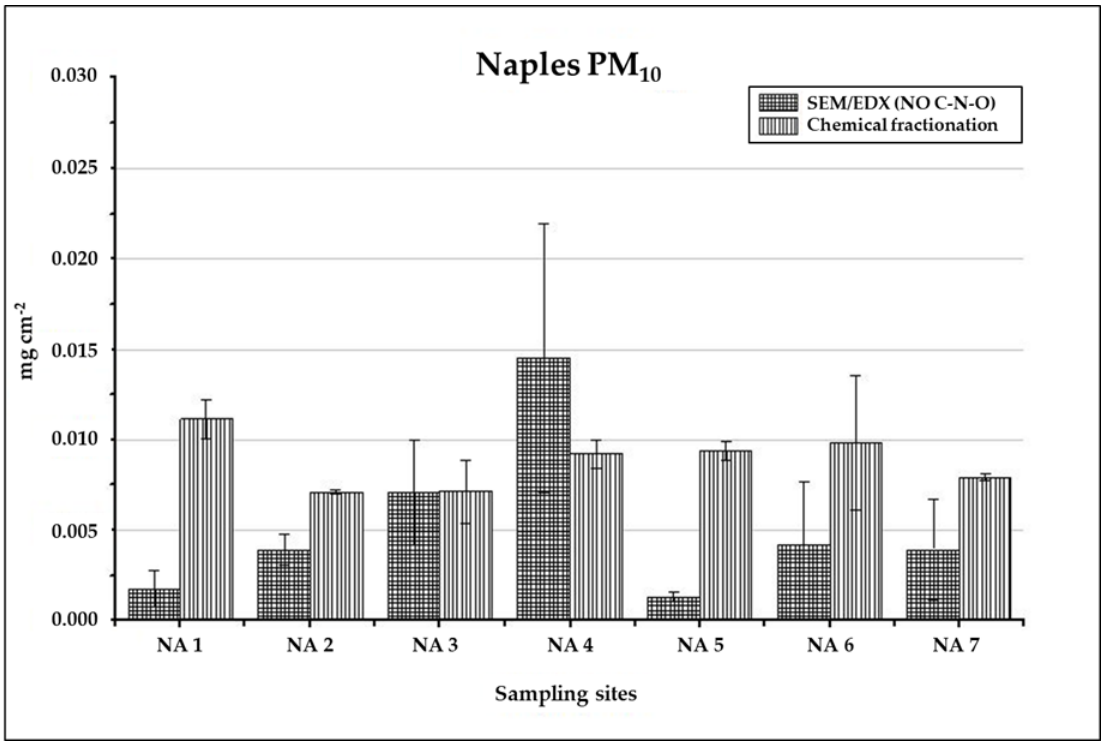

Fig. 7. Comparison between total PM load (mg cm^{-2}) detected through the chemical fractionation procedure (Soluble + Insoluble fraction) and through SEM/EDX, in Naples samples. Each bar represents the mean of N=2 replicates ± standard deviations.

WSOC has been excluded by the total PM_{10} load estimation, since it is impossible to discriminate biological soluble organic species produced by the plant from organic species related to leaf deposited PM. The PM_{10} loads obtained by analysing leaves collected at the same sampling sites by SEM/EDX are also reported in Figure 7, for comparison. For the same reason as above, the relative percentages of C, N and O have been excluded by the calculation of PM_{10} loads also in this case [31]. Most interestingly, the PM_{10} loads obtained

by the two techniques are in the same order of magnitude at every site, thus confirming the reliability of our fractionation procedure in estimating PM load. Differences in the total PM_{10} load determination among the two techniques are obtained at sites NA 1 and NA 5, where the SEM/EDX PM loads are significantly lower not only in comparison to the corresponding chemical fractionation ones but also to all the SEM/EDX loads obtained at the other sites. As shown previously, sites NA 1 and NA 5 are windward with respect to the marine breeze and are characterized by high levels of Na and Cl and low Fe concentration, this could lead to an underestimation of PM load by SEM/EDX, as previously discussed [31]. Moreover, a general underestimation of fine particles ($PM_{2.5}$) is expected from SEM/EDX, due to the limitation of imaging resolution. This is further suggested by the comparison of concentrations of single elemental components: while significant correlations are obtained between the elemental concentration of Fe ($\rho = 0.91$) and Si ($\rho = 0.78$) in the insoluble fraction of coarse PM ($PM_{2.5–10}$) and in the SEM/EDX data, no significant correlations (Pearson's $\rho < 0.75$) are found when SEM/EDX results are compared with the elemental concentrations of Al, Cr, Cu, Fe, Si and Ti in the insoluble fine fraction ($PM_{2.5}$). However, as previously said, the $PM_{2.5–10}$ size class is the one which mainly drive the total PM_{10} amount. Indeed, a significant correlation ($\rho = 0.87$) is still obtained when comparing the PM_{10} Fe concentration per unit leaf area obtained by the chemical fractionation with that from SEM/EDX (Figure 8): despite the concentrations detected through the chemical fractionation are an order of magnitude lower than the ones by

SEM/EDX, an analogous behaviour of the Fe concentration as a function of the sampling site is obtained. The only exception is NA 5 site, for which an underestimation of the Fe content by SEM/EDX can be thus suggested.

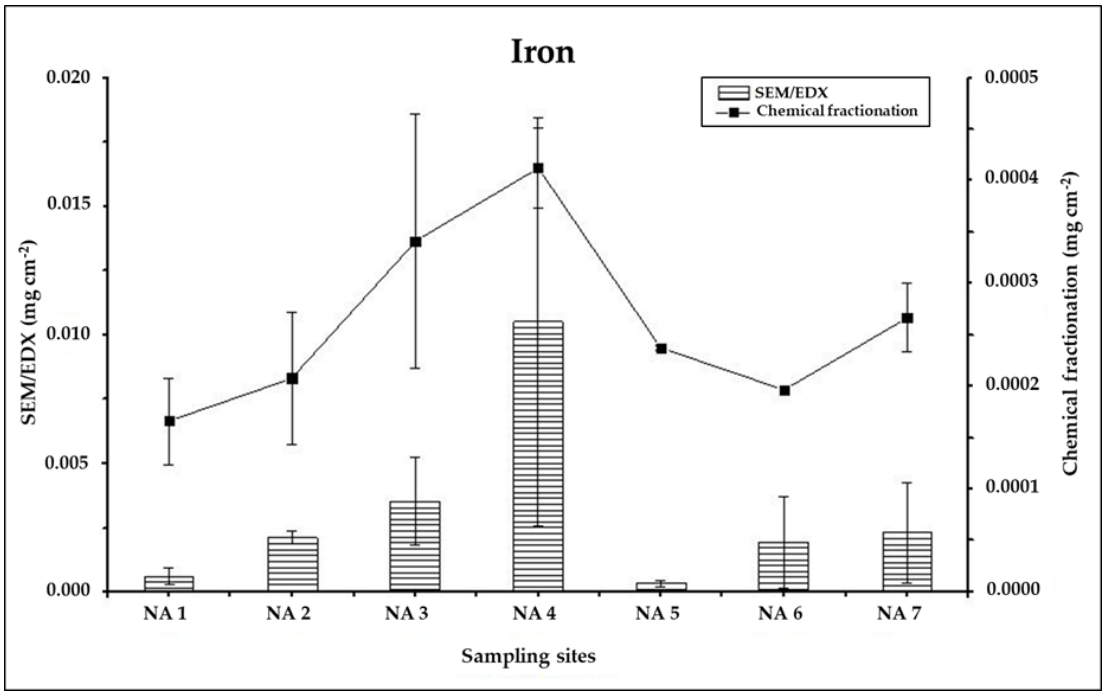

Fig. 8. Comparison between total PM load (mg cm^{-2}) detected through the chemical fractionation procedure (Soluble + Insoluble fraction) and through SEM/EDX, in Naples samples. Each bar represents the mean of N=2 replicates ± standard deviations.

4. Conclusions

This study focused on the potential of chemical fractionation procedure in the characterization of inorganic leaf deposited PM, when investigating both its water-soluble and insoluble fraction, as obtained by leaf V/F procedure. The study was composed by two sub-studies mainly aimed at evaluate the sensitivity of the proposed procedure to different PM sources (Naples data from holm oak leaves sampled at seven different sites) and the suitability of different plant species to be used as passive filters for PM monitoring (Terni data from twelve tree and four shrub species, from the same site). From the Naples campaign, we have shown that: the PM water-soluble fraction quantification obtained by the chemical fractionation procedure is proportional to the washing solution EC (K = 0.64); the quantification of the insoluble fraction of PM (by ICP-OES) is consistent with the gravimetric results for the coarse particle fractions; by summing the two fractions, PM_{10} loads consistent with those previously determined by SEM/EDX for the same sites can be obtained. Moreover, by using single elemental concentrations from both the water-soluble and insoluble fraction as input variable of a multivariate analysis, the efficiency of this analytical approach to increase the selectivity of elements as specific source tracers has been proved. From the Terni campaign, we have obtained that: for eleven over the sixteen tested species, the PM water-soluble fraction quantification obtained by the chemical fractionation procedure is still proportional to the washing solution EC, with the same conversion coefficient as above; the chemical characterization of the insoluble fraction of PM is not reliable, since it appears to be highly dependent on the amounts of organic compounds in the PM itself. Nevertheless, the single elemental concentrations as obtained by the chemical fractionation of both the water-soluble and insoluble fraction of leaf deposited PM appear to be efficient source tracers also in the case of Terni. Interestingly, some species emerge as not suitable to be used as passive filters for PM monitoring (i.e., *P. tremula*, *P. nigra*, *C. atlantica*, *T. cordata*, *R. pseudoacacia* and, to a minor extent, *M. grandiflora*), likely due to the presence of biological and organic matrices (such as honeydew and resins), as well as peculiar surface traits, on their leaves. However, these characteristics seems to increase, at the same time, their PM capturing capability. Thus, the total of our results confirms the potential of leaves as a low-cost alternative for monitoring PM pollution, suggests that EC of leaf washing solutions is a fast and easy to apply technique to estimate the water-soluble PM content, and that the proposed chemical fractionation procedure is a reliable, analytical tool to study leaf deposited PM in connection with potential sources. The main limitations of the proposed approach reside in its inability in detecting organic compounds (which may be important in the insoluble PM fraction) and in its dependency on the tree species; both deserving the need of further investigations. In particular, the interactions between airborne particles with specific chemical-physical characters and leaves with species-specific surface properties could deserve interest to develop future air pollutant-specific nature-based solutions, in which the planted tree species will be choose as a function of the affinity they have with the most abundant air pollutants and emission sources acting in the area.

Author Contributions: Conceptualization, C.B.; methodology, M.R. and C.B.; formal analysis, M.R., C.B. and L.M.; investigation, M.R., L. M. and G.S.; resources, C.B. and G.S.; writing—original draft preparation, M.R.; writing—review and editing, M.R., C.B., G.S., L.M. and C.C.; visualization, M.R. and C.B.; supervision, C.C.; project administration, C.C.; funding acquisition, C.C. All authors have read and agreed to the published version of the manuscript.

Funding: This work has been partially funded by the following projects: "ICOS"—Integrated carbon observation system, and "EUFORICC"—Establishing Urban Forest based solutions In Changing Cities (Prin 2017ERRN2S: "Projects of National Interest"), both founded by the Italian Ministry of Education, University and Research (MIUR).

Acknowledgments: The authors thank Alessandro Feliziani and Maria Grazia Agrimi from University of Tuscia for preliminary EC measurements, and Salvatore Cannistraro and Anna Rita Bizzarri from University of Tuscia for providing the conductimeter.

Conflicts of Interest: The authors declare no conflict of interest. The funders had no role in the design of the study; in the collection, analyses, or interpretation of data; in the writing of the manuscript, or in the decision to publish the results

References

1. Nowak, D.J.; Crane, D.E.; Stevens, J.C. Air pollution removal by urban trees and shrubs in the United States. Urban For. Urban Green. 2006, 4, 115–123. [CrossRef]

2. Escobedo, F.J.; Nowak, D.J. Spatial heterogeneity and air pollution removal by an urban forest. Landsc. Urban Plan. 2009, 90, 102–110. [CrossRef]

3. Nowak, D.J.; Hirabayashi, S.; Bodine, A.; Greenfield, E. Tree and forest effects on air quality and human health in the United States. Environ. Pollut. 2014, 193, 119–129. [CrossRef]

4. Davidson, C.I.; Phalen, R.F.; Solomon, P.A. Airborne Particulate Matter and Human Health: A Review. Aerosol Sci. Tech. 2005, 39, 737–749. [CrossRef]

5. Anderson, J.O.; Thundiyil, J.G.; Stolbach, A. Clearing the Air: A Review of the Effects of Particulate Matter Air Pollution on Human Health. J. Med. Toxicol. 2012, 8, 166–175. [CrossRef]

6. Kim, K.H.; Kabir, E.; Kabir, S. A review on the human health impact of airborne particulate matter. Environ. Int. 2015, 74, 136–143. [CrossRef] [PubMed]

7. Pope, C.A., III; Burnett, R.T.; Thun, M.J.; Calle, E.E.; Krewski, D.; Ito, K.; Thurston, G.D. Lung cancer, cardiopulmonary mortality, and long-term exposure to fine particulate air pollution. JAMA 2002, 287, 1132–1141. [CrossRef] [PubMed]

8. El-Fadel, M.; Massoud, M. Particulate matter in urban areas: Health-based economic assessment. Sci. Total Environ. 2000, 257, 133–146. [CrossRef]

9. Roemer, W.; Hoek, G.; Brunekreef, B.; Clench-Aas, J.; Forsberg, B.; Pekkanen, J.; Schultz, A. PM10 elemental composition and acute respiratory health effects in European children (PEACE project). Eur. Respir. J. 2000, 15, 553–559. [CrossRef]

10. Englert, N. Fine particles and human health—A review of epidemiological studies. Toxicol. Lett. 2004, 149, 235–242. [CrossRef]

11. Valavanidis, A.; Fiotakis, K.; Vlachogianni, T. Airborne Particulate Matter and Human Health: Toxicological Assessment and Importance of Size and Composition of Particles for Oxidative Damage and Carcinogenic Mechanisms. J. Environ. Sci. Health 2008, 26, 339–362. [CrossRef] [PubMed]

12. Janhall, S. Review on urban vegetation and particle air pollution e Deposition and dispersion. Atmos. Environ. 2015, 105, 130–137. [CrossRef]

13. Tong, Z.; Baldauf, R.W.; Isakov, V.; Deshmukh, P.; Zhang, K.M. Roadside vegetation barrier designs to mitigate near-road air pollution impacts. Sci. Total Environ. 2016, 541, 920–927. [CrossRef] [PubMed]

14. Petroff, A.; Mailliat, A.; Amielh, M.; Anselmet, F. Aerosol dry deposition on vegetative canopies. Part I: Review of present knowledge. Atmos. Environ. 2008, 42, 3625–3653. [CrossRef]

15. Rasanen, J.V.; Holopainen, T.; Joutsensaari, J.; Ndam, C.; Pasanen, P.; Rinnan, Å.; Kivimaenpaa, M. Effects of species-specific leaf characteristics and reduced water availability on fine particle capture efficiency of trees. Environ. Pollut. 2013, 183, 64–70. [CrossRef]

16. Wang, L.; Gong, H.; Liao, W.; Wang, Z. Accumulation of particles on the surface of leaves during leaf expansion. Sci. Total Environ. 2015, 532, 420–434. [CrossRef]

17. Chen, L.; Liu, C.; Zou, R.; Yang, M.; Zhang, Z. Experimental examination of effectiveness of vegetation as bio-filter of particulate matters in the urban environment. Environ. Pollut. 2016, 208, 198–208. [CrossRef]

18. Sgrigna, G.; Baldacchini, C.; Dreveck, S.; Cheng, Z.; Calfapietra, C. Relationships among PM capture efficiency and leaf micro-macromorphological characteristics in twelve tree species from an Italian urban-industrial environment. Sci. Total Environ. 2020. [CrossRef]

19. Litschke, T.; Kuttler, W. On the reduction of urban particle concentration by vegetation a review. Meteorol. Z. 2008, 17, 229–240. [CrossRef]

20. Rodríguez-Germade, I.; Mohamed, K.J.; Rey, D.; Rubio, B.; García, A. The influence of weather and climate on the reliability of magnetic properties of tree leaves as proxies for air pollution monitoring. Sci. Total Environ. 2014, 468–469, 892–902. [CrossRef]

21. Lorenzini, G.; Grassi, C.; Nali, C.; Petiti, A.; Loppi, S.; Tognotti, L. Leaves of Pittosporum tobira as indicators of airborne trace element and PM10 distribution in central Italy. Atmos. Environ. 2006, 40, 4025–4036. [CrossRef]

22. Mitchell, R.; Maher, B.A.; Kinnersley, A. Rates of particulate pollution deposition onto leaf surfaces: Temporal and inter-species magnetic analyses. Environ. Pollut. 2010, 158, 1472–1478. [CrossRef] [PubMed] Int. J. Environ. Res. Public Health 2020, 17, 5717 17 of 19

23. Leonard, R.J.; McArthur, C.; Hochuli, D.F. Particulate matter deposition on roadside plants and the importance of leaf trait combinations. Urban For. Urban Green. 2016, 20, 249–253. [CrossRef]

24. Umbrìa, A.; Galan, M.; Munoz, M.J.; Martìn, R. Characterization of atmospheric particles: Analysis of particles in the Campo de Gibraltar. Atmosfera 2004, 17, 191–206.

25. Thorpe, A.; Harrison, R.M. Sources and properties of non-exhaust particulate matter from road traffic: A review. Sci. Total Environ. 2008, 400, 270–282. [CrossRef] [PubMed]

26. Canepari, S.; Perrino, C.; Olivieri, F.; Astolfi, M.L. Characterisation of the traffic sources of PM through size-segregated sampling, sequential leaching and ICP analysis. Atmos. Environ. 2008, 42, 8161–8175. [CrossRef]

27. Sgrigna, G.; Baldacchini, C.; Esposito, R.; Calandrelli, R.; Tiwary, A.; Calfapietra, C. Characterization of leaf-level particulate matter for an industrial city using electron microscopy and X-ray microanalysis. Sci. Total Environ. 2016, 548–549, 91–99. [CrossRef]

28. Baldacchini, C.; Castanheiro, A.; Maghakyan, N.; Sgrigna, G.; Verhelst, J.; Alonso, R.; Amorim, J.H.; Bellan, P.; Bojovi´c, D.D.; Breuste, J.; et al. How Does the Amount and Composition of PM Deposited on Platanus acerifolia Leaves Change Across Different Cities in Europe? Environ. Sci. Technol. 2017, 51, 1147–1156. [CrossRef]

29. Rossini Oliva, S.; Fernández Espinosa, A.J. Monitoring of heavy metals in topsoils, atmospheric particles and plant leaves to identify possible contamination sources. Microchem. J. 2007, 86, 131–139. [CrossRef]

30. Hofman, J.; Samson, R. Biomagnetic monitoring as a validation tool for local air quality models: A case study for an urban street canyon. Environ. Int. 2014, 70, 50–61. [CrossRef]

31. Baldacchini, C.; Sgrigna, G.; Clarke, W.; Tallis, M.; Calfapietra, C. An ultra-spatially resolved method to quali-quantitative monitor particulate matter in urban environment. Environ. Sci. Pollut. Res. Int. 2019, 26, 18719–18729. [CrossRef] [PubMed]

32. Gratani, L.; Crescente, M.F.; Varone, L. Long-term monitoring of metal pollution by urban trees. Atmos. Environ. 2008, 42, 8273–8277. [CrossRef]

33. Moreno, E.; Sagnotti, L.; Dinares Turell, J.; Winkler, A.; Cascella, A. Biomonitoring of traffic air pollution in Rome using magnetic properties of tree leaves. Atmos. Environ. 2003, 37, 2967–2977. [CrossRef]

34. Richardson, D.H.S.; Shore, M.; Hartree, R.; Richardson, R.M. The use of X-ray fluorescence spectrometry for the analysis of plants, especially lichens, employed in biological monitoring. Sci. Total Environ. 1995, 176, 97–105. [CrossRef]

35. Power, A.L.; Worsley, A.T.; Booth, C. Magneto-biomonitoring of intra-urban spatial variations of particulate matter using tree leaves. Environ. Geochem. Health 2009, 31, 315–325. [CrossRef]

36. Dzierzanowski, K.; Popek, R.; Gawro ´nska, H.; Sæbø, A.; Gawro ´nski, S.W. Deposition of Particulate Matter of Different Size Fractions on Leaf Surfaces and in Waxes of Urban Forest Species. Int. J. Phytoremediat. 2011, 13, 1037–1046. [CrossRef]

37. Tomaševi´c, M.; Vukmirovi´c, Z.; Rajši´c, S.; Tasi´c, M.; Stevanovi´c, B. Characterization of trace metal particles deposited on some deciduous tree leaves in an urban area. Chemosphere 2005, 61, 753–760. [CrossRef]

38. Castanheiro, A.; Samson, R.; De Wael, K. Magnetic- and particle- based techniques to investigate metal deposition on urban green. Sci. Total Environ. 2016, 571, 594–602. [CrossRef]

39. Weerakkody, U.; Dover, J.W.; Mitchell, P.; Reiling, K. Quantification of the traffic-generated particulate matter capture by plant species in a living wall and evaluation of the important leaf characteristics. Sci. Total Environ. 2018, 635, 1012–1024. [CrossRef]

40. Canepari, S.; Cardarelli, E.; Giuliano, A.; Pietrodangelo, A. Determination of metals, metalloids and non-volatile ions in airborne particulate matter by a new two-step sequential leaching procedure Part A: Experimental design and optimization. Talanta 2006, 69, 581–587. [CrossRef]

41. Canepari, S.; Cardarelli, E.; Pietrodangelo, A.; Strincone, M. Determination of metals, metalloids and non-volatile ions in airborne particulate matter by a new two-step sequential leaching procedure Part B: Validation on equivalent real samples. Talanta 2006, 69, 588–595. [CrossRef] [PubMed]

42. Dinka, M.O.; Loiskandl, W.; Ndambukic, J.M. Hydrochemical characterization of various surface water and groundwater resources available in Matahara areas, Fantalle Woreda of Oromiya region. J. Hydrol. Reg. Stud. 2015, 3, 444–456. [CrossRef]

43. Rice, A.; Baird, E.W.; Eaton, R.B. APHA 2017 Standard Methods for Examination of Water and Wastewater; American Public Health Association, American Water Works Association, Water Environment Federation: Washington, DC, USA, 2017; ISBN 9780875532875.

44. Alfani, A.; Maisto, G.; Prati, M.V.; Baldantoni, D. Leaves of Quercus ilex L. as biomonitors of PAHs in the air of Naples (Italy). Atmos. Environ. 2001, 35, 3553–3559. [CrossRef]

45. Sgrigna, G.; Sæbø, A.; Gawronski, S.; Popek, R.; Calfapietra, C. Particulate Matter deposition on Quercus ilex leaves in an industrial city of central Italy. Environ. Pollut. 2015, 197, 187–194. [CrossRef] [PubMed]

46. Massimi, L.; Conti, M.E.; Mele, G.; Ristorini, M.; Astolfi, M.L.; Canepari, S. Lichen transplants as indicators of atmospheric element concentrations: A high spatial resolution comparison with PM10 samples in a polluted area (Central Italy). Ecol. Indic. 2019, 101, 759–769. [CrossRef]

47. Massimi, L.; Simonetti, G.; Buiarelli, F.; Di Filippo, P.; Pomata, D.; Riccardi, C.; Ristorini, M.; Astolfi, M.L.; Canepari, S. Spatial Distribution of Levoglucosan and Alternative Biomass Burning Tracers in an Urban and Industrial Hot-spot of Central Italy. Atmos. Res. 2020, 239, 104904. [CrossRef]

48. Capelli, L.; Sironi, S.; Del Rosso, R.; Céntola, P.; Rossi, A.; Austeri, C. Olfactometric approach for the evaluation of citizens' exposure to industrial emissions in the city of Terni, Italy. Sci. Total Environ. 2011, 409, 595–603. [CrossRef]

49. Massimi, L.; Ristorini, M.; Eusebio, M.; Florendo, D.; Adeyemo, A.; Brugnoli, D.; Canepari, S. Monitoring and Evaluation of Terni (Central Italy) Air Quality through Spatially Resolved Analyses. Atmosphere 2017, 8, 200. [CrossRef]

50. Wang, H.; Shi, H.; Wang, Y. Effects of Weather, Time, and Pollution Level on the Amount of Particulate Matter Deposited on Leaves of Ligustrum lucidum. Sci. World J. 2015, 8, 935942. [CrossRef]

51. Schneider, C.A.; Rasband, W.S.; Eliceiri, K.W. NIH Image to ImageJ: 25 years of image analysis. Nat. Methods 2012, 9, 671–675. [CrossRef]

52. Astolfi, M.L.; Marconi, E.; Protano, C.; Vitali, M.; Schiavi, E.; Mastromarino, P.; Canepari, S. Optimization and validation of a fast digestion method for the determination of major and trace elements in breast milk by ICP-MS. Anal. Chim. Acta 2018, 1040, 49–62. [CrossRef]

53. Iyasele, J.U.; Idiata, D.J. Investigation of the Relationship between Electrical Conductivity and Total Dissolved Solids for Mono-Valent, Di-Valent and Tri-Valent Metal Compounds. IJERR 2015, 3, 40–48.

54. Al Dahaan, S.; Al-Ansari, N.; Knutsson, S. Influence of Groundwater Hypothetical Salts on Electrical Conductivity Total Dissolved Solids. Engineering 2016, 8, 823–830. [CrossRef]

55. Astolfi, M.L.; Protano, C.; Marconi, E.; Massimi, L.; Brunori, M.; Piamonti, D.; Migliara, G.; Vitali, M.; Canepari, S. A new rapid treatment of human hair for elemental determination by inductively coupled mass spectrometry. Anal. Methods 2020, 12, 1906–1918. [CrossRef]

56. Huggins, F.E.; Huffman, G.E.; Robertson, J.D. Speciation of elements in NIST particulate matter SRMs 1648 and 1650. J. Hazard. Mater. 2000, 74, 1–23. [CrossRef]

57. Huggins, F.E.; Shah, N.; Huffman, G.E.; Robertson, J.D. XAFS spectroscopic characterization of elements in combustion ash and fine particulate matter. Fuel Process. Technol. 2000, 65–66, 203–218. [CrossRef]

58. Yinsong, W.; Aiguo, L.; Yuanxun, L.; Lun, W.; Yan, L.; Guilin, Z.; Yaning, X.; Jing, Z.; Yuanmao, Z.; Zuci, S. Speciation of elements in atmospheric particulate matter by XANES. J. Radioanal Nucl. Chem. 2007, 273, 247–251. [CrossRef]

59. Mészáros, E.; Barcza, T.; Gelencsér, A.; Hlavay, J.; Kiss, G.; Krivácsy, Z.; Molnár, A.; Polyák, K. Size distributions of inorganic and organic species in the atmospheric aerosol in Hungary. J. Aerosol Sci. 1997, 28, 1163–1175. [CrossRef]

60. Venkataraman, C.; Thomas, S.; Kulkarni, P. Size distribution of polycyclic aromatic hydrocarbons- gas/particle portioning to urban aerosols. J. Aerosol Sci. 1999, 30, 759–770. [CrossRef]

61. Birmili, W.; Allen, A.G.; Bary, F.; Harrison, R.M. Trace Metal Concentrations and Water Solubility in Size-Fractionated Atmospheric Particles and Influence of Road Traffic. Environ. Sci. Technol. 2006, 40, 1144–1153. [CrossRef]

62. Adachi, K.; Tainosho, Y. Characterization of heavy metal particles embedded in tire dust. Environ. Int. 2004, 30, 1009–1017. [CrossRef]

63. Blair, M.; Stevens, T.L. Steel Castings Handbook, 6th ed.; Steel Founders' Society and ASM International: Novelty, OH, USA, 1995; pp. 2–34.

64. Minguillón, M.C.; Querol, X.; Baltensperger, U.; Prévôt, A.S.H. Fine and coarse PM composition and sources in rural and urban sites in Switzerland: Local or regional pollution? Sci. Total Environ. 2012, 427–428, 191–202. [CrossRef]

65. Dongarrà, G.; Manno, E.; Varrica, D. Possible markers of traffic-related emissions. Environ. Monit. Assess. 2008, 154, 117–125. [CrossRef]

66. Gietl, J.K.; Lawrence, L.; Thorpe, A.J.; Harrison, R.M. Identification of brake wear particles and derivation of a quantitative tracer for brake dust at a major road. Atmos. Environ. 2010, 44, 141–146. [CrossRef]

67. Grigoratos, G.; Martini, G. Brake wear particle emissions: A review. Environ. Sci. Pollut. Res. Int. 2015, 22, 2491–2504. [CrossRef]

4. Application to PM biomonitoring

In the last few years, the **biomonitoring** approach has gained more and more attention by the scientific communities, as a valid alternative to conventional and instrumental air pollution monitoring. This is strictly connected to the ability of some organisms, defined as **bioindicators**, of providing crucial information on the surrounding environment and its pollution levels. As previously described in the Introduction chapter of this PhD thesis (Chapter 1), the utilization of plants to this aim, is connected to several advantages, which can result in a major abatement of costs associated to the definition of wide and dense monitoring networks and the utilization of conventional samplers. Being usually wide-spread, even in highly anthropized areas such as urban ones, plants can result also in an increase of potential sampling sites, thus potentially providing highly spatially-resolved data.

In this context, the evaluation of leaf deposited PM and its chemical and physical characterization can provide useful information on 1) the identification of specific emission sources and their differentiated impact and on 2) the risk for human health. This is especially true since each emission source is characterized by specific **emission chemical/physical fingerprints**, and therefore, each PM compounds and their specific size distribution can be used to identify them and trace back their impact at different sites. This aspect also applies to leaf deposited PM and the evaluation of their variables such as chemical composition, size distribution and morphology. It is important to underline that proper **validation** is needed to prove the efficiency of this biomonitoring approach. The validation step may include the comparison with data retrieved from already existing air quality monitoring networks.

In this PhD project, the evaluation of PM leaf deposition is tested to biomonitoring purposes of atmospheric PM pollution (A2). To this aim, leaves of *Arundo donax* L., one of the most known riparian and invasive species, are collected in six sampling sites in the city of Terni, along the river and at sites characterized by differentiated PM and river water pollution. PM leaf superficial deposition is evaluated through the comparison of the elemental concentrations detected on washed and unwashed leaves sampled from the same sites. Then, to prove the efficiency of PM leaf deposition data, for the evaluation of the impact of the emission sources acting in this study area, these are compared to the elemental data of PM_{10} membrane filters sampled in parallel at the same sites. PM_{10} membrane filters are subjected to the chemical fractionation procedure, thus obtaining detailed information on both the water-soluble and insoluble fraction of PM_{10} elemental components, useful for increasing their selectivity as specific source tracers. Furthermore, due to the hyper-accumulation ability of this riparian species, element concentrations detected in *A. donax* leaves are compared also

with those measured in river water samples, collected at the six sites, with the aim to evaluate at what extent river water contamination can affect leaves elemental composition.

4.1 (A2) Evaluation of the Efficiency of *Arundo donax* L. Leaves as Biomonitors for Atmospheric Element Concentrations in an Urban and Industrial Area of Central Italy

Atmosphere (2020), 11, 226, doi: 10.3390/atmos11030226

Martina Ristorini[1,2], Maria Luisa Astolfi[3], Maria Agostina Frezzini[3], Silvia Canepari[3] and Lorenzo Massimi[3*]

[1] Department of Bioscience and Territory, Università del Molise, Pesche (IS), 86090, Italy
[2] Institute of Terrestrial Ecosystem research – Council of National research (IRET-CNR) Via G. Marconi 2, 05010 Porano (TR), Italy
[3] Department of Chemistry, Sapienza University of Rome (Rome), 00185, Italy
* Correspondence: l.massimi@uniroma1.it; Tel.: +39-0649913742 or +39-3703022703

Abstract: Washed and unwashed *A. donax* leaves were analyzed for elements and results were compared with element concentrations detected in river water and PM_{10}. Samples were collected along a river in an urban and industrial hot-spot of Central Italy, where element concentrations show relevant spatial gradients both in air and river water. The aim of this study is to identify the role of the two environmental matrices on leaves composition. Element concentrations of washed and unwashed leaves were compared to differentiate between the superficial deposition and the uptake into leaf tissues of elements. Water-soluble and insoluble element concentrations were measured in PM_{10} samples collected on membrane filters by using innovative high spatial resolution samplers. The comparison among leaf and atmospheric concentrations of PM_{10} elements showed a similar trend for Ni, Mo, Cr, Ti and Fe, which are reliable tracers of the PM_{10} contribution by steel plant and vehicular traffic. Soluble species appeared to be mainly bounded into leaf tissues, while insoluble species were deposited on their surface. On the other hand, element concentrations detected in washed *A. donax* leaves were poorly correlated with those measured in river water samples. The obtained results proved that *A. donax* leaves can be used as reliable biomonitors for the evaluation of the atmospheric concentrations of some PM_{10} elemental components.

Keywords: air quality; biomonitoring; particulate matter; leaf deposition; source tracer

1. Introduction

Arundo donax L., commonly known as giant reed, is a tall perennial grass of the family *Poaceae*, typical of riparian areas and characterized by great productivity, growing up to 10 cm per day in optimal conditions [1-2]. Numerous studies had underlined the potential of this species for the phytoremediation of contaminated waters and soils, due to its tolerance to high concentrations of heavy metals, such as Cd, Cr, Ni [3] and its ability to absorb and bioaccumulate contaminants. In particular, *A. donax* turns out to be characterized by a root > leaf > stem translocation pattern [4], with the belowground biomass (roots and rhizomes) as the main bioaccumulation organs [5-7]. These characteristics make this species suitable to be used as bioindicator of heavy metal pollution of water and soil. Therefore, *A. donax* provides an alternative to the traditional sampling and analytical procedures applied to this task [8].

On the other hand, numerous studies underlined the potential of biomonitoring to assess airborne particulate matter (PM) pollution [9-11]. In this context, urban trees and shrubs leaves are often proposed as efficient and low-cost passive biomonitors for PM [12-14], since they are able to affect dispersion and deposition of airborne particles [15]. In particular, the evaluation of chemical and physical characteristics of particles deposited on leaves can be used to achieve information about the role and the impact of anthropogenic PM emission sources [16-17]. In fact, these characteristics can be directly influenced by the type of emission process and source [18-19]. PM is an extremely heterogenous mixture of airborne solid particles and liquid droplets, varying in size, shape, chemical composition, solubility, toxicity and origin [20]. It is considered one of the most relevant air pollutants in terms of human health effects [21-23]. In particular, PM_{10} (particles characterized by aerodynamic diameters ≤ 10 μm) includes particles that are able to interact at different levels with human respiratory system and induce negative health effects [24-25]. PM_{10} mass concentration is used as an air quality indicator, but to date, exceedances of guideline levels set for PM_{10} are still frequent in many urban and industrial areas (such as the daily limits of 50 ng m^{-3} for PM_{10} mass concentrations set by 2008/50/EC).

Dry deposition of PM on leaves is a complex and dynamic process, being influenced both by species-specific characteristics of vegetation and chemical-physical characteristics of airborne particles themselves [26-27]. To date, due to the high complexity of dry deposition processes and the heterogeneity of PM_{10}, the achievement of a complete characterization of leaf deposited particles is difficult to obtain. Numerous analytical procedures have been applied for the achievement of this task, but it is still uncertain which procedure is the most efficient. One of the main sources of uncertainty is connected to the leaf washing procedure, being still unsure whether this step should be carried out or not. In fact, the efficiency of leaf washing together with the chemical and physical characteristics of the particles, can influence their encapsulation in leaf structures (waxes layer or stomata pores) [28-29]. These factors can affect the efficiency of any analytical procedure applied in the characterization of leaf deposited particles.

This study is aimed to evaluate the influence on element concentrations of *A. donax* leaves of two types of environmental contaminations to which plants are exposed: atmospheric PM_{10} and river water pollution. To this aim, *A. donax* leaves, PM_{10} sampled filters and river water samples were collected in parallel at sites impacted by different pollution sources. Element concentrations determined in the three matrices were compared. Washed and unwashed leaves were analyzed and compared to differentiate between superficial deposition and uptake into leaf tissues of PM_{10} elements. Furthermore, due to the hyper-accumulate ability of this riparian species, element concentrations detected in *A. donax* leaves were compared with those measured in river water samples. This was aimed to evaluate at what extent river water contamination can affect leaves elemental composition.

2. Materials and methods

2.1. Study area and sampling sites

The study was carried out in Terni city, an urban and industrial hot-spot of Central Italy. The choice of Terni was mainly driven by the presence of intense local emission sources. This study area is characterized

by typical urban sources such as vehicular traffic and domestic heating, but also by a power plant for waste treatment and an extensive steel plant, occupying about 158 ha (Fig. 1). Due to its peculiar geomorphological and meteorological conditions, Terni basin is characterized by high PM_{10} mass and element concentrations, which make this area one of the most critical for human health in Central Italy [30-35]. In addition, these emission sources determine very relevant spatial variations of element concentrations in both PM_{10} and river water, making this area particularly suitable for studying correlations among biomonitors and environmental conditions. Six sampling sites (TE1, TE2, TE3, TE4, TE5, TE6) were individuated along the river Nera and chosen for the collection of *A. donax* leaves and river water samples. TE1 is located near the power plant, in the western part of the city, TE2 and TE3 near the main trafficked streets of the city center, and TE4, TE5 and TE6 are sited around the steel plant, in the eastern part of the city (Figure 1, Table 1). In particular, TE6 is located upstream from the wastewater systems for the treatment of the steel plant effluents.

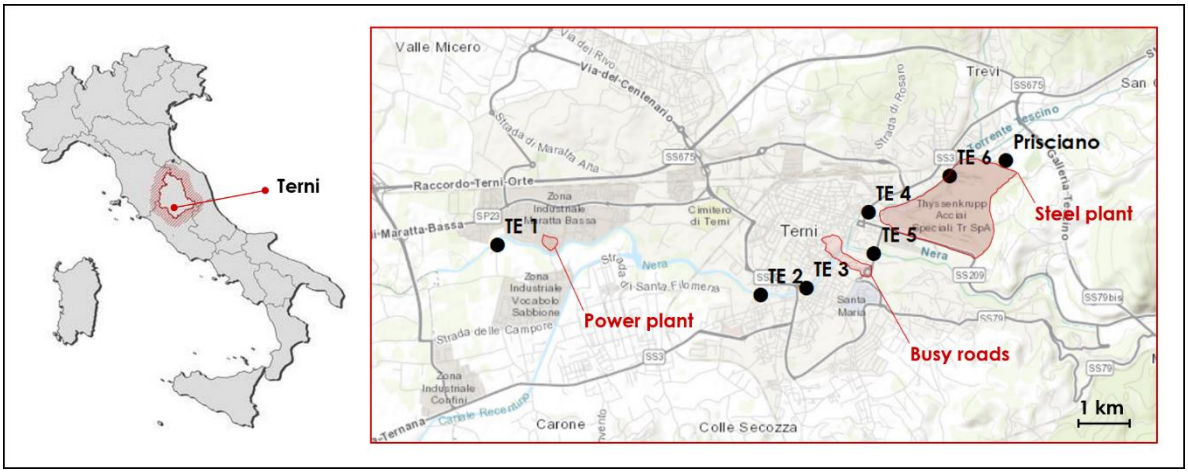

Figure 1. Sampling sites of *A. donax* leaves and river water samples along the river Nera in Terni (Central Italy) and air quality station "Prisciano" controlled by ARPA Umbria (regional agency for environmental protection). Highlighted the main PM10 anthropogenic emission sources present in the study area.

Table 1. Latitude and longitude of the six sampling sites in Terni.

SAMPLING SITES	LATITUDE	LONGITUDE
TE1	42°33'43.84"N	12°35'47.18"E
TE2	42°33'22.27"N	12°38'21.02"E
TE3	42°33'25.29"N	12°38'47.81"E
TE4	42°33'58.02"N	12°39'24.08"E
TE5	42°33'40.12"N	12°39'27.33"E
TE6	42°34'13.53"N	12°40'11.41"E

2.2. Arundo donax leaves and river water samples collection and preparation

A. donax leaves and river water samples were monthly collected at the six sampling sites (Figure 1) from March to July 2017. For each site, 3 plants were selected and 6 leaves were collected from each plant for a total of 18 leaves collected each month. Leaves were detached, at least a week after the last rainfall event, from the same internode (second-last from the top of the stems), in order to avoid youngest leaves and ensure longer exposition time to both river water and PM_{10} atmospheric pollution. Furthermore, leaves were collected at a height comparable to that of PM_{10} active samplers (about 2 meters from the ground). Leaves samples were then stored at -18 °C in paper bags, to avoid external contamination. *A. donax* leaves collected at North-East of the Terni basin (42°38'25.95"N, 12°48'34.98"E), far from the direct impact of anthropogenic emission sources, were used as background samples. Half of the collected leaves were washed thoroughly three times with 250 mL of deionized water (produced by Arioso UP 900 Integrate Water Purification System) for 5 minutes by using a rotating mixer (Rotator, Glas-Col, USA). The dry weight calculation (30 replicates) was carried out by oven drying 1 g of fresh leaves at 60 ± 2 °C until constant weight. Washed and unwashed leaves monthly collected at each site were then pulverized by grinding in a mill with Teflon balls and the obtained powders were homogenized and weighed (analytical balance Gibertini Europe 60; Gibertini Elettronica Srl, Milan, Italy). Subsequently, three replicates of about 30 mg of each sample (homogenized powders of washed or unwashed leaves monthly collected at each site) was subjected to a microwave assisted acid digestion (Ethos Touch Control with Q20 rotor, Milestone, Bergamo, Italy). The acid digestion was carried out for 30 min at 180°C by using a HNO_3/H_2O_2 mixture (2:1, v/v; 2 mL of ultrapure concentrated HNO_3 67%, Promochem, LGC Standards GmbH, Wesel, Germany; 1 mL of H_2O_2 30%, Promochem, LGC Standards GmbH, Wesel, Germany). The digested solutions were then diluted to 100 mL of deionized water. Since all the sampled plants were in close proximity to the river and the root system was often in direct contact withthe river water (frequent overflowing of the river), each month, about 50 mL of river water was collected at each sampling site, for a total of 30 water samples. River water samples were taken from 10 to 15 cm below the water surface, according to APHA, 1998 [36].

2.3. PM_{10} samples collection and preparation

PM_{10} was monthly sampled on Teflon membrane filters (PTFE membranes, 37 mm diameter, 2 μm pore size, PALL Corporation, Port Washington, New York, NY, USA) from March to July 2017 at 23 monitoring sites spread over the Terni basin by using innovative and very-low volume (0.5 l min^{-1}) PM_{10} active samplers (High spatial resolution sampler - HSRS, Fai Instruments, Fonte Nuova, Italy). The localization and the geographical coordinates of the 23 PM_{10} sampling sites as well as the characteristics of the used HSRS are deeply described in Massimi et al. 2017 and Massimi et al. 2019 [11, 31]. The monthly collected PM_{10} membrane filters were subjected to a chemical fractionation procedure, previously optimized and validated [37-38], useful to separate the water-soluble and insoluble fraction of each PM_{10} elemental component, thus increasing its selectivity as source tracer [11, 39-40]. Firstly, after removing the supporting polymethylpentene ring from each membrane filter, PM_{10} filters were extracted in 10 mL of deionized water for 30 min at 25 °C by using an ultrasonic bath (Proclean 10.0 ultrasonic cleaner, Ulsonix, Germany) and then filtered on cellulose

nitrate filters (0.45 μm pore size, Merck Millipore Ltd., Billerica, MA, USA). Secondly, both the membrane and cellulose nitrate filters were acid-digested for 30 min at 180°C in the microwave oven by using the HNO_3/H_2O_2 mixture (2:1, v/v) previously described. The digested solutions were then diluted to 50 mL with deionized water.

2.4. ICP-MS analysis

The collected river water samples and all the acid-digested solutions were filtered with syringe filters (25 mm diameter, 0.45 μm pore size, GVS Filter Technology, Morecambe, England, UK) before instrumental analysis. The concentrations of 16 elements (Ba, Cd, Cr, Cs, Cu, Fe, Li, Mn, Mo, Ni, Pb, Rb, Sb, Sn, Sr, Ti) were determined in all the samples (river water samples, water-extracted and acid-digested PM_{10}, washed and unwashed *A. donax* leaves) by a quadrupole inductively coupled plasma mass spectrometer (ICP-MS, model 820-MS; Bruker, Bremen, Germany) equipped with a glass nebulizer (0.4 mL min^{-1} ; Analytik Jena AG, Jena, Germany). External matrix-matched standard calibration curves were performed for all the analyzed elements in the 1-500 μg L^{-1} range by serially diluting standard stock solutions (1000 ± 2 mg L^{-1}; Exaxol Italia Chemical Manufacturers Srl, Genoa, Italy). To control the nebulizer efficiency, yttrium and rhodium were set at 5 μg L^{-1} as internal standards for all measurements and were prepared from standard stock solutions (1000 ± 2 mg L^{-1}; Panreac Química, Barcelona, Spain; Ultra Scientific, North Kingstown, RI, USA; Merck Millipore Ltd., Billerica, MA, USA). The values of blanks, subjected to similar sample preparation and analytical procedures, were deducted from all measurements and the limits of detection (LODs; supplementary material S1; Table S1.1, S1.2, S1.3) were set at 3 times the standard deviation (Std Dev) of 10 replicate blank determinations. Standard deviations of the replicates were all below 20%. The used instrumental conditions and the performance of the method are detailed in Astolfi et al. 2018 [41].

2.5. Data elaboration

Concentrations of the 16 elements derived from the three replicates analyses of washed and unwashed leaves, monthly collected at each site, were averaged in order to obtain a single monthly value. This was aimed to properly compare leaves element concentrations with results from the chemical analysis of PM_{10} samples (one filter monthly sampled for each site). The concentrations determined in the washed and unwashed *A. donax* leaves were divided by the dry weight of each sample (ng mg^{-1}). Then, monthly element concentrations were averaged for each monitoring site (supplementary material S2; Table S2.1, Table S2.2). The averaged element concentrations detected in washed leaves were subtracted to the unwashed ones to evaluate the elemental amount superficially deposed on leaves (SD in ng mg^{-1}). Element concentrations (μg l^{-1}) were determined in river water samples collected at each site for each of the 5 collection months (three replicates of 10 mL). Also for river water samples, results obtained from the three replicates analyses were averaged to obtain one monthly result relative to each site. Then, monthly element concentrations were averaged for each monitoring site and these are reported in supplementary material S2 (Table S2.3). The element concentrations of the water-soluble and insoluble PM_{10} were divided by the air volume sampled on each PM_{10} membrane filter

(ng m^{-3}). Total concentrations were calculated as the sum of the two solubility fractions. Since the *A. donax* leaves were collected at different sites with respect to the PM_{10} samples, ordinary kriging (OK, spherical semivariogram model) interpolation [42-43] was applied to the PM_{10} soluble, insoluble and total element concentrations monthly determined at the 23 PM_{10} sampling sites. Then, these concentrations were averaged over the 5 months collection period, in order to estimate their concentrations (supplementary material S2; Table S2.4, S2.5) at the leaves collection sites (TE1, TE2, TE3, TE4, TE5, TE6).

2.6. Statistical analysis

Normal distribution of data was tested by using the Kolmogorov-Smirnov test. Then, paired t-tests were used to assess the statistical significance of the differences between mean values of each element detected in unwashed and washed leaves. Pearson correlation was used to assess the correlations between: SD results and element concentrations in the water-soluble and insoluble fraction of PM_{10}; washed leaves element concentrations and the element concentrations in the the two fractions of $PM_{10;}$ washed leaves and river water element concentrations. Statistical analyses were carried out using IBM SPSS Statistics 25 software (IBM Corp., Armonk, NY, USA).

2.7. SEM analysis of PM_{10} samples

PM_{10} sampling on polycarbonate membranes (PCTE membranes, 37 mm diameter, 0.8 μm pore size, Sterlitech Corporation, Kent, Washington, USA) was carried out for three days, from the 2nd to the 4th of March, by using two HSRS working in parallel at the air quality station "Prisciano".The station is located in the East of the city (42°34'20.30"N 12°40'44.23"E), in the proximity of the steel plant and it is controlled by the regional agency for environmental protection (ARPA Umbria) (Fig. 1). Small portions of each polycarbonate membrane were cut, fixed to aluminum stubs by self-adhesive carbon disks (TAAB, 12mm diam.) and coated with an ultra-thin carbon layer in a vacuum evaporator (108 Carbon A; Scientific Instruments Ltd., Cressington, England, UK). Micrographs of each sample were acquired by a high-resolution field emission scanning electron microscopy (HR-FESEM; model AURIGA; Carl Zeiss Microscopy GmbH, Jena, Germany) equipped with an energy dispersive spectrometer for X-ray microanalysis (XEDS; model QUANTAX; Bruker Italia S.r.l., MI, Italy). Micrographs were acquired through the use of backscatter electron detector (BSD) at magnification ranging from 25,000x to 600,000x and at working distance (WD) ranging from 9.6 mm to 12.4 mm.

3. Results and discussion

3.1. Element concentrations in Arundo donax leaves

Figure 2 reports the concentrations of elements associated to the steel plant emission (Cr, Fe, Mo, Ni and Ti) in unwashed and washed leaves. All these elements showed a marked concentration gradient in both washed and unwashed leaves, indicating that the measured concentrations are sensitive to environmental

concentrations. A similar trend was found for all the considered elements, with higher concentrations at sites surrounding the steel plant.

Cr, Ni and Ti showed higher concentrations (ng mg^{-1}) in leaves collected at TE5 and TE6 (Figure 2a, d and e), which are the sites closest to the steel plant. Furthermore, for these elements, concentrations in unwashed leaves were significantly higher than those in washed leaves. This means that a major part of the measured concentrations in unwashed leaves is probably due to superficial deposition of atmospheric particles. PM_{10} particles containing these elements are known to be emitted at high concentrations by the steel plant [31]. Chromium is usually used to increase the steel resistance to chemical oxidation and nickel is used to increase the steel strength, ductility and toughness. Titanium is used in steelmaking for deoxidation, grain-size control, carbon and nitrogen control, and stabilization [44]. The variation among the selected sites, observed for the leaf deposition of these elements, underlined the impact of the steel plant and proved the reliability of *A. donax* leaf deposition results for the individuation of the steel plant tracers.

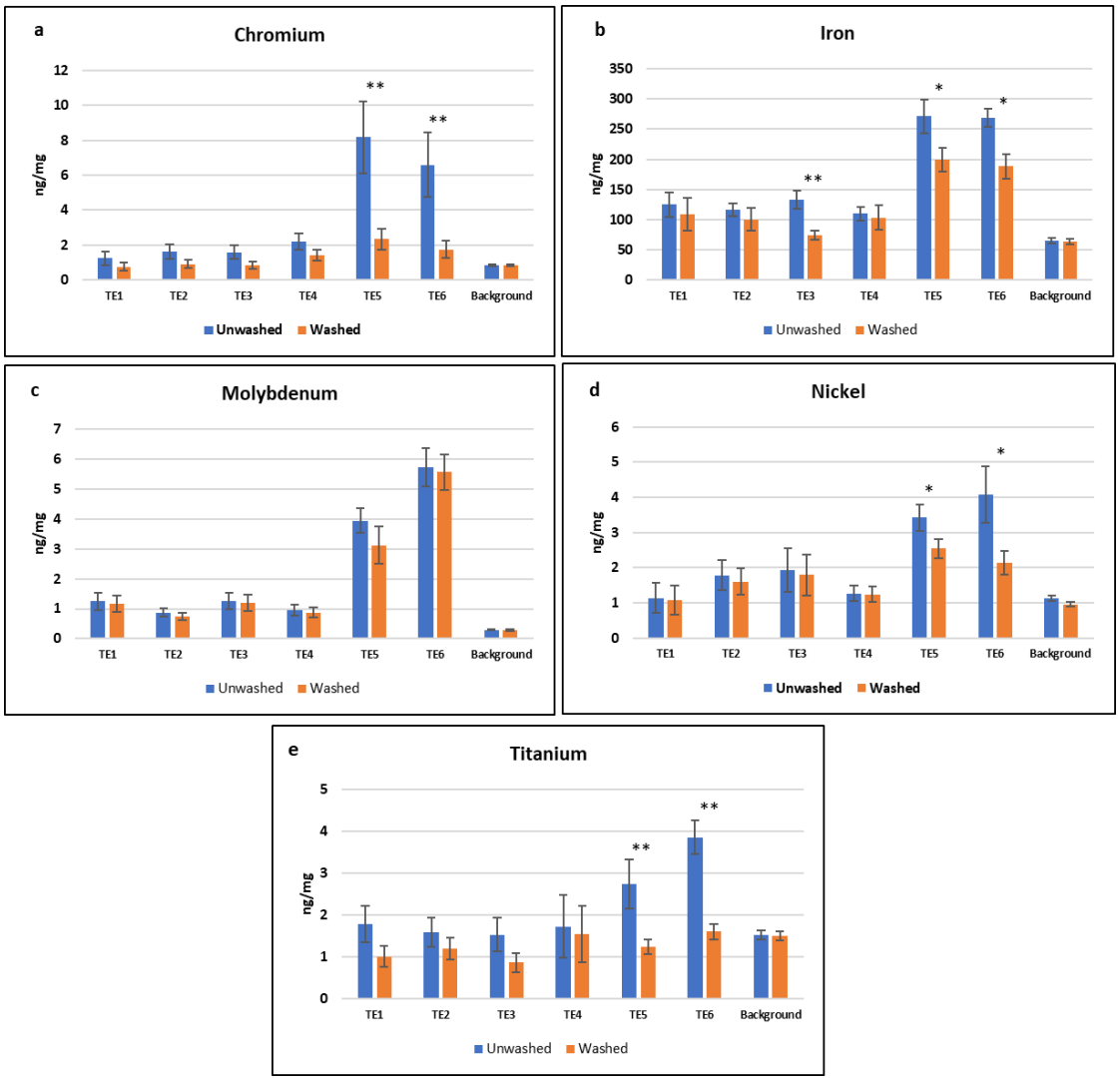

Figure 2. Comparison between averaged concentrations (ng mg^{-1}) of Cr, Fe, Mo, Ni and Ti, detected in unwashed and washed leaves at the six sites (panel a, b, c, d and e). P values obtained by applying paired sample t-test (* $p<0.05$; ** $p<0.001$) and standard deviations calculated between monthly concentrations are reported.

In panel b of Figure 2, we can observe that Fe concentrations (ng mg^{-1}) detected in unwashed leaves were higher at the sampling sites TE3, TE5 and TE6. Also in this case, concentrations were significantly higher in unwashed leaves. Iron is the principal component of stainless steel and higher deposition values in *A. donax* leaves collected at TE5 and TE6, which are the closest sites to the steel plant, confirmed its attribution to emissions from the steel plant. However, Fe is also a well-known tracer for vehicular traffic, being related to the mechanical abrasion of brakes and vehicle components [30, 45-46]. The increase of Fe concentration at TE3, located near the city center, is mainly related to its emission from the close busy roads. Therefore, the trend of Fe leaf deposition underlined the impact of two different emission sources: steel plant (at TE5 and TE6) and vehicular traffic (at TE3).

In the specific case of molybdenum, higher concentrations were found at the same collection sites (TE5 and TE6) whereby were found high concentrations of Cr, Ni and Ti, highlighting the impact of the steel plant. In fact, Mo is typically used as secondary component to improve the resistance of stainless steel [44]. However, Mo concentrations in washed and unwashed leaves were very similar, indicating that this element is deeply bound to the leaves (Figure 2c). This difference may be due to a different uptake process (i.e. root absorption from water or soil) or to the different chemical and/or physical characteristics of atmospheric particles deposited on leaves. Further details on these issues can be obtained by comparing the element concentrations in leaves with those found in atmospheric PM_{10} and river water samples.

3.2. Comparison between leaf deposition and PM_{10} element concentrations

To evaluate the potential of this biological approach, based on the evaluation of PM_{10} deposition on *A. donax* leaves for the assessment of the impact of the PM_{10} emission sources, we compared the elements superficial deposition on leaves (SD) with the spatially-resolved atmospheric element concentrations detected in the PM_{10}.

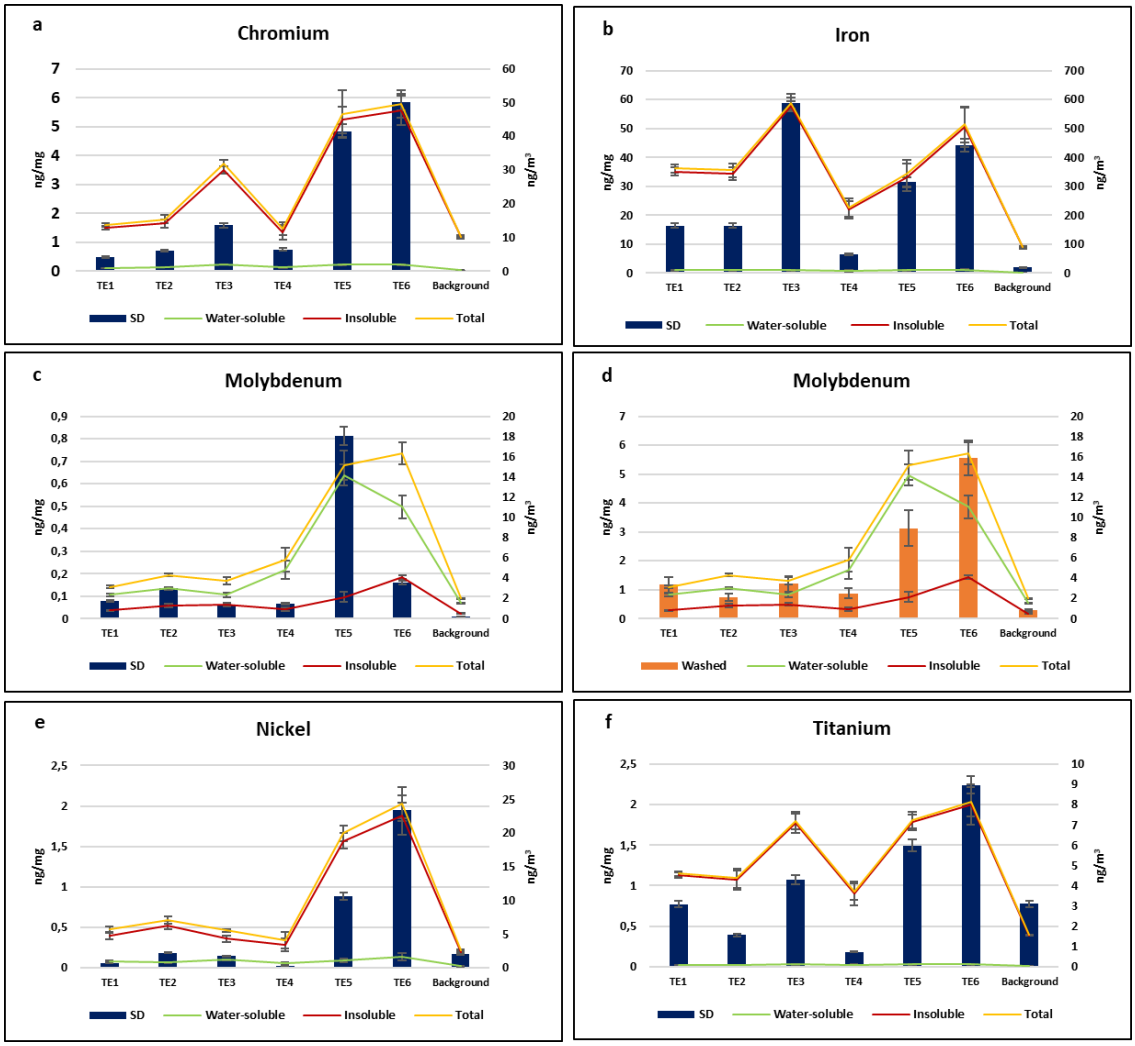

Figure 3. Comparison between averaged SD results (ng mg^{-1}) and concentrations in the water-soluble, insoluble and total fraction of PM_{10} (ng m^{-3}) of Cr, Fe, Mo, Ni and Ti (panels a, b, c, e and f). Comparison between averaged Mo concentrations in washed leaves (ng mg^{-1}) and in the water-soluble, insoluble and total fraction of PM_{10} (ng m^{-3}) (panel d). Standard deviations calculated between monthly SD values, washed leaves and PM10 interpolated concentrations are reported.

From Figure 3, we can observe that, for most of the identified steel plant tracers (Cr, Fe, Ni and Ti), the SD showed a similar trend to total concentrations in PM_{10} (Figure 3a, b, e and f). For these elements, the difference between unwashed and washed concentrations in *A. donax* leaves seems then to be reliably representative of their atmospheric concentrations. In the case of Mo, much poorer correlations between SD and PM_{10} concentrations were found (Figure 3c). For this element, we also reported the comparison between PM_{10} and washed leaves concentrations (Figure 3d), which showed a much higher correlation. In order to investigate the different behavior of Mo with respect to the other steel plant tracers, we considered the solubility and the morphological characteristics of particles emitted by the steel plant.

Indeed, dimensions and morphological characteristics of airborne particles have proven to be able to influence the deposition of PM on leaves and its interaction with leaf tissues [26, 47-48]. For this reason, we carried out SEM analyses on PM_{10} sampled on polycarbonate membranes through HSRS working near the steel plant (Figure 4).

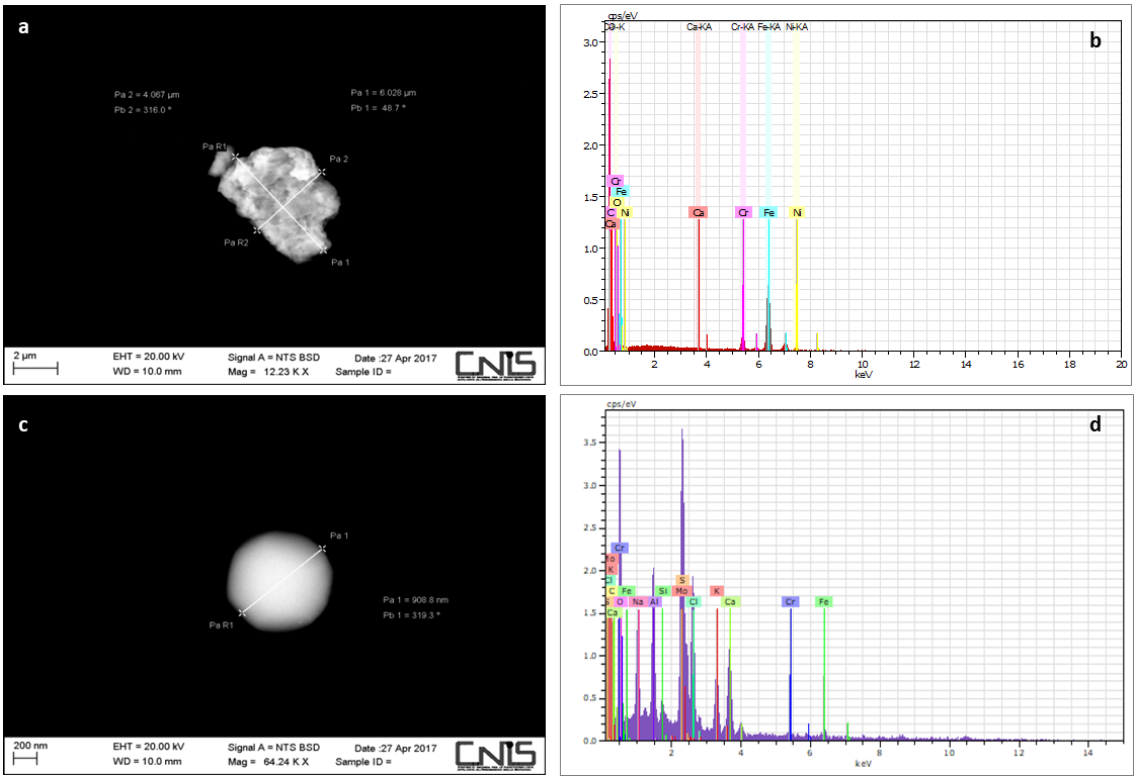

Figure 4. SEM micrograph (a) and respective EDX spectrum (b) of a steel particle (Cr, Fe and Ni) sampled near the steel plant. SEM micrograph (c) and respective EDX spectrum (d) of a Mo particle sampled near the steel plant.

From Figure 4, we can observe the micrograph (panel a) with the respective EDX spectrum (panel b) of a particle containing the basic stainless steel components: Cr, Ni and Fe. This steel particle is coarse (up to 5 µm of diameter) and is characterized by an irregular, angular and sharp morphology. The peculiar dimension and morphology of this and other analyzed coarse particles with the same chemical composition, seems to be related to mechanical-abrasive emission processes. On the other hand, in the panel c, we can observe a fine particle (with diameter smaller than 1 µm) containing Mo and spherical in shape, which is the typical morphology of airborne particles formed by high temperature processes [49-50]. Even though these two types of particles are emitted by the same emission source (steel plant), they appeared to be characterized by different dimension and morphology, revealing the presence of two different emission processes (high temperature and mechanical-abrasive processes). The different physical characteristics of these particles may be considered responsible for the different behavior observed in Figure 2 and 3. In particular, coarse particles containing Cr, Fe, and Ni seem to have been deposited on the leaf surfaces, making it easy to wash them off and to detect significant differences between washed and unwashed leaves. On the other hand, fine particles containing Mo could be more likely to get encapsulated into the waxes layer or stomata pores situated on the leaf surface, making more difficult to wash them out from the leaves [28-29]. This can results in the lowest difference between unwashed and washed leaves, detected for molybdenum concentrations. In Figure 3 we also reported water-soluble and insoluble fractions of each element in PM_{10}. As it can be noted, Cr, Fe, Ni and Ti are almost exclusively present as insoluble species, while Mo is mainly present in the water soluble fraction. Besides the

small dimensions of particles containing Mo, the different behavior observed for this element may be due to the higher solubility of species containing Mo that might be then directly absorbed by the leaf surface.

Table 2. Pearson's correlation coefficients calculated between SD and washed leaves element concentrations and their concentrations in the water-soluble and insoluble fractions of PM10. Mean monthly concentrations at each site were included in the elaboration (N=30). Positive linear correlations (Pearson's coefficient > 0.8) between the two variables are reported in red.

Pearson's	Ba	Cd	Cr	Cs	Cu	Fe	Li	Mn	Mo	Ni	Pb	Rb	Sb	Sn	Sr	Ti
SD/Water soluble PM_{10}	-0,06	0,31	0,74	0,31	-0,39	0,49	0,62	0,77	0,78	0,77	0,21	0,00	-0,65	0,34	-0,56	0,79
SD/Insoluble PM_{10}	-0,12	0,22	0,87	0,38	-0,08	0,93	0,25	0,92	0,16	0,95	-0,79	0,12	-0,74	0,53	-0,62	0,93
Washed leaves/Water soluble PM_{10}	0,01	0,18	0,49	0,10	0,08	0,31	0,67	0,73	0,90	0,63	0,02	0,51	0,45	-0,43	0,19	0,17
Washed leaves/Insoluble PM_{10}	-0,59	0,24	0,59	-0,14	0,18	0,02	-0,03	0,75	0,35	0,82	0,55	-0,08	0,43	-0,66	0,21	0,01

Table 2 reports Pearson's correlation coefficients (ρ) calculated between elements superficially deposited on leaves or bounded to leaf tissues (washed leaves) and their concentrations in the water-soluble and insoluble fractions of PM_{10}. In general, the highest positive correlations were found between concentrations in insoluble fraction of PM_{10} and SD of Cr, Fe, Ni, Mn, Ti and Zn. Most of these elements (Cr, Ni, Fe, Ti) are tracers of the steel plant; as already showed, particles containing these elements are mainly characterized by coarse dimensions. Mn is also well correlated to SD; this element is also known as a source tracer for steel producing processes [51-52] but it is also used as tracer of non-combustive emissions from vehicular traffic [18, 53]. This source produces particles scarcely soluble and belonging to the coarse dimensional fraction of PM as well [54]. It is then reasonable to hypothesize that coarse and insoluble particles are deposited on leaf surface and easily washed out during the leaf washing step. For this kind of PM contribution, the determination of SD may constitute a reliable biomonitoring procedure. In the case of Mo, as already pointed out, a good correlation was found between washed leaves and soluble fraction of PM_{10}. Mo is present in PM_{10} mainly as soluble species belonging to the fine fraction; these characteristics promote a stronger interaction with leaf structure and washing procedure is not able to detach Mo-containing particles. A positive correlation was found also between washed leaves and insoluble Ni. In this regard, it is worth noting that fine particles containing Ni were also individuated through SEM analysis (supplementary material S3; Figure S3.1). These particles are probably released by the same high temperature process but contain Ni as insoluble species. The correlation between washed leaves and Ni may indicate that the uptake into leaf tissues is mainly driven by physical interaction of small particles with waxes layer and stomata pores. In particular, dimensions of *A. donax* stomata pores are reported to be 23.2 ± 1.7 μm for length and 9.7 ± 1.2 μm for width [55]. Even if particles encapsulation in leaves structures, is reported to be a relevant mechanism for particles ≤ 10.6 μm, this process results to be dominant especially for fine particles ≤ 2.6 μm [28-29]. Correlations between SD results and PM_{10}

element concentrations were much lower for all the other analyzed elements, tracers of other PM sources, whose strength was lower than the steel plant. For example, correlations were poor for water-soluble Cd, Cs, Rb and Tl, which have been identified as reliable tracers for biomass burning in the Terni basin [56-57] and weak for insoluble Cu and Sn, which are well-known as rail network and vehicular traffic tracers [11, 31, 58-59]. Then, SD of atmospheric elements can be then considered reliable only for the evaluation of the impact of strong PM sources (steel plant and vehicular traffic).

3.3. Comparison between river water samples and A. donax leaves elemental content

To evaluate the potential influence of river water pollutants on the elemental composition of leaves, where heavy metals adsorbed by roots can be stored and transferred [60-61], we analyzed the element concentrations of water samples (Figure 1). Since metals adsorbed by roots are expected to be included in leaf tissues, element concentrations in river water were compared with the element concentrations in washed leaves (Figure 5). It is worth underlining that some of the analyzed elements are known to be micro-nutrients for this riparian species. In this context, low concentrations of Cu are known to be relevant for plant growth and development, while Mn and Zn are connected to enzymatic processes, playing essential metabolic roles [8, 62-63].

The steel plant tracers (Cr, Fe, Mo, Ni and Ti), previously individuated for PM_{10}, showed their maximum concentrations in the river water samples collected at TE5 (Figure 5). On the contrary, high concentrations were not found at TE6, where high concentrations in *A. donax* washed leaves were instead found. Indeed, wastewater systems for the treatment of the effluents from cold and hot rolling sections of the steel plant are located in the southern part of the steel industry plant, at the close proximity to TE5 [64]. We can thus hypothesize that the higher concentrations of Cr, Fe, Mo, Ni and Ti at TE5 water samples are related to local disposal of steel plant wastewater in the Nera river. Due to the heavy metal hyper-accumulate ability of this riparian species [65-66], high concentrations of these steel plant tracers in washed leaves, may be then due to the influence of river water contamination. The very relevant differences at TE6 (still strongly affected by emissions from the steel plant,) underlined the lower reliability of leaves for the evaluation of the river heavy-metal contamination.

We also calculated Pearson's correlation coefficients between element concentrations detected in river water samples and washed leaves (Table 3). Correlations were in general much lower than those related to PM_{10} concentrations. The highest correlation between these two datasets was found for Cd; this result could be explained by considering the hyper-accumulate and translocation ability of *A. donax* toward Cd [67]. However, in this set of measurements, Cd showed a low variability in both river water and washed leaves (supplementary material S2; Table S2.2, S2.3) and this is reasonably the main reason of the significant correlation found. Then, the use of this riparian species seems to have a low reliability for the evaluation of the concentration in the river water.

Table 3. Pearson's correlation coefficients calculated between river water and washed leaves element concentrations. Mean monthly concentrations at each site were included in the elaboration (N=30). Positive linear correlations (Pearson's coefficient > 0.8) between the two variables are reported in red.

Pearson's	Ba	Cd	Cr	Cs	Cu	Fe	Li	Mn	Mo	Ni	Pb	Rb	Sb	Sn	Sr	Ti
Washed leaves/ River Water	0,38	0,81	0,76	0,18	0,34	0,53	-0,20	-0,55	0,17	0,71	-0,10	-0,35	0,06	-0,20	-0,44	-0,23

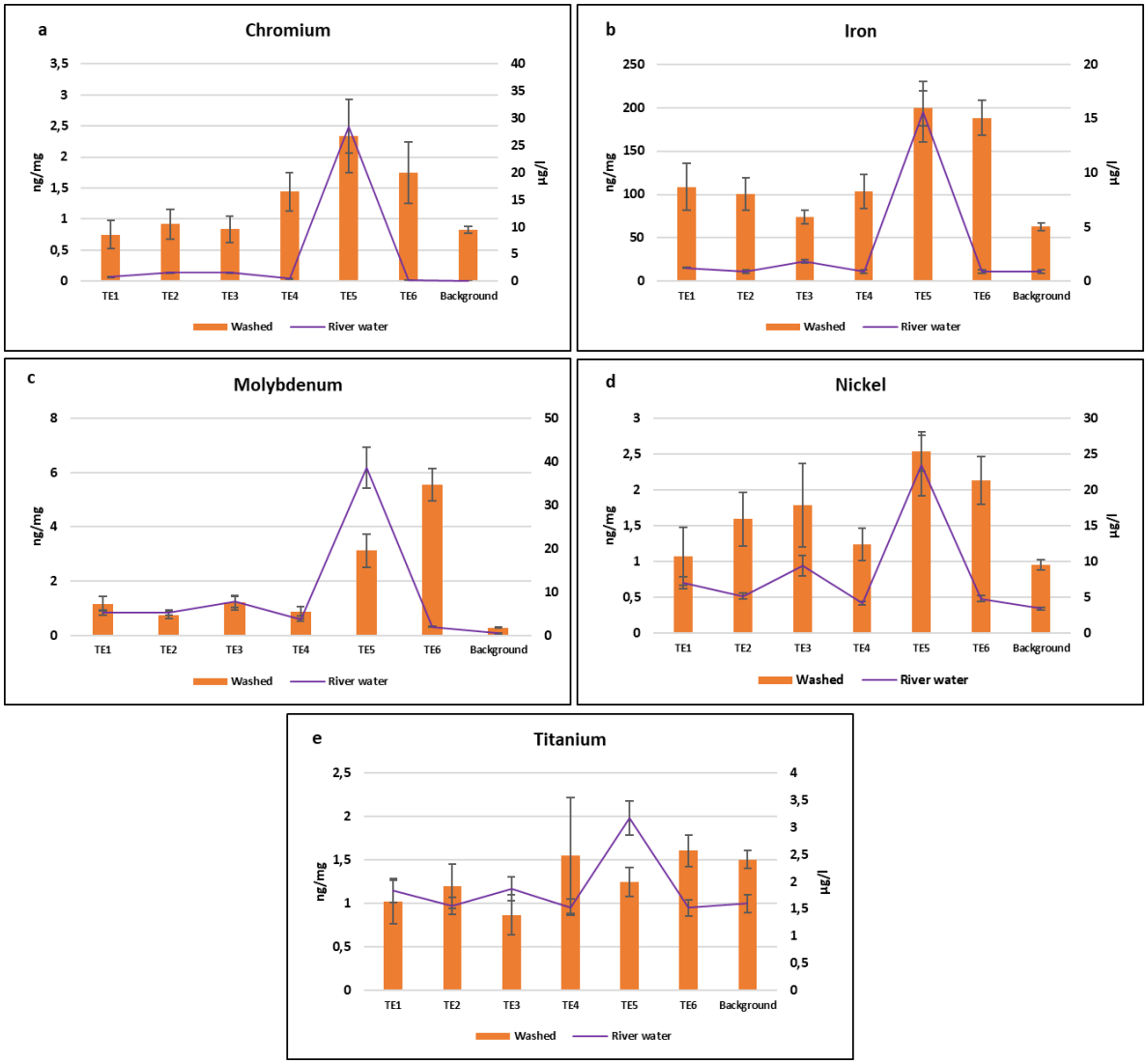

Figure 5. Comparison between averaged concentrations of Cr, Mo, Ni detected in river water samples (µg L^{-1}) and *A. donax* washed leaves (ng mg^{-1}). Standard deviations calculated between monthly concentrations are reported.

4. Conclusion

For the first time in this study, we were able to compare the different influence of PM_{10} atmospheric pollution and river contamination, acting in parallel in the study area of Terni, on the elemental content of *A. donax* leaves.

Thanks to the availability of newly developed PM_{10} samplers (HSRS), spatially-resolved element concentrations were detected in PM_{10} samples and compared to SD results. This was helpful to evaluate the

reliability of this biomonitoring approach, based on the utilization of leaves and the chemical characterization of leaf deposed PM, for the evaluation of atmospheric element concentrations. The good correlations between SD results and atmospheric PM_{10} concentrations of Cr, Fe, Ni, Mn, Zn and Ti, confirmed the reliability of these results for the evaluation of the impact related to intense local emission sources.

On the other hand, in our study washed leaves and river water element concentrations were poorly correlated, underlying a lower efficiency of this biological approach for the evaluation of the river contamination.

These preliminary results encourage further investigations on the utilization of this riparian species, largely distributed in urban areas of Italy, for future studies on PM leaf deposition. It also encourages its application as a low-cost alternative for the monitoring of atmospheric PM and its elemental components.

Supplementary Material S1.

Table S1.1. Limits of detection (LODs) of the concentrations (µg/L) detected in water samples of the analyzed elements, set at 3 times the standard deviation (SD) of 10 replicate blank determinations.

	UoM	LODs
Ba	µg/L	1.6
Cd	µg/L	0.0088
Cr	µg/L	0.24
Cs	µg/L	0.0095
Cu	µg/L	0.15
Fe	µg/L	1.8
Li	µg/L	0.011
Mn	µg/L	0.11
Mo	µg/L	0.99
Ni	µg/L	0.14
Pb	µg/L	0.02
Rb	µg/L	0.026
Sb	µg/L	0.0094
Sn	µg/L	0.043
Sr	µg/L	0.7
Ti	µg/L	0.079
Zn	µg/L	4.3

Table S1.2. Limits of detection (LODs) of the concentrations (µg/L) detected in PM_{10} samples, of the water-soluble and insoluble fraction of the analyzed elements, set at 3 times the standard deviation (SD) of 10 replicate blank determinations.

	UoM	LODs Water-soluble Fraction	LODs Insoluble Fraction
Ba	µg/L	3.7	0.44
Cd	µg/L	0.0038	0.0031
Cr	µg/L	0.081	0.86
Cs	µg/L	0.0033	0.0017
Cu	µg/L	0.2	0.24
Fe	µg/L	3	9.6
Li	µg/L	0.0063	0.004
Mn	µg/L	0.17	0.17
Mo	µg/L	0.049	0.012
Ni	µg/L	0.35	0.17
Pb	µg/L	0.1	0.15
Rb	µg/L	0.031	0.023
Sb	µg/L	0.0094	0.0094
Sn	µg/L	0.013	0.027
Sr	µg/L	0.2	0.57
Ti	µg/L	0.15	0.4
Zn	µg/L	15	47

Table S1.3. Limits of detection (LODs) of the concentrations (µg/L) detected in washed and unwashed *A. donax* leaves, of the water-soluble and insoluble fraction of the analyzed elements, set at 3 times the standard deviation (SD) of 10 replicate blank determinations.

	UoM	LODs *A. donax* leaves
Ba	µg/L	6.7
Cd	µg/L	0.33
Cr	µg/L	0.22
Cs	µg/L	0.0021
Cu	µg/L	0.12
Fe	µg/L	30
Li	µg/L	0.014
Mn	µg/L	1.1
Mo	µg/L	0.13
Ni	µg/L	0.18
Pb	µg/L	0.059
Rb	µg/L	0.028
Sb	µg/L	0.011
Sn	µg/L	0.019
Sr	µg/L	0.63
Ti	µg/L	0.47
Zn	µg/L	4.2

Supplementary Material S2.

Table S2.1. Average mean (AM) values and standard deviations of element concentrations detected in unwashed *A. donax* leaves at the six monitoring sites.

***A. donax* Unwashed Leaves Element Concentrations**													
		TE1		**TE2**		**TE3**		**TE4**		**TE5**		**TE6**	
	UoM	**AM**	**SD**	**AM**	**SD**	**AM**	**SD**	**AM**	**SD**	**AM**	**SD**	**AM**	**SD**
Ba	ng/mg	13	1.1	5	0.2	16	1.7	16	1.8	32	3.5	47	5.2
Cd	ng/mg	0.26	0.047	1.6	0.28	3.4	0.61	1.6	0.29	3.9	0.7	0.26	0.047
Cr	ng/mg	1.2	0.053	1.6	0.092	1.6	0.2	2.2	0.17	6.2	0.98	6.6	1.2
Cs	ng/mg	0.18	0.032	0.23	0.034	0.2	0.022	0.078	0.0097	0.071	0.008	0.031	0.0015
Cu	ng/mg	5.7	0.59	6.6	0.79	5.2	0.49	5.1	0.47	8.9	1.4	11	2.3
Fe	ng/mg	125	14	117	12	133	15	110	11	271	47	269	48
Li	ng/mg	0.037	0.0043	0.047	0.0067	0.053	0.0086	0.036	0.0041	0.055	0.009	0.086	0.014
Mn	ng/mg	36	3.4	26	1.9	15	0.63	51	7.1	31	2.6	128	18
Mo	ng/mg	1.2	0.15	0.87	0.073	1.3	0.15	0.94	0.085	3.9	0.77	5.7	0.97
Ni	ng/mg	1.1	0.08	1.8	0.19	1.9	0.23	1.3	0.098	3.4	0.51	4.1	0.45
Pb	ng/mg	0.2	0.033	0.15	0.012	0.18	0.027	0.35	0.063	0.3	0.042	0.33	0.053
Rb	ng/mg	30	5.6	36	4.7	33	4.2	31	6.2	25	4.1	26	4.2
Sb	ng/mg	0.021	0.0033	0.009	0.0007	0.039	0.0078	0.01	0.0007	0.009	0.0007	0.024	0.0044
Sn	ng/mg	0.053	0.0062	0.055	0.0066	0.051	0.0058	0.06	0.008	0.055	0.0066	0.058	0.0075
Sr	ng/mg	17	1.1	22	1.8	23	2	32	3.8	28	2.9	53	10
Ti	ng/mg	1.8	0.16	1.6	0.13	1.5	0.12	1.7	0.15	2.7	0.39	3.8	0.42
Zn	ng/mg	26	4	36	7.5	34	6.9	27	4.2	36	4	51	10

Table S2.2. Average mean (AM) values and standard deviations (SD) of element concentrations detected in washed *A. donax* leaves at the six monitoring sites.

***A. donax* Washed Leaves Element Concentrations**													
		TE1		**TE2**		**TE3**		**TE4**		**TE5**		**TE6**	
	UoM	**AM**	**SD**	**AM**	**SD**	**AM**	**SD**	**AM**	**SD**	**AM**	**SD**	**AM**	**SD**
Ba	ng/mg	5.3	0.22	5.4	0.22	5.3	0.21	16	2	31	4.3	46	6.9
Cd	ng/mg	0.26	0.047	1.1	0.21	3.3	0.59	1.6	0.29	3.8	0.68	0.26	0.046
Cr	ng/mg	0.75	0.051	0.92	0.077	0.84	0.063	1.4	0.19	2.3	0.49	1.7	0.19
Cs	ng/mg	0.16	0.029	0.21	0.036	0.16	0.027	0.078	0.04	0.069	0.0084	0.022	0.0008
Cu	ng/mg	5.2	0.55	6.5	0.85	5.1	0.53	4.5	0.4	7.4	1.1	8.7	1.5
Fe	ng/mg	109	14	100	12	74	6.4	103	12	199	20	188	42
Li	ng/mg	0.026	0.0028	0.029	0.0035	0.03	0.0038	0.033	0.0046	0.045	0.0088	0.062	0.01
Mn	ng/mg	35	3.4	24	1.7	14	0.53	48	6.7	27	2	121	17
Mo	ng/mg	1.2	0.14	0.74	0.058	1.2	0.15	0.88	0.081	3.1	0.56	5.6	0.72
Ni	ng/mg	1.1	0.093	1.6	0.2	1.8	0.26	1.2	0.12	2.5	0.25	2.1	0.36
Pb	ng/mg	0.14	0.022	0.047	0.0025	0.18	0.036	0.13	0.021	0.29	0.038	0.25	0.045
Rb	ng/mg	29	5.4	36	4.6	34	4.1	30	6	25	4	25	4.2
Sb	ng/mg	0.02	0.003	0.009	0.001	0.0089	0.001	0.0093	0.0011	0.0092	0.0011	0.0089	0.001
Sn	ng/mg	0.016	0.0013	0.015	0.0013	0.017	0.0012	0.048	0.0076	0.017	0.0013	0.016	0.0012
Sr	ng/mg	16	0.99	18	1.3	15	0.93	31	3.9	27	3	52	5.2
Ti	ng/mg	1	0.089	1.2	0.12	0.87	0.065	1.5	0.21	1.2	0.13	1.6	0.22
Zn	ng/mg	26	4.1	35	3.8	22	2.9	26	4.3	35	4.3	51	6.1

Table S2.3. OK (ordinary kriging) interpolated concentrations of water-soluble fraction of atmospheric elements at the six monitoring sites.

Water-soluble Interpolated Atmospheric Element Concentrations							
	UoM	**TE1**	**TE2**	**TE3**	**TE4**	**TE5**	**TE6**
Ba	ng/m^3	6.1	4.7	4.1	4.7	5.3	4.8
Cd	ng/m^3	0.03	0.047	0.052	0.032	0.039	0.05
Cr	ng/m^3	0.88	1.3	2	1.1	1.9	1.9
Cs	ng/m^3	0.012	0.017	0.017	0.015	0.015	0.016
Cu	ng/m^3	2.5	2.6	2.7	1.5	2.5	1.9
Fe	ng/m^3	9.8	11	10	7.5	9.9	12
Li	ng/m^3	0.059	0.088	0.12	0.085	0.11	0.12
Mn	ng/m^3	4.2	4.3	2.6	3.8	4.8	5.6
Mo	ng/m^3	2.3	3.0	2.4	4.8	14	11
Ni	ng/m^3	0.92	0.81	1.2	0.68	1.1	1.7
Pb	ng/m^3	0.32	0.41	0.42	0.4	0.29	0.36
Rb	ng/m^3	0.34	0.43	0.4	0.3	0.36	0.37
Sb	ng/m^3	0.45	0.35	0.26	0.51	0.31	0.29
Sn	ng/m^3	0.25	0.16	0.18	0.15	0.16	0.17
Sr	ng/m^3	1.7	2.1	1.4	1.7	1.9	1.8
Ti	ng/m^3	0.08	0.091	0.12	0.089	0.1	0.13
Zn	ng/m^3	13	14	21	13	16	18

Table S2.4. OK (ordinary kriging) interpolated concentrations of insoluble fraction of atmospheric elements at the six monitoring sites.

Insoluble Interpolated Atmospheric Element Concentrations							
	UoM	**TE1**	**TE2**	**TE3**	**TE4**	**TE5**	**TE6**
Ba	ng/m³	7.3	6.9	4.9	6.2	6.5	4
Cd	ng/m³	0.006	0.022	0.016	0.021	0.025	0.026
Cr	ng/m³	13	14	30	12	45	48
Cs	ng/m³	0.021	0.03	0.035	0.025	0.031	0.032
Cu	ng/m³	8.9	7.3	9.3	4.7	11	6.6
Fe	ng/m³	351	344	577	218	332	504
Li	ng/m³	0.12	0.1	0.15	0.087	0.15	0.1
Mn	ng/m³	6.3	7.1	3.5	5.3	11	14
Mo	ng/m³	0.8	1.3	1.4	0.96	2.1	4.1
Ni	ng/m³	4.8	6.3	4.3	3.4	19	23
Pb	ng/m³	3	3.3	4.6	3	4.5	3.4
Rb	ng/m³	0.45	0.32	0.43	0.16	0.44	0.3
Sb	ng/m³	0.66	0.4	0.3	0.64	0.73	0.25
Sn	ng/m³	2	1.7	2.1	0.85	2.3	1
Sr	ng/m³	1.2	1.4	1	2.4	2.3	1.3
Ti	ng/m³	4.5	4.3	7.1	3.6	7.1	8
Zn	ng/m³	30	32	57	26	40	34

Table S2.5. Average mean (AM) values and standard deviations of element concentrations detected in river water samples at the six monitoring sites.

River Water Element Concentrations													
		TE1		**TE2**		**TE3**		**TE4**		**TE5**		**TE6**	
	UoM	**AM**	**SD**	**AM**	**SD**	**AM**	**SD**	**AM**	**SD**	**AM**	**SD**	**AM**	**SD**
Ba	µg/l	96	11.2	66	5.3	71	6.0	60	4.3	95	11	86	9.0
Cd	µg/l	0.012	0.00057	0.013	0.00065	0.019	0.0014	0.033	0.0042	0.036	0.0050	0.034	0.0044
Cr	µg/l	0.84	0.022	1.56	0.077	1.61	0.082	0.53	0.0089	28	5.4	0.30	0.0028
Cs	µg/l	0.15	0.016	0.14	0.014	0.20	0.028	0.10	0.0068	0.24	0.038	0.11	0.0077
Cu	µg/l	1.4	0.19	0.84	0.065	1.4	0.18	0.93	0.079	2.15	0.42	1.28	0.15
Fe	µg/l	1.2	0.068	1.9	0.16	1.9	0.16	1.9	0.17	16	2.8	1.9	0.17
Li	µg/l	6.3	1.1	4.9	0.65	7.2	1.4	5.4	0.79	7.9	0.87	4.7	0.6
Mn	µg/l	0.12	0.014	0.13	0.014	0.13	0.014	0.057	0.0028	0.14	0.016	0.12	0.013
Mo	µg/l	5.2	0.59	5.2	0.59	7.8	1.3	3.6	0.28	39	4.6	2.0	0.087
Ni	µg/l	7.1	0.83	5.2	0.45	9.4	1.5	4.2	0.29	23	4.2	4.9	0.39
Pb	µg/l	0.14	0.017	0.035	0.0029	0.053	0.0066	0.037	0.0032	0.029	0.0019	0.037	0.0032
Rb	µg/l	3.3	0.56	1.7	0.15	2.3	0.27	1.8	0.16	2.6	0.35	2.0	0.20
Sb	µg/l	0.094	0.016	0.055	0.0054	0.091	0.015	0.051	0.0047	0.19	0.026	0.055	0.0055
Sn	µg/l	0.20	0.028	0.23	0.030	0.0094	0.00020	0.012	0.00035	0.024	0.0013	0.053	0.0064
Sr	µg/l	978	172	859	133	1084	211	904	147	986	175	900	146
Ti	µg/l	1.8	0.22	1.6	0.15	1.9	0.22	1.5	0.15	3.2	0.32	1.5	0.15
Zn	µg/l	4.4	0.18	4.4	0.017	5.4	0.26	4.5	0.18	5.3	0.26	4.3	0.17

Acknowledgments

This work was funded by the project 2017 RG11715C7C8801CF (Principal Investigator Dr. S. Canepari) and the project 2018 AR1181641E22B570 (Principal Investigator Dr. L. Massimi) financed by Sapienza University of Rome.

The authors gratefully thank FAI Instruments (Fonte Nuova, Rome, Italy), the citizens of Terni and the Terni district of ARPA Umbria (regional agency for environmental protection), with special regard to Giancarlo Caiello, Caterina Austeri and Marco Pompei, for the support in the installation and management of the sampling equipment as well as for the help in the choice of the sampling sites and Iqra Javed for providing language help.

Author Contributions: S. Canepari and L. Massimi conceived and planned the monitoring and the experiments; M. Ristorini and L. Massimi performed the samplings; M. L. Astolfi and L. Massimi performed the chemical analyses; M. Ristorini and L. Massimi elaborated the data; M. Ristorini wrote the manuscript; S. Canepari and L. Massimi coordinated the group and supervised the manuscript.

Conflicts of Interest: The authors declare no conflicts of interest.

References

Perdue: R. E. Arundo donax—Source of musical reeds and industrial cellulose 1958, Econ Bot, 12: 368. https://doi.org/10.1007/BF02860024

Bell, G. P. Ecology and management of Arundo donax, and approaches to riparian habitat restoration in Southern California 1997, Plant Invasions: studies from North America and Europe, pp. 103-113.

Papazoglou, E. G.; Karantounias, G. A.; Vemmos S. N.; Bouranis, D. L. Photosynthesis and growth responses of giant reed (Arundo donax L.) to the heavy metals Cd and Ni 2005, Environ. Int. 31(2), 243-249. https://doi.org/10.1016/j.envint.2004.09.022

Nsanganwimana, F.; Marchand, L.; Douay, F.; Mench, M. Arundo donax L., a candidate for phytomanaging water and soils contaminated by trace elements and producing plant-based feedstock. A review 2014, Int J Phytoremediation 16, 982–1017. DOI: 10.1080/15226514.2013.810580

Bonanno, G. Comparative performance of trace element bioaccumulation and biomonitoring in the plant species Typha domingensis, Phragmites australis and Arundo donax 2013, Ecotoxicol. Environ. Saf. 97, 124-130. https://doi.org/10.1016/j.ecoenv.2013.07.017

Bonanno, G.; Borg, J. A.; Di Martino, V. Levels of heavy metals in wetland and marine vascular plants and their biomonitoring potential: A comparative assessment 2017, Sci. Total Environ. 576, 796-806. https://doi.org/10.1016/j.scitotenv.2016.10.171

Fiorentino, N.; Ventorino, V.; Rocco, C.; Cenvinzo, V.; Agrelli, D.; Gioia, L.; Di Mola, L.; Adamo, P.; Pepe, O.; Fagnano, M. Giant reed growth and effects on soil biological fertility in assisted phytoremediation of an industrial polluted soil 2017, Sci. Total Environ. 575, 1375-1383. https://doi.org/10.1016/j.scitotenv.2016.09.220

Bonanno, G. Arundo donax as a potential biomonitor of trace element contamination in water and sediment 2012, Ecotoxicol. Environ. Saf. 80, 20–27. doi:10.1016/j.ecoenv.2012.02.005

Szczepaniak, K.; Biziuk, M. Review: Ecotoxicology, Aspects of the biomonitoring studies using mosses and lichens as indicators of metal pollution 2003, Environ. Res 93, 221–230. doi:10.1016/S0013-9351(03)00141-5

Abril, G. A.; Wannaz, E. D.; Mateos, A. C.; Pignata, M. L. Biomonitoring of airborne particulate matter emitted from a cement plant and comparison with dispersion modelling results 2014 Atmos. Environ. 8, 154-163, https://doi.org/10.1016/j.atmosenv.2013.10.020

Massimi, L.; Conti, M. E.; Mele, G.; Ristorini, M.; Astolfi, M. L.; Canepari, S. Lichen Transplants as Indicators of Atmospheric Element Concentrations: a High Spatial Resolution Comparison with PM10 Samples in a Polluted Area (Central Italy) 2019, Ecol. Indic. 101, 759-769. DOI: 10.1016/j.ecolind.2018.12.051

Urbat, M.; Lehndorff, E.; Schwark, L., Biomonitoring of air quality in the Cologne conurbation using pine needles as a passive sampler—Part I: magnetic properties 2004, Atmos. Environ. 38 (23), 3781-3792 https://doi.org/10.1016/j.atmosenv.2004.03.061

Lin, V. S. Research highlights: natural passive samplers – plants as biomonitors 2015. Environ. Sci.: Processes Impacts 17, 1137-1140. DOI: 10.1039/C5EM90016F

Sgrigna, G.; Baldacchini, C.; Esposito, R.; Calandrelli, R.; Tiwary, A.; Calfapietra, C. Characterization of leaf-level particulate matter for an industrial city using electron microscopy and X-ray microanalysis 2016, Sci Total Environ 548–549, 91–99. http://dx.doi.org/10.1016/j.scitotenv.2016.01.057

Janhall, S. Review on urban vegetation and particle air pollution e Deposition and dispersion 2015, Atmos. Environ. 105, 130-137. http://dx.doi.org/10.1016/j.atmosenv.2015.01.052

Gratani, L.; Crescente, M. F.; Varone L. Long-term monitoring of metal pollution by urban trees 2008, Atmos. Environ. 42, 8273–8277, doi:10.1016/j.atmosenv.2008.07.032.

Baldacchini, C.; Sgrigna, G.; Clarke, W.; Tallis, M.; Calfapietra, C. An ultra-spatially resolved method to quali-quantitative monitor particulate matter in urban environment 2019, Environ Sci Pollut Res Int. 26 (18), 18719-18729. doi: 10.1007/s11356-019-05160-8.

Thorpe, A.; Harrison, R. M., Sources and properties of non-exhaust particulate matter from road traffic: A review 2008, Sci. Total Environ. 400 270-282. doi:10.1016/j.scitotenv.2008.06.007

Slezakova, K.; Pires, J. C. M.; Pereira, M. C.; Martins, F. G.; Alvim-Ferraz, M. C. Influence of traffic emissions on the composition of atmospheric particles of different sizes—Part 2: SEM–EDS characterization 2008, J. Atmos. Chem. 60 (3), 221–236. https://doi.org/10.1007/s10874-008-9117-y

Pope III, C. A.; Burnett, R. T.; Thun, M. J.; Calle, E. E.; Krewski, D.; Ito, K.; Thurston, G. D. Lung cancer, cardiopulmonary mortality, and long-term exposure to fine particulate air pollution 2002, Jama, 287(9), 1132-1141.

Ebelt, S.T.; Petkau, A.J.; Vedal, S.; Fisher, T.V.; Brauer, M. Exposure of chronic obstructive pulmonary disease patients to particulate matter: relationships between personal and ambient air concentrations 2000, Journal of the Air and Waste Management Association 50 (7), 1081–1094.

Chen, L. C.; Lippmann, M. Effects of Metals within Ambient Air Particulate Matter (PM) on Human Health 2009, Inhal. Toxicol. 21(1), 1-31, DOI: 10.1080/08958370802105405

Anderson, J. O.; Thundiyil, J. G.; Stolbach, A. Clearing the Air: A Review of the Effects of Particulate Matter Air Pollution on Human Health 2012, J. Med. Toxicol. 8, 166–175 DOI 10.1007/s13181-011-0203-1

Pope III, C. A.; Dockery, D. W. Acute Health Effects of PM10 Pollution on Symptomatic and Asymptomatic Children 1992, AJRCCM Issues 145 (5). https://doi.org/10.1164/ajrccm/145.5.1123

Donaldson, K.; MacNee, W. Potential mechanisms of adverse pulmonary and cardiovascular effects of particulate air pollution (PM10) 2010, Int. J. Hyg. Environ. Health 203 (5-6), 411-415. https://doi.org/10.1078/1438-4639-00059

Sæbø, A.; Popek, R.; Nawrot, B.; Hanslin, H.M.; Gawronska, H.; Gawronski, S.W.; Plant species differences in particulate matter accumulation on leaf surfaces 2012, Sci Total Environ 427–428, 347–354. doi:10.1016/j.scitotenv.2012.03.084

Petroff, A.; Mailliat, A.; Amielh, M.; Anselmet, F.; Aerosol dry deposition on vegetative canopies. Part I: Review of present knowledge 2008, Atmos. Environ. 42, 3625–3653. doi:10.1016/j.atmosenv.2007.09.043

Terzaghi, E.; Wild, E.; Zacchello, G.; Cerabolini, B. E. L.; Jones, K. C.; Di Guardo, A. Forest Filter Effect: Role of leaves in capturing/releasing air particulate matter and its associated PAHs 2013, Atmos. Environ. 74, 378-384. https://doi.org/10.1016/j.atmosenv.2013.04.013

Hofman, J.; Wuyts, K.; Van Wittenberghe, S.; Brackx, M.; Samson, R. On the link between biomagnetic monitoring and leaf-deposited dust load of urban trees: Relationships and spatial variability of different particle size fractions 2014, Environ. Poll. 189, 63-72. https://doi.org/10.1016/j.envpol.2014.02.020

Sgrigna, G.; Sæbø, A.; Gawronski, S.; Popek, R.; Calfapietra, C. Particulate matter deposition on Quercus ilex leaves in an industrial city of central Italy 2015, Environ. Pollut. 197, 187–194. http://dx.doi.org/10.1016/j.envpol.2014.11.030

Massimi, L.; Ristorini, M.; Eusebio, M.; Florendo, D.; Adeyemo, A.; Brugnoli, D.; Canepari, S. Monitoring and evaluation of Terni (Central Italy) air quality through spatially resolved analyses 2017, Atmosphere 8(10), 200. doi:10.3390/atmos8100200

Moroni, B.; Ferrero, L.; Crocchianti, S.; Perrone, M. G.; Sangiorgi, G.; Bolzacchini, E.; Cappelletti, D. Aerosol dynamics upon Terni basin (Central Italy): results of integrated vertical profile measurements and electron microscopy analyses 2013, Rendiconti Lincei 24 (4) 319–328. doi: 10.1007/s12210-013-0230-8

Manigrasso, M.; Protano, C.; Astolfi, M. L.; Massimi, L.; Avino, P.; Vitali, M.; Canepari, S. Evidences of copper nanoparticle exposure in indoor environments: Long-term assessment, high-resolution field emission scanning electron microscopy evaluation, in silico respiratory dosimetry study and possible health implications 2017, Sci Total Environ 653, 1192-1203. https://doi.org/10.1016/j.scitotenv.2018.11.044

Zona. A.; Pasetto, R.; Fazzo, L.; Iavarone, I.; Bruno, C.; Pirastu, R.; Comba, P. Fifth report S.E.N.T.I.E.R.I 2019, Epidemiologia & Prevenzione, Rivista dell'Associazione italiana di epidemiologia 2-3, 43, Supplement 1, http://www.epiprev.it/materiali/2019/EP2-3_Suppl1/SENTIERI_FullText.pdf

https://www.arpa.umbria.it/monitoraggi/aria/Default.aspx

APHA, (1998) Standard methods for examination of water and waste water (20th. Ed.). Washington DC: American Public Health Association

Canepari, S.; Cardarelli, E.; Giuliano, A.; Pietrodangelo, A. Determination of metals, metalloids and non-volatile ions in airborne particulate matter by a new two-step sequential leaching procedure Part A: Experimental design and optimization 2006, Talanta 69, 581–587. doi:10.1016/j.talanta.2005.10.023

Canepari, S.; Cardarelli, E.; Pietrodangelo, A.; Strincone, M. Determination of metals, metalloids and non-volatile ions in airborne particulate matter by a new two-step sequential leaching procedure Part B: Validation on equivalent real samples 2006, Talanta 69, 588–595. doi:10.1016/j.talanta.2005.10.024

Canepari, S.; Pietrodangelo, A.; Perrino, C.; Astolfi, M. L.; Marzo, M. L. Enhancement of source traceability of atmospheric PM by elemental chemical fractionation 2009, Atmos. Environ. 43 (31), 4754-4765. https://doi.org/10.1016/j.atmosenv.2008.09.059

Piacentini, D.; Falasca, G.; Canepari, S.; Massimi, L. Potential of PM-selected components to induce oxidative stress and root system alteration in a plant model organism 2019, Environ. Int. 132, 105094. https://doi.org/10.1016/j.envint.2019.105094

Astolfi, M. L.; Marconi, E.; Protano, C.; Vitali, M.; Schiavi, E.; Mastromarino, P.; Canepari, S. Optimization and validation of a fast digestion method for the determination of major and trace elements in breast milk by ICP-MS 2018, Anal. Chim. Acta 1040, 49-62. https://doi.org/10.1016/j.aca.2018.07.037

Cressie, N. Spatial Prediction and Ordinary Kriging 1988, Math. Geol. 20 (4), 405–421. https://doi.org/10.1007/BF00892986

Cressie, N. The origins of kriging 1990, Math. Geol. 22 (3),239–252. https://doi.org/10.1007/BF00889887

Blair, M.; Stevens, T.L. Steel Castings Handbook, 6th ed.; Steel Founders' Society and ASM International: Novelty, OH, USA, 1995; pp. 2–34.

Adachi, K.; Tainosho, Y. Characterization of heavy metal particles embedded in tire dust 2004, Environ. Int. 30 (8), 1009-1017. https://doi.org/10.1016/j.envint.2004.04.004

Birmili, W.; Allen, A. G.; Bary, F.; Harrison, R. M. Trace Metal Concentrations and Water Solubility in Size-Fractionated Atmospheric Particles and Influence of Road Traffic 2006, Environ. Sci. Technol. 40, 1144-1153. DOI: 10.1021/es0486925

Litschke, T.; Kuttler, W. On the reduction of urban particle concentration by vegetation – a review 2008, Meteorol. Z. 17, (3), 229-240. DOI: 10.1127/0941-2948/2008/0284

Morakinyo, T. E.; Lam, Y. F. Simulation study of dispersion and removal of particulate matter from traffic by road-side vegetation barrier 2016, Environ Sci Pollut Res 23, 6709–6722. DOI 10.1007/s11356-015-5839-y.

Umbrìa, A.; Galan, M.; Munoz, M.J.; Martìn, R. Characterization of atmospheric particles: analysis of particles in the Campo de Gibraltar 2004, Atmosfera 17 (4), 191-206. ISSN 0187-6236.

Bouhsina, S.; Cazier, F.; Noual, H.; Dewaele, D.; Delbende A.; Courcot, D.; Aboukais, A. Characteristics of suspended particulate matter emitted from an iron and steel company – A multi technique approach for search of tracers 2008, Chem. Eng. Trans. 16:79.

Tunno, B. J.; Dalton, R.; Michanowicz, D. R.; Shmool, J. L. C.; Kinnee, E.; Tripathy, S.; Cambal, L.; Clougherty, J. E. Spatial patterning in PM2.5 constituents under an inversion-focused sampling design across an urban area of complex terrain 2016, J Expo Sci Environ Epidemiol 26, 385–396. doi:10.1038/jes.2015.59

Thurston, G. D.; Ito, K.; Lall, R. A source apportionment of U.S. fine particulate matter air pollution 2011, Atmos. Environ. 45 (24) 3924-3936. https://doi.org/10.1016/j.atmosenv.2011.04.070

Song, F.; Gao, Y. Size distributions of trace elements associated with ambient particular matter in the affinity of a major highway in the New Jersey–New York metropolitan area 2011, Atmospheric Environ. 45 (37), 6714-6723. https://doi.org/10.1016/j.atmosenv.2011.08.031

Canepari, S.; Perrino, C.; Olivieri, F.; Astolfi, M. L. Characterisation of the traffic sources of PM through size-segregated sampling, sequential leaching and ICP analysis 2008, Atmospheric Environ. 42(35), 8161-8175. https://doi.org/10.1016/j.atmosenv.2008.07.052

Shakoor, S. A.; Soodan, A. M.; Kumar, K. Morphological Diversity and Frequency of Phytolith Types in Gaint Reed Arundo donax (L.) 2014, World Appl. Sci. J. 29 (7) 926-932. DOI: 10.5829/idosi.wasj.2014.29.07.14

Simonetti, G.; Buiarelli, F.; Di Filippo, P.; Pomata, D.; Riccardi, C.; Ristorini, M.; Astolfi, M. L.; Canepari, S. Spatial Distribution of Levoglucosan and Alternative Biomass Burning Tracers in an Urban and Industrial Hot-spot of Central Italy, ATMOSRES- paper under review

Minguillón, M. C.; Querol, X.; Baltensperger, U.; Prévôt, A. S. H. Fine and coarse PM composition and sources in rural and urban sites in Switzerland: Local or regional pollution? 2012, Sci Total Environ 427–428, 191-202. https://doi.org/10.1016/j.scitotenv.2012.04.030

Gietl, J. K.; Lawrence, L.; Thorpe, A., J.; Harrison, R. M. Identification of brake wear particles and derivation of a quantitative tracer for brake dust at a major road 2010, Atmos. Environ. 44 (2), 141-146. https://doi.org/10.1016/j.atmosenv.2009.10.016

Dongarrà, G.; Manno, E.; Varrica, D. Possible markers of traffic-related emissions 2008, Environ. Monit. Assess. 154:117. https://doi.org/10.1007/s10661-008-0382-7

Mirza, N.; Pervez, A.; Mahmood, Q.; Shah, M. M.; Shafqat, M. N. Ecological restoration of arsenic contaminated soil by Arundo donax L 2011, Ecol. Eng. 37, 1949– 1956. doi:10.1016/j.ecoleng.2011.07.006

Barbosa, B.; Boléo, S.; Sidella, S.; Costa, J.; Duarte, M.; Mendes, B.; Cosentino, S. L.; Fernando A. L. Phytoremediation of Heavy Metal-Contaminated Soils Using the Perennial Energy Crops Miscanthus spp. and Arundo donax L. 2015, Bioenerg. Res. 8, 1500–1511. DOI 10.1007/s12155-015-9688-9

Carranza-Álvarez, C.; Alonso-Castro, A. J.; Alfaro-De La Torre, M. C; García-De La Cruz, R. F. Accumulation and Distribution of Heavy Metals in Scirpus americanus and Typha latifolia from an Artificial Lagoon in San Luis Potosí, México 2007, Water Air Soil Pollut. 188, 297–309. DOI 10.1007/s11270-007-9545-3

Kabata-Pendias, A.; Mukherjee, A. B. Trace Elements from Soil to Human 2007, Springer. ISBN 978-3-540-32714-1

Capelli, L.; Sironi, S.; Del Rosso, R.; Céntola, P.; Rossi, A.; Austeri, C. Olfactometric approach for the evaluation of citizens' exposure to industrial emissions in the city of Terni, Italy 2011, Sci. Total Environ. 409 (3), 595-603. https://doi.org/10.1016/j.scitotenv.2010.10.054

Sabeen, M.; Mahmood, Q.; Irshad, M.; Fareed, I.; Khan, A.; Ullah, F.; Hussain, J.; Hayat, Y.; Tabassum S. Cadmium Phytoremediation by Arundo donax L. from Contaminated Soil and Water 2013, BioMed Research International, 9 pages http://dx.doi.org/10.1155/2013/324830

Atma, W.; Larouci, M.; Meddah, B.; Benabdeli, K.; Sonnet, P. Evaluation of the phytoremediation potential of Arundo donax L. for nickel-contaminated soil 2017, Int J Phytoremediat 19 (4), 377-386, DOI:10.1080/15226514.2016.1225291

Fiorentino, N.; Fagnano, M.; Adamo, P.; Impagliazzo, A.; Mori, M.; Pepe, O.; Ventorino, V.; Zoina, A. Assisted phytoextraction of heavy metals: compost and Trichoderma effects on giant reed (Arundo donax L.) uptake and soil N-cycle microflora 2013, Italian J. Agronomy 8, 244-254. doi:10.4081/ija.2013.e29

5. Nature-based solutions and air quality regulation

The umbrella concept of **Nature-based solutions** (**NbS**) is defined as cost-effective solutions that are inspired and supported by nature, providing simultaneously environmental, social and economic benefits. This concept includes several solutions, varying from greening of grey surfaces, afforestation, urban parks, and street trees.

The design, implementation, and maintenance of NbS in highly anthropized areas, such as cities, industrial and post-industrial sites, is related to the potential provision of **ecosystem services** (**ES**), thus comprising all the benefits that human can derive from nature.

To our interest, and among the different ESs, vegetation can certainly play an important role in improving air quality, through the removal of gaseous pollutants via stomatal uptake and particulate ones mainly via **dry** and **wet deposition**. However, the provision of these air-quality related ESs is affected by several factors, which are connected to the specific urban context, the NbS type and species-specific functional traits of the vegetation. Therefore, being able to properly evaluate the affinity of NbS and plants species involved in their implementation is certainly important to evaluate their efficiency and to increase the comparability between different solutions. Moreover, and through a proper evaluation, it is also possible to provide relevant information which can be used at any stage of the NbS implementation, from design to management of new and to-be implemented solutions, which are expected to be more and more efficient. To date, most of the evaluation attempts have focused only on single NbSs or ES, thus lacking a comprehensive and integrated evaluation of the simultaneous and cross-cutting provision of co-benefits.

The NbS implementation is also connected to the **biomonitoring** concept and to the fact that these solutions may be used themselves as low-cost and alternative monitoring stations able to provide information on the environmental quality of the areas where they are implemented. NbS can act as living laboratories where additional environmental monitoring procedures can be carried out. Few examples of the potential application of the NbS concept as **biomonitoring tool** are described and reported in a published book chapter, together with a detailed description of some of the main methodologies and key indicators used for the evaluation of their provision of air quality, soil and water related ESs (A3).

In this PhD project, the evaluation of the efficiency of a specific NbS, a renatured landfill in the city of Dortmund, towards the provision of air-quality and carbon related ESs is described (A4). Specifically, the species-specific affinity of tree species planted within this NbS, towards the removal via leaf deposition of atmospheric PM is evaluated by means of **SEM/EDX leaf microanalysis**, with details on number density, elemental composition, and weight of removed particles. These

experimental results are then integrated with the ones obtained by the application of the ***i-Tree eco* model**, one of the most used for the evaluation of ES provided by the vegetation. The *i-Tree eco* model is also employed for the species-specific modelling of the removal of typically urban gaseous pollutants (SO_2, NO_2 and O_3), together with the modelling of the species-specific carbon mitigation potential. SEM/EDX $PM_{2.5}$ results are then compared with the modelled ones, to evaluate the efficiency of the two approaches, both the experimental and the modelled one and to highlight their potential limitations.

Within the context of the **Horizon 2020 project – ProGIreg**, the atmospheric PM abatement of specific NbSs is evaluated again through the application of SEM/EDX leaf microanalysis, as a function of plant species and size fraction of PM. In this PhD project, preliminary results related to three NbSs are presented, a renatured lake shore in the city of Ningbo (China), an urban forest and productive gardens in the city of Turin (Italy). Specifically for the two Turin NbSs, PM leaf deposition results are integrated with data retrieved from the chemical fractionation of PM_{10} membrane filters sampled at high proximity from each NbS, to identify and evaluate the impact of PM emission acting in the study area.

5.1 (A3) Nature-Based Solutions as Tools for Monitoring the Abiotic and Biotic Factors in Urban Ecosystems

In: Catalano C., Andreucci M. B., Guarino R., Bretzel F., Leone M., Pasta S. (eds) Urban Services to Ecosystems. Future City, 17. Springer, doi: 10.1007/978-3-030-75929-2_7

Federica Larcher[1], Chiara Baldacchini[2,3], Chiara Ferracini[1], Monica Vercelli[1], Martina Ristorini[4], Luca Battisti[1], and Carlo Calfapietra[3]

[1] Department of Agricultural, Forest and Food Sciences, University of Turin, Turin, Italy
[2] Department of Ecological and Biological Sciences, University of Tuscia, Viterbo, Italy
[3] Research Institute on Terrestrial Ecosystems (IRET), Headquarter of Porano, Italian National Research Council (CNR), Terni, Italy
[4] Department of Bioscience and Territory, University of Molise, Campobasso, Italy

Abstract Nature-based solutions (NBS) include a wide spectrum of situations: natural and seminatural green spaces, urban forests, designed gardens and parks, green road lines and roundabouts, bio-swales, productive gardens, green roofs and walls. In each site, the challenge is to provide the best solution according to the environmental and cultural context and the citizens' demand. The urban horticulture in synergy with NBS provides to design, realise and manage green solutions for specific problems in the urban context. NBS supplies actions able to improve urban resilience and many opportunities for improving urban quality, optimising the delivering of a mixed range of ecosystem services (ES). This chapter highlights that NBS can be used for monitoring, soil, air and water quality, water matrices and pollinator diversity. We therefore describe methods for monitoring the quality of soil, air, water matrices and pollinator diversity and abundance. In conclusion, we point out some key aspects, under an interdisciplinary perspective, in order to promote further and deeper knowledge in the application of NBS in the urban environments.

Keywords Air quality · Water quality · Soil fertility · Pollinators · Urban horticulture

7.1 Introduction

The International Union for the Conservation of Nature (IUCN 2020) considers nature-based solutions (NBS) as an umbrella concept for ecosystem-related approaches. NBS can be adopted especially in urban ecosystems that are altered and complex systems designed to mainly provide citizens with a range of economic and social services, rather than ecosystem services (Melles 2005). NBS address several societal challenges, contributing to green growth, improving human well-being and economic opportunities and creating ecologically, economically and socially resilient cities (van den Bosch and Sang 2017; Keesstra et al. 2018). Specifically, NBS

can be a tool for combining biological information with planning methodologies (Pickett et al. 2004) in order to provide a pleasant environment for local residents and to protect the downstream environment. With regard to the benefits for wildlife and living organisms, NBS can maintain or increase the level of genetic, biological, habitat and landscape diversity in cities,
often higher than in several seminatural or rural areas out of the urban context (Savard et al. 2000; Niemelä 1999). This colonisation, which involves pollinators as well, is also related to the presence of different green areas with a rich variety of flowers and trees in the urbanised environment. Regarding human well-being, NBS are strictly linked to the concept of ecosystem
services (ES). ES have been framed into four different categories: provisioning (food, timber, fresh water), regulating (air quality regulation, pollination, pest control and climate control), cultural (psychological and cognitive benefits, sense of place, aesthetic value, tourism) and supporting (biogeochemistry, nutrient cycling) (MEA 2005; TEEB 2011). The ES concept, strongly anthropocentric (Hunter et al. 2014), was mainly based on economic and ecological disciplines (Chaudhary et al. 2015), but research in this area has considerably evolved. The supply/demand balance of ES was previously poorly considered (Baró et al. 2015). In addition, citizens do not always directly benefit from urban nature, but sometimes there is a disservice, considered as damages, costs and negative effects of nature on human well-being (e.g. allergies, human and plant pathogens, greenhouse gasses emission) derived from processes and functions of urban ecosystems (Shapiro and Báldi 2014; Shackleton et al. 2016). Specific applications of NBS could reduce such disservices supporting synergies among ES. The extreme selective pressures exerted by human environmental changes suggest that the evolution of urban ecosystems is likely to be the evolution under unbalanced conditions in rapidly changing environments (Collins et al. 2000). The NBS concept supplies actions able to improve urban resilience, intended as the ability of a system to return to a previous or improved set of dynamics following a shock, strengthening the ability of a city to mitigate, adapt and recover from internal and external stresses (United Nations Conferences on Housing and Sustainable Urban Development 2017). The way in which an urban ecosystem recovers from a disturbing event can be drastically or positively influenced by human intervention. NBS have an integrative and systemic approach and include the experience of several stakeholders, so that positive actions contribute to achieving all dimensions of sustainability (Nesshöver et al. 2017). Urban greening represents a specific kind of NBS, facing the challenge of climate change adaptation and improving human well-being through the supply of ES (Panno et al. 2017). In the next paragraphs, some specific characteristics of NBS in urban areas are analysed. In particular, the topics of environmental and ecological monitoring are investigated.

7.1.1 Urban Horticulture

The cultivation of vegetables and ornamental plants in cities is called urban horticulture (UH). Commonly, it is easy to identify UH practice in urban gardens and parks, thus influencing and modifying their structure and use. Therefore, like the UH concept, the concept of urban gardens and urban parks has evolved over time,

conceiving the new green areas as spaces that must provide ES, thus focusing on ecological aspects and ensuring human well-being. As stated in the introduction section, currently there seems to be a tendency to conceive the green areas as spaces that must provide ES, focused to ecological aspects and to guarantee human well-being. The tendency to construct new buildings is decreasing in favour of re-using the existing ones; similarly, many industrial areas around the world are being transformed into urban parks (e.g. Dora Park in Turin, Landschaftspark Duisburg in northwestern Germany or Freshkills Park in New York). Therefore, in order to achieve these objectives, NBS is necessary and a new and attentive UH is the key for proper management. In Turin (Italy), a good example is the birth in 2019 of a new public-private area of community gardens called *Orti generali*, located in the neighbourhood of Mirafiori, the former headquarters of the ex-FIAT car company (now STELLANTIS Group) (Fig. 7.1), managed with an innovative economic, ecological and social approach (www.ortigenerali.it). In such contexts, UH plays an important role in providing or maintaining multiple ES. In the last years, therefore, UH is applied to design, realise and manage green solutions for specific problems in the urban context (NBS) so authors introduced the concept of environmental horticulture as the application of environmentally sustainable practices in urban greening (Cameron and Hitchmough 2016). In this context, many opportunities to promote NBS as tools for improving urban quality – optimising the delivering of a mixed range of ES – can be developed.

Fig. 7.1 Example of NBS Community gardens *Orti generali* at Mirafiori neighbourhood in Turin

Box 1: NBS for the urban environment

Since 2016, the European Union, with the Horizon Research and Innovation Programme, funded several large-scale demonstrative projects in cities as living labs for NBS for driving urban sustainable development. As preliminary results issuing from some of these projects, catalogues and applied examples of NBS have been proposed (URBANGREENUP, URBiNAT, CLEVER, ThinkNature, proGIreg, EdiCitNET). Some important and common solutions aim at supporting biodiversity in cities and enhancing the quality of the urban environment. In this chapter, we outline some aspects describing NBS as tools for monitoring, in particular, soil, air, water matrices and pollinator diversity. The NBS realisation starts with a particular attention to preserve the soil capital and improve soil ES (Morel et al. 2015). Experimental research with new regenerated soils are going to be performed in Turin (Italy), while some interesting examples in France are already available as 'Le Jardin des Joyeux est' in Aubervilliers, by the Wagon landscaping studio (www.wagon-landscaping.fr). Moreover, the issue of air quality in urban areas is more and more perceived by citizens. As the effectiveness of air purification service mostly depends on the complexity of the structure of the vegetation found in green
areas, wooded areas play a major role. Otherwise managed and other vegetation types, like lawns and single trees, appear to be less effective in mitigating climate changes and improving air purification (Vieira et al. 2018).

7.2 NBS as Environmental Monitoring Tools

The evaluation of the benefits related to the NBS implementation in urban areas is a crucial aspect for assessing their efficiency, for increasing the measurability of their effects and the comparability between different nature-based approaches (Sparks et al. 2011). However, the assessment of these benefits still represents a challenge, since existing systems are rarely able to address the cross-sectoral benefits provided simultaneously by NBS (Ordóñez et al. 2019). To this aim, several key indicators, monitoring parameters and recommended methods have been developed and applied. Furthermore, the definition of standardised protocols for the monitoring of NBS environmental benefits would also bring, and in few cases have already brought, to the use of NBS themselves as suitably designed monitoring stations in urban context.

7.2.1 Monitoring and Indicators of Local Climate and Air Quality Regulation Provided by NBS

Climate change is expected to worsen climate conditions of cities, due to the so-called urban heat islands effect (UHI) (IPCC 2014). NBS can ameliorate urban microclimatic conditions, mainly by shading and/or regulating evapotranspiration (Vieira et al. 2018).), thus reducing air temperature, mitigating extreme heat-wave events and, as a consequence, reducing urban energy use (McDonald et al. 2016). The cooling effect of several NBS can be evaluated through direct measurements, meteorological modelling of air temperature or key indicators,

such as mean and maximum daily temperatures (NCAR & UCAR n.d.). Cameron et al. (2014) investigated the performances of different green wall types for air temperature reduction, proving the efficiency of green walls by measuring ambient air temperature, irradiance and humidity through weather stations and temperature sensors. Largest temperature differentials were recorded at mid-late afternoon, when air close to green walls was 3 °C cooler than the one near to non-vegetated walls. Interestingly, the relevance of the species selection for increasing the cooling efficiency of NBS was also reported. Green infrastructure also plays an important role in urban air pollution abatement (Abhijith et al. 2017). The interaction between vegetation and air pollutants is mainly driven by the leaf stomata uptake of gaseous pollutants and by the leaf deposition of particulate matter (PM) (Tong et al. 2015; Jayasooriya et al. 2017). The NBS impact on air quality can be evaluated by monitoring the concentrations of atmospheric pollutants such as PM_{10}, $PM_{2.5}$, O_3, NO_2, CO and SO_2 and toxic metals (As, Cd, Ni, Pb and Hg), as retrieved from monitoring stations or during experimental campaigns (ISO, 2018). Net fluxes of air pollutants can be either measured by eddy covariance (Guidolotti et al. 2017) or estimated through the application of air quality models (such as the i-Tree Eco model, USDA Forest Service, 2019). However, these approaches have been proven to be effective more at the city scale, rather than at the NBS scale (Selmi et al. 2016). Air quality mitigation at the NBS level should be assessed through experimental techniques able to determine the pollutant uptake at the single tree scale (or lower). To this aim, several approaches have been already proposed to assess PM removal at the single leaf scale and applied to green roofs, green walls and urban parks. The vacuum filtration procedure, described in Dzierżanowski et al. (2011), is a widely used gravimetric technique able to assess leaf-deposited PM amount, into different size fractions (e.g. PM10, PM2.5). Saturation isothermal remanent magnetisation (SIRM) signals allow to assess the amount of magnetic PM on leaves (Power et al. 2009), and SIRM has been successfully used to evaluate the removal of traffic-related PM from a street tree canyon in Gent
(Belgium) (Kardel et al. 2012). Finally, the analysis of leaf surfaces by scanning electron microscopy combined with energy dispersed X-ray (SEM/EDX) can provide a detailed characterisation of leaf-deposited PM in terms of particle size distribution and elemental composition (Baldacchini et al. 2017) and also a reliable quantification of leaf-deposited PM (Baldacchini et al. 2019). Weerakkody et al. (2018) analysed by SEM/EDX microanalysis the leaves of a green wall situated in a busy road of Stoke-on-Trent, UK, thus estimating an average number of $122.08 \pm 6.9 \times 10^7$ PM_1, $8.24 \pm 0.72 \times 10^7$ $PM_{2.5}$ and $4.45 \pm 0.33 \times 10^7$ PM_{10} captured
on 100 cm2 of the living wall. The use of SEM allowed also to highlight differences between the PM capturing efficiencies of the living wall species, likely due to specific leaf surface characteristics, as further confirmed also on tree species (Sgrigna et al. 2020).

7.2.2 Indicators of the NBS Impact on Soil Fertility and Stability

Soil sealing, connected to the urbanisation process, can increase the risk of floods following intense rain events, which are becoming increasingly frequent in the climate change scenario (Marafuz et al. 2015). This process

is also responsible for a significant reduction of soil-atmosphere gas exchanges (Weltecke and Gaertig 2012), soil organic carbon, basal respiration and microbial activity, thus limiting soil fertility and the overall provision of ecosystem services (Fini et al. 2017). NBS can counteract these negative effects, providing several benefits on soil stability, fertility and resilience towards the impacts of climate change. Carbon storage can be used as an indicator of the increased resilience and mitigation potential against climate change impacts provided by specific NBS such as green roofs (Getter et al. 2009). Whittinghill et al. (2014) evaluated the differences in carbon storage and sequestration potential of various in-ground or green roof systems. Green areas composed by woody plants (shrubs), or herbaceous perennials and grasses, resulted to have higher content of carbon stored (up to 78.75 kg m^{-2}), while green roof systems were less efficient in this sense. The NBS-induced soil physical resilience can be evaluated by measuring its organic matter content, texture, structure and permeability. Oldfield et al. (2014) investigated the potential of afforestation procedures in increasing soil quality in an urban park in Queens, NYC. Data analysis underlined positive effects on soil quality provided by trees in combination with specific procedure of soil preparation (weeding, rototilling and the use of compost). These practices determined significant changes on soil properties and resulted effective in improving soil traits that are critical for ecosystem services such as water infiltration and nutrient retention.

7.2.3 Monitoring and Indicators of the Impact of NBS on Water Quality and Management

Urbanisation leads to changes of surface cover that are able to affect negatively also the hydrological cycle, reducing the interception, storage and infiltration of rainwater and increasing the volume of storm water runoff and the risks of local flooding (Zölch et al. 2017). Runoff waters are often characterised by the presence of several pollutants (US EPA 2009) that are able to cause the degradation of downstream ecosystems (Pennino et al. 2016). In this context, NBS represent an efficient alternative to grey infrastructures for the mitigation of runoff water and for the improvement of water quality, being also able to control the circulation of pollutants (Tiwary and Kumar 2014). As a result, specific NBS defined also as storm water control measures (SCMs), such as rain gardens, detention ponds and green roofs, have been
implemented in order to help mitigate flooding and water quality problems in urban areas (Jayasooriya and Ng 2014). Zölch et al. (2017) reported quantitative evidences of NBS efficiency, using an integrated hydrological simulation tool (MIKE SHE) for the modelling of future scenarios based on different variations of green cover in a high-density population
area of Munich (Germany). Results obtained revealed the high efficiency of NBS (trees and green roofs) for the regulation and the management of storm waters. In order to quantify the effects of NBS implementation on water quality, the concentrations of nutrients and metal pollutants are monitored (Reedyk and Forsyth 2006). To this aim, test kits or ion selective electrodes (ISEs) can be used, thus providing rapid but usually less accurate results. Other known chemical pollution indicators are the biogeochemical oxygen demand (BOD) and the chemical oxygen demand (COD). Total suspended solids (TSS) or turbidity (% or total) measurements can be used to assess the reduction of sediment runoff, before and after the NBS

implementation. TSS is typically calculated through a gravimetric approach based on the filtration of water samples and subsequent drying and weighting of the sediments removed. Leroy et al. (2016) reported the evaluation of the efficiency of vegetated swales for the improvement of water quality, taking into account 12 different storm events and carrying out measurements of parameters such as TSS, COD, BOD, total phosphorus (TP), trace elements and polycyclic aromatic hydrocarbons (PAHs). Results underlined the efficiency of swales planted with macrophytes in reducing trace metals and PAH concentrations from 17% up to 45%.

7.2.4 NBS as Living Monitoring Stations for Environmental Quality Parameters

The efficiency and the high spatial resolution of some of the techniques developed to monitor and assess the NBS benefits have suggested that NBS could be used as monitoring stations within the urban context (Baldacchini et al. 2019; Cherqui et al. 2019). This results in the potential of having high-spatial resolution networks useful for environmental monitoring and in the decreasing need of on-site stations. To date, very few research studies have focused on this aspect. In Baldacchini et al. (2019), leaves are proposed as passive samplers, proving their efficiency for low-cost and in situ urban PM biomonitoring. The chemical and physical characterisation obtained through SEM/EDX microanalysis of leaf surfaces allowed to obtain information useful to identify the impact of PM emission sources. As shown in Fig. 7.2, the proposed approach efficiently discriminated the different impacts of sources on leaves of seven different *Quercus ilex* L. trees located within an urban park of Naples (about 6 ha): PM collected on the trees close to the street was characterised by high levels of traffic pollutants (such as Fe, site 2 and 4); PM deposited on leaves from trees exposed to the marine breeze (sites 1, 5 and 7), with high levels of ions linked to salt-spray exposure (Na and Cl), was observed; elements from the crustal component (namely, Si and Al) were mostly abundant in the leaf-deposited PM recorded in the remaining sites.

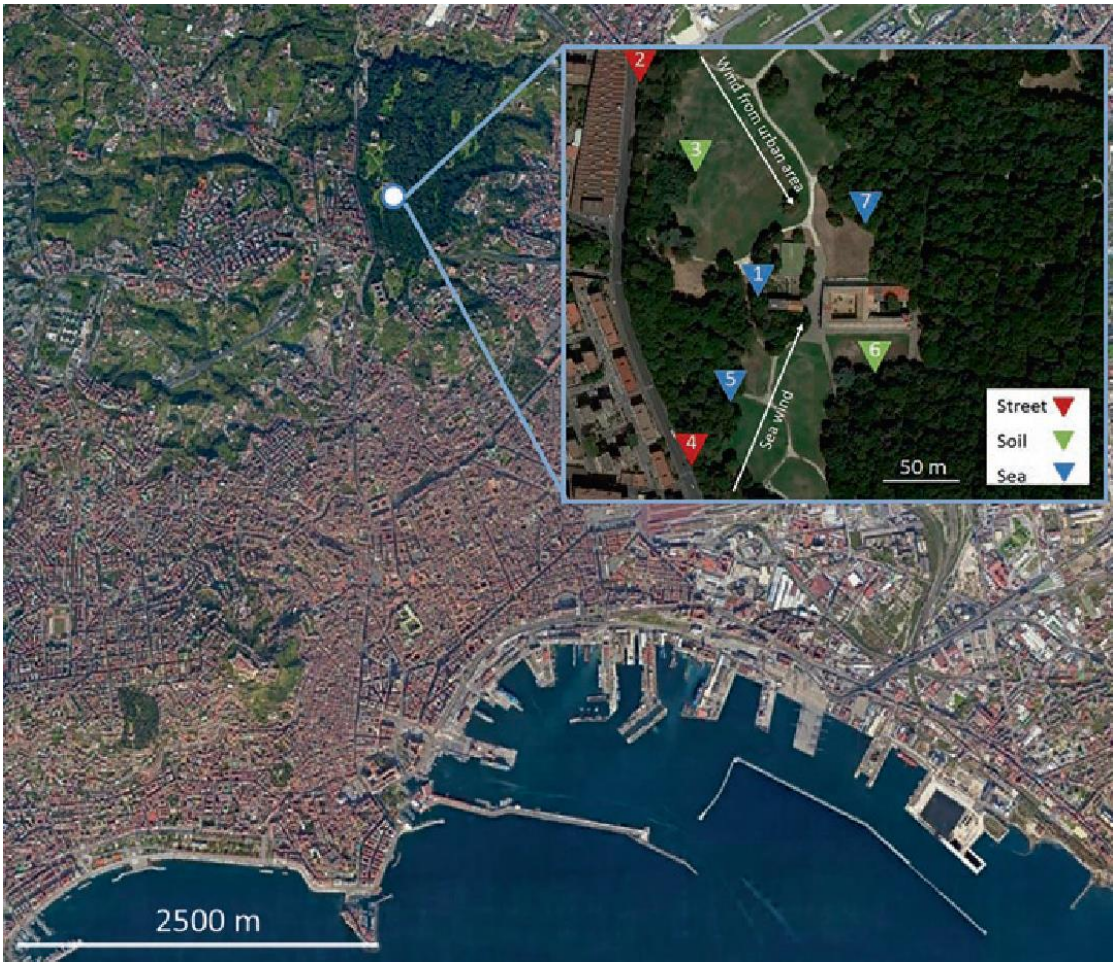

Fig. 7.2 Air pollution source apportionment issued from the SEM/EDX analysis of the PM deposited

A similar approach has been proposed by Cherqui et al. (2019) for water management: the use of a micro-controller (e.g. based on easy-to-use hardware and software) applied to specific SCMs, in combination with open-access monitoring data, with the purpose of designing a monitoring system. This innovative approach results to be useful for the achievement of information with high spatial resolution that can be used for the management of storms and flood events in urban areas**.**

7.3 NBS as Arthropod Diversity Monitoring Tool

A wide range of insect taxa can potentially play a crucial role as pollinators in ecosystem services, even if the most effective ones are bees (Hymenoptera: Apoidea) (Potts et al. 2016). Among non-bee flower-visitor insects, hoverflies (Diptera: Syrphidae), tachinids (Diptera: Tachinidae), butterflies (Lepidoptera), beetles (Coleoptera), sphecids (Hymenoptera: Ampulicidae, Sphecidae and Crabronidae) and wasps (Hymenoptera: Chalcidoidea) may provide key ecosystem services, such as pollination and biological control (Ferracini and Alma 2007; Corcos et al. 2019). Pollination is an important ecosystem service, providing food production and enabling plants to reproduce. Over 80% of wild and cultivated plants grown in

Europe strictly depend on insect pollinators, mainly bees. In 2005, this pollination service represented over 153 billion € throughout the world and over 14.2 billion euros in Europe, with about 84% of all crops that have been studied depending on, or benefiting from, insect pollination (Gallai et al. 2009; Ferrazzi et al. 2017). Moreover, other beneficial arthropods (e.g. predators and parasitoids) may sustain easily their populations when they have access to non-prey foods as pollen and nectar (Picciau et al. 2019). In urban green areas, pollination and biological control represent very impressive examples for NBS supported by and using nature to provide environmental benefits. Unfortunately, the impact of urbanisation on pollinators is poorly studied. Although landscape changes, due to increasing urbanisation, have been identified as drivers of pollinator decline, there is evidence of the biological value and ecological importance of cities providing nutritional resources and suitable habitats for pollinators, thus helping in conserving biodiversity (Hicks et al. 2016; Hall et al. 2017). Bees, and in particular honey bees, are good indicators of biodiversity in cities, and any type of biomonitoring aiming to census and quantify them is an effective method to evaluate the ecosystem supply of urban environments. Urban green spaces include a range of habitat types. Habitats with greater vegetation complexity often benefit natural enemies by providing resources, such as alternative preys and hosts, nectar and pollen for omnivores, suitable microclimates and habitat for multiple life stages (Parsons and Frank 2019). A positive correlation between flower numbers and pollinator abundance has been demonstrated (Pardee et al. 2014). Awareness of the role of wild pollinators has significantly grown in recent years. According to Underwood et al. (2017), training initiatives for local authorities and procurement policies for green space management to adopt pollinator-friendly management strategies are needed. Besides floral abundance and richness, beneficial arthropods are positively affected by increased mulch and leaf litter cover, larger garden size, perennials and increased structural diversity (Arnold et al. 2019). Several research comparing pollinator communities in urban and non-urban landscapes demonstrated that cities can support higher bee species richness compared to agricultural and natural ecosystems (Matteson et al. 2008; Kennedy et al. 2013; Goulson et al. 2015; Baldock et al. 2019; Wenzel et al. 2020). Bees include both solitary and eusocial species, especially cavity nesters and pollen generalist species (Hernandez et al. 2009; Cariveau and Winfree 2015), and specialised species indicative of high-quality habitats, even though specialist bees are rare in cities (Tonietto et al. 2011). In particular, urban areas can host greater species richness of bumblebees than rural or natural landscapes, and green roofs can be also used by pollinators as foraging and nesting habitat (Ksiazek et al. 2012; MacIvor et al. 2015). Diverse urban bee communities also may provide a benefit by pollinating urban crops and garden plants (Larcher et al. 2017). Numerous lists of 'pollinator-friendly' plants are available, even if most of them are not well grounded in empirical data, nor they do specify the taxonomic composition of pollinator assemblages attracted by particular plant species (Mach and Potter 2018). Studies on floral resources and pollinators have traditionally focused on flower strips, urban gardens, parks and allotments (Somme et al. 2016). Besides, the urban foraging sources provided by urban areas may be consistent as investigated in the city of Turin (NW Italy) (Vercelli and Ferrazzi 2014). Several broadleaved trees, shrubs and herbs give an opportunity to urban beekeeping, also allowing to produce local monofloral and multifloral honey (Fig. 7.3) (MV, personal investigations).

Regarding the pollination process, the correlation between high visitation rates and increased fruit and seed set in urban areas was demonstrated by several authors (Lowenstein et al. 2015). Concern for bees' survival among the general public has led to an increase in the numbers of beekeepers and pollinator-friendly gardens in cities. The introduction of bee-friendly gardening (artificial nests and bee flora) to enhance and support wild pollinators is quite a widespread practice in conservation programmes (MacIvor and Packer 2015; Bortolotti et al. 2016). Bee hotels are specialised nesting devices that can be installed in urban areas (Fig. 7.4). Using a variety of untreated materials and varying tunnel diameters will bring a diversity of bee species, even if mason bees (*Osmia* spp.) and leafcutter bees (*Megachile* spp.) are considered the most common ones. Regarding urban beekeeping, it has recently become almost a fashion, with hives on the roofs of historic or prestigious buildings, as in Paris, London, Turin and many other European cities (Moore and Kosut 2013; Vercelli and Ferrazzi 2014) (Fig. 7.5). The blooming scalarity allows to maintain a high number of hives in the cities. This environment proves to be favourable for bees together with the heat islands effect, which ensures survival and reproduction during winter. Furthermore, a feasible management without chemical treatments may positively affect pollinators' life. A growing body of research, national and international initiatives and citizen science activities have been carried out to monitor the support provided by cities to conserve and restore biodiversity (Quaranta et al. 2004, 2018; Van Swaay et al. 2010; Nieto et al. 2014; Potts et al. 2016; Roy et al. 2016; Underwood et al. 2017; Bonelli et al. 2018; Maes et al. 2019).

Fig. 7.3 Typical pollinator-friendly species of the urban environment

Fig. 7.4 An urban nesting device, also called “bee hotel”

Fig. 7.5 Urban beekeeping in Turin

A variety of sampling methods is available for arthropod census, even if some methods can be biased, and their performance varies widely (Rega et al. 2018). Direct counts of individuals, sweep-netting and trapping

methods (pan traps, malaise traps and sticky traps) are commonly used (McCravy 2018). Bee presence is measured in terms of diversity and abundance in several habitats using the estimate methods proposed by several authors (Westphal et al. 2008; O'Connor et al. 2019; Bartholomée and Lavorel 2019). The most common sampling methods for bees and beneficial insects are resumed in Table 7.1. To assess the total bee species richness and abundance, a combination of transect walks conducted by trained bee collectors and pan trap sampling is suggested. The indirect indicators of biodiversity, represented by food source availability in urban environments and the consequent bee foraging activity, can be measured through field surveys and melissopalynological analyses of the bee products.

Table 7.1 Typology and description of the most common estimated methods to monitoring bees and beneficial insect diversity and abundance [methods proposed by Westphal et al. (2008) and subsequently modified in terms of length, width and time of transect walk, and placing time of pan traps (Dennis et al. 2012; O'Connor et al. 2019)]

Typology	Description
Observation plots	Ten equally sized rectangular (1m long × 2 m wide) plots were located according to a random design. During a 6-min observational period, every bee visiting a flower is recorded and then identified checking wings or collected for further identification. The observations are conducted throughout the main flowering period
Standardised transect walk	Permanently marked (250 m long × 4 m wide) corridor divided into ten 25-m-long subunits is used for the standardised transect walks. Each subunit is surveyed for 5 min during which all bees visiting flowers are registered or collected (i.e. 50-min recording time for the whole standardised transect)
Variable transect walk	1-ha plot adjacent to the area where the other sampling methods are undertaken is identified. In the variable transect plot surveyors are allowed to search actively for bees throughout the plot by slowly walking around for 30 minutes
Pan traps	15 pan traps set up in five clusters separated by 15 m are established in the study area. Each cluster contains three UV-bright pan traps, coloured in white, yellow and blue taking account for different colour preferences of bee species. The pan traps are mounted on a wooden pole at vegetation height, filled with 400 mL of water and a drop of liquid dishwashing detergent and left active for 48 hours
Trap nests	Ten poles are mounted in the study area containing five trap nests each. Two types of trap nests are used: (1) traps made of ca. 150 stems of common reed *Phragmites australis* internodes each, with 2–10 mm in diameter and 15–20 cm in length, and (2) trap nests filled with paper tubes of distinct diameters, 6.5, 8 and 10 mm, respectively. Each pole carries two trap nests with common reed internodes and three paper tube nests

Nectar and pollen forage activity may be defined in relation to flower visitation rate, pollen loads and honeys. Furthermore, pollen transfer, pollination success and harvest for human consumption are used to measure the pollination capacity (Bartholomée and Lavorel 2019). The abundance and diversity of native bee species in urban landscapes underline the biological value and ecological importance of cities. In this context, conserving pollinator assemblages may be essential for ecosystem restoration, and the urban environment with its variety

of forage and nesting sites can act as a refuge for insect pollinators. In the last decades, research on bees and beneficial arthropods in cities showed that diverse populations live in urban landscapes (Somme et al. 2016; Wenzel et al. 2020). Bees, and in particular honey bees, are good indicators of biodiversity in cities, and any type of biomonitoring to census and quantify them is an effective method to evaluate the ecosystem supply of urban environments. Further evidence comes from the analysis of honey bees and wild bees and related products. Specific ecological green space management plans are needed, encouraging the use of native flowering plants and the combination of annuals and perennials, in field margins and flowerbeds. Weed species provide many important resources for beneficial insects such as pollen or nectar as well as microhabitats. The possibility to combine beekeeping and the use of flowers highlights the importance of adopting melliferous plants when designing urban areas, and also properly managing the practices for the urban green spaces (e.g. reduced lawn mowing practices) can significantly affect insect biodiversity.

7.4 Concluding Remarks

In conclusion, we point out some key aspects, under an interdisciplinary perspective, in order to promote further and deeper knowledge in the application of NBS in the urban environments.

NBS can be used as low-cost tools for the environmental monitoring in urban areas. New strategies are needed in order to upscale the information achieved through the measurements of parameters and key indicators described in the previous paragraphs. In order to enhance the functioning and health of urban ecosystems, a larger engagement and a stronger connection of citizens and stakeholders to nature are desirable, for example, regarding the raising awareness on the decline of pollinators and biodiversity. The more citizens comprehend the value of nature and participate reasonably in the codesign and co-management processes, the more NBS will achieve self-standing and long-term results. In this contest, the various forms of collective use of green spaces are essential for creating a nature-based educated population, promoting a more ecologically responsible behaviour (Colding and Barthel 2013; Battisti et al. 2017; Larcher et al. 2017). Finally, since decisions concerning management can affect conservation of threatened and endangered species, we argue that a multifunctional approach to conserve and restore cities using NBS should be adopted.

References

Abhijith KV, Kumar P, Gallagher J, McNabola A, Baldauf R, Pilla F, Broderick B, Di Sabatino S, Pulvirenti B (2017) Air pollution abatement performances of green infrastructure in open road and built-up street canyon environments. Atmos Environ 162:71–86

Arnold JE, Egerer M, Daane KM (2019) Local and landscape effects to biological controls in urban agriculture – a review. Insects 10:215

Baldacchini C, Castanheiro A, Maghakyan N, Sgrigna G, Verhelst J, Alonso R, Amorim JH, Bellan P, Bojović DD, Breuste J, Bühler O, Cântar IC, Cariñanos P, Carriero G, Churkina G, Dinca L, Esposito R, Gawroński SW, Kern M, Le Thiec D, Moretti M, Ningal T, Rantzoudi EC, Sinjur I, Stojanova B, Aničić Urošević M, Velikova V, Živojinović I, Sahakyan L, Calfapietra C, Samson R (2017) How does the amount and composition of PM deposited on Platanus acerifolia leaves change across different cities in Europe? Environ Sci Technol 51(3):1147–1156

Baldacchini C, Sgrigna C, Clarke W, Tallis M, Calfapietra C (2019) An ultra-spatially resolved method to quali-quantitative monitor particulate matter in urban environment. Environ SciPollut Res 26:18719–18729

Baldock KCR, Goddard MA, Hicks DM, Kunin WE, Mitschunas N, Morse H, Osgathorpe LM, Potts SG, Robertson KM, Scott AV, Staniczenko PPA, Stone GN, Vaughan IP, Memmott J (2019) A systems approach reveals urban pollinator hotspots and conservation opportunities. Nature Ecology & Evolution 3:363–373

Baró F, Haase D, Gómez-Baggethun E, Frantzeskaki N (2015) Mismatches between ecosystem services supply and demand in urban areas: a quantitative assessment in five European cities. Ecol Indic 55:146–158
Bartholomée O, Lavorel S (2019) Disentangling the diversity of definitions for the pollination ecosystem service and associated estimation methods. Ecol Indic 107:105576
Battisti L, Larcher F, Devecchi M (2017) L'orto come strumento di educazione ambientale e inclusione sociale. esperienze multidisciplinari nella città di Torino. Memorie Geografiche 15:453–459
Blicharska M, Andersson J, Bergsten J, Bjelke U, Hilding-Rydevik T, Johansson F (2016) Effects of management intensity, function and vegetation on the biodiversity in urban ponds. Urban For Urban Green 20:103–112
Bonelli S, Casacci LP, Barbero F, Cerrato C, Dapporto L, Sbordoni V, Scalercio S, Zilli A, Battistoni A, Teofili C, Rondinini C, Balletto E (2018) The first red list of Italian butterflies. Insect Conserv & Diversity 11(5):506–521
Bortolotti L, Bogo G, de Manincor N, Fisogni A, Galloni M (2016) Integrated conservation of bee pollinators of a rare plant in a protected area near Bologna, Italy. Conservation Evidence 13:51–56
Bretzel F, Vannucchi F, Romano D, Malorgio F, Benvenuti S, Pezzarossa B (2016) Wildflowers: from conserving biodiversity to urban greening- a review. Urban For Urban Green 20:428–436
Cameron R, Hitchmough J (2016) Environmental horticulture science and management of green landscapes. CABI, Oxfordshire, p 250. ISBN 1780641389
Cameron RWF, Taylor JE, Emmett MR (2014) What's 'cool' in the world of green façades? How plant choice influences the cooling properties of green walls. Build Environ 73:198–207
Cariveau D, Winfree R (2015) Causes of variation in wild bee responses to anthropogenic drivers. Curr Opinion Insect Sci 10:104–
Chaudhary S, McGregor A, Houston D, Chettri N (2015) The evolution of ecosystem services: a time series and discourse-centered analysis. Environ Sci Policy 54:25–34
Cherqui F, Szota C, Poelsma P, James R, Burns MJ, Fletcher T, Bertrand-Krajewski JL (2019) How to manage nature-based assets such as storm-water control measures? Conference Paper LESAM 2019, Vancouver
Colding J, Barthel S (2013) The potential of 'urban Green commons' in the resilience building of cities. Ecol Econ 86:156–166
Collins JP, Kinzig A, Grimm NB, Fagan WF, Hope D, Wu J, Borer ET (2000) A new urban ecology. Am Sci 5(88):416–425
Corcos D, Cerretti P, Caruso V, Mei M, Falco M, Marini L (2019) Impact of urbanization on predator and parasitoid insects at multiple spatial scales. PLoS One 14(4):e0214068
Dennis P, Herzog F, Jeanneret P, Arndorfer M, Bailey D, Bogers MMB, et al (2012) BIOBIO: biodiversity in organic and low-input farming systems. Handbook for recording key indicators. Wageningen, Alterra, Alterra-Report 2308. 92 pp
Dzierżanowski K, Popek R, Gawrońska H, Sæbø A, Gawroński SW (2011) Deposition of particulate matter of different size fractions on leaf surfaces and in waxes of urban Forest species. Int J Phytoremediation 13(10):1037–1046
Ferracini C, Alma A (2007) Evaluation of the community of native eulophid parasitoids on Cameraria ohridella Deschka and Dimic in urban areas. Environ Entomol 36:1147–1153
Ferrazzi P, Vercelli M, Chakir A, Romane A, Mattana M, Consonni R (2017) Pollination effects on antioxidant content of Perilla frutescens seeds analysed by NMR spectroscopy. Nat Prod Res 31(23):2705–2711
Fini A, Frangi P, Mori J, Donzelli D, Ferrini F (2017) Nature based solutions to mitigate soil sealing in urban areas: results from a 4-year study comparing permeable, porous, and impermeable pavements. Environ Res 156:443–454
Gallai N, Salles JM, Settele J, Vaissière BE (2009) Economic valuation of the vulnerability of world agriculture confronted with pollinator decline. Ecol Econ 68:810–821
Getter KL, Rowe DB, Robertson GP, Cregg BM, Andresen JA (2009) Carbon sequestration potential of extensive Green roofs. Environ Sci Technol 43:7564–7570
Goulson D, Nicholls E, Botías C, Rotheray EL (2015) Bee declines driven by combined stress from parasites, pesticides, and lack of flowers. Science 347(6229):1255957
Guidolotti G, Calfapietra C, Pallozzi E, De Simoni G, Esposito R, Mattioni M, Nicolini G, Matteucci G, Brugnoli E (2017) Promoting the potential of flux-measuring stations in urban parks: an innovative case study in Naples, Italy. Agric For Meteorol 233:153–162
Hall DM, Camilo GD, Tonietto RK, Ollerton J, Ahrné K, Arduser M, Ascher JS, Baldock KCR, Fowler R, Frankie G, Goulson D, Gunnarsson B, Hanley ME, Jackson JI, Langellotto G, Lowenstein D, Minor ES, Philpott SM, Potts SG, Sirohi MH, Spevak EM, Stone GN, Threlfall C (2017) The city as a refuge for insect pollinators. Conserv Biol 31:24–29
Hernandez JL, Frankie GW, Thorp RW (2009) Ecology of urban bees: a review of current knowledge and directions for future study. Cities Environ 2(1):1–15
Hicks DM, Ouvrard P, Baldock KCR, Baude M, Goddard MA, Kunin WE, Mitschunas N, Memmott J, Morse H, Nikolitsi M, Osgathorpe LM, Potts SG, Robertson KM, Scott AV, Sinclair F, Westbury DB, Stone GN (2016) Food for pollinators: quantifying the nectar and pollen resources of urban flower meadows. PLoS One 11(6):e0158117
Hunter ML, Redford KH, Lindenmayer DB (2014) The complementary niches of anthropocentric and biocentric conservationists: Anthropocentrists and biocentrists. Conserv Biol 28:641–645
Intergovernmental Panel on Climate Change (IPCC) (2014) Climate Change 2014–Synthesis Report– Summary for Policy Makers. http://www.ipcc.ch/report/ar5/syr/. (Last accessed: February 10, 2020)
International Organization for Standardization (ISO) (2018) Sustainable cities and communities — Indicators for city services and quality of life (ISO 37120:2018).. https://www.iso.org/ standard/68498.html. (last accessed: February 10, 2020)
International Union for Conservation of Nature – IUCN (2020) Available online: https://www. iucn.org/commissions/commission-ecosystem- management/ our-work/ nature-based- solutions. (Last accessed: February 09, 2020)
Jayasooriya VM, Ng AWM (2014) Tools for modeling of stormwater management and economics of green infrastructure practices: a review. Water Air Soil Pollut 225(8):1–20
Jayasooriya VM, Ng AWM, Muthukumaran S, Perera BJC (2017) Green infrastructure practices for improvement of urban air quality. Urban For Urban Green 21:34–47
Kardel F, Wuyts K, Maher BA, Samson R (2012) Intra-urban spatial variation of magnetic particles: monitoring via leaf saturation isothermal remanent magnetisation (SIRM). Atmos Environ 55:111–120
Keesstra S, Nunes J, Novara A, Finger D, Avelar D, Kalantari Z, Cerdà A (2018) The superior effect of nature based solutions in land management for enhancing ecosystem services. Sci Total Environ 610-611:997–1009

Kennedy CM, Lonsdorf E, Neel MC, Williams NM, Ricketts TH, Winfree R, Bommarco R, Brittain C, Burley AL, Cariveau D, Carvalheiro LG, Chacoff NP, Cunningham SA, Danforth BN, Dudenhöffer JH, Elle E, Gaines HR, Garibaldi LA, Gratton C, Holzschuh A, Isaacs R, Javorek SK, Jha S, Klein AM, Krewenka K, Mandelik Y, Mayfield MM, Morandin L, Neame LA, Otieno M, Park M, Potts SG, Rundlöf M, Saez A, Steffan-Dewenter I, Taki H, Viana BF, Westphal C, Wilson JK, Greenleaf SS, Kremen C (2013) A global quantitative synthesis of local and landscape effects on wild bee pollinators in agroecosystems. Ecol Lett 16(5):584–599
Ksiazek K, Fant J, Skogen K (2012) An assessment of pollen limitation on Chicago green roofs. Landsc Urban Plan 107(4):401–408
Larcher F, Devecchi M, Battisti L, Vercelli M (2017) Urban horticulture and ecosystem services: challenges and opportunities for greening design and management. Italus Hortus 24(1):33–39
Leroy M, Portet-Koltal F, Legras M, Lederf M, Moncond'huy V, Polaerte I, Marcotte S (2016) Performance of vegetated swales for improving road runoff quality in a moderate traffic urban area. Sci Total Environ 566-567:113–121
Lowenstein DM, Matteson KC, Minor ES (2015) Diversity of wild bees supports pollination services in an urbanized landscape. Oecologia 179:811–821
Mach BM, Potter DA (2018) Quantifying bee assemblages and attractiveness of flowering woody landscape plants for urban pollinator conservation. PLoS One 13(12):e0208428
MacIvor JS, Packer L (2015) "Bee hotels" as tools for native pollinator conservation: a premature verdict? PLoS One 10(3):e0122126
MacIvor JS, Ruttan A, Salehi B (2015) Exotics on exotics: pollen analysis of urban bees visiting Sedum on a green roof. Urban Ecosyst 18:419–430
Maes D, Verovnik R, Wiemers M, Brosens D, Beshkov S, Bonelli S, Buszko J, Cantú Salazar L, Cassar LF, Collins S, Dincă V, Djuric M, Dusej G, Elven H, Franeta F, Garcia Pereira P, Geryak Y, Goffart P, Gór A, Hiermann U, Höttinger H, Huemer P, Jakšić P, John E, Kalivoda H, Kati V, Komac B, Kőrösi A, Kulak AV, Kuussaari M, L'Hoste L, Lelo S, Mestdagh X, Micevski N, Mihut S, Monasterio León Y, Munguira ML, Murray T, Nielsen PS, Ólafsson E, Õunap E, Pamperis L, Pavlíčko A, Pettersson LB, Popov S, Popović M, Ryrholm N, Šašić M, Pöyry J, Savenkov N, Settele J, Sielezniew M, Sinev S, Stefanescu C, Švitra G, Tammaru T, Tiitsaar A, Tzirkalli E, Tzortzakaki O, van Swaay CAM, Viborg AL, Wynhoff I, Zografou K, Warren MS (2019) Integrating national red lists for prioritising conservation actions for European butterflies. J Insect Conserv 23(2):301–330
Marafuz I, Rodrigues C, Gomes A (2015) Analysis and assessment of urban flash floods on areas with limited available altimetry data (Arounca, NW Portugal): a methodological approach. Environ Earth Sci 73:2937–2949
Matteson KC, John S, Ascher G, Langellotto A (2008) Bee richness and abundance in new York City urban gardens. Ann Entomol Soc Am 101:140–150
McCravy KW (2018) A review of sampling and monitoring methods for beneficial arthropods in Agroecosystems. Insects 9:170
McDonald R, Kroeger T, Boucher T, Longzhu W, Salem R, Adams J, Bassett S, Edgecomb M, Garg S (2016) Planting healthy air: a global analysis of the role of urban trees in addressing particulate matter pollution and extreme heat. The Nature Conservancy, Arlington
Melles SJ (2005) Urban bird diversity as an Indicator of human social diversity and economic inequality in Vancouver, British Columbia. Urban Habitats 1(3):25–48
Millennium Ecosystem Assessment (Program) (Ed.) (2005) Ecosystems and human well-being: synthesis. Island Press, Washington, DC
Moore LJ, Kosut M (2013) Buzz: urban beekeeping and the power of the bee. NYU Press, New York
Morel JL, Chenu C, Lorenz K (2015) Ecosystem services provided by soils of urban, industrial, traffic, mining, and military areas (SUITMAs). J Soil Sediment 15:1659–1666
National Center for Atmospheric Research (NCAR) & University Corporation for Atmospheric Research (UCAR). (n.d.). Weather Research and Forecasting (WRF) Model Users' Page.. http://www2.mmm.ucar.edu/wrf/users/. (Last accessed: January 21, 2020)
Nesshöver C, Assmuth T, Irvine KN, Rusch GM, Waylen KA, Delbaere B, Haase D, Jones-Walters L, Keune H, Kovacs E, Krauze K, Külvik M, Rey F, van Dijk J, Inge Vistad O, Wilkinson ME, Wittmer H (2017) The science, policy and practice of nature-based solutions: an interdisciplinary perspective. Sci Total Environ 579:1215–1227 Niemela J (1999) Is there a need for a theory of urban ecology? Urban Ecosyst 3:57–65
Nieto A, Roberts SPM, Kemp J, Rasmont P, Kuhlmann M, García Criado M, Biesmeijer JC, Bogusch P, Dathe HH, De la Rúa P, De Meulemeester T, Dehon M, Dewulf A, Ortiz-Sánchez FJ, Lhomme P, Pauly A, Potts SG, Praz C, Quaranta M, Radchenko VG, Scheuchl E, Smit J, Straka J, Terzo M, Tomozii B, Window J, Michez D (2014) European red list of bees. IUCN, Luxembourg
O'Connor RS, Kunin WE, Garratt MPD, Potts SG, Roy HE, Andrews C, Jones CM, Peyton J, Savage J, Harvey M, Morris RKA, Roberts SPM, Wright I, Vanbergen AJ, Carvell C (2019) Monitoring insect pollinators and flower visitation: the effectiveness and feasibility of different survey methods. Methods Ecol Evol 10:2129–2140
Oldfield EE, Felson AJ, Wood SA, Hallett RA, Strickland MS, Bradford MA (2014) Positive effects of afforestation efforts on the health of urban soils. For Ecol Manage 313:266–273
Ordóñez C, Grant A, Millward A, Steenberg J, Sabetski V (2019) Developing performance indicators for nature-based solution projects in urban areas: the case of trees in revitalized commercial spaces. Cities And The Environment (CATE) 12(1):1–23
Panno A, Carrus G, Lafortezza R, Mariani L, Sanesi G (2017) Nature-based solutions to promote human resilience and wellbeing in cities during increasingly hot summers. Environ Res 159:249–256
Pardee GL, Philpott SM (2014) Native plants are the bee's knees: local and landscape predictors of bee richness and abundance in backyard gardens. Urban Ecosyst 17:641–659
Parsons SE, Frank SD (2019) Urban tree pests and natural enemies respond to habitat at different spatial scales. J Urban Ecol 5(1):1–15
Pennino MJ, McDonald RI, Jaffe PR (2016) Watershed-scale impacts of stormwater green infrastructure on hydrology, nutrient fluxes, and combined sewer overflows in the mid-Atlantic region. Sci Total Environ 565:1044–1053
Picciau L, Alma A, Ferracini C (2019) Effect of different feeding sources on lifespan and fecundity in the biocontrol agent Torymus sinensis. Biol Control 134:45–52
Pickett STA, Cadenasso ML, Grove JM (2004) Resilient cities: meaning, models, and metaphor for integrating the ecological, socio-economic, and planning realms. Landsc Urban Plan 69:369–384
Potts SG, Imperatriz-Fonseca V, Ngo HT, Aizen MA, Biesmeijer JC, Breeze TD, Dicks LV, Garibaldi LA, Hill R, Settele J, Vanbergen AJ (2016) Safeguarding pollinators and their values to human Well-being. Nature 540:220–229

Power AL, Worsley AT, Booth C (2009) Magneto-biomonitoring of intra-urban spatial variations of particulate matter using tree leaves. Environ Geochem Health 31(2):315–325
Quaranta M, Ambroselli S, Barro P, Bella S, Carini A, Celli G, Cogoi P, Comba L, Comoli R, Felicioli A, Floris I, Intoppa F, Longo S, Maini S, Manino A, Mazzeo G, Medrzycki P, Nardi E, Niccolini L, Palmieri N, Patetta A, Piatti C, Piazza MG, Pinzauti M, Porporato M, Porrini C, Ricciardelli Dalbore G, Romagnoli F, Ruiu L, Satta A, Zandigiacomo P (2004) Wild bees in agroecosystems and semi-natural landscapes. 1997–2000 collection period in Italy. Bull Insectol 57(1):11–61
Quaranta M, Cornalba M, Biella P, Comba M, Battistoni A, Rondinini C, Teofili C (2018) Lista Rossa IUCN delle api italiane minacciate. IUCN, Roma
Reedyk S, Forsyth A (2006) Using field chemistry kits for monitoring nutrients in surface water. Publication number PRO-121-2006-1. Ottawa, Ontario, Canada: Agriculture and Agri-Food Canada PFRA
Rega C, Bartual AM, Bocci G, Sutter L, Albrecht M, Moonen A-C, Jeanneret P, van der Werf W, Pfister SC, Holland JM, Paracchini ML (2018) A pan-European model of landscape potential to support natural pest control services. Ecol Indic 90:653–664
Roy HE, Baxter E, Saunders A, Pocock MJO (2016) Correction: focal plant observations as a standardised method for pollinator monitoring: opportunities and limitations for mass participation citizen science. PLoS One 11(5):e0155571
Savard J-PL, Clergeau P, Mennechez G (2000) Biodiversity concepts and urban ecosystems. Landsc Urban Plan 48:131–142
Selmi W, Weber C, Rivière E, Blonda N, Mehdi L, Nowak D (2016) Air pollution removal by trees in public green spaces in Strasbourg city, France. Urban Forestry & Urban Greening 17:192–201
Sgrigna G, Baldacchini C, Dreveck S, Cheng Z, Calfapietra C (2020) Relationships between air particulate matter capture efficiency and leaf traits in twelve tree species from an Italian urban-industrial environment. Sci Total Environ 718:137310
Shackleton CM, Ruwanza S, Sinasson Sanni GK, Bennett S, De Lacy P, Modipa R, Mtati N, Sachikonye M, Thondhlana G (2016) Unpacking Pandora's box: understanding and categorising ecosystem disservices for environmental management and human wellbeing. Ecosystems 19:587–600
Shapiro J, Báldi A (2014) Accurate accounting: how to balance ecosystem services and disservices. Ecosyst Serv 7:201–202
Somme L, Moquet L, Quinet M, Vanderplanck M, Michez D, Lognay G, Jacquemart A-L (2016) Food in a row: urban trees offer valuable floral resources to pollinating insects. Urban Ecosyst 19:1149–1161
Sparks TH, Butchard SHM, Balmford A, Bennun L, Stanwell-Smith D, Walpole M, Bates NR, Bomhard B, Buchanan GM, Chenery AM, Collen B, Csirke J, Diaz RJ, Dulvym NK, Fitzgerald C, Kapos V, Mayaux P, Tierney M, Waycott M, Wood L, Green RE (2011) Linked indicator sets for addressing biodiversity loss. Oryx 45(03):411–419
TEEB – The Economics of Ecosystems and Biodiversity (2011) TEEB manual for cities: ecosystem services in urban management. www.teebweb.org
Tiwary A, Kumar P (2014) Impact evaluation of green–grey infrastructure interaction on builtspace integrity: an emerging perspective to urban ecosystem service. Sci Total Environ 487:350–360
Tong Z, Whitlow TH, Macrae PF, Landers AJ, Harada Y (2015) Quantifying the effect of vegetation on near-road air quality using brief campaigns. Environ Pollut 201:141–149
Tonietto R, Fant J, Ascher J, Ellis K, Larkin D (2011) A comparison of bee communities of Chicago green roofs, parks and prairies. Landsc Urban Plan 103:102–108
Underwood E, Darwin G, Gerritsen E (2017) Pollinator initiatives in EU Member States: Success factors and gaps. Report for European Commission under contract for provision of technical support related to Target 2 of the EU Biodiversity Strategy to 2020 – maintaining and restoring ecosystems and their services ENV.B.2/SER/2016/0018. Institute for European Environmental Policy, Brussels.
United Nations Conferences on Housing and Sustainable Urban Development (2017) Habitat III policy papers: policy paper 8 urban ecology and resilience. United Nations, New York. https:// www.habitat3.org
United States Department of Agriculture (USDA) Forest Service (2019) I-tree eco manual. Northern Research Station. https://www.itreetools.org/resources/manuals/Ecov6_ManualsGuides/ Ecov6_UsersManual.pdf. (Last accessed: January 23, 2020)
US EPA (2009) National Water Quality Inventory. 2004 report. EPA-841-R-02-001. Environmental Protection Agency, Washington, DC
van den Bosch M, Ode Sang Å (2017) Urban natural environments as nature-based solutions for improved public health – a systematic review of reviews. Environ Res 158:373–384
Van Swaay C, Cuttelod A, Collins S, Maes D, López Munguira M, Šašić M, Settele J, Verovnik R, Verstrael T, Warren M, Wiemers M, Wynhof I (2010) European red list of butterflies. Publications Office of the European Union, Luxembourg
Vercelli M, Ferrazzi P (2014) Melliferous potential yield of Torino city (Piedmont, Northwestern Italy). In: 2nd ApiEcoFlora & Biodiversity. Proceedings of Apimondia Symposium, 6–7 November 2014, Roma
Vieira J, Matos P, Mexia T, Silva P, Lopes N, Freitas C, Correia O, Santos-Reis M, Branquinho C, Pinho P (2018) Green spaces are not all the same for the provision of air purification and climate regulation services: the case of urban parks. Environ Res 160:306–313
Weerakkody U, Dover JW, Mitchell P, Reiling K (2018) Quantification of the traffic-generated particulate matter capture by plant species in a living wall and evaluation of the important leaf characteristics. Sci Total Environ 635:1012–1024
Weltecke K, Gaertig T (2012) Influence of soil aeration on rooting and growth of the Beuys-trees in Kassel, Germany. Urban For Urban Green 11:329–338
Wenzel A, Grass I, Belavadi VV, Tscharntke T (2020) How urbanization is driving pollinator diversity and pollination – a systematic review. Biol Conserv 241:108321
Westphal C, Bommarco R, Carré G, Lamborn E, Morison N, Petanidou T, Potts SG, Roberts SPM, Szentgyörgyi H, Tscheulin T, Vaissière BE, Woyciechowski M, Biesmeijer JC, Kunin WE, Settele J, Steffan-Dewenter I (2008) Measuring bee diversity in different European habitats and biogeographical regions. Ecol Monogr 78(4):653–671
Whittinghill LJ, Rowe DB, Schutzki R, Cregg BM (2014) Quantifying carbon sequestration of various green roof and ornamental landscape systems. Landsc Urban Plan 123:41–48
Zölch T, Henze L, Keilholz P, Pauleit S (2017) Regulating urban surface runoff through nature-based solutions – an assessment at the micro-scale. Environ Res 157:135–144

5.2 (A4) Nature-based solutions in post-industrial sites: integrated evaluation of atmospheric pollution abatement and carbon uptake in a German city

Urban Climate – Submitted

Martina Ristorini[1,2], Gabriele Guidolotti[2], Gregorio Sgrigna[2], Mais Jafari[3], Dagmar Knappe[3], Vittorio Garfì[1], Chiara Baldacchini[2,4,*], Axel Timpe[5], Carlo Calfapietra[2]

[1] Department of Bioscience and Territory, University of Molise, 86090 Pesche (IS), Italy
[2] Institute of Research on Terrestrial Ecosystems (IRET), National Research Council (CNR), 05010 Porano (TR), Italy
[3] City of Dortmund, Department of Urban Renewal, Kampstraße 47, 44137 Dortmund, Germany
[4] Biophysics and Nanoscience Centre, Department of Ecological and Biological Sciences (DEB), Università degli Studi della Tuscia, 01100 Viterbo, Italy
[5] Institute of Landscape Architecture, RWTH Aachen University, Jakobstraße 2, 52056 Aachen, Germany
1. Corresponding author (baldacchini@unitus.it)

Abstract: The evaluation of ecosystem services (ESs) provided by nature-based solutions (NbS) is crucial to assess their efficiency and plan their management. This study is focused on the abatement of atmospheric pollutants and on the carbon mitigation potential of tree species located in a recultivated landfill in Dortmund (DE). Leaves collected from four different tree species are analysed by Scanning Electron Microscopy coupled with Energy Dispersive X-Ray Spectroscopy (SEM/EDX): surface density, elemental composition and weight of leaf deposited PM are assessed as a function of particle size fraction and tree species. $PM_{0.2\text{-}10}$ removal results in a maximum of 3.8 ± 0.4 μg cm^{-2} of leaf unit area, detected for *Salix alba L.*. $PM_{2.5}$ results are compared with those obtained, by the *i-Tree Eco* model. Also modelled removals of O_3, SO_2 and NO_2 are presented, as well as carbon uptake. A carbon storage of 352.6 ± 88.9 tons ha^{-1} and a carbon gross sequestration of 12.8 ± 2.4 tons ha^{-1} $year^{-1}$ are estimated for this NbS, with *S. alba* L. resulting again as the most efficient species. Our study proves the efficiency of this large NbS for the provision of regulating ESs related to air quality amelioration and climate change mitigation.

Keywords: *Nature-based solutions; ecosystem services; air quality; particulate matter; carbon impact.*

1. Introduction

Urban emission sources, such as vehicular traffic, domestic heating and industrial activities determine frequent exceedances of air quality standards, which are defined for gaseous and particulate atmospheric pollutants (Rafael et al., 2018; EEA, 2016). Combustion processes related to these anthropogenic sources are responsible for the emission of gaseous pollutants, such as SO_2 and NO_2. These gases contribute to acidic depositions and being highly reactive, are known precursors of secondary atmospheric particulate matter (PM), with severe consequences on human health and radiative forcing (Ferm and Svanberg, 1998; Meng et al., 2008). Atmospheric PM, an extremely heterogeneous mixture of solid and liquid particles, represents one of the greater concerns for human health, thus accounting for 5% of lung cancer death globally (Cohen et al., 2005). In addition to this, combustion related NOx (nitrogen oxides, both NO_2 and N_2O) are known precursors of tropospheric ozone (O_3), with severe consequences on human and ecosystems health (Jacob, 2000). Increasing urban emissions of air pollutants such as carbon monoxide (CO) and carbon dioxide (CO_2) are also related to

climate change, being known greenhouse gases (GHGs). Atmospheric concentrations of these long-lived GHGs have increased dramatically in the last decades (Marble et al., 2011; IPCC, 2007), and this has been associated not only to a substantial rise in global average temperatures (Florides, 2008; Douglas, 2004) but also to the increased strength and frequency of extreme events (Oliveira et al., 2011; Nowak, 2000).

Therefore, the identification of new and sustainable strategies for the improvement of air quality and climate change mitigation in urban environments is extraordinarily important. Since 2015, the newly developed concept of Nature-based Solutions (NbS) has been introduced by the European Commission (EC) and later defined by the International Union for Conservation of Nature (IUCN) as "actions to protect, sustainably manage, and restore natural or modified ecosystems" (EC, 2015; Cohen-Shacham, 2016). This concept and its application are connected to the addressing of several and cross-cutting environmental, social, and economic challenges, in a sustainable and cost-efficient way (Faivre et al., 2017). Indeed, NbS implementation is not only related to the increase of urban resilience, but also to economic and sustainable development, improvement of environmental quality and therefore human health and wellbeing (Carrus et al., 2015; Ruangpan et al., 2020). In this context, the recultivation and afforestation of post-industrial sites is gaining more and more attention from local authorities, stakeholders and scientists (Escobedo et al., 2019; Panno et al., 2017; Song et al., 2019). Among these sites, landfills are a common element of post-industrial landscapes that can be transformed from environmental nuisance into elements of urban green infrastructure, through the NbS concept. Initially located on the periphery of cities, landfills have become more integrated into the urban fabric. This is extremely relevant, if the different environmental risks associated to them are considered. For instance, abandoned landfills are releasing gases, mainly CH_4 and CO_2, due to the rotting process of the waste, and washing out of pollutants into the groundwater, due to the penetration of rainwater. Securing these sites could include different combinations of technical and NbSs. Water infiltration, gas, dust, and smell emissions are mainly controlled by sealing layers. Water run-off is often collected, and ground sealing and groundwater monitoring can be used to prevent water pollution.

Once safeness is ensured, landfills present a potential for being integrated into the urban green infrastructure by a wider use of NbS, thus being able to provide several ecosystem services (ESs), defined as "benefits that humans derive directly and indirectly from the processes and functions of an ecosystem" (Costanza et al., 1997). Air pollution abatement is one of the best-known ES and its provision is linked to the potential of plants to remove gaseous pollutants through stomatal uptake and PM through wet or dry deposition on their foliage (MEA, 2005; Nowak et al., 2006), thus determining an improvement of urban air quality (Janhall, 2015; Currie and Bass, 2008). PM leaf dry deposition is a complex and dynamic mechanism influenced by the chemical-physical characteristics of PM and leaves' micro- and macro-morphology, such as leaf shape, margin and surface structures, and meteorological conditions (Saebo et al., 2012; Wang et al., 2015; Sgrigna et al., 2020; Ristorini et al., 2020). GHGs mitigation (Baro' et al., 2014), due to the atmospheric CO_2 sequestration and carbon storage in the biomass through the photosynthetic activity (Myeong et al., 2006), is another important

ES provided by NbSs. In this case, species-specific characteristics such as tree growth rate, leaf area index, and plant biomass can influence the restorative efficiency of the NbS (Nowak et al., 2002).

The correct assessment of these ESs by specific NbSs allows to measure their impact, and to compare different solutions (Calliari et al., 2019). However, this task is very complex, and it rarely accounts of the integrative and cross-sectoral approach of the NbS concept, often addressing single ES or challenges (Ordóñez et al., 2019; Farrugia et al., 2015).

To this aim, we focused on the experimental and modelled assessment of the atmospheric pollutants abatement and the carbon impact of a specific NbS, a recultivated landfill located in Dortmund (DE). The study proves the efficiency of this large NbS, providing fundamental information on the species-specific affinity towards the provision of these specific ESs. All this information can be considered for the design and management processes of future NbSs, which need to be increasingly suitable and efficient in the improvement of urban life quality and citizen health and well-being.

2. Materials and methods

2.1 Study area

The former landfill of Deusen is in the Northwest of the city (51°32'48" N, 7°25'8" E), in the borough of Huckarde, characterized by the presence of a former mining site and a coking plant, and the district Deusen, from which it takes its name (Fig. 1). Since the beginning of the 20th century, urban waste has been disposed on this site and until its closure in 1992, the Deusen landfill reached a height of 55 m above the surroundings, with 11,000,000 m^3 of waste. Basic recultivation started in 1997, with the plantation of about 150000 trees and shrubs, after drainage and soil cover operations.

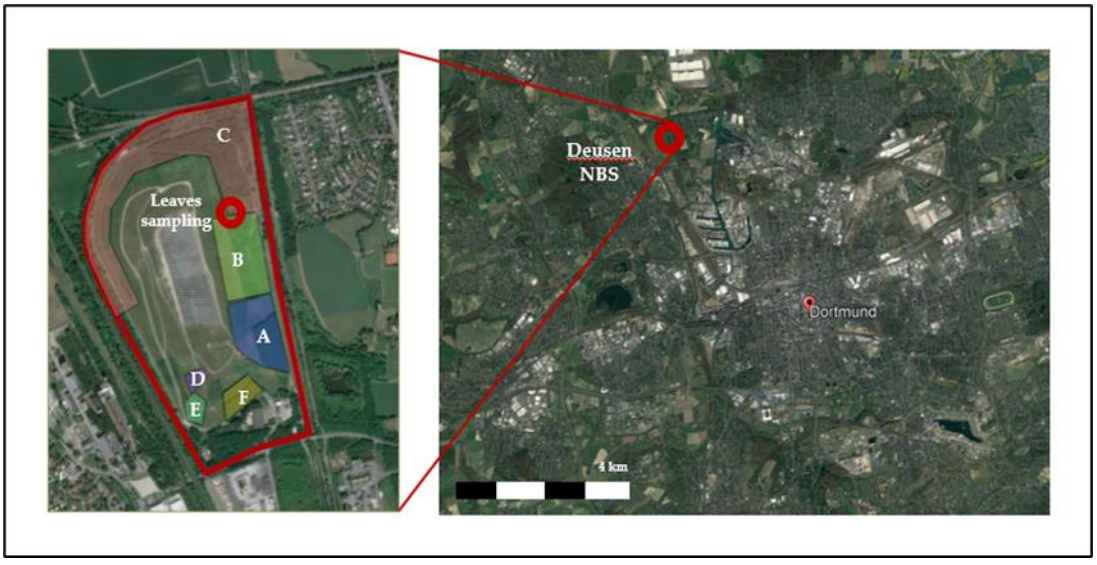

Figure 1. Deusen previous landfill location and zoomed image, with shown leaves sampling site and zonation by plant species composition as used for the *i-Tree Eco* modelling.

The initial recultivation of the site has been enhanced in stages towards a multifunctional greenspace and it will be further improved within the Horizon 2020 Innovation Action - proGIreg (productive Green Infrastructure for post-industrial urban regeneration) (Jafari et al., 2020). To date, the solutions implemented on the Deusen landfill include different elements as shown in Figure 2. While during proGIreg new ones will be added, the benefits of the already implemented ones, such as the recultivated areas, can be already scientifically assessed.

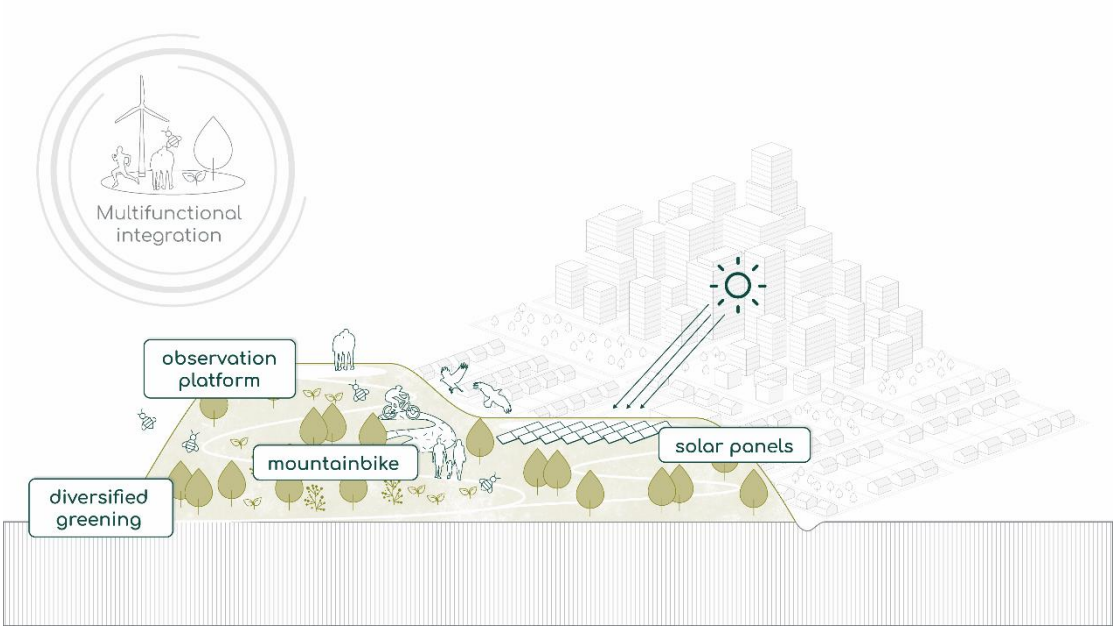

Fig. 2 Different NbSs and other measures combined to make the Deusen landfill a multifunctional green infrastructure: greening with trees and shrubs, accessibility of vistas by steps and walkways, a mountain biking parkours, solar panels and diversified greening for enhancing pollinator friendliness.

2.2 Experimental evaluation of the atmospheric PM abatement

2.2.1 Leaf sampling

The potential of this NbS towards the abatement of airborne PM was assessed through the characterization of leaf deposited particles. Fully-grown leaves were collected from four different tree species: *Acer campestre* L., *Betula pendula* Roth, *Carpinus betulus* L. and *Salix alba* L.. The leaf sampling was carried out on the 18th of September 2019, one month after the last intense precipitation event (see Section 2.3.2 for details) (Climate Data Center - Deutscher Wetterdienst - https://cdc.dwd.de/portal/). For each species, six leaves were sampled from trees in the East part of the NbS (51°32'51.88"N, 7°25'7.82"E; see Figure 1) (Sgrigna et al., 2020; Tomašević et al., 2005). These were collected from the external part of the crown with different cardinal exposures, at 2 meters height from ground level. To ensure homogeneity, only the youngest leaves at the top of each branch were selected for SEM/EDX microanalysis.

2.2.2 SEM/EDX microanalysis of leaf surfaces

A total of 24 leaves (6 leaves per species) were analysed by a Phenom ProX (PhenomWorld, The Netherlands) scanning electron microscope, equipped with an X-ray analyser (SEM/EDX). Two sections of 0.5 cm^2 (adaxial and abaxial surface) were cut from the same leaf part and mounted on aluminium stubs, by using double coated carbon conductive PELCO Tabs (Ted Pella, Inc.). The two sections were slightly fluxed with compressed air, as recommended by the user manual, and then inserted in the SEM with a charge reduction sample holder, suitable for biological samples. Then, operating in backscattering electron mode, with an incident electron energy of 5 keV, ten micrographs of 150 x 150 μm width (1024 x 1024 pixels resolution) were acquired from each section, for a total of 120 micrographs for each species (60 micrograph for the adaxial and 60 for the abaxial surfaces). Gwyddion v. 2.49 (Nečas and Klapetek, 2012) was used to acquire the number of particles and their equivalent sphere diameter (d_{eq}) (Baldacchini et al., 2017; Merkus, 2009). Therefore, particles density for each species (expressed as the number of particles per unit leaf area in mm^2), was obtained for adaxial (AD) and abaxial (AB) surfaces as a function of size fraction (specifically $PM_{0.2\text{-}1}$, particles with aerodynamic diameters from 0.2 μm to 1.0 μm, $PM_{1\text{-}2.5}$ with 1.0 μm ≤ a. d. ≤ 2.5 μm, and $PM_{2.5\text{-}10}$ with 2.5 μm ≤ a. d. ≤ 10 μm), thus averaging density values obtained from the 60 corresponding micrographs. Standard deviations were also calculated. More detailed information is reported in Baldacchini et al. 2017 (Baldacchini et al., 2017). Due to the high density of trichomes in the AB surfaces of *S. alba* L., these surfaces were excluded from the SEM/EDX analysis. For this species, AB particle densities were thus estimated calculating the AD/AB ratio of the other three species, averaging it for each size fraction, and multiplying it for the *S. alba* AD results.

Five micrographs of 50 x 50 μm width and same resolution as before were also acquired, with an incident electron energy of 15 keV. From each one, 10 particles were randomly selected for the EDX spectrum acquisition, for a total of 600 particles analysed for each species. Relative percentages of the main (Na, Mg, Al, Si, Cl, K, Ca and Fe) and trace (P, S, Ti, Cr, Mn, Ni, Cu an Zn) elemental components were acquired. The weighted volume percentage ($W_{\%xi}$) occupied by each element (*x*) was calculated for each particle (*i*), by taking in account the particle volume ($V_i = 4/3\ \pi\ (d_{eqi}/2)^3$) and the element relative percentage (Baldacchini et al., 2017). For this part, d_{eq} was obtained through the ImageJ software (Schneider et al., 2012). Then, by averaging these results, mean elemental composition $W_{\%n}$ for each leaf sample (*n*) and standard deviations, for each size fraction and each species, were obtained. The weight of leaf deposited particles per unit leaf area (μg cm^{-2}) was then calculated taking in account the $W_{\%n}$ of each element, multiplied by the total volume of SEM analysed particles, per each sample, and the corresponding elemental atomic mass per volume (https://www.webelements.com/periodicity/density/), as reported in Baldacchini et al. 2019. These values and standard deviations were calculated for each species and size fraction, thus averaging and combining results from both the AD and the AB surfaces.

2.3 i-Tree Eco *model*

2.3.1 Biometric, meteorological, and atmospheric pollutants concentrations data

In 2019, data on biometric and health status of trees located in the Deusen NbS were collected. These are required by the *i-Tree Eco* model as input data for the modelling of the NbS provision of ESs (*i-Tree Eco* User Manual, 2021) To assess the different pollutant removal and carbon impact of the NbS species and combination of them, the site was subdivided in six zones (Figure 1), and for each of them trees were surveyed. The collected information was then averaged over the total number of trees for each species and within each zone (Suppl. Materials S1). According to the model input requirements (*i-Tree Eco* User Manual, 2021) essential data for estimating parameters such as the leaf area (LA) and the plant dry biomass were collected (Pace et al., 2018): tree height, diameter of the trunk at the breast height (DBH, approximately 1.3 meters from the ground), crown base height and width, percentage of crown missing, crown health and light exposure.

The *i-Tree Eco* model also requires hourly meteorological and atmospheric pollutants concentrations data that are retrieved from stations included in the *i-Tree Eco* model database. The closest station to the sampling area have been selected: the Dortmund city airport provided atmospheric concentrations of O_3, NO_2 and $PM_{2.5}$, the station of Recklinghausen (30 km from Dortmund) provided SO_2 concentration, while the nearest station with a complete meteorological data was the station in Maastricht airport (National Center of Environmental Information, NCEI ID: 063800-99999; 170 km from Dortmund). The most recent available data in the *i-Tree Eco* database were referred to the year 2014.

2.3.2 Modelled removal of O_3, SO_2, NO_2, $PM_{2.5}$ and comparison with experimental $PM_{2.5}$ SEM/EDX results

The *I-Tree Eco* model estimates the removal of O_3, SO_2, NO_2 and $PM_{2.5}$ by the vegetation via deposition or stomatal uptake throughout the year. Pollutant flux (F; expressed in g m^{-2} s^{-1}) of gaseous pollutants is calculated as the product of each pollutant deposition velocity (V_d in m s^{-1}) and their atmospheric concentration (C in g m^{-3}) (Hirabayashi et al., 2012) The V_d for gaseous pollutants (O_3, SO_2, NO_2) are calculated as the inverse sum of the aerodynamic resistance (R_a), quasi-laminar boundary layer resistance (R_b) and canopy resistance (R_c). R_a is calculated using meteorological data, while R_b and R_c are calculated separately for each pollutant (Pace et al., 2018). $PM_{2.5}$ flux and V_d calculations are mainly affected by wind speed and LA (Nowak et al., 2013). Each modelled pollutant flux is multiplied for the modelled LA, to achieve the mass removed through dry deposition ($PM_{2.5}$) or stomatal uptake (gaseous pollutants) by the vegetation. The removed mass of each pollutant in one year, by single trees of each species and by the total number of trees located in this NbS were finally obtained. For those species that have been reported to have trees with different biometric characteristics and/or health status, results were summed together (Suppl. Materials S1), obtaining a single value for each species. To assess the potential removal of different combinations of tree species and properly compare them, we decided to normalize the removal values of each zone and of the total NbS (Suppl. Materials S1), by their areas in hectares, obtaining the kg of pollutants removed throughout the year per unit area (kg ha^{-1} $year^{-1}$). For each modelled value obtained (single tree, zone upscale, total NbS) the associated uncertainty was calculated. Specifically, percentage uncertainties were calculated as the square root of the sum of squared percentage uncertainties for each single factor considered in the modelling and in the upscale. The single factor

uncertainties were estimated by the experimental data dispersion or by the standard deviation, depending on the data structure.

Finally, modelled removal results of $PM_{2.5}$ were compared with the experimental ones obtained from SEM/EDX. The comparison concerned only the species analysed by SEM/EDX. Species-specific mass concentrations of $PM_{2.5}$ obtained through the SEM/EDX procedure were multiplied for the LA (in cm^2) modelled by *i-Tree Eco* for single trees of *Acer campestre* L., *Betula pendula* Roth, *Carpinus betulus* L. and *Salix alba* L.. These latter results were considered representative of about one-month PM leaf dry deposition, due to the occurrence of last intense precipitation event in Dortmund city (15^{th} of August 2019) before the leaf sampling date (Climate Data Center - Deutscher Wetterdienst - https://cdc.dwd.de/portal/.) The precipitation event was characterized by a cumulative rain amount of 12 mm with a maximum intensity of 6.5 mm/h enough to wash-off more than 70% of leaf deposited PM (Xu et al., 2017). To finalize the comparison, the yearly *i-Tree Eco* $PM_{2.5}$ outputs were normalized accounting a leafy period length of eight months.

2.3.3 Carbon storage and carbon gross sequestration

Carbon storage describes the amount of carbon stored in the plant dry biomass via photosynthesis, while carbon gross sequestration is the yearly rate of carbon removal from the atmosphere (Martina et al., 2012). The above-ground plant dry biomass is calculated through DBH and allometric equations. To estimate the total biomass (above and below ground), a root to shoot ratio of 0.26 was applied. Since the allometric equations are diameter-based and developed for closed canopies, biomass was reduced by a factor of 0.8, to account the influence of urban open-growth conditions on the above ground biomass (Pace et al., 2018).
The modelled carbon gross sequestration is calculated thus considering a standard diameter growth of tree which accounts of the tree light exposure and the number of frost days in the year considered (Nowak and Crane, 2002; Nowak, 1994).
As for the removal of atmospheric pollutants, the individual tree results for carbon storage and gross sequestration (expressed in kg and kg $year^{-1}$, respectively) were then upscaled for the total number of trees for each species. Results of each zone and of the total NbS were furtherly normalized by their areas in hectares, obtaining the kg ha^{-1} of carbon stored/sequestrated in one year. Also, for these parameters, uncertainties were calculated as reported in section 2.3.2.

3. Results and discussion

3.1 PM abatement estimated by SEM/EDX microanalysis

3.1.1 Density of leaf deposited PM

The averaged species-specific particle densities (number of particles per unit leaf area in mm^2), with standard deviations were obtained by the SEM images of the adaxial (AD) and abaxial (AB) leaf surfaces, for three size

fractions, ultrafine ($PM_{0.2-1}$) from fine ($PM_{1-2.5}$) and coarse ($PM_{2.5-10}$) PM (Suppl. Materials, S2). The particle density on the AB side was about the 70% of that on the AD side, per each tree species and each size fraction (Suppl. Materials, S2). This difference between AD and AB leaf sides is largely described in literature as a direct consequence of peculiar micromorphology and leaf orientation and, therefore, different interaction with wind turbulence (Baldacchini et al., 2017; Ottele et al., 2010; Shi et al., 2008). In our study, the $PM_{0.2-1}$ was the most abundant one in terms of particles density, ranging from 90% to 93.1% for AD sides (respectively for *A. campestre* and *S. alba*) and from 91.7% to 93.6% for AB sides (respectively for *B. pendula* and *S. alba*). The $PM_{1-2.5}$ was represented by percentages ranging from 6.3% (*S. alba*) to 8.8% (*A. campestre*) in the AD surfaces, while for the AB ones, these percentages ranged from 6.0% (*A. campestre*) to 7.5% (*B. pendula*). Finally, the AD coarse particles ($PM_{2.5-10}$) ranged from 0.5% (*B. pendula*) to 1.1% (*A. campestre*), comparable to the range of AB ones (0.5% - 0.8%). If the total leaf deposited particles were considered, no appreciable differences were detected between the four species. *A. campestre* resulted to be the species with the highest density of $PM_{2.5-10}$ in the AD side ($362 \pm 47 * 10^4$ particles mm^{-2}), while particles densities of this size fraction on the AB sides of all the species were in the same range, with a mean value of $(134 \pm 34) * 10^4$ particles mm^{-2} (Suppl. Materials, S2). Our findings agreed with those obtained by Baldacchini et al. 2019 for deposited PM on *Q. ilex* L. (oak holm) leaves collected in a southern Italian city, and they were in the same range reported by Weerakkody et al., 2017 for leaves of 17 green wall species, and by Baldacchini et al. 2017 for leaves of *Platanus acerifolia* L. belonging to 28 different urban areas.

3.1.2 Elemental composition of leaf deposited PM

For all the considered size fractions and species, sodium (Na), magnesium (Mg), aluminium (Al), chlorine (Cl), potassium (K), calcium (Ca) and iron (Fe) were the main components of leaf deposited particles. Some general trends could be described for the size distribution of these elemental components. All the accounted species were characterized by a decrease of $W_{\%}$ for elements such as Na, Cl, Mg, Al, and Si, from coarse particles ($PM_{2.5-10}$) to ultrafine ones ($PM_{0.2-1}$) (Fig. 3). These elements are typical crustal components used as tracers for natural soil resuspension (Abhijith and Kumar, 2020). The size distribution detected for these elements was in total agreement with previous studies, which described higher aerodynamic diameters due to their mechanical and abrasive origin (Amato et al., 2009). On the other hand, Fe, which is often associated to anthropogenic emission sources (Massimi et al., 2020; Ristorini et al., 2020), was mostly abundant in the ultrafine particles fraction (Fig. 3), as well as trace elements such as titanium (Ti), chromium (Cr) and manganese (Mn) (data not shown); this suggesting that may be emitted by combustion related processes, such the ones associated to urban vehicular (Massimi et al., 2019; Davila et al., 2006).

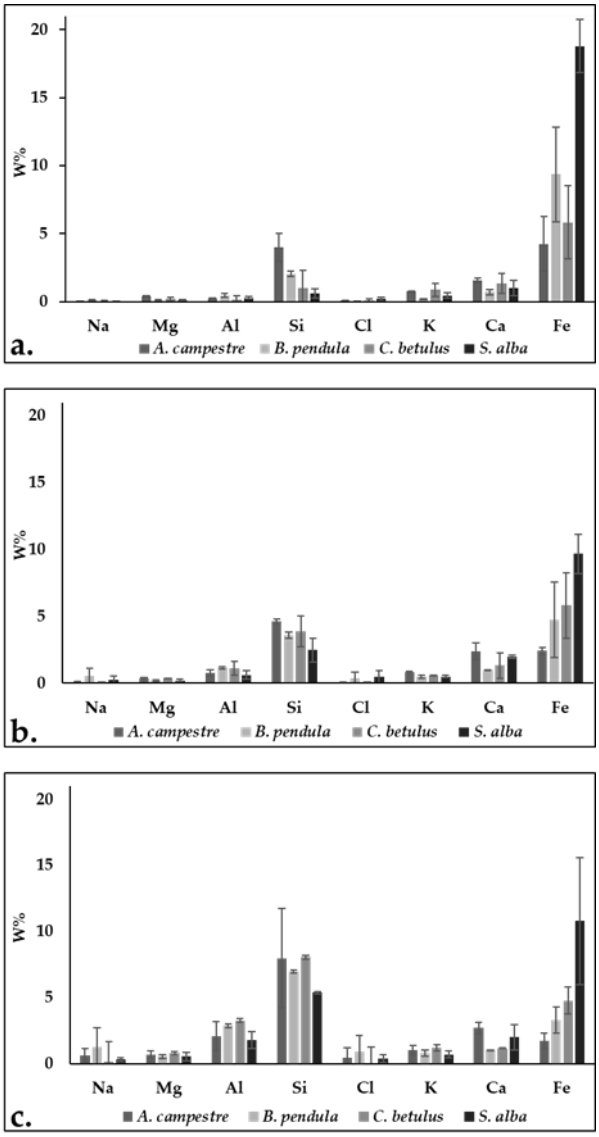

Figure 3. Relative elemental composition and standard deviations, as estimated by the W% obtained from the SEM/ EDX analysis, for the three PM size fractions (a. $PM_{0.2\text{-}1}$; b. $PM_{1\text{-}2.5}$; c. $PM_{2.5\text{-}10}$), for all the species.

Interestingly, differences between the elemental composition of PM were detected across the four tree species. *S. alba* leaves had the highest number of iron-containing particles, in both $PM_{2.5\text{-}10}$ and $PM_{0.2\text{-}1}$ fractions, with a Fe W% of 10.8% and 18.8%, respectively. These were the highest percentages measured for all the species and for all the fractions (Fig. 3). *S. alba* confirmed this trend in $PM_{1\text{-}2.5}$ fraction also for others trace elements, such as chromium (Cr, W% = 0.19%) and titanium (Ti, W% = 0.26%). Instead, *S. alba* $PM_{2.5\text{-}10}$ was characterized by the lowest relative W% of soil-related Si (W% = 5.37%). On the other hand, *A. campestre* leaves were characterized by $PM_{0.2\text{-}1}$ with a significantly higher concentrations of Si (W% = 3.99%) and Ca (W% = 1.58%). No significant differences were found between the W% of the other elemental components, for all the size fractions.

3.1.2 Mass concentration of leaf deposited PM

The mass of removed PM per unit leaf area (µg cm^{-2}), for each species and size fraction, is shown in Figure 4. *S. alba* and *A. campestre* had the highest total $PM_{0.2-10}$ mass accumulated on their leaves, corresponding to 3.84 ± 0.36 µg cm^{-2} and 3.23 ± 0.23 µg cm^{-2} respectively, while *C. betulus* leaves were the less efficient, with a mean load of 1.92 ± 0.14 µg cm^{-2}. The same trend was obtained for the coarse PM size fraction ($PM_{2.5-10}$), which is known to mainly drive the mass load of $PM_{0.2-10}$ (Cai et al., 2017). Instead, for both $PM_{1.2,5}$ and $PM_{0.2-1}$ fractions, only *S. alba* leaves showed a particle load that was significantly higher than the others (0.68 ± 0.11 µg cm^{-2} for $PM_{0.2-1}$ and 1.07 ± 0.13 µg cm^{-2} for the $PM_{1.2,5}$).

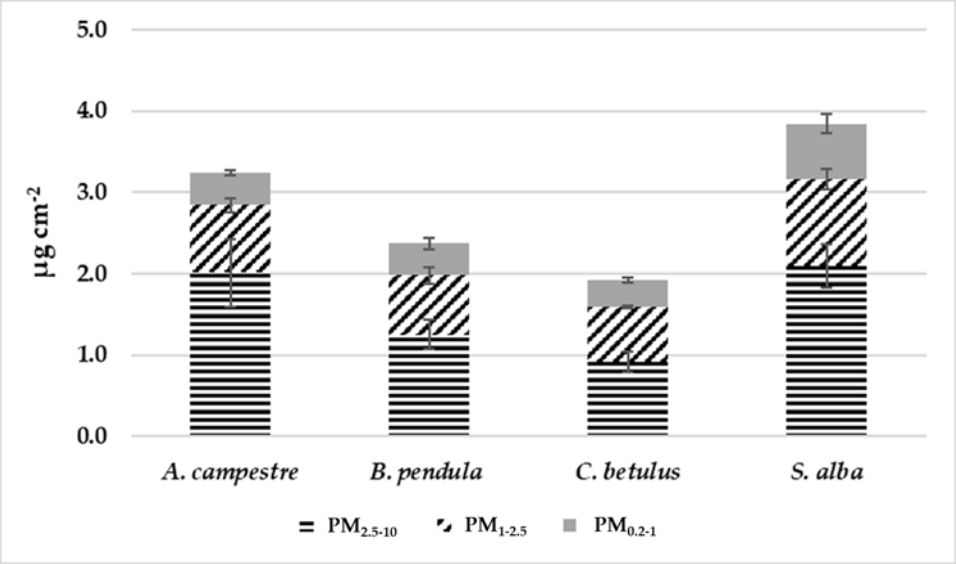

Figure 4. PM mass concentration on leaves (µg cm^{-2}), as obtained from SEM/EDX, through the combination of PM density and elemental composition results, as averaged values over the six leaves per each species. Standard deviations are given for each size fraction and each species.

Overall, *S. alba* resulted to be the species with the highest mass of leaf deposited particles, for all the studied size fractions, likely due to the affinity shown by *S. alba* leaves towards heavy metal containing particles (section 3.1.2). This result could be used as a valid proxy for its potential removal affinity towards airborne PM. Instead, the high PM mass concentrations detected for total PM ($PM_{0.2-10}$) and coarse fraction ($PM_{2.5-10}$) in *A. campestre* leaves could be explained by the high particle densities detected on its leaf samples for the coarse size fraction (section 3.1.1). *C. betulus* and *B. pendula* were then the species with the lowest accumulated PM loads, for every considered size fraction. Results described in previous studies confirmed the low capacity of *C. betulus* leaves for capturing both PM_{10} and $PM_{2.5}$, due the smooth surface of its leaves (He et al., 2020; Przybysz et al., 2019). Moreover, the high accumulation of coarse particles in *A. campestre* leaves was also described in Dzierżanowski et al. 2011, which reported a high accumulation of $PM_{2.5-10}$ particles both in superficial part of leaves and in waxes. The observed differences in PM load between these four species was likely due to micro and macro-morphological differences of leaves, and their impact on the deposition of airborne PM (Sgrigna et al., 2020; Hofman et al., 2013). However, inter-specific variability was lower than

expected, and often not significant. This may be explained by the proximity of the sampled plants in a densely forested area, which could have determined a quite homogeneous conditions of leaf exposure to airborne PM.

3.2 i-Tree Eco *model evaluation of atmospheric pollutant removal (O_3, SO_2, NO_2 and $PM_{2.5}$)*

Modelled results relative to the removal of O_3, SO_2, NO_2 and $PM_{2.5}$ by single trees showed a high inter-specific variability (Table 1). For $PM_{2.5}$, the highest removal efficiency was observed for *S. alba*, followed by *R. pseudoacacia*, *C. betulus* and *A. campestre*, while *S. aucuparia*, *B. pendula* and *T. cordata* were the less efficient species. Yearly removal of $PM_{2.5}$ ranged from a minimum of 0.10 ± 0.02 g, detected for single trees of *S. aucuparia* to a maximum of 11.8 ± 2.1 g for *S. alba* (Tab. 1). Similar trend could be observed also for O_3, SO_2 and NO_2, confirming *S. alba* as the most efficient species with removal values up to 162.8 ± 27.4 g for O_3, 93.1 ± 27.4 g for NO_2 and 8.6 ± 1.5 g of SO_2 were modelled (Tab. 1). Modelled and species-specific removal of atmospheric pollutants, both gaseous and particulate ones, proved the impact of tree growth and health conditions on the described specific affinity towards the provision of this air quality related ES. The described approach may be considered to deduce which species are the more adapt to survive and grow in urban environments, thus providing relevant information for the preliminary stages of NbS design and for the selection of the most efficient tree species.

Table 1. *I-Tree Eco* modelled potential removal of atmospheric pollutants O_3, SO_2, NO_2 and $PM_{2.5}$. Single tree results for each species (g of pollutant removed $year^{-1}$) together with zone and total NbS results (kg of pollutant removed ha^{-1} $year^{-1}$) are presented. The uncertainties associated to each value are also presented.

g per single tree $year^{-1}$	**$PM_{2.5}$**	**O_3**	**NO_2**	**SO_2**
S. alba L.	11.8 ± 2.1	162.8 ± 27.4	93.1 ± 15.0	8.6 ± 1.5
***R. pseudoacacia* L.**	5.5 ± 1.0	76.5 ± 12.9	43.7 ± 7.1	4.0 ± 0.7
***C. betulus* L.**	4.5 ± 0.8	61.6 ± 10.4	35.2 ± 5.7	3.3 ± 0.6
***A. campestre* L.**	2.5 ± 0.4	34.5 ± 5.8	19.7 ± 3.2	1.8 ± 0.3
***B. pendula* Roth**	1.2 ± 0.2	16.3 ± 2.7	9.3 ± 1.5	0.9 ± 0.2
***T. cordata* MILL.**	0.6 ± 0.1	9.2 ± 1.5	5.2 ± 0.8	0.4 ± 0.1
***S. aucuparia* L.**	0.10 ± 0.02	1.4 ± 0.2	0.8 ± 0.1	0.10 ± 0.02
Kg per hectare $year^{-1}$	**$PM_{2.5}$**	**O_3**	**NO_2**	**SO_2**
Zone A	9.6 ± 2.0	132 ± 26	75.6 ± 14.7	7.0 ± 1.4
Zone B	3.4 ± 0.7	47.9 ± 9.6	27.4 ± 5.3	2.3 ± 0.5
Zone C	1.7 ± 0.3	22.7 ± 4.5	13.0 ± 2.5	1.2 ± 0.2
Zone D	0.4 ± 0.1	6.8 ± 1.3	3.9 ± 0.7	0.4 ± 0.1
Zone E	13.7 ± 2.9	190 ± 38	109 ± 21	9.7 ± 2.0
Zone F	2.9 ± 0.6	40.2 ± 7.6	23.0 ± 4.2	2.1 ± 0.4
Total NbS	3.4 ± 0.8	46.4 ± 10.7	26.5 ± 6.0	2.4 ± 0.6

Zone E, characterized by the co-presence of two different types of *B. pendula* trees (Tab. 1), was the most effective towards the removal of $PM_{2.5}$, followed by Zone A and B. Likewise, Zone E confirmed as the one

with the highest annual removal of gaseous pollutants that was 189.8 ± 38.0 kg ha^{-1}, 109.2 ± 21.2 kg ha^{-1}, 9.7 ± 2.0 kg ha^{-1} for O_3, NO_2 and SO_2, respectively (Tab. 1). Conversely, Zone D, characterized by two different types of *S. aucuparia* trees, was the least efficient one (6.8 ± 1.3 kg ha^{-1} of O_3, 3.9 ± 0.7 kg ha^{-1} of NO_2 and 0.4 ± 0.1 kg ha^{-1} of SO_2 removed each year). In Zone E, the high tree density overcame the limited removal of its main species (*B. pendula*), while the high removal values obtained for zone A and B, may be due to the presence of highly removing species, *i.e. R. pseudoacacia* (zone A) and *S. alba* (zone B). The sum of the various zones provides the pollution removal by the total NbS: 46.4 ± 10.7 kg ha^{-1} of O_3, 26.5 ± 6.0 kg ha^{-1} of NO_2, 2.4 ± 0.6 kg ha^{-1} of SO_2 and 3.4 ± 0.8 kg ha^{-1} of $PM_{2.5}$, for a total of 78.7 ± 15.7 kg ha^{-1} of pollutants removed (Tab. 1).

As previously described (Section 2.3.2), the *i-Tree Eco* modelling of air pollutant removal is strongly affected by the field data collection used to calculate the LA of each single tree. The plants with a highest modelled LAs have also the highest removal potentials. Indeed, when trees were surveyed in this NbS, *S. alba* trees were the most healthful and grown ones, thus showing the highest values for each biometric or health status category, such as DBH, crown width, health, and light exposure, and on the other hand, lower percentages of crown missing (Suppl. Materials S1). On the contrary, *S. aucuparia* trees significantly differed from the others, having the lowest recorded biometric values. Also trees from *B. pendula* and *T. cordata* species were characterized by low crown width (1.5 meter), low light exposure and a high percentage of crown missing (up to 50%), thus resulting in a low removal efficiency. It is important to underline that the species-specific affinity towards the removal of atmospheric pollutants, described in this section, as well the carbon impact described later in this study, may change over time, if the different growth rates of the trees species are considered.
The *i-Tree Eco* model has been often applied to assess air pollution mitigation at the city level, while very few examples of NbS modelling can be found. In our case, the identification of the recultivated landfill of Deusen as study area, allowed the evaluation of this regulating ES at this smaller scale (NbS one), thus providing a quantitative estimation of the provision of these air quality related benefits by the vegetation. One of the most impressive examples of *i-Tree Eco* model evaluation of air pollutant removal can be found in Nowak et al. 2006, that collected data for the green areas of 55 U.S.A. cities. Even if the use of no-local meteorological data may have affected the total annual O_3, NO_2 and SO_2 removal estimation obtained for the Deusen Nbs, these resulted to be within the ranges reported in this study (Nowak et al., 2006). This is an important result considering the high number of factors affecting air pollution removal such as tree species, plants health status, meteorological conditions and finally pollutants atmospheric concentrations (Guidolotti et al., 2016).

3.3 Intercomparison between SEM/EDX and i-Tree Eco *$PM_{2.5}$ removal results*

The amount of $PM_{2.5}$ removed in one month by single trees of *A. campestre*, *B. pendula*, *C. betulus* and *S. alba* in the Deusen NbS was estimated starting from the *i-Tree Eco* modelled values (see Section 2.3.2). Similarly, the upscale of the removed $PM_{2.5}$ was performed from the loads estimated by SEM/EDX, for all the four species considered and for the same size fraction. The two scaled up values, per each tree species, are compared

in Figure 5. Although the general trend showed by the two techniques was similar, the modelled values were always lower than those assessed by SEM/EDX, especially in the case of *S. alba*.

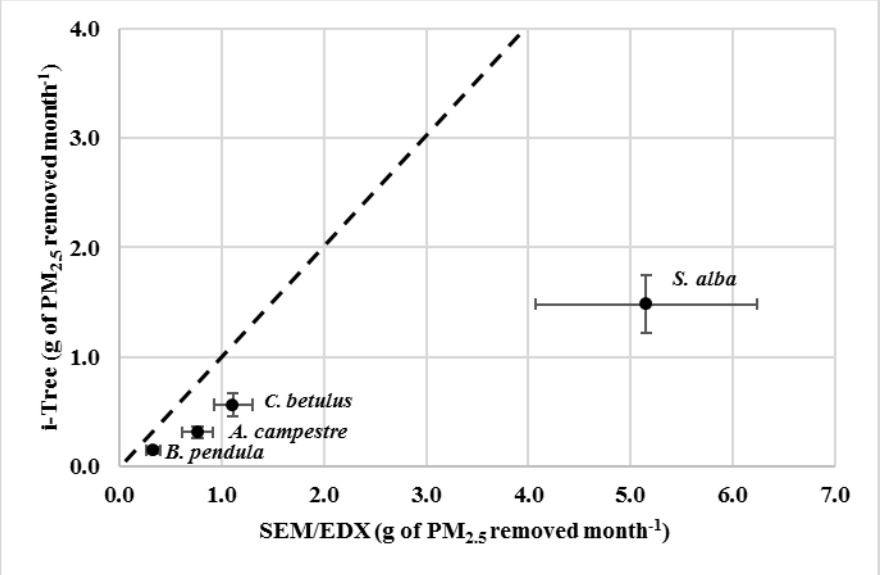

Figure 5. Kg of $PM_{2.5}$ removed in one month by single trees of the four considered species (*A. campestre*, *B. pendula*, *C. betulus* and *S. alba).* Standard deviations calculated for SEM/EDX experimental mass concentrations and uncertainties calculated for the *i-Tree Eco* modelling results are also reported. The dashed line represents the 1:1.

This could be explained by the presence of some gross approximations in the *i-Tree Eco* model. Firstly, the modelling of the atmospheric pollutant removal in the model is based on a V_d that is dependent on the pollutant type and not on the tree species, thus neglecting that species-specific traits and their impact on PM leaf deposition such as leaf morphological traits (Sæbø et al., 2012; Sgrigna et al., 2020; Dzierżanowski et al., 2011) and structure of the vegetation as a function of height and density (Abhijith and Kumar, 2020). This may be connected to the larger underestimation detected especially for single trees of *S. alba*, which among the other species is characterized by peculiar characteristic both in terms of crown structure and morphology both in terms of leaf micromorphology (presence of trichomes). Then, the model assumes that hourly meteorological and atmospheric pollutants concentration data are homogeneous over a region (Cabaran et al., 2013), this implying that only one station can be sourced for each type of data, within the model database. Riondato et al. 2020 evidenced how this aspect may be relevant in influencing the modelling of the air quality improvement by urban trees, through the comparison between modelled results of $PM_{2.5}$ removal and data from field monitoring stations, with only half of the real air quality improvement predicted by the model. A better parameterization of the *i-Tree Eco* model, accounting for species-specific deposition velocities, together with a wider set of usable meteorological/pollution stations may guarantee a more accurate estimation and a better validation with experimental data (Pace et al., 2021). Despite these limitations, the open-source *i-Tree Eco* model certainly represents an important tool for the evaluation of ESs provided by urban vegetation.

3.4 i-Tree Eco *model evaluation of carbon storage and gross sequestration*

The Deusen NbS showed a total dry biomass of 352.6 ± 88.9 tons ha^{-1} and an annual carbon gross sequestration of 12.8 ± 2.4 tons ha^{-1} $year^{-1}$. Carbon storage of single trees ranged from a minimum of 17.7 ± 4.5 kg for *S. aucuparia* to a maximum of 4844.2 ± 1223.6 kg for *S. alba* (Tab. 2). This latter species, with 3500 trees on a total of 63000 trees, accounted for 82% of the total NbS carbon storage, followed by relatively small percentages of *B. pendula* (7.5%) and *R. pseudoacacia* (4.6%). Also in this case, the results were strongly dependent on the field data collection, in particular DBH, as described in Section 2.3.3. Indeed, the higher values obtained for *S. alba* trees corresponded the highest DBH values among all the studied species.

Table 2. *I-Tree Eco* modelled carbon storage and sequestration. Single tree results (respectively expressed in kg and in kg $year^{-1}$) together with zone and total NbS results (tons ha^{-1} and tons ha^{-1} $year^{-1}$) are presented with calculated uncertainties.

Kg per single tree	**C storage**	**C sequestration per year**
***Salix alba* L.**	4844 ± 1224	110 ± 20
***Betula pendula* Roth**	80.7 ± 20.3	11.6 ± 2.1
***Robinia pseudoacacia* L.**	62.0 ± 15.6	6.0 ± 1.1
***Carpinus betulus* L.**	49.3 ± 12.4	7.4 ± 1.4
***Acer campestre* L.**	45.3 ± 11.4	3.5 ± 0.6
***Tilia cordata* L.**	39.0 ± 9.8	3.5 ± 0.6
***Sorbus aucuparia* L.**	17.7 ± 4.5	4.2 ± 0.8
Tons per hectare	**C storage**	**C sequestration per year**
Total NbS	353 ± 89	12.8 ± 2.4
Zone A	105 ± 26	7.6 ± 1.4
Zone B	985 ± 248	20.0 ± 3.7
Zone C	225 ± 57	8.2 ± 1.5
Zone D	84 ± 21	13.8 ± 2.6
Zone E	1277 ± 322	130 ± 24
Zone F	218 ± 55	19.6 ± 3.6

The carbon gross sequestration (expressed as kg $year^{-1}$) was directly influenced by the crown light exposure (Suppl. Materials S1). The *i-Tree Eco* model assigns to this parameter a high influence on trees growth and therefore their ability to sequestrate atmospheric carbon. Indeed, this was connected to the 110.3 ± 20.4 kg $year^{-1}$ detected also in this case, for *S. alba,* followed by *B. pendula* (11.6 ± 2.1 Kg $year^{-1}$), *C. betulus* (7.4 ± 1.4 kg $year^{-1}$) and *R. pseudoacacia* (6.0 ± 1.1 kg year $^{-1}$) (Tab. 2). For all these species, higher light crown exposures were reported, with values ranging between 4 and 4.5. As in the case of air pollutant removal, the species-specific affinity towards these carbon related ESs, which are directly influenced by the tree health and grown status, may indirectly provide information on the adaptability of single species to this specific urban context. This is true since the most grown plants are expected to be also the ones with higher adaptability to the highly stressful living conditions of these environments. The highest tree density detected in the NbS and

the massive presence of *B. pendula* trees in the Zone E, determined higher values per unit area for both carbon storage and carbon sequestration (1277.4 ± 322.1 tons ha^{-1} and 130.2 ± 24.0 tons ha^{-1} $year^{-1}$, respectively). Also Zone B, composed by 5500 trees distributed between *A. campestre* and *S. alba*, resulted in high carbon storage (984.7 ± 248.5 tons ha^{-1}) and sequestration (20.0 ± 3.7 tons ha^{-1} $year^{-1}$) (Tab. 2).

Lately, Song et al. 2020 evaluated the provision of various ESs by four different urban green areas in Luohe city (China), through the application of the *i-Tree Eco* model and the acquisition of high-resolution aerial images: for a total of 3320 hectares of urban green areas and a density of about 750 trees ha^{-1}, they estimated a total carbon storage and sequestration of 16 tons ha^{-1} and 1.5 tons ha^{-1} $year^{-1}$, respectively. The impact of the Deusen NbS it was much larger, with a carbon storage and sequestration per unit area of 352.6 ± 88.9 tons ha^{-1} and 12.8 ± 2.4 tons ha^{-1} $year^{-1}$, respectively. This was probably linked to the higher tree density (average of 1050 trees ha^{-1}) and its specific tree composition. Numerous studies, investigating the carbon of urban green areas, underlined the need of comparing these data to urban carbon emissions data, to evaluate their real impact. The Global Covenant of Mayors for Climate and Energy, which gathers a multitude of local governments engaged in the reduction of GHGs emissions, reported for Dortmund city a baseline (referred to the year 2008) of GHGs emission of about 9 million tons (https://www.globalcovenantofmayors.org/.). The Deusen NbS, that is only one of the several green area of the city of Dortmund covering about the 0.21% of the city, was able to store in its dry biomass the 0.22% of the carbon emitted that is within the range of 0.12%-2.75% reported from Barò et al., 2015 for green areas of different European cities. Taking in account previously described results, it is worth noticing that if this urban forest was exclusively composed by *S. alba* trees, the ones with the higher adaptability, it would be able to store up to 3.4% of carbon emitted, with about 305 thousand tons stored in its biomass. This underlines the importance of a proper selection of species, based on an accurate quantification of their affinity towards the provision of ESs and their adaptability, in the design of highly efficient NbS. For a proper assessment of the climate change mitigation potential of urban green areas, it would be necessary to consider the whole carbon balance (Kabisch et al., 2017; Nicese et al., 2021) thus accounting also for all GHG emissions connected to the NbS implementation and maintenance (e.g soil preparation, pruning, etc), decomposition rate of removed plants and also the role of soil as natural carbon sink and source.

4. Conclusions

This study is focused on the evaluation of the atmospheric pollutants removal and the carbon impact of an NbS implemented on a former landfill in Dortmund (DE). The experimental SEM/EDX results on PM removal are used as proxy for the species-specific affinity towards the removal via leaf deposition, with *Salix alba* being the most efficient one. The experimental removal of PM is compared with the output obtained by *i-Tree Eco* model, with the confirmation of the species-specific trend despite the modelled data were systematically underestimated. Additionally, the modelling outputs demonstrate how plant density can compensate for lower tree PM removal efficiency. The carbon impact of the tree species located within the NbS is also evaluated through *i Tree Eco*, and the results give important information about carbon storage and gross sequestration

that are directly connected to the amount of dry biomass and the trees rate of growth. Among the tree species, *S. alba* plants emerged as those having the major impact for all the ESs analysed in this study, likely due to the best adaptability of this species in the study area. Finally, our study underlines some of the main advantages which may be connected to the implementation of NbS, such as the afforestation of post-industrial sites, and presented results could be extremely relevant, for the management of already implemented NbS, and for the design of new ones, which are expected to increasingly efficient in the future.

Supplementary materials

Supplementary materials S1. Zonation of the NbS, species-specific composition, number of trees, and relative biometric/health status information. Reported information were averaged over the total number of trees surveyed for each zone.

Zone	Ha	Species	Nr. of trees	Height (m)	DBH (cm)	Crown base height (m)	Crown width (m)	Crown missing	Crown health	Crown light exposure
A	9	*R. pseudoacacia* L. 1	1400	15	20	4	5	40%	17.5%	4
		R. pseudoacacia L. 2	12600	15	20	4	5	20%	5%	1
B	10	*A. campestre* L.	3500	8	15	3	5	20%	17.5%	4
		S. alba L. 1	2000	11	80	1	7.5	20%	40%	4.5
C	35	*B. pendula* Roth 1	3500	13	15	6	3	5%	5%	4.5
		S. alba L. 2	1500	10	80	3	8	30%	5%	4
		C. betulus L.	7000	6	15	2	6	10%	5%	4.5
D	0,8	*S. aucuparia* L. 1	350	4.5	10	0.5	1	40%	5%	4
		S. aucuparia L. 2	3150	4.5	10	0.5	1	20%	5%	1
E	1	*B. pendula Roth* 2	1400	9	15	3	3	40%	5%	4
		B. pendula Roth 3	12600	9	15	3	3	20%	5%	3
F	2,5	*T. cordata* MILL. 1	1400	12	15	5	1.5	40%	5%	2
		T. cordata MILL. 1	12600	12	15	5	1.5	50%	5%	2

Supplementary materials S2. Mean species-specific particle densities (number of particles * 10^4 * mm^{-2}), with standard deviations, on the adaxial (AD) and abaxial (AB) sides, for the three PM size fractions ($PM_{0.2-1}$, $PM_{1-2.5}$, $PM_{2.5-10}$). Results averaged over the four species are also reported as mean NbS values. *S. alba* AB values have been estimated (*) thus averaging the AD/AB ratio detected in the other three species.

AD					
10^4 particles/mm^2	***A. campestre***	***B. pendula***	***C. betulus***	***S. alba***	**Mean NbS**
$PM_{0,2-1}$	3.02 ± 0.65	2.58 ± 0.45	2.76 ± 0.33	2.30 ± 0.23	2.67 ± 0.30
$PM_{1-2,5}$	0.29 ± 0.04	0.18 ± 0.06	0.22 ± 0.05	0.15 ± 0.03	0.21 ± 0.06
$PM_{2,5-10}$	0.040 ± 0.005	0.010 ± 0.003	0.02 ± 0.01	0.010 ± 0.001	0.02 ± 0.01
$PM_{0,2-10}$	3.35 ± 0.69	2.77 ± 0.51	3.00 ± 0.38	2.47 ± 0.23	2.90 ± 0.37
AB					
$PM_{0,2-1}$	2.08 ± 0.25	1.83 ± 0.50	1.79 ± 0.31	1.57 ± 0.16*	1.82 ± 0.21
$PM_{1-2,5}$	0.13 ± 0.02	0.15 ± 0.03	0.13 ± 0.03	0.10 ± 0.02*	0.13 ± 0.02
$PM_{2,5-10}$	0.020 ± 0.001	0.020 ± 0.003	0.010 ± 0.004	0.010 ± 0.0006*	0.010 ± 0.003
$PM_{0,2-10}$	2.23 ± 0.26	2.00 ± 0.53	1.92 ± 0.34	1.67 ± 0.16*	1.96 ± 0.23

Author Contributions: Conceptualization, C.B.; methodology, M.R., G.G., and C.B.; formal analysis, M.R., G. S., C.B. and G.G; investigation, M.R., G.G. and G.S.; resources, M.J., D.K., A.T..; writing—original draft preparation, M.R.; writing—review and editing, C.B., G.G., V.G., A.T., C.C.; visualization, M.R., C.B. and A.T.; supervision, C.C.; project administration, A.T., C.C.; funding acquisition, C.C., A. T. All authors have commented read and agreed to the final version of the manuscript.

Funding: The research leading to these results has received funding from the European Union's Horizon 2020 innovation action program under Grant Agreement no. 776528. The sole responsibility for the content lies with the proGIreg project and in no way reflects the views of the European Union.

Acknowledgments: The authors thank Arianna Calabresi for preliminary measurements and Dania Valli for supporting data acquisition.

Conflicts of Interest: The authors declare no conflict of interest. The funders had no role in the design of the study; in the collection, analyses, or interpretation of data; in the writing of the manuscript, or in the decision to publish the results.

References

1. Rafael, S.; Vicente, B.; Rodrigues, V.; Miranda, A. I.; Borrego, C.; Lopes, M., 2018. Impacts of green infrastructures on aerodynamic flow and air quality in Porto's urban area. Atmospheric Environment 190, 317–330. https://doi.org/10.1016/j.atmosenv.2018.07.044
2. European Environment Agency (EEA), 2016. Air Quality in Europe — 2016 Report. Publications Office of the European Union, Luxembourg ISBN 978-92-9213-847-9.
3. Ferm, M.; Svanberg, P., 1998. Cost-efficient techniques for urban- and background measurements of SO2 and NO2, Atmospheric Environment 32 (8), 1377-1381, ISSN 1352-2310, https://doi.org/10.1016/S1352-2310(97)00170-2.
4. Meng, Z. Y.; Ding, G. A.; Xu, X. B.; Xu, X. D.; Yu, H. Q.; Wang, S. F., 2008. Vertical distributions of SO2 and NO2 in the lower atmosphere in Beijing urban areas, China, Science of The Total Environment, 390 (2–3), 456-465, ISSN 0048-9697, https://doi.org/10.1016/j.scitotenv.2007.10.012.
5. Cohen, A. J.; Anderson, H. R.; Ostro, B.; Pandey, K. D.; Krzyzanowski, M.; Künzli, N.; Gutschmidt, K.; Pope, A.; Romieu, I.; Samet, J. M.; Smith, K., 2005. The global burden of disease due to outdoor air pollution. J Toxicol Environ Health A., Jul 9-23; 68 (13-14):1301-7. doi: 10.1080/15287390590936166.
6. Jacob, D. J., 2000. Heterogeneous chemistry and tropospheric ozone, Atmospheric Environment 34 (12–14), 2131-2159, ISSN 1352-2310, https://doi.org/10.1016/S1352-2310(99)00462-8.
7. Marble, S. C.; Prior, S. A.; Runion, G. B.; Torbert, H. A.; Gilliam, C. H.; Fain, G. B., 2011. The Importance of Determining Carbon Sequestration and Greenhouse Gas Mitigation Potential in Ornamental Horticulture. HORTSCIENCE, 46(2):240–244. 2011. https://doi.org/10.21273/HORTSCI.46.2.240
8. IPCC., 2007. Contribution of Working Group II to the Fourth Assessment Report of the Intergovernmental Panel on Climate Change. Parry, M.L., O.F. Canziani, J.P. Palutikof, P.J. van der Linden, and C.E. Hanson (eds.). Cambridge University Press, Cambridge, UK.
9. Florides, G. A.; Christodoulides. P., 2008. Global warming and carbon dioxide through sciences. J. Environ. Intl., 35:390–401.
10. Douglas, L., 2004. Global warming. Facts on File Inc., New York, NY. ISBN: 0816051372
11. Oliveira, S.; Andrade, H.; Vaz, T., 2011. The cooling effect of green spaces as a contribution to the mitigation of urban heat: A case study in Lisbon, Building and Environment, 46 2186-2194. doi:10.1016/j.buildenv.2011.04.034
12. Nowak, D.J., 2000. The interactions between urban forests and global climate change. In: Abdollahi, K.K.; Ning, Z.H. Appeaning, A. (Eds.), Global Climate Change and the Urban Forest. GCRCC and Franklin Press, Baton Rouge, LA, pp. 31–44.
13. European Commission, 2015. Nature-based solutions & re-naturing cities. Final report of the horizon 2020 28 expert group on 'Nature-Based solutions and Re-Naturing cities'. https://doi.org/10.2777/765301
14. Cohen-Shacham, E.; Walters, G.; Janzen, C.; Maginnis, S., 2016. Nature-based Solutions to address global societal challenges. Gland, Switzerland: IUCN xiii + 97pp. http://dx.doi.org/10.2305/IUCN.CH.2016.13.en
15. Faivre, N.; Fritz, M.; Freitas, T.; de Boissezon, B.; Vandewoestijne, S. 2017. Nature-Based Solutions in the EU: Innovating with nature to address social, economic and environmental challenges, Environmental Research , 159, 509–518. http://dx.doi.org/10.1016/j.envres.2017.08.032
16. Carrus, G.; Scopelliti, M.; Lafortezza, R.; Colangelo, G.; Ferrini, F.; Salbitano, F.; Agrimi, M.; Portoghesi, L.; Semenzato, P.; Sanesi, G., 2015. Go greener, feel better? The positive effects of biodiversity on the well-being of individuals visiting urban and peri-urban green areas. Landsc. Urban Plan., 134, 221–228. http://dx.doi.org/10.1016/j.landurbplan.2014.10.022
17. Ruangpan, L.; Vojinovic, Z.; Di Sabatino, S.; Leo, L. S.; Capobianco, V.; Oen, A. M. P.; McClain, M. E.; Lopez-Gunn, E.,2020. Nature-based solutions for hydro-meteorological risk reduction: a state-of-the-art review of the research area. Natural Hazards and Earth System Sciences, 20: 243–270. 49 doi:10.5194/nhess-20-243-2020.2020.
18. Escobedo, F. J.; Giannico, V.; Jim, C. Y.; Sanesi, G.; Lafortezza, R., 2019. Urban forests, ecosystem services, green infrastructure and nature-based solutions: Nexus or evolving metaphors? Urban Forestry & Urban Greening, 37 3–12. https://doi.org/10.1016/j.ufug.2018.02.011
19. Panno, A.; Carrusa, G.; Lafortezza, R.; Mariani, L.; Sanesi G., 2017. Nature-based solutions to promote human resilience and wellbeing in cities during increasingly hot summers. Environmental Research, 159, 249–256. http://dx.doi.org/10.1016/j.envres.2017.08.016

20. Song, Y.; Kirkwood, N.; Maksimović, C.; Zheng, X.; O'Connor, D.; Jin, Y.; Hou, D., 2019. Nature based solutions for contaminated land remediation and brownfield redevelopment in cities: A review. Science of The Total Environment, 663, 568-579. https://doi.org/10.1016/j.scitotenv.2019.01.347
21. Costanza, R.; d'Arge, R.; de Groot, R.; Farber, S.; Grasso, M.; Hannon, B.; Limburg, K.; Naeem, S.; O'Neill, R. V.; Paruelo, J.; Raskin, R. G.; Sutton, P.; van den Belt, M., 1997. The value of the world's ecosystem services and natural capital. Nature, 387, 253–260. https://doi.org/10.1038/387253a0
22. Millennium Ecosystem Assessment (Program), 2005. Ecosystems and human well-being. Washington, D.C: Island Press.
23. Nowak, D. J.; Crane, D. E.; Stevens, J. C., 2006. Air pollution removal by urban trees and shrubs in the United States, Urban Forestry & Urban Greening, 4, 115–123. doi:10.1016/j.ufug.2006.01.007
24. Janhall, S., 2015. Review on urban vegetation and particle air pollution: Deposition and dispersion. Atmospheric Environment, 105, 130-137. http://dx.doi.org/10.1016/j.atmosenv.2015.01.052
25. Currie, B. A.; Bass, B., 2008. Estimates of air pollution mitigation with green plants and green roofs using the UFORE model. Urban Ecosystems, 11, 409–422. DOI: 10.1007/s11252-008-0054-y
26. Sæbø, A.; Popek, R.; Nawrot, B.; Hanslin, H. M.; Gawronska, H.; Gawronski, S. W., 2012. Plant species differences in particulate matter accumulation on leaf surfaces. Science of the Total Environment, 427–428, 347–354.
27. Wang, H.; Shi, H.; Wang, Y., 2015. Effects of Weather, Time, and Pollution Level on the Amount of Particulate Matter Deposited on Leaves of Ligustrum lucidum. Hindawi Publishing Corporation, Scientific World Journal, Article ID 935942, 8 pages http://dx.doi.org/10.1155/2015/935942
28. Sgrigna, G.; Baldacchini, C.; Dreveck, S.; Cheng, Z.; Calfapietra, C., 2020. Relationships between air particulate matter capture efficiency and leaf traits in twelve tree species from an Italian urban-industrial environment. Science of the Total Environment, 718, 137310. https://doi.org/10.1016/j.scitotenv.2020.137310
29. Ristorini, M.; Baldacchini, C.; Massimi, L.; Sgrigna, G.; Calfapietra, C., 2020 Innovative Characterization of Particulate Matter Deposited on Urban Vegetation Leaves through the Application of a Chemical Fractionation Procedure. Int. J. Environ. Res. Public Health, 17, 5717. https://doi.org/10.3390/ijerph17165717
30. Baro´, F.; Chaparro, L.; Gomez-Baggethun, E.; Langemeyer, J.; Nowak, D. J.; Terradas, J., 2014. Contribution of Ecosystem Services to Air Quality and Climate Change Mitigation Policies: The Case of Urban Forests in Barcelona, Spain. AMBIO, 43:466–479 DOI 10.1007/s13280-014-0507-x
31. Myeong, S.; Nowak, D. J.; Duggin, M. J., 2006. A temporal analysis of urban forest carbon storage using remote sensing. Remote Sensing of Environment, 101, 277 – 282. doi:10.1016/j.rse.2005.12.001
32. Nowak, D. J.; Stevens, J. C.; Sisinni, S. M.; Luley, C. J., 2002. Effects of urban tree management and species selection on atmospheric carbon dioxide. Journal of Arboriculture, 28(3): 113-122.
33. Calliari E.; Staccione A.; Mysiak J., 2019. An assessment framework for climate-proof nature-based solutions, Science of The Total Environment, 656, 15 March 2019, Pages 691-700, https://doi.org/10.1016/j.scitotenv.2018.11.341
34. Ordóñez, C.; Grant, A.; Millward, A.; Steenberg, J.; Sabetski, V., 2019. Developing Performance Indicators for Nature-Based Solution Projects in Urban Areas: The Case of Trees in Revitalized Commercial Spaces. Cities And The Environment (CATE), 12 (1).
35. Farrugia, S.; Hudson, M. D.; McCulloch, L., 2015. An evaluation of flood control and urban cooling ecosystem services delivered by urban green infrastructure, International Journal of Biodiversity Science, Ecosystem Services & Management, 9 (2), 136–145, http://dx.doi.org/10.1080/21513732.2013.782342
36. Jafari, M.; Knappe, D.; Rehkop, N.; Runte, J.; Morgenstern, R.; Störzner, A.; Pölling, B., 2021. Dortmund Living Lab Implementation Plan, Deliverable No. 3.2, proGIreg. Horizon 2020 Grant Agreement No 776528, European Commission. Accessed April 03, 2021. https://progireg.eu/resources/planning-implementing-nbs/
37. Climate Data Center - Deutscher Wetterdienst - https://cdc.dwd.de/portal/
38. M. Tomašević, Z. Vukmirović, S. Rajšić, M. Tasić, B. Stevanović, 2005. Characterization of trace metal particles deposited on some deciduous tree leaves in an urban area, Chemosphere, Volume 61, Issue 6, Pages 753-760, ISSN 0045-6535, https://doi.org/10.1016/j.chemosphere.2005.03.077.
39. Nečas, D., Klapetek, P., 2012. Gwyddion: an open-source software for SPM data analysis. Open Phys 10, 181–188. https://doi.org/10.2478/s11534-011-0096-2.
40. Baldacchini, C.; Castanheiro, A.; Maghakyan, N.; Sgrigna, G.; Verhelst, J.; Alonso, R.; Amorim, J.H.; Bellan, P.; Bojović, D.D.; Breuste, J.; et al., 2017. How Does the Amount and Composition of PM Deposited on Platanus acerifolia Leaves Change Across Different Cities in Europe? Environ. Sci. Technol., 51, 1147–1156. https://doi.org/10.1021/acs.est.6b04052
41. Merkus, H.G., 2009. Particle size measurements. In: Springer, S. (Ed.), Particle Technology
42. Schneider CA, Rasband WS, Eliceiri KW (2012) NIH Image to ImageJ: 25 years of image analysis. Nat Methods 9:671–675
43. https://www.webelements.com/periodicity/density/
44. Baldacchini, C.; Sgrigna, G.; Clarke, W.; Tallis, M.; Calfapietra, C., 2019. An ultra-spatially resolved method to quali-quantitative monitor particulate matter in urban environment. Environ Sci Pollut Res, 26, 18719–18729. https://doi.org/10.1007/s11356-019-05160-8
45. i-Tree Eco v.6.0, User Manual. https://www.itreetools.org/support/resources-overview/i-tree-manuals-workbooks
46. Pace, R.; Biber, P.; Pretzsch, H.; Grote, R., 2018. Modeling Ecosystem Services for Park Trees: Sensitivity of i-Tree Eco Simulations to Light Exposure and Tree Species Classification. Forests, 9, 89; doi:10.3390/f9020089
47. Hirabayashi, S.; Kroll, C. N.; Nowak, D. J, 2012. i-Tree Eco Dry Deposition Model Descriptions.
48. Nowak, D.J.; Hirabayashi, S.; Bodine, A.; Hoehn, R., 2013. Modeled PM2.5 removal by trees in ten US cities and associated health effects. Environ. Pollut., 178, 395–402.

49. Xu, X.; Zhang, Z.; Bao, L.; Mo, L.; Yu, X.; Fan, D.; Lun, X., 2017. Influence of rainfall duration and intensity on particulate matter removal from plant leaves, Science of The Total Environment, Volume 609, Pages 11-16, ISSN 0048-9697, https://doi.org/10.1016/j.scitotenv.2017.07.141.
50. Martin, N. A.; Chappelka, A. H.; Loewenstein, E. F.; Keever, G. J., 2012. Comparison of carbon storage, carbon sequestration, and air pollution removal by protected and maintained urban forests in Alabama, USA, International Journal of Biodiversity Science, Ecosystem Services & Management 8:3, 265-272, DOI: 10.1080/21513732.2012.712550
51. Nowak, D.J.; Crane, D. E., 2002. Carbon storage and sequestration by urban trees in the USA. Environ Pollut., 116(3):381–389. PII: S0269-7491(01)00214-7
52. Nowak, D.J., 1994. Atmospheric Carbon Dioxide Reduction by Chicago's urban forest. In Chicago's Urban Forest Ecosystem: Results of the Chicago Urban Forest Climate Project; McPherson, E.G., Nowak, D.J., Eds.; US Department of Agriculture, Forest Service, Northeastern Forest Experiment Station: Radnor, PA, USA, 1994; pp. 83–94.
53. Ottele, M.; van Bohemen, H. D.; Fraaij, A. L. A., 2010. Quantifying the deposition of particulate matter on climber vegetation on living walls. Ecol. Eng., 36, 154-162. https://doi.org/10.1016/j.ecoleng.2009.02.007.
54. Shi, J.; Zhang, G.; An, H.; Yin, W.; Xia, X., 2008. Quantifying the particulate matter accumulation on leaf surfaces of urban plants in Beijing, China. Atmospheric Pollution Research, 8, 836-842. http://dx.doi.org/10.1016/j.apr.2017.01.011
55. Weerakkody, U.; Dover, J. W.; Mitchell, P.; Reiling, K, 2017. Particulate matter pollution capture by leaves of seventeen living wall species with special reference to rail-traffic at a metropolitan station, Urban Forestry & Urban Greening 27, 173-186, ISSN 1618-8667, https://doi.org/10.1016/j.ufug.2017.07.005.
56. Abhijith, K.V.; Kumar, P.; 2020. Quantifying particulate matter reduction and their deposition on the leaves of green infrastructure, Environmental Pollution. https://doi.org/10.1016/j.envpol.2020.114884.
57. Amato, F.; Pandolfi, M.; Viana, M.; Querol, X.; Alastuey, A.; Moreno, T., 2009. Spatial and chemical patterns of PM10 in road dust deposited in urban environment. Atmospheric Environment, 43, 9, 1650-1659. https://doi.org/10.1016/j.atmosenv.2008.12.009
58. Bencharif-Madani, F.; Ali-Khodj, H.; Kemmouche, A.; Terrouche, A.; Lokorai, K.; Naidja, L.; Bouziane, M., 2019. Mass concentrations, seasonal variations, chemical compositions and element sources of PM10 at an urban site in Constantine, northeast Algeria. Journal of Geochemical Exploration, 206, 106356. https://doi.org/10.1016/j.gexplo.2019.106356
59. Massimi, L.; Ristorini, M.; Astolfi, M. L.; Perrino, C.; Canepari, S., 2020. High resolution spatial mapping of element concentrations in PM10: A powerful tool for localization of emission sources, Atmospheric Research, 244, 105060. https://doi.org/10.1016/j.atmosres.2020.105060.
60. Ristorini, M.; Astolfi, M.L.; Frezzini, M.A.; Canepari, S.; Massimi, L., 2020. Evaluation of the Efficiency of Arundo donax L. Leaves as Biomonitors for Atmospheric Element Concentrations in an Urban and Industrial Area of Central Italy. Atmosphere, 11, 226. https://doi.org/10.3390/atmos11030226
61. Massimi, L.; Conti, M. E.; Mele, G.; Ristorini, M.; Astolfi, M. L.; Canepari, S., 2019. Lichen transplants as indicators of atmospheric element concentrations: a high spatial resolution comparison with PM10 samples in a polluted area (Central Italy), Ecological Indicators, 101, 759-769, https://doi.org/10.1016/j.ecolind.2018.12.051.
62. Davila, A. F.; Rey, D.; Mohamed, K.; Rubio, B.; Guerra, A. P., 2006. Mapping the Sources of Urban Dust in a Coastal Environment by Measuring Magnetic Parameters of Platanus hispanica Leaves. Environ. Sci. Technol., 40, 3922−3928
63. Cai, M.; Xin, Z.; Yu, X., 2017. Spatio-temporal variations in PM leaf deposition: A meta-analysis. Environ Pollut., 231(Pt 1), 207-218. doi: 10.1016/j.envpol.2017.07.105.
64. He, C., Qiu, K. & Pott, R., 2020. Reduction of urban traffic–related particulate matter—leaf trait matters. Environ Sci Pollut Res 27, 5825–5844. https://doi.org/10.1007/s11356-019-07160-0
65. Przybysz, A., Nersisyan, G. & Gawroński, S.W., 2019. Removal of particulate matter and trace elements from ambient air by urban greenery in the winter season. Environ Sci Pollut Res 26, 473–482. https://doi.org/10.1007/s11356-018-3628-0
66. Dzierżanowski, K.; Popek, R.; Gawrońska, H.; Sæbø, H.; Gawroński, S. W., 2011. Deposition of Particulate Matter of Different Size Fractions on Leaf Surfaces and in Waxes of Urban Forest Species. International Journal of Phytoremediation, 13:10, 1037-1046, DOI: 10.1080/15226514.2011.552929
67. Hofman, J.; Stokkaer, I.; Snauwaert, L.; Samson, R., 2013. Spatial distribution assessment of particulate matter in an urban street canyon using biomagnetic leaf monitoring of tree crown deposited particles, Environmental Pollution, 183, 123-132, ISSN 0269-7491, https://doi.org/10.1016/j.envpol.2012.09.015.
68. Guidolotti, G.; Salviato, M.; Calfapietra, C., 2016. Comparing estimates of EMEP MSC-W and UFORE models in air pollutant reduction by urban trees. Environ Sci Pollut Res Int. 2016 23(19):19541-50. doi: 10.1007/s11356-016-7135-x. Epub Jul 8. PMID: 27392620.
69. Cabaraban, M. T. I.; Kroll, C. N.; Hirabayashi, S.; Nowak, D. J., 2013. Modeling of air pollutant removal by dry deposition to urban trees using a WRF/CMAQ/i-Tree Eco coupled system, Environmental Pollution 176, 123-133, https://doi.org/10.1016/j.envpol.2013.01.006.
70. Riondato, E.; Pilla, F.; Basu, A. S.; Basu, B., 2020. Investigating the effect of trees on urban quality in Dublin by combining air monitoring with i-Tree Eco model, Sustainable Cities and Society 61, 102356, ISSN 2210-6707, https://doi.org/10.1016/j.scs.2020.102356.
71. Pace, R.; Guidolotti, G.; Baldacchini, G.; Pallozzi, E.; Grote, R.; Nowak, D. J.; Calfapietra, C., 2021. Comparing i-Tree Eco Estimates of Particulate Matter Deposition with Leaf and Canopy Measurements in an Urban Mediterranean Holm Oak Forest. Environmental Science & Technology, 55, 6613-6622. DOI: 10.1021/acs.est.0c07679

72. Song, P.; Kim, G.; Mayer, A.; He, R.; Tian, G., 2020. Assessing the Ecosystem Services of Various Types of Urban Green Spaces Based on i-Tree Eco. Sustainability, 12, 1630. https://doi.org/10.3390/su12041630
73. https://www.globalcovenantofmayors.org/. Accessed on 26 April 2021
74. Baró, F.; Haase, D.; Gómez-Baggethun, E.; Frantzeskaki, N., 2015. Mismatches between ecosystem services supply and demand in urban areas: a quantitative assessment in five European cities. Ecol Indic, 55, 146–158.
75. Kabisch, N.; Korn, H.; Stadler, J.; Bonn, A., 2017. Nature-based solutions to climate change adaptation in urban areas - linkages between science, policy and practice. Cham: Springer doi:10.1007/978-3-319-56091-5_1.
76. Nicese, F. P.; Colangelo, G.; Comolli, R.; Azzini, L.; Lucchetti, S.; Marziliano, P. A.; Sanesi, G., 2021. Estimating CO2 balance through the Life Cycle Assessment prism: A case – Study in an urban park, Urban Forestry & Urban Greening, Volume 57, 126869, ISSN 1618-8667, https://doi.org/10.1016/j.ufug.2020.126869.

5.3 Ningbo Living Lab case study: SEM/EDX evaluation of leaf deposited PM

Preliminary results

Within the context of ProGIreg, the defined Ningbo Living Lab (28 ha) is mainly located in the so-called Moon Lake Park, a shallow lake in the centre of the city (geographical coordinates: 29°51'52.5"N, 121°32'37.1"E). The lake has the ecological functions of storing and purifying water, providing habitats for animals and plants, and regulating the nearby climate to reduce the urban heat island effect. In recent years, severe eutrophication events have occurred frequently, and seasonal polluted and malodorous water has appeared locally. The water quality has gradually deteriorated, greatly reducing the ecological and social benefits of the urban lake. SEM/EDX evaluation of leaf deposited PM and potential abatement of this atmospheric pollutant is focused on a specific NbS implemented at the Moon Lake, which consists on the planting of aquatic plants along the shore of the lake (Baldacchini, 2021). To this aim, three sampling sites are individuated along the lakeshore for leaves collection (Fig. 1).

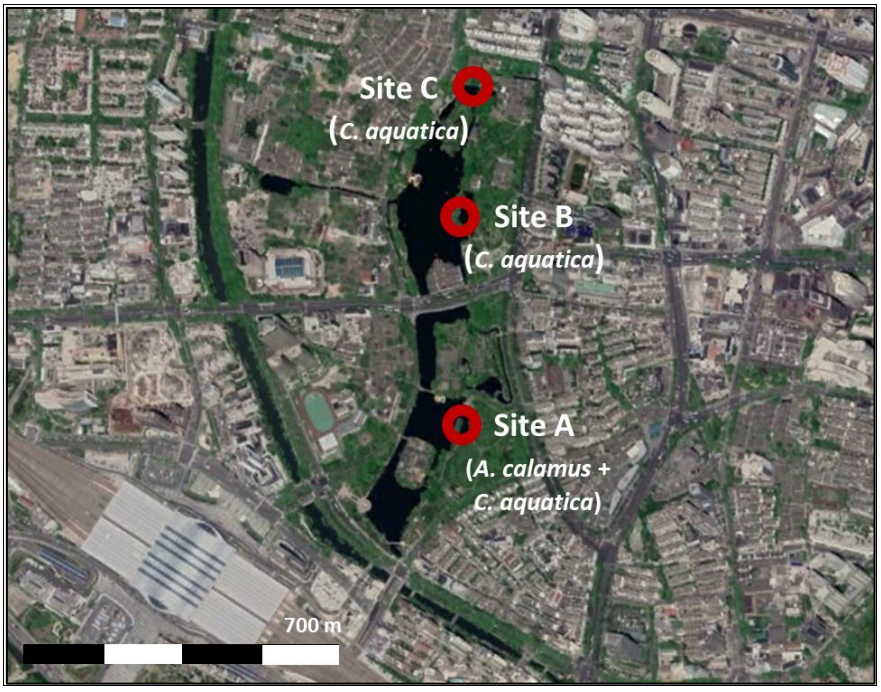

Figure 1. Leaf sampling sites in Ningbo NbS for PM biomonitoring task.

Fully grown leaves have been collected in August 2020, after one week of no precipitations, from two herbaceous and aquatic species, namely *Acorus calamus* L. and *Canna aquatica* L.. Two leaves from three different plants of *A. calamus* L. (for a total of six leaves) and two leaves from three different plants of *C. aquatica* L. (for a total of six leaves) have been sampled in a first sampling

location along the shore (Site A, Figure 1). Then for *C. aquatica* L., additional leaves have been also sampled in other two locations (Site B and C Figure 1), thus always collecting two leaves from three different plants in each sites. Leaves have been always collected from the external part of the plants. In this specific case, it was possible not only to evaluate the species-specific PM abatement of the two species, but also to retrieve potential site-specific information on PM pollution and the impact of local emission sources (only for *C. aquatica* L.).

In Figure 2, results related to the density of leaf deposited particles (number of particles per mm^2 of leaf area unit), as a function of species, sites for *C. aquatica,* size fractions ($PM_{0.3-1}$, $PM_{1-2.5}$ and $PM_{2.5-10}$) are presented. Density results are also described with details on the upper (adaxial, AD) and lower (abaxial, AB) leaf surfaces.

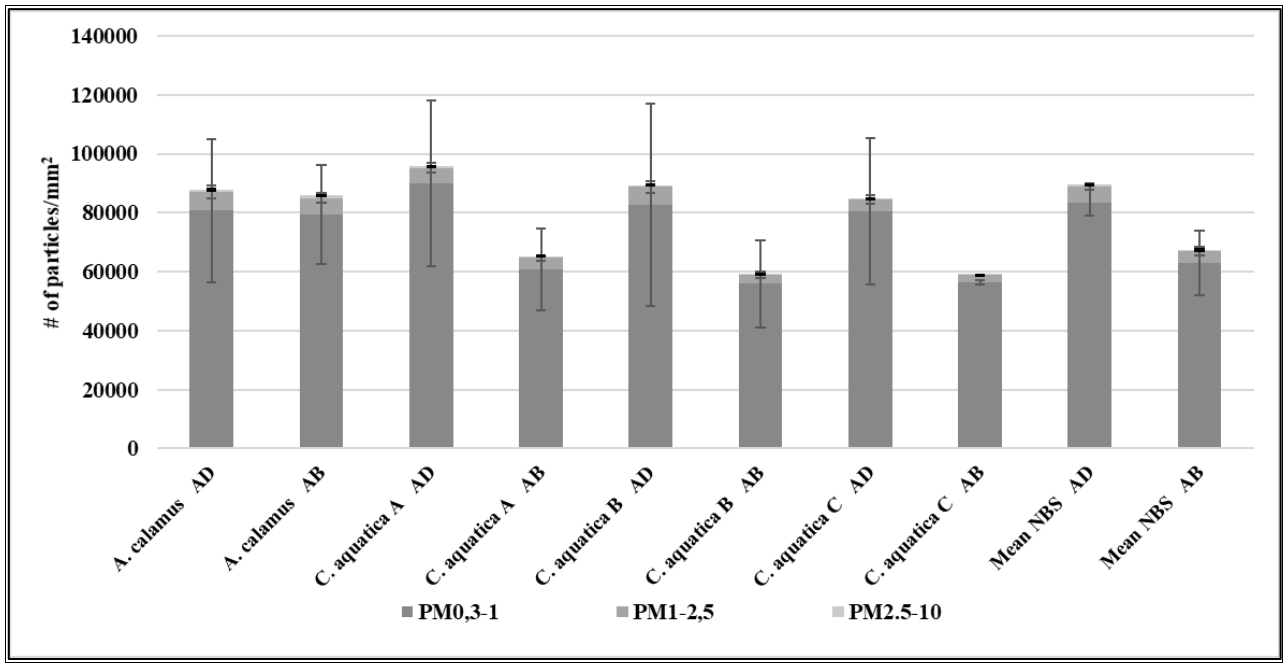

Figure 2. Mean species-specific and site particle densities (number of particles * mm^{-2}), with standard deviations, on the adaxial (AD) and abaxial (AB) sides, for the three PM size fractions ($PM_{0.3-1}$, $PM_{1-2.5}$, $PM_{2.5-10}$). Results averaged over the two species are also reported as mean NBS values.

Interestingly, no differences are detected between the AD and AB leaf surfaces. Lower deposition values for AB surfaces are usually described in literature, because of the impact of micromorphological leaf traits (such as trichomes or stomata) and also of their specific orientation towards the air flow, thus being able to affect the deposition of airborne particles (Ottele et al., 2010; Shi et al., 2008). This result may be explained taking in account the peculiar leaf orientation of these aquatic species, which usually have a more vertical development in comparison to what is usually

described for trees. This may determine a more homogeneous exposure of the two leaf surfaces to the air flow and therefore quite homogeneous deposition rate of atmospheric PM.

As expected, the $PM_{0.3-1}$ size fraction is the most abundant one in terms of particles density, ranging from 91.9% to 94.7% for AD sides (respectively for *A. calamus* and *C. aquatica* in site C) and from 92.4% to 95.3% for AB sides (respectively for *A. calamus* and *C. aquatica* in site C). The $PM_{1-2.5}$ is represented by percentages ranging from 4.8% (*C. aquatica* in site C) to 7.1% (*A. calamus*) in the AD surfaces, while for the AB ones, these percentages range from 4.2% (*C. aquatica* in site C) to 6.7% (*A. calamus*). Finally, the AD coarse particles ($PM_{2.5-10}$) ranged from 0.5% (*C. aquatica* in site C) to 0.9% (*A. calamus*), same as the range of AB ones. If the total leaf deposited particles ($PM_{0.3-10}$) are considered, no appreciable differences are detected between the two aquatic species and for *C. aquatica* at the three sampling sites. *C. aquatica* leaves sampled at the so-called site C, result as the ones characterized in their AB surfaces by the lowest particles densities in all the three size fractions, respectively being for $PM_{0.3-1}$, 56313 ± 765 particles per mm^2, for $PM_{1-2.5}$, 2508 ± 139 particles mm^2 and for $PM_{2.5-10}$, 281 ± 24 particles per unit leaf area in mm^2. These results being significantly different only with the ones detected in each size fraction for *A. calamus* in site A. Instead, no appreciable differences are found between AB surfaces of *C. aquatica* sampled at the three sites (A, B and C) and for all the considered AD surfaces, both *A. calamus* and both *C. aquatica*. Mean NbS values for AD surfaces result in 83439 ± 4480 particles per mm^2 for $PM_{0.3-1}$, 5418 ± 990 for $PM_{1-2.5}$ and 612 ± 184 for $PM_{2.5-10}$.

For what concerns the chemical composition of leaf deposited particles, relative percentages (W%) of the main elemental components of total $PM_{0.3-10}$ are shown in Figure 3. Also for this chemical parameters, if the total $PM_{0.3-10}$ is considered no appreciable differences are detected between the two sampled species *A. calamus* and *C. aquatica*, and at the three sampling sites for *C. aquatica*. This is true for all the main elemental components characterized by W% higher than 2%, with the exception of iron (Fe). For this element, *A. calamus* results to be the one with higher W% of 24.9%, in respect to an averaged value of 5.6% calculated for *C. aquatica.* This is confirmed by the relative W% of Fe in each size fraction considered, the ultrafine ($PM_{0.3-1}$, 26.5%), fine ($PM_{1-2.5}$, 18.3%) and coarse one ($PM_{2.5-10}$, 25.8%). This species is also characterized by significantly higher percentages of trace elemental components (with W% ≤ 2%), copper (Cu = 1.3%) and chromium (Cr = 1.4%) in the ultrafine fraction and also titanium (Ti = 1.3%) in the fine one (data not shown). In the specific case of iron (Fe), higher relative W% percentages detected especially in the ultrafine ($PM_{0.3-1}$) and coarse fraction ($PM_{2.5-10}$) confirms the duplicity of its origin, thus being related both 1) to natural and soil resuspension mechanisms (in the coarse fraction) and both 2) to anthropogenic combustive and traffic

related processes (Massimi et al., 2020; Ristorini et al., 2020), confirmed also by higher percentages in the ultrafine fraction of Cu and Cr, known tracers of vehicular traffic .

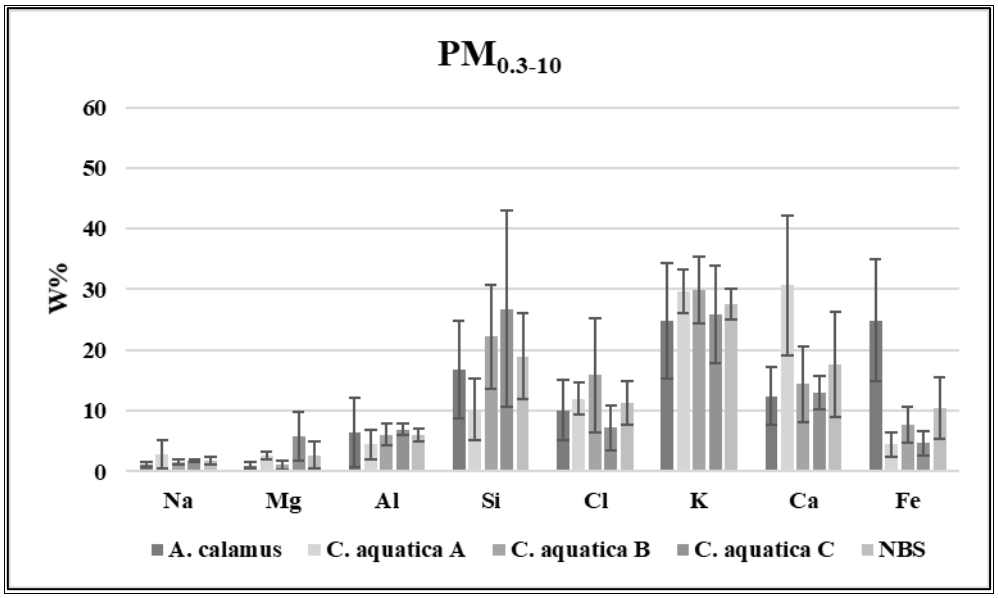

Figure 3. Relative elemental composition and standard deviations of total $PM_{0.3\text{-}10}$, as estimated by the W% obtained from the SEM/EDX analysis, for all the species and all the sites together with averaged NbS ones.

Unfortunately, no appreciable and chemical differences are detected between the three sites of *C. aquatica*, for both main and trace elemental components and for each size fractions (data not shown). However, obtained chemical data by SEM/EDX, result to be effective for highlighting the different species-specific affinity toward the deposition of particles with a specific chemical composition, which may be emitted by specific emission sources. On the other hand, the lack of a clear spatial variability between the chemical composition of leaf deposited PM at three selected sites, may be connected to the vicinity of the three sites or may underline quite homogeneous PM pollution levels over the study area, without the direct impact of local emission source.

Finally, the mass of removed PM per unit leaf area (μg cm^{-2}), for each species, sampling site and size fraction is shown in Figure 4, obtained as reported in Chapter 2, Section 2.3.1 of this PhD thesis.

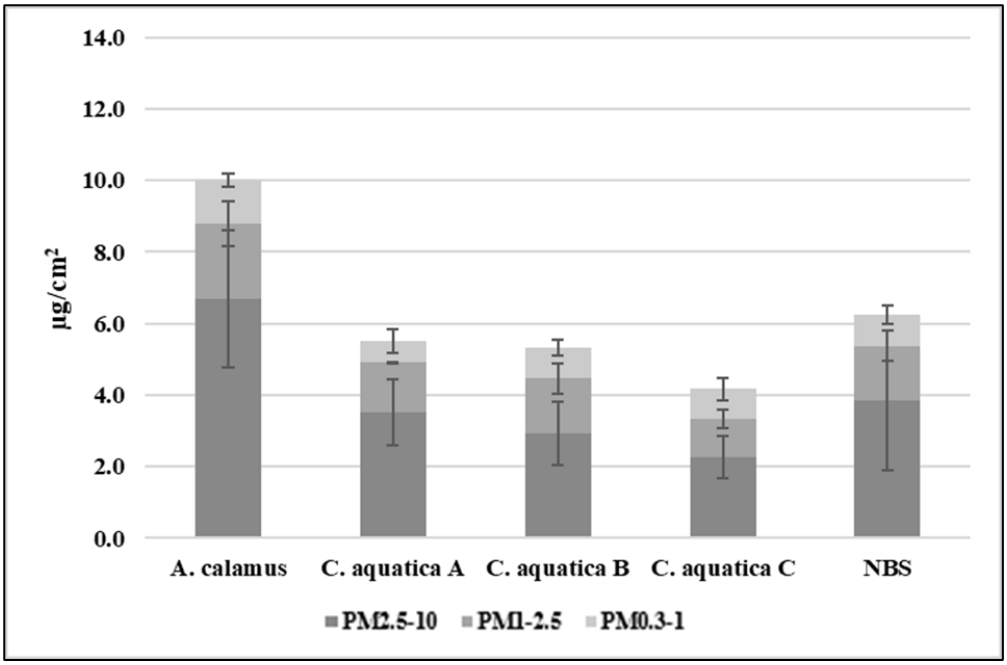

Figure 4. Weight of PM removed (µg cm^{-2}), as obtained from SEM/EDX, through the combination of PM density and chemical composition results. Results averaged over the two species are also reported as mean NBS values. Standard deviations are given for each size fraction and each species/sites.

A. calamus has the highest total $PM_{0.3-10}$ mass accumulated on its leaves, corresponding to 10.0 ± 2.7 µg cm^{-2}. The same trend is obtained for the coarse PM size fraction ($PM_{2.5-10}$), which is known to mainly drive the mass load of $PM_{0.3-10}$ (Cai et al., 2017), while for ultrafine $PM_{0.3-1}$, higher values for *A. calamus* (1.2 ± 0.2 µg cm^{-2}) are confirmed only in respect to *C. aquatica* sampled in site A, and for fine $PM_{1-2.5}$ (2.1 ± 0.6 µg cm^{-2}) only in respect to *C. aquatica* sampled in site A and Site C. The highest mass of leaf deposited PM detected for *A. calamus* may be connected to the affinity shown by the species towards the deposition of heavy metal containing particles, which are known to be characterized by higher atomic masses (Chapter 2, Section 2.3.1). Again, also the mass of PM removed by *C. aquatica* at the three sampling sites, does not underline specific spatial trend, thus confirming what obtained from chemical data. The Moon Lake NbS results to be characterized by averaged values of $PM_{0.3-10}$ removed by means of leaf deposition of 6.3 ± 2.6 µg cm^{-2} of unit leaf area. This value will be needed to be upscaled to the total leaf area of the NbS, to properly evaluate the role of this specific solution to reduce PM pollution levels.

Even if results presented in this section are at a preliminary stage, they represent an important example of the application of SEM/EDX leaf microanalysis for the evaluation of PM leaf deposition, and the assessment of the efficiency of NbS for the removal of this hazardous atmospheric pollutant and the improvement of urban air quality. PM abatement by leaf deposition on aquatic species employed in the implementation of this NbS in Ningbo (China) will be furtherly integrated with other

environmental data, which are connected to water quality, soil contamination and biodiversity, to present a comprehensive evaluation of the provided ESs.

5.4 Turin Living Lab case study: SEM/EDX evaluation of leaf deposited PM and atmospheric concentrations of PM elemental components as specific source tracers

Preliminary results

Within the Turin Living Lab, always defined in the context of ProGIreg, SEM/EDX evaluation of PM abatement has been carried out at two NbSs, with details also in this case, on plant species and PM size distribution, and as a function of particles density, chemical composition and finally weight of removed particles. The first NbS (Fig. 1) consists of a newly implemented urban forest (New Forest) of 2000 m^2 along the banks of the Sangone river, implemented using regenerated soil (New Soil), based on excavated material with the addition of compost, zeolites and innovative bio stimulants. The new soil realization has been completed in February 2020 (Baldacchini, 2021)
The second Turin NbS taken in account are productive gardens (Orti Generali; Fig. 1), which are born with the aim of building a model of enterprise for the transformation and management of post-industrial and metropolitan residual agricultural areas based on ecological sustainability and social equity. The implementation of this NBS has been concluded in November 2019, in an area of 12000 m^2 in the "Mirafiori Sud" district.

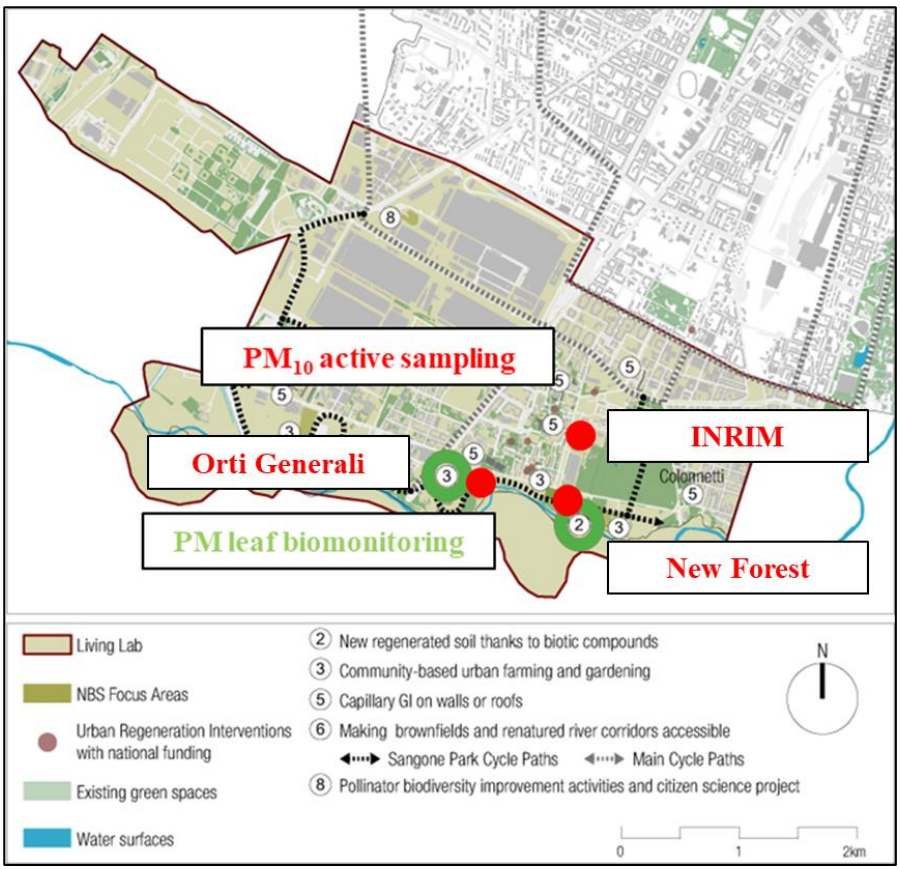

Figure 1. Leaf sampling sites for the PM biomonitoring task (in green) and PM_{10} active sampling sites at the Turin Living Lab (in red).

Leaf sampling procedures for the evaluation of PM abatement have been conducted the 10th July 2020, after one-week rainless period.

In the New Forest NbS, PM abatement has been assessed for newly-planted species, namely *Celtis australis* L., *Malus evereste* L. and *Quercus ilex*. L.. At the Orti Generali NbS, leaves have been sampled from *Malus domestica* L., *Morus nigra* and *Prunus* spp.. From each of these species, three plants have been individuated and two branches from each of them were collected from the external part of the crown. To reduce and exclude as much as possible the potential influence of soil resuspension on the detected PM leaf deposition, all the sampled branches have been collected at the top of the plants (about 2 meters from the ground). Then, to ensure homogeneity, one fully grown leaf was selected for subsequent SEM/EDX analysis at the top of each branch, for a total of six leaves for each species. Biometric data relative to height and DBH (diameter at the breast heigh of the trunk, measured at 1.3 meter from the ground) of the sampled plants have been also randomly collected, for upscale purposes.

In Figure 2, results related to the density of leaf deposited particles (number of particles per mm^2 of leaf area), as a function of species and size fractions ($PM_{0.3-1}$, $PM_{1-2.5}$ and $PM_{2.5-10}$) at the two NbSs (New Forest and Orti Generali), are presented. Again, density results are also described with details on the upper (adaxial, AD) and lower (abaxial, AB) leaf surfaces.

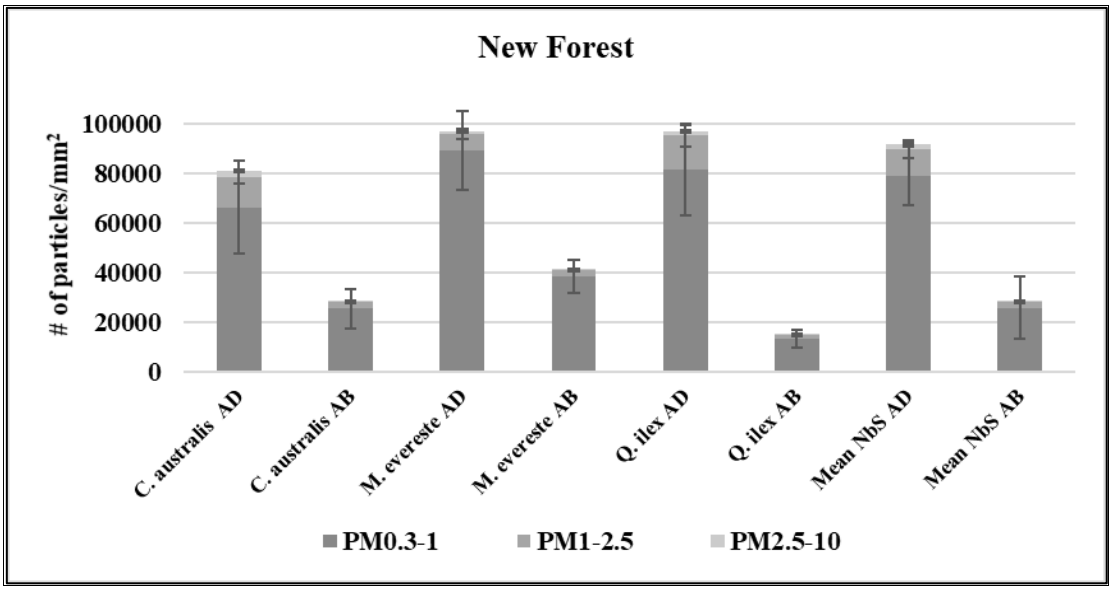

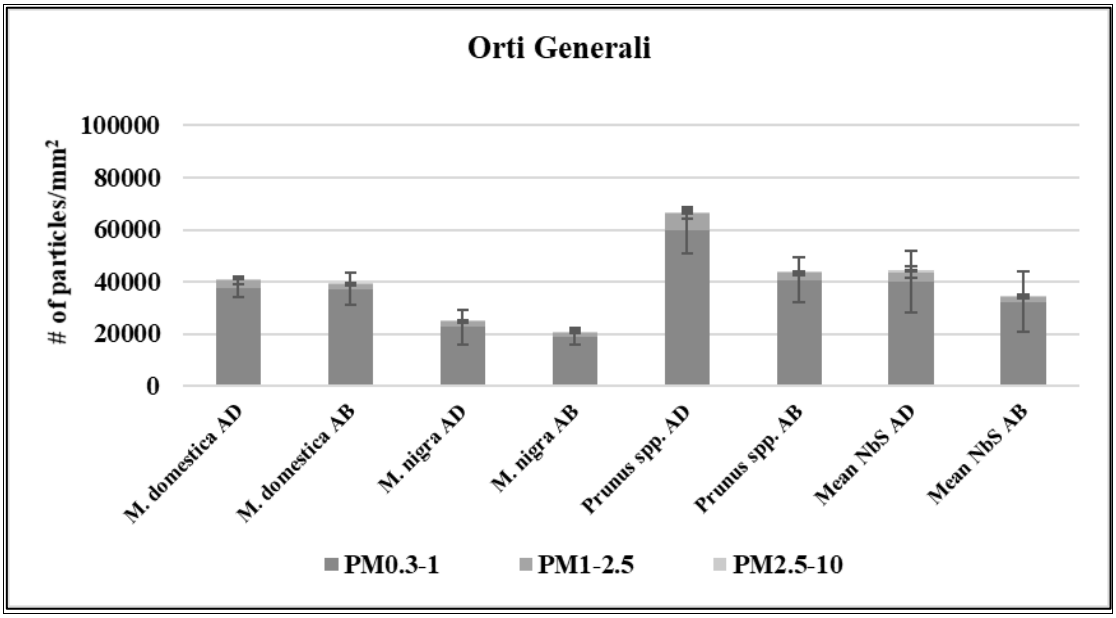

Figure 2. Mean species-specific particle densities (number of particles * mm^{-2}), with standard deviations, on the adaxial (AD) and abaxial (AB) sides, for the three PM size fractions ($PM_{0.3-1}$, $PM_{1-2.5}$, $PM_{2.5-10}$). Results averaged over the three species at each NbS are also reported.

While in the New Forest NbS, for all the species and size fraction considered, it is possible to underline clear differences between the particle densities of AD leaf surfaces and the AB ones, same output is not highlighted takin in account the results of species sampled from the Orti Generali NbS. Specifically, for the New Forest NbS, AB particles densities result to be ranging from a minimum of 13.8% for *Q. ilex* to a maximum of 39.7% for *M. evereste* of AD leaf surfaces, thus confirming what is usually expected and described in literature (Ottele et al., 2010; Shi et al., 2008), due to the peculiar characteristics of abaxial leaf surfaces, both in terms of micromorphological traits and both in terms of orientation.

At the New Forest NbS (Fig.2), the AB surfaces of *Q. ilex* result as the ones characterized by lower $PM_{0.3-10}$ density values of 14984 ± 4142 particles per unit leaf area in mm^2. This trend is also confirmed by results obtained in the fine ($PM_{1-2.5}$, with 1529 ± 458 particles per mm^2) and coarse fraction ($PM_{2.5-10}$, with 200 ± 54 particles per mm^2). On the other hand, and for AD leaf surfaces, *M. evereste* is the species with higher density of leaf deposited particles, both in the fine fraction ($PM_{1-2.5}$, with 6784 ± 1966 particles per mm^2) and in the coarse one ($PM_{2.5-10}$, with 960 ± 435 particles per mm^2).

At the Orti Generali NbS (Fig. 2), *Prunus* spp is the one with higher density values for total $PM_{0.3-10}$ both in the AD and the AB leaf surfaces (respectively 66806 ± 8730, and 43742 ± 9092 particles per mm^2) and only for the AD surfaces in the ultrafine size fraction (59780 ± 9030 particles per mm^2). The less efficient species in terms of density of leaf deposited particle is on the other hand, *M. nigra*,

with regard to the total $PM_{0.3-10}$ and ultrafine $PM_{0.3-1}$ size fraction. No significant differences are detected for both the AD and both the AB leaf surfaces of the other size fractions considered, coarse ($PM_{2.5-10}$) and fine one ($PM_{1-2.5}$).

In Figure 3, results related to the main chemical composition (W%) of total $PM_{0.3-10}$ deposited on each species at the two Turin NbSs are reported. At this preliminary stage, it is not possible to underline any significant differences for what concerns the chemical composition of leaf deposited PM among the species sampled at each NbS. For this size fraction, this is also true for trace elemental components (W% ≤ 2%; data not shown). Unfortunately, also if the averaged NbS percentages are considered, no significant differences can be highlighted for the chemical composition of leaf deposited at the two sites, for both main (Figure 3) and trace PM elemental components. Therefore, at this stage it is not possible to describe any species-specific affinity or neither a differential impact of specific emission sources at the two NbSs. However and to this aim, further elaborations are needed, focused on the chemical composition of specific PM size fractions. Moreover, chemical W% data obtained from the application of SEM/EDX microanalysis of leaves sampled at the Turin Living Lab and at the two NbSs, the New Forest and the Orti Generali, will be furtherly analysed thanks to the application of the *Positive Matrix Factorization* (PMF; Norris et al., 2014) model. As previously described, this modelling approach is applicable to source apportionment purposes, for the identification of chemical profiles of specific PM sources, and to the assessment of their mass contribution. To our knowledge and as one of first attempts PMF model will be employed on PM leaf deposition data by means of SEM/EDX.

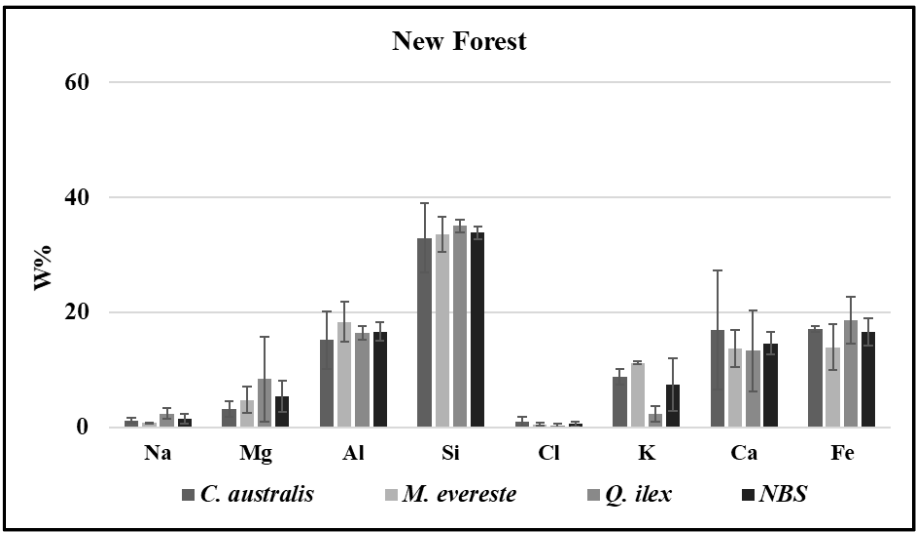

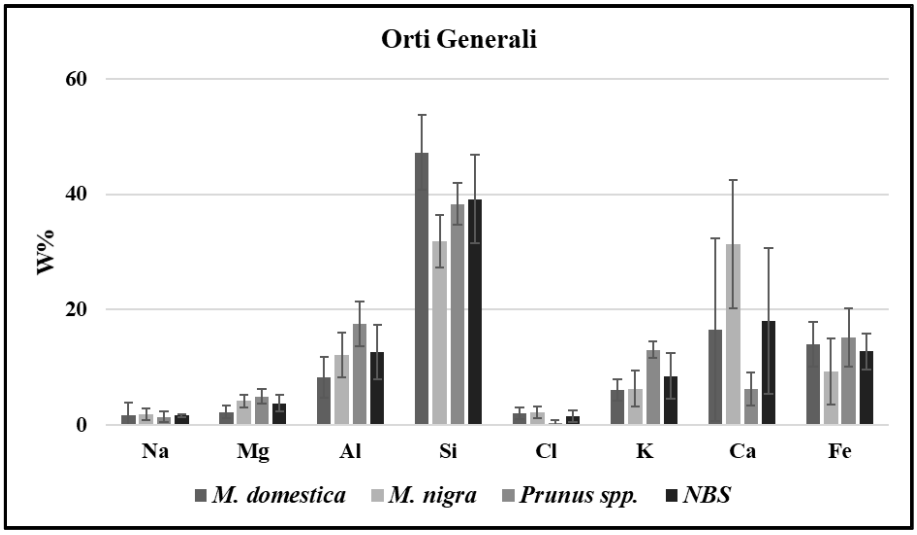

Figure 3. Relative elemental composition and standard deviations of total $PM_{0.3\text{-}10}$, as estimated by the W% obtained from the SEM/ EDX analysis, for all the species and averaged NbS one.

Finally, the mass of removed PM per unit leaf area (µg cm^{-2}), for each species, size fraction, at the two Turin NbSs, is shown in Figure 4.

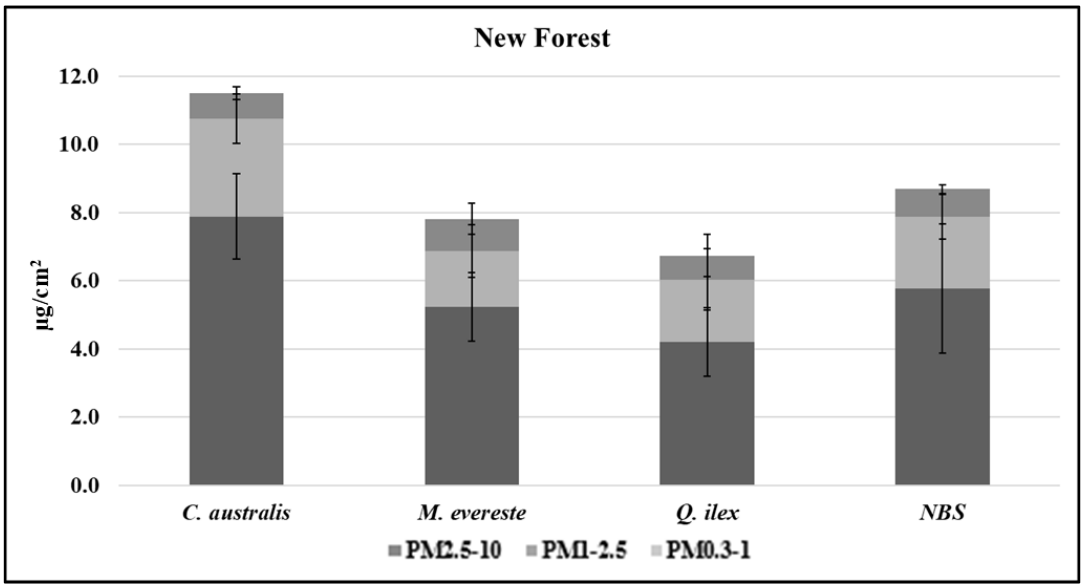

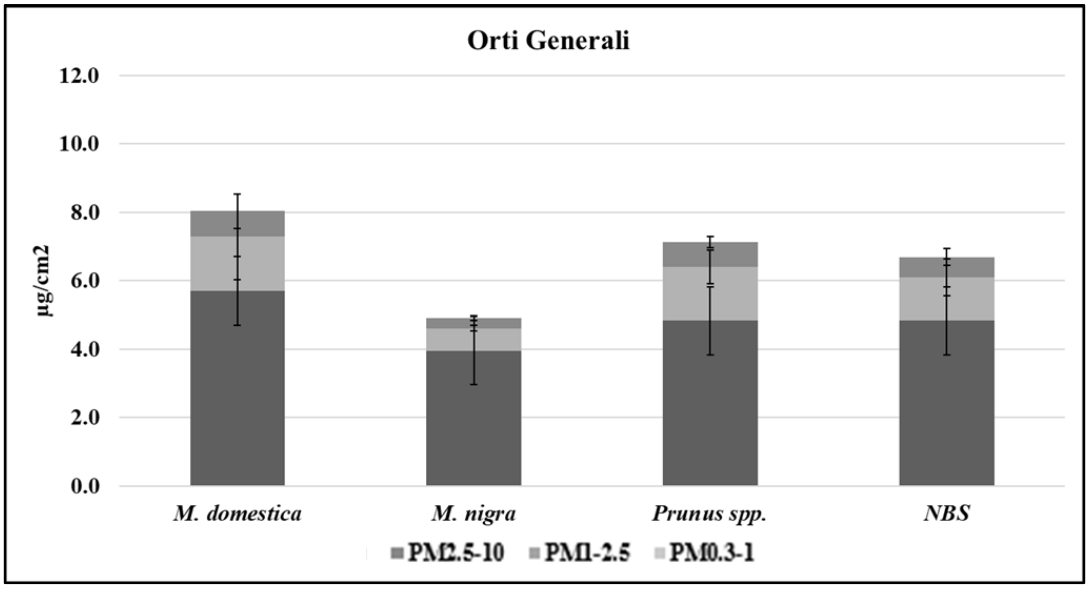

Figure 4. Weight of PM removed (µg cm^{-2}) by each species at the two Turin NbSs, as obtained from SEM/EDX, through the combination of PM density and chemical composition results (W%). Results averaged over the three species are also reported as mean NBS values. Standard deviations are given for each size fraction and each species.

At the New Forest NbS (Figure 4), *C. australis* results as the most efficient species in terms of weight of PM removed for both the total $PM_{0.3\text{-}10}$ and the coarse fraction ($PM_{2.5\text{-}10}$), respectively resulting in 11.5 ± 0.3 µg cm^2 and 7.9 ± 1.2 µg cm^2. On the other hand, species-specific values of removed PM in the other two size fractions, fine ($PM_{1\text{-}2.5}$) and ultrafine one ($PM_{0.3\text{-}1}$), result to be quite similar. Averaged NbS values for these two latter size fractions correspond to 2.1 ± 0.7 µg cm^2 of $PM_{1\text{-}2.5}$ removed and 0.8 ± 0.3 µg cm^2 of $PM_{0.3\text{-}1}$ removed.

At the Orti Generali, the weight of removed total $PM_{0.3\text{-}10}$ and coarse $PM_{2.5\text{-}10}$ are in the same range, thus not highlighting any specific efficiency towards the removal of PM by means of leaf deposition. Averaged NbS values for these two size fractions correspond to 6.7 ± 1.6 µg cm^2 of $PM_{0.3\text{-}10}$ removed and 4.8 ± 0.9 µg cm^2 of $PM_{2.5\text{-}10}$ removed. For what concerns the removal of fine $PM_{1\text{-}2.5}$ the only significant differences are detected between *M. nigra* and *Prunus* spp., respectively being characterized by a removal of 0.7 ± 0.1 µg cm^2 and 1.6 ± 0.5 µg cm^2. Same trend is also highlighted if the results related to ultrafine $PM_{0.3\text{-}1}$ are considered (*M. nigra* 0.3 ± 0.1 µg cm^2; *Prunus* spp. 0.7 ± 0.2 µg cm^2). Lower removal of ultrafine particles by this species, may be explained taking in account the lower particle density previously detected for this specific size fraction.

Also in this case, PM mass removal values will be furtherly upscaled to the total leaf area of each NbS, calculated through the tree biometric information randomly collected at the two NbSs, and the

application of the *i-Tree eco* model, to properly evaluate the role of these specific solutions to reduce PM pollution levels and improve urban air quality.

Uniquely at the Turin Living Lab, additional atmospheric PM_{10} active samplings have been performed, in collaboration with the Department of Chemistry of University of Rome "La Sapienza", Orti Generali Association, Fondazione Bela Rosin and INRIM (National Institute of Metrologic Research). Active samplings have been performed in three monitoring sites (namely New Forest, Orti and INRIM) as shown in Figure 1, at high proximity to the New Forest and the Orti Generali NbS, for a total of 12 months. Samplings have started from July 2019 to April 2020, then due to the establishment of the Covid-19 lockdown, they have been stopped and restarted from July to November 2020.

HSRS - High Spatial Resolution Samplers (FAI INSTRUMENTS, Fonte Nuova (RM), Italy) with a flow rate of 0.5 l/min, have been employed in each site for two-months sampling periods. Teflon (PTFE) filters have been used for the characterization of inorganic elemental components of PM_{10}, through the application of the chemical fractionation procedure and with details on both the water-soluble and insoluble fraction. Main goals of this additional monitoring campaign are 1) achieving additional data on the atmospheric concentrations of PM, which could be furtherly compared with SEM/EDX leaf deposition ones and 2) thanks to the application of the chemical fractionation, being able to identify and assess the impact of specific PM emission sources (both natural and both anthropogenic) and their seasonality.

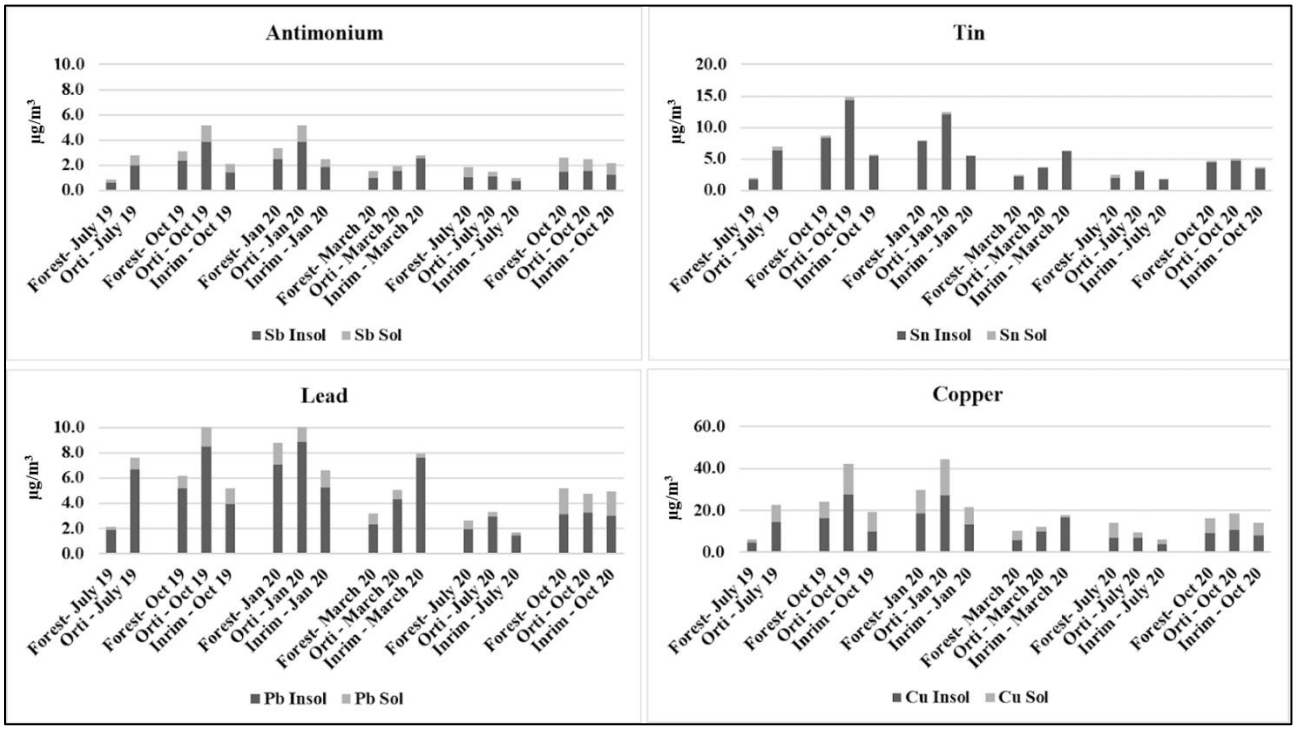

Figure 5. Water-soluble and insoluble concentration of antimuonium (Sb), tin (Sn), lead (Pb) and copper (Cu) obtained by the chemical fractionation of PM_{10} membrane filters sampled at the three sites in Turin Living Lab.

The concentrations of PM_{10} elemental components such as antimuonium (Sb), tin (Sn), lead (Pb) and copper (Cu) (Fig. 5) as well as nickel (Ni), chromium (Cr) and zinc (Zn), are characterized by a strong prevalence in their insoluble fraction, as obtained through the application of the chemical fractionation procedure. The insoluble fraction of these element is a known tracer for the non-exhaust emission process associated to vehicular traffic. Indeed, these heavy metals are commonly used as components of brake pads' wear, disks and tires, and their emission can be associated to the mechanical abrasion of these vehicles components (Massimi et al., 2020; Namgung et al., 2016). Same emission source for these components is confirmed by their similar spatial and temporal trends. Even if the concentrations of these elements appear to be quite similar at the three monitoring sites (Forest, Orti and INRIM), slightly higher concentrations are found at the Orti site, thus underlining a more significant impact of this specific emission sources. Interestingly, if the temporal variability is taken in account, higher concentrations are found for all these elements in 2019, previous to the establishment of Covid-19 regulation. This may underline the impact of this unique regulation in the abatement, or at least reduction of this anthropogenic emission source.

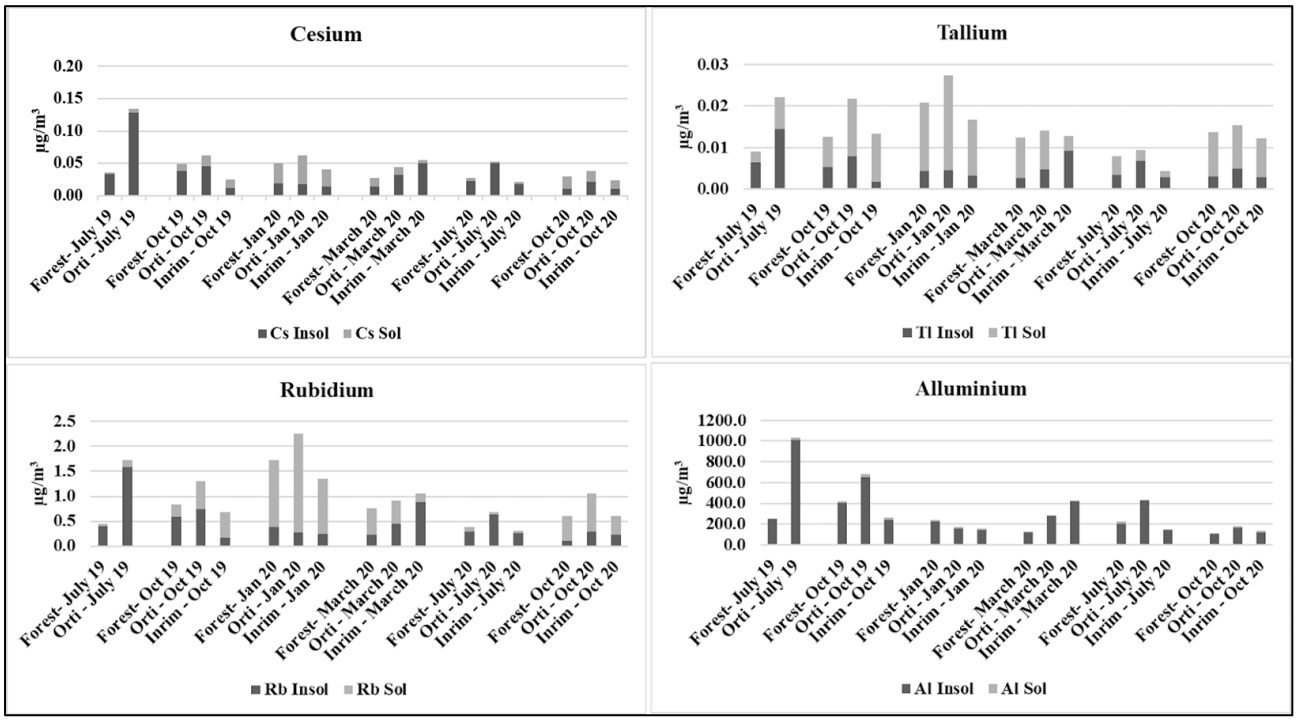

Figure 6. Water-soluble and insoluble concentration cesium (Cs), tallium (Tl), rubidium (Rb) and alluminium (Al) obtained by the chemical fractionation of PM_{10} membrane filters sampled at the three sites in Turin Living Lab.

Same spatial distribution and seasonal variability of other elemental components, such as cesium (Cs), thallium (Tl), rubidium (Rb) and aluminium (Al) in their insoluble fractions underlines the potential impact of the same emission sources (Fig. 6). Indeed, these insoluble concentrations result to be higher during summer samplings (especially July 2019), and at the Orti site, which is the only site characterized by unpaved roads, and as previously described, the one most affected by the traffic. These elements are typically contained in soil, and used as elemental tracers for soil resuspension. Moreover, especially in warm and dry periods, the traffic and the passage of vehicles, may favours soil resuspension (Simonetti et al., 2018; Bencharif-Madani et al., 2019). The impact of vehicular traffic as vector for the soil resuspension is also partly confirmed by the reduction of the insoluble concentrations of these soil related elements during summer 2020 (July 2020), after the establishment of Covid-19 regulations as previously described for the vehicular traffic tracers (Fig. 5 and Fig. 6). Interestingly, the water-soluble fractions of Cs, Rb and Tl (Fig. 6) are instead clearly higher during the winter period (October 2019 and January 2020) thus showing a different seasonal variability than their insoluble fractions. Same spatial and seasonal variability is also obtained for other PM_{10} elemental components, such as water-soluble potassium (K) and cadmium (Cd). All of these elements in their water-soluble fraction are known tracers of biomass burning (Massimi et al., 2020; Perrino et al., 2010) and are usually applied for the evaluation of its impact. Higher concentrations detected again and also for these elemental tracers at the Orti site, may underline the impact of domestic biomass burning appliances, but also combustion and farming related events at these productive gardens. As expected, after the establishment of Covid-19 regulations, which mostly affected urban traffic and mobility, no abatement is detected for these biomass combustion tracers, with similar concentrations in the fall/winter samplings, both in 2019 and in 2020.

Finally, spatial and temporal differences detected between the two solubility fractions of the same PM_{10} elemental components confirms their different origin and the impact of different emission sources, thus also proving the effectiveness of chemical fractionation procedure to increase the selectivity of elements as specific source tracers (Canepari et al., 2009; Massimi et al., 2017).

6. Spatially resolved analyses of PM for localization and impact assessment of emission sources

Spatially resolved information on the concentration, size, and form of the various PM chemical components can be of great help in providing useful information for the identification of its main **emission sources**, both natural and anthropogenic ones, the evaluation of their **impact**, the assessment of particles **dispersion** and the identification of **human health** negative effects. This is also relevant for properly plan effective control and mitigation strategies, toward this hazardous atmospheric pollutant.

However, due to the very high complexity of PM and its emission sources, being able to properly evaluate the **spatial and temporal variability of PM** and its **chemical components** still represents a challenge.

The development of extensive and dense monitoring networks would certainly be crucial to this aim. However, as previously described, conventional and instrumental monitoring stations are associated to very high costs, and for this reason, they are usually employed in very few spots, thus not ensuring a complete coverage of the study area and its emission sources.

To this aim, automatic and **very-low volume** device for PM sampling on membrane filters, the **High Spatial Resolution Samplers** (HSRS; FAI Instruments, Fonte Nuova, Rome, Italy) has been developed with the purpose of allowing spatially-resolved determination of PM chemical components. HSRS assure long-term (1-2 months) collection of PM and being placed at short distance between each other, they can ensure the coverage even of large areas with a substantial reduction of costs.

During this PhD project and in addition to the case studies already described, the HSRS are employed in a wide and dense network of 23 monitoring sites across Terni, an urban and industrial hot spot of Central Italy, for 15 consecutive months, during which the spatial distribution of PM_{10} mass and elements is evaluated and mapped (A5). To increase the selectivity of PM elemental components, the **chemical fractionation** procedure is employed for the characterization of sampled PM_{10} membrane filters. As already mentioned, this procedure ensures a better accuracy in the use of **tracers** for the identification of PM sources, and it constitutes a precious key tool for evaluating their strength and impact. Same monitoring network in Terni and obtained chemical fractionated data are also employed for the individuation of the spatial relationships between **oxidative potential** (OP) data and PM sources and for identifying the relative contribution of single emission sources in building up OP values (A6). Since a larger spatial resolution is also ensured by the **biomonitoring approach** and the utilization of biondicators, in the same study area, lichen transplants of *E. prunasti* are tested and

validated for the evaluation of the spatial variability of persistent organic pollutants (POPs), through the comparison with results obtained by bulk deposition samplers (A7).

Always with the final aim to identify and to evaluate the impact of specific emission sources, source apportionment technique is also employed. The receptor model **Positive Matrix Factorization** (PMF), is applied to PM_{10} chemical data, related to the pre-lockdown, lockdown and post-lockdown periods (A8). A specific PM monitoring campaign carried out at three sampling sites in the Rome area, in which 24-h PM_{10} samples are collected and chemically characterized. The contribution to PM_{10} mass concentration and composition of emission sources during these three periods, are assessed by applying the PMF, thus offering a unique opportunity to also quantify the abatement of typical PM anthropogenic sources. As previously described, all of these additional aspects are certainly relevant in the individuation of new approaches for obtain high spatially resolved data on PM and its main elemental components with source apportionment aims. This is also important for properly validate the utilization of leaves as low-cost and passive PM samplers, and of the evaluation of leaf deposited particles, both chemical and physical, for PM biomonitoring purposes.

6.1 (A5) High resolution spatial mapping of element concentrations in PM_{10}: A powerful tool for localization of emission sources

Atmospheric Research (2020), 244, 105060, doi: 10.1016/j.atmosres.2020.105060

Lorenzo Massimi[1,*], Martina Ristorini[2], Maria Luisa Astolfi[1], Cinzia Perrino[3], Silvia Canepari[1]

[1] Department of Chemistry, Sapienza University of Rome, P. le Aldo Moro, 5, Rome 00185, Italy;
[2] Department of Bioscience and Territory, University of Molise, Pesche (IS), 86090, Italy;
[3] C.N.R. Institute of Atmospheric Pollution Research, Via Salaria, Km 29,300, Monterotondo St. (Rome), 00015, Italy.

*Correspondence: **l.massimi@uniroma1.it**

Keywords: PM_{10} element; chemical fractionation; source tracer; spatial variability; seasonal variation; size distribution.

Abstract: A very-low volume sampler of particulate matter (PM) on membrane filters, recently developed with the purpose of allowing spatially-resolved determination of PM and of its chemical components, was employed from December 2016 to February 2018 in a wide and dense monitoring network across Terni, an urban and industrial hot-spot of Central Italy (23 sampling sites, about 1 km between each other). Terni basin can be considered as an open air laboratory for studying the spatial distribution of PM, as it includes several spatially disaggregated sources. PM_{10} samples were chemically characterized for the water-soluble and insoluble fraction of 33 elements (Al, As, Ba, Bi, Ca, Cd, Ce, Co, Cr, Cs, Cu, Fe, Ga, K, La, Li, Mg, Mn, Mo, Na, Nb, Ni, Pb, Rb, Sb, Sn, Sr, Ti, Tl, U, W, Zn, Zr). Spatial variability of the element concentrations across Terni was then mapped by using the ordinary kriging interpolation method. Spatial distribution of the analyzed elements successfully traced the various PM_{10} sources. In particular, the spatial mapping of Ba (water-soluble fraction), Bi, Cu, Sb, Sn and Zr (insoluble fraction) traced PM_{10} emission from the rail network and vehicular traffic, Ce, Cs, La, Li, Rb, Sr and U (insoluble fraction) traced soil resuspension, Cd, Cs, K, Rb and Tl (water-soluble fraction) biomass burning and Co, Cr, Mn, Nb, Ni, Pb (insoluble fraction), As, Cr, Ga, Li, Mo, Mn, W and Zn (water-soluble fraction) the steel industry pole. Principal component analysis was performed on the spatially-resolved chemical data to cluster the elements tracing the main PM_{10} sources. The winter and summer size distribution of the water-soluble and insoluble elements was analyzed to verify their link with the emission sources. The proposed experimental approach promises to be very effective for the assessment of population exposure to different PM_{10} sources.

1. Introduction

Particulate matter air pollution is a serious threat to human health (Lubczyńska et al., 2017). The World Health Organization estimates that PM air pollution contributes to approximately 800,000 premature deaths each year (Anderson et al., 2012). Various epidemiological studies have spotlighted strong correlations between exposure to PM and the onset of cardiovascular and respiratory diseases (Pope and Dockery, 2006). Urban and industrial PM is known to increase morbidity and mortality due to cardiopulmonary diseases related to

inflammatory processes and genotoxic effects (Perez et al., 2009, Zanobetti and Schwartz, 2009). Therefore, the identification, quantification and apportionment of PM sources is necessary to facilitate their reduction through proper management plans (Taiwo et al., 2014).

The study of the spatial distribution of PM chemical compounds is essential for a reliable identification of emission sources, the evaluation of particle dispersion over the territory and the assessment of personal exposure. However, due to the very high cost of a network based on traditional PM samplers, ambient air quality assessment and epidemiological studies are usually based on measurements taken at a few sampling points (Hoek et al., 2002; Minguillón et al., 2012; Mangia et al., 2013). Consequently, to obtain a reliable assessment of population exposure, the information collected at these few points needs to be extended to wider areas by evaluating the dispersion properties of pollutants (Setton et al., 2010; Kloog et al., 2013; Minguillón et al., 2014). Typically, PM dispersion is estimated through mathematical models (Irwin, 2014; Vitali et al., 2016; Kim et al., 2017), which may not be able to properly describe the complexity of PM transport and transformation processes. Indeed, since PM dispersion varies as a function of the particle dimension, shape, chemical composition and density (Yu et al., 2018; Meng et al., 2019), its evaluation through mathematical models is a quite complex issue in particularly polluted areas, where PM sources are various and variable. Moreover, the reliability of dispersion models needs to be in any case verified through the acquisition of experimental data.

For these reasons, in the last few years, a self-powered, automatic and very-low volume device (High spatial resolution sampler, HSRS; FAI Instruments, Fonte Nuova, Rome, Italy) for PM sampling on membrane filters (suitable for subsequent chemical analyses) has been developed with the purpose of allowing spatially-resolved determination of PM and of its chemical components. The sampler can be employed for the construction of wide and dense air quality monitoring networks across urban and industrial areas. In addition, it can work autonomously for long periods of time (1-2 months), thus allowing a good data representativeness and a substantial reduction of maintenance costs of the monitoring network.

In this study, the HSRS was employed to evaluate the winter and summer spatial variability of PM_{10} mass and element concentrations at 23 sampling sites (approximately 1 km of distance between each other) in Terni (Central Italy), during a 15-month monitoring period. Terni is located in an intra-mountain depression characterized by quite intensive urban PM emissions (vehicular traffic, rail network, domestic heating) and a high density of industrial activities (power plant for waste treatment, steel industry pole), which makes it the most industrialized city of Central Italy (Capelli et al., 2011; Guerrini, 2012). The peculiar meteorological conditions of the Terni basin reduce air mixing and air pollutants transport, favoring their accumulation (Ferrero et al., 2012). These factors have been associated with an increase of morbidity and mortality due to the onset of cardiopulmonary environment-related diseases, which made this area of national interest for environmental remediation (SENTIERI-ReNaM, 2016). Therefore, the Terni basin was found to be particularly suitable for the application of the high spatial resolution sampling technique.

This work is aimed to identify reliable tracers for the main PM_{10} sources in Terni and to map their winter and summer spatial distribution through the experimental approach here described.

2. Materials and Methods

2.1 Study Area

Terni is a medium-sized city of around 112,000 inhabitants (Sgrigna et al., 2015), located in a basin in the southwest of the Umbria region (42°34′N; 12°39′E), Central Italy. The territory of Terni is a wide plain of 211.90 km^2 surrounded by the Apennine mountains, which limit the dispersion of air pollutants (Ferrero et al., 2012), reducing air mixing, especially during the severe winter episodes of atmospheric stability (Moroni et al., 2013; Curci et al., 2015). The weather is characterized by very-low winds, whose predominantly direction is from North-East (Capelli et al., 2011).

According to the Köppen climate classification (Peel et al., 2007), the area of Terni belongs to the temperate climate of the middle latitudes. The winter is cold and rainy, spring and autumn are mild and humid, while summer is hot, humid, muggy and not rainy (Morini et al., 2016).

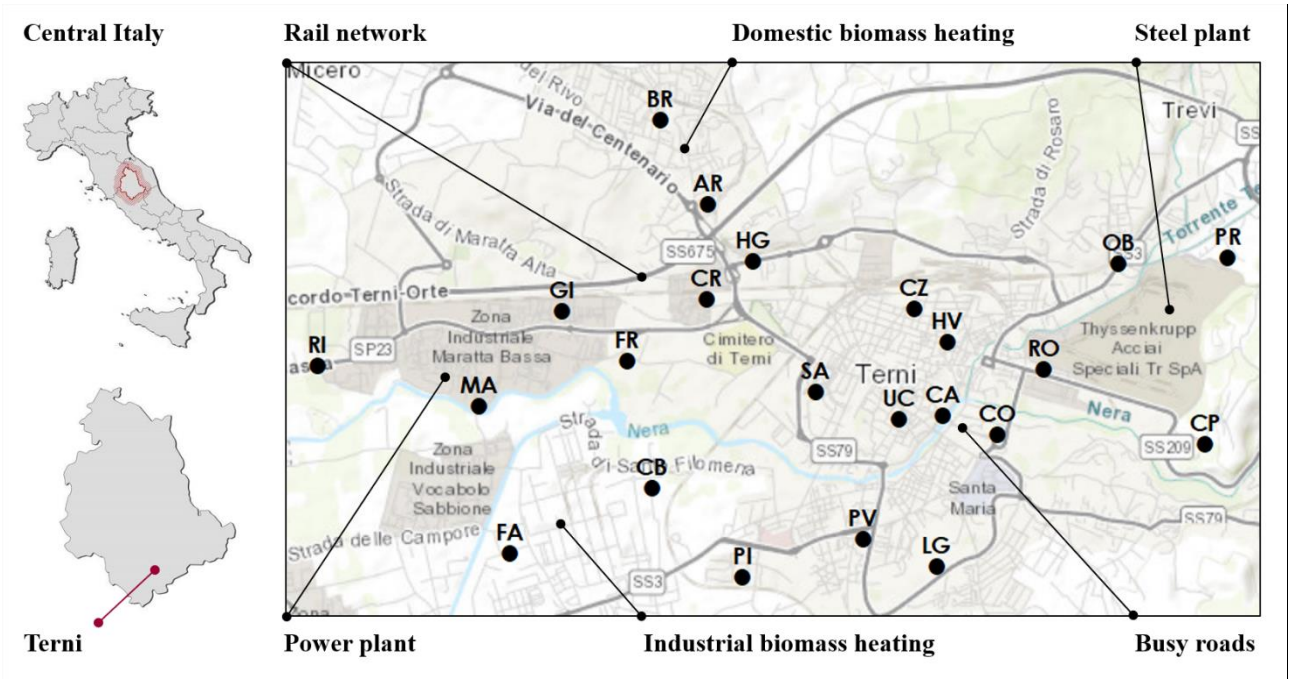

Fig. 1. Map of the 23 sampling sites in the study area (Terni, Central Italy) with the location of the main local PM_{10} emission sources (ArcMap 10.3.1, ArcGis Desktop; ESRI, Redlands, CA, USA).

2.2 Sampling Sites

The first phase of the study required great commitment and large amount of time for selecting appropriate sites for the deployment of the 23 HSRS. The sampling sites were chosen, with the support and help of the Terni district of the Environmental Protection Agency (ARPA) of Umbria (Italy). ARPA Umbria provided us with

a particulate matter dispersion grid that was used as a reference system and recommended us the best locations for the installation of the devices, according to their previous PM_{10} monitoring and analyses. Samplers were deployed in order to cover the whole basin with a spatial resolution of about 1 km and to be as close as possible to potential local PM_{10} sources, allowing us to represent the contribution of the main emission sources of the study area (Fig. 1). In particular:

1. power plant for waste treatment in the West of the city: RI, MA;
2. railway in the North-West of the city: GI, CR, HG;
3. trafficked streets in the city center: CZ, HV, SA, UC, CA, CO;
4. industrial biomass heating (carpentry and craftsmanship lab) in the South-West of the city: FA, CB;
5. domestic biomass heating (townhouses frequently heated by biomass burning appliances) in the North and in the South of the city: FR, BR, AR, PI, PV, LG;
6. very extensive steel plant in the East of the city: RO, OB, PR, CP.

To ensure homogeneous sampling conditions, all the HSRS were deployed within 4 m above ground level and with southern exposition to be exposed to sun rays as much as possible, since they were powered by solar panels and a recharchable battery. The geographical coordinates of the 23 sites (RI, MA, FA, GI, FR, CB, PI, BR, AR, CR, HG, SA, PV, LG, CZ, HV, UC, CA, CO, RO, OB, PR, CP) are reported in supplementary material S1 and additional characteristics about the sampling sites are detailed in Massimi et al. (2017, 2019, 2020).

The 15-month monitoring campaign was carried out from November 19th 2016 to February 19th 2018.

2.3 Sampling Equipment

2.3.1 High Spatial Resolution Sampler

The High spatial resolution sampler (HSRS; FAI Instruments, Fonte Nuova, Rome, Italy) operates with a flow rate of 0.5 L min^{-1}. It was equipped with PM_{10} sampling head filter system and worked with 1-month temporal resolution.

The HSRS was evaluated by Catrambone et al. (2019) in terms of efficiency and repeatability and it showed very good sampling efficiency for stable and fine PM_{10} chemical compounds (such as the elements) and high repeatability, especially for metals and metalloids (5.6–16%). In addition, the HSRS was already employed in the area of Terni and was found to be effective for the construction of wide and dense monitoring networks and for the evaluation of the spatial variability of PM_{10} chemical components (Massimi et al., 2017, 2019, 2020).

The very-low volume samplers were deployed at the 23 sites. They worked in parallel for 12 sampling periods: seven samplings during the winter (November 2016 - March 2017 and October 2017 - February 2018) and five samplings during the summer (April - October 2017). The start and stop dates of each period are reported

in supplementary material S2. The HSRS were equipped with 37 mm Teflon membrane filters (2 μm pore size, PALL Corporation, Port Washington, NY, USA).

2.3.2 Micro-Orifice Uniform Deposition Impactor

The Micro-orifice uniform deposition impactor (MOUDI; model 110-NR; MSP Corporation, Shoreview, MN, USA) is a low-pressure cascade impactor for the collection of size-segregated PM samples. It operates ~~at the~~ with a flow rate of 30 L min^{-1} and it has 10 impaction stages, low internal-loss characteristics and sharp cut-size aerodynamic diameters of 0.18, 0.32, 0.56, 1.0, 1.8, 3.2, 5.6, 10 and 18 μm. ~~MOUDI~~ Size-segregated PM samples used for PM mass and elemental concentration measurements were collected on 47 mm Teflon membranes (2 μm pore size, PALL Corporation, Port Washington, NY, USA) by using three MOUDI working in parallel at three different sites (one impactor per site). The MOUDI were employed at PR (East of the city), CA (city center) and MA (West of the city) for 20 days during the winter (February 15th - March 6th, 2018) and 16 days during the warm season (September 15th - 30th, 2017), allowing us to obtain information on the winter and summer size distribution of the PM mass and of the water-soluble and insoluble fraction of the elements. Size-segregated PM was also collected on aluminum foils (47 mm, MSP Corporation, Shoreview, MN, USA) during a 3-day period (February 12nd - 14th 2018) at PR (East of the city).

2.4 Analytical Procedure

Teflon membrane filters were weighed before and after sampling, in order to determine PM mass concentrations.

PM_{10} samples and size-segregated PM samples were chemically characterized for the water-soluble and insoluble fraction of the elements by using a chemical fractionation procedure, previously optimized and validated (Canepari et al., 2006a, 2006b). Chemical fractionation consists in the water extraction of PM membrane filters followed by digestion of the residue, combined with the determination of the element concentrations in the two obtained fractions. This procedure allowed us to assess the chemical form in which each element was released, which may be typical of its emission source (Templeton et al., 2000), thus increasing the selectivity of the elements as source tracers (Canepari et al., 2009; Perrino et al. 2010).

Briefly, the supporting polymethylpentene ring was removed from each membrane filter, which was subjected to an ultrasound assisted extraction for 30 min in 10 mL of deionized water (Arioso UP 900 Integrate Water Purification System, Cole-Parmer Co Ltd., Saint Neots, England, UK). The extracted solution was then filtered on a cellulose nitrate filter (0.45 μm pore size, Merck Millipore Ltd., Billerica, MA, USA). Subsequently, both the membrane filter and the cellulose nitrate filter were subjected to a microwave assisted acid digestion (Ethos Touch Control with Q20 rotor, Milestone, Bergamo, Italy) by using 2 mL of ultrapure concentrated HNO_3 (67%; Promochem, LGC Standards GmbH, Wesel, Germany) and 1 mL of H_2O_2 (30%; Promochem, LGC Standards GmbH, Wesel, Germany). The digested solution was then diluted to 50 mL with deionized water and filtered with syringe filters (25 mm diameter, 0.45 μm pore size, GVS Filter Technology, Morecambe, England, UK). After the two-step sequential leaching, the concentrations of 33 elements (Al, As, Ba, Bi, Ca,

Cd, Ce, Co, Cr, Cs, Cu, Fe, Ga, K, La, Li, Mg, Mn, Mo, Na, Nb, Ni, Pb, Rb, Sb, Sn, Sr, Ti, Tl, U, W, Zn, Zr) in the water-soluble and insoluble fraction of each sample was determined by a quadrupole inductively coupled plasma mass spectrometer (ICP-MS; model 820-MS; Bruker, Bremen, Germany) equipped with a glass nebulizer (0.4 mL min^{-1}; Analytik Jena AG, Jena, Germany). For each element, external standard calibration curve was performed in the 1-500 µg L^{-1} range by serially diluting standard stock solutions (1000 ± 2 mg L^{-1}; Exaxol Italia Chemical Manufacturers Srl, Genoa, Italy; Ultra Scientific, North Kingstown, RI, USA; Merck Millipore Ltd., Billerica, MA, USA). To control the nebulizer efficiency, yttrium (1000 ± 2 mg L^{-1}; Panreac Química, Barcelona, Spain) was set at 5 µg L^{-1} as internal standard for all the measurements (Astolfi et al., 2018; Conti et al., 2018). The limits of detection (LODs; supplementary material S3) were set at 3 times the standard deviation (SD) of 10 replicate blank determinations.

The instrumental conditions and the performance of the method are detailed in Astolfi et al. (2018) and in Canepari et al. (2009), respectively.

2.5 Spatial Mapping

The winter and summer spatial distribution of the water-soluble and insoluble elements was mapped by the software ArcMap 10.3.1 (ArcGis Desktop; ESRI, Redlands, CA, USA).

To create a continuous surface from the 23 measured sample points and predict the values at unmeasured locations (Kumar et al., 2007), the element concentrations determined at the 23 sampling sites were interpolated by using the ordinary kriging (OK) method (Johnston et al., 2001). Kriging is based on the assumption that the parameter being interpolated can be treated as a regionalized variable and its estimator is given by a linear combination of the observed values with weights, which are derived from the kriging equations using a semivariogram function (Xie et al., 2011). In the OK the data are assumed to be generated from a stochastic process which is split into a constant but unknown trend component and an error component (Beelen et al., 2009).

As the skewed dataset showed clear trends of the element concentrations, log transformation was applied. The variogram was computed on the transformed data, and the experimental semivariances were fitted by a spherical function (spherical semivariogram model), by weighted least-squares approximation (Jian et al., 1996). This function was then used for the kriging.

2.6 Multivariate Statistical Analyses

To cluster the tracers of the main PM_{10} emission sources in Terni, principal component analysis (PCA) was performed on the spatially-resolved data of PM_{10} mass concentration and water-soluble and insoluble fraction of elements. Performance and uncertainty of PCA approach and other source apportionment models in characterization of PM sources are detailed in Belis et al. (2015).

The matrix of the data (9384 data) used for the PCA is composed of 276 samples (23 samples for each of the 12 sampling periods) and of 34 selected variables: PM_{10} mass concentration and 33 water-soluble (_s) and/or insoluble (_i) element concentrations (As_s, Ba_s, Bi_i, Cd_s, Ce_i, Co_i, Cr_i, Cr_s, Cs_i, Cs_s, Cu_i, Fe_i,

Ga_s, K_s, La_i, Li_i, Li_s, Mn_i, Mn_s, Mo_s, Nb_i, Ni_i, Pb_i, Rb_i, Rb_s, Sb_i, Sn_i, Sr_i, Tl_s, U_i, W_s, Zn_s, Zr_i). The variables were selected depending on the ability (widely documented in previous studies; Canepari et al., 2014, 2019; Massimi et al., 2017, 2020) of the elements (water-soluble and/or insoluble fraction) to selectively trace PM_{10} emission sources. Before performing the PCA, the matrix of the data was transformed by column mean centering and row and column autoscaling in order to correct for variations of the data due to the different scaling of the examined variables (Conti et al., 2007; Massimi et al., 2017, 2018). Multivariate statistical analyses were performed using the statistical software R (R-project for statistical computing, Ver. 3.0, 32-bit).

2.7 Scanning Electron Microscopy Characterization

A small portion of the samples collected by MOUDI (about 0.8 cm^2) on aluminum foils was cut in the center, fixed to aluminum stubs by self-adhesive carbon discs (TAAB, 12 mm diameter) and coated with an ultra-thin carbon layer (5 nm) by a vacuum evaporator (108 Carbon A; Scientific Instruments Ltd., Cressington, England, UK). Subsequently, PM samples in the range 3.2-5.6 µm and 0.32-0.56 µm were morphologically characterized by a High resolution field emission scanning electron microscopy (HR-FESEM; model AURIGA; Carl Zeiss Microscopy GmbH, Jena, Germany), equipped with an energy dispersive spectrometer for X-ray microanalysis (XEDS; model QUANTAX; Bruker Italia S.r.l., MI, Italy), to qualitative describe the morphology and elemental composition of particles released by the steel plant in the fine and coarse fraction. HR-FESEM XEDS acquisitions were performed under high vacuum (10^{-6} hPa) at 20 keV accelerating voltage. Micrographs were acquired by secondary electron detector (SED) at magnification, working distance (WD), tilt angle, and spot size conditions properly adjusted on a case-sensitive scale to optimize image resolution. The microanalysis was performed at WD ranging from 9.6 mm to 12.4 mm and at magnification ranging from 25,000x to 600,000x.

3. Results and Discussion

3.1 PM_{10} and elemental concentration

Spatially-resolved data, obtained by sampling in parallel at the 23 sites, were used to evaluate the spatial variability of PM_{10} mass concentration in Terni. The seasonal mean (AM) concentrations of the PM_{10} mass determined in the winter and summer were considered.

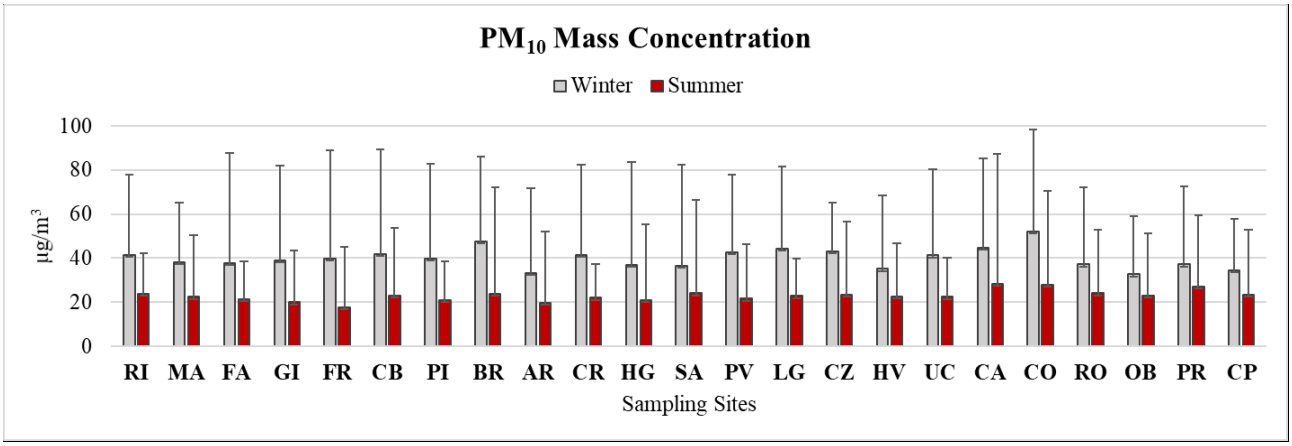

Fig. 2. Winter and summer mean PM_{10} mass concentrations ($\mu g/m^3$) recorded at the 23 sampling sites in Terni. Error bars represent the monthly variability in PM_{10} mass concentration at each site for the summer and winter monitoring periods.

From Fig. 2, we can observe that a clear increase in PM_{10} mass concentration occurred at all the sampling sites during the winter. This can be explained by a combination of two factors: the increase in the strength of some typical winter sources, such as domestic biomass burning, and the frequent temperature inversions occurring during the cold season, which leads to a less efficient mixing of the lower atmosphere and to severe episodes of atmospheric stability (Moroni et al., 2013; Curci et al., 2015).

Mean PM_{10} mass concentration at all the sites during the winter was 40 $\mu g/m^3$, while during the summer it was 23 $\mu g/m^3$. The highest PM_{10} mass concentration (52 $\mu g/m^3$) was found during the winter at CO, which is located between high-speed roads and the steel plant. High winter PM_{10} mass concentration was recorded also at CA (close to CO; 45 $\mu g/m^3$) and at BR (48 $\mu g/m^3$), where domestic biomass heating systems were largely used during the cold season. During the summer, the lowest PM_{10} mass concentration was recorded at FR (urban background site; 18 $\mu g/m^3$), while higher concentrations were found at sites close to busy roads (CO, CA) and to the steel industry pole (RO, OB, PR, CP), sources whose strength increased probably because of the more easily resuspension of vehicle components and steel particles in the warm and dry season.

Winter and summer mean concentrations of all the measured elements in their water-soluble and insoluble fraction are reported in Supplementary Materials S3. As already observed for PM_{10}, the average concentration of most elements was higher during the winter. A different behaviour was observed only for elements that are generally considered as released by the soil (Ce_i, Cs_i, La_i, Li_s, Rb_i, Sr_i), whose resuspension is favoured during the dry season.

The data in S3 also show that at all the 23 sites the solubility percentages of the elements were fairly constant. For example, Cd, Mo, Rb and Tl were found, at all sites, mainly in their soluble fraction, while Al, Bi, Ce, Co, Cr, Fe, Ga, La, Nb, Ni, Pb, Sn, Ti, U and Zr were found in the residual fraction. This indicates that the relative strength of the sources of each element did not change in the whole area of the Terni basin. For some elements (Cd, Cs, Rb, Tl), however, we observed great seasonal differences in the solubility percentage, which indicate the activity of seasonal sources.

It is worth noting that at all the sampling sites the yearly average concentration of As, Cd and Pb in PM_{10} was well below the values set by the European Union (EU 2008/50/CE) as target value (As, Cd) or limit value (Pb). The yearly average concentration of Ni, instead, was above the EU target value (20 ng/m^3) in all the East area of the city, where the steel industry pole is located. The maximum Ni concentration was found at RO, where it was almost five times the target value (98 ng/m^3). The identification and characterization of the source/s responsible for these high values constitutes a valuable tool for planning the mitigation measures that are necessary to protect citizens health in the area of study.

3.2 Spatial Mapping of the Water-soluble and Insoluble Element Concentrations

The winter and summer spatial distribution of the water-soluble and/or insoluble fraction of the 33 selected elements are reported in supplementary material S4. The maps allow an easy identification of the location and strength of the local sources of each element. They also give reliable indications about the horizontal diffusion of the particles in which the elements are contained.

For some elements (Cr, Cs, Li, Mn, Rb), the spatial maps of the soluble and of the residual fraction were different. As an example, in Fig. 3 (panels a-d) we report the spatial distribution of Cs_s and Cs_i. The concentration of Cs_s was clearly higher during the winter period in all the residential area. The highest values were recorded at FA, which is close to the carpentry, and at sites close to townhouses frequently heated by biomass burning appliances, such as BR. The spatial distribution of Cs_s (panels a,b) was practically identical to those of K_s, which is widely recognized as a robust tracer of biomass burning, and of Cd_s, Rb_s and Tl_s, which also have been identified as possible biomass burning tracers (Frasca et al., 2018; Simonetti et al., 2018a; Massimi et al., 2019).

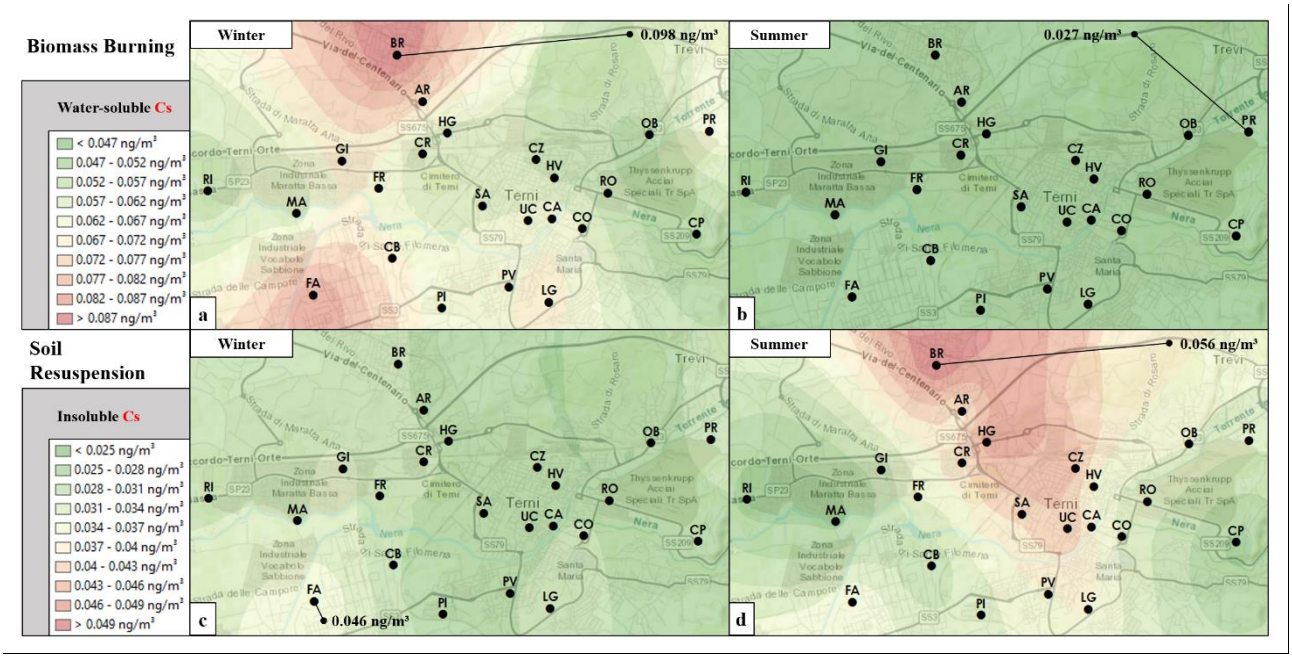

Fig. 3. Map of the winter and summer spatial distribution of water-soluble (panels a,b) and insoluble Cs (panels c,d).

The insoluble fraction of Cs (panels c,d), instead, showed a completely different spatial distribution and seasonal variability. In fact, its concentration was higher during the summer and its maximum values were recorded at the sites most affected by traffic, particularly those close to high-speed roads. A similar spatial pattern was observed also for elements that are typically contained in soil (Ce_i, Cs_i, La_i, Li_i, Rb_i, Sr_i, U_i), as the traffic favours their resuspension, particularly during warm and dry periods (Amato et al., 2009; Simonetti et al., 2018a; Bencharif-Madani et al., 2019; Soleimanian et al., 2019). It is thus clear that insoluble and soluble species of Cs were released into the environment by different sources. This confirms the effectiveness of the chemical fractionation based on solubility in increasing the selectivity of the elements as source tracers (Canepari et al., 2009; Perrino et al., 2010; Massimi et al., 2017).

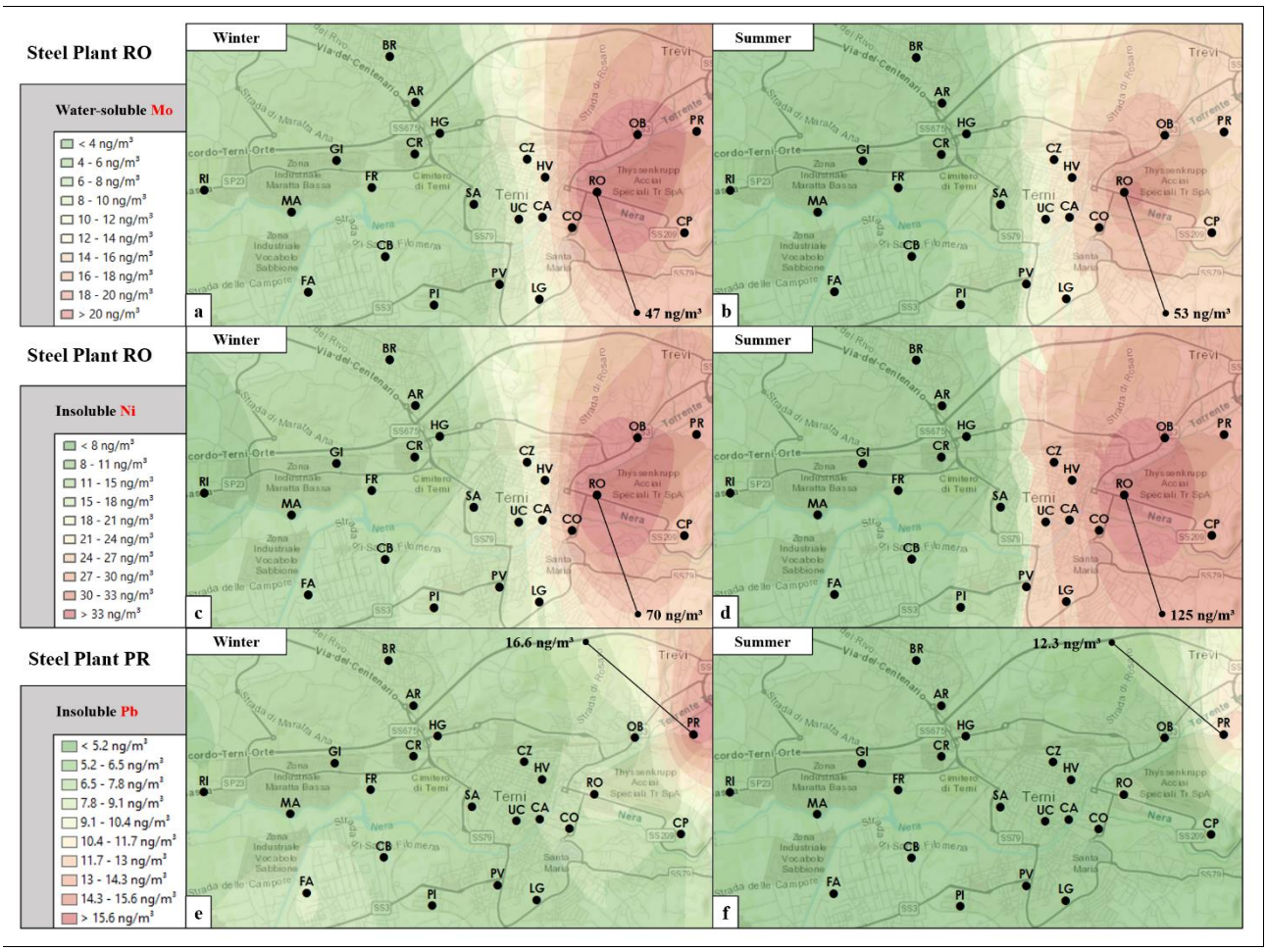

Fig. 4. Map of the winter and summer spatial distribution of water-soluble Mo (panels a,b), insoluble Ni (panels c,d) and Pb (panels e,f).

The concentration of some elements (Co, Cr, Fe, Mn, Mo, Nb, Ni, Pb, W) was, as expected, higher in the Eastern area of the basin, where the steel plant is located. All these elements are used in steel production: Cr, Fe and Ni are basic components of steel, while Co, Mn, Mo, Nb, Ni and W are used to increase its toughness, ductility, tensile strength and corrosion resistance (Querol et al., 2007; Owoade et al., 2015; Massimi et al., 2017; Marcias et al., 2018). In Fig. 4 we report the spatial maps of Mo_s, Ni_i and Pb_i, obtained during the

winter and summer periods. These examples show that during the winter months the spatial distribution of Mo_s and Ni_i were practically identical, suggesting the existence of a common main source (Fig. 4, panels a,c). For both these elements, the maximum concentration was measured at RO, very close to the steel rolling plants; this activity seems therefore to be the main cause of the measured values. Also during the summer period, the maximum concentrations of Mo_s and Ni_i were measured at RO, but their seasonal variability showed some differences (Fig. 4, panels b,d). In both cases, during the summer the strength of the local sources at the hot spot site (RO) was higher with respect to the winter period, but the summer increase was definitely more remarkable in the case of Ni_i (average concentrations were 70 ng/m^3 during the winter and 125 ng/m^3 during the summer) than in the case of Mo_s (average concentrations were 47 ng/m^3 and 53 ng/m^3, respectively). Furthermore, the spatial diffusion of Mo_s was lower during the summer than during the winter, while the opposite was observed for Ni_i. These observations suggest the possible coexistence of two different types of emission in the same area, which are differently affected by seasonal variations of the meteorological conditions.

High concentrations of Pb_i (Fig. 4, panels e,f) were recorded at PR, which is the closest site to the furnaces for the annealing of the cold rolled product of the steel industry pole (Capelli et al., 2011) and to the steel waste storage site. A similar behavior was observed also for Cr_s, Li_s, Ga_s, Mn_s and Zn_s (supplementary material S4). Also these elements were then probably emitted by steel plant related sources, but the involved processes should be different from those releasing Ni and Mo. In fact, for these elements, the mean concentrations at PR and in the whole basin were higher during the winter. This indicates a contribution to PM that is not seasonal and that is then susceptible to the conditions of stronger atmospheric stability which are typical of the cold period.

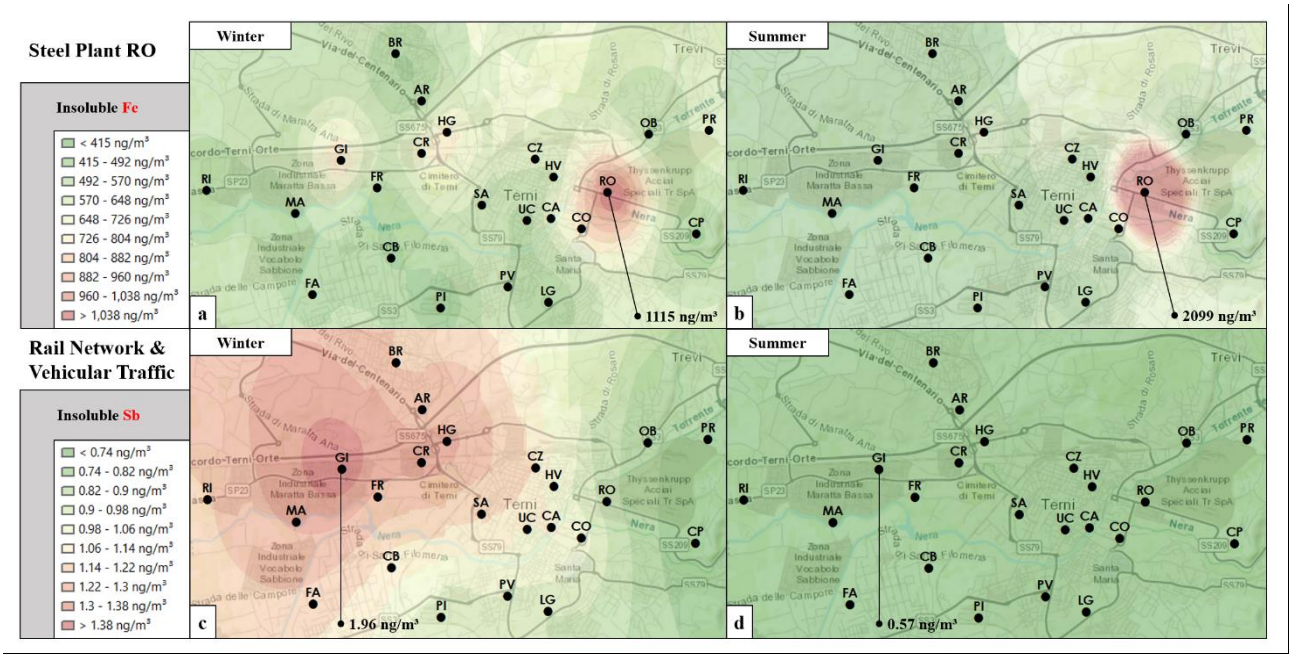

Fig. 5. Map of the winter and summer spatial distribution of insoluble Fe (panels a,b) and Sb (panels c,d).

Similarly to Ni_i, also Fe_i showed the maximum concentrations at RO (Fig. 5, panels a,b), where summer concentration was much higher than winter values (2099 ng/m^3 and 1115 ng/m^3, respectively). Ni and Fe are among the main components of stainless steel; it is thus possible that they were both released by mechanical processes such as brushing and polishing operations on rolled steel (Noe et al., 1996). This release could be more important during the dry summer period (Canepari et al., 2008; Pant and Harrison, 2013; Simonetti et al., 2018a). Mainly during the winter months, the spatial distribution of Fe_i showed the existence of additional intensive sources, mostly sited along the railway (GI, CR, HG) and probably due to abrasion of rolling stock. The contribution of the railway is very clear also for Sb_i, as well as for Bi_i, Sn_i and Zr_i, summer and winter maps for this element are shown in Fig. 5 (panels c,d; maps for Bi_i, Sn_i, and Zr_i are reported in supplementary material S4). It is worth noting that these elements are generally considered as robust tracers of non-exhaust emission from vehicular traffic, as they are contained in high concentration in brake pads. Our spatial maps show that the rail network, which employs brake systems similar to those used by vehicles, can be considered a much more important source of these elements with respect to vehicular traffic. In particular, the highest release of dust by abrasion of rolling stock was found at GI, located at approximately 3 km of distance to the station, where the trains start breaking for the entrance to the residential area of the city.

3.3 Principal Component Analysis

To cluster the tracers of the main PM_{10} emission sources in Terni, principal component analysis was performed on the spatially-resolved chemical data recorded at the 23 sampling sites.

Four significant components accounting for 80.6% were obtained (the scores and loadings are shown in supplementary material S5); the variance explained by each component is: 40.1%, 19.2%, 15.2% and 6.1%. First component (PC1), which explains the 40.1% of the total variance, well separates the samples (scores) whereby the highest element concentrations (loadings) were found from the others. However, PC1 does not cluster the elements released by the different emission sources. On the contrary, PC2, PC3 and PC4 well separate the elements depending on their concentration variability among the sampling sites (the loading plots of PC1/PC2 and of PC2/PC3 are shown in supplementary material S5). Along the PC3 are clustered the insoluble elements released by soil resuspension. PC2 well separates the elements at high concentrations in the samples of the sites where the impact of the rail network, vehicular traffic and biomass burning was higher (GI, CR, HG, CZ, HV, SA, UC, CA, CO, FA, CB, FR, BR, AR, PI, PV, LG) from the elements released by the steel plant (RO, PR). However, PC2 does not separate the elements released by the railway and vehicular traffic from the water-soluble elements released by biomass burning, which are well clustered along the PC4. Therefore, PC2 and PC4, which explain the 25.3% of the total variance, were represented in the loading plot of Fig. 6, since they better reflect the spatial variability of the PM_{10} mass and element concentrations in the study area.

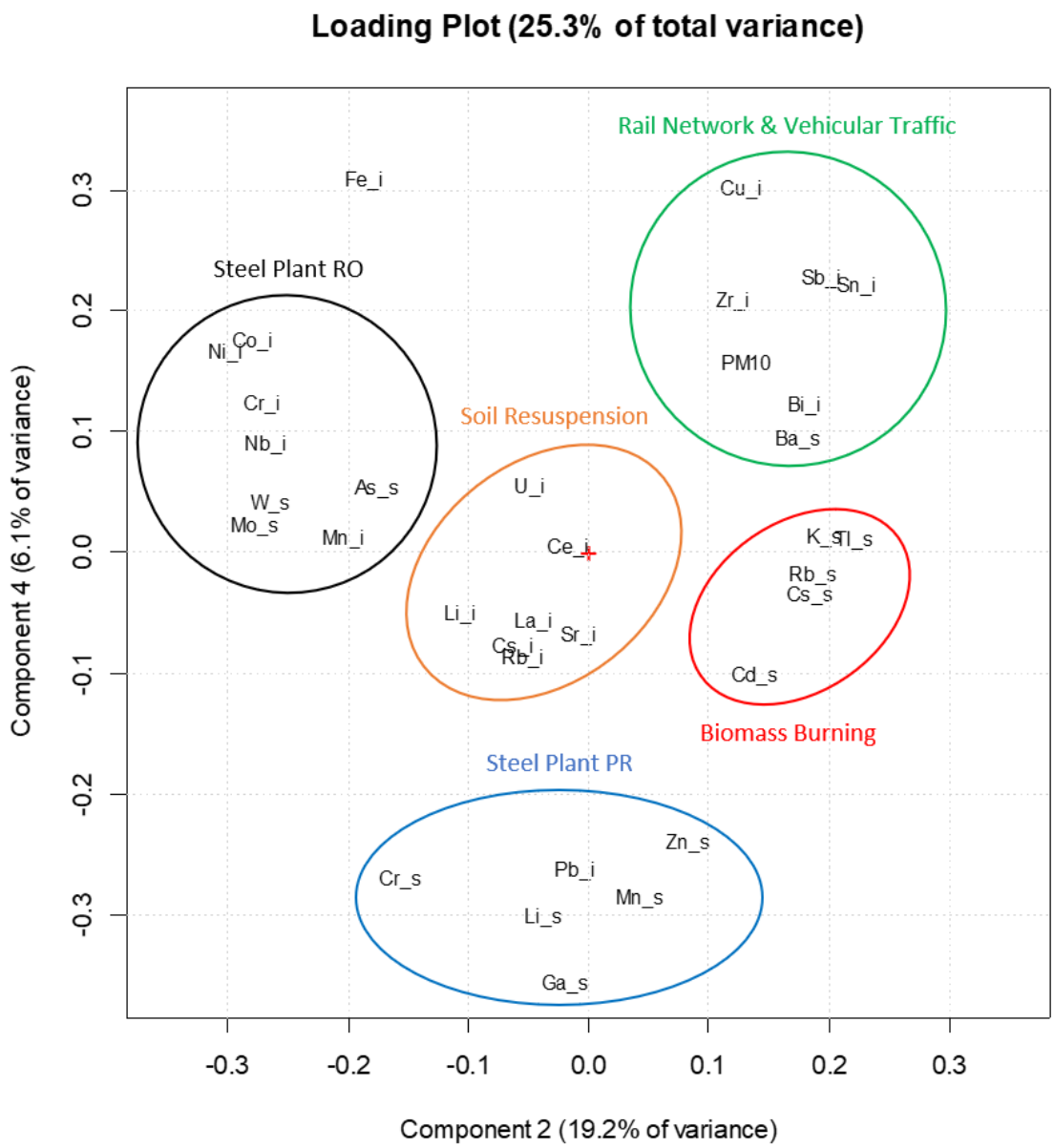

Fig. 6. Loading plot of the PCA (PC2/PC4) performed on the concentration data of the PM_{10} mass and of the 33 selected water-soluble and/or insoluble elements, determined at the 23 collection sites.

From Fig. 6, we can observe that the water-soluble and/or insoluble elements are clustered in five main groups, each one containing tracers of a specific emission source. The first group, on the left upper part of the loading plot, is composed of elements found at high concentrations at RO (As_s, Co_i, Cr_i, Mn_i, Mo_s, Nb_i, Ni_i, W_s). RO is the closest site to the rolling plants of the steel industry pole and it is in the close proximity to the plant for the treatment of the effluents from casting and hot rolling section. All these elements, which are present in stainless steel as basic components (Cr, Fe, Ni) or to increase its toughness, ductility, tensile strength and corrosion resistance (Co, Mn, Mo, Nb, Ni, W; Querol et al., 2007; Owoade et al., 2015; Massimi et al., 2017; Marcias et al., 2018), can be reasonably used as tracers for the steel rolling emission from the steel plant

(Taiwo et al., 2014). The second group, on the lower part of the loading plot, is composed of elements released at PR (Cr_s. Ga_s, Li_s, Mn_s, Pb_i, Zn_s), probably by primary emission from the close furnaces for the annealing of the cold rolled product (Capelli et al., 2011). These elements appeared to be efficient tracers for the combustion emission from the steel industry.

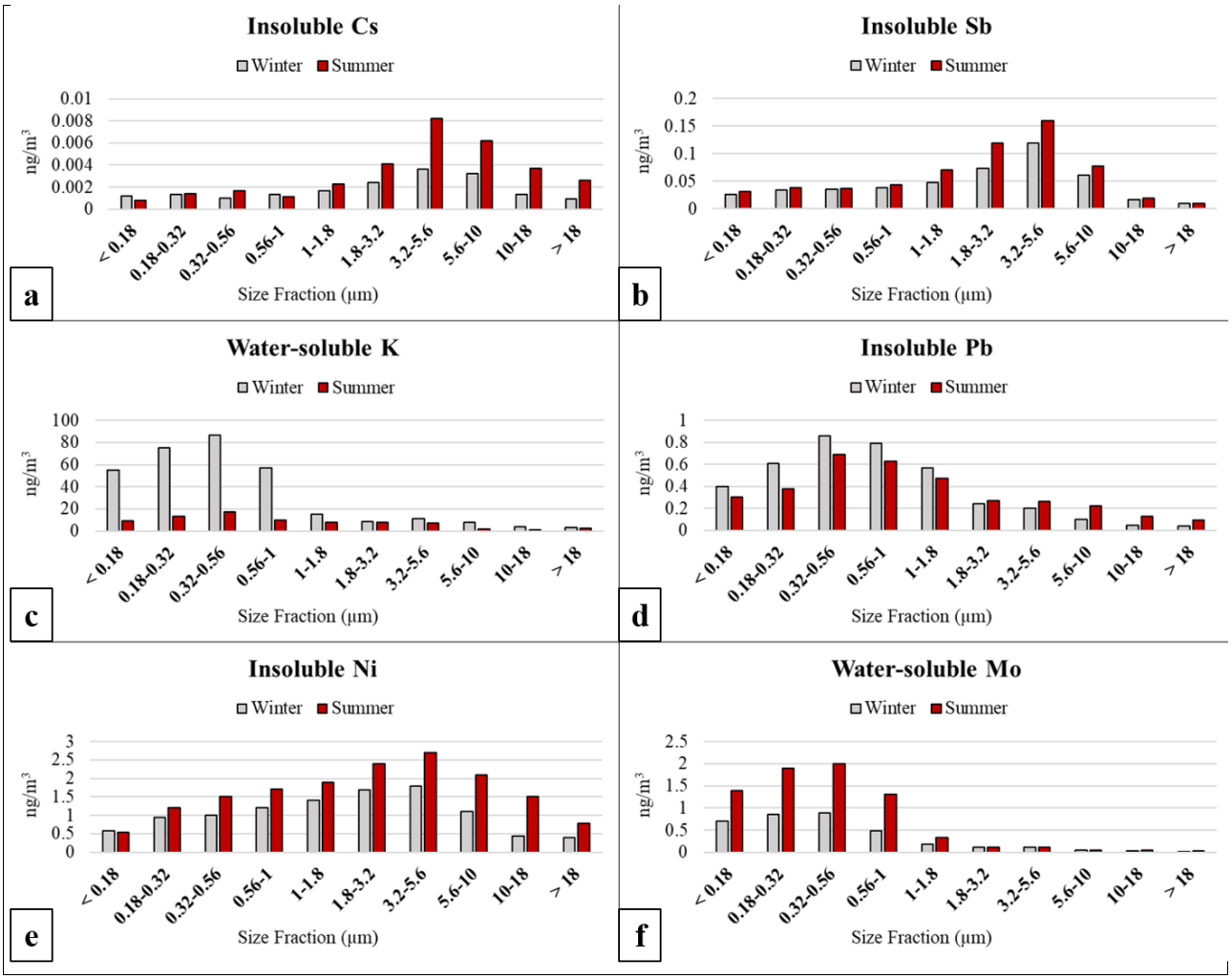

Fig. 7. Size distribution of the winter and summer insoluble Cs, Sb, Pb, Ni (panels a,b,d,e) and water-soluble K and Mo (panels c,f).

The third group, on the central part of the loading plot, is composed of elements (Ce_i, Cs_i, La_i, Li_i, Rb_i, Sr_i, U_i) originated from resuspension of soil dust from dry surfaces by vehicular traffic (Canepari et al., 2008; Pant and Harrison, 2013). The fourth group, on the central right part of the loading plot, is composed of water-soluble elements (Cd_s, Cs_s, K_s, Rb_s, Tl_s) reasonably released by biomass burning related sources (Cvjetko et al., 2010; Canepari et al., 2014; Karbowska, 2016; Simonetti et al., 2018a; Frasca et al., 2018) such as industrial biomass heating (carpentry at FA and craftsmanship lab at CB) and domestic biomass burning (townhouses frequently heated by biomass burning appliances are present at FR, BR, AR, PI, PV, LG). The fifth group, on the right upper part of the loading plot, is composed of elements (Ba_s, Bi_i, Cu_i, Sb_i, Sn_i, Zr_i) generally considered as tracers of railway and vehicular traffic emissions, as they are usually released by mechanical abrasion and resuspension of vehicle/train components (brake disks and pads lining, tires;

Weckwerth, 2001; Abbasi et al., 2012; Querol et al., 2012; Kam et al., 2013; Namgung et al., 2016). Insoluble Fe (Fe_i) is between this group and the group of tracers for the steel rolling emission from the steel plant as it is affected by both contributions. Finally, PM_{10} mass concentration (PM10) is in this last group of vehicular traffic tracers and it is in the same direction of the biomass burning tracers along PC2; this because PM mass is constituted for a relevant fraction (20-60%) by carbon-containing compounds, which are generally released in large amount by vehicular traffic and biomass burning (Perrino et al., 2007, 2009; Canepari et al., 2009; Massimi et al., 2019, 2020). Overall, low values of loadings (supplementary material S5.5) were found respect to typical values found in some previous studies (Cesari et al., 2016). As a consequence of these low loads, the communalities seem to be relatively low, indicating that the components do not explain the majority of the variances of the different elements. In fact, items with low communality may indicate additional factors which will be explored in further studies focused on source apportionment by measuring additional items.

3.4 Size Distribution of Water-soluble and Insoluble Element Concentrations

Given the well-known relationship between size distribution of PM and its emission processes, we carried out elemental analysis of size-segregated PM samples to verify their link with the emission sources in the Terni basin. The behavior of some elements representative of the PCA clusters are shown in Fig. 7 (size distribution of the other elements is reported in supplementary material S6). We can observe that the concentration of Cs_i (panel a), as well as of the other elements originated from resuspension of soil dust by vehicular traffic (Ce_i, La_i, Li_i, Rb_i, Sr_i, U_i), was particularly high in the coarse mode, with a maximum in the size fraction 3.2-5.6 µm, in agreement with PM production by mechanical abrasion. Moreover, the concentration of these elements was higher in the summer, when the higher temperature and the lower rainfall led to a major dryness of the road surfaces and to an easier resuspension of soil dust. The same considerations (size distribution and seasonal pattern) are to be maintained for Sb_i (panel b) and the other elements that trace PM production by abrasion from railway and non-exhaust vehicular traffic emissions (Ba_s, Bi_i, Cu_i, Sn_i, Zr_i).

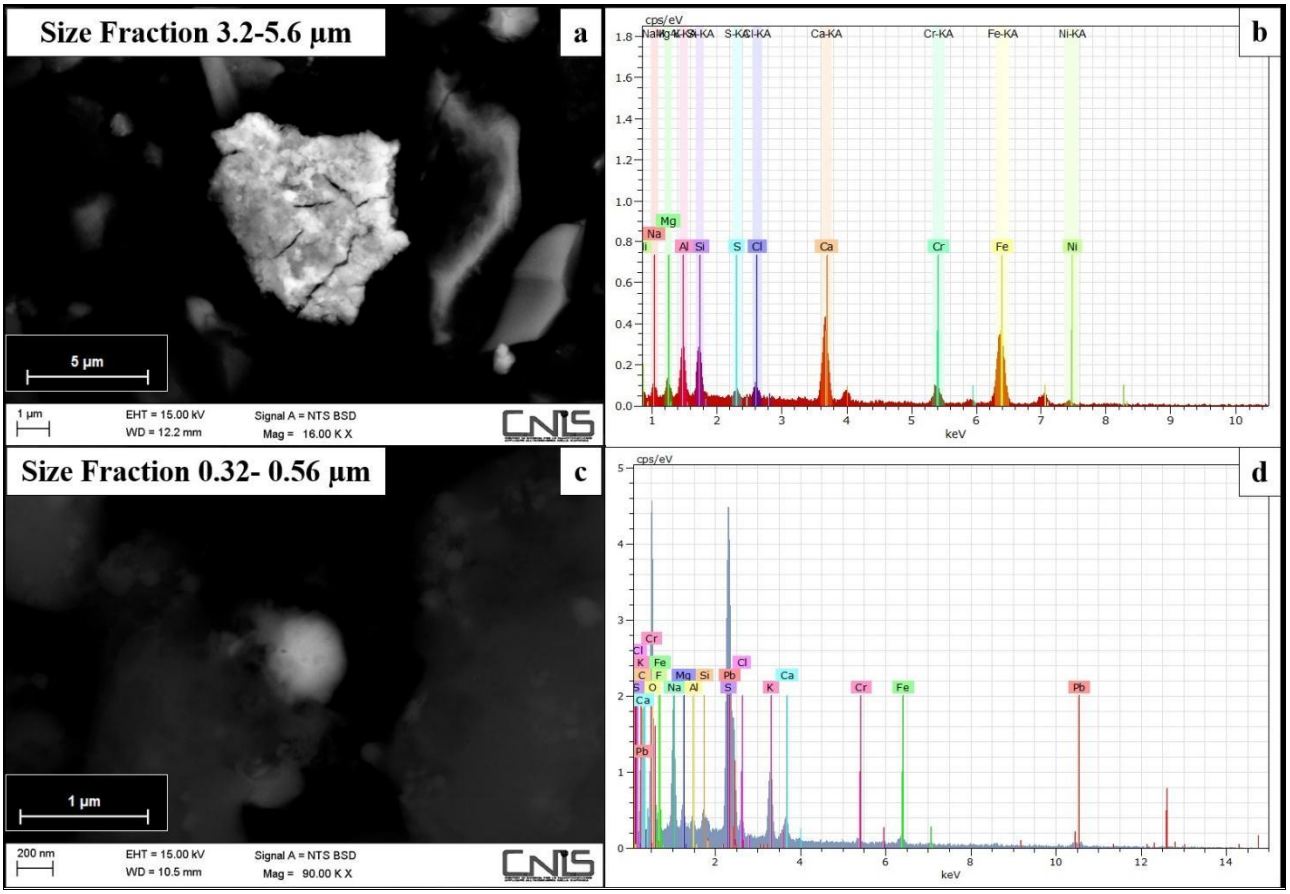

Fig. 8. HR-FESEM micrographs (panels a,c) and XEDS microanalyses (panels b,d) of particles emitted by the steel plant in the size fractions 3.2-5.6 µm (panels a,b) and 0.32-0.56 µm (panels c,d), collected at PR by MOUDI on aluminum foils during a 3-day period (February 12nd - 14th 2018).

On the other hand, K_s (panel c), as well as the other identified biomass burning tracers (Cd_s, Cs_s, Rb_s, Tl_s), was found mostly in particles below 1 µm, at much higher concentration during the winter. This is consistent with an emission by combustion sources whose strength increases during the cold period (biomass burning).

Insoluble Pb (Pb_i; panel d) and the other elements reasonably released by primary emission from the furnaces for the annealing of the cold rolled product at PR (Cr_s, Ga_s, Li_s, Mn_s, Zn_s), were likewise all found in fine particles in the winter as well as in the summer. Consequently, their size distribution is in agreement with the combustion emission from the steel industry.

Finally, the different size distribution of the elements identified as tracers for the steel rolling emission (cluster "Steel Plant RO" in Fig. 6) revealed the presence of two different types of emission acting in this area. Water-soluble Mo (Mo_s; panel e), as well as As_s and W_s (supplementary material S6), were found in particles smaller than 1 µm, indicating that they were released by hot works, such as casting and hot rolling. Instead, Ni_i (panel f) together with Co_i, Cr_i, Mn_i and Nb_i, showed also a relevant coarse fraction, indicating a main role of cold processes (abrasion, brushing and polishing of rolled steel).

3.5 HR-FESEM characterization

HR-FESEM observation and XEDS microanalyses were performed on the 3.2-5.6 µm and 0.32-0.56 µm size-segregated PM samples collected at PR, which is in the close proximity of the steel industry pole, to qualitative describe the morphology and elemental composition of the coarse and fine particles released by the steel plant. Fig. 8 shows two particles that contain elements typically released by the steel industry and that are representative of two types of emission. The first particle, belonging to the size fraction 3.2-5.6 µm (panel a), was about 5 µm of diameter, irregular in shape and its microanalysis (panel b) showed the basic components of stainless steel: Cr, Fe and Ni. This particle seems to have been originated from mechanical abrasion of steel. The second one (size fraction 0.32-0.56 µm, about 0.4 µm in diameter, panel c) showed a regular and spherical shape and was composed of Cr, Fe and different elements used in steel processing-related activities, including Pb (panel d). It may be attributed to condensation of supersaturated vapors (Džiugys and Peters, 2001). Panel d shows the presence of Pb, O and S, suggesting the possibility that Pb was released in the form of lead oxide (PbO) or as lead sulphate ($PbSO_4$).

The morphological characterization of the size-segregated PM samples confirmed that the coarse particles originated from the steel industry pole may have been emitted by abrasive machining of steel from the rolling plants, while the fine ones, containing Pb_i and Cr_s, Ga_s, Li_s, Mn_s, Zn_s, may have been released by combustive processes from the furnaces for the annealing of the cold rolled product.

4. Conclusions

The winter and summer spatial and size distribution of the water-soluble and insoluble elements allowed a reliable identification and localization of the main local PM_{10} sources in the Terni basin. It was also possible to evaluate the diffusion capacity of the emitted particles. A clear increase in PM_{10} mass concentration occurred at all the sites during the winter, due to the strength of winter PM sources (such as domestic biomass heating) and the temperature inversion during the cold season.

By clustering the analyzed elements and by observing their spatial distribution, we identified reliable and selective source tracers for rail network and vehicular traffic (Ba_s, Bi_i, Cu_i, Sb_i, Sn_i, Zr_i), soil resuspension (Ce_i, Cs_i, La_i, Li_i, Rb_i, Sr_i, U_i), biomass burning (Cd_s, Cs_s, K_s, Rb_s, Tl_s) and steel plant (As_s, Co_i, Cr_i, Cr_s, Ga_s, Li_s, Mo_s, Mn_i, Mn_s, Nb_i, Ni_i, Pb_i, W_s, Zn_s).

Furthermore, size distribution of source tracers and HR-FESEM characterization allowed us to distinguish between contributes originated by mechanical abrasion processes (resuspension of soil, abrasion of vehicle/train components and steel particles), characterized by particles belonging to the coarse mode, and contributes associated to combustion processes or hot works (biomass burning, combustion emission and annealing of the cold rolled product from the steel industry), which typically produce fine particles.

Each identified source showed characteristic winter and summer spatial distributions, depending on the different persistence in atmosphere of coarse and fine particles and on the seasonal variation of meteorological conditions and sources strength.

The described experimental approach enabled us to overcome the limits connected to the study of PM dispersion through the use of mathematical models and the limits associated to the high cost of a monitoring

network based on traditional PM samplers. This kind of high spatial resolution chemical data also promises to be effective for the optimization and validation of dispersion models and is a powerful tool for a reliable geo-referenced assessment of population exposure to PM. This last aspect could also constitute an appealing starting point in studies aimed to deepen the relationship between health effects and PM chemical composition and sources.

Acknowledgments

This work was funded by the project 2017 RG11715C7C8801CF (Principal Investigator Dr. S. Canepari) and the project 2018 AR1181641E22B570 (Principal Investigator Dr. L. Massimi) financed by Sapienza University of Rome.
The authors gratefully thank FAI Instruments (Fonte Nuova, Rome, Italy), the citizens of Terni and the Terni district of ARPA Umbria (regional agency for environmental protection), with special regard to Giancarlo Caiello, Caterina Austeri and Marco Pompei, for the support in the installation and management of the sampling equipment as well as for the help in the choice of the sampling sites.

Author Contributions: L. Massimi and S. Canepari conceived and planned the monitoring and the experiments; L. Massimi and M. Ristorini performed the samplings; L. Massimi, M. Ristorini and M. L. Astolfi performed the chemical analyses; L. Massimi elaborated the data and wrote the manuscript; C. Perrino and S. Canepari coordinated the group and supervised the manuscript.

Conflicts of Interest: The authors declare no conflicts of interest.

Table S1.1. Type of site, main local PM emission sources and geographical coordinates of the 23 sampling sites in Terni.

	Type of Site & Main Local PM Emission Sources	Latitude	Longitude
RI	Industrial Site - Power Plant (West of the City)	42°33′52.02″ N	12°35′21.94″ E
MA	Industrial Site - Power Plant (West of the City)	42°33′41.42″ N	12°36′19.05″ E
FA	Industrial Site - Industrial Biomass Heating (West of the City)	42°33′03.19″ N	12°36′29.76″ E
GI	Urban Site - Rail Network (North-West of the City)	42°34′06.28″ N	12°36′48.27″ E
FR	Urban Site - Domestic Biomass Heating (West of the City)	42°33′53.22″ N	12°37′11.44″ E
CB	Industrial Site - Industrial Biomass Heating (West of the City)	42°33′20.30″ N	12°37′20.45″ E
PI	Urban Site - Domestic Biomass Heating (South of the City)	42°32′56.96″ N	12°37′52.26″ E
BR	Urban Site - Domestic Biomass Heating (North of the City)	42°34′56.19″ N	12°37′23.30″ E
AR	Urban Site - Domestic Biomass Heating (North of the City)	42°34′34.23″ N	12°37′39.88″ E
CR	Urban Site - Rail Network (North-West of the City)	42°34′09.49″ N	12°37′39.81″ E
HG	Urban Site - Rail Network (North-West of the City)	42°34′19.32″ N	12°37′56.02″ E
SA	Urban Site - Trafficked Streets (City Centre)	42°33′45.16″ N	12°38′18.45″ E
PV	Urban Site - Domestic Biomass Heating (South of the City)	42°33′06.96″ N	12°38′35.20″ E
LG	Urban Site - Domestic Biomass Heating (South of the City)	42°32′59.75″ N	12°39′01.16″ E
CZ	Urban Site - Trafficked Streets (City Centre)	42°34′06.90″ N	12°38′52.97″ E
HV	Urban Site - Trafficked Streets (City Centre)	42°33′58.33″ N	12°39′04.74″ E
UC	Urban Site - Trafficked Streets (City Centre)	42°33′38.09″ N	12°38′47.62″ E
CA	Urban Site - Trafficked Streets (City Centre)	42°33′39.01″ N	12°39′03.11″ E
CO	Urban Site - Trafficked Streets (City Centre)	42°33′34.23″ N	12°39′22.62″ E
RO	Industrial Site - Steel Plant (East of the City)	42°33′51.16″ N	12°39′39.15″ E
OB	Industrial Site - Steel Plant (East of the City)	42°34′18.64″ N	12°40′05.57″ E
PR	Industrial Site - Steel Plant (East of the City)	42°34′20.30″ N	12°40′44.23″ E
CP	Industrial Site - Steel Plant (East of the City)	42°33′31.65″ N	12°40′36.04″ E

Table S2.1. Start and stop dates of the 12 HSRS samplings during the 15-month monitoring campaign in Terni.

Start and Stop Dates of the Twelve Samplings			
Season	**Sampling**	**Start Date**	**Stop Date**
Winter	**1°**	19/11/2016	12/12/2016
	2°	17/12/2016	12/01/2017
	3°	21/01/2017	20/02/2017
	4°	25/02/2017	27/03/2017
Summer	**5°**	01/04/2017	01/05/2017
	6°	06/05/2017	05/06/2017
	7°	10/06/2017	17/07/2017
	8°	22/07/2017	28/08/2017
	9°	02/09/2017	02/10/2017
Winter	**10°**	21/10/2017	20/11/2017
	11°	25/11/2017	15/01/2018
	12°	20/01/2018	19/02/2018

Table S3.1. Limits of detection (LODs) of the concentrations (µg/L) of the water-soluble and insoluble fraction of the analyzed elements set at 3 times the standard deviation (SD) of 10 replicate blank determinations.

	UoM	LODs Water-soluble Fraction	LODs Insoluble Fraction
Al	µg/L	3.4	3.8
As	µg/L	0.086	0.18
Ba	µg/L	3.7	0.44
Bi	µg/L	0.0011	0.0017
Ca	µg/L	370	932
Cd	µg/L	0.0038	0.0031
Ce	µg/L	0.0096	0.033
Co	µg/L	0.0073	0.0022
Cr	µg/L	0.081	0.86
Cs	µg/L	0.0033	0.0017
Cu	µg/L	0.2	0.24
Fe	µg/L	3	9.6
Ga	µg/L	0.0018	0.0021
K	µg/L	64	827
La	µg/L	0.0033	0.016
Li	µg/L	0.0063	0.004
Mg	µg/L	3.9	8.8
Mn	µg/L	0.17	0.17
Mo	µg/L	0.049	0.012
Na	µg/L	19	23
Nb	µg/L	0.00082	0.012
Ni	µg/L	0.35	0.17
Pb	µg/L	0.1	0.15
Rb	µg/L	0.031	0.023
Sb	µg/L	0.0094	0.0094

Sn	µg/L	0.013	0.027
Sr	µg/L	0.2	0.57
Ti	µg/L	0.15	0.4
Tl	µg/L	0.00012	0.00062
U	µg/L	0.00092	0.00062
W	µg/L	0.0015	0.0037
Zn	µg/L	15	47
Zr	µg/L	0.00052	0.28

Table S3.2. Average (AM) PM_{10} mass and insoluble element concentrations determined at the 23 sampling sites for the winter monitoring period.

Winter - PM_{10} Mass and Insoluble Element Concentrations (AM)																								
	UoM	**RI**	**MA**	**FA**	**GI**	**FR**	**CB**	**PI**	**BR**	**AR**	**CR**	**HG**	**SA**	**PV**	**LG**	**CZ**	**HV**	**UC**	**CA**	**CO**	**RO**	**OB**	**PR**	**CP**
PM_{10}	µg/m³	41	38	38	39	40	42	40	48	33	41	37	37	43	44	43	35	41	45	52	37	33	37	34
Al	ng/m³	130	204	166	184	144	136	268	130	233	154	144	190	164	209	119	238	156	191	199	151	146	290	193
As	ng/m³	0.33	0.43	0.64	0.47	0.41	0.67	0.47	0.55	0.41	0.36	0.45	0.44	0.48	0.42	0.65	0.48	0.46	0.47	0.51	0.67	0.49	0.67	0.58
Ba	ng/m³	16	15	19	17	13	16	16	17	15	26	19	18	18	14	21	16	17	16	23	12	11	18	12
Bi	ng/m³	0.35	0.29	0.42	0.39	0.36	0.27	0.23	0.31	0.27	0.43	0.41	0.3	0.31	0.28	0.32	0.27	0.3	0.37	0.34	0.23	0.18	0.29	0.17
Ca	ng/m³	1057	980	1241	1090	764	1032	1064	854	726	654	1721	563	912	574	1136	902	1108	991	799	945	821	1641	1009
Cd	ng/m³	0.067	0.035	0.115	0.058	0.08	0.08	0.054	0.048	0.028	0.054	0.069	0.065	0.066	0.11	0.042	0.076	0.085	0.074	0.13	0.1	0.1	0.15	0.08
Ce	ng/m³	0.27	0.27	0.34	0.31	0.24	0.28	0.24	0.25	0.21	0.29	0.38	0.26	0.29	0.27	0.37	0.28	0.27	0.31	0.31	0.22	0.23	0.27	0.26
Co	ng/m³	0.18	0.18	0.25	0.26	0.2	0.24	0.21	0.2	0.22	0.23	0.24	0.25	0.26	0.23	0.24	0.29	0.33	0.39	0.48	1.23	0.45	0.67	0.28
Cr	ng/m³	19	21	25	32	23	25	22	25	24	29	28	27	29	24	28	34	38	42	52	124	57	88	38
Cs	ng/m³	0.029	0.026	0.046	0.034	0.03	0.026	0.021	0.028	0.025	0.031	0.029	0.024	0.029	0.031	0.027	0.023	0.025	0.028	0.035	0.024	0.022	0.036	0.022
Cu	ng/m³	12	11	11	21	14	9	7.6	10	10	19	20	12	11	9.2	14	9.4	9.3	15	16	11	8.2	12	6.7
Fe	ng/m³	449	458	473	816	466	399	335	416	449	717	766	547	490	393	590	570	454	633	801	1115	491	612	377
Ga	ng/m³	0.066	0.083	0.091	0.09	0.072	0.072	0.081	0.07	0.082	0.077	0.077	0.078	0.082	0.09	0.072	0.096	0.084	0.1	0.11	0.14	0.11	0.21	0.096
K	ng/m³	1161	1352	1297	1335	940	1018	1495	1747	1838	1335	1815	1293	1356	1258	1876	1270	1187	1702	1141	1198	972	1338	1338
La	ng/m³	0.15	0.13	0.18	0.15	0.11	0.18	0.13	0.1	0.11	0.13	0.17	0.12	0.14	0.13	0.2	0.15	0.14	0.15	0.15	0.1	0.12	0.13	0.15
Li	ng/m³	0.09	0.08	0.13	0.11	0.09	0.09	0.08	0.09	0.10	0.1	0.1	0.08	0.09	0.1	0.09	0.08	0.09	0.1	0.11	0.1	0.09	0.13	0.08
Mg	ng/m³	43	38	67	53	41	48	41	44	42	46	51	44	45	48	55	47	50	57	53	46	41	85	48
Mn	ng/m³	8.3	9.7	11	15	11	9.8	7.4	7.6	9.8	12	12	10	8.7	7.6	10	9.9	9.5	11	13	24	12	27	9.4
Mo	ng/m³	2.7	2.9	4.4	4.4	4.1	4.4	4.7	5.3	4.5	3.7	3.8	5.0	5.3	5.5	4	4.3	6.1	7.1	7.1	14.9	7.7	9.6	5
Na	ng/m³	199	273	352	305	241	286	240	319	171	188	231	250	291	254	326	280	270	407	251	322	229	309	234
Nb	ng/m³	0.089	0.085	0.12	0.13	0.1	0.1	0.1	0.11	0.12	0.13	0.13	0.13	0.12	0.11	0.14	0.16	0.16	0.2	0.26	0.66	0.25	0.57	0.14
Ni	ng/m³	6.2	6.7	11	9.7	8.2	12	12	10	11	9.3	9.6	11	11	10	10	13	15	18	28	70	24	37	14
Pb	ng/m³	5.2	5.4	8.1	6.2	5.8	6.0	5.3	5.7	5.6	5.5	5.5	5.8	5.8	5.7	5.5	5.8	5.8	6.7	6.9	8.6	6.8	16.6	6.2
Rb	ng/m³	0.28	0.24	0.41	0.31	0.26	0.3	0.22	0.27	0.25	0.26	0.35	0.25	0.27	0.28	0.25	0.22	0.21	0.3	0.28	0.19	0.19	0.37	0.2
Sb	ng/m³	1.1	1.3	1.2	2	1.1	0.93	0.73	1	1	1.5	1.7	1.2	1	0.77	1.2	0.80	0.88	1.3	1.4	0.75	0.65	0.80	0.48
Sn	ng/m³	6.2	6.2	5.9	8.6	6.1	4.6	4.1	6.7	6.5	7.5	8.5	5.8	5	4.2	6.2	4.5	4.3	5.7	5.5	3.2	3.1	3.2	2.6
Sr	ng/m³	1.6	1.3	2.1	2.2	1.3	1.7	1.5	1.2	1.6	1.7	2.2	1.4	1.7	1.5	2.5	1.5	1.9	1.8	1.9	1.5	1.2	2.4	1.5
Ti	ng/m³	3.7	4.4	6.2	5.3	3.9	4.1	3.5	4.1	4.6	5.9	5.4	4.3	5.3	4.9	4.4	4.3	4.1	4.7	5.9	5.9	5.2	11	3.8
Tl	ng/m³	0.046	0.044	0.082	0.065	0.056	0.051	0.039	0.062	0.044	0.056	0.048	0.051	0.052	0.045	0.04	0.038	0.05	0.054	0.063	0.041	0.035	0.045	0.028
U	ng/m³	0.0082	0.0072	0.01	0.0096	0.0073	0.0067	0.0066	0.0069	0.0068	0.0084	0.0098	0.0069	0.008	0.0075	0.0081	0.007	0.0075	0.0081	0.01	0.0084	0.0072	0.01	0.0058
W	ng/m³	0.074	0.08	0.11	0.2	0.09	0.1	0.084	0.1	0.091	0.089	0.090	0.1	0.081	0.089	0.091	0.088	0.091	0.12	0.15	0.28	0.12	0.16	0.095
Zn	ng/m³	30	32	78	43	34	38	53	30	32	34	67	28	43	30	50	43	44	49	39	41	41	82	42
Zr	ng/m³	0.77	0.76	0.8	1.2	0.77	0.52	0.46	0.62	0.73	1.2	1.2	0.76	0.67	0.57	0.88	0.51	0.49	0.76	0.87	0.52	0.43	0.57	0.38

Table S3.3. Average (AM) water-soluble element concentrations determined at the 23 sampling sites for the winter monitoring period.

Winter - Water-soluble Element Concentrations (AM)																							
	UoM	**RI**	**MA**	**FA**	**GI**	**FR**	**CB**	**PI**	**BR**	**AR**	**CR**	**HG**	**SA**	**PV**	**LG**	**CZ**	**HV**	**UC**	**CA**	**CO**	**RO**	**OB**	**PR**	**CP**
Al	ng/m³	7.9	9.1	11	8.7	12	8.0	8.7	9.2	12	7.3	9.5	9.6	9.3	9.1	8.7	8.7	8.2	12	9.3	13	9.5	27	7.8
As	ng/m³	0.33	0.33	0.42	0.29	0.32	0.32	0.37	0.29	0.37	0.28	0.38	0.34	0.37	0.35	0.39	0.37	0.34	0.47	0.52	1.08	0.47	0.61	0.36
Ba	ng/m³	6.6	6.5	6.4	9.1	5.3	4.4	4.9	7.6	9.5	9.4	9.2	8.3	7.6	6.9	9.2	6.6	6.4	7.5	7.4	5.8	4.4	5.5	4.9
Bi	ng/m³	0.023	0.02	0.028	0.018	0.016	0.018	0.017	0.017	0.022	0.015	0.02	0.016	0.017	0.02	0.017	0.019	0.017	0.021	0.017	0.022	0.018	0.029	0.016
Ca	ng/m³	924	864	1270	825	809	843	599	752	715	820	910	720	974	852	925	711	670	898	1163	921	725	1295	564
Cd	ng/m³	0.14	0.17	0.25	0.18	0.16	0.18	0.19	0.24	0.23	0.13	0.16	0.17	0.18	0.2	0.17	0.20	0.16	0.24	0.14	0.2	0.19	0.26	0.16
Ce	ng/m³	0.013	0.023	0.019	0.015	0.012	0.011	0.019	0.035	0.021	0.014	0.029	0.017	0.024	0.021	0.019	0.015	0.015	0.017	0.016	0.013	0.016	0.018	0.063
Co	ng/m³	0.043	0.038	0.045	0.048	0.039	0.039	0.045	0.035	0.043	0.036	0.046	0.042	0.044	0.039	0.049	0.048	0.053	0.067	0.054	0.065	0.049	0.046	0.036
Cr	ng/m³	1.4	1.4	1.4	1.4	1.4	1.6	2.2	1.6	2.0	1.3	1.6	1.8	1.9	1.7	1.8	1.9	1.9	1.8	2.4	4.6	2.8	5.8	2.1
Cs	ng/m³	0.052	0.055	0.092	0.07	0.066	0.07	0.062	0.098	0.073	0.054	0.059	0.061	0.066	0.07	0.055	0.055	0.062	0.07	0.061	0.053	0.049	0.069	0.044
Cu	ng/m³	3.4	4	3.2	7.4	3.3	2.3	2	2.8	4.2	5.1	6.6	3.7	2.9	2.4	5	3	2.4	4.2	3.6	2.7	2.6	2.6	2
Fe	ng/m³	10	13	14	24	12	14	18	13	22	18	22	12	13	12	18	12	10	13	13	17	12	14	11
Ga	ng/m³	0.0082	0.0094	0.012	0.010	0.0078	0.01	0.011	0.0096	0.014	0.0097	0.012	0.0094	0.0096	0.01	0.013	0.011	0.01	0.015	0.013	0.018	0.017	0.030	0.017
K	ng/m³	488	468	722	554	630	534	518	722	572	495	545	532	531	556	451	463	502	681	496	419	391	462	351
La	ng/m³	0.0081	0.012	0.0098	0.0073	0.0074	0.0071	0.0076	0.018	0.01	0.0077	0.014	0.0086	0.015	0.012	0.011	0.0081	0.0066	0.0089	0.0089	0.0070	0.0098	0.0094	0.035
Li	ng/m³	0.11	0.12	0.17	0.13	0.13	0.15	0.14	0.16	0.16	0.12	0.14	0.14	0.15	0.16	0.15	0.15	0.15	0.19	0.19	0.25	0.2	0.36	0.16
Mg	ng/m³	53	48	81	58	53	63	57	66	73	56	65	59	61	61	72	62	62	57	69	76	65	117	57
Mn	ng/m³	6	7.8	8.9	9.5	9	7.6	6.7	8.1	9.2	8	9.1	7.9	7.2	7.2	8.8	7.8	7.2	9.1	8.6	10	10	19	8.2
Mo	ng/m³	4	4.1	4.9	4.3	4.4	4.7	4.2	4	5.3	4.5	5.3	5.3	5.3	5.4	5.9	6.2	7.2	9.5	15	47	16	21	8.4
Na	ng/m³	361	295	531	374	365	397	358	450	489	336	409	335	331	369	450	372	379	342	410	369	373	450	340
Nb	ng/m³	0.0019	0.0031	0.0024	0.0029	0.0019	0.0023	0.0019	0.0021	0.003	0.0022	0.0026	0.0026	0.0019	0.002	0.0029	0.003	0.0024	0.0037	0.0047	0.018	0.0084	0.025	0.0051
Ni	ng/m³	0.96	0.7	0.78	1.1	0.91	0.86	1.1	0.98	1.3	0.99	0.89	0.99	0.95	0.82	1	1.1	1.2	1.5	1.2	3.8	1.6	1.7	1.1
Pb	ng/m³	0.72	1	1.6	0.94	0.93	1.1	1.2	1.5	1.8	0.7	0.89	0.98	1	1.3	0.99	1.1	1	1.2	0.75	1.3	1.3	2.7	1.5
Rb	ng/m³	1.4	1.1	1.8	1.3	1.7	1.4	1.2	1.9	1.5	1	1.2	1.1	1.2	1.3	1	1	1.1	1.3	1.1	0.9	0.86	1	0.77
Sb	ng/m³	0.43	0.63	0.68	0.47	0.43	0.43	0.33	0.34	0.43	0.39	0.46	0.4	0.36	0.32	0.47	0.39	0.33	0.49	0.4	0.4	0.34	0.53	0.28
Sn	ng/m³	0.17	0.23	0.2	0.2	0.15	0.12	0.085	0.084	0.15	0.19	0.26	0.11	0.11	0.11	0.19	0.15	0.087	0.16	0.21	0.31	0.2	0.22	0.14
Sr	ng/m³	2.4	2.1	3.1	2.3	2.3	2.2	2	2.2	2.0	2.4	2.6	2.4	2.6	2.6	2.4	2.1	2.3	2.5	3.0	3.3	1.7	2.6	1.5
Ti	ng/m³	0.1	0.11	0.11	0.079	0.083	0.094	0.056	0.087	0.092	0.079	0.13	0.084	0.097	0.086	0.11	0.087	0.086	0.1	0.16	0.25	0.18	0.48	0.11
Tl	ng/m³	0.11	0.14	0.22	0.17	0.15	0.15	0.15	0.24	0.18	0.12	0.14	0.14	0.14	0.15	0.12	0.12	0.13	0.14	0.11	0.09	0.098	0.092	0.09
U	ng/m³	0.0012	0.0014	0.0017	0.0012	0.0011	0.0013	0.0011	0.0012	0.0018	0.001	0.0014	0.0011	0.0011	0.0012	0.002	0.0015	0.0011	0.0012	0.0011	0.0015	0.0018	0.0017	0.0015
W	ng/m³	0.054	0.058	0.077	0.061	0.076	0.064	0.054	0.058	0.071	0.058	0.067	0.067	0.065	0.075	0.072	0.068	0.082	0.10	0.13	0.46	0.14	0.18	0.085
Zn	ng/m³	31	33	45	34	32	40	34	36	39	29	36	32	34	35	35	33	31	40	33	39	38	77	36
Zr	ng/m³	0.076	0.026	0.02	0.023	0.012	0.016	0.012	0.017	0.031	0.012	0.029	0.014	0.012	0.014	0.016	0.01	0.0079	0.014	0.011	0.034	0.03	0.021	0.024

Table S3.4. Average (AM) PM_{10} mass and insoluble element concentrations determined at the 23 sampling sites for the summer monitoring period.

Summer - PM_{10} Mass and Insoluble Element Concentrations (AM)																								
	UoM	**RI**	**MA**	**FA**	**GI**	**FR**	**CB**	**PI**	**BR**	**AR**	**CR**	**HG**	**SA**	**PV**	**LG**	**CZ**	**HV**	**UC**	**CA**	**CO**	**RO**	**OB**	**PR**	**CP**
PM_{10}	µg/m³	24	22	21	20	18	23	21	24	20	22	21	24	22	23	24	23	22	28	28	24	23	27	24
Al	ng/m³	154	192	269	189	192	176	244	309	311	237	271	288	185	263	250	271	190	266	253	204	189	249	271
As	ng/m³	0.23	0.33	0.39	0.36	0.4	0.26	0.30	0.42	0.44	0.29	0.27	0.32	0.24	0.33	0.52	0.44	0.33	0.33	0.35	0.67	0.33	0.2	0.31
Ba	ng/m³	6.8	4	5.2	6.3	4.5	2.7	2.1	2.7	3.4	8.3	7.2	4.9	4	4.7	7.2	5.9	4.1	3.4	3.2	2.6	1.9	1.2	1
Bi	ng/m³	0.077	0.11	0.09	0.12	0.073	0.038	0.048	0.085	0.095	0.21	0.22	0.11	0.11	0.083	0.15	0.075	0.099	0.13	0.12	0.095	0.075	0.11	0.062
Ca	ng/m³	1489	1593	1232	1507	1359	1156	911	1368	1259	986	1387	1664	1297	1258	1087	884	975	783	1296	1026	976	1433	1012
Cd	ng/m³	0.022	0.018	0.029	0.023	0.032	0.015	0.02	0.024	0.025	0.02	0.033	0.024	0.017	0.02	0.022	0.024	0.039	0.024	0.014	0.036	0.023	0.045	0.021
Ce	ng/m³	0.22	0.25	0.31	0.24	0.39	0.31	0.32	0.39	0.32	0.3	0.35	0.39	0.31	0.34	0.35	0.29	0.31	0.34	0.46	0.3	0.32	0.29	0.27
Co	ng/m³	0.075	0.1	0.13	0.11	0.13	0.13	0.13	0.13	0.12	0.13	0.16	0.17	0.13	0.13	0.14	0.14	0.26	0.24	0.29	1.98	0.2	0.28	0.1
Cr	ng/m³	9.3	16	16	15	14	19	17	18	16	18	19	19	16	15	15	15	22	46	41	206	23	42	16
Cs	ng/m³	0.023	0.023	0.039	0.029	0.035	0.027	0.033	0.056	0.036	0.04	0.05	0.04	0.036	0.038	0.046	0.033	0.044	0.038	0.033	0.032	0.035	0.032	0.023
Cu	ng/m³	5.3	7.4	6.3	8.4	4.8	4	4.5	5.2	5.8	8.1	13	6	7.2	5.2	8.7	5.3	5.6	7.5	8.1	11.1	5.7	5.9	3.5
Fe	ng/m³	254	349	312	426	269	290	283	329	321	410	591	371	383	306	447	394	396	531	537	2080	343	424	213
Ga	ng/m³	0.026	0.045	0.071	0.04	0.044	0.041	0.054	0.072	0.056	0.057	0.078	0.066	0.041	0.063	0.058	0.057	0.064	0.083	0.076	0.145	0.055	0.12	0.061
K	ng/m³	331	651	611	430	505	276	390	761	443	377	894	709	387	508	830	636	937	1079	376	314	417	264	517
La	ng/m³	0.14	0.16	0.2	0.15	0.25	0.18	0.16	0.24	0.21	0.2	0.23	0.22	0.18	0.18	0.22	0.17	0.16	0.21	0.25	0.17	0.17	0.15	0.17
Li	ng/m³	0.1	0.13	0.15	0.1	0.13	0.12	0.13	0.19	0.15	0.16	0.19	0.14	0.11	0.14	0.16	0.1	0.13	0.17	0.15	0.16	0.11	0.14	0.1
Mg	ng/m³	54	65	72	59	63	56	70	95	84	72	96	82	57	68	82	64	62	72	76	61	58	99	61
Mn	ng/m³	4.9	6.6	7	8.4	6.8	6.4	6.1	6.9	7.2	8.5	10	7.6	6.4	6.1	8.5	6.8	7.9	9.8	9.9	32.3	7.2	19.2	6.3
Mo	ng/m³	0.88	1.7	1.4	1.3	1.2	1.5	1.9	0.99	0.96	1.2	1.6	1.4	1.3	1.4	1.3	1.2	3.1	3	4	15	1.9	2.3	1
Na	ng/m³	207	292	256	226	269	274	259	467	375	354	375	256	285	389	353	357	253	334	339	278	255	226	334
Nb	ng/m³	0.025	0.037	0.061	0.043	0.049	0.063	0.071	0.059	0.046	0.056	0.087	0.087	0.059	0.054	0.068	0.058	0.12	0.13	0.18	1.3	0.16	0.59	0.075
Ni	ng/m³	3.2	6.2	6.4	5.1	5.3	7.4	7.7	4.9	6	5.9	5.9	7.5	6.9	7.9	6.6	5.9	14	18	22	125	13	17	5.6
Pb	ng/m³	2.1	2.8	2.9	2.6	2.8	2.6	2.6	2.8	2.7	2.8	3.1	3.0	2.9	2.9	3.8	3.2	3.6	4.1	3.2	5.7	3.5	12	3.2
Rb	ng/m³	0.28	0.47	0.47	0.34	0.41	0.39	0.44	0.62	0.42	0.48	0.57	0.54	0.41	0.48	0.53	0.22	0.36	0.45	0.5	0.31	0.32	0.35	0.27
Sb	ng/m³	0.41	0.61	0.5	0.57	0.43	0.35	0.27	0.42	0.44	0.63	0.96	0.56	0.41	0.3	0.67	0.3	0.38	0.48	0.54	0.5	0.24	0.32	0.15
Sn	ng/m³	1.5	1.8	1.5	2.1	1.3	0.93	1	1.5	1.6	2.1	3.5	1.5	1.5	0.93	2.3	1.2	1.3	1.6	1.8	1.4	0.84	1.1	0.61
Sr	ng/m³	1.9	1.8	2	1.8	1.8	1.5	1.8	2.6	2	1.8	2.4	2	1.9	1.8	2.3	1.8	1.5	2.3	2.2	1.4	1.3	1.7	1.8
Ti	ng/m³	3.5	5	7.9	4.1	5.3	4.7	4.6	7.1	4.8	7.8	7.7	6.3	4.4	4.6	6.5	4.1	5	6.3	6.1	8.9	5.4	17	4
Tl	ng/m³	0.011	0.0098	0.018	0.017	0.02	0.0095	0.0097	0.012	0.014	0.015	0.017	0.014	0.008	0.009	0.016	0.012	0.017	0.0095	0.0057	0.0076	0.008	0.0087	0.0055
U	ng/m³	0.0053	0.0054	0.0078	0.0064	0.0066	0.006	0.0074	0.011	0.0079	0.0087	0.012	0.011	0.0075	0.0078	0.0094	0.0066	0.0098	0.0083	0.0073	0.0081	0.0081	0.0092	0.0052
W	ng/m³	0.021	0.028	0.036	0.181	0.035	0.031	0.031	0.04	0.036	0.037	0.047	0.042	0.033	0.029	0.041	0.027	0.061	0.04	0.05	0.368	0.05	0.074	0.02
Zn	ng/m³	30	34	35	42	34	36	31	41	39	28	34	48	36	34	32	26	31	52	37	34	29	53	30

Zr	ng/m³	0.66	0.56	0.51	0.65	0.48	0.32	0.31	0.52	0.49	0.70	1.03	0.58	0.58	0.43	0.76	0.56	0.49	0.66	0.59	0.49	0.39	0.6	0.24

Table S3.5. Average (AM) water-soluble element concentrations determined at the 23 sampling sites for the summer monitoring period.

Summer - Water-soluble Element Concentrations (AM)																								
	UoM	**RI**	**MA**	**FA**	**GI**	**FR**	**CB**	**PI**	**BR**	**AR**	**CR**	**HG**	**SA**	**PV**	**LG**	**CZ**	**HV**	**UC**	**CA**	**CO**	**RO**	**OB**	**PR**	**CP**
Al	ng/m³	5.2	6.8	12.9	7.1	7.5	4.5	6	5.7	13.2	6.6	4.7	4.8	5.7	5.7	5.9	5.3	4.7	5.9	4.4	8	6.6	12.9	5.6
As	ng/m³	0.17	0.18	0.21	0.21	0.15	0.19	0.15	0.2	0.21	0.23	0.2	0.22	0.19	0.19	0.26	0.26	0.26	0.29	0.29	0.8	0.23	0.3	0.17
Ba	ng/m³	4.8	5.0	3.1	4.8	3.7	3.7	4	3.6	4.1	5.7	5.9	3.7	3.8	4.3	5.2	4	2.9	3.7	3.9	4	3.5	3.9	3
Bi	ng/m³	0.0054	0.0063	0.0071	0.0065	0.0044	0.006	0.0078	0.011	0.01	0.0091	0.0072	0.0058	0.0059	0.0076	0.0096	0.0067	0.0070	0.011	0.0048	0.0082	0.0094	0.0099	0.0072
Ca	ng/m³	787	754	931	768	820	759	607	769	781	864	648	702	886	718	834	673	653	741	764	949	939	1573	548
Cd	ng/m³	0.026	0.032	0.034	0.049	0.042	0.04	0.037	0.036	0.055	0.044	0.039	0.041	0.039	0.04	0.045	0.044	0.045	0.055	0.036	0.085	0.051	0.031	0.037
Ce	ng/m³	0.021	0.014	0.013	0.026	0.013	0.0085	0.017	0.019	0.036	0.029	0.02	0.018	0.013	0.014	0.015	0.022	0.017	0.014	0.011	0.013	0.016	0.0087	0.011
Co	ng/m³	0.025	0.024	0.028	0.028	0.032	0.022	0.034	0.033	0.033	0.03	0.032	0.035	0.028	0.031	0.033	0.036	0.037	0.045	0.028	0.08	0.039	0.027	0.025
Cr	ng/m³	0.7	0.97	0.89	0.99	0.95	1	1.2	0.86	1.1	1.1	0.98	1.2	1.3	1.4	1.4	1.4	1.6	2.4	1.7	5.2	2.1	3.9	1.3
Cs	ng/m³	0.0089	0.012	0.013	0.014	0.011	0.01	0.013	0.013	0.02	0.015	0.012	0.013	0.014	0.012	0.016	0.017	0.016	0.017	0.012	0.021	0.016	0.027	0.011
Cu	ng/m³	1.8	2.3	1.5	2.9	1.6	1.3	1.8	1.9	2.5	2.8	3.5	1.9	2.8	2	3.1	2	1.7	2.8	2.2	2.5	1.9	1.2	1.2
Fe	ng/m³	9.8	9.4	9.4	14	9.2	9.1	8.5	9	11	11	11	8.1	10	9.1	11	8.7	8	11	8.8	19	12	15	7.2
Ga	ng/m³	0.0032	0.007	0.0061	0.0043	0.0075	0.0048	0.0081	0.0075	0.008	0.0066	0.0054	0.005	0.0069	0.0067	0.0079	0.0088	0.0074	0.0076	0.0052	0.0079	0.0084	0.0155	0.01
K	ng/m³	89	111	130	136	129	119	118	122	165	153	125	119	133	132	144	122	146	130	111	150	149	162	108
La	ng/m³	0.013	0.012	0.0085	0.014	0.0093	0.0095	0.012	0.012	0.027	0.019	0.009	0.013	0.0076	0.0096	0.0093	0.011	0.0078	0.0063	0.0067	0.0079	0.0081	0.0079	0.0058
Li	ng/m³	0.047	0.065	0.073	0.067	0.070	0.067	0.072	0.06	0.073	0.075	0.064	0.076	0.09	0.085	0.099	0.097	0.092	0.13	0.091	0.21	0.13	0.23	0.085
Mg	ng/m³	44	48	53	48	48	52	60	60	74	63	56	59	68	60	75	62	60	66	58	87	73	113	61
Mn	ng/m³	3	4	4.1	5.9	4.9	3.8	3.8	4.3	5.1	5.7	4.7	4.4	4.4	4.3	5.5	4.7	4.4	5.6	4.2	7.2	6	8.5	4.7
Mo	ng/m³	1.7	3.2	3.3	2.5	3	4.1	3.9	2.3	2.6	2.9	2.4	4.1	5.3	5.7	3.7	4	7.1	11	12	53	11	9	3.5
Na	ng/m³	275	294	321	259	271	309	380	385	481	382	336	337	390	350	458	369	356	345	320	375	370	382	340
Nb	ng/m³	0.0021	0.003	0.0029	0.0028	0.003	0.003	0.0041	0.0035	0.0033	0.003	0.0033	0.0031	0.0043	0.0039	0.0038	0.0041	0.005	0.0074	0.006	0.0329	0.0076	0.0196	0.0063
Ni	ng/m³	0.83	0.93	0.62	0.73	1.2	0.76	0.98	0.68	0.86	0.8	0.71	0.92	0.92	0.93	0.85	0.86	1.1	1.6	1.1	5.9	1.8	1.1	0.76
Pb	ng/m³	0.28	0.35	0.32	0.36	0.28	0.44	0.48	0.37	0.55	0.36	0.3	0.41	0.38	0.38	0.43	0.42	0.36	0.54	0.29	0.61	0.64	1.3	0.47
Rb	ng/m³	0.27	0.31	0.35	0.38	0.36	0.3	0.33	0.39	0.48	0.4	0.33	0.33	0.38	0.35	0.39	0.38	0.41	0.4	0.29	0.42	0.38	0.52	0.25
Sb	ng/m³	0.29	0.43	0.54	0.35	0.44	0.42	0.29	0.38	0.43	0.45	0.37	0.36	0.35	0.31	0.41	0.32	0.34	0.54	0.27	0.41	0.3	0.33	0.28
Sn	ng/m³	0.22	0.24	0.2	0.21	0.2	0.18	0.18	0.25	0.25	0.23	0.21	0.16	0.17	0.17	0.22	0.17	0.15	0.21	0.15	0.2	0.19	0.21	0.13
Sr	ng/m³	1.7	1.8	2	1.8	1.8	1.7	1.7	1.9	2.1	2.1	1.7	1.9	2.3	2	2.3	1.7	1.6	1.8	1.8	2.2	2.1	3	1.5
Ti	ng/m³	0.071	0.084	0.097	0.119	0.089	0.082	0.089	0.11	0.144	0.21	0.079	0.079	0.095	0.12	0.12	0.11	0.094	0.13	0.1	0.15	0.13	0.24	0.12
Tl	ng/m³	0.024	0.029	0.035	0.041	0.024	0.027	0.028	0.033	0.044	0.033	0.029	0.026	0.027	0.022	0.035	0.035	0.031	0.026	0.016	0.021	0.024	0.017	0.017
U	ng/m³	0.0018	0.0022	0.0023	0.0018	0.0021	0.0015	0.0022	0.0030	0.0028	0.0025	0.0027	0.0019	0.0021	0.0022	0.0028	0.0023	0.0021	0.0024	0.0020	0.0023	0.0021	0.0024	0.0021
W	ng/m³	0.024	0.036	0.042	0.036	0.035	0.042	0.043	0.025	0.029	0.035	0.031	0.042	0.055	0.057	0.044	0.046	0.074	0.11	0.1	0.51	0.099	0.093	0.03
Zn	ng/m³	10	16	15	21	14	16	15	14	17	16	13	16	18	17	17	16	15	24	16	26	23	27	20

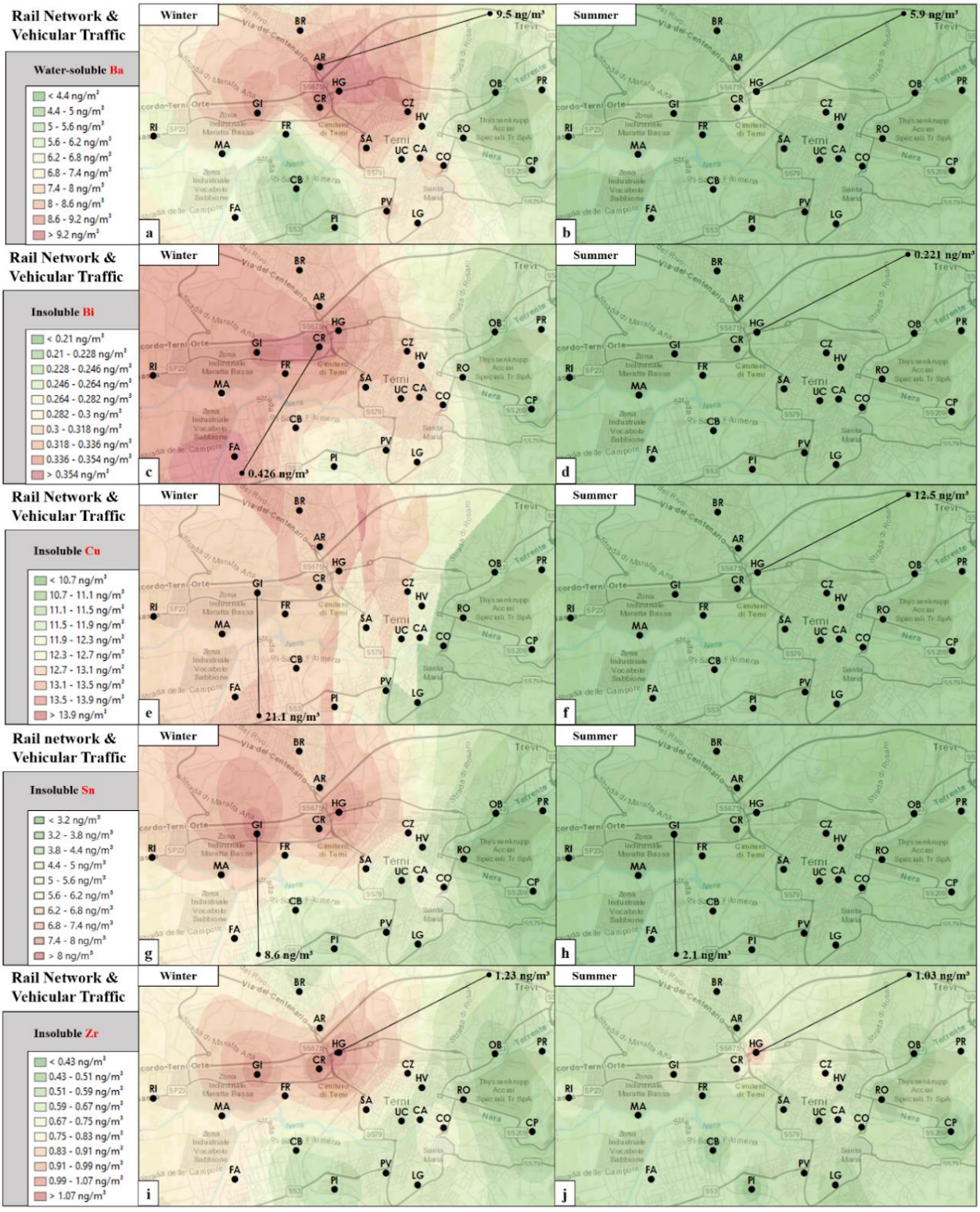

Fig. S4.1. Map of the winter and summer spatial distribution of water-soluble Ba (panels a,b), insoluble Bi (panels c,d), Cu (panels e,f), Sn (panels g,h) and Zr (panels i,j)

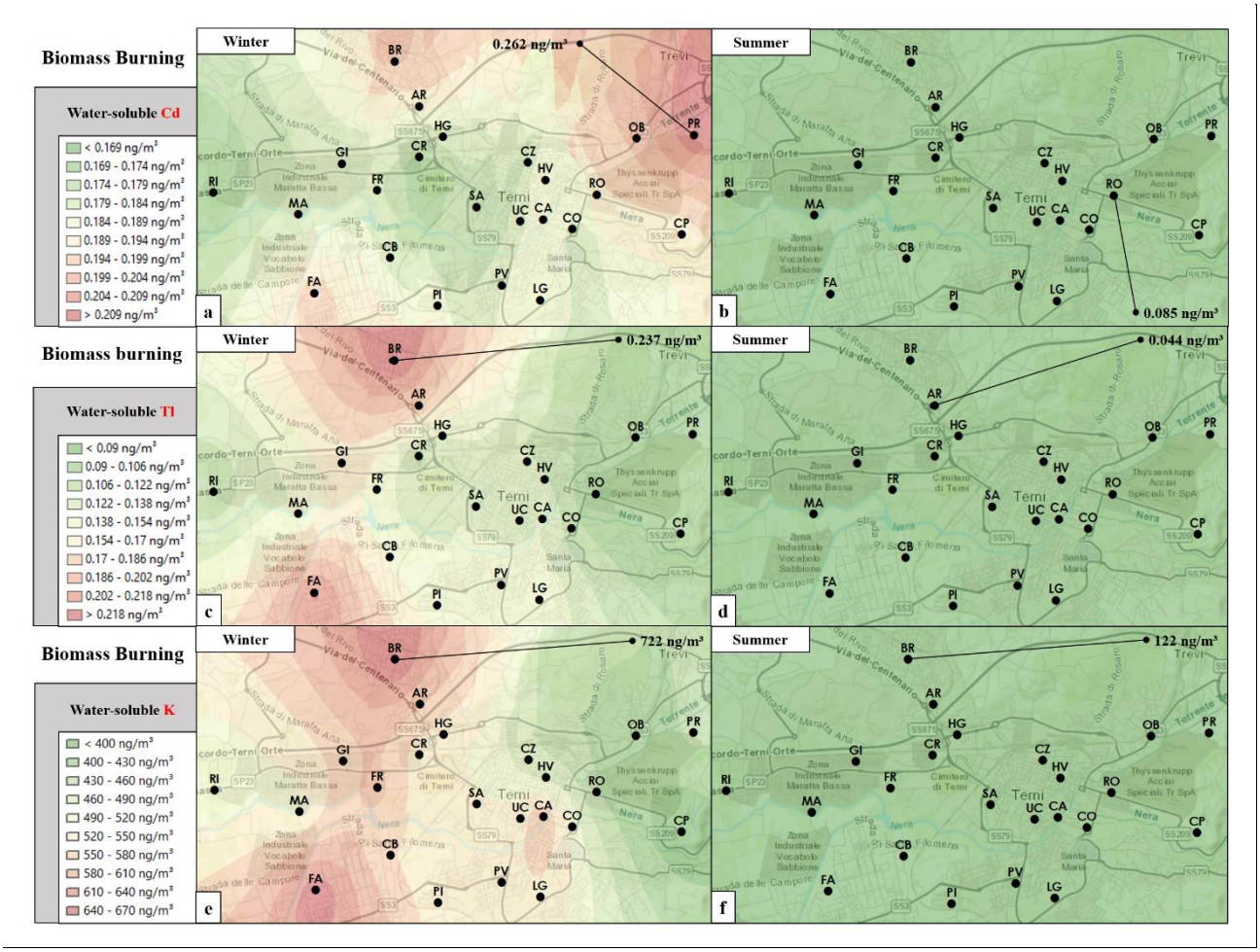

Fig. S4.2 Map of the winter and summer spatial distribution of water-soluble Cd (panels a,b), Tl (panels c,d) and K (panels e,f).

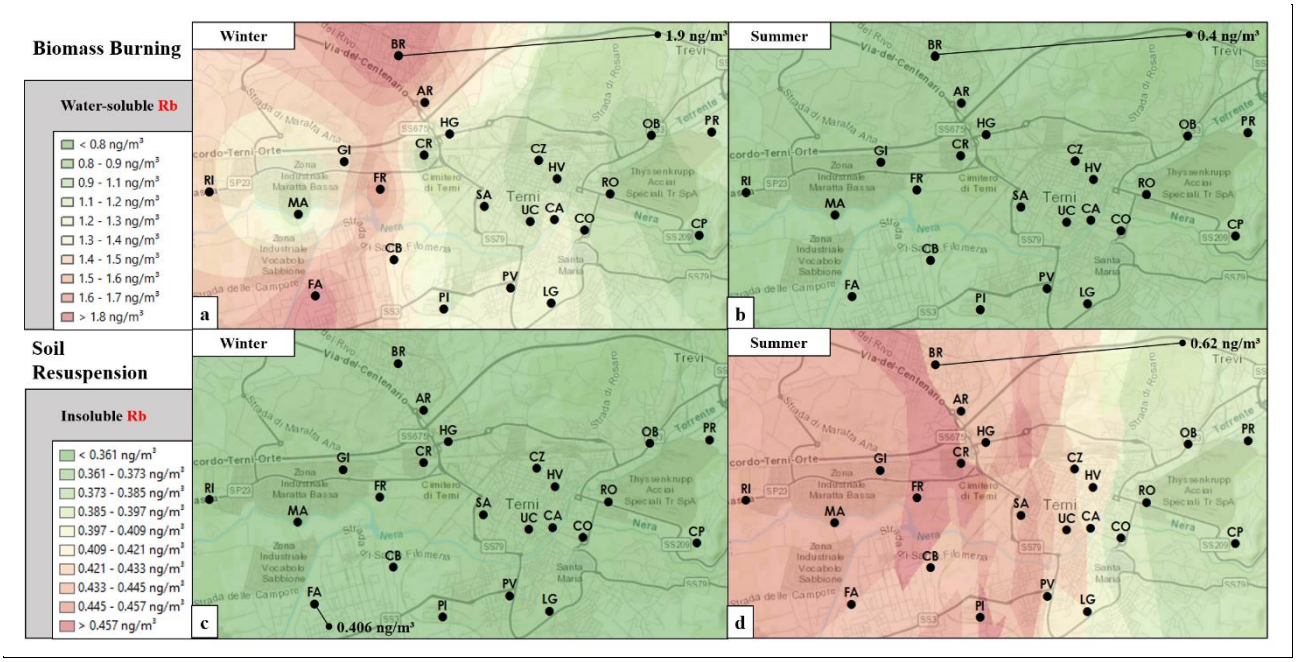

Fig. S4.3. Map of the winter and summer spatial distribution of water-soluble (panels a,b) and insoluble Rb (panels c,d).

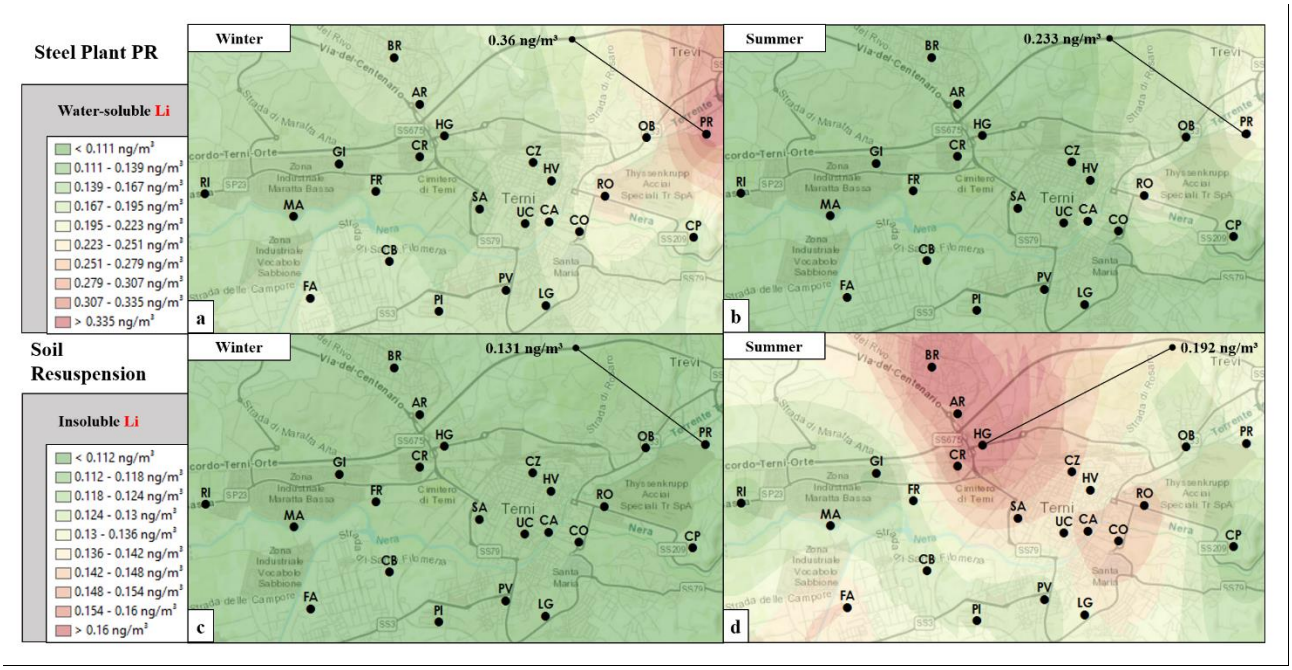

Fig. S4.4. Map of the winter and summer spatial distribution of water-soluble (panels a,b) and insoluble Li (panels c,d).

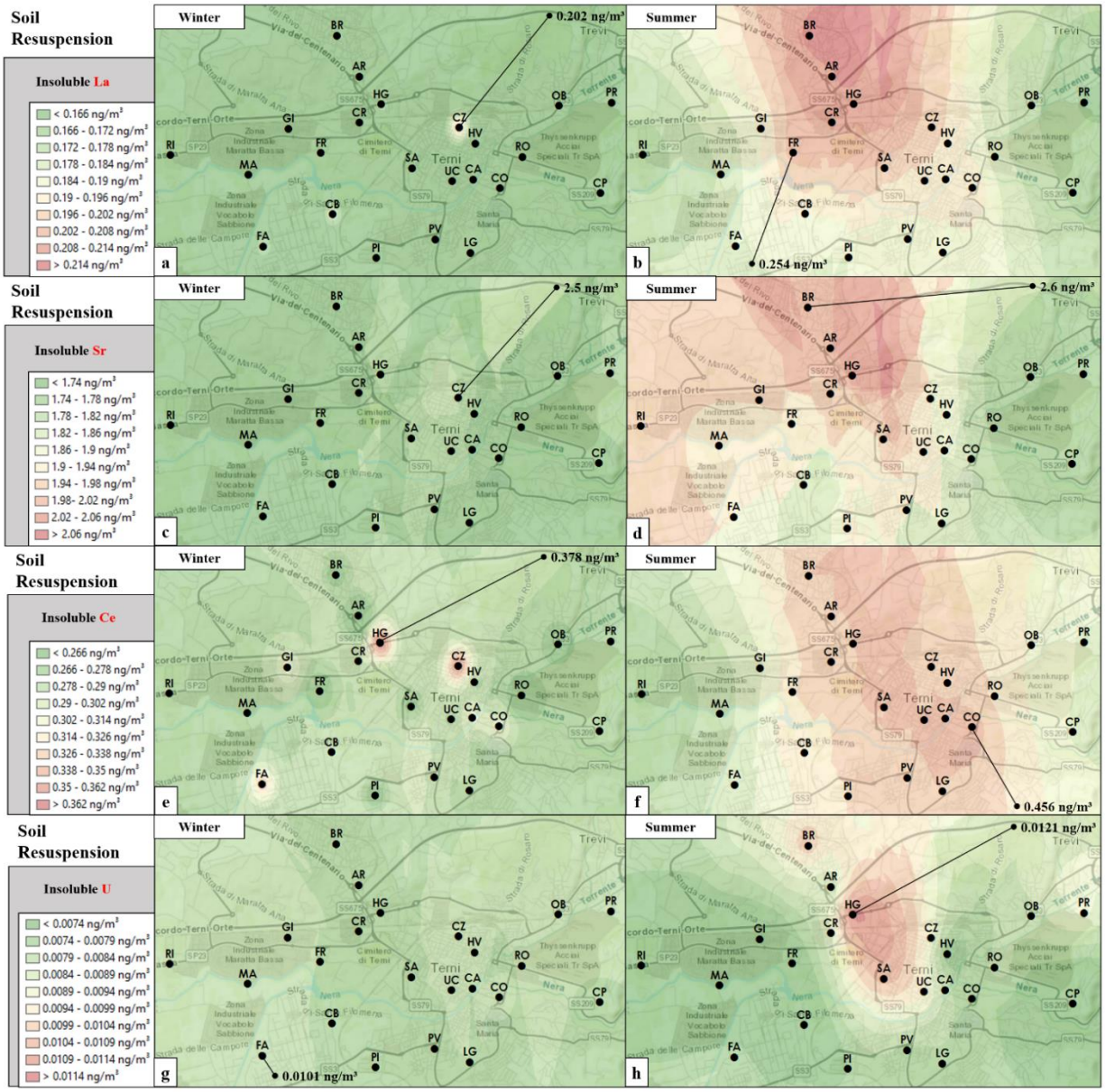

Fig. S4.5. Map of the winter and summer spatial distribution of insoluble La (panels a,b), Sr (panels c,d), Ce (panels e,f) and U (panels g,h).

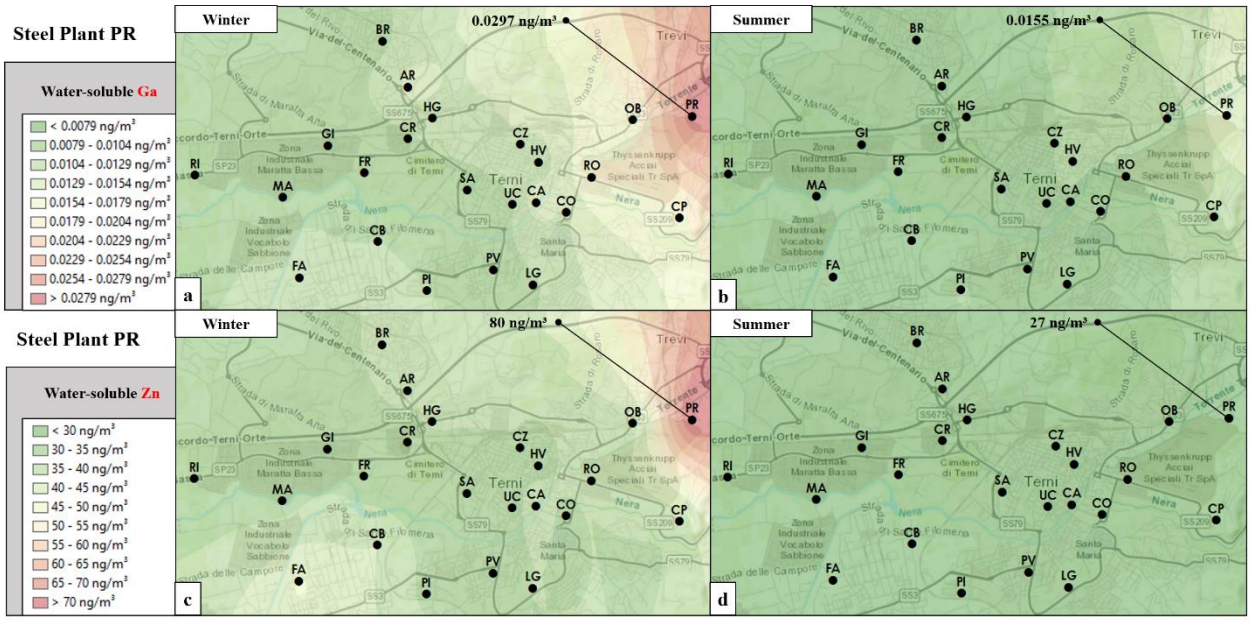

Fig. S4.6. Map of the winter and summer spatial distribution of water-soluble Ga (panels a,b) and Zn (panels c,d).

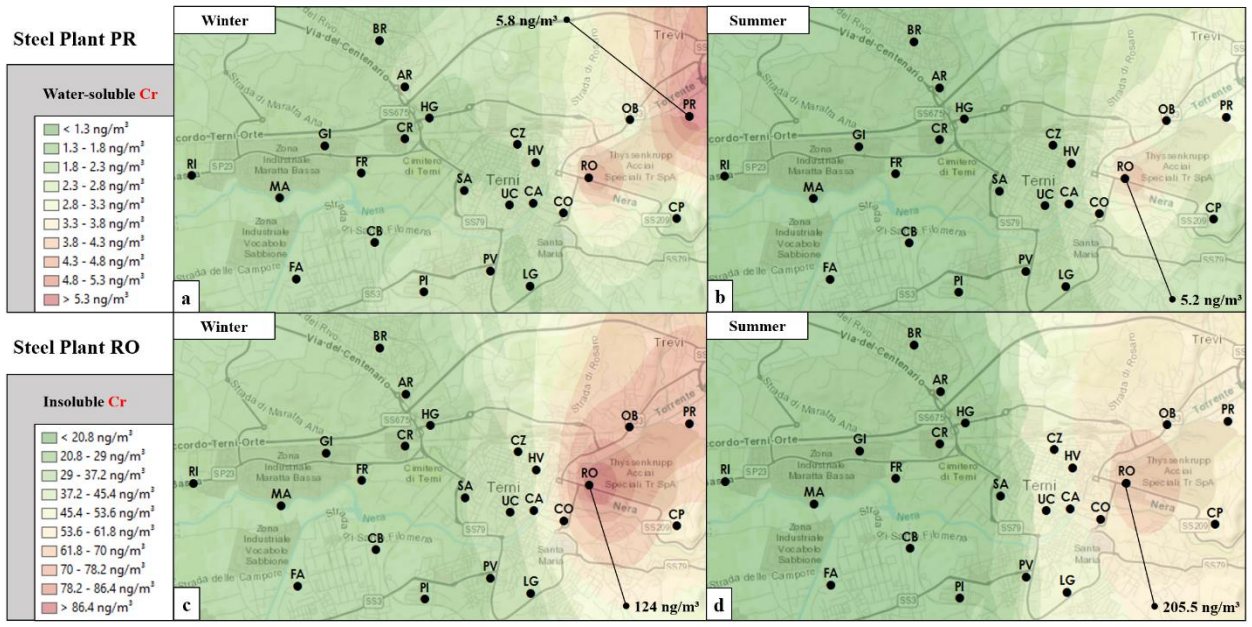

Fig. S4.7. Map of the winter and summer spatial distribution of water-soluble (panels a,b) and insoluble Cr (panels c,d).

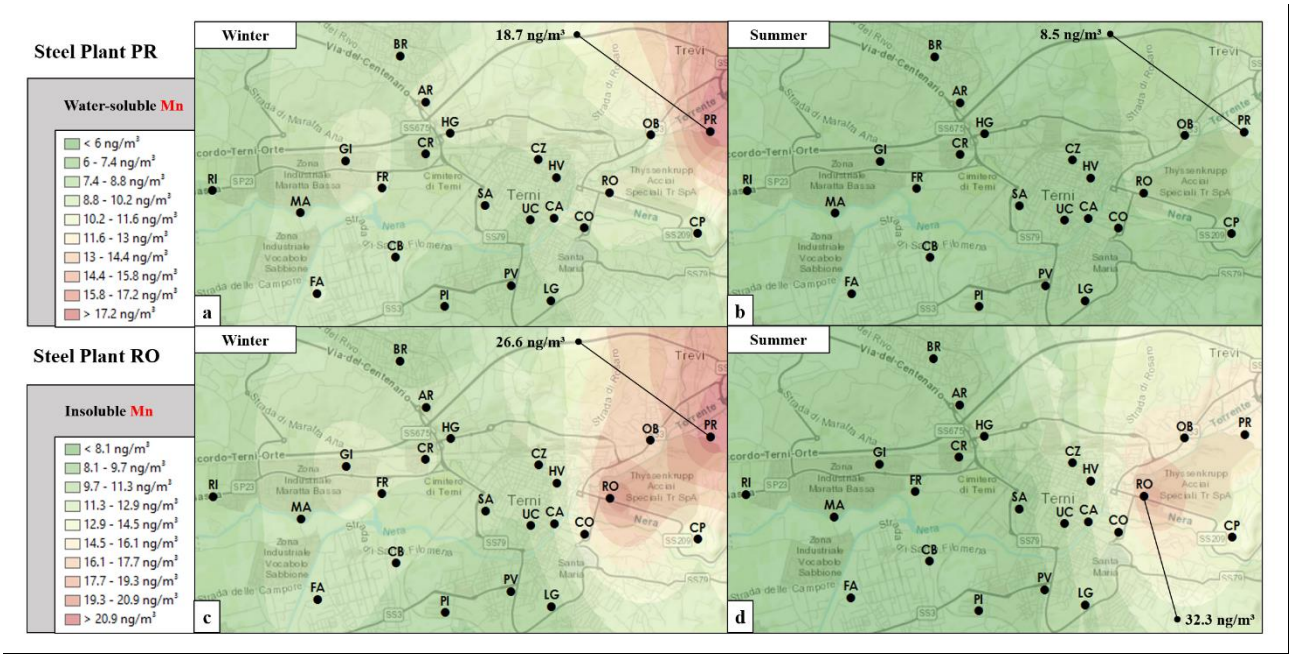

Fig. S4.8. Map of the winter and summer spatial distribution of water-soluble (panels a,b) and insoluble Mn (panels c,d).

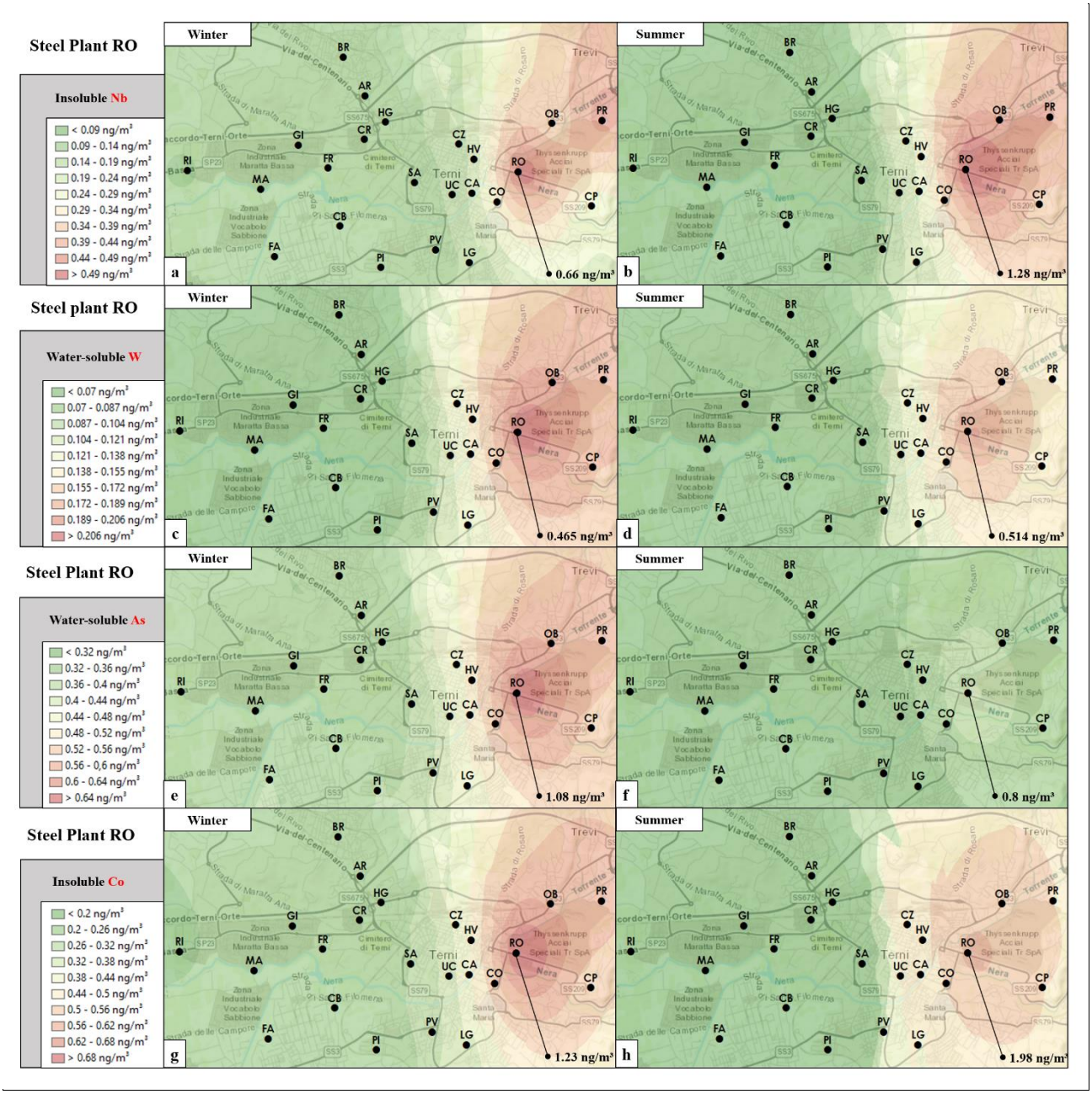

Fig. S4.9. Map of the winter and summer spatial distribution of insoluble Nb (panels a,b), Co (panels g,h), water-soluble W (panels c,d) and As (panels e,f).

Table S5.1. Scores of the four significant components (accounting for 80.6%) obtained by performing the PCA on the matrix of the data composed of 276 samples (23 samples for each of the 12 samplings) and 34 selected variables: PM_{10} mass concentration and 33 water-soluble (_s) and insoluble (_i) element concentrations.

Scores 1° Sampling Month					Scores 2° Sampling Month					Scores 3° Sampling Month				
Site	**PC1**	**PC2**	**PC3**	**PC4**	**Site**	**PC1**	**PC2**	**PC3**	**PC4**	**Site**	**PC1**	**PC2**	**PC3**	**PC4**
RI_1	4.661	3.213	-1.530	0.916	**RI_2**	4.392	3.601	1.428	1.259	**RI_3**	1.252	2.293	0.382	1.336
MA_1	3.792	2.576	-0.506	1.094	**MA_2**	3.699	3.182	1.168	0.655	**MA_3**	0.190	1.772	1.510	0.743
FA_1	2.592	1.399	-3.333	0.176	**FA_2**	4.888	3.262	0.752	-0.474	**FA_3**	0.048	1.571	1.531	-0.221
GI_1	6.863	3.588	-3.354	2.572	**GI_2**	4.806	3.313	-0.347	2.756	**GI_3**	0.330	1.715	-1.316	3.505
FR_1	4.627	3.130	0.449	1.406	**FR_2**	6.369	4.154	1.184	1.206	**FR_3**	0.975	2.136	0.694	1.102
CB_1	4.037	1.811	0.802	-0.834	**CB_2**	4.478	2.345	-2.998	-0.236	**CB_3**	-2.501	0.794	1.834	0.342
PI_1	2.601	1.779	0.847	0.026	**PI_2**	3.229	2.191	0.070	-1.054	**PI_3**	-1.173	1.221	1.587	-0.294
BR_1	4.115	3.345	1.675	-0.282	**BR_2**	4.421	4.109	2.198	0.979	**BR_3**	-0.055	2.073	1.012	0.996
AR_1	7.132	3.206	-0.890	-1.368	**AR_2**	3.025	2.270	2.842	0.034	**AR_3**	-2.713	1.369	1.661	1.368
CR_1	6.946	3.735	-1.714	2.496	**CR_2**	6.999	3.490	-0.724	2.812	**CR_3**	-3.169	1.076	1.533	1.779
HG_1	7.329	3.244	-5.274	1.581	**HG_2**	5.176	3.056	0.402	1.997	**HG_3**	1.493	2.527	0.802	1.791
SA_1	5.407	2.531	-0.668	0.953	**SA_2**	6.453	2.812	0.441	1.180	**SA_3**	-2.726	0.726	1.674	1.143
PV_1	3.302	1.641	0.169	-0.172	**PV_2**	4.089	2.197	0.296	-0.218	**PV_3**	0.790	1.304	0.701	-0.031
LG_1	3.620	1.805	0.474	-0.303	**LG_2**	4.634	2.896	0.681	-0.453	**LG_3**	0.293	1.596	1.129	-0.284
CZ_1	6.217	2.664	-3.612	1.180	**CZ_2**	5.031	2.136	-0.134	1.040	**CZ_3**	0.326	1.475	1.122	0.613
HV_1	5.106	2.083	-1.950	0.778	**HV_2**	3.842	0.780	2.758	0.161	**HV_3**	-0.196	0.707	1.368	-0.513
UC_1	3.756	1.384	-0.840	-0.129	**UC_2**	5.191	2.059	0.266	0.805	**UC_3**	-0.050	0.201	-0.210	0.672
CA_1	7.935	2.246	-1.487	1.160	**CA_2**	9.080	3.310	-0.440	0.616	**CA_3**	1.815	0.645	0.689	0.639
CO_1	7.317	1.194	-2.902	1.889	**CO_2**	6.895	0.982	-0.465	1.474	**CO_3**	1.941	-0.431	1.651	0.407
RO_1	6.234	-4.616	2.931	-0.952	**RO_2**	6.792	-3.794	2.566	-0.216	**RO_3**	5.677	-7.516	4.301	1.691
OB_1	3.050	-1.223	1.936	-1.870	**OB_2**	3.258	-1.647	2.415	-1.790	**OB_3**	2.128	-0.759	1.765	-0.742
PR_1	9.111	-2.297	1.131	-3.862	**PR_2**	7.741	-3.453	3.100	-3.253	**PR_3**	3.549	-3.354	-0.999	-0.018
CP_1	2.123	-0.362	1.609	-1.796	**CP_2**	2.469	0.556	1.267	-1.571	**CP_3**	0.650	-0.866	1.510	-2.464

Table S5.2. Scores of the four significant components (accounting for 80.6%) obtained by performing the PCA on the matrix of the data composed of 276 samples (23 samples for each of the 12 samplings) and 34 selected variables: PM_{10} mass concentration and 33 water-soluble (_s) and insoluble (_i) element concentrations.

Scores 4° Sampling Month				
Site	**PC1**	**PC2**	**PC3**	**PC4**
RI_4	-3.428	0.569	-0.026	1.144
MA_4	-3.272	0.370	-0.742	1.205
FA_4	-3.879	-0.044	-0.792	0.279
GI_4	-2.598	0.135	-1.424	1.552
FR_4	-3.472	0.060	-0.003	0.728
CB_4	-3.360	0.306	1.081	0.023
PI_4	-3.892	0.281	1.807	-0.156
BR_4	-3.828	0.175	-0.037	0.329
AR_4	-4.194	0.089	0.848	0.452
CR_4	-2.259	0.451	-1.702	2.098
HG_4	-2.429	0.581	-1.414	1.999
SA_4	-3.504	0.111	1.401	0.482
PV_4	-2.822	0.291	1.233	0.119
LG_4	-3.471	-0.085	-0.096	0.339
CZ_4	-5.025	0.531	2.453	0.135
HV_4	-3.850	-0.195	0.167	0.378
UC_4	-4.019	-0.337	1.832	0.437
CA_4	-2.016	-0.379	-0.876	1.314
CO_4	-1.776	-0.817	-1.287	1.702
RO_4	0.609	-5.334	0.524	1.992
OB_4	-3.055	-1.170	0.276	0.654
PR_4	0.687	-3.472	-1.603	0.513
CP_4	-3.347	-0.641	-0.537	-0.042

Scores 5° Sampling Month				
Site	**PC1**	**PC2**	**PC3**	**PC4**
RI_5	-3.776	0.981	1.689	0.488
MA_5	-2.892	0.317	0.134	0.488
FA_5	-3.724	0.305	1.525	-0.153
GI_5	-2.757	0.712	2.118	0.095
FR_5	-5.378	0.126	2.285	0.046
CB_5	-3.700	0.166	2.200	-0.553
PI_5	-4.229	-0.036	2.572	-0.705
BR_5	-4.489	0.091	1.321	-0.017
AR_5	-4.245	0.382	2.213	-0.275
CR_5	-3.555	0.569	2.240	-0.053
HG_5	-2.890	0.651	1.517	0.809
SA_5	-3.799	-0.006	2.099	-0.381
PV_5	-3.516	0.293	1.923	0.005
LG_5	-3.990	0.005	2.295	-0.490
CZ_5	-3.714	0.282	2.046	-0.260
HV_5	-4.167	0.251	2.650	-0.884
UC_5	-3.570	-0.287	1.528	0.033
CA_5	-2.706	-0.327	1.991	0.025
CO_5	-2.609	-0.364	2.323	0.022
RO_5	1.430	-5.567	4.082	0.657
OB_5	-3.029	-0.588	2.679	-0.884
PR_5	0.039	-1.978	1.768	-2.316
CP_5	-3.922	-0.099	2.391	-1.172

Scores 6° Sampling Month				
Site	**PC1**	**PC2**	**PC3**	**PC4**
RI_6	-3.509	0.495	0.223	0.500
MA_6	-3.881	0.366	1.130	0.225
FA_6	-4.120	-0.163	0.226	0.009
GI_6	-3.259	0.476	0.564	0.560
FR_6	-4.433	-0.107	0.918	-0.299
CB_6	-3.875	-0.395	0.842	-0.509
PI_6	-5.017	-0.383	0.410	-0.099
BR_6	-4.894	0.211	1.692	-0.382
AR_6	-4.136	0.010	1.173	-0.085
CR_6	-3.577	0.113	0.477	0.242
HG_6	-3.944	0.553	1.596	0.543
SA_6	-4.214	0.198	1.928	-0.588
PV_6	-4.022	0.097	1.584	-0.060
LG_6	-4.198	-0.304	0.982	-0.395
CZ_6	-3.873	-0.118	1.158	-0.058
HV_6	-4.042	-0.174	1.655	-0.423
UC_6	-3.809	-1.056	-0.206	0.081
CA_6	-1.933	-1.528	0.109	-0.137
CO_6	-2.066	-1.414	-0.129	0.632
RO_6	5.747	-12.439	4.574	3.146
OB_6	-4.243	-0.158	2.280	-0.483
PR_6	-1.411	-1.877	1.607	-1.295
CP_6	-4.384	-0.329	1.201	-0.897

Table S5.3. Scores of the four significant components (accounting for 80.6%) obtained by performing the PCA on the matrix of the data composed of 276 samples (23 samples for each of the 12 samplings) and 34 selected variables: PM_{10} mass concentration and 33 water-soluble (_s) and insoluble (_i) element concentrations.

Scores 7° Sampling Month				
Site	**PC1**	**PC2**	**PC3**	**PC4**
RI_7	-4.593	-0.139	-0.245	0.009
MA_7	-2.570	-0.178	-1.135	-0.774
FA_7	-2.069	-1.495	-4.910	-0.938
GI_7	-3.285	-0.504	-2.100	-0.186
FR_7	-1.413	-1.391	-5.866	-1.893
CB_7	-5.205	-0.116	1.086	-0.248
PI_7	-1.906	-1.331	-2.595	-1.753
BR_7	-1.638	-2.111	12.022	-2.004
AR_7	-2.009	-0.881	-4.244	-0.997
CR_7	-1.303	-0.311	-3.364	-0.508
HG_7	-0.060	-0.128	-5.946	-0.868
SA_7	-2.316	-0.918	-3.471	-0.126
PV_7	-1.627	-1.260	-4.685	-0.707
LG_7	-2.304	-1.305	-3.163	-1.257
CZ_7	-1.309	-0.835	-5.023	-1.162
HV_7	-3.152	-0.788	-1.470	-1.229
UC_7	-0.889	-1.975	-2.028	-1.383
CA_7	-1.044	-2.803	-5.595	-1.003
CO_7	-2.095	-4.317	-7.484	-0.182
RO_7	-6.253	-11.370	-0.240	-2.234
OB_7	-0.410	-2.949	-4.439	-1.777
PR_7	-2.202	-3.329	-1.977	-3.273
CP_7	-1.924	-1.300	-2.233	-2.319

Scores 8° Sampling Month				
Site	**PC1**	**PC2**	**PC3**	**PC4**
RI_8	-4.087	-0.377	-0.906	-0.063
MA_8	-3.461	-0.547	-1.345	-0.189
FA_8	-3.130	-0.761	-2.016	-0.303
GI_8	-2.455	0.049	-1.298	-0.307
FR_8	-2.943	-0.626	-2.268	-0.705
CB_8	-2.311	-1.736	-4.991	-0.923
PI_8	-3.010	-1.164	-3.860	-0.244
BR_8	-3.708	-1.570	-6.044	-0.015
AR_8	-2.294	-0.935	-3.998	-0.939
CR_8	-2.084	-1.111	-5.002	-0.001
HG_8	-1.045	-1.342	-8.676	-1.728
SA_8	-1.805	-2.014	-6.931	-0.151
PV_8	-2.353	-1.158	-2.861	-0.330
LG_8	-2.556	-1.209	-3.295	-0.610
CZ_8	-0.882	-0.734	-4.786	-0.165
HV_8	-2.032	-0.980	-1.598	-0.242
UC_8	-2.808	-1.672	-1.335	-0.270
CA_8	-1.189	-2.034	-2.443	-0.455
CO_8	-1.653	-2.343	-3.415	-0.845
RO_8	-6.584	-12.930	-1.722	-4.372
OB_8	-3.147	-1.526	-0.826	-0.473
PR_8	-0.381	-2.677	-2.476	-1.531
CP_8	-3.797	-0.881	-0.266	-0.827

Scores 9° Sampling Month				
Site	**PC1**	**PC2**	**PC3**	**PC4**
RI_9	-3.662	-0.208	-0.228	-0.219
MA_9	-2.753	-0.454	-0.884	-0.269
FA_9	-2.632	-0.384	-0.842	-0.009
GI_9	-1.273	0.289	-0.303	-0.602
FR_9	-2.574	-0.250	-0.902	-0.248
CB_9	-2.949	-1.153	-0.103	-0.054
PI_9	-3.241	-0.504	-0.766	-0.591
BR_9	-3.560	0.197	-1.307	-0.309
AR_9	-1.721	0.083	-0.743	-0.419
CR_9	-1.310	0.063	-1.754	-0.760
HG_9	-0.875	-0.128	-3.641	-1.299
SA_9	-1.794	-0.642	-2.567	-0.023
PV_9	-2.742	-0.281	-0.515	-0.246
LG_9	-2.649	-0.745	-1.390	-0.428
CZ_9	-0.192	-0.154	-3.671	-0.630
HV_9	-1.170	-0.621	-1.356	-0.251
UC_9	-1.699	-0.867	-0.935	-0.096
CA_9	-1.801	-1.625	-0.400	-0.092
CO_9	-4.986	-0.626	-1.398	-0.521
RO_9	-9.406	-15.877	-3.021	-6.499
OB_9	-1.797	-1.423	-0.614	-1.054
PR_9	-1.097	-2.535	-0.653	-2.546
CP_9	-4.132	-0.369	-1.133	-0.588

Table S5.4. Scores of the four significant components (accounting for 80.6%) obtained by performing the PCA on the matrix of the data composed of 276 samples (23 samples for each of the 12 samplings) and 34 selected variables: PM_{10} mass concentration and 33 water-soluble (_s) and insoluble (_i) element concentrations.

Scores 10° Sampling Month				
Site	**PC1**	**PC2**	**PC3**	**PC4**
RI_10	-3.077	0.146	-0.130	0.433
MA_10	-2.002	0.690	1.336	0.187
FA_10	-2.013	0.063	0.373	0.007
GI_10	1.485	1.876	0.303	1.380
FR_10	-1.970	0.463	0.384	-0.548
CB_10	-2.056	-0.343	1.077	0.016
PI_10	-1.808	0.087	1.766	-0.176
BR_10	0.313	1.676	0.393	-0.261
AR_10	0.691	0.987	0.463	-0.008
CR_10	-0.372	1.197	0.008	1.808
HG_10	-0.270	0.895	-0.493	1.409
SA_10	-1.449	0.428	0.805	0.488
PV_10	-2.196	0.194	0.728	0.527
LG_10	-1.888	0.237	0.561	-0.458
CZ_10	-1.180	0.399	-2.585	0.424
HV_10	-1.286	-0.727	1.200	0.365
UC_10	-1.025	-0.532	1.518	-0.342
CA_10	-0.870	-0.174	1.762	-0.072
CO_10	1.329	-1.929	1.043	2.467
RO_10	5.177	-8.827	3.368	1.931
OB_10	-1.007	-1.263	1.494	-0.609
PR_10	0.676	-1.532	1.670	-3.059
CP_10	-2.449	-0.350	1.033	-1.390

Scores 11° Sampling Month				
Site	**PC1**	**PC2**	**PC3**	**PC4**
RI_11	-1.419	1.214	0.259	0.077
MA_11	0.240	2.281	0.649	-0.280
FA_11	10.477	5.155	-2.603	-1.385
GI_11	4.103	4.082	0.767	2.128
FR_11	0.161	2.014	1.525	0.641
CB_11	2.308	2.492	0.889	-0.746
PI_11	-0.909	1.549	2.198	-1.318
BR_11	-0.621	2.409	2.110	-0.854
AR_11	1.795	2.833	2.254	-1.086
CR_11	0.546	1.943	0.434	1.817
HG_11	2.624	2.462	-0.273	1.628
SA_11	0.506	2.105	1.590	-0.061
PV_11	1.149	2.685	0.647	0.633
LG_11	-0.257	1.850	1.872	-0.541
CZ_11	0.944	1.275	-0.240	0.331
HV_11	-0.973	0.965	2.137	-1.059
UC_11	-0.633	1.333	2.189	-0.517
CA_11	0.808	1.405	1.864	-0.542
CO_11	1.252	-0.190	0.889	0.062
RO_11	6.973	-7.314	4.221	0.705
OB_11	1.828	-1.545	2.345	-1.675
PR_11	17.175	-4.320	-0.734	-12.843
CP_11	-0.293	-0.015	1.750	-1.202

Scores 12° Sampling Month				
Site	**PC1**	**PC2**	**PC3**	**PC4**
RI_12	-0.502	1.412	0.610	0.132
MA_12	0.414	1.610	-0.960	-0.188
FA_12	5.446	3.382	-0.822	-0.598
GI_12	5.324	3.259	-0.725	-1.160
FR_12	0.335	1.577	1.203	-0.409
CB_12	0.828	1.416	0.961	-1.479
PI_12	1.417	1.035	0.765	-0.957
BR_12	6.660	4.943	1.196	-0.318
AR_12	4.228	2.518	-0.019	-1.182
CR_12	2.463	2.226	-0.194	0.985
HG_12	2.640	1.986	-0.907	-1.287
SA_12	1.543	1.902	0.384	-0.196
PV_12	1.926	1.440	-0.476	-0.523
LG_12	1.029	1.442	-0.720	-0.325
CZ_12	1.495	1.453	-0.051	-0.157
HV_12	0.900	1.098	0.994	-1.148
UC_12	0.716	0.641	1.197	-0.862
CA_12	1.172	0.639	1.133	-0.521
CO_12	2.179	-0.466	-0.973	-0.051
RO_12	8.523	-7.089	-2.769	-0.451
OB_12	1.858	-0.599	-2.064	-1.725
PR_12	3.763	-0.664	-2.298	-3.802
CP_12	-0.754	-0.220	-1.988	-0.896

Table S5.5. Loadings of the four significant components (accounting for 80.6%) obtained by performing the PCA on the matrix of the data composed of 276 samples (23 samples for each of the 12 samplings) and 34 selected variables: PM_{10} mass concentration and 33 water-soluble (_s) and insoluble (_i) element concentrations.

	Loadings								
Variable	**PC1**	**PC2**	**PC3**	**PC4**	**Variable**	**PC1**	**PC2**	**PC3**	**PC4**
PM_{10}	0.162	0.131	0.031	0.158	**Li_s**	0.235	-0.036	0.047	-0.299
As_s	0.189	-0.175	0.121	0.054	**Mn_i**	0.209	-0.204	-0.020	0.012
Ba_s	0.162	0.175	0.006	0.094	**Mn_s**	0.232	0.043	0.017	-0.285
Bi_i	0.193	0.180	-0.036	0.123	**Mo_s**	0.142	-0.277	0.118	0.024
Cd_s	0.202	0.139	0.084	-0.100	**Nb_i**	0.147	-0.268	0.035	0.090
Ce_i	0.068	-0.017	-0.349	0.006	**Ni_i**	0.140	-0.302	0.070	0.166
Co_i	0.165	-0.279	0.027	0.176	**Pb_i**	0.219	-0.011	0.008	-0.261
Cr_i	0.173	-0.271	0.069	0.124	**Rb_i**	0.008	-0.054	-0.370	-0.086
Cr_s	0.205	-0.157	0.055	-0.269	**Rb_s**	0.187	0.187	0.055	-0.017
Cs_i	0.040	-0.063	-0.372	-0.076	**Sb_i**	0.188	0.193	-0.052	0.228
Cs_s	0.225	0.185	0.052	-0.035	**Sn_i**	0.195	0.224	-0.014	0.221
Cu_i	0.198	0.127	-0.068	0.302	**Sr_i**	0.088	-0.008	-0.299	-0.066
Fe_i	0.181	-0.186	-0.028	0.308	**Tl_s**	0.193	0.222	0.068	0.012
Ga_s	0.198	-0.019	-0.046	-0.356	**U_i**	0.080	-0.049	-0.352	0.056
K_s	0.213	0.197	0.060	0.014	**W_s**	0.158	-0.264	0.093	0.042
La_i	0.003	-0.044	-0.318	-0.056	**Zn_s**	0.227	0.084	0.058	-0.239
Li_i	0.040	-0.107	-0.374	-0.049	**Zr_i**	0.146	0.121	-0.238	0.209

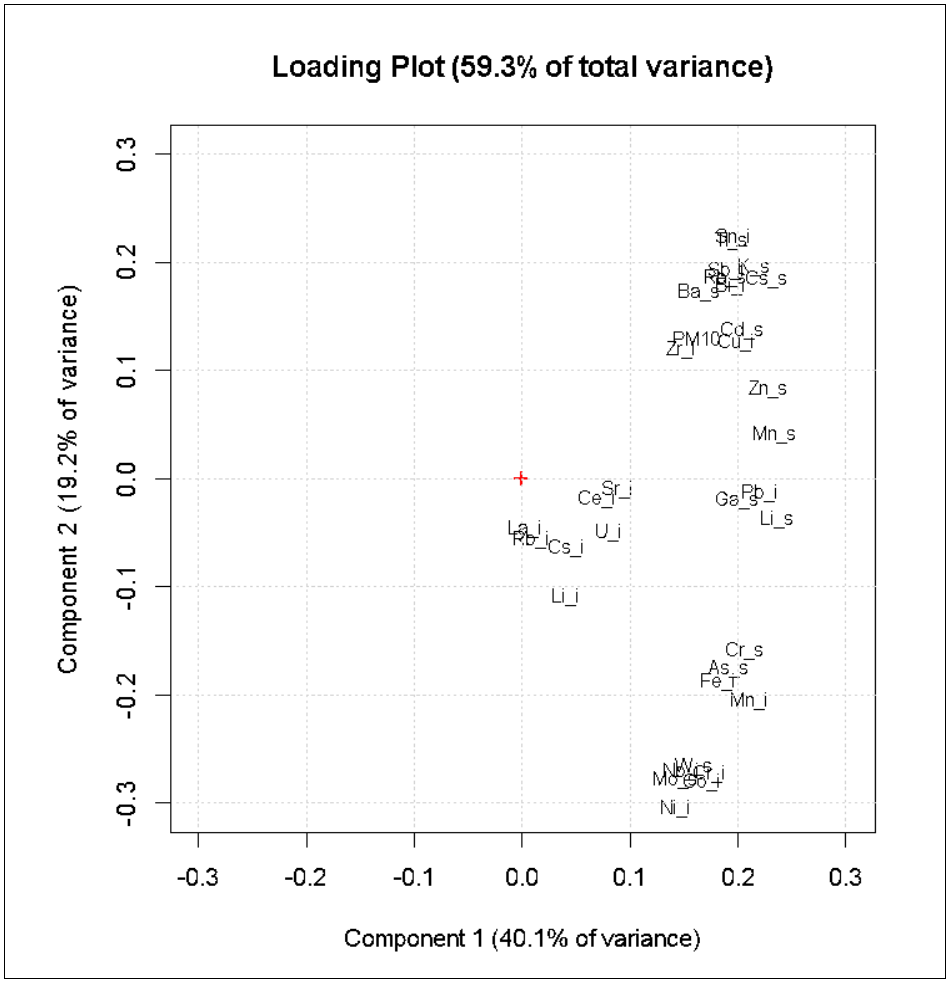

Fig. S5.1. Loading plot of PC1/PC2 performed on the matrix of the data composed of 276 samples (23 samples for each of the 12 samplings) and 34 selected variables: PM_{10} mass concentration and 33 water-soluble (_s) and insoluble (_i) element concentrations.

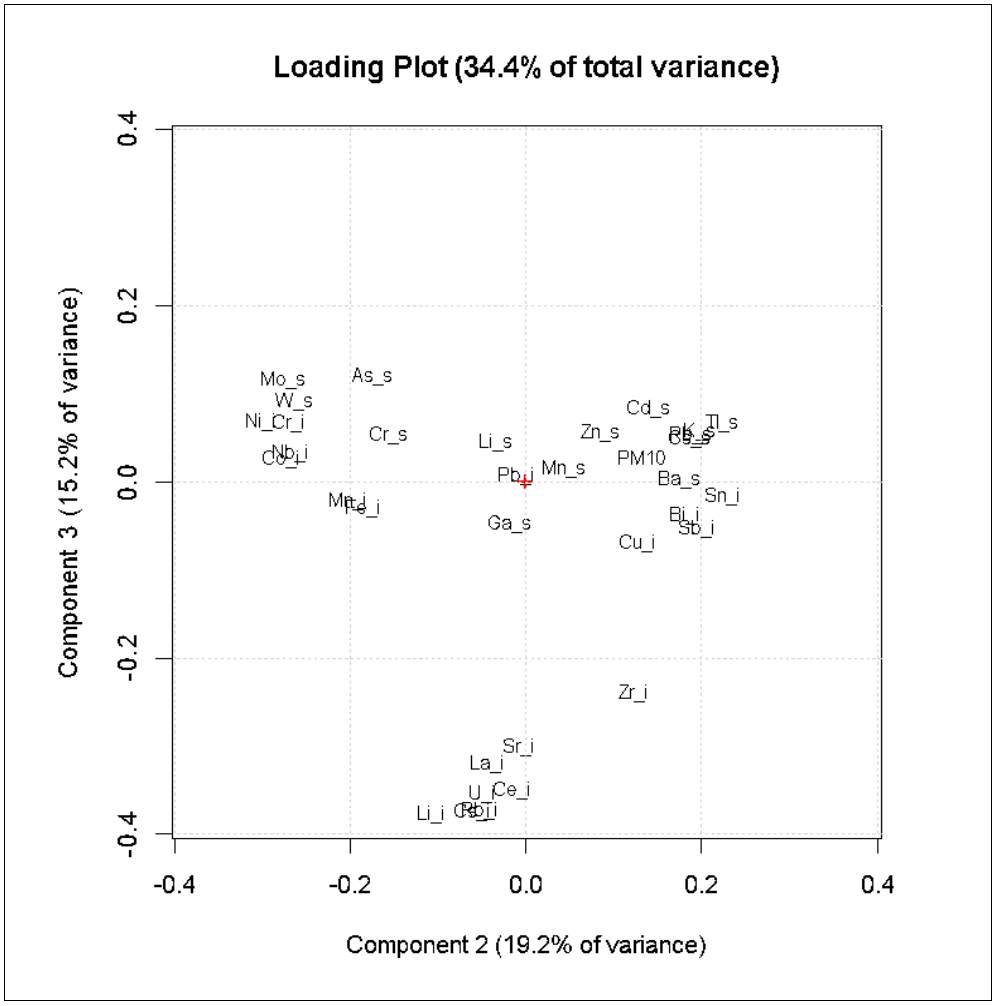

Fig. S5.2. Loading plot of PC2/PC3 performed on the matrix of the data composed of 276 samples (23 samples for each of the 12 samplings) and 34 selected variables: PM_{10} mass concentration and 33 water-soluble (_s) and insoluble (_i) element concentrations.

Table S6.1. Average (AM) PM mass, insoluble and water-soluble element concentrations determined in size-segregated PM samples for the winter monitoring period.

		Winter - Size Distribution (μm) of PM Mass and Insoluble Element Concentrations (AM)										Winter - Size Distribution (μm) of Water-soluble Element Concentrations (AM)									
	UoM μm	**<0.18**	**0.18 - 0.32**	**0.32 - 0.56**	**0.56 - 1**	**1 - 1.8**	**1.8 - 3.2**	**3.2 - 5.6**	**5.6 - 10**	**10 - 18**	**>18**	**<0.18**	**0.18 - 0.32**	**0.32 - 0.56**	**0.56 - 1**	**1 - 1.8**	**1.8 - 3.2**	**3.2 - 5.6**	**5.6 - 10**	**10 - 18**	**>18**
PM	μg/m³	2.8	3.3	3.9	4.4	2	3.1	3.8	1.8	1	1.0										
Al	ng/m³	1.3	1.4	1.9	2	6.2	12	18	13	6	5.4	0.18	0.33	0.57	0.58	0.71	0.56	0.49	0.44	0.26	0.21
As	ng/m³	0.041	0.042	0.043	0.043	0.04	0.040	0.04	0.029	0.023	0.021	0.077	0.071	0.073	0.062	0.021	0.0097	0.0048	0.0053	0.0049	0.0062
Ba	ng/m³	0.71	0.46	0.76	0.68	0.95	1.8	2	1.7	1.5	1.1	0.056	0.055	0.1	0.12	0.14	0.23	0.53	0.27	0.085	0.069
Bi	ng/m³	0.013	0.013	0.013	0.018	0.019	0.021	0.026	0.014	0.0059	0.0032	0.0025	0.0037	0.0059	0.0074	0.0032	0.00037	0.00052	0.00016	0.00051	0.000094
Ca	ng/m³	24	12	25	19	29	54	99	72	53	38	7.1	5.8	7.5	18	38	60	92	79	27	21
Cd	ng/m³	0.0051	0.0064	0.006	0.0066	0.0061	0.0032	0.0028	0.0009	0.0024	0.0041	0.024	0.029	0.033	0.025	0.0099	0.0013	0.0014	0.00081	0.00055	0.00033
Ce	ng/m³	0.0016	0.002	0.002	0.001	0.002	0.0065	0.02	0.011	0.0025	0.00058	0.014	0.021	0.002	0.0019	0.0012	0.00068	0.0012	0.00069	0.00064	0.00019
Co	ng/m³	0.01	0.011	0.014	0.023	0.029	0.032	0.036	0.023	0.0098	0.0088	0.0022	0.0032	0.0038	0.004	0.003	0.0023	0.0018	0.0011	0.00052	0.00038
Cr	ng/m³	1.3	1.2	1.5	3	3.8	4.2	5	3	1.3	0.89	0.44	0.47	0.48	0.38	0.11	0.02	0.022	0.013	0.0035	0.0023
Cs	ng/m³	0.0012	0.0013	0.001	0.0013	0.0017	0.0024	0.0036	0.0032	0.0013	0.00092	0.011	0.012	0.011	0.0081	0.0019	0.00014	0.00014	0.00011	0.00008	0.00004
Cu	ng/m³	0.26	0.28	0.4	0.44	0.56	1.3	1.5	0.86	0.29	0.22	0.15	0.11	0.14	0.22	0.23	0.25	0.28	0.11	0.036	0.023
Fe	ng/m³	6.7	7	11	20	41	67	81	49	19	18	0.94	1.9	2.9	4.8	3.1	0.67	1.1	0.75	0.42	0.24
Ga	ng/m³	0.0047	0.0053	0.0063	0.0091	0.0066	0.0047	0.0038	0.0032	0.0022	0.001	0.0022	0.005	0.007	0.0086	0.002	0.000092	0.00006	0.00005	0.00004	0.00003
K	ng/m³	40	49	50	62	45	45	47	40	33	40	55	75	87	57	15	8.8	11	8.1	3.8	3.1
La	ng/m³	0.0018	0.002	0.0022	0.0025	0.0025	0.0041	0.0079	0.0037	0.0019	0.00028	0.011	0.012	0.00084	0.0011	0.00067	0.00041	0.00069	0.00053	0.00046	0.00015
Li	ng/m³	0.0043	0.0044	0.003	0.0064	0.0079	0.012	0.015	0.01	0.0049	0.0044	0.044	0.04	0.028	0.017	0.0061	0.0024	0.0038	0.002	0.00069	0.00047
Mg	ng/m³	0.94	0.82	1.2	1.7	4.8	8.3	11	9	4.7	5.1	0.54	0.66	0.97	2.3	4.5	6	10	5	1.4	1.1
Mn	ng/m³	0.35	0.55	0.88	1.2	1.3	1.6	2	1.2	0.53	0.48	0.45	0.81	1.3	1.9	0.81	0.19	0.28	0.21	0.064	0.049
Mo	ng/m³	1.1	0.9	0.86	0.64	0.34	0.25	0.24	0.15	0.062	0.059	0.7	0.85	0.88	0.48	0.18	0.12	0.11	0.053	0.022	0.019
Na	ng/m³	7.2	7.9	9	9	17	25	32	34	10	13	7.2	8.9	10	15	31	43	83	37	9.7	8.8
Nb	ng/m³	0.0011	0.0011	0.0022	0.0064	0.017	0.022	0.044	0.026	0.0087	0.008	0.00013	0.00017	0.00031	0.00064	0.00051	0.00041	0.00039	0.00029	0.00028	0.00026
Ni	ng/m³	0.59	0.94	1	1.2	1.4	1.7	1.8	1.1	0.44	0.39	0.11	0.11	0.16	0.25	0.12	0.037	0.053	0.013	0.007	0.0084
Pb	ng/m³	0.4	0.61	0.86	0.79	0.57	0.24	0.2	0.1	0.045	0.038	0.36	0.47	0.62	0.59	0.22	0.013	0.01	0.0041	0.0056	0.0025
Rb	ng/m³	0.01	0.012	0.014	0.018	0.022	0.027	0.042	0.034	0.019	0.013	0.17	0.23	0.22	0.12	0.033	0.0059	0.011	0.0038	0.00073	0.00066
Sb	ng/m³	0.026	0.034	0.036	0.038	0.047	0.073	0.12	0.061	0.017	0.01	0.035	0.045	0.055	0.048	0.027	0.02	0.01	0.0051	0.0013	0.00082
Sn	ng/m³	0.22	0.22	0.2	0.24	0.24	0.27	0.35	0.19	0.057	0.044	0.018	0.017	0.022	0.022	0.011	0.0027	0.0031	0.0011	0.0011	0.00033
Sr	ng/m³	0.064	0.059	0.069	0.069	0.13	0.24	0.34	0.26	0.17	0.13	0.015	0.015	0.02	0.042	0.093	0.14	0.2	0.13	0.044	0.032
Ti	ng/m³	0.027	0.024	0.046	0.11	0.34	0.61	1.1	0.85	0.43	0.42	0.0035	0.0052	0.0069	0.013	0.012	0.011	0.013	0.0072	0.0054	0.0025
Tl	ng/m³	0.001	0.0058	0.0059	0.0048	0.0013	0.00082	0.00064	0.00025	0.000087	0.00016	0.041	0.044	0.033	0.02	0.0034	0.00029	0.00026	0.00012	0.000039	0.000039

U	ng/m$_3$	0.0001	0.0001	0.000057	0.000042	0.00017	0.00063	0.0012	0.00081	0.00028	0.00021	0.00011	0.000095	0.00011	0.00014	0.00011	0.00013	0.00017	0.00013	0.000063	0.000039
W	ng/m$_3$	0.004	0.004	0.0047	0.0061	0.0052	0.0051	0.0063	0.0041	0.0018	0.0015	0.021	0.025	0.024	0.021	0.011	0.001	0.0016	0.0012	0.00035	0.00026
Zn	ng/m$_3$	1.5	1.7	2.7	3.7	3.2	2.9	2.7	1.6	1.4	1.4	2.5	2.9	3.9	6.4	4.7	0.84	0.64	0.31	0.14	0.11
Zr	ng/m$_3$	0.0065	0.0058	0.009	0.021	0.052	0.1	0.12	0.07	0.029	0.024	0.0002	0.00035	0.0009	0.0076	0.0038	0.0019	0.0012	0.00067	0.00017	0.001

Table S6.2. Average (AM) PM mass, insoluble and water-soluble element concentrations determined in size-segregated PM samples for the summer monitoring period.

		Summer - Size Distribution (µm) of PM_{10} Mass and Insoluble Element Concentrations (AM)										Summer - Size Distribution (µm) of Water-soluble Element Concentrations (AM)									
	UoM µm	<0.18	0.18 - 0.32	0.32 - 0.56	0.56 - 1	1 - 1.8	1.8 - 3.2	3.2 - 5.6	5.6 - 10	10 - 18	>18	<0.18	0.18 - 0.32	0.32 - 0.56	0.56 - 1	1 - 1.8	1.8 - 3.2	3.2 - 5.6	5.6 - 10	10 - 18	>18
PM_{10}	µg/m³	1.5	1.5	1.6	1.4	1.3	2	4.2	3.8	1.9	1.7										
Al	ng/m³	1.6	2.3	4	3	8.3	15	26	25	13	9.8	2.6	0.51	1.6	1	1.4	0.56	0.7	0.76	1.4	2.1
As	ng/m³	0.019	0.022	0.026	0.024	0.027	0.027	0.03	0.027	0.022	0.0068	0.07	0.058	0.041	0.029	0.018	0.0068	0.0034	0.0048	0.0018	0.0036
Ba	ng/m³	0.28	0.28	0.4	0.35	0.87	1.5	2	1.7	0.78	0.66	0.13	0.13	0.11	0.16	0.29	0.29	0.33	0.26	0.25	0.19
Bi	ng/m³	0.0063	0.0063	0.0065	0.0096	0.018	0.025	0.032	0.024	0.0093	0.004	0.0022	0.0024	0.0035	0.0035	0.0018	0.00025	0.00016	0.00013	0.00014	0.0004
Ca	ng/m³	24	42	32	24	42	89	210	259	154	125	40	32	29	34	49	87	122	109	105	91
Cd	ng/m³	0.00021	0.0049	0.0061	0.0025	0.0033	0.00068	0.0018	0.0014	0.0012	0.00081	0.011	0.014	0.028	0.013	0.0061	0.0037	0.003	0.003	0.004	0.0035
Ce	ng/m³	0.0073	0.009	0.011	0.0075	0.017	0.032	0.063	0.063	0.03	0.021	0.0016	0.0022	0.0026	0.003	0.002	0.0018	0.0019	0.0019	0.0017	0.0023
Co	ng/m³	0.01	0.018	0.022	0.023	0.038	0.053	0.072	0.076	0.042	0.027	0.0048	0.0061	0.0047	0.0051	0.0041	0.0036	0.0045	0.0029	0.0055	0.0026
Cr	ng/m³	1	2.2	2.4	2.6	4.6	7	7.9	8.4	4.8	2.7	0.58	0.59	0.41	0.41	0.23	0.12	0.17	0.11	0.44	0.15
Cs	ng/m³	0.0008	0.0014	0.0017	0.0011	0.0023	0.0041	0.0082	0.0062	0.0037	0.0026	0.0036	0.0034	0.0037	0.003	0.00067	0.00018	0.00021	0.00021	0.00022	0.00029
Cu	ng/m³	0.21	0.41	0.51	0.35	0.87	1.7	2.3	1.9	0.66	0.44	0.14	0.18	0.25	0.26	0.39	0.21	0.16	0.091	0.042	0.06
Fe	ng/m³	7.5	12	26	28	68	113	151	120	78	69	1.7	2.7	3.2	3.5	2.7	1.5	2.1	1.4	3.5	1.5
Ga	ng/m³	0.0022	0.0039	0.0038	0.0046	0.0066	0.0077	0.012	0.01	0.0044	0.0028	0.0016	0.0038	0.0042	0.0028	0.00085	0.00012	0.00011	0.0001	0.00018	0.00014
K	ng/m³	18	20	19	21	22	28	50	56	23	17	9	13	17	10	8	8	7	1.9	1.3	2.4
La	ng/m³	0.0022	0.0063	0.0064	0.0059	0.011	0.019	0.035	0.035	0.017	0.011	0.0012	0.0013	0.0011	0.0018	0.0011	0.0011	0.0012	0.0014	0.0011	0.0014
Li	ng/m³	0.0057	0.0066	0.0052	0.0031	0.0084	0.015	0.027	0.026	0.011	0.0076	0.018	0.024	0.023	0.019	0.0063	0.0053	0.0064	0.0074	0.0053	0.006
Mg	ng/m³	1.3	2	2.2	1.4	4.7	7.6	14	19	10	8.6	1.2	0.98	2	2.1	5.1	8.8	15	7	3.2	2.1
Mn	ng/m³	0.27	0.6	0.8	0.75	1.4	1.8	2.7	3	1.5	1	0.22	0.46	0.89	0.68	0.45	0.3	0.41	0.22	0.19	0.11
Mo	ng/m³	0.65	1	0.94	0.32	0.30	0.3	0.33	0.36	0.14	0.091	1.4	1.9	2	1.3	0.33	0.11	0.11	0.045	0.042	0.031
Na	ng/m³	11	14	13	10	16	17	18	30	12	11	6.2	6.7	11	10	27	49	84	36	11	7
Nb	ng/m³	0.0024	0.0021	0.0072	0.0048	0.017	0.024	0.054	0.064	0.036	0.029	0.0006	0.00044	0.00083	0.0008	0.00047	0.00053	0.00067	0.00034	0.00035	0.00025
Ni	ng/m³	0.53	1.2	1.5	1.71	1.9	2.4	2.7	2.1	1.5	0.79	0.16	0.27	0.32	0.49	0.28	0.098	0.14	0.081	0.26	0.11
Pb	ng/m³	0.3	0.38	0.69	0.63	0.47	0.27	0.26	0.22	0.13	0.091	0.22	0.29	0.4	0.38	0.074	0.0079	0.0056	0.007	0.0062	0.0088
Rb	ng/m³	0.0092	0.013	0.016	0.014	0.019	0.031	0.076	0.08	0.031	0.023	0.049	0.052	0.052	0.039	0.015	0.013	0.012	0.0082	0.011	0.0071
Sb	ng/m³	0.032	0.038	0.037	0.044	0.071	0.12	0.16	0.078	0.019	0.01	0.075	0.077	0.098	0.066	0.039	0.013	0.011	0.0047	0.0033	0.0029
Sn	ng/m³	0.1	0.12	0.13	0.13	0.18	0.28	0.4	0.27	0.064	0.032	0.083	0.057	0.051	0.037	0.012	0.0021	0.0019	0.00084	0.00074	0.0015
Sr	ng/m³	0.047	0.076	0.071	0.054	0.14	0.23	0.46	0.58	0.27	0.21	0.059	0.05	0.074	0.083	0.13	0.21	0.32	0.19	0.14	0.11
Ti	ng/m³	0.07	0.072	0.1	0.1	0.35	0.69	1.8	2.2	1.3	0.85	0.013	0.016	0.02	0.021	0.015	0.011	0.011	0.011	0.019	0.0088
Tl	ng/m³	0.0047	0.0058	0.0022	0.00086	0.0008	0.00086	0.0011	0.0015	0.00048	0.0004	0.029	0.014	0.0059	0.0044	0.00078	0.00031	0.0003	0.00016	0.00015	0.00014
U	ng/m³	0.0003	0.00024	0.00031	0.00026	0.0008	0.0015	0.003	0.0032	0.0016	0.0011	0.0002	0.00016	0.00015	0.0002	0.00016	0.00016	0.00019	0.00019	0.00016	0.0002
W	ng/m³	0.01	0.01	0.01	0.0098	0.0083	0.0088	0.017	0.012	0.0065	0.0035	0.025	0.02	0.014	0.01	0.0028	0.0021	0.0013	0.00081	0.0008	0.00056
Zn	ng/m³	1.1	3.2	3.6	3.5	3.7	4.1	4.4	3.7	2.8	2.1	2.2	2.6	4.4	4.7	3.5	2	1.6	1.2	1.1	1.6
Zr	ng/m³	0.016	0.013	0.015	0.02	0.069	0.13	0.18	0.15	0.063	0.046	0.0014	0.0014	0.0029	0.0035	0.0041	0.002	0.0033	0.0022	0.0021	0.0024

References

Abbasi, S., Olander, L., Larsson, C., Olofsson, U., Jansson, A., Sellgren, U. 2012. A field test study of airborne wear particles from a running regional train. Proceedings of the Institution of Mechanical Engineers, Part F: Journal of Rail and Rapid Transit, 226(1), 95-109.

Almeida, S. M., Pio, C. A., Freitas, M. C., Reis, M. A., Trancoso, M. A. 2005. Source apportionment of fine and coarse particulate matter in a sub-urban area at the Western European Coast. Atmospheric Environment, 39(17), 3127-3138.

Amato, F., Pandolfi, M., Viana, M., Querol, X., Alastuey, A., Moreno, T. 2009. Spatial and chemical patterns of PM10 in road dust deposited in urban environment. Atmospheric Environment, 43(9), 1650-1659.

Anderson, J. O., Thundiyil, J. G., & Stolbach, A. 2012. Clearing the air: a review of the effects of particulate matter air pollution on human health. Journal of Medical Toxicology, 8(2), 166-175.

Astolfi, M. L., Marconi, E., Protano, C., Vitali, M., Schiavi, E., Mastromarino, P., Canepari, S. 2018. Optimization and validation of a fast digestion method for the determination of major and trace elements in breast milk by ICP-MS. Analytical Chimica Acta, 1040, 49-62.

Beelen, R., Hoek, G., Pebesma, E., Vienneau, D., de Hoogh, K., Briggs, D. J. 2009. Mapping of background air pollution at a fine spatial scale across the European Union. Science of the Total Environment, 407(6), 1852-1867.

Belis, C. A., Karagulian, F., Amato, F., Almeida, M., Artaxo, P., Beddows, D. C. S., ... & Hopke, P. K. 2015. A new methodology to assess the performance and uncertainty of source apportionment models II: The results of two European intercomparison exercises. Atmospheric Environment, 123, 240-250.

Bencharif-Madani, F., Ali-Khodja, H., Kemmouche, A., Terrouche, A., Lokorai, K., Naidja, L., Bouziane, M. 2019. Mass concentrations, seasonal variations, chemical compositions and element sources of PM10 at an urban site in Constantine, northeast Algeria. Journal of Geochemical Exploration, 206, 106356.

Canepari, S., Cardarelli, Giuliano, A., E., Pietrodangelo, A. 2006a. Determination of metals, metalloids and non-volatile ions in airborne particulate matter by a new two-step sequential leaching procedure Part A: Experimental design and optimization. Talanta, 69(3), 581-587.

Canepari, S., Cardarelli, E., Pietrodangelo, A., Strincone, M. 2006b. Determination of metals, metalloids and non-volatile ions in airborne particulate matter by a new two-step sequential leaching procedure: Part B: Validation on equivalent real samples. Talanta, 69(3), 588-595.

Canepari, S., Perrino, C., Olivieri, F., Astolfi, M.L. 2008. Characterisation of the traffic sources of PM through size-segregated sampling, sequential leaching and ICP analysis. Atmospheric Environment, 42(35), 8161-8175.

Canepari, S., Pietrodangelo, A., Perrino, C., Astolfi, M. L., Marzo, M. L. 2009. Enhancement of source traceability of atmospheric PM by elemental chemical fractionation. Atmospheric Environment, 43(31), 4754-4765.

Canepari, S., Astolfi, M. L., Farao, C., Maretto, M., Frasca, D., Marcoccia, M., Perrino, C. 2014. Seasonal variations in the chemical composition of particulate matter: a case study in the Po Valley. Part II: concentration and solubility of micro-and trace-elements. Environmental Science and Pollution Research, 21(6), 4010-4022.

Canepari, S., Astolfi, M. L., Catrambone, M., Frasca, D., Marcoccia, M., Marcovecchio, F., Massimi, L., Rantica, E., Perrino, C. 2019. A combined chemical/size fractionation approach to study winter/summer variations, ageing and source strength of atmospheric particles. Environmental Pollution, 253, 19-28.

Capelli, L., Sironi, S., Del Rosso, R., Céntola, P., Rossi, A., Austeri, C. 2011. Olfactometric approach for the evaluation of citizens' exposure to industrial emissions in the city of Terni, Italy. Science of the Total Environment, 409(3), 595-603.

Catrambone, M., Canepari, S., Cerasa, M., Sargolini, T., Perrino, C. 2019. Performance evaluation of a very-low-volume sampler for atmospheric particulate matter. Aerosol Air Quality Research.

Cesari, D., Amato, F., Pandolfi, M., Alastuey, A., Querol, X., Contini, D. 2016. An inter-comparison of PM_{10} source apportionment using PCA and PMF receptor models in three European sites. Environmental Science and Pollution Research, 23(15), 15133-15148.

Conti, M. E., Canepari, S., Finoia, M. G., Mele, G., Astolfi, M. L. 2018. Characterization of Italian multifloral honeys on the basis of their mineral content and some typical quality parameters. Journal of Food Composition and Analysis, 74, 102-113.

Curci, G., Ferrero, L., Tuccella, P., Barnaba, F., Angelini, F., Bolzacchini, E., Carbone, C., Denier van der Gon, H. A. C., Facchini, M. C., Gobbi, G. P., Kuenen, J. P. P., Landi, T. C., Perrino, C., Perrone, M. G., Sangiorgi, G., Stocchi, P. 2015. How much is particulate matter near the ground influenced by upper-level processes within and above the PBL? A summertime case study in Milan (Italy) evidences the distinctive role of nitrate. Atmospheric Chemistry and Physics, 15(5), 2629-2649.

Cvjetko, P., Cvjetko, I., Pavlica, M. 2010. Thallium toxicity in humans. Archives of Industrial Hygiene and Toxicology, 61(1), 111-119.

Džiugys, A., and Peters, B. 2001. An approach to simulate the motion of spherical and non-spherical fuel particles in combustion chambers. Granular matter, 3(4), 231-266.

Ferrero, L., Cappelletti, D., Moroni, B., Sangiorgi, G., Perrone, M. G., Crocchianti, S., Bolzacchini, E. 2012. Wintertime aerosol dynamics and chemical composition across the mixing layer over basin valleys. Atmospheric Environment, 56, 143-153.

Frasca, D., Marcoccia, M., Tofful, L., Simonetti, G., Perrino, C., Canepari, S. 2018. Influence of advanced wood-fired appliances for residential heating on indoor air quality. Chemosphere, 211, 62-71.

Guerrini, R. 2012. Qualità dell'aria nella provincia di Terni tra il 2002 e il 2011. Quad ARPA Umbria, 81-87.

Hoek, G., Meliefste, K., Cyrys, J., Lewné, M., Bellander, T., Brauer, M., Fischer, P., Gehring, U., Heinrich, J., Van Vliet, P., Brunekreef, B. 2002. Spatial variability of fine particle concentrations in three European areas. Atmospheric Environment 36, 4077-4088.

Irwin, J. S. 2014. A suggested method for dispersion model evaluation. Journal of the Air & Waste Management Association, 64(3), 255-264.

Jacobson, M. Z., Seinfeld, J. H. 2004. Evolution of nanoparticle size and mixing state near the point of emission. Atmospheric Environment, 38(13), 1839-1850.

Janhäll, S., Olofson, K. F. G., Andersson, P. U., Pettersson, J. B., Hallquist, M. 2006. Evolution of the urban aerosol during winter temperature inversion episodes. Atmospheric Environment, 40(28), 5355-5366.

Jian, X., Olea, R. A., & Yu, Y. S. 1996. Semivariogram modeling by weighted least squares. Computers & Geosciences, 22(4), 387-397.

Johnston, K., Ver Hoef, J. M., Krivoruchko, K., Lucas, N. 2001. Using ArcGIS geostatistical analyst (Vol. 380). Redlands: Esri.

Kam, W., Delfino, R. J., Schauer, J. J., Sioutas, C. 2013. A comparative assessment of $PM_{2.5}$ exposures in light-rail, subway, freeway, and surface street environments in Los Angeles and estimated lung cancer risk. Environmental Science: Processes & Impacts, 15(1), 234-243.

Karbowska, B. 2016. Presence of thallium in the environment: sources of contaminations, distribution and monitoring methods. Environmental monitoring and assessment, 188(11), 640.

Kim, B. U., Bae, C., Kim, H. C., Kim, E., Kim, S. 2017. Spatially and chemically resolved source apportionment analysis: Case study of high particulate matter event. Atmospheric Environment, 162, 55-70.

Kloog, I., Ridgway, B., Koutrakis, P., Coull, B.A., Schwartz, J.D. 2013. Long- and short term exposure to $PM_{2.5}$ and mortality using novel exposure models. Epidemiology 24, 555-561.

Kumar, A., Maroju, S., Bhat, A. 2007. Application of ArcGIS geostatistical analyst for interpolating environmental data from observations. Environmental Progress, 26(3), 220-225.

Li, R., Wiedinmyer, C., & Hannigan, M. P. 2013. Contrast and correlations between coarse and fine particulate matter in the United States. Science of the Total Environment, 456, 346-358.

Lubczyńska, M. J., Sunyer, J., Tiemeier, H., Porta, D., Kasper-Sonnenberg, M., Jaddoe, V. W., Xavier Basagaña, X., Dalmau-Bueno, A., Forastiere, F., Wittsiepe, J., Hoffmann, B., Nieuwenhuijsen, M., Hoek, G., de Hoogh, K., Brunekreef, B., Guxens, M. 2017. Exposure to elemental composition of outdoor PM2. 5 at birth and cognitive and psychomotor function in childhood in four European birth cohorts. Environment international, 109, 170-180.

Mangia, C., Gianicolo, E. A., Bruni, A., Vigotti, M. A., Cervino, M. 2013. Spatial variability of air pollutants in the city of Taranto, Italy and its potential impact on exposure assessment. Environmental monitoring and assessment, 185(2), 1719-1735.

Massimi, L., Ristorini, M., Eusebio, M., Florendo, D., Adeyemo, A., Brugnoli, D., Canepari, S. 2017. Monitoring and evaluation of Terni (Central Italy) air quality through spatially resolved analyses. Atmosphere, 8(10), 200.

Massimi, L., Giuliano, A., Astolfi, M.L., Congedo, R., Masotti, A., Canepari, S. 2018. Efficiency evaluation of food waste materials for the removal of metals and metalloids from complex multi-element solutions. Materials, 11(3), 334.

Massimi, L., Conti, M. E., Mele, G., Ristorini, M., Astolfi, M. L., Canepari, S. 2019. Lichen transplants as indicators of atmospheric element concentrations: a high spatial resolution comparison with PM_{10} samples in a polluted area (Central Italy). Ecological Indicators, 101, 759-769.

Massimi, L., Simonetti, G., Buiarelli, F., Di Filippo, P., Pomata, D., Riccardi, C., Ristorini, M., Astolfi, M. L., Canepari, S. 2020. Spatial distribution of levoglucosan and alternative biomass burning tracers in atmospheric aerosols, in an urban and industrial hot-spot of Central Italy. Atmospheric Research, 104904.

Meng, X., Wu, Y., Pan, Z., Wang, H., Yin, G., Zhao, H. 2019. Seasonal characteristics and particle-size distributions of particulate air pollutants in Urumqi. International Journal of Environmental Research and Public Health, 16(3), 396.

Minguillón, M.C., Rivas, I., Aguilera, I., Alastuey, A., Moreno, T., Amato, F., Sunyer, J., Querol, X. 2012. Within-city contrasts in PM composition and sources and their relationship with nitrogen oxides. Journal of Environmental Monitoring 14, 2718-2728.

Minguillón, M. C., Cirach, M., Hoek, G., Brunekreef, B., Tsai, M., de Hoogh, K., Jedynskag, A., Kooterg, I. M., Nieuwenhuijsen, M., Querol, X. 2014. Spatial variability of trace elements and sources for improved exposure assessment in Barcelona. Atmospheric Environment, 89, 268-281.

Morini, E., Touchaei, A., Castellani, B., Rossi, F., Cotana, F. 2016. The impact of albedo increase to mitigate the urban heat island in Terni (Italy) using the WRF model. Sustainability, 8(10), 999.

Moroni, B., Ferrero, L., Crocchianti, S., Perrone, M. G., Sangiorgi, G., Bolzacchini, E., & Cappelletti, D. 2013. Aerosol dynamics upon Terni basin (Central Italy): Results of integrated vertical profile measurements and electron microscopy analyses. Rendiconti Lincei, 24(4), 319-328.

Namgung, H. G., Kim, J. B., Woo, S. H., Park, S., Kim, M., Kim, M. S., Bae, G. N., Park, D., Kwon, S. B. 2016. Generation of nanoparticles from friction between railway brake disks and pads. Environmental Science and Technology, 50(7), 3453-3461.

Noe, R., Noe, A., & Baukloh, D. 1996. U.S. Patent No. 5,554,235. Washington, DC: U.S. Patent and Trademark Office.

Owoade, K. O., Hopke, P. K., Olise, F. S., Ogundele, L. T., Fawole, O. G., Olaniyi, B. H., Jegede, O. O., Ayoola, M. A., & Bashiru, M. I. 2015. Chemical compositions and source identification of particulate matter (PM2.5 and PM2.5–10) from a scrap iron and steel smelting industry along the Ife–Ibadan highway, Nigeria. Atmospheric Pollution Research, 6(1), 107-119.

Pant, P., Harrison, R.M. 2013. Estimation of the contribution of road traffic emissions to particulate matter concentrations from field measurements: a review. Atmospheric Environment 77, 78-97.

Peel, M. C., Finlayson, B. L., McMahon, T. A. 2007. Updated world map of the Köppen-Geiger climate classification. Hydrology and earth system sciences discussions, 4(2), 439-473.

Perez, L., Medina-Ramón, M., Künzli, N., Alastuey, A., Pey, J., Pérez, N., Garcia, R., Tobias, A., Querol, X., Sunyer, J. 2009. Size fractionate particulate matter, vehicle traffic, and case-specific daily mortality in Barcelona, Spain. Environmental Science and Technology 43, 4707-4714.

Perrino, C., Canepari, S., Cardarelli, E., Catrambone, M., Sargolini, T. 2007. Inorganic constituents of urban air pollution in the Lazio region (Central Italy), Environmental Monitoring and Assessment, 128, 133-151.

Perrino, C., Canepari S., Catrambone, M., Dalla Torre, S., Rantica, E., Sargolini, T. 2009. Influence of natural events on the concentration and composition of atmospheric particulate matter. Atmospheric Environment 43, 4766–4779.

Perrino, C., Canepari, S., Pappalardo, S., Marconi, E. 2010. Time-resolved measurements of water-soluble ions and elements in atmospheric particulate matter for the characterization of local and long-range transport events. Chemosphere, 80(11), 1291-1300.

Pope III, C. A., Dockery, D. W. 2006. Health effects of fine particulate air pollution: lines that connect. Journal of the air and waste management association, 56(6), 709-742.

SENTIERI-ReNaM, GdL, Binazzi, A., Mangone, L. 2016. SENTIERI - Epidemiological study of residents in national priority contaminated sites: incidence of mesothelioma. Epidemiologia e prevenzione, 40(5Suppl1), 1-116.

Querol, X., Viana, M., Alastuey, A., Amato, F., Moreno, T., Castillo, S., Pey, J., de la Rosa, J., Sánchez de la Campa, A., Artíñano, B., Salvador, P., García Dos Santos, S., Fernández-Patier, R., Moreno-Grau, S., Negral, L., Minguillón, M. C., Monfort, E., Gil, J. I., Inza, A., Ortega, L. A., Santamaría, J. M., & Zabalza, J. 2007. Source origin of trace elements in PM from regional background, urban and industrial sites of Spain. Atmospheric Environment, 41(34), 7219-7231

Querol, X., Moreno, T., Karanasiou, A., Reche, C., Alastuey, A., Viana, M., Font, O., Gil, J., de Miguel, E., Capdevila, M. 2012. Variability of levels and composition of PM_{10} and $PM_{2.5}$ in the Barcelona metro system. Atmospheric Chemistry and Physics, 12(11), 5055-5076.

Setton, E., Marshall, J.D., Brauer, M., Lundquist, K.R., Hystad, P., Keller, P., Cloutier Fisher, D. 2010. The impact of daily mobility on exposure to traffic-related air pollution and health effect estimates. Journal of Exposure Science and Environmental Epidemiology 21, 42-48.

Simonetti, G., Frasca, D., Marcoccia, M., Farao, C., Canepari, S. 2018a. Multi-elemental analysis of particulate matter samples collected by a particle-into-liquid sampler. Atmospheric Pollution Research, 9(4) 747-754.

Simonetti, G., Conte, E., Perrino, C., Canepari, S. 2018b. Oxidative potential of size-segregated PM in an urban and an industrial area of Italy. Atmospheric Environment, 187, 292-300.

Sgrigna, G., Sæbø, A., Gawronski, S., Popek, R., Calfapietra, C. 2015. Particulate Matter deposition on Quercus ilex leaves in an industrial city of central Italy. Environmental Pollution, 197, 187-194.

Soleimanian, E., Taghvaee, S., Mousavi, A., Sowlat, M. H., Hassanvand, M. S., Yunesian, M., Naddafi, K., Sioutas, C. 2019. Sources and Temporal Variations of Coarse Particulate Matter (PM) in Central Tehran, Iran. Atmosphere, 10(5), 291.

Taiwo, A. M., Harrison, R. M., Shi, Z. 2014. A review of receptor modelling of industrially emitted particulate matter. Atmospheric environment, 97, 109-120.

Templeton, D. M., Ariese, F., Cornelis, R., Danielsson, L. G., Muntau, H., van Leeuwen, H. P., Lobinski, R. 2000. Guidelines for terms related to chemical speciation and fractionation of elements. Definitions, structural aspects, and methodological approaches (IUPAC Recommendations 2000). Pure and applied chemistry, 72(8), 1453-1470.

Vitali, L., Morabito, A., Adani, M., Assennato, G., Ciancarella, L., Cremona, G., Giua, R., Pastore, T., Piersanti, A., Righini, G., Russo, F., Spagnolo, S., Tanzarella, A., Tinarelli, G., Zanini, G. 2016. A Lagrangian modelling approach to assess the representativeness area of an industrial air quality monitoring station. Atmospheric Pollution Research, 7(6), 990-1003.

Weckwerth, G. 2001. Verification of traffic emitted aerosol components in the ambient air of Cologne (Germany). Atmospheric Environment, 35(32), 5525-5536.

Xie, Y., Chen, T. B., Lei, M., Yang, J., Guo, Q. J., Song, B., & Zhou, X. Y. 2011. Spatial distribution of soil heavy metal pollution estimated by different interpolation methods: Accuracy and uncertainty analysis. Chemosphere, 82(3), 468-476.

Yu, F., Wang, Q., Yan, Q., Jiang, N., Wei, J., Wei, Z., Yin, S. 2018. Particle size distribution, chemical composition and meteorological factor analysis: A case study during wintertime snow cover in Zhengzhou, China. Atmospheric research, 202, 140-147.

Zanobetti, A., Schwartz, J. 2009. The effect of fine and coarse particulate air pollution on mortality: a national analysis. Environmental health perspectives, 117(6), 898-90.

Zhang, K. M., Wexler, A. S. 2002. Modeling the number distributions of urban and regional aerosols: theoretical foundations. Atmospheric Environment, 36(11), 1863-1874.

6.2 (A6) Spatial mapping and size distribution of oxidative potential of particulate matter released by spatially disaggregated sources

Environmental Pollution (2020), 266, 115271, doi: 10.1016/j.envpol.2020.115271

Lorenzo Massimi[1,*], Martina Ristorini[2], Giulia Simonetti[1], Maria Agostina Frezzini[1], Maria Luisa Astolfi[1], Silvia Canepari[1]

[1] Department of Chemistry, Sapienza University of Rome, P. le Aldo Moro, 5, Rome 00185, Italy;
[2] Department of Bioscience and Territory, University of Molise, Pesche (IS), 86090, Italy.
*Corresponding author

Keywords: Spatial variability; Size distribution; PM source; Ascorbic acid (OP^{AA}) assay; 1,4-dithiothreitol (OP^{DTT}) assay; 2',7'-dichlorodihydrofluorescein (OP^{DCFH}) assay

Abstract

The ability of particulate matter (PM) to induce oxidative stress is frequently estimated by acellular oxidative potential (OP) assays, such as ascorbic acid (AA) and 1,4-dithiothreitol (DTT), used as proxy of reactive oxygen species (ROS) generation in biological systems, and particle-bound ROS measurement, such as 2',7'-dichlorodihydrofluorescein (DCFH) assay. In this study, we evaluated the spatial and size distribution of OP results obtained by three OP assays (OP^{AA}, OP^{DCFH} and OP^{DTT}), to qualitative identify the relative relevance of single source contributions in building up OP values and to map the PM potential to induce oxidative stress in living organisms. To this aim, AA, DCFH and DTT assays were applied to size-segregated PM samples, collected by low-pressure cascade impactors, and to PM_{10} samples collected at 23 different sampling sites (about 1 km between each other) in Terni, an urban and industrial hot-spot of Central Italy, by using recently developed high spatial resolution samplers of PM, which worked in parallel during three monitoring periods (February, April and December 2017). The sampling sites were chosen for representing the main spatially disaggregated sources of PM (vehicular traffic, rail network, domestic heating, power plant for waste treatment, steel plant) present in the study area. The obtained results clearly showed a very different sensitivity of the three assays toward each local PM source. OP^{AA} was particularly sensitive toward coarse particles released from the railway, OP^{DCFH} was sensible to fine particles released from the steel plant and domestic biomass heating, and OP^{DTT} was quite selectively sensitive toward the fine fraction of PM released by industrial and biomass burning sources.

1. Introduction

Particulate matter (PM) air pollution is one of the major risk factors for human health worldwide (Anderson et al., 2012; Lubczyńska et al., 2017). Various epidemiological studies have spotlighted strong correlations between exposure to PM and the onset of cardiovascular and respiratory diseases (Pope and Dockery, 2006). Indeed, over the years, it has been associated to a great number of adverse outcomes for human health, such as respiratory and cardiovascular diseases, cancer, diabetes, metabolic disorders, atherosclerosis and neurodegenerative diseases (Strak et al., 2012; Gupta et al., 2019; Øvrevik et al., 2019). Several

epidemiological studies have spotlighted strong correlations between PM exposure and the onset of cardiopulmonary diseases (Brunekreef et al, 2002; Pope et al, 2006). However, most of the studies use PM mass concentration as exposure indicator, which misestimates the overall impact of PM, since it does not take into account the multiple toxicological effects of the different pollutants that make up particulate matter. This limitation can be overcome by identifying possible relationships between PM toxicity and its specific physic-chemical properties. In fact, during the last few decades, the complex and variable composition of PM has been widely investigated and many studies have revealed that several PM properties, such as chemical composition and particle dimension, influence its health and environmental effects (Ricci and Cirillo, 1985; Hlavay et al., 2001; Kelly et al., 2012). Nevertheless, not enough evidence that associates each property to specific outcomes has been yet identified (WHO, 2013).

Nowadays, there is a growing scientific consensus in affirming that generation of reactive oxygen species (ROS) is one of the major mechanisms by which PM exerts its adverse biological effects (Li et al., 2015), leading to oxidative stress responses and thus to different chronic and acute systemic inflammations (Li et al., 2003; Esposito et al., 2014; Pirrino et al., 2017). Indeed, PM ability to generate oxidative stress in biological systems has been demonstrated to contribute to genotoxicity and cytotoxic mechanisms responsible for cell damages (Marcoccia et al., 2017; Piacentini et al., 2019). PM capacity to trigger damaging oxidative reactions and inflammations is defined as oxidative potential (OP), which is a measure of PM ability to oxidise target molecules, by generating ROS in acellular environments. Over the last years, OP has been proposed as a biologically relevant metric for addressing PM exposure (Yang et al., 2016; Simonetti et al., 2018a, 2018b; Gao et al., 2020), since it appeared to be more reliable than PM mass concentration (Delfino et al., 2011; Gupta et al., 2019). However, the variability in chemical composition of PM and in the contributions of different sources, reduces the correlation with health outcomes and may thus limit the potential of OP as a global toxicological indicator.

To date, various acellular assays for the measurement of OP, such ascorbic acid (AA), 1,4-dithiothreitol (DTT) and 2',7'-dichlorodihydrofluorescein (DCFH), have been used to estimate the toxicity of PM released by different emission sources (Bates et al., 2019). Ascorbic acid and 1,4-dithiothreitol ($HSCH_2CH(OH)CH(OH)CH_2SH$) are strong reducing agents; DTT and AA assays involve the controlled incubation of the anti-oxidant (DTT or AA) in PM aqueous extracts under controlled conditions and the measurement of its depletion over time (Cho et al., 2005; Stoeger et al., 2008; Fang et al., 2016; Campbell et al., 2019). The antioxidant loss rate represents the capacity of PM reactive species to catalyze the transfer of electrons from AA or DTT to oxygen, providing an estimation of the OP. On the other hand, 2',7'-dichlorodihydrofluorescein assay, formerly developed for the in-vitro determination of ROS in biological cells (Lebel et al., 1992; Wang and Joseph, 1999; Halliwell and Whiteman, 2004), is today one of the most used methods for particle-bound ROS measurement in PM (Venkatachari et al., 2005, 2007). It is based on the oxidation of DCFH, a non-fluorescent reagent, to DCF, a fluorescent compound, in the presence of ROS and horseradish peroxidase (HRP), a redox enzyme that primarily reacts with hydrogen peroxide and organic hydroperoxides. The measured fluorescence intensity is converted into hydrogen peroxide equivalents, which

is used as an indicator of the ROS reactivity (Hung and Wang, 2001; Perrone et al., 2016). However, each of these methods has been deemed sensible toward PM coming from different emission sources and characterized by very different physic-chemical properties (Ayres et al., 2008; Simonetti et al., 2018b; Frezzini et al., 2019; Piacentini et al., 2019). Therefore, none of the OP assays can be a-priori considered as representative of ROS generation pathways in biological organisms (Fang et al., 2015).

The knowledge of the relative relevance of the single source contributions in building up OP values can be of great help for the identification of the emission sources mainly responsible for ROS generation. Source apportionment of OP results from field campaigns have been attempted in some studies, but conflicting results were found (Fang et al., 2016; Perrone et al., 2016; Chirizzi et al., 2017; Calas et al., 2018). Therefore, this study was aimed to improve the knowledge about the existing relationships between OP values and sources of PM, useful to properly address PM mitigation measures to protect citizens health. In this study, we describe an innovative experimental approach, transferable to other monitoring campaigns, for the spatial mapping of OP^{AA}, OP^{DCFH} and OP^{DTT}, which represents a powerful tool for geo-referenced assessment of PM potential to induce oxidative stress and harmful effects on human health. This innovative approach, allows to qualitatively evaluate possible associations between OP values and different sources of PM, overcoming the use of receptor models, often used to investigate the contribution of sources to measured OP with different assays (Cesari et al., 2019). To this aim, we applied the AA, DCFH and DTT assays to the aqueous extracts of PM_{10} sampled by a recently developed very-low volume device (Massimi et al., 2017, 2019; Ristorini et al., 2020), in a wide and dense monitoring network (23 sampling sites, about 1 km between each other) across Terni (Central Italy). The study area includes various spatially disaggregated intensive local PM sources (vehicular traffic, rail network, domestic heating, power plant for waste treatment, steel plant) (Capelli et al., 2011; Guerrini, 2012; Massimi et al., 2020a, 2020b) and is characterized by peculiar meteorological conditions that reduce air pollutants transport, thus favoring their accumulation (Ferrero et al., 2012). These factors have been associated with an increase of morbidity and mortality due to the onset of cardiovascular and respiratory environment-related diseases, which made this area of national interest for environmental remediation (SENTIERI-ReNaM, 2016) and particularly suitable for the spatial mapping of the OP of PM released by different sources. To our knowledge, the comparison of the three OP assays applied to PM_{10} spatially-resolved samples has never been undertaken so far.

To obtain a more reliable identification of the sources responsible for OP, the evaluation of the spatial variability was supported by the study of the size distribution of OP, able to provide information on the relative relevance of combustive and abrasive-mechanical sources in building up OP values (Simonetti et al., 2018a; Manigrasso et al., 2020). Furthermore, size distribution analysis of OP of PM provides information on the penetration capacity of particles responsible for OP in the respiratory system, thus resulting considerably valuable for the evaluation of exposure to PM and relative health risk.

2. Materials and Methods

2.1 Study Area

The study area is the city of Terni, of 211.90 km^2 and of about 112,000 inhabitants (Sgrigna et al., 2015), located in a basin of the Region Umbria (42° 34'N; 12°39' E), in Central Italy. The peculiar geomorphology of the Terni basin, limits air mixing and air pollutants transport, especially during the frequent winter episodes of atmospheric stability (Morini et al., 2016; Curci et al., 2015; Ferrero et al., 2012).

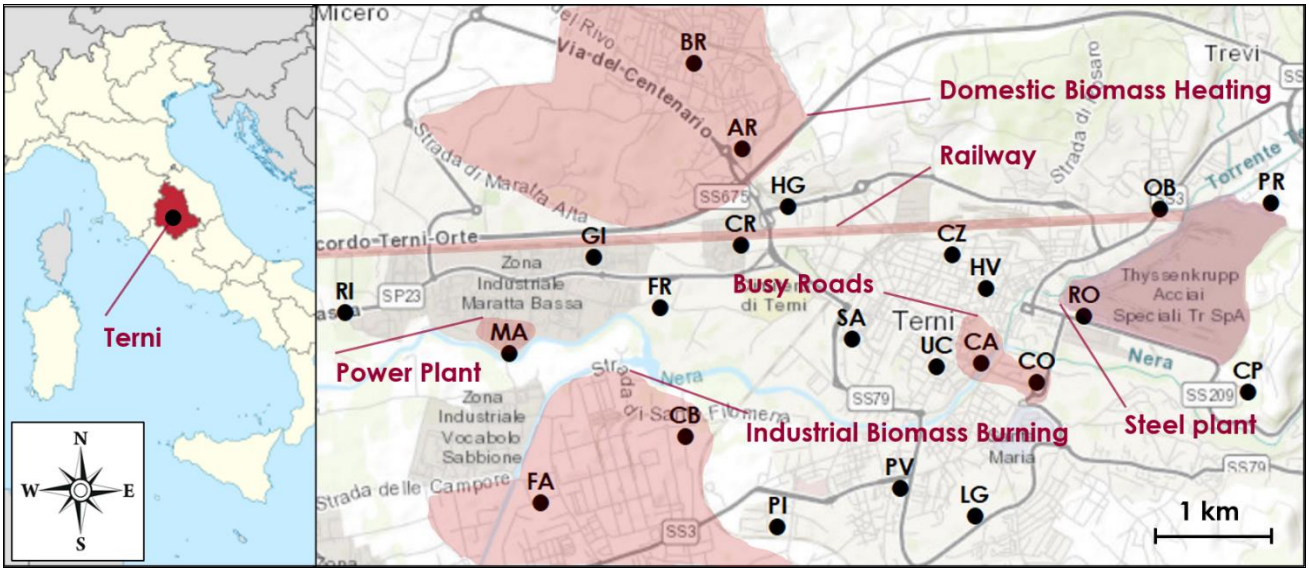

Fig. 1. Map of the 23 sampling sites in the study area (Terni, Central Italy; latitude: 42.5681, longitude: 12.6508, decimal degrees) with the location of the main local PM_{10} emission sources (ArcMap 10.3.1, ArcGis Desktop; ESRI, Redlands, CA, USA).

In Fig. 1 are shown the 23 sampling sites that were selected to cover the whole area with around 1 km spatial resolution and to study the contributions of the main local PM_{10} emission sources. In detail: RI and MA sites are located in the West of the city, near the power plant for waste treatment; GI, CR and HG are situated in the close proximity to the railway, in the North-West of the city; CZ, HV, SA, UC, CA and CO are located in the city center, between the rail network and busy roads; FA and CB, in the South-West of the city, are close to a carpentry and a craftsmanship lab and, along with PI, PV and LG, are affected by industrial biomass burning, such as the burning of carpentry waste products; FR, BR and AR, in the North of the city, are situated near townhouses frequently heated by biomass burning appliances; finally, RO, OB, PR, CP are located around the steel plant in the East of the city.

The 23 sampling sites (RI, MA, FA, GI, FR, CB, PI, BR, AR, CR, HG, SA, PV, LG, CZ, HV, UC, CA, CO, RO, OB, PR, CP) have already been studied (Massimi et al., 2017, 2019) and spatial variability of element concentrations in PM_{10} has been widely evaluated (Massimi et al., 2017, 2020a, 2020b). Spatial maps of elements tracing the main local PM_{10} sources in Terni have been obtained (Massimi et al., 2020b); therefore, localization and spatial distribution of the emission sources in the study area is well known.

2.2 Sampling Equipment

2.2.1 High Spatial Resolution Sampler

The High spatial resolution sampler (HSRS; FAI Instruments, Fonte Nuova, Rome, Italy) operates with a very-low flow rate (0.5 L min^{-1}), it is self-powered (with a rechargeable battery and a solar panel), assures long-term (1-2 months) collection of PM_{10} and has very good sampling efficiency and high repeatability for stable and fine PM_{10} chemical compounds (Catrambone et al., 2019).

23 HSRS, equipped with 37 mm Polytetrafluoroethylene (PTFE) membrane filters (2 μm pore size, PALL Corporation, Port Washington, NY, USA), were used to collect PM_{10} samples and worked in parallel at the 23 sites for three monitoring periods: February (January 21st - February 20th, 2017; 30-day sampling), April (April 1st - May 1st, 2017; 31-day sampling) and December (November 25th, 2017 - January 15th, 2018; 51-day sampling) 2017, allowing the collection of 23 PM_{10} samples per monitoring period.

2.2.2 Micro-Orifice Uniform Deposition Impactor

The Micro-orifice uniform deposition impactor (MOUDI; model 110-NR; MSP Corporation, Shoreview, MN, USA) is a low-pressure cascade impactor (flow rate of 30 L min^{-1}) for the collection of size-segregated PM samples through 10 impaction stages, with cut-size aerodynamic diameters of 0.18, 0.32, 0.56, 1.0, 1.8, 3.2, 5.6, 10 and 18 μm.

Three MOUDI, equipped with 47 mm PTFE membranes (2 μm pore size, PALL Corporation, Port Washington, NY, USA), were used to collect PM samples with different size fractions and worked in parallel in the center (CA), West (MA) and East (PR) of the city for 20 days (February 15th - March 6th, 2018).

Sampling efficiency and repeatability of MOUDI were assessed in Canepari et al., 2019 and in Simonetti et al., 2018a. The relative repeatability for all the considered variables was found to be below 10%.

It is worth noting that long-duration samplings carried out by MOUDI may lead to bouncing-off phenomena that can be responsible for a modification of the original size distribution of atmospheric particles (Canepari et al., 2019). However, to our knowledge, there are no solid and recognized methods to correct the data for this artefact; furthermore, PTFE membrane filters are generally considered as a suitable sampling material able to minimize the bouncing-off (Giorio et al., 2013).

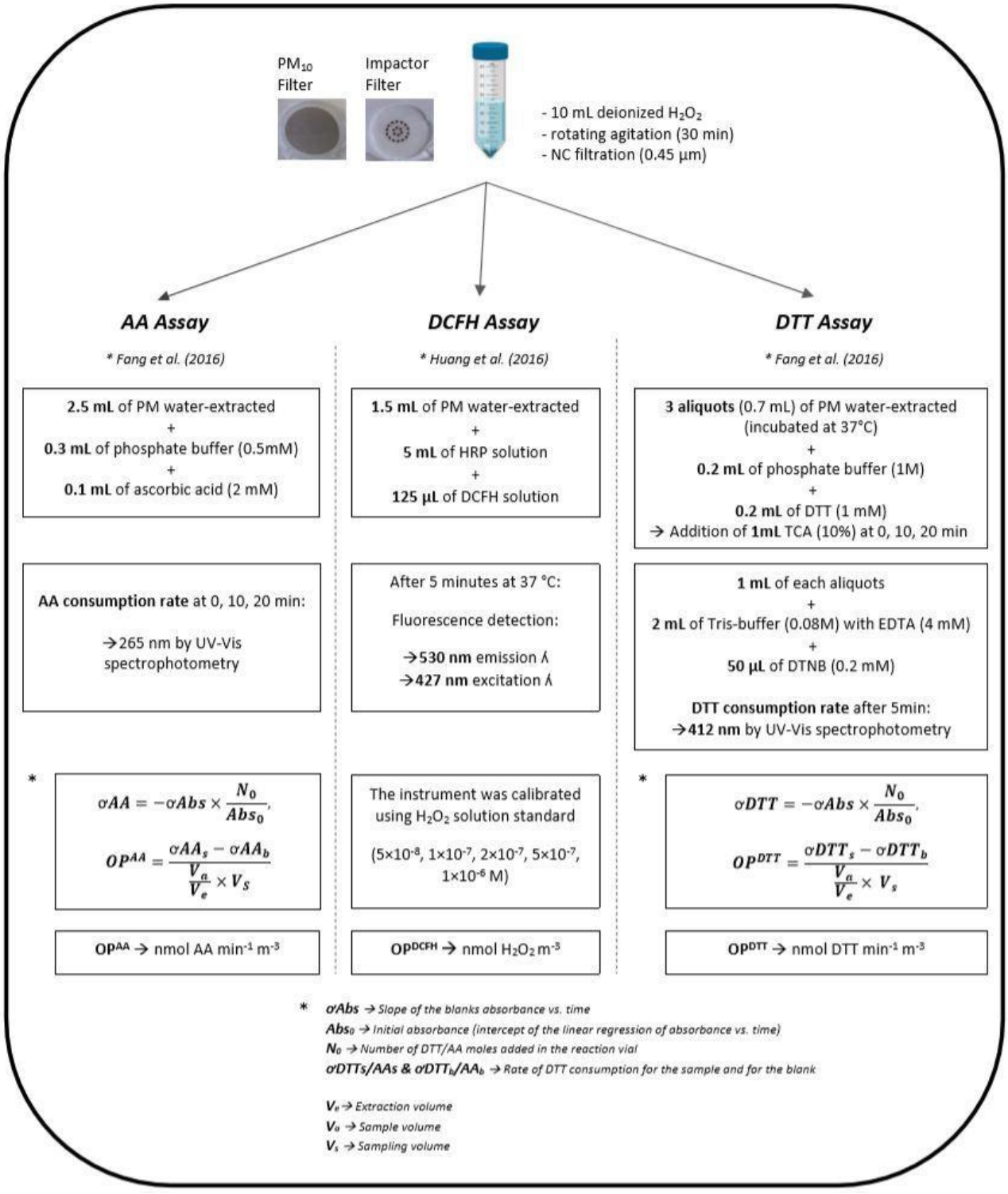

Fig. 2. Block diagram of the conducted samples preparation and OP analytical procedures for the AA, DCFH and DTT assays applied to the PM aqueous extracts.

2.3 Analytical Procedures

PTFE membrane filters were weighed before and after sampling, in order to determine PM mass concentrations. Mass concentration was determined gravimetrically by using an automated microbalance (1 mg sensitivity, mod. ME5, Sartorius AG, Goettingen, Germany). Membrane filters were equilibrated for 2

days at 20 °C and 50% RH before and after sampling. Subsequently, PM field samples were treated by following the procedure detailed in Massimi et al. (2017, 2020a, 2020b). Briefly, after the removal of the supporting polymethylpentene ring from the PTFE membrane filter, each field filter was extracted in 10 mL of deionized water (produced by Arioso UP 900 Integrate Water Purification System, USA) by rotating agitation (60 rpm; Rotator; Glas-Col, USA) for 30 minutes, to avoid ROS generation upon ultrasonic irradiation, commonly used to efficiently extract the PM from the filters. In fact, ultrasonic waves triggers the formation and collapse of cavitation bubbles in the solution, inside which high temperatures and pressures can be reached. These conditions may lead to pyrolysis of the molecules present inside the cavitation bubbles, which results in the production of free radicals (Mutzel et al., 2013; Khurshid et al., 2014; Miljevic et al., 2014). After the extraction by rotating agitation, the obtained solution was filtered through a nitrocellulose filter (NC; pore size 0.45 µm; Merck Millipore Ltd., Billerica, MA, USA). The water-extracted solution was then split in proper aliquots for the different OP analytical procedures. Conducted samples preparation and OP analytical procedures for the AA, DCFH and DTT assays applied to the PM aqueous extracts are summarized in the block diagram of Fig. 2. Further details on the followed AA, DCFH and DTT analytical procedures and used reagents are reported in supplementary material S1. For the quality control and assurance in AA, DCFH and DTT measurements (evaluated in Simonetti et al., 2018a, 2018b and in Piacentini et al., 2019), different tests to assess the repeatability and efficiency of the three OP assays were performed in our lab on a large amount of PM field filters not stored, stored for 15 days in the fridge, in the freezer (-20°C) and at constant ambient temperature, and then extracted by ultrasonic irradiation, rotating agitation (60 rpm) and by using the vortex (2000 rpm). The obtained results showed high repeatability (10-15 %) of the OP values obtained by applying the three OP assays to the PM field samples extracted by rotating agitation.

2.4 Spatial Mapping

Spatial mapping of OP^{AA}, OP^{DCFH} and OP^{DTT} was performed by the software ArcMap 10.3.1 (ArcGis Desktop; ESRI, Redlands, CA, USA). The OP^{AA}, OP^{DCFH} and OP^{DTT} values obtained at the 23 sampling sites for each monitoring period were interpolated by using the spherical semivariogram model (Jian et al., 1996) of the ordinary kriging (OK) method (Johnston et al., 2001), in order to create a continuous surface from the 23 measured sample points and to predict the values at unmeasured locations (Kumar et al., 2007). OK is one of the most used kriging techniques for describing data spatial continuity (Gia Pham et al., 2019). The used OK estimator is given by a linear combination of the observed values with weights, which are derived from the kriging equations, using experimental semivariances fitted by a spherical function (Xie et al., 2011).

3. Results and Discussion

3.1 PM_{10} Mass Concentration

Spatially-resolved data obtained by sampling in parallel at the 23 sites during the three monitoring periods allowed us to evaluate the spatial variability of PM_{10} mass concentration in Terni. PM_{10} mass concentrations determined in February, April and December 2017 are reported in Table 1.

From Table 1, we can observe that the concentration increased at all the sampling sites in the winter monitoring periods (February and December). Mean PM_{10} mass concentration was: 41 ± 7 μg m^{-3} in February, 19 ± 5 μg m^{-3} in April and 33 ± 7 μg m^{-3} in December. This behavior is mostly due to frequent temperature inversions during the colder season, which lead to severe episodes of atmospheric stability (Moroni et al., 2013; Curci et al., 2015), and to the major strength of typical winter sources, such as domestic biomass heating. In fact, in both February and December, high PM_{10} mass concentration was recorded at sites located near townhouses heated by biomass burning appliances (FR, BR and AR).

Table 1. PM_{10} mass concentration determined at the 23 sampling sites in the three monitoring periods (February, April and December 2017).

Site	PM_{10} Mass Concentration (μg m^{-3})		
	February	**April**	**December**
RI	52	21	44
MA	38	22	32
FA	33	21	38
GI	39	15	23
FR	46	12	32
CB	31	23	24
PI	40	18	34
BR	51	24	48
AR	34	14	36
CR	38	21	32
HG	53	10	35
SA	29	15	22
PV	47	21	34
LG	47	28	36
CZ	48	15	39
HV	45	16	35
UC	33	20	24
CA	46	20	36
CO	44	20	35
RO	40	16	29
OB	41	21	30
PR	32	30	26
CP	32	20	24
Mean	**41**	**19**	**33**
SD	**7**	**5**	**7**

3.2 Spatial Mapping of OP

Spatial variability of OP^{AA}, OP^{DCFH} and OP^{DTT} was evaluated, the OP values obtained at the 23 sites in the three monitoring periods are reported in supplementary material S2. Spatial mapping of OP^{AA}, OP^{DCFH} and

OP^{DTT} allowed us to assess spatial relationships between the three OP assays and local emission sources of PM.

From Fig. 3, we can observe that high OP^{AA} values were recorded at sites close to the railway. In particular, the highest OP^{AA} values were found at the sites located near the rail station (GI, CR and HG), where trains brake entering the residential area of the city, releasing the highest amount of dust by abrasion of rolling stock (Massimi et al., 2020b). Therefore, AA assay seems to be particularly sensitive toward particles released from the rail network by mechanical abrasion of train brakes. This source releases particles rich in some transition metals, such as Cu, Fe and Mn (Abbasi et al., 2012; Querol et al., 2012; Kam et al., 2013; Namgung et al., 2016). In various studies, OP^{AA} was found to be sensitive to transition metals (Vidrio et al., 2008; Charrier and Anastasio, 2011; Simonetti et al., 2018b; Piacentini et al., 2019) and has been strongly positively correlated with the main elements tracing non-exhaust traffic emission, such as Cu, Fe and Mn (Shiraiwa et al., 2017; Pietrogrande et al., 2018a, 2018b; Bates et al., 2019). However, these elements, generally considered as robust tracers of vehicular traffic, in Terni were found to be released at much higher concentration from the railway (Massimi et al., 2020b). Moreover, these results confirmed the high OP^{AA} activity shown at underground station in Gupta et al. (2019). It is worth nothing that relative high OP^{AA} values were recorded at the sites influenced by the rail network emission in all the monitoring periods, in accordance with the non-seasonal character of this source. In April (panel b), the OP^{AA} response to particles released from the railway, turned out to be higher and more localized at GI, CR and HG, presumably because of the more efficient mixing of the lower atmosphere during the warmer season, which led to a less horizontal diffusion of the released particles.

On the other hand, in Fig. 4 we can note that high OP^{DCFH} values were recorded at sites close to the steel plant (RO, OB, PR and CO) in all the monitoring periods and at sites near townhouses frequently heated by biomass burning appliances (BR, AR and CR) in winter (panels a and c). In this case, the high OP^{DCFH} values recorded at BR, AR and CR in February (panel a) and December (panel c), confirmed the relationships between OP^{DCFH} and PM released by domestic biomass heating. In fact, in previous studies, the same sites were identified as the most impacted by biomass burning contributions (Massimi et al., 2020a; 2020b). Relative high OP^{DCFH} values were also recorded at RO, OB, PR and CO in all the monitoring periods. These sites are close to the steel plant and have proven to be the most affected by particles released from the steel plant by abrasive machining of steel from the rolling plants and/or by combustive processes from the furnaces for the annealing of the cold rolled product (Massimi et al., 2020b). The relevance of steel plant related emissions on OP^{DCFH} values is particularly evident in April (panel b), when the strength of biomass burning emissions is weaker. Hence, DCFH assay seems to be particularly sensitive toward particles released from the steel plant and partly from domestic biomass heating. It is worth mentioning that in February, increased OP^{DCFH} values were also measured at sites near the railway (GI, CR and HG); this indicates a contribution to OP^{DCFH} also from particles released by abrasion of rolling stock. These results are in agreement with the findings of See et al. (2007) and Wang et al. (2010), which have shown a positive correlation between ROS and both transition metals (including Fe) and organic concentrations.

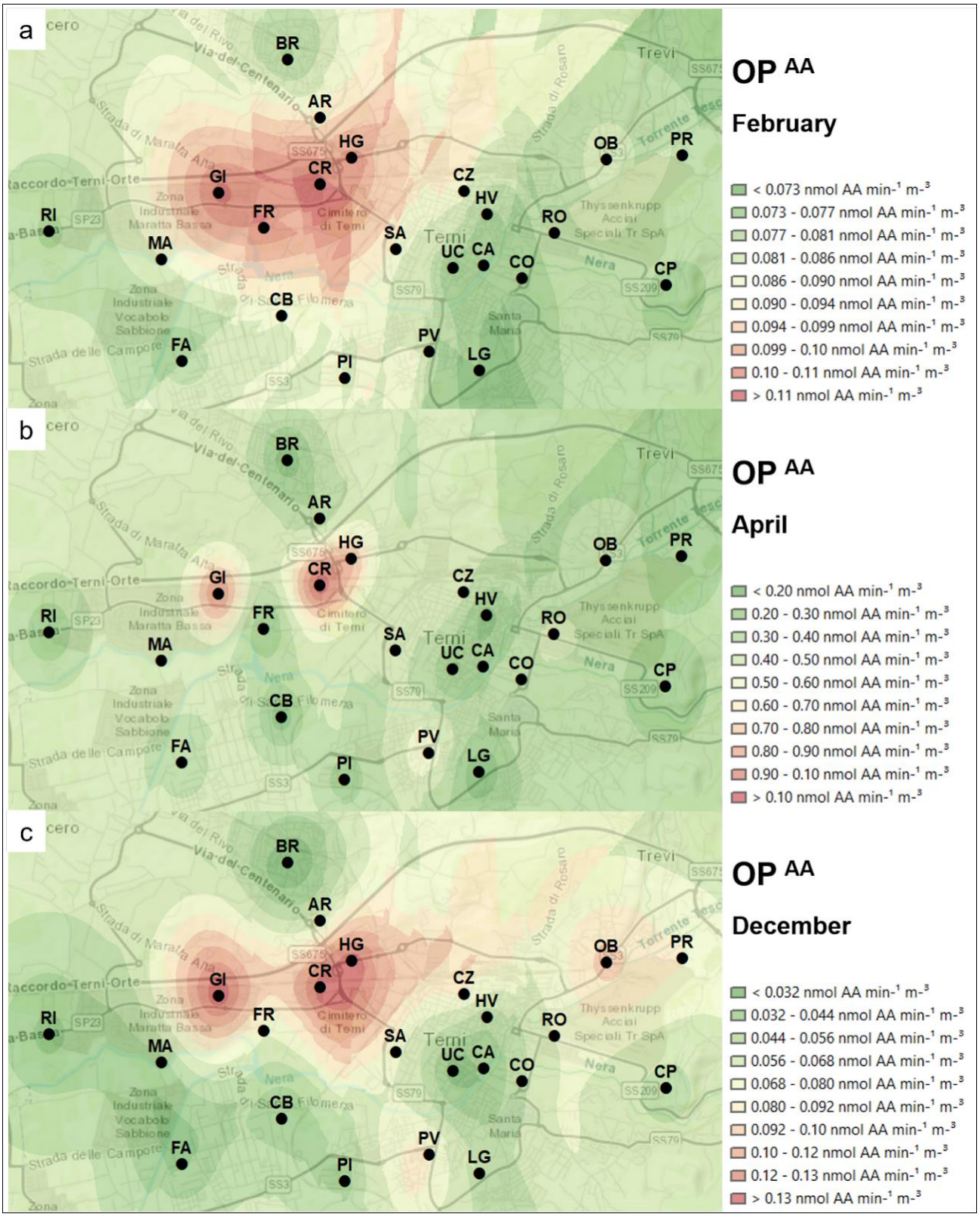

Fig. 3. Spatial mapping of OP^{AA} in February (panela a), April (panel b) and December (panel c) 2017.

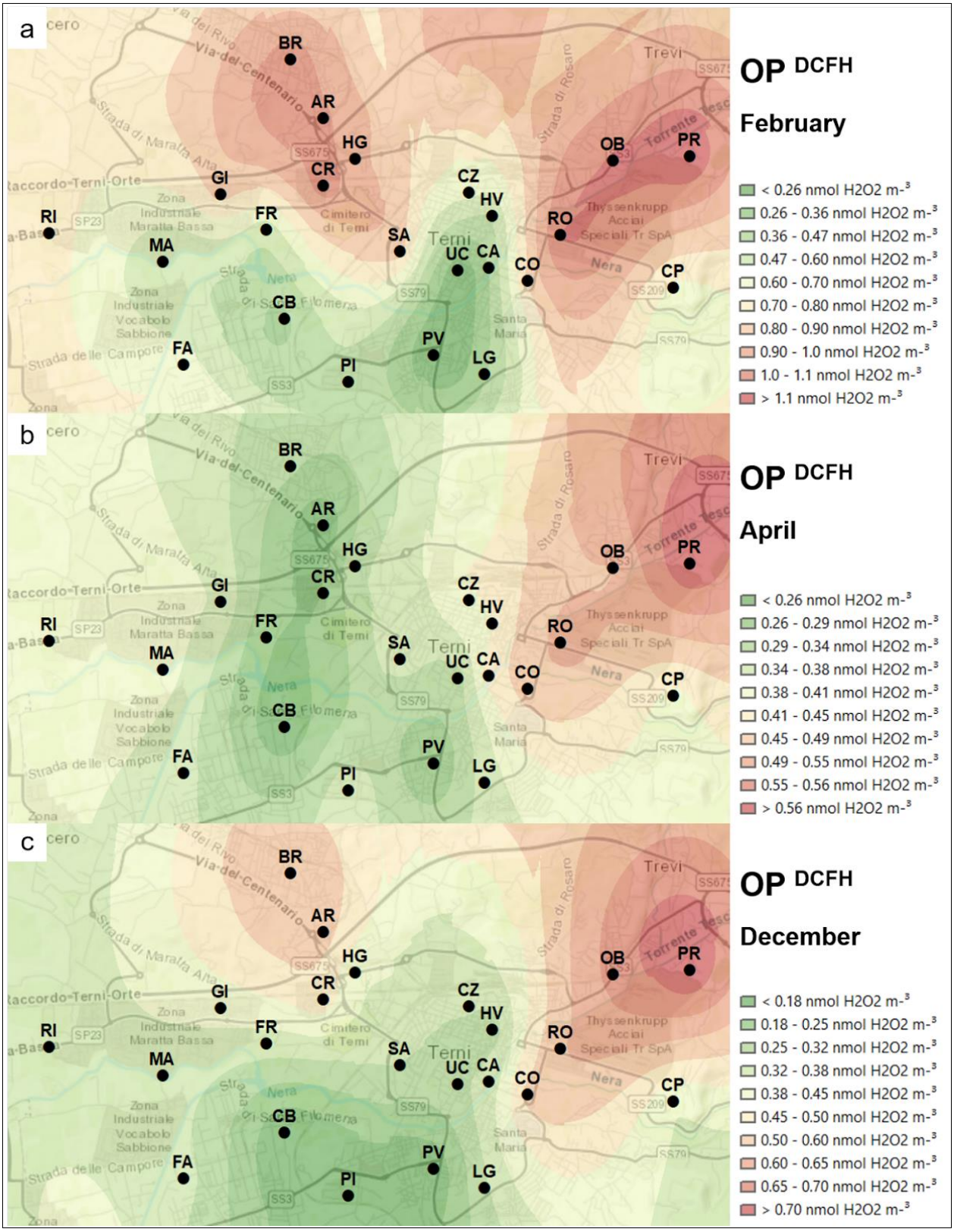

Fig. 4. Spatial mapping of OP^{DCFH} in February (panela a), April (panel b) and December (panel c) 2017.

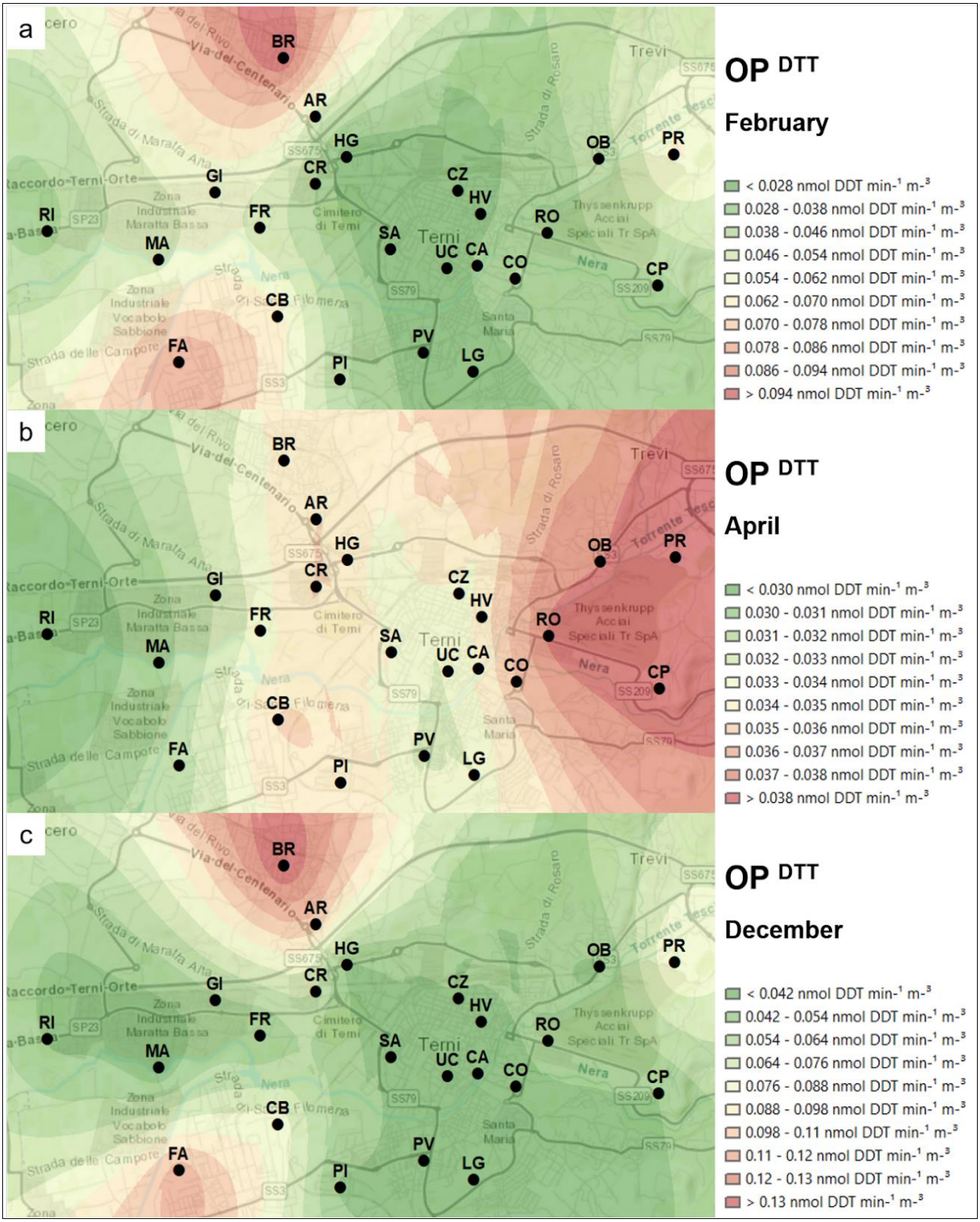

Fig. 5. Spatial mapping of OP^{DTT} in February (panela a), April (panel b) and December (panel c) 2017.

Finally, from Fig. 5, we can observe that in February (panel a) and December (panel c), the highest OP^{DTT} values were recorded at sites close to townhouses where domestic biomass heating systems are prevalent (BR

and AR) and at FA and CB. Previous studies demonstrated that these sites were affected by the emissions from burning of carpentry waste products (Massimi et al., 2020a; 2020b). Moreover, relative high OP^{DTT} values (supplementary material S2) occurred in all the monitoring periods at PR, which is the site most impacted by a source related to combustive processes associated to the steel production, such as casting, annealing and hot rolling of steel. This source releases particles rich of water-soluble Cr, Ga, Li, Mn and Zn (Massimi et al., 2020b). In April (panel b), when biomass burning appliances are not used, OP^{DTT} values turned out to be lower in all the Terni basin, except for the area affected by the steel plant (RO, OB, PR, CO and CP), where the highest OP^{DTT} values were recorded. Therefore, in general, DTT assay appears to be sensitive to combustion sources, in particular toward particles released by both industrial (panel b) and biomass burning (panel a and c) emissions. However, since biomass burning has a seasonal trend, a strong variability of the OP^{DTT} values at the sites influenced by this source is observed in the three monitoring periods, due to the stronger biomass burning contribution in the colder season. In fact, biomass burning and secondary organic aerosols are deemed to be the largest contributors to the OP^{DTT} (Verma et al., 2018). To corroborate this, despite various chemical components in atmospheric aerosols have been demonstrated to be well-correlated with OP^{DTT}, including water-soluble transition metal ions, water-soluble organic compounds and quinones (Wong et al., 2019), numerous studies have shown strong correlations of OP^{DTT} with K, a robust biomass burning tracer, and organic compounds, such as levoglucosan, associated to wood combustion sources (Pietrogrande et al., 2018a; Bates et al., 2019; Wang et al., 2019; Hakimzadeh et al., 2020).

3.3 Size *Distribution of OP*

Size distribution of OP^{AA}, OP^{DCFH} and OP^{DTT} was evaluated by analyzing size-segregated PM samples collected at CA, MA and PR. The OP^{AA}, OP^{DCFH} and OP^{DTT} values recorded in each size fraction at CA, MA and PR are reported in supplementary material S3.

Fig. 6 shows the mean concentration of the PM mass and the mean size distribution of the OP in Terni. Size distribution of PM mass concentration showed a bimodal profile, while OP^{AA}, OP^{DCFH} and OP^{DTT} size profiles were substantially unimodal, since AA, DCFH and DTT assays responded selectively to fine or coarse particles. In fact, from Fig. 6, we can observe that AA assay was found to be mainly sensitive to coarse particles (1.8-10 μm), showing a broad maximum in the size range 3.2-5.6 μm, while DCFH and DTT assays turned out to be more sensitive toward the fine fraction of PM (0.18-1.8 μm), with the highest OP values in the size fractions 0.56-1 μm and 0.32-0.56 μm, respectively. These findings are in line with previous publications, which have demonstrated higher OP^{AA} sensitivity toward redox active components in coarse aerosols (Godri et al., 2011; Manigrasso et al., 2020) and higher OP^{DCFH} and OP^{DTT} values in the fine fraction of PM (De Vizcaya-Ruiz et al., 2006; Ntziachristos et al., 2007; Steenhof et al., 2011; Janssen et al., 2014). Moreover, these results confirmed the findings of paragraph 3.2. In fact, particles released by re-suspension of dust and mechanical processes, such as brake abrasion, to whom OP^{AA} was found to be more sensitive, are typically present in the coarse fraction of PM. On the contrary, combustion processes (such as biomass burning and hot works from the furnaces of the steel plant), to whom OP^{DCFH} and OP^{DTT} appeared to be more sensitive, mainly

produce particles belonging to the fine fraction of PM (Shiraiwa et al., 2017; Canepari et al., 2019), which contain water-soluble metals and organics, generally associated with higher intrinsic redox activity.

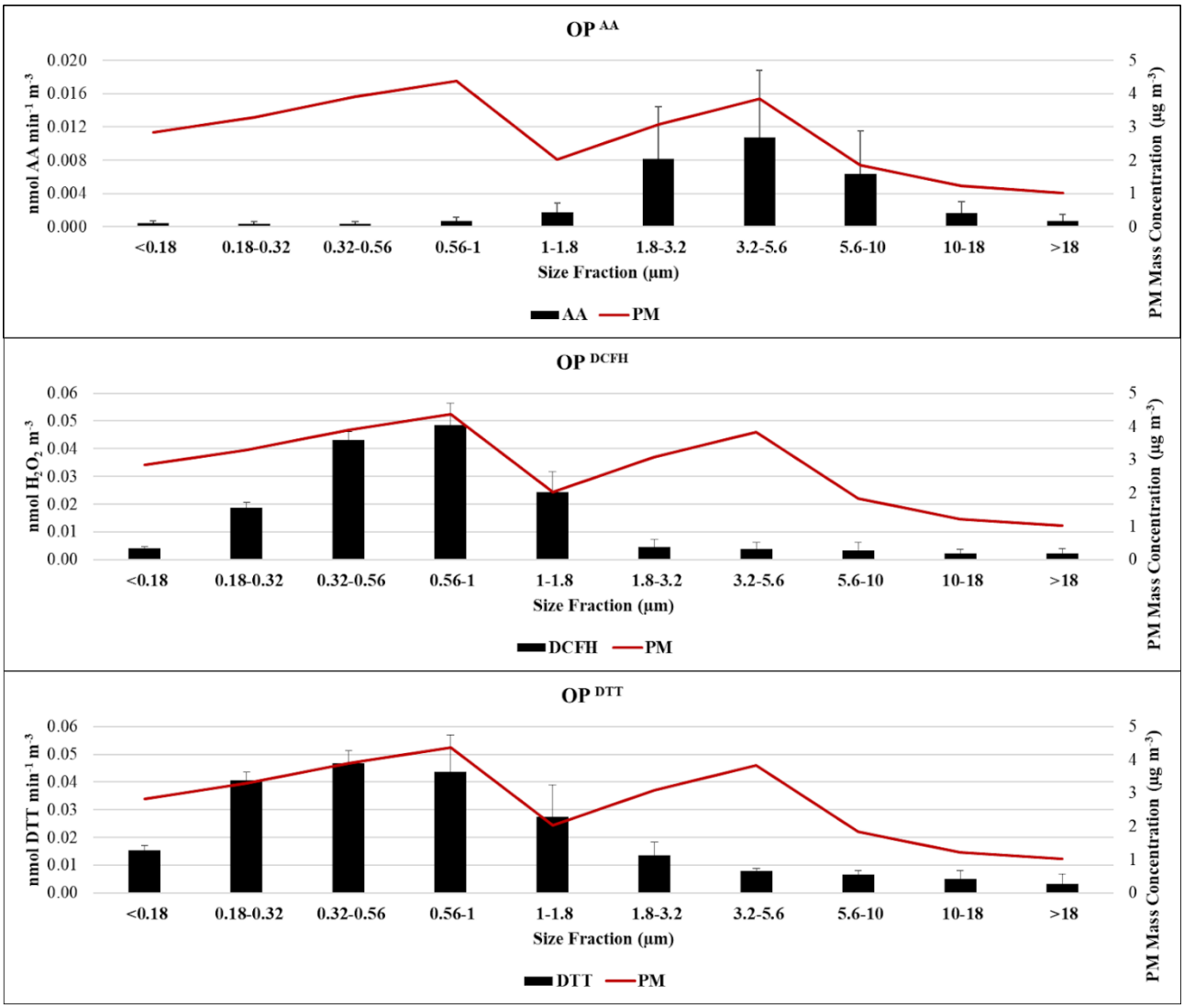

Fig. 6. Mean concentration of the PM mass and mean OP^{AA}, OP^{DCFH} and OP^{DTT} values of size-segregated PM samples collected at CA, MA and PR.

4. Conclusions

In this study, an innovative experimental approach, based on the spatial mapping of OP^{AA}, OP^{DCFH} and OP^{DTT}, for geo-referenced assessment of PM potential to induce oxidative stress, was described. This approach allowed us to map the spatial variability of OP^{AA}, OP^{DCFH} and OP^{DTT}, proving to be a powerful tool, transferable to other monitoring campaigns, for the individuation of spatial relationships between oxidative potential of PM and its chemical composition and sources. The obtained results showed that OP^{AA} was particularly sensitive toward coarse particles (1.8-10 µm) released from the rail network (GI, CR and HG) by abrasion of train brakes. On the contrary, OP^{DCFH} appeared to be particularly sensitive to fine particles (0.18-1.8 µm) released from the steel plant (RO, OB, PR and CO) and domestic biomass heating (BR, AR and CR), while OP^{DTT} was found to be specifically sensitive toward the fine fraction of PM (0.18-1.8 µm) released by both

industrial and biomass burning sources, such as domestic biomass heating (BR and AR) and the burning of carpentry waste products (FA and CB). Overall, these results showed that biomass burning may play a key role in PM potential to generate ROS.

The described approach promises to be very effective for the identification and localization of the emission sources mainly responsible for ROS generation and provides a reliable tool for spatially-resolved evaluation of exposure to PM and relative health risk.

Author Contributions: L. Massimi and S. Canepari conceived and planned the monitoring and the experiments; L. Massimi and M. Ristorini performed the samplings; L. Massimi, M. Ristorini and G. Simonetti performed the OP analyses; L. Massimi and G. Simonetti elaborated the data; L. Massimi wrote the manuscript; M. A. Frezzini and M. L. Astolfi reviewed a previous version of the manuscript; L. Massimi and S. Canepari coordinated the group and supervised the manuscript.

Supplementary Materials

Details on the followed OP analytical procedures for the AA, DCFH and DTT assays applied to the PM aqueous extracts and used reagents.

S1.1 AA Procedure

AA procedure is described by Fang et al. (2016). First, 0.3 mL of 0.5 mM phosphate buffer and 0.1 mL of 2 mM ascorbic acid were added to 2.5 mL of water-extracted solution from each sample. The absorbance of the solutions was analyzed by using UV-Vis absorption spectrometry (UV-Vis, Varian Cary 50 UV-Vis Spectrometer) at 265 nm wavelength and at different reaction times (0, 10, and 20 minutes) to acquire the depletion rate of AA. OP^{AA} was calculated as the depletion rate per volume unit (nmol AA min^{-1} m^{-3}) using the following equations:

$$\sigma AA = -\sigma Abs \times N0Abs0, \quad OPAA = \sigma AAs - \sigma AAbVa\ Ve\ VS$$

where σAbs is the slope of the absorbance of blanks vs. time (min^{-1}), Abs_0 is the initial absorbance calculated from the intercept of the linear regression of absorbance vs. time, N_0 is the number of AA moles added in the reaction vial (200 nmol), σAA_s and σAA_b are the rate of AA consumption for the sample and for the blank, respectively (nmol min^{-1}), V_e and V_a are the extraction volume (10 mL) and sample volume added to the reaction vial (2.5 mL) respectively, and V_s is the sampling volume (m^3) for each PM sample.

S1.2 DCFH Procedure

The DCFH assay applied on PM field samples was adapted from Huang et al. (2016). Firstly, operating in the dark, 4.873 mg of 2',7'-dichlorodihydrofluorescein diacetate (DCFH-DA, Sigma-Aldrich, USA) was dissolved in 5 mL of ethanol and mixed with 20 mL of 0.01 M NaOH, in order to promote the de-acetalization. Then the solution was kept for 30 minutes in a dark room. The HRP solution was prepared dissolving 3.15 mg of HRP (Type VI, essentially salt-free, lyophilized powder, ≥ 250 units/mg solid) in 1 L of phosphate buffer 25 mM at pH 7.4. Aliquots of 1.5 mL of the water-extracted solution from each PM sample was mixed with 5 mL of HRP solution and with 125 µL of DCFH solution and then kept for 5 minutes at 37 °C. The mixture was then analyzed with a fluorescence detector (Jasco FP-920) at 530 nm wavelength (427 nm excitation wavelength). The instrument was calibrated using standard H_2O_2 solution (30%; Promochem, LGC Standards GmbH, Wesel, Germany; 5×10^{-8}, 1×10^{-7}, 2×10^{-7}, 5×10^{-7} and 1×10^{-6} M). The calibration curve was used to convert the obtained fluorescence intensity of the samples into H_2O_2 equivalents and to acquire OP^{DCFH} values (nmol H_2O_2 m^{-3}) for each of them.

S1.3 DTT procedure

According to the method reported in Fang et al. (2016), 0.2 mL of 1M phosphate buffer and 0.1 mL of 1 mM DTT were mixed with three aliquots (0.7 mL) of the water-extracted solution from each PM sample, then incubated at 37 °C in a thermostatic bath (HAAKE DC3, Fisons). At regular intervals (0, 10 and 20 minutes), 1 mL of trichloroacetic acid 10% was added to one of the aliquots to stop the reaction. Then, 1 mL of each solution was taken and mixed with 2 mL of Tris-buffer (0.08M, containing EDTA 4 mM) and with

50 µL of 5,50-dithiobis-2-nitrobenzoic acid (DTNB) 0.2 mM. After 5 minutes, the absorbance of the solutions was measured at 412 nm by UV-Vis spectrophotometry. An operative blank was always measured in parallel. OP^{DTT} was calculated as DTT consumption rate per volume unit (nmol DTT min^{-1} m^{-3}) using the following equations:

$$\sigma DTT = -\sigma Abs \times N0Abs0\ ,\ OPDTT = \sigma DTTs - \sigma DTTbVa\ Ve\ Vs$$

where σAbs is the slope of the absorbance of blanks vs. time (min^{-1}), Abs_0 is the initial absorbance calculated from the intercept of the linear regression of absorbance vs. time, N_0 is the number of DTT moles added in the reaction vial (100 nmol), σDTT_s and σDTT_b are the rate of DTT consumption for the sample and for the blank, respectively (nmol min^{-1}), V_e and V_a are the extraction volume (10 mL) and sample volume added to the reaction vial (0.7 mL) respectively, and V_s is the sampling volume (m^3) for each PM sample.

Table S2.1. OP^{AA}, OP^{DCFH} and OP^{DTT} values determined at the 23 sampling sites in the three monitoring periods (February, April and December 2017).

Site	OP^{AA} (nmol AA min^{-1} m^{-3})			OP^{DCFH} (nmol H_2O_2 m^{-3})			OP^{DTT} (nmol DTT min^{-1} m^{-3})		
	February	**April**	**December**	**February**	**April**	**December**	**February**	**April**	**December**
RI	0.048	0.17	0.012	0.73	0.38	0.35	0.034	0.027	0.041
MA	0.078	0.49	0.025	0.46	0.40	0.34	0.050	0.029	0.030
FA	0.040	0.29	0.014	0.61	0.36	0.37	0.087	0.030	0.12
GI	0.18	0.97	0.19	0.82	0.39	0.42	0.056	0.031	0.051
FR	0.12	0.16	0.052	0.50	0.28	0.34	0.050	0.029	0.041
CB	0.060	0.11	0.025	0.34	0.22	0.040	0.066	0.041	0.084
PI	0.075	0.23	0.026	0.44	0.40	0.13	0.039	0.039	0.040
BR	0.031	0.10	0.0032	1.1	0.54	0.61	0.10	0.035	0.14
AR	0.078	0.33	0.043	1.0	0.47	0.58	0.050	0.038	0.10
CR	0.15	1.1	0.17	1.1	0.42	0.55	0.037	0.041	0.064
HG	0.13	0.85	0.16	0.90	0.50	0.33	0.024	0.030	0.039
SA	0.081	0.43	0.073	0.83	0.38	0.33	0.021	0.034	0.038
PV	0.11	0.61	0.10	0.15	0.25	0.051	0.025	0.028	0.041
LG	0.036	0.10	0.042	0.35	0.36	0.31	0.021	0.029	0.034
CZ	0.13	0.43	0.10	0.61	0.41	0.36	0.023	0.028	0.042
HV	0.024	0.14	0.032	0.46	0.40	0.16	0.026	0.038	0.040
UC	0.050	0.18	0.0032	0.17	0.30	0.33	0.025	0.032	0.034
CA	0.079	0.24	0.029	0.36	0.45	0.31	0.030	0.033	0.036
CO	0.079	0.39	0.058	0.80	0.47	0.62	0.038	0.038	0.037
RO	0.082	0.44	0.070	1.1	0.50	0.60	0.035	0.042	0.045
OB	0.11	0.42	0.11	1.1	0.47	0.69	0.040	0.036	0.040
PR	0.082	0.19	0.085	1.2	0.61	0.87	0.063	0.041	0.087
CP	0.066	0.20	0.042	0.65	0.38	0.32	0.034	0.039	0.042
Mean	**0.083**	**0.37**	**0.064**	**0.69**	**0.41**	**0.39**	**0.043**	**0.034**	**0.055**

Table S3.1. Mean concentration of the PM mass and OP^{AA}, OP^{DCFH} and OP^{DTT} values of size-segregated PM samples collected at CA, MA and PR.

Size Fraction (µm)	PM Mass Concentration (µg m^{-3})	OP^{AA} (nmol AA min^{-1} m^{-3})					OP^{DCFH} (nmol H_2O_2 m^{-3})					OP^{DTT} (nmol DTT min^{-1} m^{-3})				
		CA	**MA**	**PR**	**Mean**	***SD***	**CA**	**MA**	**PR**	**Mean**	***SD***	**CA**	**MA**	**PR**	**Mean**	***SD***
<0.18	2.8	0.00046	0.00067	0.00015	**0.00042**	*0.00026*	0.0032	0.0039	0.0047	**0.0039**	*0.0007*	0.014	0.015	0.017	**0.015**	*0.001*
0.18-0.32	3.3	0.00068	0.00023	0.00016	**0.00035**	*0.00028*	0.017	0.019	0.021	**0.019**	*0.002*	0.038	0.041	0.043	**0.041**	*0.003*
0.32-0.56	3.9	0.00063	0.00040	0.00018	**0.00041**	*0.00023*	0.041	0.046	0.043	**0.043**	*0.003*	0.043	0.052	0.045	**0.047**	*0.005*
0.56-1	4.4	0.0010	0.00088	0.00022	**0.00071**	*0.00043*	0.046	0.058	0.042	**0.048**	*0.008*	0.046	0.056	0.029	**0.044**	*0.013*
1-1.8	2.0	0.0021	0.0026	0.00043	**0.0017**	*0.0012*	0.023	0.032	0.018	**0.024**	*0.007*	0.031	0.037	0.015	**0.027**	*0.011*
1.8-3.2	3.1	0.013	0.011	0.0010	**0.0082**	*0.0063*	0.0019	0.0049	0.0071	**0.0046**	*0.0026*	0.014	0.018	0.0088	**0.014**	*0.005*
3.2-5.6	3.8	0.016	0.014	0.0015	**0.011**	*0.008*	0.0017	0.0032	0.0065	**0.0038**	*0.0024*	0.0071	0.0080	0.0089	**0.0080**	*0.0009*
5.6-10	1.8	0.0092	0.0095	0.00053	**0.0064**	*0.0051*	0.0016	0.0013	0.0068	**0.0032**	*0.0031*	0.0052	0.0062	0.0083	**0.0066**	*0.0016*
10-18	1.2	0.0022	0.0026	0.000077	**0.0016**	*0.0014*	0.0016	0.0013	0.0038	**0.0022**	*0.0014*	0.0045	0.0026	0.0082	**0.0051**	*0.0028*
>18	1.0	0.00056	0.0015	0.000047	**0.00071**	*0.00074*	0.0011	0.0014	0.0043	**0.0023**	*0.0018*	0.0012	0.0012	0.0073	**0.0032**	*0.0035*

References

Abbasi, S., Olander, L., Larsson, C., Olofsson, U., Jansson, A., Sellgren, U. 2012. A field test study of airborne wear particles from a running regional train. Proceedings of the Institution of Mechanical Engineers, Part F: Journal of Rail and Rapid Transit, 226(1), 95-109.

Anderson, J. O., Thundiyil, J. G., Stolbach, A. 2012. Clearing the air: a review of the effects of particulate matter air pollution on human health. Journal of Medical Toxicology, 8(2), 166-175.

Ayres, J. G., Borm, P., Cassee, F. R., Castranova, V., Donaldson, K., Ghio, A., Harrison, R.M., Hider, R., Kelly, F., Kooter, I.M., Marano, F., Maynard, R.L., Mudway, I., Nel, A., Sioutas, C., Smith, S., Baeza-Squiban, A., Cho, A., Duggan, S., Froines, J. 2008. Evaluating the toxicity of airborne particulate matter and nanoparticles by measuring oxidative stress potential - a workshop report and consensus statement. Inhalation Toxicology, 20(1), 75-99.

Bates, J. T., Fang, T., Verma, V., Zeng, L., Weber, R. J., Tolbert, P. E., Abrams, J. Y., Sarnat, S. E., Klein, M., Mulholland, J. A., Russell, A. G. 2019. Review of acellular assays of ambient particulate matter oxidative potential: Methods and relationships with composition, sources, and health effects. Environmental Science & Technology, 53(8), 4003-4019.

Brunekreef, B., Holgate, S. T. 2002. Air Pollution and Health. Lancet 360, 1233–1242.

Calas, A., Uzu, G., Kelly, F., Houdier, S., Martins, J., Thomas, F., Molton, F., Charron, A., Dunster, C., Oliete, A., Jacob, V., Besombes, J., Chevrier, F., Jaffrezo, J. 2018. Comparison between five acellular oxidative potential measurement assays performed with detailed chemistry on PM10 samples from the city of Chamonix (France). Atmospheric Chemistry and Physics, 18, 7863–7875.

Campbell, S. J., Utinger, B., Lienhard, D. M., Paulson, S. E., Shen, J., Griffiths, P. T., Stell, A.C., Kalberer, M. 2019. Development of a physiologically relevant online chemical assay to quantify aerosol oxidative potential. Analytical Chemistry, 91(20), 13088-13095.

Canepari, S., Astolfi, M. L., Catrambone, M., Frasca, D., Marcoccia, M., Marcovecchio, F., Massimi, L., Rantica, E., Perrino, C. 2019. A combined chemical/size fractionation approach to study winter/summer variations, ageing and source strength of atmospheric particles. Environmental Pollution, 253, 19-28.

Capelli, L., Sironi, S., Del Rosso, R., Céntola, P., Rossi, A., Austeri, C. 2011. Olfactometric approach for the evaluation of citizens' exposure to industrial emissions in the city of Terni, Italy. Science of the Total Environment, 409(3), 595-603.

Catrambone, M., Canepari, S., Cerasa, M., Sargolini, T., Perrino, C. 2019. Performance evaluation of a very-low-volume sampler for atmospheric particulate matter. Aerosol Air Quality Research, 19, 2160-2172.

Cesari, D., Merico, E., Grasso, F. M., Decesari, S., Belosi, F., Manarini, F., De Nuntiis, P., Rinaldi, M., Volpi, F., Gambaro, A., Morabito, E., Contini, D. 2019. Source apportionment of PM2.5 and of its oxidative potential in an industrial suburban site in south Italy. Atmosphere, 10(12), 758.

Charrier, J. G., Anastasio, C. 2011. Impacts of antioxidants on hydroxyl radical production from individual and mixed transition metals in a surrogate lung fluid. Atmospheric Environment, 45 (40), 7555− 7562.

Chirizzi, D., Cesari, D., Guascito, M. R., Dinoi, A., Giotta, L., Donateo, A., Contini, D. 2017. Influence of Saharan dust outbreaks and carbon content on oxidative potential of water-soluble fractions of PM2.5 and PM10. Atmospheric Environment, 163, 1–8.

Cho, A. K., Sioutas, C., Miguel, A. H., Kumagai, Y., Schmitz, D. A., Singh, M., Fernandez, F.A., Froines, J. R. 2005. Redox activity of airborne particulate matter at different sites in the Los Angeles Basin. Environmental Research, 99(1), 40-47.

Curci, G., Ferrero, L., Tuccella, P., Barnaba, F., Angelini, F., Bolzacchini, E., Carbone, C., Denier van der Gon, H. A. C., Facchini, M. C., Gobbi, G. P., Kuenen, J. P. P., Landi, T. C., Perrino, C., Perrone, M. G., Sangiorgi, G., Stocchi, P. 2015. How much is particulate matter near the ground influenced by upper-level processes within and above the PBL? A summertime case study in Milan (Italy) evidences the distinctive role of nitrate. Atmospheric Chemistry and Physics, 15(5), 2629-2649.

Delfino, R. J., Staimer, N., Vaziri, N. D. 2011. Air pollution and circulating biomarkers of oxidative stress. Air Quality, Atmosphere & Health, 4(1), 37-52.

De Vizcaya-Ruiz, A., Gutiérrez-Castillo, M. E., Uribe-Ramirez, M., Cebrián, M. E., Mugica-Alvarez, V., Sepúlveda, J., Rosas, I., Salinas, E., Garcia-Cue´llar, C., Martinez, F., Alfaro-Moreno, E., Torres-Flores, V., Osornio-Vargas, A., Sioutas, C., Fine, P.M., Singh, M., Geller, M.D., Kuhn, T., Miguel, A.H., Eiguren-Fernandez, A., Schiesti, R.H., Reliene, R., Froines, J. 2006. Characterization and in vitro biological effects of concentrated particulate matter from Mexico City. Atmospheric Environment, 40, 583-592.

Fang, T., Verma, V., Bates, J. T., Abrams, J., Klein, M., Strickland, M. J., Sarnat, S. E., Chang, H. H., Mulholland, J. A., Tolbert, P. E., Russell, A. G. 2015. Oxidative potential of ambient water-soluble PM 2.5 measured by Dithiothreitol (DTT) and Ascorbic Acid (AA) assays in the southeastern United States: contrasts in sources and health associations. Atmospheric Chemistry & Physics Discussions, 15(21) 30609-30644.

Fang, T., Verma, V., Bates, J. T., Abrams, J., Klein, M., Strickland, M. J., Stefanie E., Sarnat, S. E., Chang, H. H., Mulholland, J. A., Tolbert, P. E., Russell, A. G., Weber, R. J. 2016. Oxidative Potential of Ambient Water-Soluble PM2.5 in the Southeastern United States: Contrasts in Sources and Health Associations between Ascorbic Acid (AA) and Dithiothreitol (DTT) Assays. Atmospheric Chemistry, 16, 3865–3879.

Ferrero, L., Cappelletti, D., Moroni, B., Sangiorgi, G., Perrone, M. G., Crocchianti, S., Bolzacchini, E. 2012. Wintertime aerosol dynamics and chemical composition across the mixing layer over basin valleys. Atmospheric Environment, 56, 143-153.

Frezzini, M. A., Castellani, F., De Francesco, N., Ristorini, M., Canepari, S. 2019. Application of DPPH Assay for Assessment of Particulate Matter Reducing Properties. Atmosphere, 10(12), 816.

Gao, D., Mulholland, J. A., Russell, A. G., Weber, R. J. 2020. Characterization of water-insoluble oxidative potential of PM2.5 using the dithiothreitol assay. Atmospheric Environment, 224, 117327.

Gia Pham, T., Kappas, M., Van Huynh, C., Hoang Khanh Nguyen, L. 2019. Application of ordinary kriging and regression kriging method for soil properties mapping in hilly region of Central Vietnam. ISPRS International Journal of Geo-Information, 8(3), 147.

Giorio, C., Tapparo, A., Scapellato, M.L., Carrieri, M., Apostoli, P., Bartolucci, G.B. 2013. Field comparison of a personal cascade impactor sampler, an optical particle counter and CEN-EU standard methods for PM10, PM2.5 and PM1 measurement in urban environment. Journal of Aerosol Science, 65, 111-120.

Godri, K. J., Harrison, R. M., Evans, T., Baker, T., Dunster, C., Mudway, I. S., Kelly, F. J. 2011. Increased oxidative burden associated with traffic component of ambient particulate matter at roadside and urban background schools sites in London. PloS one, 6(7).

Guerrini, R. 2012. Qualità dell'aria nella provincia di Terni tra il 2002 e il 2011. Quad ARPA Umbria, 81-87.

Gupta, T., Singh, S. P., Rajput, P., Agarwal, A. K. 2019. Measurement, Analysis and Remediation of Environmental Pollutants. Springer.

Hakimzadeh, M., Soleimanian, E., Mousavi, A., Borgini, A., De Marco, C., Ruprecht, A. A., Sioutas, C. 2020. The impact of biomass burning on the oxidative potential of PM2. 5 in the metropolitan area of Milan. Atmospheric Environment, 224, 117328.

Halliwell, B., Whiteman, M. 2004. Measuring reactive species and oxidative damage *in vivo* and in cell culture: How should you do it and what do the results mean? British Journal of Pharmacology, 142, 231–255.

Hlavay, J., Polyak, K., Weisz, M. 2001. Monitoring of the natural environment by chemical speciation of elements in aerosol and sediment samples. Presented at the Whistler 2000 Speciation Symposium, Whistler Resort, BC, Canada, June 25–July 1, 2000. Journal of Environmental Monitoring, 3(1), 74-80.

Huang, W., Zhang, Y., Zhang, Y., Fang, D., Schauer, J. J., 2016. Optimization of the Measurement of Particle-Bound Reactive Oxygen Species with 2',7'-dichlorofluorescin (DCFH), Water Air Soil Pollution, 227, 164.

Hung, H. F., Wang, C. S. 2001. Experimental determination of reactive oxygen species in Taipei aerosols. Journal of Aerosol Science, 32, 1201–1211.

Janssen, N. A., Yang, A., Strak, M., Steenhof, M., Hellack, B., Gerlofs-Nijland, M. E., Kuhlbusch T., Kelly, F., Harrison R., Brunekreef, B., Cassee, F., Hoek, G. 2014. Oxidative potential of particulate matter collected at sites with different source characteristics. Science of the Total Environment, 472, 572-581.

Jian, X., Olea, R. A., Yu, Y. S. 1996. Semivariogram modeling by weighted least squares. Computers & Geosciences, 22(4), 387-397.

Johnston, K., Ver Hoef, J. M., Krivoruchko, K., Lucas, N. 2001. Using ArcGIS geostatistical analyst (Vol. 380). Redlands: Esri.

Kam, W., Delfino, R. J., Schauer, J. J., Sioutas, C. 2013. A comparative assessment of PM2.5 exposures in light-rail, subway, freeway, and surface street environments in Los Angeles and estimated lung cancer risk. Environmental Science: Processes & Impacts, 15(1), 234-243.

Kelly, F. J., Fuller, G. W., Walton, H. A., Fussell, J. C. 2012. Monitoring air pollution: Use of early warning systems for public health. Respirology, 17(1), 7-19.

Khurshid, S. S., Siegel, J. A., Kinney, K. A. 2014. Indoor particulate reactive oxygen species concentrations. Environmental research, 132, 46-53.

Kumar, A., Maroju, S., Bhat, A. 2007. Application of ArcGIS geostatistical analyst for interpolating environmental data from observations. Environmental Progress, 26(3), 220-225.

Lebel, C. P., Ischiropoulos, H., Bondy, S. C. 1992. Evaluation of the probe 2',7'-dichlorofluorescin as an indicator of reactive oxygen species formation and oxidative stress. Chemical Research in Toxicology, 5, 227–231.

Li, R., Kou, X., Geng, H., Xie, J., Yang, Z., Zhang, Y., Cai, Z., Dong, C. 2015. Effect of ambient PM 2.5 on lung mitochondrial damage and fusion/fission gene expression in rats. Chemical Research in Toxicology, 28, 408-418.

Lubczyńska, M. J., Sunyer, J., Tiemeier, H., Porta, D., Kasper-Sonnenberg, M., Jaddoe, V. W., Xavier Basagaña, X., Dalmau-Bueno, A., Forastiere, F., Wittsiepe, J., Hoffmann, B., Nieuwenhuijsen, M., Hoek, G., de Hoogh, K., Brunekreef, B., Guxens, M. 2017. Exposure to elemental composition of outdoor PM2.5 at birth and cognitive and psychomotor function in childhood in four European birth cohorts. Environment international, 109, 170-180.

Manigrasso, M., Simonetti, G., Astolfi, M. L., Perrino, C., Canepari, S., Protano, C., Antonucci, A., Avino, P., Vitali, M. 2020. Oxidative Potential Associated with Urban Aerosol Deposited into the Respiratory System and Relevant Elemental and Ionic Fraction Contributions. Atmosphere, 11(1), 6.

Marcoccia, M., Ronci, L., De Matthaeis, E., Setini, A., Perrino, C., Canepari, S. 2017. In-vivo assesment of the genotoxic and oxidative stress effects of particulate matter on *Echinogammarus veneris*. Chemosphere, 173, 124–134.

Massimi, L., Ristorini, M., Eusebio, M., Florendo, D., Adeyemo, A., Brugnoli, D., Canepari, S. 2017. Monitoring and evaluation of Terni (Central Italy) air quality through spatially resolved analyses. Atmosphere, 8(10), 200.

Massimi, L., Conti, M. E., Mele, G., Ristorini, M., Astolfi, M. L., Canepari, S. 2019. Lichen transplants as indicators of atmospheric element concentrations: a high spatial resolution comparison with PM_{10} samples in a polluted area (Central Italy). Ecological Indicators, 101, 759-769.

Massimi, L., Simonetti, G., Buiarelli, F., Di Filippo, P., Pomata, D., Riccardi, C., Ristorini, M., Astolfi, M.L., Canepari, S. 2020a. Spatial distribution of levoglucosan and alternative biomass burning tracers in atmospheric aerosols, in an urban and industrial hot-spot of Central Italy. Atmospheric Research, 104904.

Massimi, L., Ristorini, M., Astolfi, M.L., Perrino, C., Canepari, S. 2020b. High Resolution Spatial Mapping of Element Concentrations in PM_{10}: a Powerful Tool for Localization of Emission Sources. Atmospheric Research, 105060.

Miljevic, B., Hedayat, F., Stevanovic, S., Fairfull-Smith, K. E., Bottle, S. E., Ristovski, Z. D. 2014. To sonicate or not to sonicate PM filters: Reactive oxygen species generation upon ultrasonic irradiation. Aerosol science and technology, 48(12), 1276-1284.

Morini, E., Touchaei, A. G., Castellani, B., Rossi, F., Cotana, F. 2016. The impact of albedo increase to mitigate the urban heat island in Terni (Italy) using the WRF model. Sustainability, 8(10), 999.

Mutzel, A., Rodigast, M., Iinuma, Y., Böge, O., Herrmann, H. 2013. An improved method for the quantification of SOA bound peroxides. Atmospheric Environment, 67, 365-369.

Namgung, H. G., Kim, J. B., Woo, S. H., Park, S., Kim, M., Kim, M. S., Bae, G. N., Park, D., Kwon, S. B. 2016. Generation of nanoparticles from friction between railway brake disks and pads. Environmental Science and Technology, 50(7), 3453-3461.

Ntziachristos, L., Froines, J. R., Cho, A. K., Sioutas, C. 2007. Relationship between redox activity and chemical speciation of size-fractionated particulate matter. Particle and Fibre Toxicology, 4(1), 5.

Øvrevik, J. 2019. Oxidative potential versus biological effects: A review on the relevance of cell-free/abiotic assays as predictors of toxicity from airborne particulate matter. International Journal of Molecular Sciences, 20, 4772.

Perrone, M. G., Zhou, J., Malandrino, M., Sangiorgi, G., Rizzi, C., Ferrero, L., Dommen, J., Bolzacchini, E. 2016. PM chemical composition and oxidative potential of the soluble fraction of particles at two sites in the urban area of Milan, Northern Italy. Atmospheric Environment, 128, 104-113.

Pietrogrande, M. C., Perrone, M. R., Manarini, F., Romano, S., Udisti, R., Becagli, S. 2018a. PM10 oxidative potential at a Central Mediterranean Site: Association with chemical composition and meteorological parameters. Atmospheric Environment, 188, 97-111.
Pietrogrande, M. C., Dalpiaz, C., Dell'Anna, R., Lazzeri, P., Manarini, F., Visentin, M., Tonidandel, G. 2018b. Chemical composition and oxidative potential of atmospheric coarse particles at an industrial and urban background site in the alpine region of northern Italy. Atmospheric Environment, 191, 340-350.
Piacentini, A., Falasca, G., Canepari, S., Massimi, L. 2019. Potential of PM-selected components to induce oxidative stress and root system alteration in a plant model organism. Environment International, 132, 105094.

Pope III, C. A., Dockery, D. W. 2006. Health effects of fine particulate air pollution: Lines that connect. Journal of the Air & Waste Management Association, 56, 709–742.

Querol, X., Moreno, T., Karanasiou, A., Reche, C., Alastuey, A., Viana, M., Font, O., Gil, J., de Miguel, E., Capdevila, M. 2012. Variability of levels and composition of PM10 and PM2.5 in the Barcelona metro system. Atmospheric Chemistry and Physics, 12(11), 5055-5076.

Ricci, P. F., Cirillo, M. C. 1985. Uncertainty in health risk analysis. Journal of Hazardous Materials, 10(2-3), 433-447.

Ristorini, M., Astolfi, M.L., Frezzini, M.A., Canepari, S., Massimi, L. 2020. Evaluation of the efficiency of Arundo donax L. leaves as biomonitors for atmospheric element concentrations in an urban and industrial area of Central Italy. Atmosphere, 11(3), 226.

See, S. W., Wang, Y. H., Balasubramanian, R. 2007. Contrasting reactive oxygen species and transition metal concentrations in combustion aerosols. Environmental Research, 103(3), 317-324.

SENTIERI-ReNaM, GdL, Binazzi, A., Mangone, L. 2016. SENTIERI - Epidemiological study of residents in national priority contaminated sites: incidence of mesothelioma. Epidemiologia e Prevenzione, 40 (5 Suppl1), 1-116.

Sgrigna, G., Sæbø, A., Gawronski, S., Popek, R., Calfapietra, C. 2015. Particulate Matter deposition on Quercus ilex leaves in an industrial city of central Italy. Environmental Pollution, 197, 187-194.

Shiraiwa, M., Ueda, K., Pozzer, A., Lammel, G., Kampf, C. J., Fushimi, A., Enami, S., Arangio, A.M., Fröhlich-Nowoisky, J., Fujitani,, Y., Furuyama, A., Lakey, P.S.J., Lelieveld, J., Lucas, K., Morino, Y., Pöschl, U., Takahama, S., Takami, A., Tong, H., Weber, B., Yoshino, A., Sato, K. 2017. Aerosol health effects from molecular to global scales. Environmental Science & Technology, 51(23), 13545-13567.

Simonetti, G., Conte, E., Perrino, C., Canepari, S. 2018a. Oxidative potential of size-segregated PM in a urban and an industrial area of Italy. Atmospheric Environment, 187, 292–300.

Simonetti, G., Conte, E., Massimi, L., Frasca, D., Perrino, C., Canepari, S. 2018b. Oxidative potential of particulate matter components generated by specific emission sources. Journal of Aerosol Sciences, 126, 99-109.

Steenhof, M., Gosens, I., Strak, M., Godri, K. J., Hoek, G., Cassee, F. R., Mudway, I.S., Kelly, F.J., Harrison, R.M., Lebret, E., Brunekreef, B., Janssen, N.A., Pieters, R.H. 2011. In vitro toxicity of particulate matter (PM) collected at different sites in the Netherlands is associated with PM composition, size fraction and oxidative potential-the RAPTES project. Particle and fibre toxicology, 8(1), 26.

Stoeger, T., Takenaka, S., Frankenberger, B., Ritter, B., Karg, E., Maier, K., Shulz, H., Schmid, O. 2009. Deducing in vivo toxicity of combustion-derived nanoparticles from a cell-free oxidative potency assay and metabolic activation of organic compounds. Environmental Health Perspectives, 117(1), 54-60.

Strak, M., Janssen, N. A., Godri, K. J., Gosens, I., Mudway, I. S., Cassee, F. R., Lebret, E., Kelly, F.G., Harrison, M.R., Brunekreef, B., Steenhof, M., Hoek, G. 2012. Respiratory health effects of airborne particulate matter: the role of particle size, composition, and oxidative potential - the RAPTES project. Environmental Health Perspectives, 120(8), 1183-1189.

Venkatachari, P., Hopke, P. K., Grover, B. D., Eatough, D. J. 2005. Measurement of particle-bound reactive oxygen species in rubidoux aerosols. Journal of Atmospheric Chemistry, 50, 49–58.

Venkatachari, P., Hopke, P. K., Brune, W. H., Ren, X., Lesher, R., Mao, J., Mitchell, M. 2007. Characterization of wintertime reactive oxygen species concentrations in Flushing, New York. Aerosol Science and Technology, 41, 97–111.

Verma, V., Sioutas, C., Weber, R. J. 2018. Oxidative Properties of Ambient Particulate Matter - An Assessment of the Relative Contributions from Various Aerosol Components and Their Emission Sources. Multiphase Environmental Chemistry in the Atmosphere, 389–416.

Vidrio, E., Jung, H., Anastasio, C. 2008. Generation of hydroxyl radicals from dissolved transition metals in surrogate lung fluid solutions. Atmospheric Environment, 42 (18), 4369−4379.

Wang, H., Joseph, J. A. 1999. Quantifying cellular oxidative stress by dichlorofluorescein assay using microplate reader. Free Radical Biology & Medicine, 27, 612–616.

Wang, Y., Arellanes, C., Curtis, D. B., Paulson, S. E. 2010. Probing the source of hydrogen peroxide associated with coarse mode aerosol particles in Southern California. Environmental Science & Technology, 44(11), 4070-4075.

Wang, M., Beelen, R., Eeftens, M., Meliefste, K., Hoek, G., Brunekreef, B. 2012. Systematic evaluation of land use regression models for NO_2. Environmental Science & Technology, 46(8), 4481-4489.

Wang, J., Lin, X., Lu, L., Wu, Y., Zhang, H., Lv, Q., Liu, W., Zhang Y., Zhuang, S. 2019. Temporal variation of oxidative potential of water soluble components of ambient PM2. 5 measured by dithiothreitol (DTT) assay. Science of The Total Environment, 649, 969-978.

WHO 2013. Review of evidence on health aspects of air pollution – REVIHAAP. First Results. WHO's Regional Office for Europe, Copenhagen, 28 pp., http://www.euro.who.int/ data/ assets/pdf file/0020/182432/e96762-final.pdf, 2013.

Wong, J. P., Tsagkaraki, M., Tsiodra, I., Mihalopoulos, N., Violaki, K., Kanakidou, M., Sciare, J., Nenes, A., Weber, R. J. 2019. Effects of atmospheric processing on the oxidative potential of biomass burning organic aerosols. Environmental Science & Technology, *53*(12), 6747-6756.

Xie, Y., Chen, T. B., Lei, M., Yang, J., Guo, Q. J., Song, B., Zhou, X. Y. 2011. Spatial distribution of soil heavy metal pollution estimated by different interpolation methods: Accuracy and uncertainty analysis. Chemosphere, 82(3), 468-476.

Yang, A., Janssen, N. A., Brunekreef, B., Cassee, F. R., Hoek, G., Gehring, U. 2016. Children's respiratory health and oxidative potential of PM2.5: the PIAMA birth cohort study. Journal of Occupational and Environmental Medicine, 73(3), 1

6.3 (A7) Lichen transplants for high spatial resolution biomonitoring of Persistent Organic Pollutants (POPs) in a multi-source polluted area of Central Italy

Ecological Indicators (2021), 120, 106921, doi: 10.1016/j.ecolind.2020.106921

Lorenzo Massimi[1], Federica Castellani[2,3], Carmela Protano[2*], Marcelo Enrique Conti[4], Arianna Antonucci[2], Maria Agostina Frezzini[1], Mara Galletti[5], Giustino Mele[4], Andrea Pileri[5], Martina Ristorini[6], Matteo Vitali[2], Silvia Canepari[1]

[1] Department of Chemistry, University of Rome La Sapienza, P.le Aldo Moro, 5, 00185 Rome, Italy;
[2] Department of Public Health and Infectious Diseases, University of Rome La Sapienza, P.le Aldo Moro, 5, 00185 Rome, Italy;
[3] Department of Ecological and Biological Sciences, Tuscia University, Largo dell'Università snc, 01100 Viterbo, Italy
[4] Department of Management, University of Rome La Sapienza, Viale del Castro Laurenziano 9, 00161 Rome, Italy;
[5] ARPA Umbria, Via Carlo Alberto dalla Chiesa, 23, 05100, Terni, Italy
[6] Department of Bioscience and Territory, University of Molise, Pesche (IS), 86090, Italy;
*Corresponding author

Keywords: Biomonitor; *Evernia prunastri*; Polychlorinated dibenzodioxins; Polychlorinated dibenzofurans; Polychlorinated biphenyl

Abstract

The ability of lichen transplant *Evernia prunastri* (L.) Ach. to reflect air concentration and spatial distribution of 7 polychlorinated dibenzodioxins (PCDDs), 10 polychlorinated dibenzofurans (PCDFs), and 23 polychlorinated biphenyls (PCBs) was evaluated through the construction of a wide and dense biomonitoring network. For this purpose, 23 lichen transplants were placed in a highly polluted area in Central Italy, characterized by the presence of different local emission sources such as a power plant, a steel plant, vehicular traffic, and domestic heating. The high spatial resolution data obtained from lichens were used to map the spatial distribution of the studied compounds, useful to identify the location and strength of target compounds sources over the territory. The maps showed that the highest concentrations of the pollutants were detected, as expected, in the sites close to the power plant and to the steel plant, confirming their important role as persistent pollutants emission sources. The statistical analysis performed on the spatially resolved data allowed us to identify the steel plant as the main source of PCDD/Fs, while PCBs were emitted by both the steel plant and the power plant. Finally, the efficiency of lichen transplants to reflect PCDD/Fs and PCBs atmospheric concentrations was assessed by comparing lichen data with POPs deposition measured by bulk deposition samplers at sites impacted by intensive emission sources; good results were achieved from the comparison (R^2 > 0.79). Lichen transplants have demonstrated to be suitable biomonitors of POPs, allowing to obtain a high spatial monitoring network. The low-cost biomonitoring and experimental approach described in this study can be applied to other monitoring campaigns for identifying localizing emission sources of POPs in areas contaminated by several disaggregated sources.

1. Introduction

The International Agency for the Research on Cancer (IARC) classified outdoor air pollution as Group 1 carcinogen (i.e., carcinogenic to humans) (IARC, 2016), confirming the great concern for public health due to air quality issue. Air pollutants are a complex mixture of inorganic and organic compounds, and many of them are of toxicological interest. A relevant group of air pollutants is the so-called Persistent Organic Pollutants (POPs), including polychlorinated dibenzodioxins (PCDDs), polychlorinated dibenzofurans (PCDFs) and polychlorinated biphenyls (PCBs) (Avino and Russo, 2018). These compounds are released into the environment from different combustion sources, such as domestic heating, vehicle and industrial emissions (e.g., waste-to-energy plants), but also from processes of metal forming and machining that involve elemental chlorine (Alcock et al., 2001 Yu et al., 2006; Eckhardt et al., 2007; Li et al., 2010; Thacker et al., 2010; Protano et al., 2015). When PCDD/Fs and PCBs are released in the atmosphere, they are distributed between gas and particulate phases depending on concentration, chemical-physical properties, meteorological parameters (e.g., temperature, wind speed, humidity), and air particulate matter (PM) levels (Hoff et al., 1996; Mi et al., 2012; Barbas et al., 2018).

The relevance of PCDD/Fs and PCBs as air pollutants is due to their toxicity and ability to persist in the environment for a long time and to biomagnify through the food chain (Thakur and Pathania, 2020). Therefore, the study of the spatial distribution of POPs over the territory is essential to assess environment-related human health risks (Vitali et al., 2019). However, to date, some limitations reduce the possibility to perform appropriate environmental monitoring campaigns for these pollutants. The main restriction is related to sampling duration and volume flow rate (24h and 2.3 $m^3 h^{-1}$, usually), that do not permit to detect low air levels of target pollutants (Augusto et al., 2013). Besides, conventional air samplers and/or bulk deposition samplers cannot be placed in numerous sites due to their expensiveness and logistic problems (Gao et al. 2015; Kardel et al. 2018). Consequently, POPs dispersion over the territory is typically estimated through mathematical models, often revealing limitations due to the complexity of the represented system (Irwin, 2014; Vitali et al., 2016; Kim et al., 2017). The development of "smart" and low-cost air monitoring systems that allow overcoming the described limitations could be useful for refining dispersion model predictions. For this reason, over the last decades, the development of methods using plants, algae, lichens, and mosses as biomonitors generated increasing interest due to their easy in operation, rapidity, and inexpensiveness (Conti and Cecchetti, 2001; Protano et al., 2015; Massimi et al., 2019; Ndlovu et al., 2019). Lichens are considered effective tools for a long-term sampling of air pollutants because of their ability to accumulate many different contaminants and their suitability for different scenarios (Sett et al., 2016). Accumulation of detectable amounts of air pollutants in lichens depends on several factors, such as chemical-physical properties of the compound (e.g., solubility in water and vapor pressure), its air concentration, atmospheric conditions over the sampling period (e.g., temperature, rainfall) and the lichen species. Biomonitoring campaign may be carried out by using native (i.e., lichens already present in the area) or transplanted lichens (i.e., species collected from unpolluted sites and transplanted into the study area; Bergamaschi et al., 2007; Augusto et al., 2013; Van der Wat and Forbes, 2014). However, lichen transplants are more suitable to achieve an extended monitoring network that allows

studying the spatial distribution of atmospheric pollutants (Protano et al., 2014; Conti et al., 2016; Lucadamo et al., 2016; Vannini et al., 2017).

Bulk deposition sampler, a passive monitoring method that allows collecting both wet and dry atmospheric depositions, is another monitoring tool frequently used to assess outdoor air quality(Jones and Duarte-Davidson, 1997; Fang et al., 2011; Argiriadis et al., 2014; Qu et al., 2019) Although it could be reductive to consider lichens just passive collectors, due to the complexity of the processes governing the bioaccumulation, numerous studies suggest that lichen thalli might reflect the air pollutants deposition from the atmosphere (Tyler, 1989; Sloof, 1995; Reis et al., 1999; Bari et al., 2001; Godinho et al., 2008). Therefore, in this study, POPs accumulation in transplanted lichens was compared with POPs deposition measured by bulk deposition samplers at sites impacted by the most intensive emission sources of the study area. The aim of this study is to use the low-cost lichen transplants for obtaining high spatial resolution data of POPs and mapping their spatial distribution, in order to evaluate the efficiency of lichen transplants to reflect PCDD/Fs and PCBs atmospheric concentrations and to assess PCDD/Fs and PCBs spatial variability according to the different strength of the sources present over the territory. To this aim, we built a wide and dense biomonitoring network (i.e. 23 biomonitoring sites, about 1 km between each other) across Terni, a very polluted area in Central Italy, characterized by the presence of numerous and diversified emission sources of air pollutants, and we performed a long-term air monitoring campaign by using transplanted lichens.

2. Materials and methods

2.1 Study area

Lichen transplants (*E. prunastri*) were placed at 23 monitoring sites in Terni, one of the most polluted areas of Central Italy (Moroni et al., 2013). Terni is a small city (212 km^2) characterized by the presence of several urban and industrial emission sources (vehicular traffic, domestic heating, a power plant for waste treatment and a steel plant) (Guerrini, 2012) and by peculiar meteorological conditions, which limit air mixing and air pollutants transport (Ferrero et al., 2012). The biomonitoring campaign was carried out for 13 months, from December 17th, 2016 to January 15th, 2018.

2.2. Sampling sites

The individuation of the most appropriate monitoring sites, as described in Massimi et al. (2017, 2020a, 2020b), was challenging and time-consuming. Indeed, the 23 monitoring sites were selected with the aim to represent the contribution of the emission sources present over the territory. The sampling sites were chosen with the support and help of ARPA Umbria (regional agency for environmental protection), which provided us a PM_{10} dispersion grid that was used as a reference system and recommended us the best locations for the deployment of the lichen transplants, according to their previous PM and POPs monitoring and analyses. The lichen transplants were deployed in order to cover the whole basin with a spatial resolution of about 1 km and to be as close as possible to potential local POPs sources. For each selected monitoring site, geographical coordinates, type of site, and main local emission sources are reported in Table 1. In each of the 23 sites, a

lichen transplant was deployed. At 4 of the 23 monitoring sites (Ind-MA, Ind-PR, Urb-LG, Res-BR), selected on a geographical approach (respectively, one for each north, south, east and west direction) and on the basis of different levels of air pollution previously measured by ARPA Umbria, data of bulk deposition samplers for monitoring POPs concentrations were used and compared with lichen data to assess their efficiency (Figure 1).

Table 1. Name, type of site, main local emission sources, and geographical coordinates of the 23 monitoring sites in Terni city.

		Geographical Coordinates	
Site	**Type of site and main emission source**	**Latitude**	**Longitude**
Ind-RI	Industrial, power plant	42° 33′ 52.02" N	12° 35′ 21.94" E
Ind-MA	Industrial, power plant	42° 33′ 41.42" N	12° 36′ 19.05" E
Ind-FA	Industrial, power plant	42° 33′ 03.19" N	12° 36′ 29.76" E
Ind-GI	Industrial, power plant	42◦ 34′ 06.28" N	12° 36′ 48.27" E
Ind-FR	Industrial, power plant	42° 33′ 53.22" N	12° 37′ 11.44" E
Ind-CB	Industrial, power plant	42° 33′ 20.30" N	12° 37′ 20.45" E
Res-PI	Residential, domestic heating	42° 32′ 56.96" N	12° 37′ 52.26" E
Res-BR	Residential, domestic heating	42° 34′ 56.19" N	12° 37′ 23.30" E
Res-AR	Residential, domestic heating	42° 34′ 34.23" N	12° 37′ 39.88" E
Ind-CR	Industrial, power plant	42° 34′ 09.49" N	12° 37′ 39.81" E
Urb-HG	Urban, vehicular traffic	42° 34′ 19.32" N	12° 37′ 56.02" E
Urb-SA	Urban, vehicular traffic	42° 33′ 45.16" N	12° 38′ 18.45" E
Urb-PV	Urban, vehicular traffic	42° 33′ 06.96" N	12° 38′ 35.20" E
Urb-LG	Urban, vehicular traffic	42° 32′ 59.75" N	12° 39′ 01.16" E
Urb-CZ	Urban, vehicular traffic	42° 34′ 06.90" N	12° 38′ 52.97" E
Urb-HV	Urban, vehicular traffic	42° 33′ 58.33" N	12° 39′ 04.74" E
Urb-UC	Urban, vehicular traffic	42° 33′ 38.09" N	12° 38′ 47.62" E
Urb-CA	Urban, vehicular traffic	42° 33′ 39.01" N	12° 39′ 03.11" E
Ind-CO	Industrial, steel plant	42° 33′ 34.23" N	12° 39′ 22.62" E
Ind-RO	Industrial, steel plant	42° 33′ 51.16" N	12° 39′ 39.15" E
Ind-OB	Industrial, steel plant	42° 34′ 18.64" N	12° 40′ 05.57" E
Ind-PR	Industrial, steel plant	42° 34′ 20.30" N	12° 40′ 44.23" E
Ind-CP	Industrial, steel plant	42° 33′ 31.65" N	12° 40′ 36.04" E

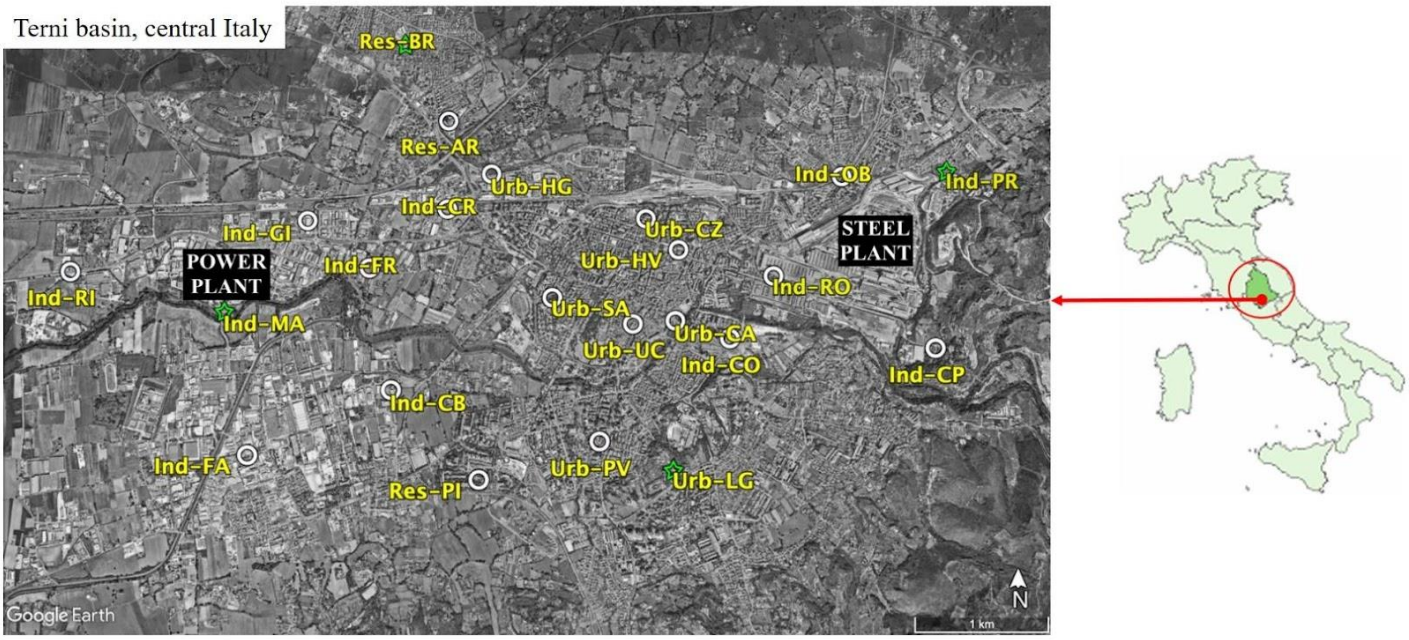

Figure 1. Map of the 23 monitoring sites (Ind-RI, Ind-MA, Ind-FA, Ind-GI, Ind-FR, Ind-CB, Res-PI, Res-BR, Res-AR, Ind-CR, Urb-HG, Urb-SA, Urb-PV, Urb-LG, Urb-CZ, Urb-HV, Urb-UC, CA, Ind-CO, Ind-RO, Ind-OB, Ind-PR, Ind-CP) in Terni. The sites where deposition samplers and lichen transplants are both present are marked with a green star (Ind-PR, Res-BR, Urb-LG, Ind-MA; Google Earth).

2.3 Lichen collection and transplant

The suitability of *E. prunastri* to subsist in diverse environments over time was previously tested (Conti et al., 2004). However, as recommended by VDI (Verein Deutscher Ingenieure; the Association of German Engineers)a pre-conditioning study was conducted to minimize the effects of additional factors than air pollution (Castellani et al., 2020; VDI, 1991, 1995). Thalli were previously transplanted for three months at the same collection sites (i.e., two or three trees in which we installed lichen transplants) of the National Park of Abruzzo (Boudreault et al., 2013). At the end of this control study, lichens looked healthy, and the sample loss was negligible (< 5% of samples).

Lichen collection was extensively described in Massimi et al. (2019). Briefly, in November 2016, *E. prunastri* thalli were collected at National Park of Abruzzo (Central Italy; 41°48′30.2″N; 13°47′11.3″E), an unpolluted area sited 120 km away from Terni. All thalli were gathered from trees stumps with inclination < 10%, at the height of 1–2 m above the terrain. Then, 10 g of thalli was split into two parts of 5 g, fixed on a support composed of two plastic nets and transplanted at the 23 selected monitoring sites (Figure 1). Standard deviations of distributions of the POPs analyzed in the two subsamples were all below 20% and results confirmed data homogeneity for subsamples. Thus, we merged data of the analyzed subsamples. To ensure homogeneous and representative sampling conditions, all biomonitors were located 2 m above the ground with the same southern exposition. After the exposure period (13 months), the transplanted lichens were collected, stored in a cooler, and transported to the laboratory. In the laboratory, as described in Conti et al. (2004),

unwashed lichen samples were sorted to remove as much extraneous material (i.e., soil, mosses, other lichen species, etc.) and stored in the dark at < -10 °C in closed containers. Once taken out of the freezer, thermal equilibrium with the external temperature was established and then the samples were dried for 48 h at 35°C until constant weight and extracted following the EPA 1613: 1994 method. The samples were then pulverized by using a ball mill.

2.4 Deposition samples

Atmospheric depositions of organic pollutants were assessed by using bulk collectors, that allow the sampling of both wet and dry depositions. Each collector, consisting of a funnel connected to a polytetrafluoroethylene bottle, was exposed to the atmosphere for one month. Considering the whole duration of the monitoring campaign (13 months), 13 deposition samples were collected at each of the 4 monitoring sites (Ind-PR, Res-BR, Urb-LG, Ind-MA; Figure 1).

2.5 Analytical determinations

2.5.1 Analytical determination for lichen samples

Lichen samples were analyzed immediately after the collection from the unpolluted site, in order to obtain PCDD/Fs and PCBs initial concentration (blank), and after 13 months of exposure.

The set of analyses was carried out by the laboratory of the Terni district of the Environmental Protection Agency of Umbria (Italy), accredited in accordance with ISO/IEC 17025 standards. The determination of target analytes was performed by using a gas chromatograph coupled to high resolution magnetic sector mass spectrometry (DFS Magnetic Sector GC-HRMS) (Thermo Scientific, Bremen, Germany). All the lichen samples were extracted by accelerated solvent extraction (ASE; Thermo Scientific Dionex ASE 350 Accelerated Solvent Extractor). Briefly, 3 g of grinded thalli were added with 50 µL of $^{13}C_{12}$-labelled polychlorinated biphenyls surrogates standard solutions at 10 ng mL^{-1} in isoctane (PCB-28, PCB-31, PCB-44, PCB-52, PCB-77, PCB-95, PCB-99, PCB-101, PCB-105, PCB-110, PCB-118, PCB-123, PCB-128, PCB-138, PCB-146, PCB-149, PCB-151, PCB-153, PCB-157, PCB-167, PCB-170, PCB-180, PCB-187) and 50 µL of $^{13}C_{12}$-labelled dioxins/furans surrogates standard solutions at 4-8 ng mL^{-1} in isoctane (2,3,7,8-TCDD, 1,2,3,7,8-PeCDD, 1,2,3,4,7-HxCDD, 1,2,3,6,7,8-HxCDD, 1,2,3,7,8,9-HxCDD, 1,2,3,4,6,7,8-HpCDD, OCDD, 2,3,7,8-TCDF, 2,3,4,7,8-PeCDF, 1,2,3,7,8-PeCDF, 1,2,3,4,7,8-HxCDF, 1,2,3,6,7,8-HxCDF, 1,2,3,7,8,9-HxCDF, 2,3,4,6,7,8-HxCDF, 1,2,3,4,6,7,8-HpCDF, 1,2,3,4,7,8,9-HpCDF, OCDF). After isotopic enrichment, samples were extracted with two consecutive ASE cycles at 150°C and 1500 psi by a mixture hexane/acetone (50:50). Extracts (about 20 mL each) were then purified to minimize interferences by a multilayer column (Na_2SO_4, silica, $NaHCO_3$ - Na_2SO_4 mixture, 12 mL H_2SO_4 96% - 20 g celite mixture, Na_2SO_4). The column was eluted with 70 mL hexane, the eluate was concentrated by rotary evaporator to about 2 mL, quantitatively transferred to the top of a second column packed with basic alumina. This second column was washed with 10 mL hexane (not collected) and eluted with 40 mL of n-hexane-dichloromethane

mixture (50:1) to collect PCBs and then with 60 mL of n-hexane-dichloromethane mixture (50:50) to collect PCDD/Fs. Both eluates were evaporated to dryness under a gently nitrogen flux and, finally, recovered with 50 μL of 2,2,4-trimethylpentane. The quantification of all the analytes and $^{13}C_{12}$-surrogate/internal standards was performed by isotopic dilution technique applied on the two most abundant product ions for native and ^{13}C-labelled standard, respectively.

Despite the complexity of the applied analytical determination, the recoveries for all the analyzed compounds were between 60% and 120%, in accordance with EPA method 1613:1994.

2.5.2 Analytical determination for deposition samples

The 13 deposition samples collected in each of the four selected sites were analyzed for their content in PCDD/Fs and PCBs. Briefly, all samples were spiked with 50 μL of $^{13}C_{12}$-labelled PCBs and 50 μL of $^{13}C_{12}$-labelled PCDD/Fs surrogate standard solutions, the same used for lichen samples. After the isotopic enrichment, samples were filtered by glass fiber filters, the filtrate was added with dichloromethane (DCM; 20:1 v/v; 50 mL of DCM each liter of filtrate), and the organic phase was collected. The glass fiber filters were then extracted by ASE, applying the same conditions used for lichens. The two final extracts (the organic phase and the ASE extract of each deposition sample) were then gathered together, treated, and analyzed, as previously indicated for lichen extracts.

2.6 Meteorological Records

Meteorological data were recorded in Terni by a WatchDog 2000 Series weather Station (model 2700; Spectrum Technologies Ltd., Bridgend, Wales, UK) located on the top of a building at Urb-AR sampling site, 30 m above ground level, in order to avoid street canyon interference effects on the wind speed and direction. Wind speed (m/s), wind direction (degrees) and wind gust (m/s) were recorded during all the monitoring campaign, from December 17th, 2016 to January 15th, 2018. The wind rose for the entire monitoring period was created using the software WRPLOT View 7.0 – Freeware (Lakes Environmental Consultants Inc., Waterloo, ON, Canada).

2.7 Data elaboration and statistical analysis

2.7.1 Spatial mapping of POPs

Concentrations of PCDD/Fs and PCBs found in lichen samples after 13 months of exposure in the 23 sampling sites were mapped by using the ArcMap 10.3.1 software (ArcGis Desktop; ESRI, Redlands, CA, USA). Ordinary kriging (OK) was used to estimate pollutant concentrations in the unmeasured locations in order to obtain a continuous surface (Johnston et al., 2001; Kumar et al., 2007). Kriging is a geostatistical interpolation technique that considers both the distance and the degree of variation between known data points to estimate values in unknown areas (Paramasivam and Venkatramanan, 2019). In the OK, data derives from a stochastic process, which is divided into a constant but unknown trend component and an error component (Beelen et al., 2009). The OK estimator is given by a linear combination of the observed values with weights, which are

derived from the kriging equations using a semivariogram function (Xie et al., 2011). The experimental semivariances were fitted by a spherical function, by weighted least-squares approximation (Jian et al., 1996). This function was then used for the kriging.

2.7.2 Multivariate statistical analysis

Multivariate statistical analysis was carried out by using the statistical software R (R-project for statistical computing, Ver. 3.0, 32-bit). Principal component analysis (PCA) was performed on the spatially resolved concentrations of PCDD/Fs and PCBs to cluster the tracers of the main emission sources over the territory. Before performing the PCA, the matrix of the data was transformed by column mean centering and row and column autoscaling in order to correct for different variable scaling and units.

3. Results and discussion

3.1 Accumulation of POPs in lichen transplants

Tables 2 (PCBs) and 3 (PCDD/Fs) report the concentrations (ng kg^{-1} dw) of the monitored compounds found in the blank sample and in the 23 exposed lichens, the limits of detection (LOD), calculated at the concentration at which signal to noise ratio (S/N) of each compound is > 3, and the sum of concentrations of the compounds recorded at each site.

Table 2. Limits of detection (LOD), concentrations of single congeners (ng kg^{-1} dw), and the sum of concentrations (ng kg^{-1} dw) of PCBs determined in the blank sample and the 23 exposed lichens in Terni.

ng kg^{-1}	LOD	Blank	Ind-RI	Ind-MA	Ind-FA	Ind-GI	Ind-FR	Ind-CB	Res-PI	Res-BR	Res-AR	Ind-CR	Urb-HG	Urb-SA	Urb-PV	Urb-LG	Urb-CZ	Urb-HV	Urb-UC	Urb-CA	Ind-CO	Ind-RO	Ind-OB	Ind-PR	Ind-CP
PCB-28	0.61	19	67	134	90	124	68	92	73	112	144	130	51	104	69	96	151	63	85	173	57	108	92	182	42
PCB-31	0.61	137	<LOD	<LOD	<LOD	<LOD	<LOD	<LOD	<LOD	<LOD	<LOD	<LOD	<LOD	<LOD	<LOD	<LOD	3.8	<LOD	<LOD	2.6	<LOD	<LOD	<LOD	9.5	<LOD
PCB-44	0.61	2.1	34	93	46	48	26	41	21	37	36	51	16	40	18	28	119	19	31	48	31	60	41	64	20
PCB-52	0.61	30	20	131	36	48	10	32	11	24	26	49	<LOD	32	0,97	23	165	16	18	40	18	62	42	68	6.1
PCB-77	0.15	25	<LOD	3.1	<LOD	19	3.4	<LOD	<LOD	<LOD	<LOD	<LOD	<LOD	<LOD	<LOD	1.2	<LOD	1.2	<LOD	5.1	<LOD	26	2.2	27	<LOD
PCB-95	0.61	46	<LOD	96	8.6	29	<LOD	<LOD	<LOD	<LOD	<LOD	23	<LOD	<LOD	<LOD	2.2	77	<LOD	<LOD	15	<LOD	62	33	55	<LOD
PCB-99	0.61	17	12	73	16	34	13	18	3.6	6.1	2.8	24	<LOD	3.6	<LOD	13	30	6.1	16	24	8.9	47	32	54	5.5
PCB-101	0.61	88	<LOD	136	<LOD	45	<LOD	<LOD	<LOD	<LOD	<LOD	26	<LOD	<LOD	<LOD	0.51	35	3.5	<LOD	13	<LOD	95	50	100	<LOD
PCB-105	0.15	15	131	314	124	137	188	114	103	151	137	140	90	121	16	101	82	123	181	246	135	1076	229	406	93
PCB-110	0.61	<LOD	134	334	132	209	131	152	43	93	72	173	76	86	42	97	131	96	134	174	102	326	224	332	88
PCB-118	0.15	74	93	342	78	290	182	131	77	57	47	150	30	44	<LOD	79	62	94	113	175	59	512	198	376	31
PCB-123	0.15	<LOD	5.3	12	4.6	17	9.3	7.4	7.4	5.5	5.2	8.8	2.9	5.7	0.61	5.5	5.5	8.1	6.8	11	5.9	37	10	14	3.6
PCB-128	0.61	<LOD	20	77	38	7.3	42	23	<LOD	<LOD	3.3	16	20	6.7	4.8	15	12	0.34	28	21	1.8	80	15	72	29
PCB-138	0.61	8.6	128	358	129	282	154	162	107	100	83	196	88	94	33	85	78	117	141	197	106	427	250	403	98
PCB-146	0.61	41	<LOD	<LOD	<LOD	<LOD	<LOD	<LOD	<LOD	<LOD	<LOD	<LOD	<LOD	<LOD	<LOD	<LOD	<LOD	<LOD	<LOD	<LOD	<LOD	5.3	<LOD	8.1	<LOD
PCB-149	0.61	13	64	177	89	140	71	66	43	50	41	101	37	48	17	44	58	60	85	101	55	201	148	187	53
PCB-151	0.61	7.2	11	37	20	28	12	12	6.2	9.9	5.8	21	5.1	7.4	<LOD	7.7	13	7.2	17	20	9.7	44	34	40	9.8
PCB-153	0.61	62	59	236	80	186	77	87	36	42	23	122	25	25	<LOD	44	34	14	87	127	48	291	182	291	38
PCB-157	0.15	1.4	8.9	34	10	40	17	19	13	9.4	10	24	8.6	9.1	1.1	6.5	2.9	9,1	14	20	11	107	20	40	7.3

PCB-167	0.15	2.3	9.1	31	8.6	26	14	13	9.8	8.6	7.1	16	6.4	7.3	0.79	5.9	4.1	5.3	9.7	16	7.5	54	19	34	5.2
PCB-170	0.61	1.7	92	177	95	198	114	129	93	86	61	139	85	71	32	60	68	64	110	133	95	342	189	306	100
PCB-180	0.61	33	75	193	94	202	110	129	83	90	65	142	66	58	10	55	112	15	119	152	93	356	193	301	100
PCB-187	0.61	10	35	102	58	86	55	47	41	55	34	70	28	33	12	32	54	67	69	77	46	138	90	132	49
ΣPCBs	-	634	1000	3092	1157	2197	1298	1275	772	937	802	1621	636	794	258	802	1295	791	1263	1791	890	4456	2092	3503	776

Table 3. Limits of detection (LOD), concentrations of single congeners (ng kg^{-1} dw), and the sum of concentrations (ng kg^{-1} dw) of PCDFs and PCDDs determined in the blank sample and the 23 exposed lichens in Terni.

ng kg^{-1}	**LOD**	**Blank**	**Ind-RI**	**Ind-MA**	**Ind-FA**	**Ind-GI**	**Ind-FR**	**Ind-CB**	**Res-PI**	**Res-BR**	**Res-AR**	**Ind-CR**	**Urb-HG**	**Urb-SA**	**Urb-PV**	**Urb-LG**	**Urb-CZ**	**Urb-HV**	**Urb-UC**	**Urb-CA**	**Ind-CO**	**Ind-RO**	**Ind-OB**	**Ind-PR**	**Ind-CP**
2,3,7,8-TCDF	0.061	0.33	0.23	0.078	0.29	0.49	0.27	0.49	0.38	0.39	0.21	0.24	0.15	0.11	<LOD	0.41	<LOD	0.52	0.38	0.61	0.17	0.52	0.44	1.6	<LOD
1,2,3,7,8-PCDF	0.061	<LOD	0.41	0.21	0.35	0.48	0.44	0.58	0.55	0.47	0.37	0.48	0.37	0.33	0.089	0.31	0.24	0.58	0.66	0.56	0.35	0.61	0.53	1.4	0.21
2,3,4,7,8-PCDF	0.031	0.041	0.43	0.29	0.35	0.84	0.46	0.62	0.58	0.47	0.42	0.63	0.39	0.31	0.098	0.47	0.23	0.61	0.58	0.71	0.35	0.67	0.71	1.8	0.24
1,2,3,4,7,8-HxCDF	0.061	0.13	0.28	0.17	0.22	0.73	0.31	0.41	0.45	0.29	0.26	0.34	0.27	0.22	<LOD	0.29	0.12	0.41	0.35	0.51	0.27	0.49	0.39	1.1	0.097
1,2,3,6,7,8-HxCDF	0.061	0.11	0.29	0.19	0.47	0.58	0.29	0.36	0.41	0.28	0.26	0.37	0.27	0.23	<LOD	0.29	0.13	0.35	0.36	0.46	0.27	0.48	0.46	1.1	0.084
2,3,4,6,7,8-HxCDF	0.061	0.21	0.18	0.084	0.14	0.64	0.19	0.33	0.29	0.25	0.18	0.34	0.16	0.11	<LOD	0.19	<LOD	0.27	0.29	0.31	0.22	0.37	0.27	0.84	<LOD
1,2,3,7,8,9-HxCDF	0.061	<LOD	0.066	<LOD	<LOD	0.17	0.076	0.12	0.11	0.068	0.11	0.15	0.086	<LOD	<LOD	0.061	<LOD	0.12	0.13	0.22	0.061	0.15	0.14	0.29	<LOD
1,2,3,4,6,7,8-HpCDF	0.061	0.34	0.65	0.53	0.77	1.3	0.69	1.1	1.3	0.81	0.82	1.1	0.82	0.49	<LOD	0.57	0.24	1.1	0.95	1.1	0.95	1.2	1.2	2.2	0.33
1,2,3,4,7,8,9-HpCDF	0.061	0.071	0.086	<LOD	0.21	0.24	0.093	0.29	0.35	0.57	0.086	0.12	0.29	<LOD	<LOD	0.17	<LOD	0.16	0.084	0.085	0.15	0.12	0.11	0.29	0.19
OCDF	0.061	<LOD	0.26	0.51	0.38	0.48	0.57	0.41	0.35	0.29	0.33	0.44	0.38	0.24	0.19	0.22	0.16	0.39	0.44	0.52	0.47	0.42	1.1	0.69	0.21
ΣPCDFs	-	1.2	2.9	2.1	3.2	6.1	3.4	4.8	4.7	3.9	3.1	4.2	3.2	2.1	0.38	3.1	1.1	4.6	4.2	5.1	3.3	5.1	5.3	11	1.4
2,3,7,8-TCDD	0.031	0.031	<LOD	<LOD	0.037	0.13	<LOD	<LOD	<LOD	0.039	<LOD	<LOD	<LOD	<LOD	<LOD	<LOD	<LOD	0.038	0.11	0.053	0.042	<LOD	<LOD	0.073	<LOD
1,2,3,7,8-PCDD	0.031	<LOD	0.076	0.034	0.081	0.075	0.12	0.089	0.12	0.095	0.089	0.087	0.11	0.068	<LOD	0.11	0.049	0.099	0.14	0.086	0.076	0.12	0.068	0.24	<LOD

1,2,3,4,7,8-HxCDD	0.091	<LOD	<LOD	<LOD	<LOD	0.23	<LOD	<LOD	<LOD	0.092	<LOD	<LOD	<LOD	<LOD	<LOD	<LOD	<LOD	<LOD	<LOD	<LOD	<LOD	<LOD	0.11	<LOD
1,2,3,6,7,8-HxCDD	0.091	<LOD	0.15	<LOD	<LOD	0.19	0.11	0.14	0.12	0.095	<LOD	0.11	<LOD	<LOD	<LOD	<LOD	<LOD	0.11	0.11	0.14	<LOD	0.17	0.14	0.31	<LOD
1,2,3,7,8,9-HxCDD	0.091	<LOD	<LOD	<LOD	<LOD	<LOD	<LOD	0.12	0.093	<LOD	0.11	0.14	<LOD	<LOD	<LOD	<LOD	<LOD	0.11	0.13	0.11	<LOD	0.12	0.16	0.22	<LOD
1,2,3,4,6,7,8-HpCDD	0.061	0.15	0.59	0.51	0.77	1.3	0.91	1.1	1.1	0.79	0.64	0.93	0.73	0.45	0.34	0.49	0.31	1.1	1.1	1.1	0.79	1.1	0.97	1.2	0.32
OCDD	0.061	0.17	1.3	1.2	2.7	6.6	6.3	2.6	2.7	1.7	1.5	2.2	1.8	1.4	2.1	1.3	0.92	2.8	3.5	2.7	1.8	2.8	4.2	2.3	0.74
ΣPCDDs	-	0.35	2.1	1.8	3.6	8.5	7.5	4.1	4.1	2.8	2.3	3.5	2.7	1.9	2.4	1.9	1.3	4.3	5.2	4.2	2.7	4.2	5.6	4.4	1.1

The most abundant PCB congeners detected in the study area were PCB-105, PCB-118, and PCB-138 (Table 2). These compounds were quite widespread in the territory, but the highest concentrations were recorded at the industrial sites (Ind-MA, Ind-RO, Ind-PR), confirming the power plant and the steel plant as relevant sources of these compounds (Choi et al., 2008; Liu et al., 2013). Regarding PCDDs and PCDFs (Table 3), the most abundant congeners were 1,2,3,4,6,7,8-HpCDD, OCDD, and 1,2,3,4,6,7,8-HpCDF. This profile is in good agreement with that found by Aristizabal et al. (2011) in an urban environment, and the small discrepancy could be attributed to the different sources of emission present over the two territories.

Table 4 shows the comparison between concentrations (ng kg^{-1} dw) of ΣPCDD/Fs and ΣPCBs measured in Terni and those previously reported for other urban and industrial sites of different geographical areas (Augusto et al., 2009; Protano et al., 2015; Augusto et al., 2016; Vitali et al., 2019).

Table 4. Lowest and highest concentrations (ng kg^{-1} dw) of ΣPCDD/Fs and ΣPCBs in lichens in Terni (present study) and other urban and industrial sites of different geographical areas.

				ΣPCDD/Fs		**ΣPCBs**	
References	**Study Area**	**Lichen Species**	**Exposition Time**	**min**	**max**	**min**	**max**
Augusto et al., 2004	Portugal	Native *Xantoria parietina*	-	73	1913		
Augusto et al., 2007	Portugal	Native *Ramalina canariensis*	-	198	1219		
Augusto et al., 2009	Portugal	Native *Xantoria parietina*	-	171	345	-	-
		Native *Ramalina canariensis*	-	392	1059	-	-
Suutari et al., 2010	Finland	Native *Cladonia* sp.	-	3.3	8.3		
		Native *Bryoria fuscescens*	-	6.5	7.1		
		Native *Usnea* sp.	-	19			
Augusto et al., 2015	Portugal	Native *Xantoria parietina*	-	19	75		
		Native *Ramalina canariensis*	-	12	86		
Protano et al., 2015	Italy	Transplanted *Pseudevernia furfuracea*	3 months for PCBS, 6 months for PCDDs/Fs	60	109	3298	4631
Augusto et al., 2016	Portugal	Transplanted *Ramalina canariensis*	7 months	35	64	-	-
Vitali et al., 2019	Italy	Native *Xantoria parietina*	-	14	114	868	7685
This work	Italy	Tranplanted *Evernia prunastri*	13 months	2.4	16	285	4456

As we can observe from Table 4, the sum of PCDD/Fs (ng kg^{-1} dw) accumulated in lichens in this work is much lower than the levels recorded in the previous studies. Also, PCBs show lower concentrations, despite the fact that the differences are less pronounced and clear, because of the lack of literature data. This difference

between concentrations may be attributed to different sampling conditions, such as the use of different lichen species, the use of native or transplanted biomonitor, and to the different exposure time (Augusto et al., 2013). Moreover, these lower concentrations can also be attributed to the introduction of severe emission limits for European waste incinerator and for industrial plants (Directive 2000/76/EG, 2000) which seem to have been efficiently reduced industrial emission of PCDD/Fs (Bruckmann et al., 2013; Augusto et al., 2015). Although this Directive also deals with PCBs, their decrease in the environment is less pronounced and mostly affects less chlorinated congeners, probably because of their higher gas-phase reactivity (Bruckmann et al., 2013). However, it should be noted that the effects of the Directive on the reduction of the POPs emissions could be successfully evaluated over a very long time, given the persistence of this class of compounds.

3.3 Spatial mapping by using lichen transplants

Concentration data obtained at the 23 monitoring sites (as reported in Tables 3 and 4) were used to map the spatial distribution of the target analytes. The spatial maps represent a simple and efficient method to identify the location and strength of the sources of the studied compounds over the territory (Massimi et al., 2020a; 2020b). Moreover, they provide reliable information about horizontal diffusion of the studied POPs, allowing the assessment of their distribution over the territory.

Figure 3 shows the spatial maps of the sum of $\sum_7$PCDDs (panel a), $\sum_{10}$PCDFs (panel b) and $\sum_{23}$PCBs (panel c).

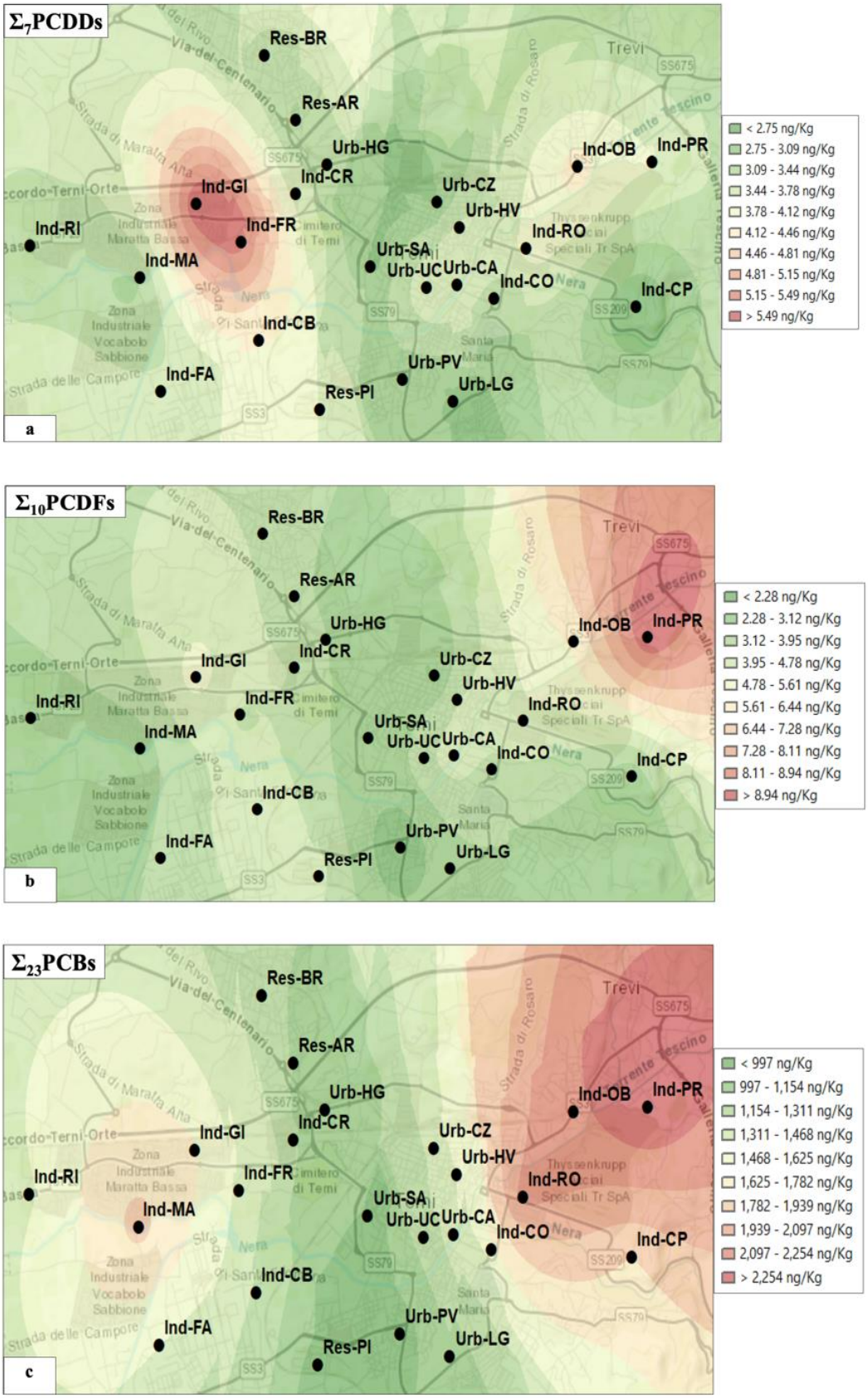

Figure 3. Maps of the spatial distribution of PCDDs (panel a), PCDFs (panel b), and PCBs (panel c) accumulated in lichen transplants after 13 months of exposure.

As shown in Figure 3, the highest concentrations of PCDFs (panel b) (11 ng kg^{-1}, Table 3) were recorded at Ind-PR, located in the proximity to the steel plant (Figure 1). Indeed, steel plants are well known as emission sources of these pollutants, due to several metallurgical processes such as sintering and blast furnace iron making (Choi et al., 2008). High concentrations of PCDD/Fs (8.5 and 6.1 ng $kg^{-1,}$ respectively; Table 3) were also recorded at Ind-GI, sited about 1 km north-east from the power plant. The higher levels found at Ind-GI respect to those recorded at Ind-MA (8.5 vs. 1.8 ng kg^{-1} for PCDDs and 6.1 vs. 2.1 ng kg^{-1} for PCDFs; Table 3), which is the closest site to the power plant, may be attributed to wind-transport. In fact, the Ind-GI area is affected by air currents that can transport the pollutants from Ind-MA (South-West) to Ind-GI (North-East), according to the wind rose obtained by using the acquired meteorological data (Figure 4).

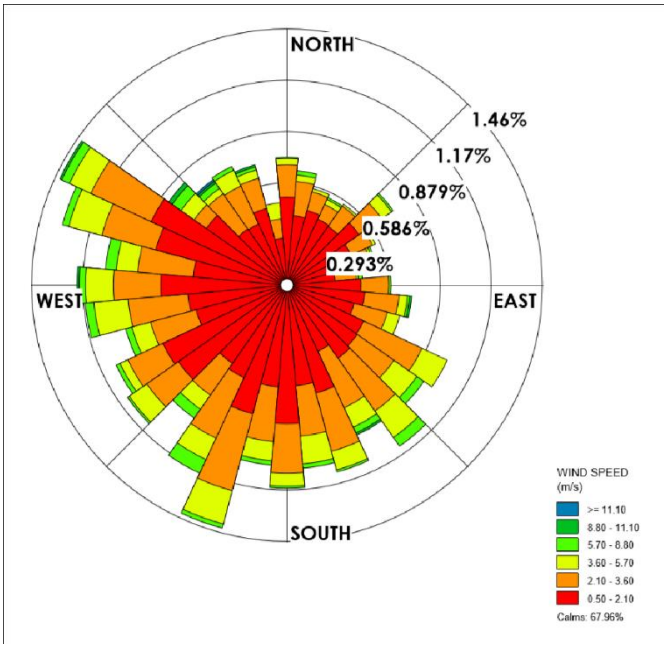

Figure 4. The wind rose of the 13-month monitoring period (WRPLOT View 7.0 – Freeware; Lakes Environmental Consultants Inc., Waterloo, ON, Canada)

The meteorological data confirmed that the weather of Terni is characterized by very-low winds (wind speed lower than 11.10 m/s), whose predominant directions are from South-West to North-East (more intense) and from North-West to South-East. The local circulation is often weak, and this leads to reduced atmospheric layers mixing, which is generally responsible of higher concentrations of air pollutants. This would also explain the elevated concentrations of PCDDs recorded at Ind-FR (7.5 ng kg^{-1}; Table 3). However, except for the two industrial areas, the concentrations of PCDDs and PCDFs were homogeneous in all the city.

Regarding PCBs, high concentrations were recorded at Ind-RO (4456 ng kg^{-1}; Table 2) and Ind-PR (3503 ng kg^{-1}; Table 2), the two prevailing impact sites of the steel plant (Massimi et al., 2019, 2020b). Also, for this class of compounds, the steel plant was confirmed to be a relevant source of organic pollutants, deriving from various thermal processes in the iron and steel industry (Aries et al., 2004). Elevated concentrations of PCBs were also recorded at Ind-MA, underlining the influence of waste incineration as a relevant emission source.

It worth be noting that PCBs are mainly present in the atmospheric gas phase and have a lower residence time in the atmosphere, thus being less horizontally diffused. Differently, PCDD/Fs are mostly coated on PM particles and more easily affected by wind transport (Barbas et al., 2018).

3.4. Principal component analysis on concentrations measured in lichens

PCA was applied to cluster the POPs (loadings) tracing the main emission sources in Terni, according to their different spatial distribution among the 23 sampling sites (scores) during the 13-month monitoring period. The PCA was performed for source identification based on the spatial variability of POPs concentrations; since we had many variables from many different locations, PCA was used to reduce the dimensionality of this data, making much simpler identifying the important spatial patterns and to confirm the results obtained by the spatial mapping of POPs concentrations.

Five significant components accounting for 89.3% were obtained; the variance explained by each component is 59.61%, 15.57%, 6.14%, 5.08% and 2.87% (Table 7). The first and the second PCs (PC1 and PC2) explain the 75.2% of the total variance, were considered. PCA results are summarized in the biplot of Fig. 5, while loadings and scores are shown in Tables 6 and 7, respectively. The biplot well separates 4 clusters of monitoring sites, each characterized by its emission profile. The first cluster, in the central part of the biplot (Figure 5), consists of samples of several monitoring sites (Ind-RI, Ind-FA, Ind-GI, Ind-FR, Ind-CB, Res-PI, Res-BR, Res-AR, Ind-CR, Urb-HG, Urb-SA, Urb-PV, Urb-LG, Urb-CZ, Urb-HV, Urb-UC, CA, Ind-CO, Ind-OB, Ind-CP) and is characterized by the presence of different organic pollutants (PCB-28, PCB-31, PCB-77, PCB-146, 1,2,3,7,8,9-HxCDF, 1,2,3,4,7,8,9-HpCDF, OCDF, 2,3,7,8-TCDD, 1,2,3,4,7,8-HxCDD, 1,2,3,6,7,8-HxCDD, OCDD), which do not show high variance among the samples. This is probably due to the high diffusion in the study area of the POPs characterizing this cluster, mainly released by widespread sources such as vehicular traffic and/or domestic heating and thus showing low concentration variability across the sites. On the contrary, the second and the third cluster are characterized by the presence of the two major impact sites of the steel plant, Ind-RO (on the lower right of the biplot) and Ind-PR (at the top right of the biplot). The monitored geographical area is characterized by the presence of two different organic pollutants emission sources related to the steel plant: Ind-RO, characterized by the prevailing emission of PCBs, and Ind-PR, characterized by the predominant emissions of PCDD/Fs. This emissions trend could be attributed to different steel processes, that probably occur at different temperatures, promoting the formation of one class of compounds rather than another one (Xu et al., 2018). The fourth cluster identified by the biplot is characterized by the presence of the power plant site (Ind-MA) and was dominated by the prevailing emission of PCBs.

Overall, the PCA confirmed the identification, localization and impact assessment of local POPs emission sources, which were individuated in the paragraph 3.3. These results encourage the use of the biomonitoring and experimental approach described in this study in other monitoring campaigns for the individuation and localization of POPs emission sources in areas contaminated by several disaggregated sources.

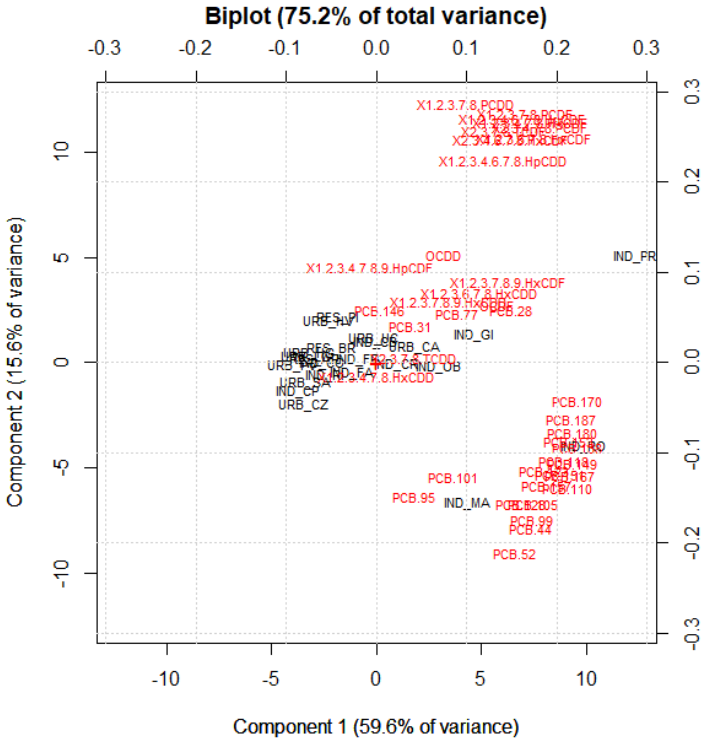

Figure 5. Biplot of the PCA (PC1 and PC2) performed on the concentration data yielded at each monitoring site after 13 months of exposure.

Table 6. Loadings of the five components obtained by the PCA performed on the concentration data yielded at each monitoring site after 13 months of exposure.

	PC1	PC2	PC3	PC4	PC5
2,3,7,8-TCDF	0.14	0.26	0.14	0.087	0.048
1,2,3,7,8-PeCDF	0.16	0.28	0.057	0.072	0.046
2,3,4,7,8-PeCDF	0.18	0.26	0.078	-0.02	0.0033
1,2,3,4,7,8-HxCDF	0.17	0.27	0.0058	0.00089	-0.087
1,2,3,6,7,8-HxCDF	0.17	0.25	0.053	-0.04	-0.022
2,3,4,6,7,8-HxCDF	0.15	0.25	-0.0093	0.018	-0.053
1,2,3,7,8,9-HxCDF	0.15	0.089	0.13	-0.12	-0.14
1,2,3,4,6,7,8-HpCDF	0.16	0.27	-0.027	-0.04	-0.11
1,2,3,4,7,8,9-HpCDF	-0.0064	0.11	0.13	0.26	-0.15
OCDF	0.13	0.064	-0.12	-0.47	0.29
2,3,7,8-TCDD	0.041	0.0047	-0.12	-0.05	0.069
1,2,3,7,8-PeCDD	0.11	0.29	0.052	0.26	0.19
1,2,3,4,7,8-HxCDD	0.00077	-0.014	-0.11	-0.07	-0.016
1,2,3,6,7,8-HxCDD	0.11	0.077	0.18	0.031	0.13
1,2,3,7,8,9-HxCDD	0.081	0.068	0.16	-0.051	0.27
1,2,3,4,6,7,8-HpCDD	0.14	0.22	-0.31	-0.15	-0.22
OCDD	0.075	0.12	-0.48	-0.34	0.11
PCB-28	0.15	0.058	0.25	-0.18	-0.57
PCB-52	0.15	-0.21	0.25	-0.21	-0.19
PCB-101	0.086	-0.13	0.14	0.047	0.14

PCB-153	0.21	-0.087	0.015	-0.067	0.049
PCB-138	0.22	-0.094	-0.01	-0.047	0.0011
PCB-180	0.22	-0.078	-0.07	0.066	0.045
PCB-77	0.091	0.054	-0.022	0.21	-0.021
PCB-123	0.19	-0.12	-0.31	0.18	-0.18
PCB-118	0.21	-0.11	-0.10	0.023	-0.016
PCB-105	0.17	-0.16	-0.19	0.31	-0.071
PCB-167	0.21	-0.12	-0.11	0.087	-0.082
PCB-157	0.19	-0.14	-0.25	0.23	-0.15
PCB-31	0.039	0.041	0.049	0.049	0.091
PCB-44	0.17	-0.18	0.23	-0.19	-0.27
PCB-95	0.042	-0.15	0.13	0.096	0.18
PCB-99	0.17	-0.17	0.17	-0.13	0.11
PCB-110	0.21	-0.14	0.078	-0.098	0.079
PCB-151	0.21	-0.12	0.015	-0.11	0.096
PCB-149	0.22	-0.11	-0.02	-0.12	0.055
PCB-146	0.0042	0.059	0.064	-0.025	0.015
PCB-187	0.22	-0.063	-0.04	-0.023	0.033
PCB-128	0.16	-0.16	0.12	0.17	0.21
PCB-170	0.22	-0.042	-0.09	0.084	0.065

Table 7. Variance % and scores of the five components obtained by the PCA performed on the concentration data yielded at each monitoring site after 13 months of exposure.

	PC1	**PC2**	**PC3**	**PC4**	**PC5**
Variance %	59.61	15.57	6.14	5.08	2.87
Ind-RI	-2.5	-0.62	0.22	0.33	0.38
Ind-MA	4.4	-6.7	2.4	-1.7	0.11
Ind-FA	-1.1	-0.44	0.34	-0.58	-0.14
Ind-GI	4.6	1.4	-2.1	-1.6	-0.94
Ind-FR	-0.83	0.16	-2.1	-0.85	1.2
Ind-CB	-0.054	0.96	-0.081	0.0011	-0.53
Res-PI	-1.8	2.2	-0.94	0.82	-0.71
Res-BR	-2.1	0.71	0.68	1.2	-1.1
Res-AR	-2.9	0.18	0.48	-0.22	-1.3
Ind-CR	0.94	-0.081	0.081	-1.1	-1.1
Urb-HG	-3.2	0.48	-0.23	0.67	0.58
Urb-SA	-3.4	-0.92	0.57	0.21	-0.83
Urb-PV	-3.9	-0.11	0.25	0.43	0.28
Urb-LG	-3.2	0.32	0.44	0.48	-0.38
Urb-CZ	-3.4	-2.1	0.50	0.69	0.85
Urb-HV	-2.1	2.1	-1.1	-0.32	-0.36
Urb-UC	-0.11	1.1	-0.92	-0.27	0.71
Urb-CA	1.8	0.77	0.024	-1.5	-2.1
Ind-CO	-2.6	-0.0054	-0.61	-0.18	0.21
Ind-RO	10	-4.1	-2.9	3.1	-0.39

Ind-OB	3.1	-0.21	-1.2	-3.1	1.5
Ind-PR	12	5.1	3.3	1.1	1.2
Ind-CP	-3.7	-1.3	0.15	1.2	1.1

3.2 Comparison between concentrations measured in lichens and deposition samples

POPs accumulation in transplanted lichens was compared with POPs deposition data obtained by using four deposition samplers at sites impacted by the most intensive emission sources of the study area (Ind-MA, Ind-PR, Urb-LG, Res-BG).

The concentrations found in lichens after 13 months of exposure were compared with the concentrations recorded by using 1-month-exposed bulk deposition samplers. To this aim, the levels obtained by the analysis of deposition samples were averaged to obtain 13-months concentrations. The mean concentrations and the standard deviations obtained from the analysis of the deposition samples are reported in Table 5.

Table 5. Limits of detection (LOD), average concentrations, standard deviations (Std.dev.), and the sum of concentrations of PCBs (ng m^{-2} d), PCDDs (pg m^{-2} d), and PCDFs (pg m^{-2} d), determined in deposition samples in 4 sampling sites.

Deposition samples (ng m^{-2} d)

PCB	**LOD**	**Ind-PR**	**Ind-MA**	**Res-BR**	**Urb-LG**
-28	0.091	0.27	0.14	0.11	<LOD
-31	0.045	0.32	0.17	0.12	0.096
-44	0.045	0.27	0.17	0.091	0.076
-52	0.031	0.45	0.29	0.15	0.14
-77	0.0021	0.078	0.029	0.017	0.014
-95	0.045	0.55	0.41	0.15	0.15
-99	0.018	0.31	0.21	0.063	0.059
-101	0.045	0.89	0.59	0.21	0.19
-105	0.0091	0.53	0.32	0.072	0.068
-110	0.045	1.1	0.78	0.23	0.22
-118	0.018	1.1	0.67	0.17	0.16
-123	0.0021	0.038	0.0091	0.0021	0.0031
-128	0.0051	0.27	0.19	0.048	0.036
-138	0.031	1.3	0.82	0.23	0.21
-146	0.0091	0.17	0.11	0.033	0.025
-149	0.023	0.84	0.48	0.17	0.16
-151	0.0091	0.19	0.11	0.043	0.042
-153	0.045	1.3	0.74	0.25	0.21
-157	0.0031	0.049	0.028	0.0071	0.0061
-167	0.0031	0.081	0.047	0.015	0.011
-170	0.0091	0.51	0.26	0.099	0.082
-180	0.018	1.1	0.55	0.21	0.16
-187	0.018	0.43	0.21	0.094	0.071

ΣPCBs	-	12	7.3	2.6	2.2
Std.dev.	-	0.42	0.26	0.078	0.073
Deposition samples (pg m^{-2} d)					
	LOD	**Ind-PR**	**Ind-MA**	**Res-BR**	**Urb-LG**
2,3,7,8-TCDF	0,091	2.3	1.9	1.5	1.4
1,2,3,7,8-PeCDF	0.091	0.97	0.56	0.56	0.43
2,3,4,7,8-PeCDF	0.061	1.9	0.91	0.78	0.83
1,2,3,4,7,8-HxCDF	0.091	1.4	0.79	0.81	0.78
1,2,3,6,7,8-HxCDF	0.091	1.4	0.82	0.82	0.77
2,3,4,6,7,8-HxCDF	0.091	1.9	1.1	1.1	0.91
1,2,3,7,8,9HxCDF	0.091	0.98	0.73	0.71	0.67
1,2,3,4,6,7,8-HpCDF	0.15	4.3	2.2	2.2	1.8
1,2,3,4,7,8,9-HpCDF	0.15	1.3	0.81	0.77	0.75
OCDF	0.15	3.2	2.7	2.1	1.7
ΣPCDFs	-	26	16	19	14
2,3,7,8-TCDD	0.061	0.14	0.12	0.12	0.12
1,2,3,7,8-PeCDD	0.061	0.29	0.17	0.14	0.21
1,2,3,4,7,8-HxCDD	0.091	0.76	0.61	0.61	0.61
1,2,3,6,7,8-HxCDD	0.091	1.2	0.71	0.69	0.68
1,2,3,7,8,9-HxCDD	0.091	1.1	0.66	0.67	0.65
1,2,3,4,6,7,8-HPCDD	0.15	6.9	2.9	4.3	2.5
OCDD	0.15	16	11	12	9.1
ΣPCDDs	-	20	12	11	10
Std.dev.	-	1.1	0.74	0.61	0.48

The highest concentrations of POPs were detected at Ind-PR, both for transplanted lichen (3503 ng kg^{-1} for PCBs, 4.4 ng kg^{-1} for PCDDs, 11 ng kg^{-1} for PCDFs; Table 2 and 3) and deposition samples (12 ng m^{-2} d for PCBs, 26 pg m^{-2} d for PCDDs, 20 pg m^{-2} d for PCDFs; Table 5).

Figure 2 shows the sum of the concentrations of $\sum_7$PCDDs (Figure 2, panel a), $\sum_{10}$PCDFs (Figure 2, panel b) and $\sum_{23}$PCBs (Figure 2, panel c) respectively found in lichens (ng kg^{-1}, black line) and deposition samples (pg m^{-2} d or ng m^{-2} d, white histograms) at the four monitoring sites (Ind-PR, Ind-Ma, Res-BR, and Urb-LG). Regarding $\sum_7$PCDDs and $\sum_{10}$PCDFs, lichen samples showed the lowest levels at Ind-MA (1.8 and 2.1 ng kg^{-1}, respectively; Table 3); on the contrary, the lowest concentrations in deposition samples were detected at Urb-LG. This may be explained by considering that PCDD/Fs are mainly present in atmosphere coated on PM particles (Barbas et al., 2018) and, due to a slower diffusion rate through lichen thalli, they tend to settle on lichen surface making them more susceptible to mechanical wash off phenomena, which would contribute to decrease their concentrations (Augusto et al., 2013). Moreover, lichens are probably not able to quantitatively collect PCDD/Fs when concentrations are too low, as demonstrated by the lowest concentrations found in

lichen transplants at Ind-MA, Res-BR, and Urb-LG compared to those recorded in deposition samples (Figure 2a and 2b).

Regarding PCBs, concentrations found in lichens were in good agreement with those recorded in deposition samples, except for Ind-MA, where PCBs concentration was found to be considerably higher in the lichen sample than in the correspondent deposition sample. This may be explained by considering that PCBs are mainly present in the atmospheric gas phase (Barbas et al., 2018), making bioaccumulation more efficient.

Overall, despite the described differences, the efficiency of lichen transplants to reflect PCDD/Fs and PCBs atmospheric concentrations was confirmed, as reported in Figure 2.

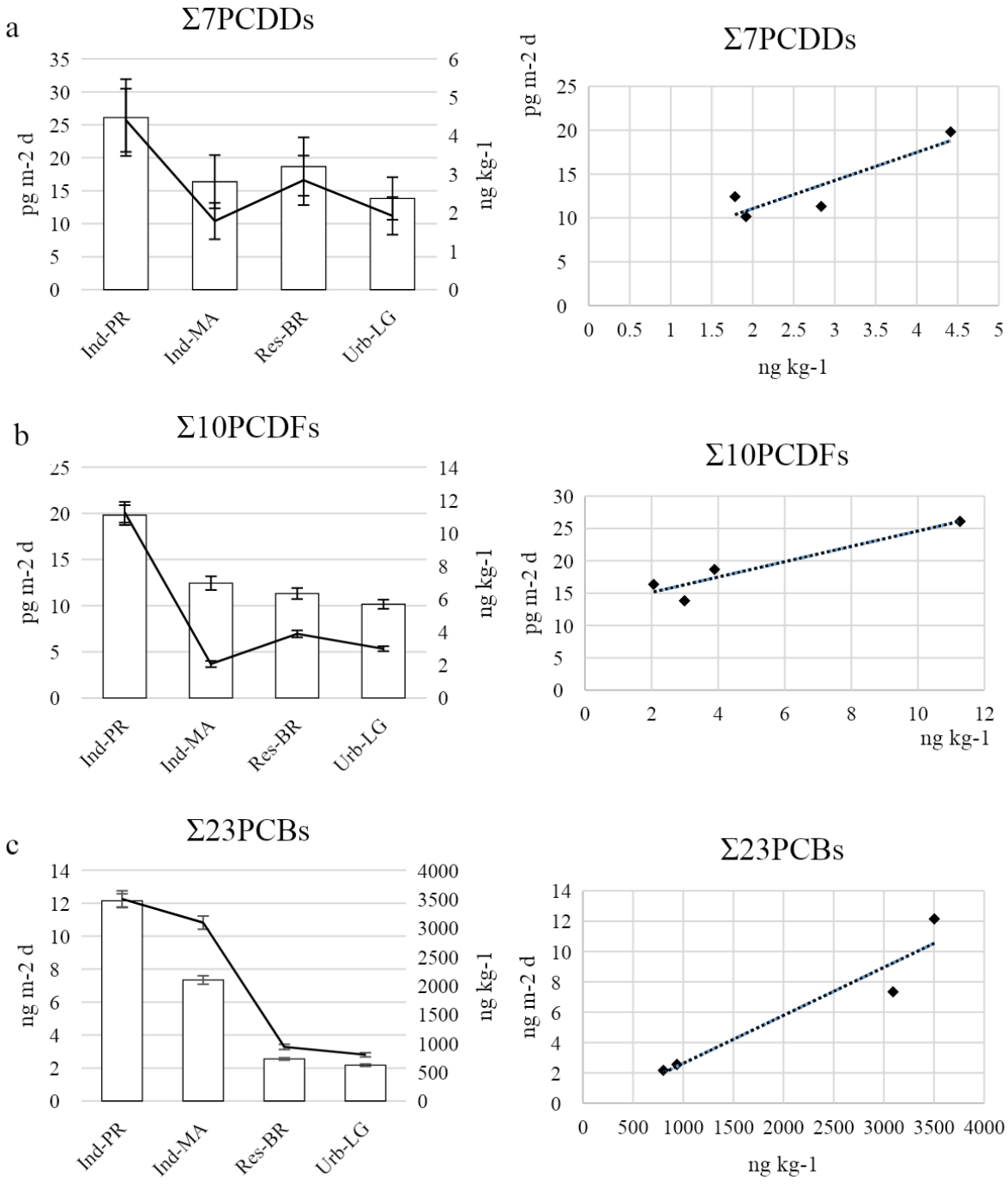

Figure 2. Comparison between the sum of the concentrations of $\sum_7$PCDDs (panel a), $\sum_{10}$PCDFs (panel b) and $\sum_{23}$PCBs (panel c) accumulated in lichens (ng kg^{-1}, black line) and collected with bulk deposition samplers (pg m^{-2} d or ng m^{-2} d, white histograms) at four monitoring sites (Ind-PR, Ind-Ma, Res-BR, and Urb-LG). The linearity response (as R^2) between POPs bioaccumulated in lichens and collected with deposition samplers is also reported.

4. Conclusions

This study demonstrates the ability of transplanted lichen *E. prunastri* to reflect the air concentration and spatial variability of PCDDs, PCDFs, and PCBs, and encourage their use as low-cost biomonitors for obtaining high spatial resolution data of POPs and mapping their spatial distribution. Power plant predominantly emitted PCBs, while steel plant was characterized by the presence of two different emission points, one characterized by the emission of PCBs and the other characterized by the emission of PCDD/Fs. This trend could be attributed to different steel processes that probably occur at different temperatures.

Lichen thalli transplants have demonstrated to be a suitable and cost-effective biomonitor of PCDDs, PCDFs, and PCBs. This approach can effectively complement the traditional air monitoring methods in order to achieve more complete monitoring networks for assessing the spatial variability of PCDDs, PCDFs, and PCBs. Moreover, we believe that the experimental approach described in this study can be applied to other monitoring campaigns for identifying and localizing POPs emission sources in areas contaminated by several disaggregated sources.

References

Alcock, R.E., Sweetman, A.J., Jones, K.C., 2001. A congener-specific PCDD/F emissions inventory for the UK: do current estimates account for the measured atmospheric burden? Chemosphere 43, 183-194. https://doi.org/10.1016/S0045-6535(00)00173-9

Argiriadis, E., Rada, E.C., Vecchiato, M., Zambon, S., Ionescu, G., Schiavon, M., Ragazzi, M., Gambaro, A., 2014. Assessing the influence of local sources on POPs in atmospheric depositions and sediments near Trento (Italy). Atmos. Environ. 98, 32-40. https://doi.org/10.1016/j.atmosenv.2014.08.035

Aries, E., Anderson, D.R., Ordsmith, N., Hall, K., Fisher, R., 2004. Development and validation of a method for analysis of ' 'dioxin-like" PCBs in environmental samples from the steel industry. Chemosphere. 54, 23–31. https://doi.org/10.1016/S0045-6535(03)00762-8

Aristizábal, B.H., Gonzalez, C.M., Morales, L., Abalos, M., Abad, E., 2011. Polychlorinated dibenzo-p-dioxin and dibenzofuran in urban air of an Andean city. Chemosphere. 85, 170–178. https://doi.org/10.1016/j.chemosphere.2011.06.035

Augusto, S., Pinho, P., Branquinho, C., Pereira, M. J., Soares, A., Catarino, F., 2004. Atmospheric dioxin and furan deposition in relation to land-use and other pollutants: a survey with lichens. J. Atmos. Chem. 49, 53-65.

Augusto, S., Máguas, C., Catarino, F., Branquinho, C., 2007. Interpreting the dioxin and furan profiles in the lichen Ramalina canariensis Steiner for monitoring air pollution. Sci. Total Environ. 377, 114-123. https://doi.org/10.1016/j.scitotenv.2007.01.089

Augusto, S, Máguas, C, Branquinho, C., 2009. Understanding the performance of different lichen species as biomonitors of atmospheric dioxins and furans: potential for intercalibration. Ecotoxicology. 18(8), 1036–42. https://doi.org/10.1007/s10646-009-0360-z

Augusto, S, Máguas, C, Branquinho, C., 2013. Guidelines for biomonitoring persistent organic pollutants (POPs), using lichens and aquatic mosses - a review. Environ. Pollut. 180, 330–8. https://doi.org/10.1016/j.envpol.2013.05.019

Augusto, S., Pinho P., Santos, A., Botelho, M.J., Palma-Oliveira, J., Branquinho, C., 2015. Declining trends of PCDD/Fs in lichens over a decade in a Mediterranean area with multiple pollution sources. Sci. Total Environ. 508, 95–100. http://dx.doi.org/10.1016/j.scitotenv.2014.11.065

Augusto, S., Pinho, P., Santos, A., Botelho, M.J., Palma-Oliveira, J., Branquinho, C., 2016. Tracking the Spatial Fate of PCDD/F Emissions from a Cement Plant by Using Lichens as Environmental Biomonitors. Environ. Sci. Technol. 50, 2434−2441. http://dx.doi.org/10.1021/acs.est.5b04873

Avino, P. and Russo, M.V., 2018. A Comprehensive Review of Analytical Methods for Determining Persistent Organic Pollutants in Air, Soil, Water and Waste. Curr. Org. Chem. 22, (10), 939-953. https://doi.org/10.2174/1385272822666180404144834

Barbas, B., de la Torre, A., Sanz, P., Navarro, I., Artíñano, B., Martínez, M.A., 2018. Gas/particle partitioning and particle size distribution of PCDD/Fs and PCBs in urban ambient air. Sci. Total Environ. 624, 170–179. https://doi.org/10.1016/j.scitotenv.2017.12.114

Bari, A., Rosso, A., Minciardi, M.R., Troiani, F., Piervittori, R., 2001. Analysis of heavy metals in atmospheric particulates in relation to their accumulation in explanted Pseudoevernia furfuracea thalli. Environ. Monit. Assess. 69, 2005-2220. https://doi.org/10.1023/A:1010757924363

Beelen, R., Hoek, G., Pebesma, E., Vienneau, D., de Hoogh, K., Briggs, D.J., 2009. Mapping of background air pollution at a fine spatial scale across the European Union. Sci. Total Environ. 407(6), 1852-1867. https://doi.org/10.1016/j.scitotenv.2008.11.048
Bergamaschi, L., Rizzio, E., Giaveri, G., Loppi, S., Gallorini, M., 2007. Comparison between the accumulation capacity of four lichen species transplanted to an urban site. Environ. Pollut. 148, 468-476. https://doi.org/10.1016/ j.envpol.2006.12.003.
Bruckmann, P, Hiester, E, Klees, M, Zetzsch, C., 2013. Trends of PCDD/F and PCB concentrations and depositions in ambient air in Northwestern Germany. Chemosphere. 93, 1471–8. https://doi.org/10.1016/j.chemosphere.2013.07.029
Boudreault, C., Coxson, D., Bergeron, Y., Stevenson, S., Bouchard, M., 2013. Do forests treated by partial cutting provide growth conditions similar to old-growth forests for epiphytic lichens? Biol. Conserv. 159, 458–467. https://doi.org/10.1016/j.biocon.2012.12.019
Castellani, F., Massimi, L., Vitali, M., Canepari, S., Guidotti, M., Conti, M. E., Protano, C., 2020. High spatial resolution analysis of polybrominated diphenyl ethers (PBDEs) using transplanted lichen Evernia prunastri: A case study in central Italy. Sci. Total Environ. 140590. https://doi.org/10.1016/j.scitotenv.2020.140590
Choi, S.D., Baek, S.Y., Chang, Y.S., 2008. Atmospheric levels and distribution of dioxin-like polychlorinated biphenyls (PCBs) and polybrominated diphenyl ethers (PBDEs) in the vicinity of an iron and steel making plant. Atmos. Environ. 42, 2479–2488. doi:10.1016/j.atmosenv.2007.12.032
Conti, M.E., Cecchetti, G., 2001. Biological monitoring: lichens as bioindicators of air pollution assessment—a review. Environ. Pollut. 114, 471-492. https://doi.org/10.1016/S0269-7491(00)00224-4
Conti, M.E., Tudino, M., Stripeikis, J., Cecchetti, G., 2004. Heavy metal accumulation in the lichen Evernia prunastri transplanted at urban, rural and industrial sites in Central Italy. J. Atmos. Chem., 49, 83-94. https://doi.org/10.1007/s10874-004-1216-9
Conti, M.E., Jasan, R., Finoia, M.G., Iavicoli, I., Plá, R., 2016. Trace elements deposition in the Tierra del Fuego region (south Patagonia) by using lichen transplants after the Puyehue-Cordón Caulle (north Patagonia) volcanic eruption in 2011. Environ. Sci. Pollut. Res., 23, 6574-6583. https://doi.org/10.1007/s11356-015-5858-8
Conti, M.E., Plà, R., Simone, C., Jasan, R., Finoia, M.G., 2020 Implementing the monitoring breakdown structure: native lichens as biomonitors of element deposition in the southern Patagonian forest connected with the Puyehue volcano event in 2011—a 6-year survey (2006–2012). Environ. Sci. Pollut. Res.. https://doi.org/10.1007/s11356-020-10001-0
Directive 2000/76/EG. Directive 2000/76/EC of the European Parliament and of the Council of December 4th 2000 on the Incineration of Waste; 2000
Eckhardt, S., Breivik, K., Manø, S., Stohl, A., 2007. Record high peaks in PCB concentrations in the Arctic atmosphere due to long-range transport of biomass burning emissions. Atmos. Chem. Phys., 7, 4527–4536, www.atmos-chem-phys.net/7/4527/2007/
Fang, M., Choi, S.D., Baek, S.Y., Park, H., Chang, Y.S., 2011. Atmospheric bulk deposition of polychlorinated dibenzo-p-dioxins and dibenzofurans (PCDD/Fs) in the vicinity of an iron and steel making plant. Chemosphere. 84(7), 894-899. https://doi.org/10.1016/j.chemosphere.2011.06.016
Ferrero, L., Cappelletti, D., Moroni, B., Sangiorgi, G., Perrone, M.G., Crocchianti, S., Bolzacchini, E., 2012. Wintertime aerosol dynamics and chemical composition across the mixing layer over basin valleys. Atmos. Environ. 56, 143–153. https://doi.org/10.1016/j.atmosenv.2012.03.071
Gao, M., Cao, J., Seto, E., 2015. A distributed network of low-cost continuous reading sensors to measure spatiotemporal variations of PM2. 5 in Xi'an, China. Environ. pollut. 199, 56-65. https://doi.org/10.1016/j.envpol.2015.01.013
Godinho, R.M., Wolterbeek, H.T., Verburg, T., Freitas, M.C., 2008. Bioaccumulation behaviour of transplants of the lichen Flavoparmelia caperata in relation to total deposition at a polluted location in Portugal. Enviro Pollut 151, 318-325. https://doi.org/10.1016/j.envpol.2007.06.034
Guerrini, R., 2012. Qualità dell'aria nella provincia di Terni tra il 2002 e il 2011. Quad ARPA Umbria 81–87
Hoff, R.M., Strachan, W.M.J., Sweet, C.W., Chan, C.H., Shackleton, M., Bidleman, T.F., Brice, K.A., Burniston, D.A., Cussion, S., Gatz, D.F., Harlin, K., Schroeder, W.H., 1996. Atmospheric Deposition of Toxic Chemicals to the Great Lakes: A Review of Data through 1994. Atmos. Environ. 30, 3505–3527. https://doi.org/10.1016/1352-2310(96)00046-5
International Agency for the research on Cancer (IARC), 2016. Outdoor Air Pollution Volume 109. Monographs on the Evaluation of Carcinogenic Risks to Humans. IARC Working Group on the Evaluation of Carcinogenic Risk to Humans. International Agency for Research on Cancer, Lyon (FR).
Irwin, J.S., 2014. A suggested method for dispersion model evaluation. J. Air Waste Manage. Assoc. 64 (3), 255–264. https://doi.org/10.1080/10962247.2013.833147
Johnston, K., Ver Hoef, J. M., Krivoruchko, K., Lucas, N., 2001. Using ArcGIS geostatistical analyst. Vol. 380. Esri.
Jones, K. C. and Duarte-Davidson, R., 1997. Transfers of Airborne PCDD/Fs to Bulk Deposition Collectors and Herbage. Environ. Sci. Technol. 1997, 31, 10, 2937-2943. https://doi.org/10.1021/es970133t
Kardel, F., Wuyts, K., De Wael, K., Samson, R., 2018. Biomonitoring of atmospheric particulate pollution via chemical composition and magnetic properties of roadside tree leaves. Environ. Sci. Pollut. R. 25(26), 25994-26004. https://doi.org/10.1007/s11356-018-2592-z
Kim, B.U., Bae, C., Kim, H.C., Kim, E., Kim, S., 2017. Spatially and chemically resolved source apportionment analysis: Case study of high particulate matter event. Atmos. Environ. 162, 55–70. https://doi.org/10.1016/j.atmosenv.2017.05.006
Kumar, A., Maroju, S., Bhat, A., 2007. Application of ArcGIS geostatistical analyst for interpolating environmental data from observations. Environmental Progress, 26(3), 220-225. https://doi.org/10.1002/ep.10223
Li, Y., Wang, P., Ding, L., Li, X., Wang, T., Zhang, Q., Yang, H., Jiang, G., Wei, F., 2010. Atmospheric distribution of polychlorinated dibenzo-p-dioxins, dibenzofurans and dioxin-like polychlorinated biphenyls around a steel plant Area, Northeast China. Chemosphere. 79 (3), 253-258. https://doi.org/10.1016/j.chemosphere.2010.01.061
Liu, G., Zheng, M., Cai, M., Nie, Z., Zhang, B., Liu, W., Du, B., Dong, S., Hu, J., Xiao, K., 2013. Atmospheric emission of polychlorinated biphenyls from multiple industrial thermal processes. Chemosphere. 90, 2453–2460. http://dx.doi.org/10.1016/j.chemosphere.2012.11.008
Lucadamo, L., Corapi, A., Loppi, S., De Rosa, R., Barca, D., Vespasiano, G., Gallo, L., 2016. Spatial Variation in the Accumulation of Elements in Thalli of the Lichen Pseudevernia furfuracea (L.) Zopf Transplanted Around a Biomass Power Plant in Italy. Arch. Environ. Con. Tox. 70, 506–521. https://doi.org/10.1007/s00244-015-0238-4

Massimi, L., Ristorini, M., Eusebio, M., Florendo, D., Adeyemo, A., Brugnoli, D., Canepari, S., 2017. Monitoring and Evaluation of Terni (Central Italy) Air Quality through Spatially Resolved Analyses. Atmosphere, 8, 200; https://doi.org/10.3390/atmos8100200
Massimi, L., Conti, M.E., Mele, G., Ristorini, M., Astolfi, M.L., Canepari, S., 2019. Lichen transplants as indicators of atmospheric element concentrations: a high spatial resolution comparison with PM10 samples in a polluted area (Central Italy). Ecol. Indic. 101, 759–769. https://doi.org/10.1016/j.ecolind.2018.12.051
Massimi, L., Simonetti, G., Buiarelli, F., Di Filippo, P., Pomata, D., Riccardi, C., Ristorini, M., Astolfi, M.L., Canepari, S. 2020a. Spatial distribution of levoglucosan and alternative biomass burning tracers in atmospheric aerosols, in an urban and industrial hot-spot of Central Italy. Atmos. Res. 104904. https://doi.org/10.1016/j.atmosres.2020.104904
Massimi, L., Ristorini, M., Astolfi, M.L., Perrino, C., Canepari, S. 2020b. Spatial Mapping of Element Concentrations in PM10: a Powerful Tool for Localization and Impact Assessment of Emission Sources. Atmos. Res. Under Review.
Mi, H.H., Wu, Z.S., Lin, L.F., Lai, Y.C., Lee, Y.Y., Wang, L.C., Chang-Chien, G.P., 2012. Atmospheric Dry Deposition of Polychlorinated Dibenzo-p-Dioxins/Dibenzofurans (PCDD/Fs) and Polychlorinated Biphenyls (PCBs) in Southern Taiwan. Aerosol Air Qual. Res. 12, 1016–1029. https://doi.org/10.4209/aaqr.2012.07.0172
Moroni, B., Ferrero, L., Crocchianti, S., Cappelletti, D., 2013. Aerosol dynamics upon Terni basin (Central Italy): Results of integrated vertical profile measurements and electron microscopy analysis. Rend. Lincei Sci. Fis. Nat. 24, 319–328. https://doi.org/10.1007/s12210-013-0230-8
Ndlovu, N.B., Frontasyeva, M.V., Newman, R.T. and Maleka, P.P., 2019. Moss and Lichen Biomonitoring of Atmospheric Pollution in the Western Cape Province (South Africa). AJAC. 10, 86-102. https://doi.org/10.4236/ajac.2019.103008
Paramasivam, C.R., Venkatramanan, S., 2019. An Introduction to Various Spatial Analysis Techniques. GIS and Geostatistical Techniques for Groundwater Science, 3, 23-30. https://doi.org/10.1016/B978-0-12-815413-7.00003-1
Protano, C., Guidotti, M., Owczarek M., Fantozzi, L., Blasi, G., Vitali, M., 2014. Polycyclic Aromatic Hydrocarbons and Metals in Transplanted Lichen (Pseudovernia furfuracea) at Sites Adjacent to a Solid-waste Landfill in Central Italy. Arch. Environ. Contam. Toxicol. 66, 471–481 https://doi.org/10.1007/s00244-013-9965-6
Protano, C., Owczarek M., Fantozzi, L., Guidotti, M., Vitali, M., 2015. Transplanted Lichen Pseudovernia furfuracea as a Multi-Tracer Monitoring Tool Near a Solid Waste Incinerator in Italy: Assessment of Airborne Incinerator-Related Pollutants. Bull. Environ. Contam. Toxicol. 95,644–653 https://doi.org/10.1007/s00128-015-1614-5
Qu, C., Albanese, S., Lima, A., Hope, D., Pond, P., Fortelli, A., Romano, N., Cerino, P., Pizzolante, A., De Vivo, B., 2019. The occurrence of OCPs, PCBs, and PAHs in the soil, air, and bulk deposition of the Naples metropolitan area, southern Italy: Implications for sources and environmental processes. Environ. Int. 124, 89-97. https://doi.org/10.1016/j.envint.2018.12.031
Reis, M.A., Alves, L.C., Freitas, M.C., Van, O., Wolterbeek, H.T., 1999. Lichens (Parmelia sulcata) time response model to environmental availability. Sci. Total Environ. 232, 105-115. https://doi.org/10.1016/S0048-9697(99)00113-8
Sett, R. and Kundu, M., 2016. Epiphytic Lichens: Their Usefulness as Bio-indicators of Air Pollution. Donnish Journal of Research in Environmental Studies Vol 3(3), 017-024. ISSN: 2984-858X
Sloof, J.E., 1995. Lichens as quantitative biomonitors for atmospheric trace-element deposition using transplants. Atmos. Environ. 29, 11-20. https://doi.org/10.1016/1352-2310(94)00221-6
Suutari, A., Ruokojärvi, P., Kiviranta, H., Verta, M., Korhonen, M., Nieminen, M., Hallikainen, A., Laaksonen, S., 2010. Airborne organic pollutants in Finnish reindeer food chain. In: E. Pongrácz, M. Hyvärinen, S. Pitkäaho, R.L. Keiski (Ed.), Clean air research at the University of Oulu (pp. 25-27). Proceeding of the SkyPro conference, June 3rd, 2010, University of Oulu, Finland. Kalevaprint, Oulu, ISBN 978-951-42-6199-2.
Tyler, G., 1989. Uptake, retention and toxicity of heavy metals in lichens. A brief review. Water Air and Soil Pollut. 47, 321-333. https://doi.org/10.1007/BF00279330
Thacker, N., Kashyap, S., Sheikh, J., Trivedi, J., Thokchom, B., Agnihotri, A., 2010. Dioxin Releases in Waste Incinerations and Thermal Processes. Bull. Environ. Contam. Toxicol. 85, 624–627. https://doi.org/10.1007/s00128-010-0137-3
Thakur, M., Pathania, D., 2020. Environmental fate of organic pollutants and effect on human health. Abatement of Environmental Pollutants. Trends and Strategies 12, 245-262. https://doi.org/10.1016/B978-0-12-818095-2.00012-6
Van der Wat, L., Forbe, P.B.C., 2015. Lichens as biomonitors for organic air pollutants. TRAC - Trends in Anal. Chem. 64, 165-172. https://doi.org/10.1016/j.trac.2014.09.006
Vannini, A., Paoli, L., Nicolardi, V., Di Lella, L.A., Loppi, S., 2017. Seasonal variations in intracellular trace element content and physiological parameters in the lichen Evernia prunastri transplanted to an urban environment. Acta Botanica Croatica 76 (2), 171–176.
VDI, 1991. VDI 3799 Blatt 2 - Zurückgezogen Messung von Immissions-Wirkungen; Ermittlung und Beurteilung phytotoxischer Wirkungen von Immissionen mit Flechten; Verfahren der standardisierten Flechtenexposition. Berlin.
VDI, 1995. VDI 3799 Blatt 1 - Zurückgezogen Messen von Immissionswirkungen - Ermittlung und Beurteilung phytotoxischer Wirkungen von Immissionen mit Flechten - Flechtenkartierung zur Ermittlung des Luftgütewertes (LGW), Berlin.
Vitali, M., Antonucci, A., Owczarek, M., Guidotti, M., Astolfi, M.L., Manigrasso, M., Avino, P., Bhattacharya, B., Protano, C., 2019. Air quality assessment in different environmental scenarios by the determination of typical heavy metals and Persistent Organic Pollutants in native lichen Xanthoria parietina. Environ. Pollut. 254, 113013. https://doi.org/10.1016/j.envpol.2019.113013
Vitali, L., Morabito, A., Adani, M., Assennato, G., Ciancarella, L., Cremona, G., Giua, R., Pastore, T., Piersanti, A., Righini, G., Russo, F., Spagnolo, S., Tanzarella, A., Tinarelli, G., Zanini, G., 2016. A Lagrangian modelling approach to assess the representativeness area of an industrial air quality monitoring station. Atmos. Pollut. Res. 7 (6), 990–1003. https://doi.org/10.1016/j.apr.2016.06.002
Xu, S., Chen, T., Li, X., Yan, J., Cen, K., 2018. Behavior of PCDD/Fs, PCBs, CBzs and PAHs during Thermal Treatment of Various Fly Ash from Steel Industry. Aerosol Air Qual. Res. 18, 1008–1018. https://doi.org/10.4209/aaqr.2017.11.0514
Yu, B.W., Jin, G.Z., Moon, Y.H., Kim M.K., Kyoung J.D., Chang Y.S., 2006. Emission of PCDD/Fs and dioxin-like PCBs from metallurgy industries in S. Korea. Chemosphere. 62, 494–501. https://doi.org/10.1016/j.chemosphere.2005.04.031

6.4 (A8) Effects of COVID-19 lockdown on PM10 composition and sources in the Rome Area (Italy) by elements' chemical fractionation-based source apportionment

Atmospheric Research (2022), 266, 105970, doi: 10.1016/j.atmosres.2021.105970

Lorenzo Massimi[1], Adriana Pietrodangelo[2*], Maria Agostina Frezzini[1,] Martina Ristorini[3], Nayma De Francesco[4], Tiziana Sargolini[2], Antonio Amoroso[5], Alessandro Di Giosa[5], Silvia Canepari[1], Cinzia Perrino[2]

[1] Department of Environmental Biology, Sapienza University of Rome, P. le Aldo Moro, 5, Rome, 00185, Italy;
[2] C.N.R. Institute of Atmospheric Pollution Research, Via Salaria, Km 29,300, Monterotondo St., Rome, 00015, Italy;
[3] Department of Bioscience and Territory, University of Molise, Pesche (IS), 86090, Italy;
[4] Department of Chemistry, Sapienza University of Rome, P. le Aldo Moro, 5, Rome, 00185, Italy;
[5] ARPA Lazio, Regional Environmental Protection Agency, Via Boncompagni 101, Rome, 00187, Italy.

*Correspondence: pietrodangelo@iia.cnr.it

Keywords: particulate matter; elements; chemical fractionation; source tracer; receptor modelling; PMF.

Abstract: During the national lockdown imposed by Italian government (from March 9th to May 18th 2020) to counter the Covid-19 pandemic, 24-h PM_{10} samples were collected at three sites in the Rome area (Central Italy), two urban (Sapienza and Via Saredo, highly impacted by vehicular traffic) and one peri-urban (Montelibretti, more impacted by biomass domestic heating). Further, at Sapienza and Montelibretti PM_{10} daily sampling had been carried out in the period immediately before lockdown, and at Via Saredo samples were additionally collected also after the end of lockdown. PM_{10} was chemically speciated for main components (major elements, inorganic ions, EC, OC, levoglucosan), and trace elements. The latter were chemically fractionated and considered for their water-soluble and insoluble fractions, which proved to be more source-selective than total element. Three datasets were thus built and analyzed by Positive Matrix Factorization (PMF), with the aim of identifying and apportioning mass contributions of sources acting in the periods before, during and after lockdown, in the Rome area. Identified emission sources were mostly from long-range advection (two different contributions of mineral dust, fresh sea spray, heavy oil combustion), while local sources (vehicular traffic and biomass burning) were strongly abated during lockdown, with respect to previous sampling period, and inorganic secondary aerosol showed a progressive increment of sulfates, driven by seasonal evolution from winter to spring. Since the lockdown interrupted all non-essential productive and work activities, thus reducing the chemical fingerprinting of local sources, this occurrence allowed to clearly describe both profiles and source contribution estimates of long-range transported PM_{10} components. Moreover, it allowed assessing the reduction of the impact of anthropogenic sources (such as vehicular traffic) and the efficiency of mitigation measures generally taken to control PM_{10} mass concentration. Acidic sulfates (bisulfate and letovicite) resulted associated to mineral dust transport events, and the role of chemically fractionated elements as source-specific tracers was further confirmed.

1. Introduction

During 2020, Coronavirus disease 2019 (Covid-19) has rapidly spread from Wuhan City of China to the rest of the world, representing the new public health threat worldwide (Coccia, 2020; Singhal, 2020; Wang et al., 2020). As a result, several lockdown-based policies have been adopted by different countries to prevent the spread of the virus, including lessening of many human activities (i.e. industries, manufacturing, transport and vehicular traffic, construction works, etc.) As a consequence, considerable decrease in anthropogenic emissions of air pollutants and outstanding changes in ambient air quality and atmospheric composition were widely observed. Therefore, over the last year, numerous studies on the air quality impacts of Covid-19 control measures have been conducted (Collivignarelli et al., 2020; Kumar et al., 2020; Guevara et al., 2021; Arregocés et al., 2021; Manchanda et al., 2021; Shen et al., 2021; Querol et al., 2021). These studies regarded several pollutants, including airborne particulate matter (PM), which is considered as one of the air pollutants exerting most harmful effects on human health (EPA, 1997; World Health Organization, WHO, 2016; Ali et al., 2019; Ramli et al., 2020; Briz-Redón et al., 2021).

Particulate matter has a very complex and variable composition and toxicology, mostly depending on local emitting sources, advected contributions and chemistry of the lower troposphere (i.e. ageing and secondary aerosol formation). Therefore, information about concentration and form of the various chemical species in PM is essential to evaluate the relative relevance of single source contributions and properly plan PM control strategies and mitigation measures to protect citizens health. In Italy, European daily limit value for PM_{10} mass concentration (50 $\mu g/m^3$ for no more than 35 days per year; EU, 2008, Directive 2008/50/EC) is often exceeded in urban areas, especially during the winter season (Tomassetti et al., 2020). As a result, in urban areas such as Rome (Central Italy), policies of traffic reduction, such as traffic stop or green zone design, are frequently taken to control and reduce the mass concentrations of PM in conditions of continue exceedance of the legal limit for several days (Cesaroni et al., 2012). Like for many urban contexts, where PM pollution mainly derives from traffic, commercial and industrial activities, biomass domestic heating and residential energy use (Borck and Pflüger, 2019; Grondys, 2019; Fan et al., 2020), the Rome area is affected by a multi-source pollution. Furthermore, contributions from natural sources, including sea-salt and mineral dust, and secondary aerosol formation significantly affect PM mass concentration in Rome (Perrino et al., 2009 and 2010). This makes a challenge to accurately assess the weight of each source contributions to PM, to the goal of properly addressing PM control strategies and mitigation measures.

To counter the Covid-19 pandemic, the Italian government imposed a national lockdown from March 9th to May 18th 2020, restricting the movement of the population except for necessity or health circumstances, interrupting all non-essential productive and work activities and closing schools and universities (DPCM 11/03/20; DPCM 26/04/20; Guzzetta et al., 2021). The 2-months stop of proactive activities and vehicle circulation offered unique and relevant opportunities to quantify the reduction of the impact of anthropogenic sources of PM due to lockdown, and to assess thus the efficiency of the mitigation measures generally adopted in Rome. Moreover, the lockdown condition of forced abatement of anthropic sources, allowed evaluating unambiguously the fingerprint of natural emissions on PM concentration and composition.

In this framework, a monitoring campaign was carried out in the urban and peri-urban area of Rome, at three sampling sites, in which PM_{10} samples were collected and chemically characterized for organic and elemental carbon, levoglucosan, ions and macro- and trace-elements. Trace elements were chemically fractionated to increase their selectivity as source tracers (Canepari et al., 2006a, 2006b). The contribution to PM_{10} mass concentration and composition of emission sources during pre-lockdown, lockdown and post-lockdown periods, was assessed by applying the Positive Matrix Factorization (PMF) to the obtained chemical data (Paatero and Tapper, 1994; Querol et al., 2007).

2. Materials and Methods

2.1 Sampling Sites

Rome (41°54'39"24 N, 12°28'54"48 E) is the largest (1300 km^2) and most populated (2.8 million of inhabitants) urban area of Italy (Perrino et al., 2019; Roma Capitale, 2019). With the absence of heavy industrial activities within its territory, vehicular traffic can be considered as the main local emission source of this area (Battista et al. 2016; Roma Capitale, 2015). In addition, seasonal influence of domestic heating, together with more frequent atmospheric stability episodes during winter, can be also considered responsible for higher PM_{10} mass concentration (Perrino et al., 2008). Due to its proximity to the Tyrrhenian coast (about 30 km), PM_{10} is also affected by the influence of marine aerosol, with natural breezes that are expected to be more frequent and intense in the daytime and during summer season (Di Bernardino et al., 2021). Previous studies have also underlined natural advection episodes of desert dust, in some cases even stronger than anthropogenic emissions (Gobbi et al., 2019).

In this urban context, daily PM_{10} samples were collected at three sampling sites, two urban sites: “Sapienza” and “Via Saredo”, and one peri-urban site: “Montelibretti” (Fig. 1). The site Sapienza is located within the Experimental Botanical Garden of Sapienza – University of Rome, in the close proximity of busy roads, bus Terminus and tram stops (at about 300 meters) and can thus be considered as a traffic site. Via Saredo is located within the facility of Environmental Protection Agency of Lazio Region (ARPA Lazio), on the building rooftop. This site is in a residential area crossed by urban arteries impacted by severe traffic conditions. Finally, Montelibretti is situated at about 30 km North-East from Rome, within the Institute of Atmospheric Pollution Research of National Research Council of Italy (CNR-IIA). This site is less affected by vehicular traffic but is located in an area where biomass domestic heating appliances are frequently used during winter.

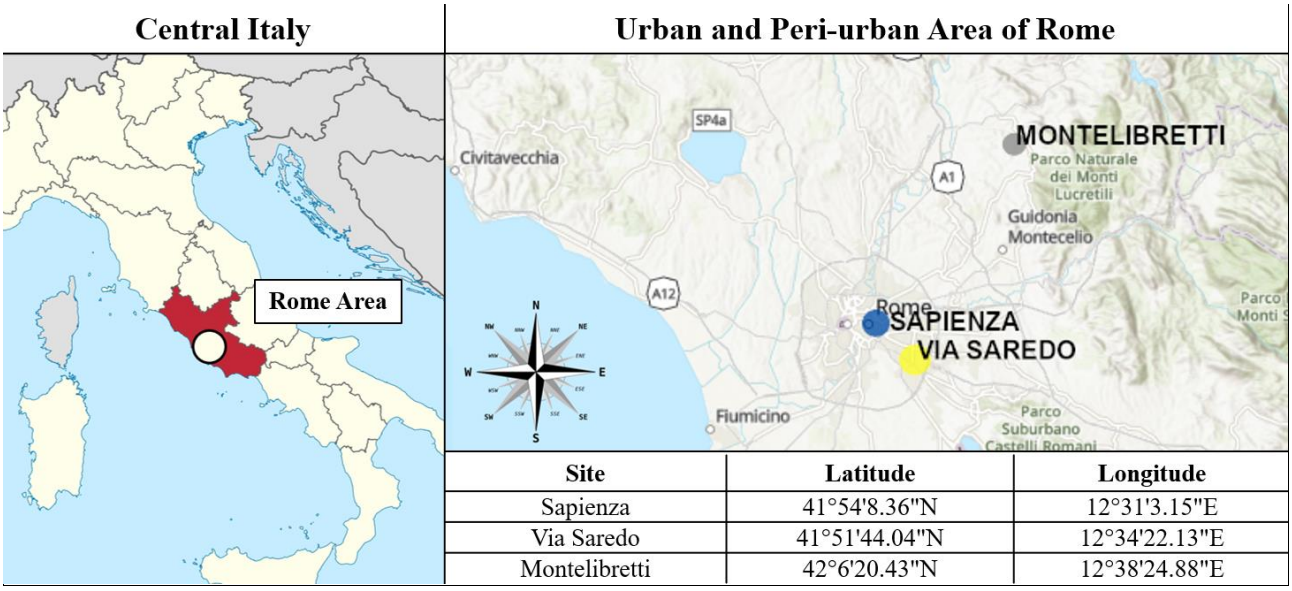

Site	Latitude	Longitude
Sapienza	41°54'8.36"N	12°31'3.15"E
Via Saredo	41°51'44.04"N	12°34'22.13"E
Montelibretti	42°6'20.43"N	12°38'24.88"E

Fig. 1. Map of the three sampling sites in the study area (Rome, Central Italy).

2.2 Sampling Periods

Daily PM_{10} filters were collected during different sampling periods at the three sites as reported in Table 1. At Sapienza, PM_{10} samples were collected from February 2nd (about one month earlier than the beginning of the national lockdown) to May 14th 2020. At Via Saredo, PM_{10} filters were collected from March 31st to June 14th 2020 (about one month later than the end of the lockdown). Finally, at Montelibretti, PM_{10} samples were collected in two separate periods, the first one from January 9th to February 7th 2020 (before lockdown), and the second one from March 14th to May 17th 2020 (during lockdown).

Table 1. PM_{10} sampling periods at the three sites during pre-lockdown, lockdown and post-lockdown.

	Pre-lockdown (before March 9th 2020)	**Lockdown (March 9th - May 18th 2020)**	**Post-Lockdown (after May 18th 2020)**
Sapienza	February 2nd - March 8th 2020	March 9th - May 14th 2020	
Via Saredo		March 31st - May 18th 2020	May 19th - June 14th 2020
Montelibretti	January 9th - February 7th 2020	March 14th - May 17th 2020	

2.2 Sampling Equipment

Sequential samplers working at the flow rate of 2.3 $m^3\ h^{-1}$ were employed at the three sampling sites for the collection of 24-h (from midnight to midnight) PM_{10} filters. A DADOLAB Gemini dual channel sampler (Dado lab srl, Cinisello B., MI, Italy), two DIGITEL DPA14 low volume aerosol samplers (Digitel Elektronik AG, Volketswil, Zurich, Switzerland), and a FAI SWAM 5a dual channel (beta attenuation automatic) monitor (Fai Instruments, Fonte Nuova, Rome, RM, Italy) were used at Sapienza, Via Saredo and Montelibretti,

respectively. All the samplers were equipped with sampling head systems for PM_{10} certified UNI EN 12341 (2014).

One of the two sampling lines at each site was equipped with Quartz membrane filters (Tissuquartz 2500QAT, 47 mm diameter, pore size 2µm, Pall Life Sciences, NY, United States), while the second line was equipped with Polytetrafluoroethylene (PTFE) membrane filters (47 mm diameter, pore size 2µm, Whatman, Maidstone, United Kingdom).

Moreover, 10 Quartz and 10 PTFE blank filters were left in the unloader of each sampler to be subsequently used for field blanks' analysis and minimum detection limits (MDL) determination.

2.3 Analytical Procedure

Daily PM_{10} filters were chemically analyzed for PM_{10} macro- and micro-components.

Quartz membrane filters were analyzed for elemental carbon (EC) and organic carbon (OC) by thermo-optical analysis (Carbon Aerosol Analyzer, Sunset Laboratory, OR, United Stated), through the application of the NIOSH-quartz temperature protocol (Perrino et al., 2014).

PTFE membrane filters were firstly used for the gravimetric assessment of PM_{10} mass concentration by using an automated microbalance with a sensitivity of 1 µg (mod. ME5, Sartorius AG, Gottingen, Germany) after conditioning the membrane filters at 20 °C and 50% of relative humidity for 48 hours. Subsequently, X-ray fluorescence (X-Lab2000, SPECTRO Analytical Instruments) was employed for the determination of sulfur (S), chloride (Cl), sodium (Na), potassium (K), magnesium (Mg), calcium (Ca), silicon (Si) and aluminum (Al).

PTFE membrane filters were then subjected to the chemical fractionation procedure, consisting in the water-extraction of PM_{10} and in the acid digestion of the residue, followed by elemental analysis of both the soluble and insoluble fractions. This procedure was already optimized (Canepari et al., 2006a, 2006b) and widely used (Astolfi et al., 2018; Massimi et al., 2020b) for increasing the selectivity of the elements as source tracers (Astolfi et al., 2006; Canepari et al., 2009; Perrino et al., 2010), since for many elements the soluble and insoluble fractions are released by different emission sources (Massimi et al., 2021). Materials and methods of the chemical fractionation are reported in Canepari et al. (2006a and b), and widely detailed in Massimi et al. (2020b). Both the water-extracted and acid-digested solutions were analyzed for 40 elements (Al, As, B, Ba, Be, Bi, Ca, Cd, Ce, Co, Cr, Cs, Cu, Fe, Ga, Ge, K, Li, Mg, Mn, Mo, Na, Nb, Ni, P, Pb, Rb, Sb, Se, Sn, Sr, Te, Ti, Tl, U, V, W, Zn, Zr) by using a quadrupole inductively coupled plasma mass spectrometer (ICP-MS; model 820-MS; Bruker, Bremen, Germany) equipped with a glass nebulizer (0.4 mL min^{-1}; Analytik Jena AG, Jena, Germany). For each element, external standard calibration curve was performed in the range 1-500 µg L^{-1} by serially diluting stock standard solutions (1000 ± 2 mg L^{-1}; Exaxol Italia Chemical Manufacturers Srl, Genoa, Italy; Ultra Scientific, North Kingstown, RI, USA; Merck Millipore Ltd., Billerica, MA, USA). To control nebulizer efficiency, Y and Rh (1000 ± 2 mg L^{-1}; Panreac Química, Barcelona, Spain) were used as internal standards for all measurements and set at 5 µg L^{-1} and 20 µg L^{-1}, respectively. The instrumental conditions are detailed in Astolfi et al. (2020).

In addition to the elements, the soluble fraction of PM_{10} was analyzed for anionic and cationic components and for levoglucosan (LVG). Ions (Ca^{2+}, Cl^-, K^+, Mg^{2+}, Na^+, NH_4^+, NO_3^-, SO_4^2) were analyzed by ion chromatography (IC; ICS1000, Dionex Co., Sunnyvale, CA, USA), while levoglucosan was analyzed by High-Performance Anion-Exchange Chromatography with Pulsed Amperometric Detection (HPAEC-PAD). Additional information about the instrument setup and analytical conditions are largely described by Perrino et al. (2019).

2.4 Positive Matrix Factorization

A receptor modelling approach (RM) based on positive matrix factorization (PMF) was employed to identify sources acting during sample collection, and apportion PM_{10} sample mass to source contributions.

The U.S. EPA-PMF v5.0 software (Norris et al., 2014) was used in this work, that is accomplished by the Multilinear Engine (ME-2) platform (Paatero, 1999).

To obtain an input data matrix suitable for PMF analyses, the number of chemical variables required to be reduced with respect to the available PM_{10} samples. The percentage of selected variables for PM_{10} source apportionment respect to the total number of PM_{10} chemical components analyzed is of 29%. The number of analyzed variables not used for PMF analysis is of 69, most of them are elements less selective in tracing different emission sources respect to those used in this study. The following variables were selected to be used for the PMF: EC, OC, levoglucosan, SO_4^-, Cl^-, Na^+, K^+, Mg^{2+}, NH_4^+, NO_3 ions, total Al, Si and Ca, soluble fraction of Cs, Ni, Rb, Tl and V, insoluble fraction of Cs, Cu, Fe, Li, Mo, Rb, Sb, Sn, Ti and V, and PM_{10} mass concentration. The variables were chosen depending on their ability to selectively trace PM_{10} emission sources, which is widely documented in previous studies (Perrino et al., 2009, Masiol et al., 2010; Tian et al., 2013; Sharma et al., 2016). To the goals of input variable selection, species determined by more than one technique (namely: ICP-MS (soluble fraction) and IC, or ICP-MS (total element) and XRF) were checked for internal consistency by linear regression. Na, K, Mg were included in PMF as ion species, while Ca, Si and Al were included as total element determined by XRF. Major species (EC, OC, levoglucosan, nitrate, sulfate and ammonium ions (NSA) were all included, while trace elements were selected for their soluble or insoluble fraction, based on previous knowledge of the role of element fraction as source tracer (Canepari et al., 2014 and 2019; Massimi et al., 2020b).

PMF analysis was performed separately at each site, to the aim of evidencing possible site-related differences of sources impact. The same chemical variables were employed for each PMF to make PMF outputs comparable among different computations on different sites. Preliminary PMF analyses of separated pre- and post-lockdown periods produced unstable solutions due to limited temporal coverage. Therefore, for each site, all samples collected in the different periods were combined in the same PMF runs. For Via Saredo, missing data were automatically replaced by median value. For Sapienza and Montelibretti, median values were calculated separately for the pre-lockdown and lockdown periods and used to replace missing data in the combined analysis. Minimum detection limit of each variable was set as mean plus 3 times the standard deviation (SD) of 10 replicate blank determinations, data below MDL were replaced with MDL/2. Percentages

of data above MDL range 80-100 for all selected variables. Uncertainties calculations were based on the approach by Polissar et al. (1998) for data below MDL, and by the equation-based method described by Norris et al. (2014) for data greater than MDL. For median-replaced data, uncertainties were calculated as four times the species median.

The final input matrices for PMF at the three sites include 29 chemical variables and 94 (Sapienza and Montelibretti) or 75 (Via Saredo) PM_{10} daily samples. MDL and descriptive statistics of the variables used for the PMF are reported in Tables 2, 3 and 4.

At all sites, the signal-to-noise (S/N) criterion (Paatero and Hopke, 2003) was ≥ 2 for all selected variables, indicating that they retain far larger signal than noise. All variables were thus categorized in the PMF model as *strong*, with the exception of PM_{10} (total variable).

PMF solutions were investigated in Q robust mode. During preliminary analysis, 5 to 9 factors were extracted at each site by initial steps of 50 consecutive runs, and approaching to local minima was monitored by the Q robust/Q expected ratio (Q_{rob}/Q_{exp}). The final number of factors was determined as best compromise between the Q_{rob}/Q_{exp} trend and the physical soundness of extracted factor profiles. Diagnostic species ratios of factor profiles were assessed to this goal. Factors describing long-range transport contributions were checked by backtrajectory analysis (HYSPLIT Trajectory Model). Final solution was obtained by 100 runs.

Error estimation of PMF factor analytic solutions was performed by classical bootstrap (BS), displacement of factor elements (DISP), and bootstrap enhanced by displacement (BS-DISP), available with the PMF v5.0 package.

3. Results and discussion

3.1 PM_{10} Mass Concentration

PM_{10} mass concentration was monitored to evaluate its variability in the study area among pre-lockdown, lockdown and post-lockdown (Tables 2, 3 and 4).

During pre-lockdown and lockdown, mean concentration at Sapienza was 29±11 μg/m³ and 20±11 μg/m³, respectively, while at Montelibretti, it was 32±15 μg/m³ and 21±10 μg/m³, respectively. The decrease in PM_{10} mass concentration (of about 10 μg/m^3) in the lockdown period can be due to different factors acting simultaneously, such as a more efficient mixing of the lower atmosphere, which is typical of the warmer period (Perrino et al., 2008), the decrease in the strength of typical winter sources like biomass domestic heating (Massimi et al., 2020a), and the decreased impact of all non-essential productive and work activities reduced during the lockdown. However, the latter factor would have been expected to lead to a larger decrease in PM_{10} mass concentration than observed. Reasons for this lower-than-expected decrease will be discussed in the following paragraphs. On the other hand, at Via Saredo, mean PM_{10} mass concentration during lockdown and post-lockdown was 19±7 μg/m³ and 20±11 μg/m³, respectively, indicating that the resumption of productive and work activities during post-lockdown leaded to a very-weak increase in PM_{10} mass concentration.

Table 2. MDL and descriptive statistics of PM_{10} mass and PM_{10} chemical compounds concentrations determined at Sapienza.

			Sapienza							
			Pre-lockdown				Lockdown			
	UoM	MDL	Mean	Std. Dev.	Median	Range (min-max)	Mean	Std. Dev.	Median	Range (min-max)
PM_{10}	µg/m³	-	29	11	30	7.2 - 48	20	11	17	8.1 - 65
OC	µg/m³	0.4	7.2	3.5	6.5	1.2 - 15	4.9	2.5	3.9	2.1 - 12
EC	µg/m³	0.12	1.8	0.88	1.6	0.31 - 3.8	0.47	0.29	0.41	0.11 - 1.4
LVG	µg/m³	0.051	0.45	0.35	0.36	0.0042 - 0.13	0.21	0.21	0.14	0.015 - 0.84
SO_4^-	µg/m³	0.011	1.1	0.6	1.1	0.11 - 2.6	1.9	1.7	1.6	0.47 - 11
Cl^-	µg/m³	0.0021	2.5	3.2	12	0.11 - 12	5.7	1.1	1.8	0.017 - 49
Na^+	µg/m³	0.0022	16	15	12	0.13 - 6.2	0.66	0.79	0.34	0.027 - 3.4
K^+	µg/m³	0.0051	0.31	0.15	0.28	0.053 - 0.65	0.19	0.15	0.15	0.057 - 0.59
Mg^{2+}	µg/m³	0.0051	0.21	0.19	0.15	0.025 - 0.77	0.11	0.11	0.064	0.016 - 0.49
NH_4^+	µg/m³	0.0021	0.42	0.53	0.21	0.016 - 2.6	0.51	0.31	0.39	0.12 - 1.3
NO_3^-	µg/m³	0.0051	3.6	2.7	3.1	0.6- 12	1.4	0.9	1.1	0.23 - 4.6
Al	µg/m³	0.012	0.057	0.028	0.056	0.001 -0.10	0.14	0.14	0.11	0.016 - 0.73
Si	µg/m³	0.011	0.18	0.089	0.18	0.0038 - 0.33	0.66	0.68	0.46	0.073 - 3.5
Ca	µg/m³	0.013	0.76	0.22	0.76	0.17 - 1.3	0.84	1.11	0.61	0.085 - 6.2
Soluble Cs	ng/m³	0.00093	0.039	0.042	0.026	0.00046 - 0.18	0.022	0.042	0.014	0.0038 - 0.11
Soluble Ni	ng/m³	0.081	0.25	0.34	0.096	0.041 - 1.5	0.28	0.21	0.21	0.041 - 0.98
Soluble Rb	ng/m³	0.021	1.2	1.1	0.96	0.011 - 4.1	0.83	0.93	0.44	0.14 - 3.3
Soluble Tl	ng/m³	0.00051	0.065	0.11	0.037	0.00025 - 0.56	0.039	0.051	0.024	0.0052 - 0.25
Soluble V	ng/m³	0.074	0.33	0.23	0.29	0.037 - 0.77	0.52	0.42	0.41	0.081 - 1.8
Soluble Cs	ng/m³	0.0016	0.049	0.022	0.051	0.014 - 0.11	0.042	0.029	0.035	0.0079 - 0.15
Insoluble Cu	ng/m³	0.86	18	10	17	4.5 - 49	3.4	1.8	2.9	0.94 - 11
Insoluble Fe	ng/m³	32	631	348	614	132 - 1792	250	156	201	50 - 818
Insoluble Li	ng/m³	0.012	0.084	0.053	0.083	0.0059 - 0.25	0.15	0.17	0.089	0.024 - 0.88

Insoluble Mo	ng/m³	0.039	1.2	0.7	1.1	0.24 - 3.7	0.37	0.21	0.31	0.061 - 0.98
Insoluble Rb	ng/m³	0.052	0.53	0.26	0.51	0.14 - 1.3	0.46	0.33	0.36	0.11 - 1.8
Insoluble Sb	ng/m³	0.23	2.1	1.9	1.7	0.31 - 11	0.59	0.49	0.42	0.12 - 1.9
Insoluble Sn	ng/m³	0.18	4.1	2.5	4.1	0.58 - 12	0.91	0.51	0.78	0.089 - 2.7
Insoluble Ti	ng/m³	0.61	5.5	2.6	5.2	1.1 - 10	6.5	5.5	5.1	1.5 - 30
Insoluble V	ng/m³	0.068	0.51	0.32	0.47	0.033 - 1.7	0.54	0.49	0.36	0.033 - 2.5

Table 3. MDL and descriptive statistics of PM_{10} mass and PM_{10} chemical compounds concentrations determined at Via Saredo.

			Via Saredo							
			Lockdown				**Post-lockdown**			
	UoM	**MDL**	**Mean**	**Std. Dev.**	**Median**	**Range (min-max)**	**Mean**	**Std. Dev.**	**Median**	**Range (min-max)**
PM_{10}	µg/m³	-	19	7	18	10.0 - 34	20	11	18	10.0 - 34
OC	µg/m³	0.4	4.6	2.2	3.8	1.6 - 9.2	3.4	0.9	3.3	1.9 - 5.6
EC	µg/m³	0.12	0.49	0.24	0.43	0.19 - 1.1	0.55	0.21	0.48	0.31 - 1.1
LVG	µg/m³	0.051	0.21	0.11	0.18	0.053 - 0.47	0.11	0.029	0.11	0.037 - 0.17
SO_4^-	µg/m³	0.011	1.9	0.9	1.6	0.47 - 3.8	1.1	0.4	1.1	0.44 - 2.5
Cl^-	µg/m³	0.0021	0.55	0.98	0.099	0.015 - 3.9	0.88	1.2	0.25	0.016 - 4.5
Na^+	µg/m³	0.0022	0.56	0.66	0.25	0.026 - 2.6	0.86	0.88	0.49	0.035 - 3.3
K^+	µg/m³	0.0051	0.18	0.091	0.15	0.071 - 0.36	0.11	0.047	0.098	0.036 - 0.22
Mg^{2+}	µg/m³	0.0051	0.085	0.076	0.054	0.016 - 0.32	0.12	0.11	0.075	0.016 - 0.41
NH_4^+	µg/m³	0.0021	0.54	0.37	0.46	0.097 - 1.3	0.24	0.11	0.23	0.065 - 0.58
NO_3^-	µg/m³	0.0051	1.3	0.6	1.3	0.25 - 2.7	1.1	0.6	0.96	0.19 - 2.9
Al	µg/m³	0.012	0.14	0.11	0.096	0.039 - 0.47	0.23	0.25	0.14	0.026 - 1.1
Si	µg/m³	0.011	0.59	0.44	0.42	0.16 - 2.1	0.96	1.11	0.58	0.11 - 4.6
Ca	µg/m³	0.013	0.67	0.36	0.62	0.18 - 1.8	0.92	0.67	0.75	0.25 - 3.5
Soluble Cs	ng/m³	0.00093	0.017	0.012	0.013	0.0031 - 0.042	0.0058	0.0035	0.0055	0.0012 - 0.017

Soluble Ni	ng/m³	0.081	0.29	0.24	0.22	0.041 - 0.85	0.13	0.14	0.11	0.041 - 0.88
Soluble Rb	ng/m³	0.021	0.62	0.39	0.48	0.19 - 1.5	0.25	0.15	0.23	0.039 - 0.75
Soluble Tl	ng/m³	0.00051	0.026	0.017	0.021	0.0036 - 0.068	0.013	0.014	0.0079	0.0013- 0.069
Soluble V	ng/m³	0.074	0.52	0.46	0.34	0.058 - 1.5	0.25	0.17	0.19	0.043 - 0.71
Soluble Cs	ng/m³	0.0016	0.044	0.019	0.041	0.018 - 0.089	0.071	0.049	0.061	0.0092 - 0.21
Insoluble Cu	ng/m³	0.86	2.8	1.1	2.6	1.3 - 5.7	4.9	2.6	3.9	1.5 - 13
Insoluble Fe	ng/m³	32	237	83	209	113 - 449	357	224	286	73 - 1151
Insoluble Li	ng/m³	0.012	0.069	0.079	0.036	0.0059 - 0.28	0.18	0.24	0.11	0.0059 - 0.98
Insoluble Mo	ng/m³	0.039	0.33	0.14	0.29	0.14 - 0.65	0.41	0.21	0.36	0.13 - 0.99
Insoluble Rb	ng/m³	0.052	0.46	0.19	0.41	0.18 - 0.79	0.71	0.52	0.58	0.079 - 2.2
Insoluble Sb	ng/m³	0.23	0.59	0.32	0.59	0.12 - 1.2	0.77	0.64	0.52	0.12 - 3.1
Insoluble Sn	ng/m³	0.18	0.95	0.39	0.93	0.41 - 2.1	1.2	0.6	1.1	0.37 - 3.1
Insoluble Ti	ng/m³	0.61	6.8	3.2	5.6	2.7 - 14	10	9	8	1.5 - 46
Insoluble V	ng/m³	0.068	0.58	0.28	0.53	0.18 - 1.4	0.82	0.62	0.65	0.21 - 3.1

Table 4. MDL and descriptive statistics of PM_{10} mass and PM_{10} chemical compounds concentrations determined at Montelibretti.

			Montelibretti							
			Pre-lockdown				Lockdown			
	UoM	MDL	Mean	Std. Dev.	Median	Range (min-max)	Mean	Std. Dev.	Median	Range (min-max)
PM_{10}	µg/m³	-	32	15	34	3.5 - 59	21	10	18	5.2 - 49
OC	µg/m³	0.4	11	5	11	1.9 - 20	4.7	2.7	3.8	1.7 - 12
EC	µg/m³	0.12	1.1	0.5	1.2	0.083 - 1.9	0.36	0.26	0.29	0.066 - 1.2
LVG	µg/m³	0.051	1.2	0.6	1.3	0.056 - 2.1	0.26	0.27	0.13	0.022 - 0.97
SO_4^-	µg/m³	0.011	0.46	0.23	0.44	0.035 - 0.92	1.8	1.2	1.6	0.41 - 7.8
Cl^-	µg/m³	0.0021	0.53	0.71	0.23	0.042 - 3.1	0.41	0.79	0.12	0.011 - 4.1
Na^+	µg/m³	0.0022	0.46	0.52	0.21	0.067 - 2.1	0.51	0.61	0.26	0.033 - 3.1
K^+	µg/m³	0.0051	0.67	0.31	0.73	0.048 - 1.1	0.24	0.17	0.19	0.048 - 0.72
Mg^{2+}	µg/m³	0.0051	0.067	0.062	0.036	0.017 - 0.25	0.082	0.078	0.054	0.013 - 0.39
NH_4^+	µg/m³	0.0021	0.79	0.51	0.77	0.031 - 2.1	0.49	0.34	0.35	0.11 - 1.6
NO_3^-	µg/m³	0.0051	3.2	1.6	3.2	0.18 - 5.9	1.2	0.8	1.1	0.065 - 4.1
Al	µg/m³	0.012	0.089	0.078	0.071	0.0091 - 0.31	0.14	0.16	0.08	0.0072 - 1.1
Si	µg/m³	0.011	0.38	0.35	0.28	0.033 - 1.3	0.61	0.69	0.36	0.038 - 4.3
Ca	µg/m³	0.013	0.61	0.29	0.62	0.072 - 1.2	0.71	0.67	0.54	0.069 - 3.4
Soluble Cs	ng/m³	0.00093	0.15	0.09	0.15	0.0073 - 0.31	0.052	0.052	0.029	0.0035 - 0.28
Soluble Ni	ng/m³	0.081	0.25	0.011	0.23	0.041 - 0.59	0.32	0.19	0.28	0.039 - 1.2
Soluble Rb	ng/m³	0.021	2.9	1.6	3.1	0.16 - 5.4	1.1	0.9	0.78	0.19 - 4.2
Soluble Tl	ng/m³	0.00051	0.092	0.046	0.11	0.0071 - 0.16	0.033	0.038	0.021	0.0041 - 0.22
Soluble V	ng/m³	0.074	0.12	0.085	0.088	0.022 - 0.34	0.39	0.29	0.31	0.049 - 1.2
Soluble Cs	ng/m³	0.0016	0.081	0.066	0.065	0.011 - 0.32	0.058	0.037	0.051	0.0093 - 0.16
Insoluble Cu	ng/m³	0.86	5.4	2.6	5.6	1.1 - 11	1.8	0.9	1.6	0.43 - 4.6

Insoluble Fe	ng/m³	32	226	103	215	44 - 494	169	137	125	16 - 736
Insoluble Li	ng/m³	0.012	0.091	0.068	0.069	0.014 - 0.31	0.14	0.16	0.081	0.017 - 0.88
Insoluble Mo	ng/m³	0.039	1.1	1.1	0.6	0.059 - 4.7	0.12	0.11	0.093	0.019 - 0.64
Insoluble Rb	ng/m³	0.052	0.41	0.21	0.38	0.091 - 0.97	0.45	0.31	0.37	0.063 - 1.5
Insoluble Sb	ng/m³	0.23	1.1	1.1	0.92	0.12 - 5.5	0.49	0.46	0.35	0.12 - 2.5
Insoluble Sn	ng/m³	0.18	1.4	0.6	1.4	0.19 - 2.6	0.48	0.29	0.42	0.089 - 1.4
Insoluble Ti	ng/m³	0.61	5.4	3.6	4.7	0.76 - 16	5.3	5.5	3.5	0.31 - 27
Insoluble V	ng/m³	0.068	0.46	0.25	0.43	0.11 - 1.2	0.45	0.43	0.34	0.033 - 2.3

3.2 Chemically Fractionated Trace Elements for Source Apportionment

Trace elements in PM are still scarcely considered as selective source markers, although their recently highlighted relevant role in identifying PM sources (Massimi et al., 2021; Perrino et al., 2020; Zhou et al., 2020). This may be due to the difficulty in discriminating tracer species that can be associated to more than one source (Querol et al., 2007). However, the chemical fractionation procedure (Canepari et al., 2006a, 2006b, 2010) allows assessing the chemical form (soluble and insoluble) in which each element is released in PM, which may be typical of its emission source (Massimi et al., 2020b), thus being very efficient for the identification of several sources (Yadav and Rajamani, 2006; Feng et al., 2009; Canepari et al., 2010; Betha et al., 2014; Li et al., 2015).

In this study, before employing chemically fractionated elements for PM_{10} source apportionment, linear correlation coefficients (R^2) were checked between reliable and commonly used source markers and trace elements in the soluble and insoluble fractions.

In Fig. 2, comparisons between the daily variability in concentration of soluble Rb and LVG (panel a), of insoluble Rb and Si (panel b), of soluble V and soluble Ni (panel c), and of insoluble V and Si (panel d), at Sapienza during lockdown (from March 14th to May 13th) are shown. LVG, Si and Ni are widely recognized as highly selective tracers of biomass burning (Chowdhury et al., 2007; Sharma et al., 2016; Massimi et al., 2020a), crustal dust (Pant and Harrison, 2012; Tian et al., 2013; Perrino et al., 2020) and heavy oil combustion (Reddy et al., 2005; Okuda et al., 2007; Moreno et al., 2010), respectively.

The temporal trend of soluble Rb (panel a) was practically identical to that of LVG (R^2 = 0.95), both showing a marked decrease from the colder to the warmer period. The same behavior was observed for soluble Cs (R^2 = 0.92; supplementary material S1), confirming the possible use of the soluble fraction of Rb and Cs as robust tracers for biomass burning sources. On the contrary, the insoluble fraction of Rb (panel b) showed a completely different trend, closely matching that of Si (R^2 = 0.81); similar behaviour is also shown by the insoluble fraction of Cs, Li and Ti (R^2 = 0.75, 0.92 and 0.88, respectively; supplementary material S1) which are contained in soil (Canepari et al., 2019; Massimi et al., 2020b), and of V (panel d). Maximum values of Si and of insoluble Rb, Cs, Li, Ti and V were observed during March 29th-30th, April 8th-10th, 18th-20th, and May 13th-14th. These days were characterized by events of mineral dust advection from desert regions (see section 3.5), thus confirming the reliability of these species as tracers of crustal dust. Moreover, since advection days occurred within the lockdown period, this presumably contributed to the lower-than-expected decrease of PM_{10} mass concentration during lockdown with respect to other periods (see section 3.1).

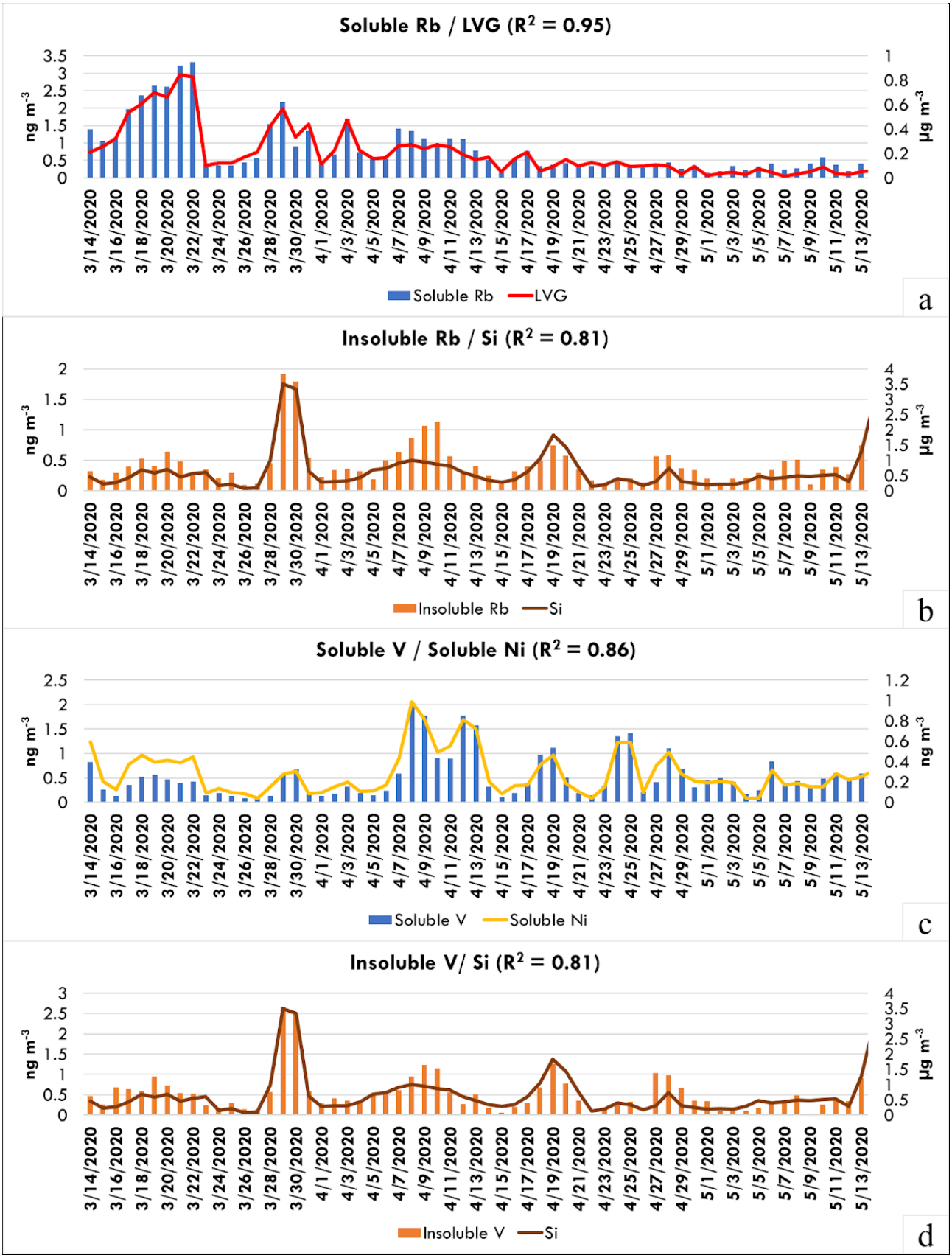
Soluble Rb / LVG (R^2 = 0.95)
ng m-3
µg m-3
Soluble Rb
LVG
a
Insoluble Rb / Si (R^2 = 0.81)
ng m-3
µg m-3
Insoluble Rb
Si
b
Soluble V / Soluble Ni (R^2 = 0.86)
ng m-3
ng m-3
Soluble V
Soluble Ni
c
Insoluble V/ Si (R^2 = 0.81)
ng m-3
µg m-3
Insoluble V
Si
d

Fig. 2. Comparison between concentrations of soluble Rb and LVG (panel a), insoluble Rb and Si (panel b), soluble V and soluble Ni (panel c), and insoluble V and Si (panel d), obtained at Sapienza from March 14th to May 13th (lockdown period).

On the other hand, from panel c, we can observe a high correlation (R^2 = 0.86) between concentrations of soluble V and soluble Ni. Both V and Ni are commonly employed in the form of total element, for their source selectivity with heavy oil combustion (Allouis et al., 2003; Moreno et al., 2010). The chemical fractionation put on evidence, in addition, that the soluble V and Ni are more involved than their insoluble fraction in describing the fingerprint of this source. Peaks of soluble V and Ni observed on the first week of April and, minor, on April 24th-28th (Fig.2, panel c) correspond to advections of heavy oil burning dust, as it will be discussed in section 3.5; however, these peaks are not observed for the insoluble V (panel d) and Ni (not reported).

For Cs, Rb and V, the solubility percentage is of 65%, 88% and 20% respectively.

Finally, Cu, Fe, Mo, Sn, Sb in their insoluble fraction, are known to be emitted by mechanical abrasion of vehicles components, since they are commonly used as components of tires, brake pads and linings (Amato et al., 2011; Tofful et al., 2020; Massimi et al., 2021). The high inter-correlation between temporal variability of insoluble Sb and Sn (supplementary material S1) confirmed their efficiency to trace brake dust (Querol et al., 2012; Kam et al., 2013; Namgung et al., 2016; Canepari et al., 2019; Massimi et al., 2020b). Moreover, the ability of chemically fractionated elements to trace different sources is supported by documented existence of very substantial differences in the size distribution of the two fractions of the considered elements (Canepari et al., 2019; Massimi et al., 2020b). These considerations encourage the use of chemically fractionated trace elements for the identification of emission sources in PM_{10} source apportionment studies (Canepari et al., 2009; Perrino et al., 2010; Massimi et al., 2021).

3.3 Source Apportionment

The most stable PMF solution extracts 7 factors at both urban traffic sites Sapienza and Via Saredo, and 8 factors at Montelibretti. Scaled residuals are within ± 3 SD for most species, with symmetrical distribution; exceptions concern, at all sites, Ca, the soluble fraction of Ni and Tl, and the insoluble fraction of Cs, Mo and Sb.

The rotation by F-peak did not improve the interpretability of factor profiles, therefore the base case with F-peak = 0 was considered as best fit (Belis et al., 2019). G-space plots were examined to exclude the presence of oblique edges between factors, and the Q_{robust}/Q_{exp} indicator was monitored. The best solution at each site showed Q_{robust}/Q_{exp} ranging 1.2-1.3.

The effect of measurement errors and of rotational ambiguity on solutions were investigated by classical bootstrap (BS), displacement of factor elements (DISP), and bootstrap enhanced by displacement (BS-DISP) tools available by EPA PMF v5.0. Regardless of data perturbation approaches, source tracers of each factor contribution show tight variability intervals, as shown in supplementary material S2, indicating that the factors extracted in the final solution are generally neither affected by uncertainties of data measurement, nor by

rotational ambiguity during PMF runs. Higher uncertainties are instead associated to species not representing source tracers, by factor, as indicated by larger intervals of variability estimated by DISP and BS-DISP analyses.

Factors identified at all sites are vehicular traffic, biomass burning, sea spray, heavy oil combustion, two different mineral dust profiles, and ammonium sulfate and organics. In addition, ammonium nitrate is extracted at Montelibretti. From Fig. 3, we can observe the chemical profiles of the factors identified by PMF at Sapienza during the entire monitoring period, while chemical profiles of the factors identified at Via Saredo and Montelibretti are reported in supplementary material S3. The related average percent source contributions to PM_{10} mass concentration for pre-lockdown, lockdown and post-lockdown are shown in Fig. 6.

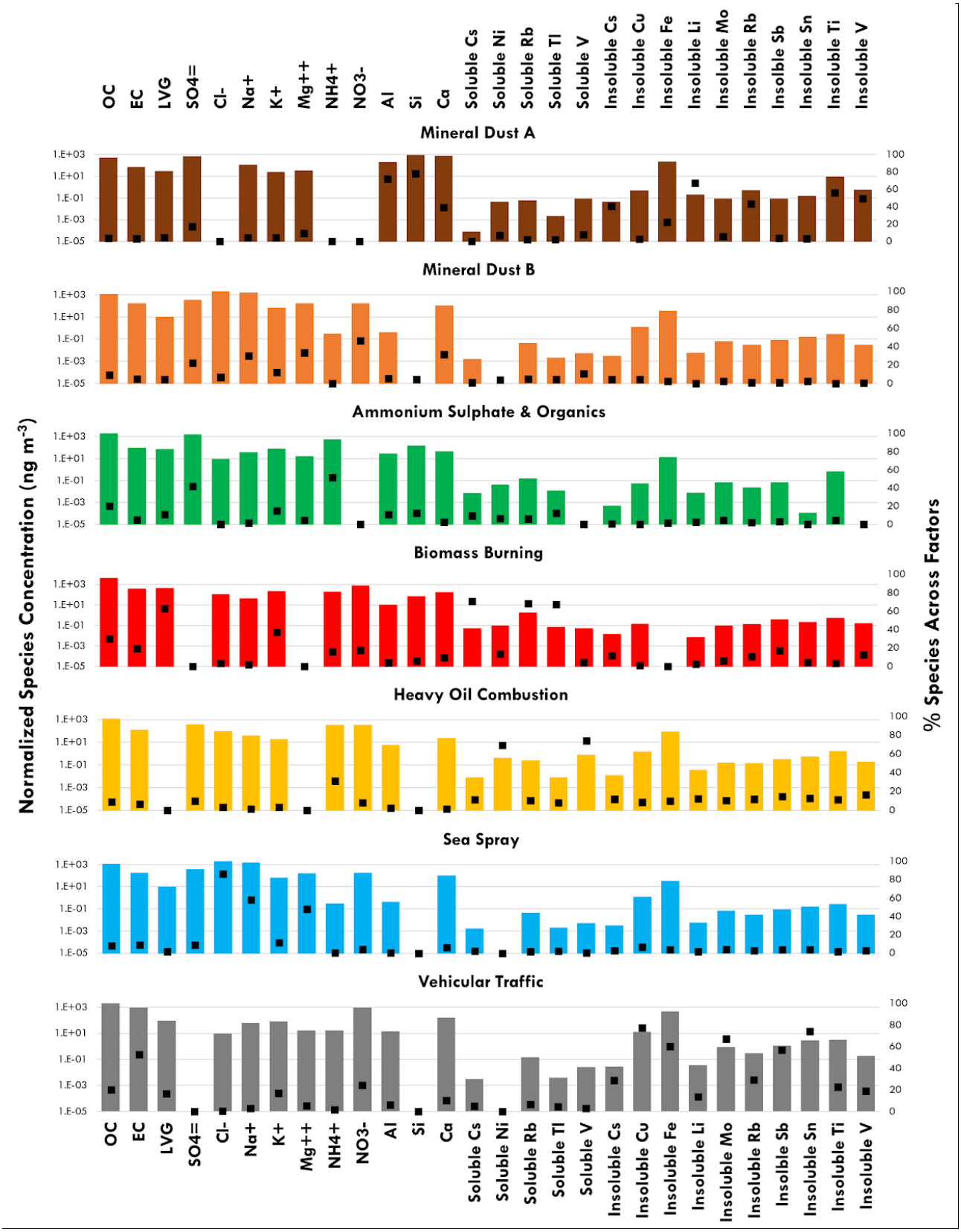

Fig. 3. Chemical profiles of the factors identified by PMF at Sapienza during the entire monitoring period.

3.3.1 Vehicular traffic

Most abundant species describing this factor are organic and elemental carbon, and to minor extent Ca and insoluble Fe. EC/OC ratios are 0.4, 0.2 and 0.1 at Sapienza, Via Saredo and Montelibretti, respectively,

comparable to the variability range of traffic profiles determined at Italian cities in recent years. In particular, traffic profiles no. 147, 265, 270, 280 and 290 (related to Milan, Genoa, Bari and Civitavecchia) of the SPECIEUROPE repository (Pernigotti et al., 2016) show EC/OC ratio ranging 0.3 – 0.8. At Montelibretti, the OC abundance in the profile is far larger than at the two urban sites, while the EC abundance is lower. Most probable explanation for this difference is the perturbation due to biomass burning, that during the first sampling period was considerably active at Montelibretti. Furthermore, it has to be noted that the non-exhaust component is also included in this factor. The PMF model was not able to disaggregate it from the exhaust part due to unavailability of selective tracers for the exhausts, whereas non-exhaust tracers were largely used. The non-exhaust is described by the presence of Ca, that is commonly related to asphalt abrasion, and of the insoluble fraction of Fe, Cu, Mo, Sb and Sn. The variability of the Ca/insoluble Fe ratio at the three sites (0.3, 0.9. and 1.1 at Sapienza, Montelibretti and Via Saredo, respectively) depends on the almost doubled abundance of Ca at Via Saredo with respect to the other sites, likely due to the presence of gravel in the public park in the nearby of sampling site, and to the lower abundance of insoluble Fe at Montelibretti. A large variability in the Ca/Fe ratio is anyway observed in traffic profiles, i.e. ranging 0.1 – 0.8 for the above cited ones. The variance of insoluble fraction of Fe, Cu, Mo, Sb and Sn is mostly explained by the vehicular traffic factor, with percent of total species ranging 60-80 %.

3.3.2 Biomass burning

This factor is mainly described by OC, EC, LVG and K^+, representing respectively the 35-50%, 4-5%, 3-5% and 2.8% of the PM_{10} mass contribution apportioned to this source. Both LVG and K^+ are widely acknowledged as selective tracers of biomass combustion (Pant and Harrison, 2012; Nguyen et al., 2013; Liu et al., 2017; Chowdhury et al., 2007; Sharma et al., 2016).

Inter-site differences of profile are very limited, which is explained by the fact that all sites are in the same area, where comparable biomass types are expected to be burned. The EC/OC, LVG/OC, K+/LVG and Cs/Rb (soluble fractions) ratios observed in the biomass burning profile of the three sites are reported in Table S3.1, with the respective variability range calculated on a number of biomass burning profiles available in SPECIEUROPE. Values of the ratios fall within the range of the available profiles.

At Via Saredo, however, either EC/OC and K+/LVG are out of the respective range, because of the lower percent abundance of EC and LVG in the biomass burning profile with respect to the other sites. This can be partly due to the almost negligible strength of this source during late spring, when samples were collected at Via Saredo. Nevertheless, at this site the LVG explained by biomass burning is 44% of total species, comparably with the 47% explained at Montelibretti (and 60% at Sapienza). It has to be noted that Cs/Rb has been rarely considered as diagnostic ratio of biomass burning. As shown in Table S3.1, with respect to other diagnostic ratios, the Cs/Rb shows narrow variability within SPECIEUROPE biomass burning profiles, ranging 0.04-0.06. At the three sites of this study, Cs/Rb values calculated on the total element (available in the extended dataset not used for PMF) fall within the above range, namely: 0.07 ± 0.01 (median 0.07; min-max: 0.05-0.1) at Montelibretti and Via Saredo, and 0.05 ± 0.01 (median 0.05; min-max: 0.03-0.08) at Sapienza. Nevertheless, using in the PMF the soluble fraction of Cs and Rb, instead of total, resulted in highly

efficient tracing of biomass burning. This indicates that soluble Cs, Rb and Tl (not shown) are far more selective tracers of biomass burning than the total element content. Indeed, by using the total element, source tracing can be perturbed by the influence of other sources, that are better marked by the insoluble fraction of same elements, as previously discussed (paragraph 3.2). Values of soluble Cs/Rb in the biomass burning profile of this study range 0.01-0.03.

3.3.3 Sea spray

Sea spray is identified by dominant abundances in the profile of Cl^-, Na^+, $SO_4^=$, Mg^{2+}, Ca and K^+, listed by decreasing order of species percent in the PM_{10} mass apportioned to factor, for the three sites. Abundances of these species strictly resemble those of fresh sea salt (Seinfeld and Pandis, 2006); this is shown in supplementary material S3, where the sea spray profiles of this study are compared with the reference profile of fresh sea salt. Diagnostic ratios between each of the above species and Na^+ are almost equal to those of the reference profile, confirming that the PMF model provided accurate estimation of the chemical fingerprint. The only exception concerns NO_3^-, the abundance of which is atypically higher than expected for this profile. Likely, this is a collinearity problem, since a significant fraction of total NO_3^- is contributed by mineral dust, in this study, and transport events observed during last part of the sampling period often include both sea spray and mineral dust contributions.

3.3.4 Heavy oil combustion

This factor is mainly described by the soluble fraction of V and Ni, and by $SO_4^=$, NH_4^+, OC, EC and the insoluble fraction of Fe. The variance of soluble Ni and V is explained by 70-80 % of total species, depending on the site, while $SO_4^=$, NH_4^+, OC, EC and insoluble Fe are explained by about 20-30%, 30-40% and 5-10% (OC, EC and insoluble Fe), respectively. The source-selective role of V and Ni as tracers of the combustion of crude oils is well acknowledged, particularly concerning exhausts from diesel engines of marine vessels (Pey et al., 2013; Corbin et al., 2018; Zhao et al., 2021). Besides V and Ni, Fe is the most abundant transition metal in exhausts of heavy oil combustion. V, Ni and Fe are indeed observed in metal-carbon inclusions (in soot, char and other carbon particles emitted by marine engines), forming crystals or microcrystals with S and Ca, and acting as nuclei for the condensation of aromatic compounds during combustion (Popovicheva et al., 2009). The V/Ni ratio associated to shipping emissions ranges 2–5, as observed in profiles available by the SPECIEUROPE repository (Pernigotti et al., 2016), and by different authors (Viana et al., 2009; Corbin et al., 2018; Zhao et al., 2021). Since in this study the soluble fraction of V and Ni was used in PMF, slightly different values of V/Ni, ranging 1.9-2.1, are observed in the heavy oil combustion profiles.

Factor identity of this profile was thus checked against literature source profiles, by using ratio-ratio scatter plots (Robinson et al., 2006) of the V/Ni and Fe/EC diagnostic ratios. In this type of plot, different source categories are expected to cluster separately from each other with respect to same source tracers, depending on the values of diagnostic ratios. The V-Ni rich profiles of this work were thus compared by ratio-ratio plot with all SPECIEUROPE source profiles (including non-shipping ones) where V, Ni, Fe and EC are available (Figures S3.4, S3.5 and S3.6).

Daily PM_{10} samples collected at each site were also included in the plots, to assess which days cluster close to literature profiles. The ratio-ratio plots confirm that the V-Ni rich factors of this study fall within the cluster of heavy oil combustion profiles. Concerning individual PM_{10} samples, those distributing closest to heavy oil combustion profiles correspond to those more contributed by the V-Ni rich PMF factor, by site.

3.3.5 Mineral Dusts

Two different mineral dust profiles have been identified, Mineral Dust A and Mineral Dust B, which will be referred to as MD-A and MD-B for the rest of this paragraph.

The MD-A is described by significantly higher abundances of Si, Ca, Al and the insoluble fractions of Fe, Ti, V, Li and Rb with respect to MD-B, while the latter is far more enriched in Na, K and Mg ions, and NO_3^-. Si, Ca, Al and insoluble Fe represent on average 10% (Si), 8% (Ca) and 2% (Al and insoluble Fe) of PM_{10} mass apportioned to MD-A, and less than half percent values, respectively, of PM_{10} apportioned to MD-B. Conversely, NO_3^- and Na, K and Mg ions are contributed by the MD-B by about one order of magnitude higher percentages than by the MD-A. It is worth mentioning that either the MD-A and the MD-B profiles are each strictly comparable among the sites. Since Montelibretti is located far from the two urban sites, this likely indicates that mineral dusts observed in this study were transported from other areas. The average percent contributions to PM_{10} mass by MD-A and MD-B are similar, both inter-site and within-site, with values of 14%, 22% and 24 % (MD-A) and 13%, 13% and 21 % (MD-B) at Montelibretti, Via Saredo and Sapienza, respectively. However, the two profiles indicate that crustal materials of MD-A and MD-B largely differ in their chemical nature, indicating different source origins. From the MD-A profile, a composition rich in silicates, Ca-rich minerals and metal oxides can be hypothesized, while the MD-B profile suggests a composition rich in nitrates and other salts. Nevertheless, most mineral dust advection episodes occurred during the same days for both MD-A and MD-B, suggesting that both contributions followed common transport pathways to receptors. In particular, the MD-A factor profile seems to be attributable to dust advection events from African deserts, given its enrichment in Ti and V (insoluble fraction), which are commonly reported in literature as source tracers of dust intrusions from Sahara and Sahel regions (Perez et al., 2008; Linares et al., 2021). However, interferences of local crustal materials on the MD-A and MD-B profiles cannot be excluded. Indeed, most dust outbreaks occurred during lockdown, when local traffic was almost turned off, and the PMF was not able, thus, to resolve the individual contributions neither of local dust re-suspension by vehicles riding, nor of short-range transport from Rome outskirts. This aspect was thus further investigated by comparison with literature profiles. A large number of Sahara and Sahel dust profiles had been previously observed to separate efficiently both from profiles of local geological areas of Rome outskirts and from road dust profiles, by ratio-ratio plot of crustal-specific diagnostic ratios (Pietrodangelo et al., 2013). Following the same approach, in this work, the Si/Al versus Ti/V plot has been thus employed to assess the distribution of MD-A and MD-B profiles with respect to local geological and Sahara/Sahel dust profiles previously analyzed. Form Fig. 4 it is evident that both MD-A and MD-B are separated from re-suspended desert topsoil, road dust, and local geological airborne dust profiles. The MD-A falls close to main group of profiles of African dust outbreaks, thus supporting the hypothesis of a transport from African deserts.

Differently, the MD-B separates from all profile groups, suggesting a non-local origin other than Sahara or Sahel regions.

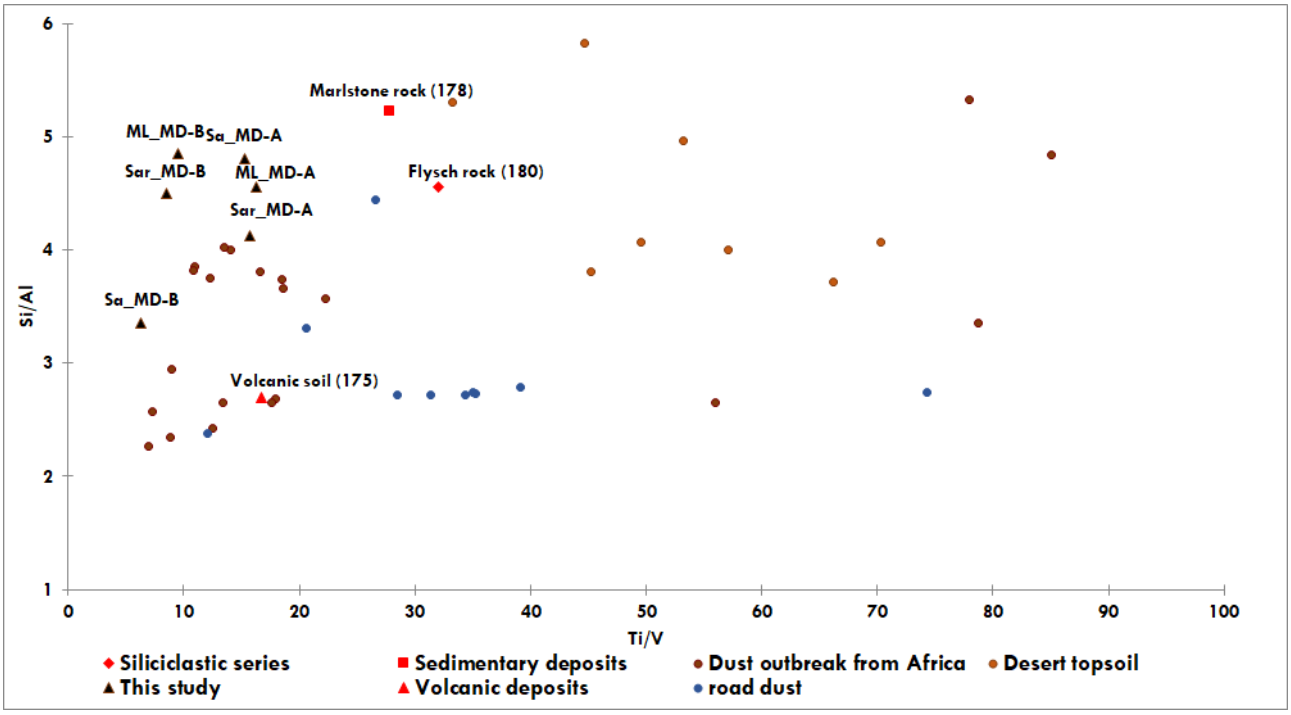

Fig. 4. Si/Al and Ti/V ratio-ratio plot comparing different African mineral dust, urban road dust and local (Latium) geological dust chemical fingerprints in the PM_{10} fraction, with the MD-A and MD-B factor profiles of this study. The following abbreviations are adopted: ***Sa*** for Sapienza, ***Sar*** for Via Saredo, and ***ML*** for Montelibretti sites. Local dust profiles are indicated by the SPECIEUROPE name and ID number.

3.3.6 Secondary Ammonium Nitrate and Sulfates

These two contributions were only identified at Montelibretti, while at Sapienza and Via Saredo stable PMF solutions extract only secondary sulfates combined to organics.

Ammonium nitrate formation is fostered by emissions of gaseous precursors from large vehicle traffic fluxes, intensive use of wood and other biomass combustion, and intensive agriculture and farming activities emitting ammonia (Amato et al., 2016). At Montelibretti, located in a country area, the latter two factors are dominant while road traffic plays a minor role. On the other side, at Sapienza and Via Saredo, which are mainly impacted by traffic emissions, these were strongly limited during most sample collection, due to lockdown. Therefore, biomass burning is expected to be the only source of ammonium nitrate precursors, in this study, and it is expected to affect Montelibretti during the first sampling period. As a matter of fact, in addition to NH_4^+ and NO_3^- , represented by this factor for the 47% and 38% respectively of total species, the ammonium nitrate profile (Fig. S3.2) is characterized by levoglucosan, EC and K^+, indicating a partial source mixing with biomass burning, and by OC, representing particulate and condensed semi-volatile organics emitted during combustion (Stefenelli et al., 2019).

The profile of secondary sulfates combined to organics is characterized by $SO_4^=$, NH_4^+ and OC, representing 15-20%, 5-7% and 25-35%, respectively, of the average PM_{10} mass apportioned to this factor. Similar source strength is observed regardless of site (Fig. 6), with increasing intensity from pre-lockdown (5% and 6%

average of total PM_{10} mass, at Sapienza and Montelibretti) to lockdown (average 15% of total PM_{10} mass at Sapienza and Via Saredo, and 25% at Montelibretti), coherently with the regional nature of this contribution and with the season-related enhanced photochemical activity. It is worth considering that the increase from the pre-lockdown to lockdown periods has to be evaluated with respect to either inorganic and organic species, since the PMF attributes 20-30% of OC variance to this profile, at all sites.

Organics in secondary sulfates profiles are frequently observed (Bernardoni et al., 2011; Amato et al., 2016; Silvern et al., 2017; Dai et al., 2020), with OC profile abundances that can reach sulfate ones. Factors giving rise to significant OC percentages in ammonium sulfates profiles are commonly ascribed to the source mixing that establishes between the ammonia- nitric acid- sulfuric acid regimes forming ammonium sulfates and nitrate (Seinfeld and Pandis, 2006) and the combustion sources emitting organics. In Fig.5 the ammonium sulfate apportioned to main forming species, and the average source contribution estimate of organic matter (OM) in the secondary sulfates profile, are shown. The total ammonium sulfate was apportioned to individual sulfates estimated by chemical equivalent ratios, considering an airborne aerosol where S-rich species are dominant (in the warm season) and form, in turn, ammonium bisulfate, letovicite and sulfate (Seinfeld and Pandis, 2006; Lehmann et al., 2007). The average source contribution estimate of organic matter was estimated as percent of total OC ascribed by PMF (by site) to secondary sulfates, multiplied by a factor α, accounting for non-C atoms in organic compounds; the α value was set to 1.8, as in previous studies in the Rome area (Perrino et al., 2019). From pre-lockdown to lockdown a significant decrease of the OM in the secondary sulfate profile is observed at Sapienza and Montelibretti (32% and 59%, respectively), suggesting that shutting down anthropic and business activities during lockdown also let to a sharp decrease of local emissions of organics and of their influence on secondary aerosol. Concerning the apportioned sulfate species, their temporal evolution and relationship with transport events are discussed in section 3.4.

As a complement of ammonium sulfate apportionment, ammonium nitrate was obtained, by NH_4^+ exceeding the neutralization of sulfates, at the three sites (Fig. 5). As expected from seasonal evolution, highest contributions are observed at Montelibretti during pre-lockdown, accounting for 9% of total PM_{10} mass, and to minor extent at Sapienza (4% of total PM_{10}), while starting from lockdown period to the end of sampling a flat contribution of about 1% is observed at all sites. The apportionment by chemical equivalent ratios allowed to assess that the PMF model overestimated the mass contribution of secondary nitrate at Montelibretti, probably due to the source mixing between secondary nitrate and biomass burning. Therefore, in Fig. 6 and Fig. 7 mass contributions of secondary nitrate are those calculated by chemical equivalents. Conversely, minor or negligible differences are observed between the secondary sulfates PMF profile and the resulting sum of calculated sulfates with OM source contribution estimate in the PMF profile (Fig. 5). Finally, the non-secondary nitrate was estimated by difference with respect to total NO_3^-. This component shows similar contributions irrespective of the period and site, representing on average 7-10%, 4-6% and 6-7% of total PM_{10}, at Sapienza, Montelibretti, and Via Saredo respectively. This areal and temporal homogeneity of mass contributions is coherent with a non-local origin, as previously supposed. Indeed, time series of this component match those of Mineral dust B, as it will be further discussed in paragraph 3.5.

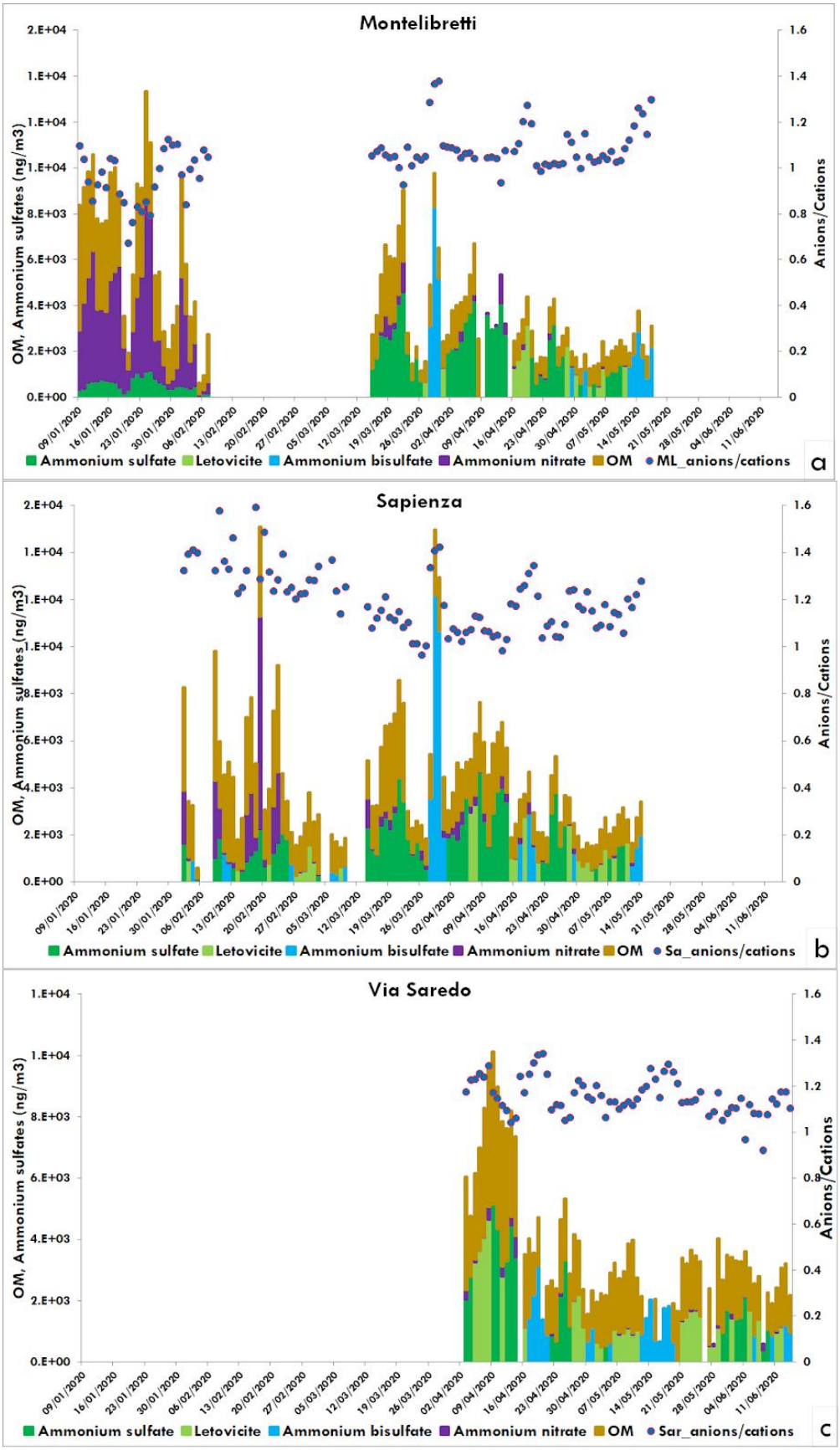

Fig. 5. Daily mass contribution of secondary nitrate, secondary sulfates and organic matter fraction attributed to secondary sulfates factor by PMF, at the three sites of this study. The anions/cations ratio is also reported on the secondary y-axis.

3.4 Ion Balance Analysis

The sum of chemical equivalents of anions and cations has been considered to evaluate the charge neutrality of samples and investigate reasons of eventual deviations from ion balance. Anions vs cations linear regression at the three sites show R^2 coefficient and slope ranging 0.91-0.98 and 1.1-1.3, respectively, indicating that acidic species were generally neutralized during the sampling periods. However, daily trends of the anions/cations ratio indicate that, during specific days, PM_{10} samples were particularly acidic, with ratio values ranging 1.4-1.6. In Fig. 5, the anions/cations ratio is compared to secondary sulfates and nitrate species apportioned by ammonia- nitric acid- sulfuric acid regimes (see paragraph 3.3.6). Highest anions/cations values clearly correspond to days where sulfates formation equilibria are dominated by ammonium bisulfate or, in minor cases, by letovicite, thus indicating that collected aerosol was significantly acidic in these days (Seinfeld and Pandis, 2006). Interestingly, these findings were similarly observed at all sites. Days affected by ammonium bisulfate-rich aerosol, namely March 28th-30th, April 17th-20th and May 12th-20th, correspond to mineral dust advection events, as discussed in paragraph 3.5, suggesting that air masses conveying mineral dusts likely run into acidic aerosols during their transport path.

3.5 Relative Relevance and Time Trend of Source Contributions to PM_{10} Mass Concentration

Relative relevance and time trend of single source contributions to PM_{10} mass concentration during pre-lockdown, lockdown and post-lockdown are shown in Fig. 6 and Fig. 7, respectively.

From Fig. 6, we can observe that the contribution to PM_{10} from vehicular traffic was considerably reduced from pre-lockdown to lockdown, as expected, due to the reduction of movement of the population during lockdown. The decrease was from 25% (panel a) to 6% (panel b) at Sapienza, and from 13% (panel e) to 6% (panel f) at Montelibretti, where the reduction was less evident due to the lower impact of this source during pre-lockdown. On the other hand, the resumption of non-essential productive and work activities after lockdown led to an increase of traffic contribution, as it can be observed at Via Saredo, where percent of PM_{10} mass concentration from vehicular traffic increased from 10% (panel c) to 19% (panel d) during post-lockdown. From Fig. 7, we can observe the time trend of the contribution from traffic in the pre- and post-lockdown periods, ranging from 0.5 to 15 μg m^{-3}, with minimum values in correspondence of the weekend days, while values were continuously very-low at all sites during lockdown.

Regarding biomass burning, the contribution to PM_{10} was reduced from pre-lockdown to lockdown at Sapienza (from 13% to 10%), as well as at Montelibretti (from 38% to 15%), where the decrease was more considerable, this site being more influenced by biomass domestic heating sources during pre-lockdown. However, in this case, the decrease in contribution during lockdown was not due to the Covid-19 quarantine but to the reduced strength of biomass heating emissions in the warmer period. In fact, from panels a and c of Fig. 7, we can observe that biomass burning contribution to PM_{10} declined a month after the lockdown restrictions began, in late March, when temperatures rose and the use of domestic heating systems was greatly reduced. Therefore, the contribution from biomass burning was reduced even more at Via Saredo (from 11% to 3%), during post-lockdown warmer months.

Transport events of sea spray mainly occurred during pre-lockdown and where more consistent during the second half of February (panel a of Fig. 7) at Sapienza, which is closer to the Tyrrhenian Sea (about 30 km)

and where marine aerosols contributed for 18% to the PM_{10} mass concentration. On the contrary, in the lockdown period, sea spray advections were less frequent and intense and occurred mainly during late April and middle May (in connection with dust events; Fig. 7), thus in this period marine aerosols contributed only for 3-8 % to total PM_{10} at all monitored sites (Fig. 6). During post-lockdown, events of sea spray occurred at the beginning of June (panel b of Fig. 7) and contributed to 11% to PM_{10} mass concentration recorded at Via Saredo (panel d of Fig. 6).

The contribution from heavy oil combustion was instead greater during lockdown at all sites, ranging from 10 to 11% to total PM_{10} (Fig. 6) and was presumably associated to events of long-distance transport of dust from coal industries and coal burning for domestic use in North African regions, in agreement with recent reporting by Kirchner et al. (2020). Transport events occurred during the first week of April and, to minor extent, during April 24th-28th. (Fig. 7). No transport of dust from heavy fuels combustion was instead recorded during pre-lockdown and post-lockdown, when this contribution was very low (ranging from 1 to 6% of total PM_{10}) at all sites.

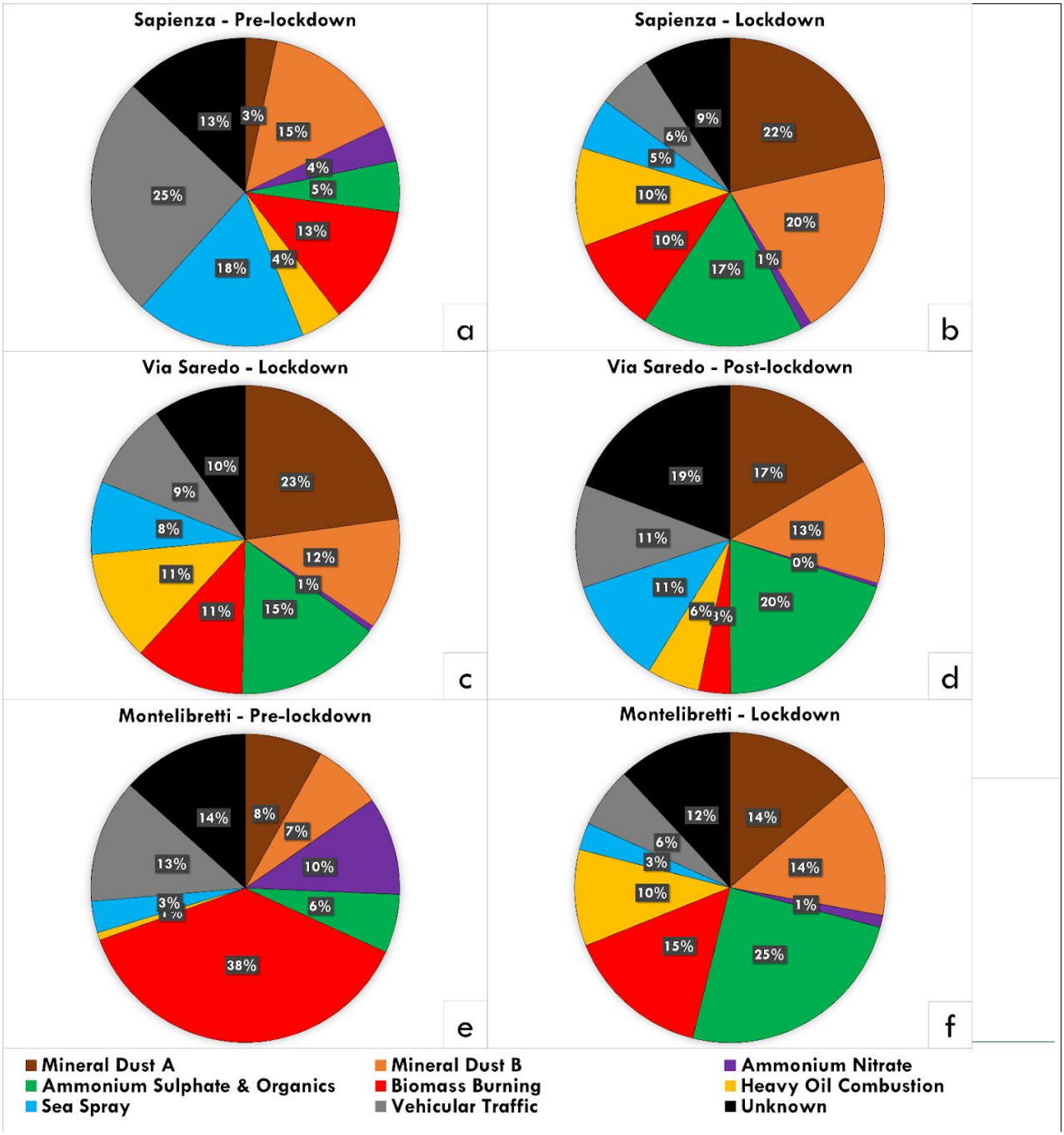

Fig. 6. Source apportionment of PM_{10} during pre-lockdown (Sapienza (panel a) and Montelibretti (panel e)), lockdown (Sapienza (panel b), Via Saredo (panel c) and Montelibretti (panel f)), and post-lockdown (Via Saredo (panel d)). Values are reported as average percent of the total measured PM_{10} mass concentration.

Regarding mineral dusts, major advection episodes of desert dust from remote regions occurred during lockdown and interested all sites, contributing together from 28 to 42% of total PM_{10} mass concentration. From Fig. 7 we can observe that MD-A and MD-B incursion events occurred during the same days, indicating common transport pathways. Moreover, this areal and temporal homogeneity is coherent with a non-local origin. The main peaks in the time trend of these factors were observed on March 28th-30th, when mass contribution from MD-B was much greater, reaching about 40 µg m^{-3} to total PM_{10} at Sapienza, and on April 17th-20th and May 12th-20th, when instead the main contribution was from MD-A. As previously discussed,

MD-A is attributable to dust advection events from African deserts, such as Sahara and Sahel, while MD-B contribution probably derived from incursion of dust from the eastern desert regions of Kazakhstan (long-range transport contributions were checked by backtrajectory analysis; HYSPLIT Trajectory Model).

Finally, high increase of ammonium sulfates due to the warm season was observed during lockdown at all sites (from 5-6 to 15-25 % of total PM_{10}), contributing, as well as mineral dust advections, to the lesser than expected decrease in PM_{10} mass concentration from pre-lockdown to lockdown. Highest contributions from ammonium nitrate were found at Montelibretti (9% of PM_{10} mass concentration) and to minor extent at Sapienza (4% of total PM_{10}) during pre-lockdown, as expected from seasonal evolution. On the contrary, from the lockdown period to the end of sampling, a flat contribution of about 1% was observed at all sites, as previously discussed. In particular, the time trend of non-secondary nitrate matches specifically with MD-B mineral dust contribution, while acidic sulfates (bisulfate and letovicite), differently from the regional distribution of ammonium sulfate, resulted associated to mineral dust transport events, likely due to collinear transport of different air masses.

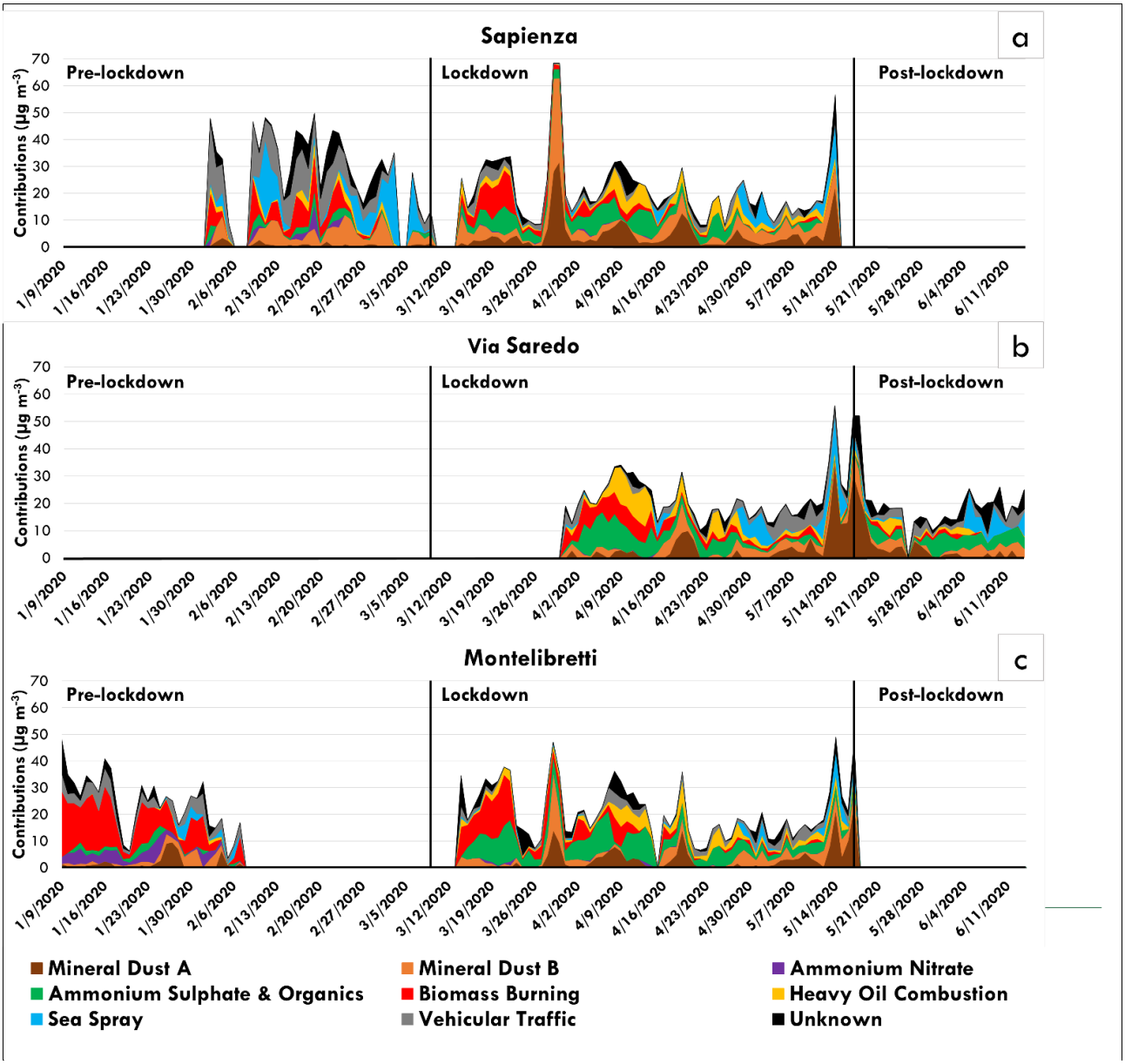

Fig. 7. Time trend of source contributions to PM_{10} mass concentration (µg m^{-3}) at Sapienza (panel a), Via Saredo (panel b) and Montelibretti (panel c) during pre-lockdown, lockdown and post-lockdown.

4. Conclusions

The impact of the lockdown-based policy adopted by Italy during 2020 to contrast the spread of the Coronavirus disease 2019 (Covid-19) was evaluated in this work for the Rome area (Italy), concerning the relative strength and time evolution of local and non-local acting sources. To this aim, daily PM_{10} samples chemically speciated, collected during pre-lockdown, lockdown and post-lockdown periods at the urban sites of Sapienza and Via Saredo, and at the peri-urban site of Montelibretti, were analyzed by PMF. Chemically fractionated elements, considered for soluble and insoluble fractions instead of total concentration, were used in the PMF input dataset, in addition to conventional analytical speciation. From pre-lockdown to lockdown, a significant abatement of local sources (vehicular traffic and biomass burning) was observed at all sites. Concerning biomass burning this is explained by the seasonal evolution from cold to warmer seasons that

overall coincides with the transition from the pre-lockdown period to the establishment of the lockdown measures (from March 9th to May 18th 2020). However, the strong reduction of vehicular traffic observed during lockdown has to be only attributed to circulation restrictions adopted by the lockdown policy, providing an experimental trial of the efficiency of PM control strategies and mitigation measures addressing vehicular traffic in the Rome area. As additional consequence of forcing the reduction of local anthropogenic activities and their source strength, the non-local source contributions (two different mineral dust - MD-A and MD-B - advected from desert regions, sea spray, and heavy oil combustion) that mainly occurred during lockdown, were poorly influenced by the chemical fingerprint of local sources. This allowed to describe their profile and estimate mass contributions more accurately than obtainable from PMF input datasets of PM collected during routine periods. The MD-A is described by significantly higher abundances of Si, Ca, Al and the insoluble fractions of Fe, Ti, V, Li and Rb with respect to MD-B, while the latter is far more enriched in Na, K and Mg ions, and non-secondary NO_3, thus indicating a composition richer in nitrates and other salts.

High overlapping of insoluble Rb, Ti, V, Cs and Li, which were previously observed to selectively trace desert dust, with Si and Al, indicate that mineral dust contributions of this study are more probably long-range transported than local. This is further supported by ratio-ratio plot comparison with profiles of African dust outbreaks, local mineral dust and road dust of the Rome area, showing that both MD-A and MD-B profiles are not assignable to local dusts and that MD-A is clearly assigned to African desert outbreaks. The sea spray profiles of this study were compared with a reference profile of fresh sea salt; diagnostic ratios showed to be almost equal to those of the reference profile. Heavy oil combustion profiles match those reported in literature for significant diagnostic ratios (V/Ni, Fe/EC). Since in this study the soluble fraction of V and Ni were used for PMF, instead of total element, the observed profile matching confirms the high selectivity of soluble V and Ni for heavy oil combustion tracing. Finally, the poor influence of local sources allowed to separate and apportion the sulfates and nitrate contributions due to secondary processes from contributions of other sources (e.g. non-secondary nitrate from MD-B dust, and non-secondary sulfates from long-range collinear transport paths).

Overall, the contribution from vehicular traffic was considerably reduced by Covid-19 lockdown; however, a more considerable decrease in PM_{10} mass concentration would have been expected during lockdown. This was not the case due to the greater strength of long-range transport events of mineral dust from desert regions during lockdown and to the increase in contribution of secondary aerosols due to seasonal evolution. Nevertheless, the forced abatement of traffic emissions (combined to season-related quenching of domestic heating) led to considerable compositional changes of PM, with strong reductions of components of health concern (EC, organics). The accurate characterization of PM obtained by combining conventional chemical speciation to non-conventional approaches (chemical fractionation by water-solubility of trace elements, apportionment of secondary inorganic species by chemical equivalent ratios) allowed to obtain enhanced information about the relative relevance of single source contributions to PM mass concentration, which is of critical importance to improve understanding of air pollution and reduce uncertainties in future air quality scenarios.

Acknowledgments

This work was funded by the project 2017 RG11715C7C8801CF (Principal Investigator Dr. S. Canepari) and the projects 2018 AR1181641E22B570 and 2019 AR11916B7027C1E6 (Principal Investigator Dr. L. Massimi) financed by Sapienza University of Rome.
The authors gratefully thank Marco Giusto, Salvatore Pareti and Elena Rantica of C.N.R. Institute of Atmospheric Pollution Research for performing part of the samplings and chemical analyses. Moreover, the authors thank the Rome Air and Physical Agents Unit of Environmental Protection Agency of Lazio Region (ARPA Lazio) for the support in the installation and management of the sampling equipment.

Author Contributions: A. Amoroso, A. Di Giosa, S. Canepari and C. Perrino conceived and planned the monitoring and the experiments; M. A. Frezzini, N. De Francesco, T. Sargolini and A. Amoroso performed the samplings; M.A. Frezzini, M. Ristorini, N. De Francesco and T. Sargolini performed part of the chemical analyses; L. Massimi and A. Pietrodangelo elaborated the data and wrote the manuscript; L. Massimi, A. Pietrodangelo, S. Canepari and C. Perrino coordinated the group and supervised the manuscript.

Conflicts of Interest: The authors declare no conflicts of interest.

Supplementary material S1

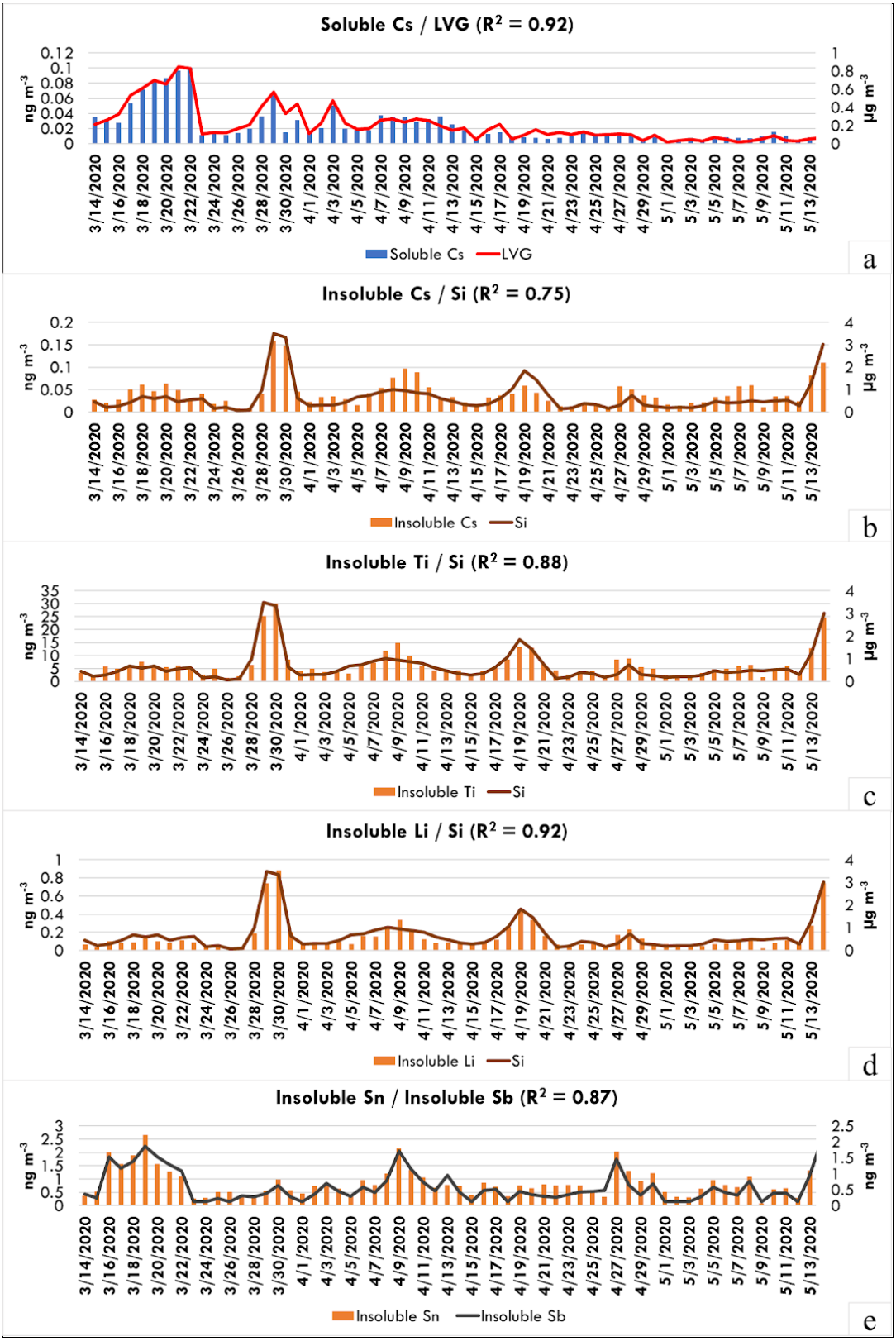

Fig. S1.1. Comparison between concentrations of soluble Cs and LVG (panel a), insoluble Cs and Si (panel b), insoluble Ti and Si (panel c), insoluble Li and Si (panel d), and insoluble Sn and insoluble Sb (panel e), obtained at Sapienza from March 14th to May 13th (lockdown period).

Supplementary material S2

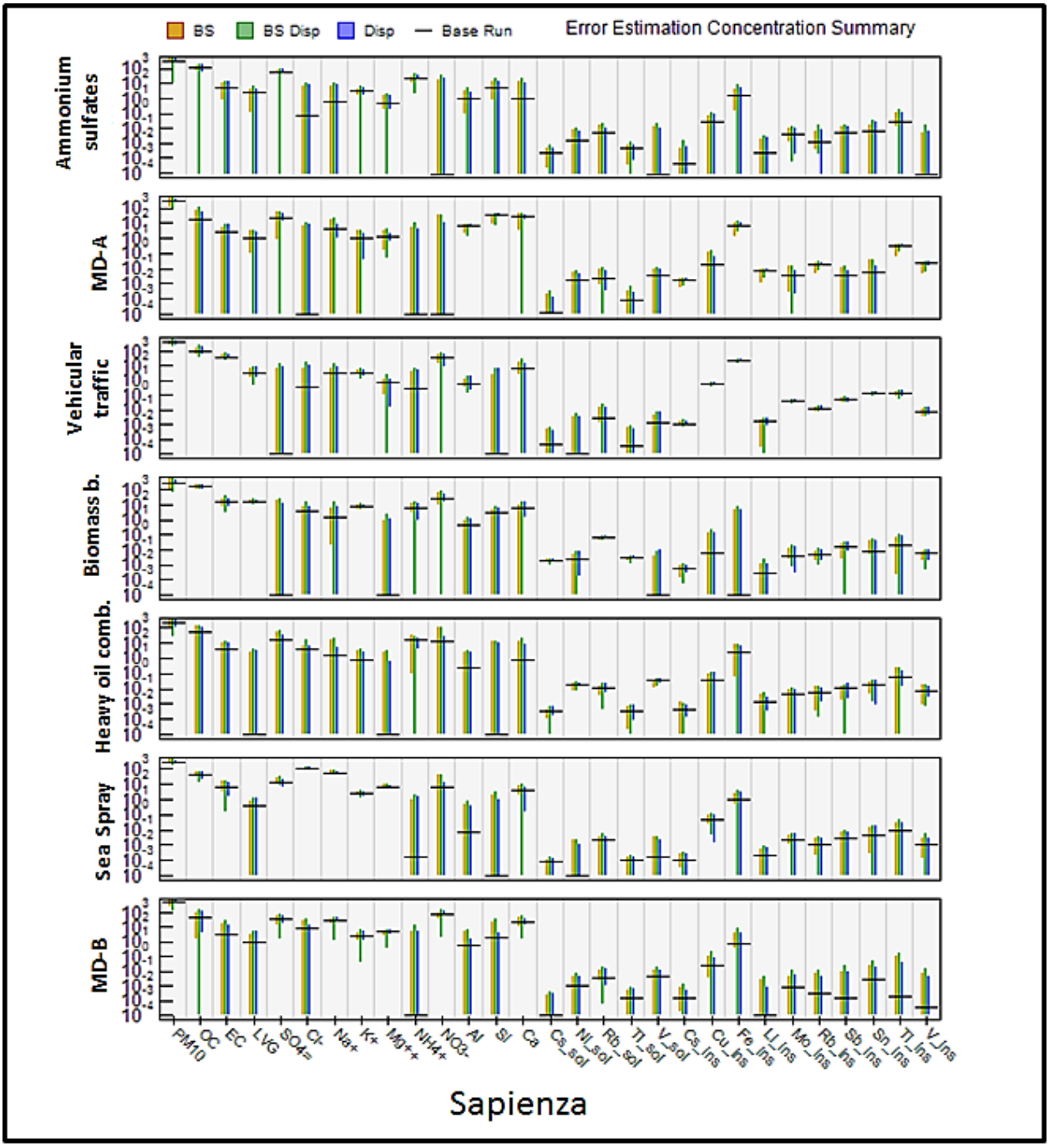

Fig. S2.1. Summary of BS, DISP and BS-DISP error estimation results at Sapienza. MD-A: Mineral dust A; MD-B: Mineral dust B; Biomass b.: biomass burning. The soluble and insoluble fraction of elements are indicated with *sol* and *ins*, respectively, to improve visualization. Concentration unit is ng m^{-3}.

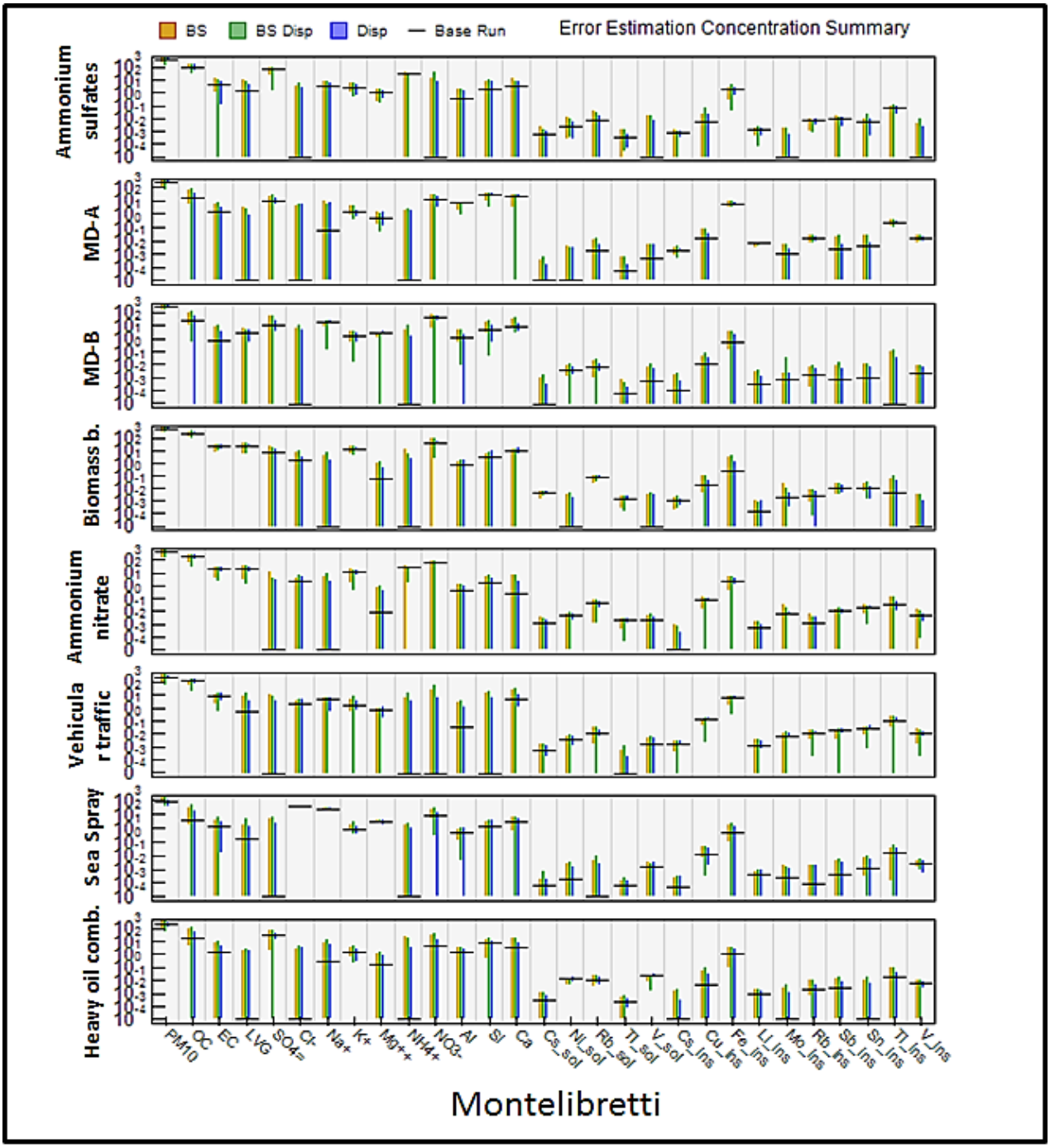

Fig. S2.2. Summary of BS, DISP and BS-DISP error estimation results at Montelibretti. MD-A: Mineral dust A; MD-B: Mineral dust B; Biomass b.: biomass burning. The soluble and insoluble fraction of elements are indicated with *sol* and *ins*, respectively, to improve visualization. Concentration unit is ng m^{-3}.

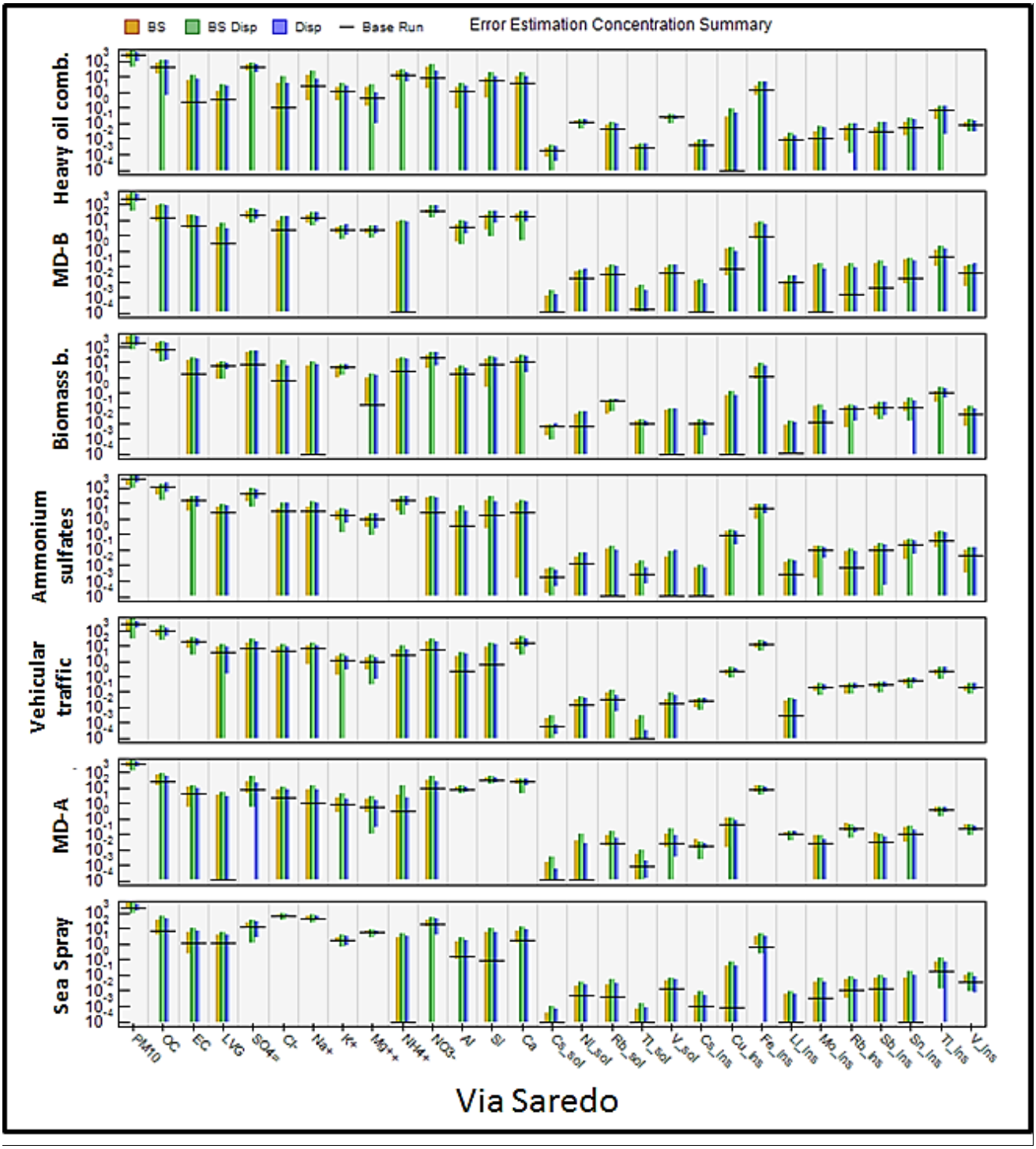

Fig. S2.3. Summary of BS, DISP and BS-DISP error estimation results at Via Saredo. MD-A: Mineral dust A; MD-B: Mineral dust B; Biomass b.: biomass burning. The soluble and insoluble fraction of elements are indicated with *sol* and *ins*, respectively, to improve visualization. Concentration unit is ng m^{-3}.

Supplementary material S3

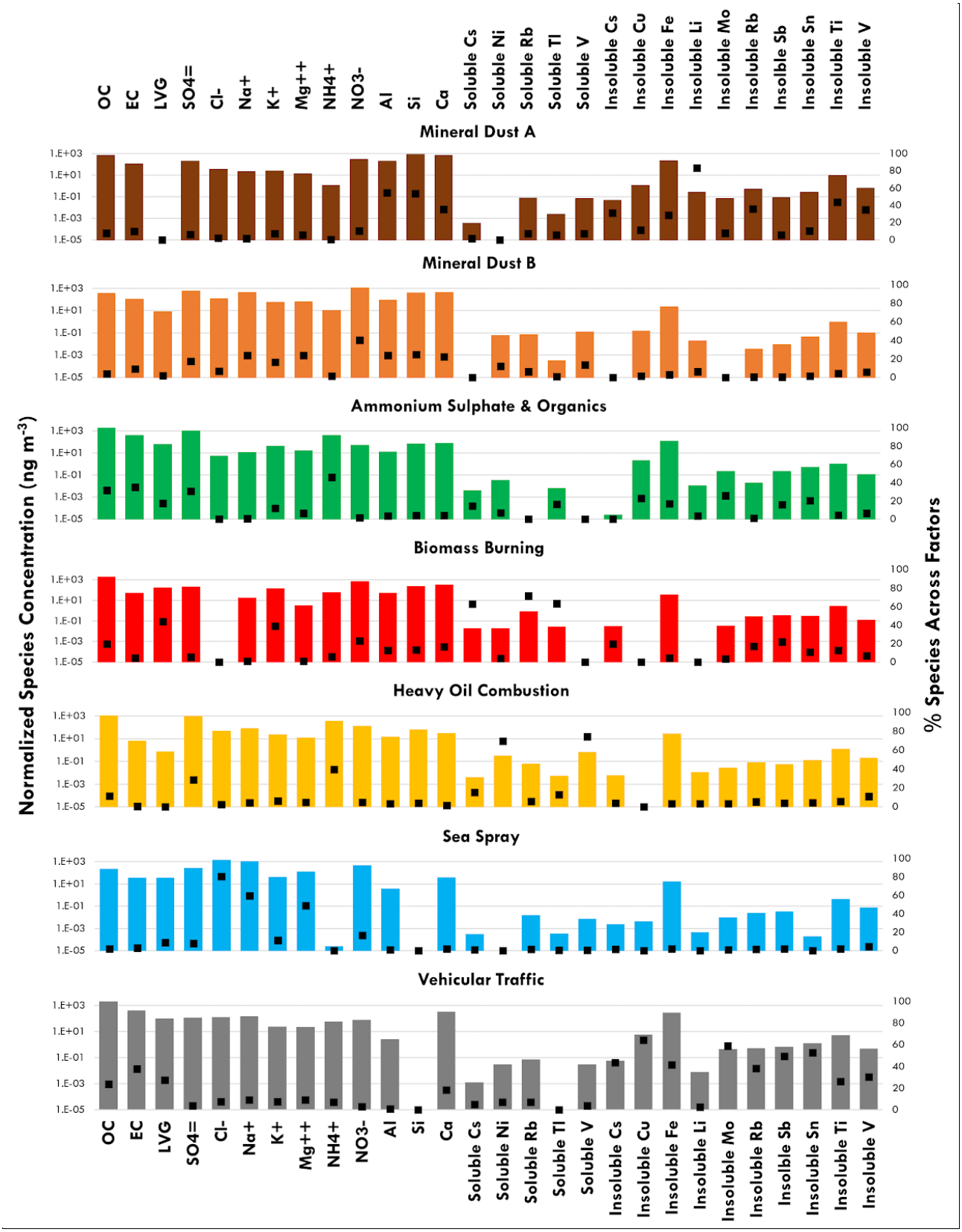

Fig. S3.1. Chemical profiles of the factors identified by PMF at Via Saredo during the entire monitoring period.

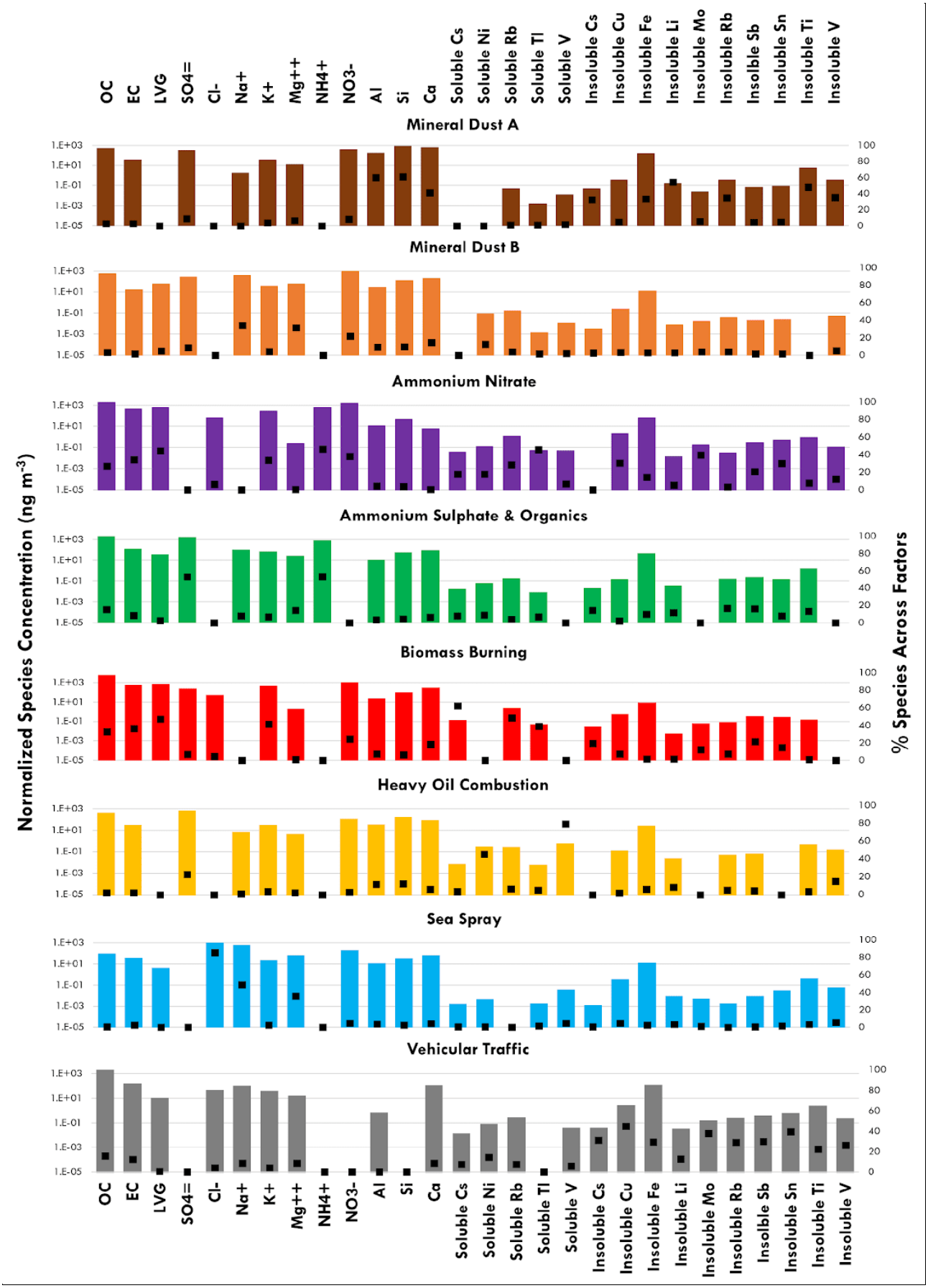

Fig. S3.2. Chemical profiles of the factors identified by PMF at Montelibretti during the entire monitoring period.

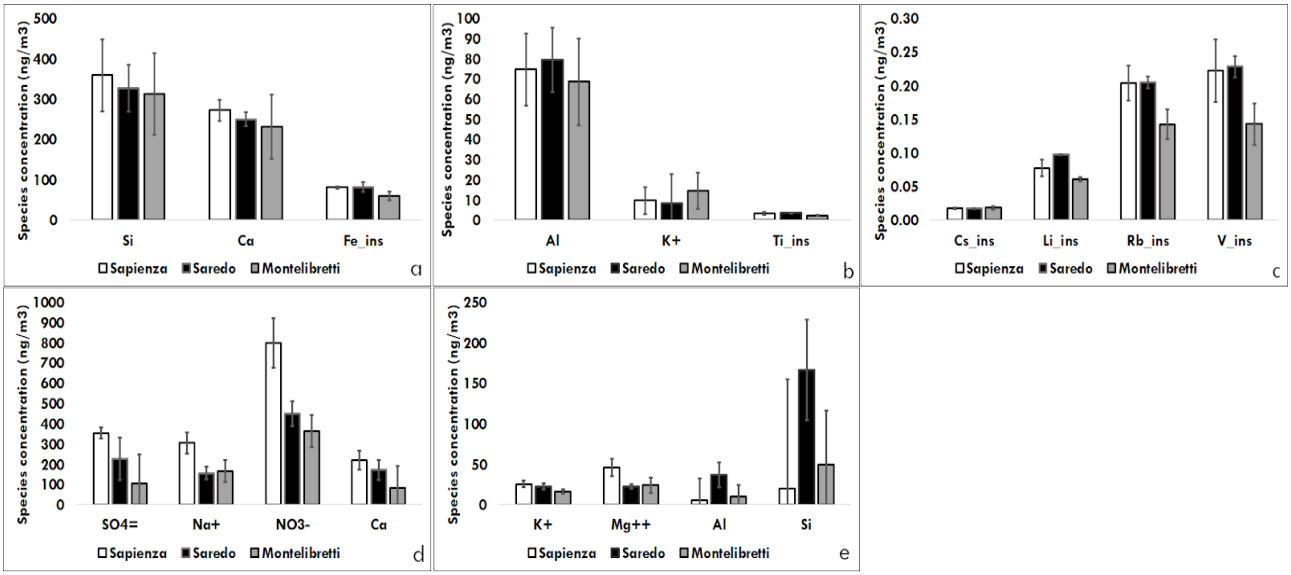

Fig. S3.3. MD-A (a, b, c) and MD-B (d, e) profiles determined at the three sites of this study. Only species for which a small-size error is estimated by at least two out of three error estimation methods (BS, DISP and BS-DISP) are reported, by each profile, for inter-site comparison. a, b, c: major, minor and trace species, respectively, of MD-A profile; d, e: major and minor species, respectively, of MD-B profile. Error bars are species uncertainties in the profile.

Table S3.1. Diagnostic ratios of the biomass burning profiles determined at the three sites by PMF are compared with the variability range of same ratios for biomass profiles available in the SPECIEUROPE repository (Pernigotti et al., 2016). All profiles used here (namely, profiles no.: 5 to 8, 67, 150, 184, 187 to 192, 224 to 226, 248 to 252) refer to PM_{10} size fraction.

	Range (min – max)	**Sapienza**	**Via Saredo**	**Montelibretti**
EC/OC	0.1 – 1	0.1	0.03	0.1
LVG/OC	0.01 – 0.3	0.1	0.1	0.1
K+/LVG	0.02 – 0.5	0.5	0.8	0.6
Cs/Rb [1]	0.04 – 0.06	0.03	0.02	0.01

[1] Calculated on the soluble fraction of Cs and Rb for the profiles determined in this study, and on the total element for the SPECIEUROPE biomass burning profiles.

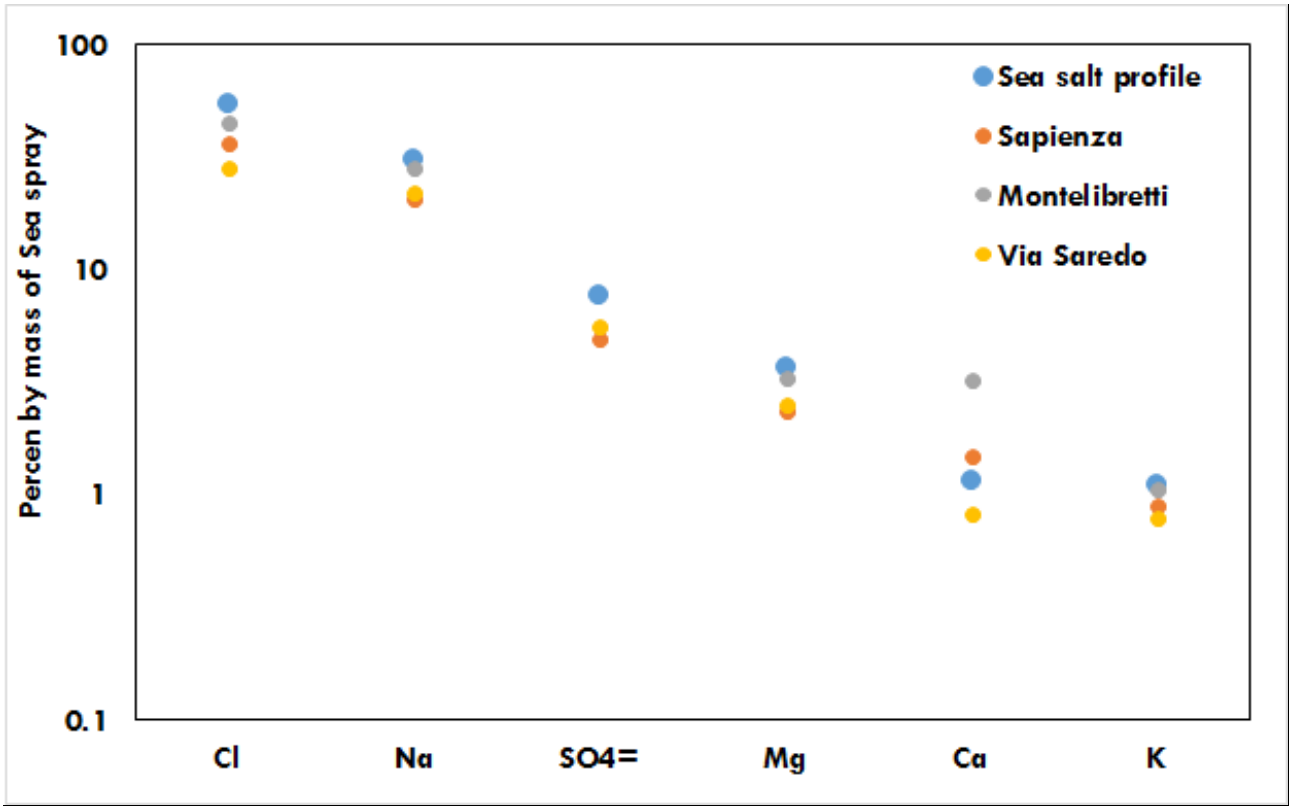

Fig. S3.4. Chemical profile of reference fresh sea salt (Seinfeld and Pandis, 2006) and of sea spray factor profiles estimated by PMF in this study. In the latter, the ion fraction of Cl, Na, Mg and K have been used. Only major species are reported.

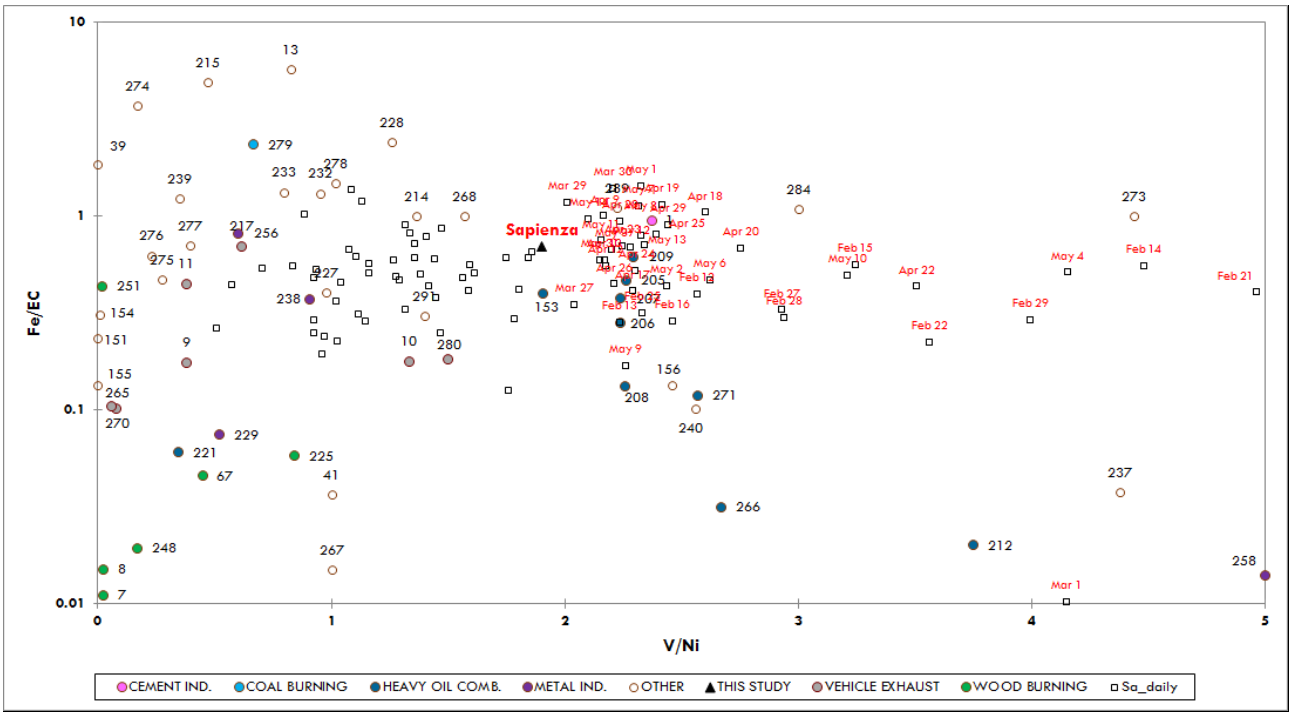

Fig. S3.5. Ratio-ratio scatter plot of selected SPECIEUROPE source profiles (identified by ID number), heavy oil combustion profile estimated by PMF at Sapienza (Sa), and daily PM_{10} samples collected at same site. The variability range of axes has been limited to the area of the plot of main interest for this work, to the aim of improving visualization of data. To same goal, dates are reported only for daily samples affected by heavy oil combustion.

Fig. S3.6. Ratio-ratio scatter plot of selected SPECIEUROPE source profiles (identified by ID number), heavy oil combustion profile estimated by PMF at Via Saredo (Sar), and daily PM_{10} samples collected at same site. The variability range of axes has been limited to the area of the plot of main interest for this work, to the aim of improving visualization of data. To same goal, dates are reported only for daily samples affected by heavy oil combustion.

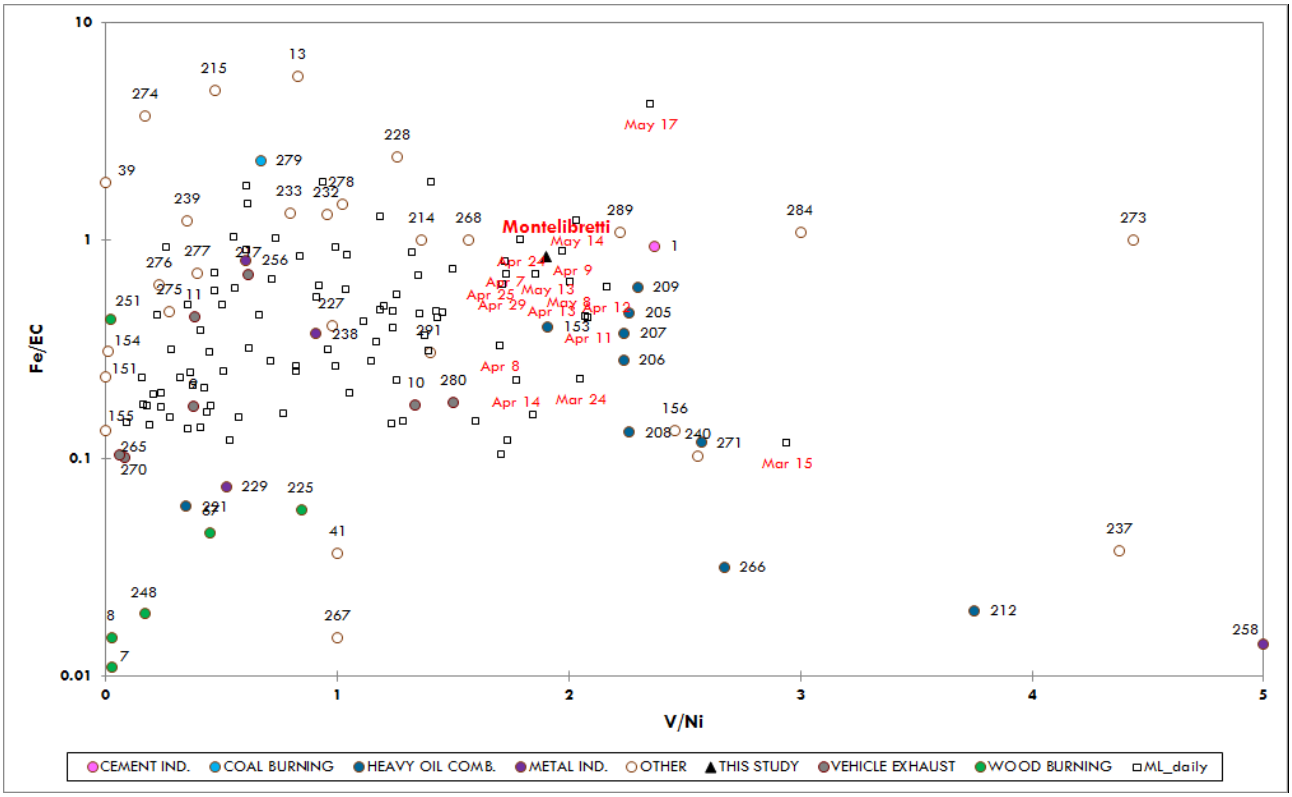

Fig. S3.7. Ratio-ratio scatter plot of selected SPECIEUROPE source profiles (identified by ID number), heavy oil combustion profile estimated by PMF at Montelibretti (ML), and daily PM_{10} samples collected at same site. The variability range of axes has been limited to the area of the plot of main interest for this work, to the aim of improving visualization of data. To same goal, dates are reported only for daily samples affected by heavy oil combustion.

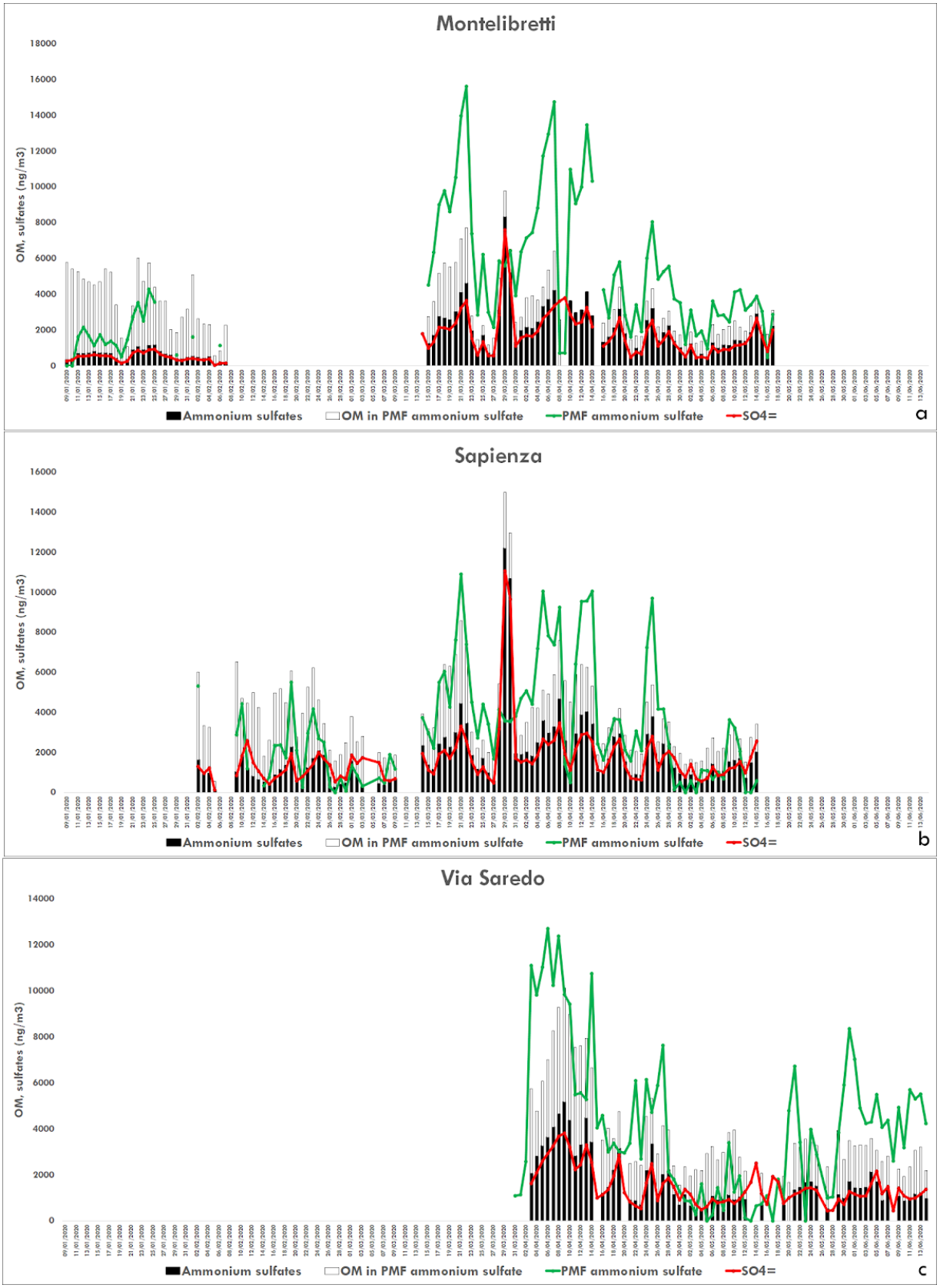

Fig. S3.8. Daily mass contribution of secondary sulfates estimated by chemical equivalent ratios and by PMF, organic matter apportioned to secondary sulfates and measured $SO_4^=$, at the three sites of this study.

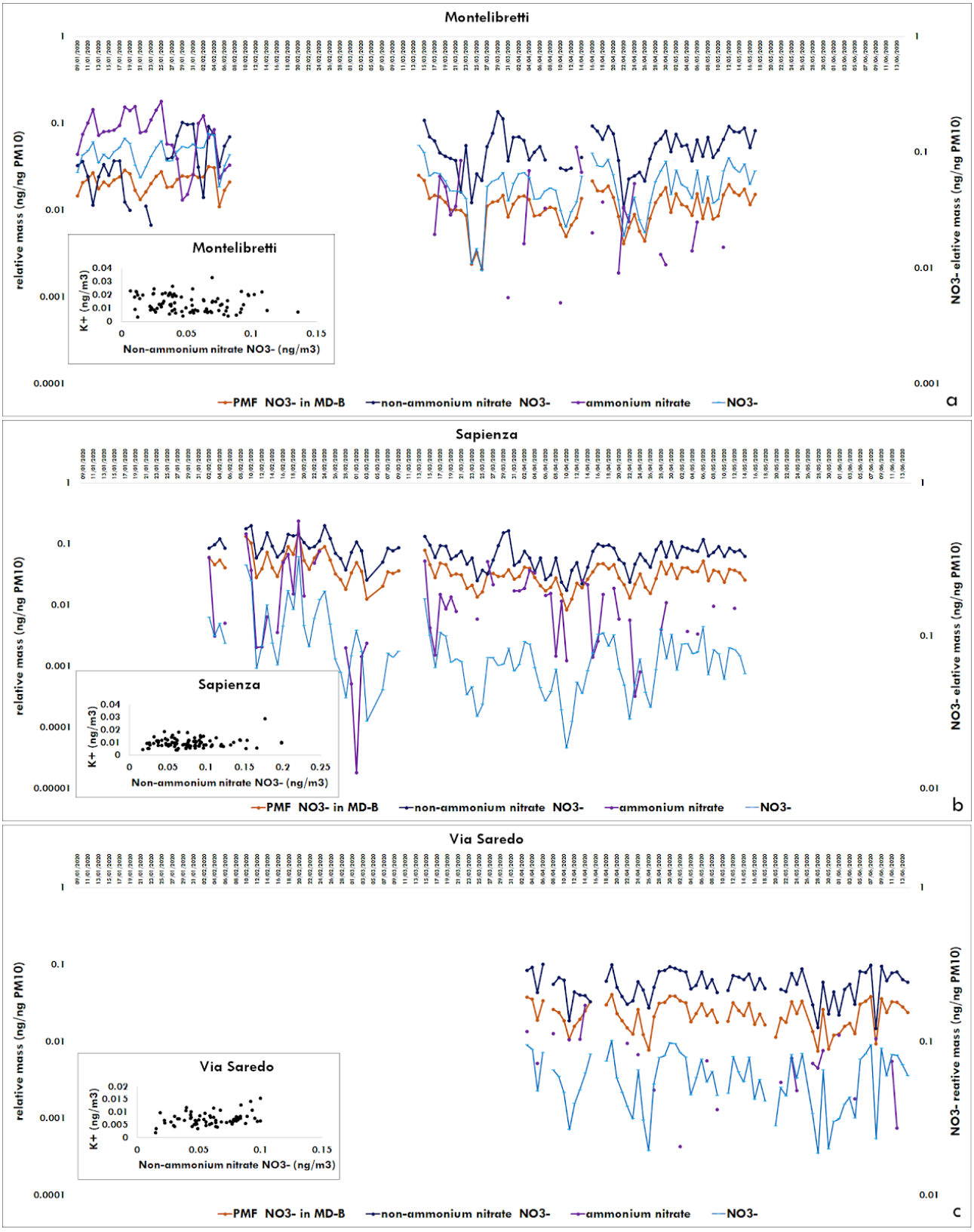

Fig. S3.9. Daily concentrations (relative mass in PM_{10}) of NO_3^- contributions estimated by chemical equivalent ratios, and of NO_3^- fraction apportioned to MD-B profile by PMF, at the three sites. Total measured NO_3^- is reported on the secondary axis, for comparison. Regression between potassium ion and non-ammonium nitrate NO_3^- is also reported at each site.

References

Ali, M. U., Liu, G., Yousaf, B., Ullah, H., Abbas, Q., Munir, M. A. M. (2019). A systematic review on global pollution status of particulate matter-associated potential toxic elements and health perspectives in urban environment. Environmental geochemistry and health, 41(3), 1131-1162.

Allouis, C., Beretta, F., D'Alessio, A. (2003). Structure of inorganic and carbonaceous particles emitted from heavy oil combustion. Chemosphere, 51(10), 1091-1096. https://doi.org/10.1016/S0045-6535(02)00714-2

Amato, F., Alastuey, A., Karanasiou, A., Lucarelli, F., Nava, S., Calzolai, G., Querol, X. (2016). AIRUSE-LIFE+: a harmonized PM speciation and source apportionment in five southern European cities. Atmospheric Chemistry and Physics, 16(5), 3289-3309.

Amato, F., Viana, M., Richard, A., Furger, M., Prévôt, A. S. H., Nava, S., Querol, X. (2011). Size and time-resolved roadside enrichment of atmospheric particulate pollutants. Atmospheric Chemistry and Physics, 11(6), 2917-2931.

Arregocés, H. A., Rojano, R., Restrepo, G. (2021). Impact of lockdown on particulate matter concentrations in Colombia during the COVID-19 pandemic. Science of the Total Environment, 764, 142874. https://doi.org/10.1016/j.scitotenv.2020.142874

Astolfi, M. L., Marconi, E., Protano, C., Vitali, M., Schiavi, E., Mastromarino, P., Canepari, S. (2018). Optimization and validation of a fast digestion method for the determination of major and trace elements in breast milk by ICP-MS. Analytica Chimica Acta, 1040, 49-62.

Astolfi, M.L., Canepari, S., Cardarelli, E., Ghighi, S. and Marzo, M.L. (2006), Chemical Fractionation of Elements in Airborne Particulate Matter: Primary Results on PM10 and PM2.5 Samples in the Lazio Region (Central Italy). Annali di Chimica, 96: 183-194. https://doi.org/10.1002/adic.200690018

Astolfi, M. L., Marconi, E., Protano, C., Canepari, S. (2020). Comparative elemental analysis of dairy milk and plant-based milk alternatives. Food Control, 116, 107327.

Battista, G., Pagliaroli, T., Mauri, L., Basilicata, C., De Lieto Vollaro, R. (2016). Assessment of the air pollution level in the city of Rome (Italy). Sustainability, 8(9), 838.

Belis, C., Favez, O., Mircea, M., Diapouli, E., Manousakas, M., Vratolis, S., Gilardoni, S., Paglione, M., Decesari, S., Mocnik, G., Mooibroek, D., Salvador, P., Takahama, S., Vecchi, R. and Paatero, P. (2019). European guide on air pollution source apportionment with receptor models, EUR 29816 EN, Publications Office of the European Union. ISBN 978-92-76-09001-4. https://doi.org/10.2760/439106, JRC117306

Bernardoni, V., Vecchi, R., Valli, G., Piazzalunga, A., Fermo, P. (2011). PM10 source apportionment in Milan (Italy) using time-resolved data. Science of the Total Environment, 409(22), 4788-4795. https://doi.org/10.1016/j.scitotenv.2011.07.048

Betha, R., Behera, S. N., Balasubramanian, R. (2014). 2013 Southeast Asian smoke haze: fractionation of particulate-bound elements and associated health risk. Environmental Science and Technology, 48(8), 4327-4335. https://doi.org/10.1021/es405533d

Borck, R., Pflüger, M. (2019). Green cities? Urbanization, trade, and the environment. Journal of Regional Science, 59(4), 743-766. https://doi.org/10.1111/jors.12423

Briz-Redón, Á., Belenguer-Sapiña, C., Serrano-Aroca, Á. (2021). Changes in air pollution during COVID-19 lockdown in Spain: a multi-city study. Journal of Environmental Sciences, 101, 16-26. https://doi.org/10.1016/j.jes.2020.07.029

Canepari, S., Cardarelli, E., Giuliano, A., Pietrodangelo, A. (2006a). Determination of metals, metalloids and non-volatile ions in airborne particulate matter by a new two-step sequential leaching procedure part A: Experimental design and optimization. Talanta, 69(3), 581–587. https://doi.org/10.1016/j.talanta.2005.10.023

Canepari, S., Cardarelli, E., Pietrodangelo, A., Strincone, M. (2006b). Determination of metals, metalloids and non-volatile ions in airborne particulate matter by a new two-step sequential leaching procedure: Part B: Validation on equivalent real samples. Talanta, 69(3), 588-595. https://doi.org/10.1016/j.talanta.2005.10.024

Canepari, S., Perrino, C., Olivieri, F., Astolfi, M. L. (2008). Characterisation of the traffic sources of PM through size-segregated sampling, sequential leaching and ICP analysis. Atmospheric Environment, 42(35), 8161-8175.

Canepari, S., Pietrodangelo, A., Perrino, C., Astolfi, M. L., Marzo, M. L. (2009). Enhancement of source traceability of atmospheric PM by elemental chemical fractionation. Atmospheric Environment, 43(31), 4754-4765.

Canepari, S., Astolfi, M. L., Moretti, S., Curini, R. (2010). Comparison of extracting solutions for elemental fractionation in airborne particulate matter. Talanta, 82(2), 834-844. https://doi.org/10.1016/j.talanta.2010.05.068

Canepari, S., Astolfi, M. L., Farao, C., Maretto, M., Frasca, D., Marcoccia, M., Perrino, C. (2014). Seasonal variations in the chemical composition of particulate matter: a case study in the Po Valley. Part II: concentration and solubility of micro-and trace-elements. Environmental Science and Pollution Research, 21(6), 4010-4022.

Canepari, S., Astolfi, M. L., Catrambone, M., Frasca, D., Marcoccia, M., Marcovecchio, F., Perrino, C. (2019). A combined chemical/size fractionation approach to study winter/summer variations, ageing and source strength of atmospheric particles. Environmental Pollution, 253, 19-28.

Cesaroni, G., Boogaard, H., Jonkers, S., Porta, D., Badaloni, C., Cattani, G., Forastiere, F., Hoek, G. (2012). Health benefits of traffic-related air pollution reduction in different socioeconomic groups: the effect of low-emission zoning in Rome. Occupational and Environmental Medicine, 69(2), 133-139. https://doi.org/10.1136/oem.2010.063750

Chowdhury Z, Zheng M, Schauer JJ, Sheesley RJ, Salmon LG, Cass GR, Russell AG (2007) Speciation of ambient fine organic carbon particles and source apportionment of PM2.5 in Indian cities. Journal of Geophysical Research 112:D15303

Coccia, M. (2020). Two mechanisms for accelerated diffusion of COVID-19 outbreaks in regions with high intensity of population and polluting industrialization: the air pollution-to-human and human-to-human transmission dynamics. MedRxiv. https://doi.org/10.1101/2020.04.06.20055657.

Collivignarelli, M. C., Abbà, A., Bertanza, G., Pedrazzani, R., Ricciardi, P., Miino, M. C. (2020). Lockdown for CoViD-2019 in Milan: What are the effects on air quality?. Science of the Total Environment, 732, 139280. https://doi.org/10.1016/j.scitotenv.2020.139280

Corbin, J. C., Mensah, A. A., Pieber, S. M., Orasche, J., Michalke, B., Zanatta, M., Czech, H., Massabò, D., Buatier de Mongeot, F., Mennucci, C., El Haddad, I., Kumar, N.K., Stengel, B., Huang, Y., Zimmermann, R., Prevot, S.H., Gysel, M. (2018). Trace metals in soot and PM2. 5 from heavy-fuel-oil combustion in a marine engine. Environmental Science and Technology, 52(11), 6714-6722. https://doi.org/10.1021/acs.est.8b01764

Dai, Q., Liu, B., Bi, X., Wu, J., Liang, D., Zhang, Y., Feng, Y., Hopke, P. K. (2020). Dispersion normalized PMF provides insights into the significant changes in source contributions to PM2. 5 after the COVID-19 outbreak. Environmental Science and Technology, 54(16), 9917-9927. https://doi.org/10.1021/acs.est.0c02776
Di Bernardino, A., Iannarelli, A. M., Casadio, S., Perrino, C., Barnaba, F., Tofful, L., Cacciani, M. (2021). Impact of synoptic meteorological conditions on air quality in three different case studies in Rome, Italy. Atmospheric Pollution Research, 12(4), 76-88.
EPA, (1997). Reference Method for the Determination of Particulate Matter as PM10 in the Atmosphere. Federal Registrer, 62, No 138, Appendix M to part 50.
EU, 2008. Directive 2008/50/EC of the European Parliament and of the Council of 21 May 2008 on ambient air quality and cleaner air for Europe. Official Journal of the European Union L152 (11/06/2008), 1–44.
Fan, H., Zhao, C., Yang, Y. (2020). A comprehensive analysis of the spatio-temporal variation of urban air pollution in China during 2014–2018. Atmospheric Environment, 220, 117066.
Feng, X. D., Dang, Z., Huang, W. L., Yang, C. (2009). Chemical speciation of fine particle bound trace metals. International Journal of Environmental Science & Technology, 6(3), 337-346.
Government of Italy. Decree of the president of the Council of Ministers 11 March 2020. March 11, 2020. https://www.gazzettaufficiale.it/eli/id/2020/03/11/20A01605/sg
Government of Italy. Decree of the president of the Council of Ministers 26 April 2020. April 26, 2020. https://www.gazzettaufficiale.it/eli/id/2020/04/27/20A02352/sg
Gobbi, G. P., Barnaba, F., Di Liberto, L., Bolignano, A., Lucarelli, F., Nava, S., Wille, H. (2019). An inclusive view of Saharan dust advections to Italy and the Central Mediterranean. Atmospheric environment, 201, 242-256.
Grondys, K. (2019). The impact of freight transport operations on the level of pollution in cities. Transportation Research Procedia, 39, 84-91. https://doi.org/10.1016/j.trpro.2019.06.010
Guevara, M., Jorba Casellas, O., Soret, A., Petetin, H., Bowdalo, D., Serradell Maronda, K., Tena, C., van der Gon, H.D., Kuenen, J., Peuch, V., Pérez García-Pando, C. (2021). Time-resolved emission reductions for atmospheric chemistry modelling in Europe during the COVID-19 lockdowns. Atmospheric Chemistry and Physics, 21, 773-779. https://doi.org/10.5194/acp-21-773-2021
Guzzetta, G., Riccardo, F., Marziano, V., Poletti, P., Trentini, F., Bella, A., Andrianou, X., Del Manso, M., Fabiani, M., Bellino, S., Boros, S., Urdiales, A.M., Vescio, M.F., Piccioli, A., COVID-19 Working Group, Brusaferro, S., Rezza, G., Pezzotti, P., Ajelli, M., Merler, S. (2021). Impact of a nationwide lockdown on Sars-cov-2 transmissibility, Italy. Emerging infectious diseases, 27(1), 267. https://dx.doi.org/ 10.3201/eid2701.202114
Hopke, P. K. (2000). A guide to positive matrix factorization, in workshop on UNMIX and PMF as applied to PM2. 5. Edited by Willis, RD, RTP, NC. EPA 600/A-00/048.
Kam, W., Delfino, R. J., Schauer, J. J., Sioutas, C. (2013). A comparative assessment of $PM_{2.5}$ exposures in light-rail, subway, freeway, and surface street environments in Los Angeles and estimated lung cancer risk. Environmental Science: Processes & Impacts, 15(1), 234-243.
Kirchner, M., Freier, K.P., Denner, P., Ratz, G., Jakobi, G., Körner, W., Ludewig, E., Schaub, M., Schramm, K.-W., Weiss, P., Moche, W. (2020). Air concentrations and deposition of chlorinated dioxins and furans (PCDD/F) at three high alpine monitoring stations: Trends and dependence on air masses. Atmospheric Environment, 223, 117199. https://doi.org/10.1016/j.atmosenv.2019.117199
Kumar, P., Hama, S., Omidvarborna, H., Sharma, A., Sahani, J., Abhijith, K. V., Debele, S.E., Zavala-Reyes, J.C., Barwise, Y., Tiwari, A. (2020). Temporary reduction in fine particulate matter due to 'anthropogenic emissions switch-off'during COVID-19 lockdown in Indian cities. Sustainable cities and society, 62, 102382. https://doi.org/10.1016/j.scs.2020.102382
Legislative Decree, 2010. Decreto Legislativo 13 agosto 2010, n. 155. Attuazione della direttiva 2008/50/CE relativa alla qualità dell'aria ambiente e per un'aria più pulita in Europa (GU n.216 del 15-9-2010 - Suppl. Ordinario n. 217).
Lehmann, C. M., Bowersox, V. C., Larson, R. S., Larson, S. M. (2007). Monitoring long-term trends in sulfate and ammonium in US precipitation: Results from the National Atmospheric Deposition Program/National Trends Network. In: Brimblecombe P., Hara H., Houle D., Novak M. (eds) Acid Rain - Deposition to Recovery. Springer, Dordrecht. https://doi.org/10.1007/978-1-4020-5885-1_7
Li, H., Wang, J., Wang, Q. G., Qian, X., Qian, Y., Yang, M., Fengying, L., Lu, H., Wang, C. (2015). Chemical fractionation of arsenic and heavy metals in fine particle matter and its implications for risk assessment: a case study in Nanjing, China. Atmospheric Environment, 103, 339-346. https://doi.org/10.1016/j.atmosenv.2014.12.065
Linares, C., Culqui, D., Belda, F., López-Bueno, J. A., Luna, Y., Sánchez-Martínez, G., Hervella, B., Diaz, J. (2021). Do Saharan Dust Intrusions Affect the Incidence and Severity of COVID-19 in Spain?. Environmental Science and Pollution Research. Preprint under consideration. https://doi.org/10.21203/rs.3.rs-180563/v1
Liu, B., Wu, J., Zhang, J., Wang, L., Yang, J., Liang, D., Dai, Q., Bi, X., Feng, Y., Zhang, Q. (2017). Characterization and source apportionment of PM2. 5 based on error estimation from EPA PMF 5.0 model at a medium city in China. Environmental Pollution, 222, 10-22.
Manchanda, C., Kumar, M., Singh, V., Faisal, M., Hazarika, N., Shukla, A., Lalchandani, V., Goel, V., Thamban, N., Ganguly, D., Tripathi, S. N. (2021). Variation in chemical composition and sources of PM2. 5 during the COVID-19 lockdown in Delhi. Environment international, 153, 106541. https://doi.org/10.1016/j.envint.2021.106541
Masiol, M., Rampazzo, G., Ceccato, D., Squizzato, S., Pavoni, B. (2010). Characterization of PM10 sources in a coastal area near Venice (Italy): an application of factor-cluster analysis. Chemosphere, 80(7), 771-778.
Massimi, L., Simonetti, G., Buiarelli, F., Di Filippo, P., Pomata, D., Riccardi, C., Ristorini, M., Astolfi, M. L., Canepari, S. (2020a). Spatial distribution of levoglucosan and alternative biomass burning tracers in atmospheric aerosols, in an urban and industrial hot-spot of Central Italy. Atmospheric Research, 239, 104904. https://doi.org/10.1016/j.atmosres.2020.104904
Massimi, L., Ristorini, M., Astolfi, M. L., Perrino, C., Canepari, S. (2020b). High resolution spatial mapping of element concentrations in PM10: A powerful tool for localization of emission sources. Atmospheric Research, 244, 105060. https://doi.org/10.1016/j.atmosres.2020.105060.
Massimi, L., Wesseling, J., van Ratingen, S., Javed, I., Frezzini, M. A., Astolfi, M. L., Canepari, S.,Vermeulen, R. (2021). Identification and spatial mapping of tracers of PM10 emission sources using a high spatial resolution distributed network in an urban setting. Atmospheric Research, 262, 105771.

Moreno, T., Querol, X., Alastuey, A., de la Rosa, J., de la Campa, A. M. S., Minguillón, M., Pandolfi, M., González-Castanedo, Y., Monfort, E., Gibbons, W. (2010). Variations in vanadium, nickel and lanthanoid element concentrations in urban air. Science of the Total Environment, 408(20), 4569-4579.
Namgung, H. G., Kim, J. B., Woo, S. H., Park, S., Kim, M., Kim, M. S., Bae, G. N., Park, D., Kwon, S. B. (2016). Generation of nanoparticles from friction between railway brake disks and pads. Environmental Science and Technology, 50(7), 3453-3461.
Nguyen, Q. T., Skov, H., Sørensen, L. L., Jensen, B. J., Grube, A. G., Massling, A., Glasius, M., and Nøjgaard, J. K. (2013). Source apportionment of particles at Station Nord, North East Greenland during 2008–2010 using COPREM and PMF analysis. Atmospheric Chemistry and Physics, 13(1), 35-49.
Norris, G., Brown, S., (2014). EPA Positive Matrix Factorization (PMF) 5.0 Fundamentals and User
Guide. EPA PMF 5.0 Manual.
Okuda, T., Nakao, S., Katsuno, M., Tanaka, S. (2007). Source identification of nickel in TSP and PM2. 5 in Tokyo, Japan. Atmospheric Environment, 41(35), 7642-7648.
Paatero, P. (1999). The multilinear engine—a table-driven, least squares program for solving multilinear problems, including the n-way parallel factor analysis model. Journal of Computational and Graphical Statistics, 8(4), 854-888.
Paatero, P., Hopke, P. K. (2003). Discarding or downweighting high-noise variables in factor analytic models. Analytica Chimica Acta, 490(1-2), 277-289.
Paatero, P. and Tapper, U. (1994), Positive matrix factorization: A non-negative factor model with optimal utilization of error estimates of data values. Environmetrics, 5, 111-126. https://doi.org/10.1002/env.3170050203
Pant, P., Harrison, R. M. (2012). Critical review of receptor modelling for particulate matter: a case study of India. Atmospheric Environment, 49, 1-12.
Perez, L., Tobias, A., Querol, X., Künzli, N., Pey, J., Alastuey, A., Viana, M., Valero, N., Gonzalez-Cabrè, M., Sunyer, J. (2008). Coarse Particles From Saharan Dust and Daily Mortality. Epidemiology, 19(6), 800-807.
Pernigotti, D., Belis, C. A., Spano, L. (2016). SPECIEUROPE: The European data base for PM source profiles. Atmospheric Pollution Research, 7(2), 307-314. http://source-apportionment.jrc.ec.europa.eu/specieurope/index.aspx
Perrino, C., Catrambone, M., Dalla Torre, S., Rantica, E., Sargolini, T., Canepari, S. (2014). Seasonal variations in the chemical composition of particulate matter: a case study in the Po Valley. Part I: macro-components and mass closure. Environmental Science and Pollution Research, 21(6), 3999-4009.
Perrino, C., Canepari, S., Catrambone, M., Dalla Torre, S., Rantica, E., Sargolini, T. (2009). Influence of natural events on the concentration and composition of atmospheric particulate matter. Atmospheric Environment, 43(31), 4766-4779. https://doi.org/10.1016/j.atmosenv.2008.06.035
Perrino, C., Catrambone, M., Canepari, S. (2020). Chemical composition of PM10 in 16 urban, industrial and background sites in Italy. Atmosphere, 11(5), 479.
Perrino, C., Catrambone, M., Pietrodangelo, A. (2008). Influence of atmospheric stability on the mass concentration and chemical composition of atmospheric particles: a case study in Rome, Italy. Environment international, 34(5), 621-628.
Perrino, C., Canepari, S., Pappalardo, S., Marconi, E. (2010). Time-resolved measurements of soluble ions and elements in atmospheric particulate matter for the characterization of local and long-range transport events. Chemosphere, 80(11), 1291-1300. https://doi.org/10.1007/s11356-014-4019-9
Perrino, C., Tofful, L., Dalla Torre, S., Sargolini, T., Canepari, S. (2019). Biomass burning contribution to PM10 concentration in Rome (Italy): Seasonal, daily and two-hourly variations. Chemosphere, 222, 839-848.
Pey, J., Pérez, N., Cortés, J., Alastuey, A., Querol, X. (2013). Chemical fingerprint and impact of shipping emissions over a western Mediterranean metropolis: Primary and aged contributions. Science of the total environment, 463, 497-507. https://doi.org/10.1016/j.scitotenv.2013.06.061
Pietrodangelo, A., Salzano, R., Rantica, E., Perrino, C. (2013). Characterisation of the local topsoil contribution to airborne particulate matter in the area of Rome (Italy). Source profiles. Atmospheric Environment, 69, 1-14. https://doi.org/10.1016/j.atmosenv.2012.11.059
Polissar, A. V., Hopke, P. K., Paatero, P., Malm, W. C., Sisler, J. F. (1998). Atmospheric aerosol over Alaska: 2. Elemental composition and sources. Journal of Geophysical Research: Atmospheres, 103(D15), 19045-19057.
Popovicheva, O., Kireeva, E., Shonija, N., Zubareva, N., Persiantseva, N., Tishkova, V., Demirdjian, B., Moldanovà, J., Mogilnikov, V. (2009). Ship particulate pollutants: Characterization in terms of environmental implication. Journal of Environmental Monitoring, 11(11), 2077-2086. https://doi.org/10.1039/B908180A
Querol, X., Viana, M., Alastuey, A., Amato, F., Moreno, T., Castillo, S., Pey, J., de la Rosa, J., Sanchez de la Campa, A., Artinano, B., Salvador, P., Garcia Dos Santos, S., Fernandez-Patier, R., Moreno-Grau, S., Negral, L., Minguillon, M.C., Gil, J.I., Inza, A., Ortega, L.A., Santamaria, J.M., Reff, A., Eberly, S. I., Bhave, P. V. (2007). Receptor modeling of ambient particulate matter data using positive matrix factorization: review of existing methods. Journal of the Air & Waste Management Association, 57(2), 146-154. https://doi.org/10.1080/10473289.2007.10465319
Querol, X., Moreno, T., Karanasiou, A., Reche, C., Alastuey, A., Viana, M., Font, O., Gil, J., de Miguel, E., Capdevila, M. (2012). Variability of levels and composition of PM_{10} and $PM_{2.5}$ in the Barcelona metro system. Atmospheric Chemistry and Physics, 12(11), 5055-5076.
Querol, X., Massagué, J., Alastuey, A., Moreno, T., Gangoiti, G., Mantilla, E., Duéguez, J.J., Escudero, M., Monfort, E., Pérez García-Pando, C., Petetin, H., Jorba, O., Vasquez, V., de la Rosa, J., Campos, A., Muñóz, M., Monge, S., Hervás, M., Javato, R., Cornide, M. J. (2021). Lessons from the COVID-19 air pollution decrease in Spain: Now what?. Science of The Total Environment, 779, 146380. https://doi.org/10.1016/j.scitotenv.2021.146380
Ramli, N. A., Yusof, N. F. F. M., Shith, S., Suroto, A. (2020). Chemical and biological compositions associated with ambient respirable particulate matter: a review. Water, Air, & Soil Pollution, 231(3), 1-14.
Reddy, M. S., Basha, S., Joshi, H. V., Jha, B. (2005). Evaluation of the emission characteristics of trace metals from coal and fuel oil fired power plants and their fate during combustion. Journal of Hazardous Materials, 123(1-3), 242-249.
Robinson, A. L., Subramanian, R., Donahue, N. M., Bernardo-Bricke, A., Rogge, W. F. (2006). Source apportionment of molecular markers and organic aerosol 1. Polycyclic aromatic hydrocarbons and methodology for data visualization. Environmental science & technology, 40(24), 7803-7810. https://doi.org/10.1021/es0510414

Roma Capitale, LA POPOLAZIONE DI ROMA. STRUTTURA E DINAMICA DEMOGRAFICA Anno 2019, (in English: Rome Population. Demographic Structure and Dinamic) Available online: https://www.comune.roma.it/web-resources/cms/documents/La_popolazione_a_Ro ma2019.pdf (accessed on 2nd June 2021)
Roma Capitale, Piano Generale del Traffico Urbano (in English: City Urban Traffic General Plan). April 2015. Available online: https://www.comune.roma.it/pcr/it/dip_mob_delibere.page (accessed on 2nd June 2021).
Seinfeld, J.H. and Pandis, S.N. (2006) Atmospheric Chemistry and Physics: From Air Pollution to Climate Change. 2nd Edition, John Wiley & Sons, New York.
Sharma, S. K., Mandal, T. K., Jain, S., Sharma, A., Saxena, M. (2016). Source apportionment of PM 2.5 in Delhi, India using PMF model. Bulletin of environmental contamination and toxicology, 97(2), 286-293.
Shen, J., Bigi, A., Marinoni, A., Lampilahti, J., Kontkanen, J., Ciarelli, G., Bianchi, F. (2021). Emerging Investigator Series: COVID-19 lockdown effects on aerosol particle size distributions in northern Italy. Environmental Science: Atmospheres, 1, 214-227. https://doi.org/10.1039/D1EA00016K
Silvern, R. F., Jacob, D. J., Kim, P. S., Marais, E. A., Turner, J. R., Campuzano-Jost, P., Jimenez, J. L. (2017). Inconsistency of ammonium–sulfate aerosol ratios with thermodynamic models in the eastern US: a possible role of organic aerosol. Atmospheric Chemistry and Physics, 17(8), 5107-5118. https://doi.org/10.5194/acp-17-5107-2017
Singhal, T. (2020). A review of coronavirus disease-2019 (COVID-19). The indian journal of pediatrics, 87(4), 281-286. https://doi.org/10.1007/s12098-020-03263-6
Stefenelli, G., Jiang, J., Bertrand, A., Bruns, E. A., Pieber, S. M., Baltensperger, U., Marchand, N., Aksoyoglu, S., Prévôt A.S.H., Slowik, J.G., Haddad, I. E. (2019). Secondary organic aerosol formation from smoldering and flaming combustion of biomass: a box model parametrization based on volatility basis set. Atmospheric Chemistry and Physics, 19(17), 11461-11484. https://doi.org/10.5194/acp-19-11461-2019
Tian, Y., Wu, J., Shi, G., Wu, J., Zhang, Y., Zhou, L., Zhang, P., Feng, Y. (2013) Long-term variation of the levels, compositions and sources of size-resolved particulate matter in a megacity in China. Science of The Total Environment, 463, 462-468, https://doi.org/10.1016/j.scitotenv.2013.06.055.
Tofful, L., Perrino, C., Canepari, S. (2020). Comparison study between indoor and outdoor chemical composition of PM2. 5 in two Italian areas. Atmosphere, 11(4), 368.
Tomassetti, L., Torre, M., Tratzi, P., Paolini, V., Rizza, V., Segreto, M., Petracchini, F. (2020). Evaluation of air quality and mobility policies in 14 large Italian cities from 2006 to 2016. Journal of Environmental Science and Health, Part A, 55(7), 886-902. https://doi.org/10.1080/10934529.2020.1752070
UNI, E., 2014. 12341: (2014). Air Quality–Determination of the PM10 fraction of suspended particulate matter. Reference method and field test procedure to demonstrate reference equivalence of measurements methods.
Viana, M., Amato, F., Alastuey, A., Querol, X., Moreno, T., Garcia Dos Santos, S., Herce, M.D., Fernández-Patier, R. (2009). Chemical tracers of particulate emissions from commercial shipping. Environmental science & technology, 43(19), 7472-7477. https://doi.org/10.1021/es901558t
Wang, C., Horby, P. W., Hayden, F. G., Gao, G. F. (2020). A novel coronavirus outbreak of global health concern. The lancet, 395(10223), 470-473. https://doi.org/10.1016/S0140-6736(20)30185-9.
World Health Organization. (2016). Ambient air pollution: A global assessment of exposure and burden of disease.
Yadav, S., Rajamani, V. (2006). Air quality and trace metal chemistry of different size fractions of aerosols in N–NW India—implications for source diversity. Atmospheric Environment, 40(4), 698-712. https://doi.org/10.1016/j.atmosenv.2005.10.005
Zhao, J., Zhang, Y., Xu, H., Tao, S., Wang, R., Yu, Q., Chen, Y., Zou, Z., Ma, W. (2021). Trace Elements From Ocean-Going Vessels in East Asia: Vanadium and Nickel Emissions and Their Impacts on Air Quality. Journal of Geophysical Research: Atmospheres, 126(8), e2020JD033984. https://doi.org/10.1029/2020JD033984
Zhou, X., Strezov, V., Jiang, Y., Yang, X., Kan, T., Evans, T. (2020). Contamination identification, source apportionment and health risk assessment of trace elements at different fractions of atmospheric particles at iron and steelmaking areas in China. PloS one, 15(4), e0230983. https://doi.org/10.1371/journal.pone.0230983

7. Conclusions and future perspectives

The present PhD research project was focused on the removal mechanism of atmospheric particulate matter (PM) by deposition on tree leaves, in urban and industrial areas. This study was aimed to identify and validate new analytical procedures for the assessment of PM leaf deposition and the chemical and physical characterization of leaf deposited PM. One of the scope of this PhD research project was related to the potential utilization of leaves as alternative, low-cost, and passive PM samplers with biomonitoring or air mitigation purposes. Moreover, PM leaf deposition was investigated with regards to the newly developed concept of nature-based solutions (NbS), to quantify species-specific affinity towards this removal mechanism, and NbS role in removing this hazardous atmospheric pollutant and improving urban air quality.

In the first part of this PhD thesis, several experimental techniques (SEM/EDX and V/F) were applied to the evaluation of PM leaf deposition and to test their efficiency obtained results were compared between each other. In this regard, the chemical fractionation procedure originally developed for the characterization of atmospheric PM membrane filters was adapted for the chemical characterization of inorganic leaf deposited PM, thus allowing to obtain information both on its water-soluble and insoluble fraction. The quantification of the water-soluble fraction of leaf deposited PM resulted to proportional to the washing solution EC, with a constant conversion coefficient K = 0.64, except for species characterized by biological and organic matrices such as honeydew in *T. cordata*. The quantification of the insoluble fraction of leaf deposited PM was consistent with the gravimetric results for the coarse particle fractions ($PM_{2.5-10}$) and PM_{10} loads were consistent with those previously determined by SEM/EDX. Moreover, by using single elemental concentrations from both the water-soluble and insoluble fraction as input variable of a multivariate analysis (PCA), the efficiency of this analytical approach to increase the selectivity of elements as specific source tracers has been proved, thus being able to underline the differentiated impact of the main emission sources acting in the two study areas considered (Terni and Naples).

The PM deposition on leaves of *A. donax* L. was then tested for PM biomonitoring purposes in the city of Terni, an urban and industrial hot-spot of Central Italy. To this aim, leaf deposition results were compared with spatially resolved atmospheric elemental concentrations detected in PM_{10} sampled collected thanks to the newly developed High Spatial Resolution Samplers (HSRS, Fai Instruments, Fonte Nuova, Italy). The good correlations between leaf deposition results and atmospheric PM_{10} concentrations of Cr, Fe, Ni, Mn, Zn and Ti, confirmed the reliability of these leaf deposition results for the evaluation of the impact related to intense local emission sources, such as

the steel plant and vehicular traffic. These results encourage further investigations on the utilization of this riparian species, largely distributed in urban areas of Italy, for future studies on PM leaf deposition and for biomonitoring application as a low-cost alternative for the monitoring of atmospheric PM.

With regards to the NbS concept, details on key indicators, monitoring parameters and recommended methods and protocols used for the evaluation of the environmental impact of NbS on soil, air and water quality) were presented together with few example on the potential utilization of NbS as monitoring tools. Within the European project ProGIreg, SEM/EDX leaf microanalysis was applied for the assessment of PM abatement of specific NbS by means of leaf deposition. In the former and renatured landfill of Dortmund city (DE), the experimental SEM/EDX results on PM removal were used as proxy for the species-specific affinity towards the removal via leaf deposition. The experimental removal of PM was compared with the outputs obtained by *i-Tree Eco* model, with the confirmation of the species-specific trend despite the modelled data were systematically underestimated. In an integrated approach, the *i Tree Eco* model was also employed for assessing the carbon impact of the tree species located within the NbS. Among the tree species, *S. alba* plants emerged as those having the major impact for all the ESs analysed in this study. This study underlined some of the main environmental advantages connected to the NbS implementation, thus also proving the importance of a proper species selection for the management of already implemented NbS, and for the design of new ones, which are expected to increasingly efficient in the future. Moreover, preliminary results on the PM abatement capability of other ProGIreg NbSs, a renatured lake shore in Ningbo (CH), together with an urban forest and productive gardens implemented in the city of Turin, are also presented. Specifically for Turin, preliminary results obtained through the utilization of HSRS installed at high proximity to the two NbS and the application of the chemical fractionation procedure, were also reported with regards to the spatial and seasonal variability of PM_{10} elemental components and known source tracers.

Finally, in the last section of this PhD thesis, new insights were provided on the acquisition of spatially-resolved data on PM_{10} mass concentrations and on atmospheric concentrations of its elemental components. The application of these innovative techniques, including the biomonitoring one, was presented to this aim, thus proving their reliability for spatially resolved analysis and their efficiency in overcoming some of the main limitations associated to conventional PM monitoring. As previously described, all of these alternative techniques resulted to be extremely functional for achieving information useful for the identification of PM emission sources and their impact, and the assessment of human health exposure and risk. However and to our interest, being able to obtain high

resolution spatial data on PM will result and, in some cases already have, in an increased availability of data to be used for the validation of the biomonitoring approach. Coherently with the aims of this PhD thesis, this proved to be true also for the PM biomonitoring based on the utilization of leaves as low-cost and passive samplers and the characterization of leaf deposited particles.

Thanks to the utilization of HSRS systems and the application of the chemical fractionation procedure it was possible to retrieve crucial information on the winter and summer spatial and size distribution of the water-soluble and insoluble PM_{10} elements. This allowed a reliable identification and localization of the main local PM_{10} sources again in the Terni basin, such as rail network and vehicular traffic, biomass burning and the steel plant. It was also possible to evaluate the diffusion capacity of the emitted particles. The described experimental approach enabled us to overcome the limits connected to the study of PM dispersion through the use of mathematical models and the limits associated to the high cost of a monitoring network based on traditional PM samplers. Then, in this same study area, an innovative experimental approach was also described, based on the spatial mapping of oxidative potential acellular assays, namely OP^{AA}, OP^{DCFH} and OP^{DTT}, for geo-referenced assessment of PM potential to induce oxidative stress,. This approach allowed us to map the spatial variability of OP^{AA}, OP^{DCFH} and OP^{DTT}, proving to be a powerful tool, transferable to other monitoring campaigns, for the individuation of spatial relationships between oxidative potential of PM and its chemical composition and sources. The described approach promises to be very effective for the identification and localization of the emission sources mainly responsible for ROS generation and provides a reliable tool for spatially-resolved evaluation of exposure to PM and relative health risk. Moreover, the efficiency of transplanted lichens of *E. prunastri* was proved towards the reflection of the air concentration and spatial variability of persistent organic pollutant (POPs), thus encouraging their use as low-cost biomonitors for obtaining high spatial resolution data and mapping their spatial distribution. Finally, the impact of the lockdown-based policy adopted by Italy during 2020 to contrast the spread of the Coronavirus disease 2019 (Covid-19) was evaluated for the Rome area (Italy), concerning the relative strength and time evolution of local and non-local acting sources. To this aim, daily PM_{10} samples chemically speciated, collected during pre-lockdown, lockdown and post-lockdown periods at three urban sites in Rome were analysed by PMF. From pre-lockdown to lockdown, a significant abatement of local sources (vehicular traffic and biomass burning) was observed at all sites. As additional consequence of forcing the reduction of local anthropogenic activities and their source strength, the non-local source contributions that mainly occurred during lockdown, were poorly influenced by the chemical fingerprint of local sources. This allowed to describe their profile and estimate mass contributions more accurately than obtainable from PMF input datasets of PM collected during routine periods. Overall, the contribution from vehicular traffic

was considerably reduced by Covid-19 lockdown; however, a more considerable decrease in PM_{10} mass concentration would have been expected during lockdown.

Future perspectives of this study will regard the upscale at the NbS and at the Living Lab level of species-specific leaf deposition results obtained by means of the SEM/EDX leaf microanalysis, as previously described. The evaluation of the PM abatement of green walls implemented outdoor and indoor in the city of Turin (Italy) and in the city of Zagreb (CR), always within the ProGIreg context, will be also carried out, to assess the efficiency of this specific NbS type, towards the provision of this air-quality related ecosystem service (ES). Results obtained for the Ningbo NbS, will be furtherly integrated with other environmental data, which are connected to water quality, soil contamination and biodiversity, to present a comprehensive evaluation of the ESs provided. Moreover, and to our knowledge for the first time, EDX data related to the chemical characterization of leaf deposited PM at the two Turin NbSs, the New Forest and the Orti Generali ones, will be employed for the application of the PMF model, to explore the application of these data to source apportionment purposes. In this context, the utilization of HSRS samplers, tested in this study for spatially resolved analysis of PM and its main elemental components used as specific source tracers, will be extremely important for validate and prove the efficiency of leaves as low-cost PM samplers and the evaluation of leaf deposited particles for biomonitoring purposes, both for the evaluation of emission sources impact and for human health exposure.